CONTENTS

Acta Technica *62*, No. 1A/2017, 1–10

Study on the passive solar house with water filled cavity[1]

Hou Gang[2], Niu Xiaoqi[2], Li Bing[3], Zhu Liyang[4]

Abstract. In order to eliminate the shortcomings of the existing solar house, a kind of passive housing structure was put forward. The principle, construction and control of this kind of housing were studied. A large number of cavities filled with water were arranged of construction. Cavities in the wall and floorslab were connected with solar collectors hanged on building exterior wall. Water could flow in circulation between solar collectors and cavities in the wall and floorslab. Thermal storage capacity and fluidity of water was used to realize a comfortable temperature of the winter room through rise temperature of walls and floorslabs uniformly. The use of this structure in summer could be further explored on the basis of the winter heating application achieved. This kind of housing was the same as the common house in terms of the internal structure, and the room temperature was more uniform because of the large amount of water used. Compared with the traditional structure, the thermal efficiency of this structure has greatly improved.

Key words. Passive solar housing, thermal storage capacity, water, structure.

1. Introduction

Energy crisis is a common problem in the world today, and how to make better use of solar energy, wind energy, geothermal energy and other clean energy has become a scientific research focus. Solar energy is inexhaustible, no pollution and cheap. With a tide of more and more attention to energy conservation and environmental protection worldwide, the development of energy-efficient buildings has become a major trend of building development in many countries. In this situation, the solar housing as a kind of energy-efficient buildings which fully exploit the potential of solar energy should receive adequate attention.

The ways of using solar energy in buildings is divided into active way and passive way. Active use of solar energy systems need to use other power sources, such as electricity, to achieve the purpose of heating or cooling. Passive mode is totally rely

[1]This work is supported by 2016 undergraduate teaching project 2016 year of Anyang Normal University.

[2]Institute of Civil Engineering, Anyang Normal University, Anyang, Henan, 455000, China

[3]Anyang Affair Co. of Water, Anyang, Henan, 455000, China

[4]Anyang Municipal Design and Research Institute Co., Ltd., Anyang, Henan, 455000, China

the power generated by solar to complete heat extraction, transportation, storage and distribution in winter, and to cool rooms by shading solar radiation, natural ventilation in the summer, through the rational arrangement and cleverly constructed of the building.

2. State of the art

The earliest patent technology of passive solar house was "black tiles" invented by an American Professor named Morse in 1881. But the research of solar house was accelerated after 1983. The first experimental solar house named MIT-1 was built by Massachusetts Institute in United State. The first article about solar heating was written by Dr. Holter in 1942. The first academic meeting about the use of solar heating was held at the Massachusetts Institute of Technology in 1950. Trombe walls obtained French patent later which had a significant contribution in the development of solar house were successfully researched by Dr. Felix Trombe director of the Institute of France odero solar who proposed first and Michel as an architect who was an collaborator. Especially after the energy crisis in 1973, it set off a climax to the study of solar house. The first research conference which theme is passive solar house was held in New Mexico May 1976. PASOLE, the passive solar house simulation program, was successfully prepared by Dr. J. D. Balcomb in United States Alamos Los National Laboratory in the same year. In the spring of 1977, Balcomb analyzed the influence of different weather conditions and structural parameters on the thermal performance of solar house used the validated program simulation. By 1980s, passive solar houses enter the practical stage from the testing phase in the world. In 1980, the Los Alamos National Laboratory published passive solar housing design manual in New Mexico, the United States. In 1982, the passive solar house magazine began publishing. In the last 20 years, the research trend of solar building has been gradually changed from theory and experiment to numerical analysis and computational simulation based on computer [1–10]. The work of practical quantitative simulation about the application technology of passive solar energy was Rapid progressed, and many of them have become commercial software, such as ENERGY, SOLA, TARP, ASEAM, DOE, BLAS, EnergyPlus, etc.

3. Methodology

Water's specific heat capacity is maximum in common substances, so water has a strong heat storage capacity. Water has good flowability at same time. If the floors and walls can be made with water, a "Water House" will be constructed in which thermal stability and temperature uniformity will be greatly improved. An ideal approach is walls and panels are made of two sheets sandwiching a layer of water. The outer sheet of exterior wall and roof is made by good insulation properties, the inner sheet of exterior wall and roof is made by good thermal conductivity. Tow sheets of interior walls and floors is made by good thermal conductivity. The water in the wall and the floor is heated by a solar collector, and the flowability and heat

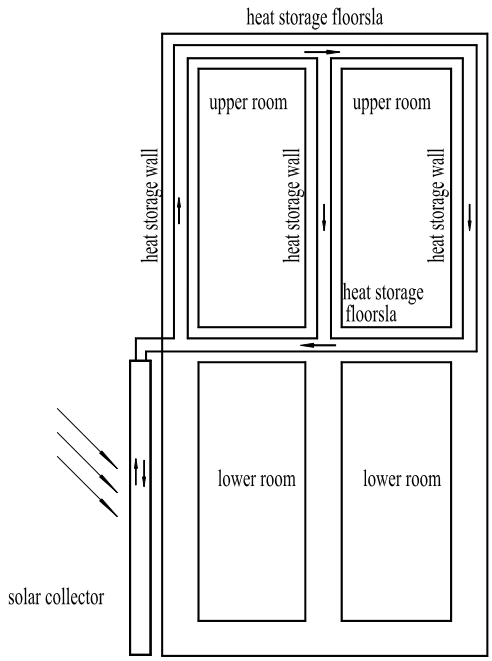

Fig. 1. The heat storage walls (floorslabs) and solar collector installed in the lower layer

storage capacity of water storage can make a suitable temperature in the room. Unfortunately, this configuration is not easy to realize and is not practical.

In fact, we can set up variety shape of cavity in the walls and floors, for example, buried pipe to form cavities. Filling with water in cavities, the wall and floor's heat storage capabilities are enhanced. They were called heat storage wall and heat storage floorslab. Being heated in the solar collector, water flows in the walls and floorslabs. In addition to improving the heat storage capacity of the wall and the floor, the water has the function of the heat medium. Heat storage walls and heat storage floorslab increase indoor temperature in winter by convection and radiation. Water is heated in solar collector, and flows into the heat storage wall (or heat storage floorslab), when heat release, cooling water flows back to solar collector. Heat storage walls (or heat storage floorslabs) are connected with the connecting pipe into the loop.

4. Installation method of solar collector

Used the installation method of Fig. 1, water flow into the heat storage wall and heat storage floorslab. Water rise to the heat storage walls and heat storage floorslab heated by solar collector, and drop back to solar collector when heat released. It has certain advantages that in the non-one-story building solar collectors are installed

next level. When there is no sunlight at night, the solar collector does not heat water, then high temperature water stays in the heat storage wall and heat storage floorslab, and the slow release of heat maintain proper thermal environment indoor. Low temperature water stays in the solar collectors. Indoor and outdoor water is no longer circulating, avoid the heat loss of hot water in the outdoor fittings. Because the solar collectors cannot install in the next layer, this method of installation will not use at first floor.

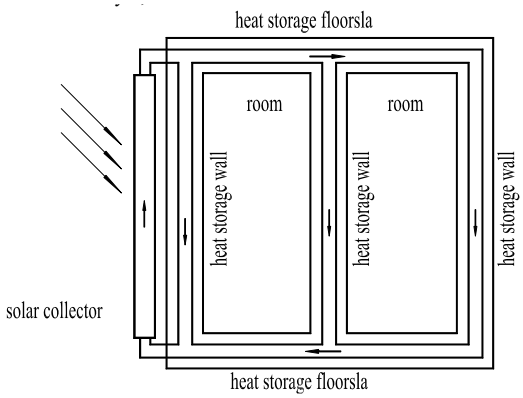

Fig. 2. The heat storage walls (floorslabs) and Solar collector installed in the same layer

Another installation of solar collectors is installed in the same layer, as shown in Fig. 2. When the outdoor temperature is low at night, water will reverse flow. As the water is still circulating in the indoor and outdoor, the corresponding portion of the heat collector should be prepared insulation to reduce heat loss. Solar collector can be set in the exterior wall having long sunshine time, which can be set at east wall and west wall, not limited to the south wall. When two or more differently oriented wall are installed solar collectors, there is a benefit using the lower installed manner, that is different orientations of solar collectors can be connected with heat storage walls and heat storage floorslabs, because the water in the heat collector is not recycled when the sun shine is not on the wall where the heat collector installed on, and heat storage walls and heat storage floorslabs could avoid being cooled for water cycle. Solar collector which the sun does not shine on will play a role of radiator if installation in the same layer is used (Of course, we can install an automatic valve, in order to close it to stop water cycle when the solar collector cannot play a role of heating).

4.1. Basic type

The basic type is depicted in Fig. 3.

The solar water heater and several heat storage wall (heat storage floorslab) are connected to form a basic system. The vent valve or the air collector is set at the highest point of the whole system to discharge air when gas gather to a certain degree

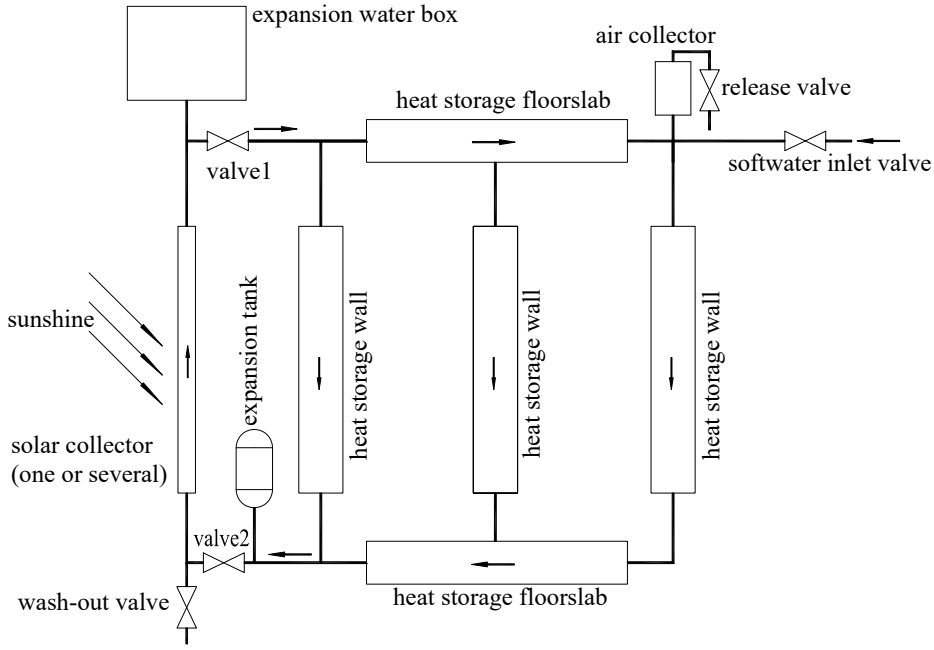

Fig. 3. Basic type- using solar energy for heating

in order to prevent the formation of air blocking effecting on water circulation. A wash-out valve is set at the lowest point of the whole system to vent water of pipe at maintenance time. Soft water is needed in order to prevent fouling. Water inlet valve can be used when the system need be filled with water, and we can also fill water into the expansion tank directly.

The basic type is only used for winter heating. The expansion water box for containing water expansion and contraction (the expansion tank can be used to discharge gas in water, so air collector is not necessary.) When weather gets warmer and it become overheating indoor, valve 1 and valve 2 which are installed between solar collector and heat storage walls (heat storage floorslabs) should be closed. So the solar heat collector is no longer supplying heat to the heat storage walls (and heat storage floorslabs). The tank contains water volume expansion and contraction in the heat storage walls and floorslabs. The basic type is only working in winter, and it is idle in summer.

4.2. Selection of heat storage wall (floorslabs)

Solar collectors installation location should be choose appropriately not to interfere with the function of the window and balcony, tough the shape of house is varies. House walls and floorslabs (floors and ceiling) can be made heat storage in whole or in part. Of course, part of a wall or a floorslab can be made also. If the heat storage walls (floorslabs) cannot be connect to a loop, some pipes can be added to

form a loop which can be laid in the walls and floorslabs. Interior walls and walls of important room have priority if partly setting heat storage. When this structure is set in building, each system is connected to only one heat storage floorslab (ceiling or floor), another heat storage floorslab is connected to the adjacent layers of the system. Figure 4 shows the heat storage system of four sides of heat storage wall and a side of heat storage floorslab (ceiling), and three solar collectors are installed on three exterior walls.

4.3. The cavity in heat storage wall (floorslab)

One side of has tow or more joints which will be connected the adjacent heat storage walls (floorslabs) or solar collector. The connecting pipe is embedded in the wall or in the floorslab. Heat pipes in the heat storage wall (floorslab) designed into a grid shape, curved shape, etc. The pipeline in heat storage floorslab can be set in the structure layer, leveling layer or other layer. The pipeline in the heat storage wall can be set combined with the construction technology of the wall in an appropriate layer in the wall. The pipeline can be produced previously in construction module and be poured (or masoned) in walls (or floorslabs) and can also be worked at the construction site. The pipeline can be poured in precast concrete parts as well.

5. Result analysis and discussion

5.1. The advantages of the passive solar housing construction

The biggest advantage of this type of construction is exactly the same as an ordinary house from the inside view is not to add additional structure or to change the space division. Water can flow to any one location house and people are free to choose any part of wall (floorslabs) as the heat storage plate. The exist of water, the heat storage capacity of wall (floorslabs) is greatly enhance, and the volatility of room temperature is reduced. It can be automatically controlled addition of a simple element.

5.2. The difference with solar floor heating

When floor heating is working, the floor is heat radiating surface, and water is heat medium. The source of solar floor heating is sunlight, and water still plays a major role of heat medium.

The structure described in this article in the form of being set a large number of cavities in the walls and floorslabs are accumulated a lot of water much more than that of the floor heating. The more use of water in this structure is its storage capacity in addition to using water as a heat medium.

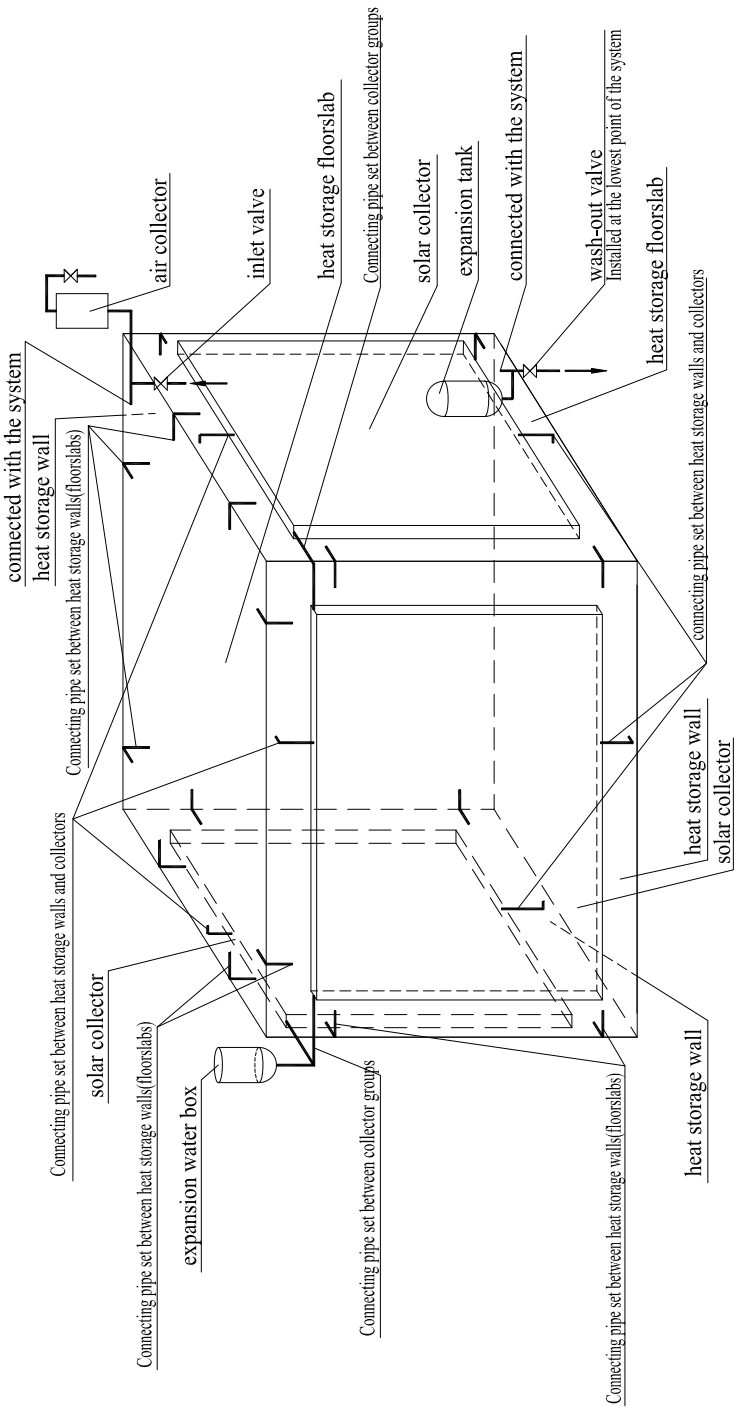

Fig. 4. Installation of solar collector and heat storage wall (floorslab)

5.3. Shortcomings and problems to be studied

This structure is not perfect, it has some drawbacks. Extensive use of water will increase the load of the building. The presence of cavity in wall or floorslab causes the increase in thickness of the wall or floorslab. The complexity of the construction increases the cost of construction. In addition, there are also some problems need to be study more deeply, and find good solutions; otherwise it is difficult to promote the construction.

Most of the water system is in the interior of walls and floodslabs, so the easy implement way is to use tubular made by some material to form seal cavity, then to fill them with water. Metal and plastic is common choose to form cavity. The material is requiremented to be able to maintain a long water-filled state without leakage. If there is leakage, maintenance will be more difficult or even not to repair. If the cavity is set in the non bearing layer, the wall or the plate can be broken open to repair, and if the cavity is set in the load bearing layer, it can not be repaired, the system will be abandon. Steel and plastics are common building materials, however, long-term contact with water the steel will rust occurs, and the plastic will appear the problem of aging.Joints of material and junctions of fitting is the weak link, where is prone to leakage. But the use of other materials with good durability which price is much higher will increase the construction costs substantially.

Fouling causes cavities thinning, pipes clogging, and because it is difficult to repair, fouling affects the using effect of this structure and service life. Even the use of soft water, prolonged use will consume part of the water, and because the remaining water ion content has increased, there is still fouling problems. To neglect leakage, fouling and other issue, to dispose pipeline in structure layer is a good idea. The pipe has been protected by concrete from the external damage. But in the structure layer, a large number of tubes will produce harmful effect to the mechanical properties of the structural layer. It is a question whether it can be achieved from mechanics' point of view to lay a lot of tubes in the structure layer, and even if it can achieve, whether it is economically reasonable is worth to explore. If the idea is rejected by the research on this issue, the cavity has to be set in other layers.

The components should be standardized in order to simplify the construction site and to improve the quality of components. The pipes can be made into standard components according to a certain modulus which can be poured or masoned directly in walls or floorslabs and can be poured into the preforms also.

In order to obtain a better temperature distribution, the water should be able to uniformly flow smoothly. The shape of the cavity should be chosen according to the hydraulic calculation.

The temperature of the water in the solar structure is suitable for the propagation of microorganisms. A large number of microbial breeding will produce a blockage in the pipeline and the problem of corrosion pipeline has become serious at same time.

In different structural forms, such as concrete structure, masonry structure, steel structure, there should be a different construction process. In cold regions, if such a structure is used, the problem of freeze in pipe may appear encountered continuous cloudy. Some work needs to be done, such as building a model room to test and

compare with traditional solar house heating effect.

6. Conclusion

Disadvantages of the traditional solar houses hinder the promotion of the passive solar house. The passive solar house with water filled cavity make well used of the fluidity and the heat storage capacity of the water, and it has the effect which the traditional solar houses are difficult to achieve. Heat storage walls (floorslabs) are built by made cavity which filled with water in walls (floorslabs). The heat storage capacity of walls and floorslabs are greatly improved for the cavities with water. Because of the mobility of the water, the heat flow between the various heat storage plates, so the uniformity of the temperature distribution of the room is greatly improved. Due to the special arrangement of the solar house which function is not dependent on the architectural space and good combination of its functional components and walls (floorslabs), the building can be constructed in the same way as an ordinary house, without increasing the structure or changing the space. Because water can be well control by valve and automatic control can be easy achieved, the indoor temperature can be adjust well. The study adds a new form of solar house. However, due to the need for further research on anti scaling, leakage prevention, standardization and other aspects, there is still a certain distance from practical application. In addition, some of the more complex automatic control can be achieved to heat in winter and to cool in summer in order to use solar energy fully.

References

[1] Li En, Liu Jiaping, Yang Liu: *Research on the passive design optimization of direct solar gain house for residential buildings Lhasa.* Industrial Construction *42* (2012), No. 2, 27–32.

[2] MA Yu-zhi, Meng Chang-zai: *The simulation analysis of passive solar houses with additional sunshine in ALaShan pastoral areas.* Energy Conservation *42* (2012), No. 5, 38–41.

[3] Chen Mingdong, Shi Yuliang, Liu Xuebing: *Heating study of passive solar house with sunspace.* Acta Energiae Solaris Sinica *33* (2012), No. 6, 944–947.

[4] Niu Run-ping, Xu Xiao-long: *Test and research on phase change energy storage floor heating system in active solar house.* Building Science *29* (2013), No. 8, 49–52.

[5] Wang Dengjia, Liu Yanfeng, Wang Bin, Chen Huiling: *Measuring study of heating performance of passive solar house with trombe wall in Qinghai-Tibet plateau.* Acta Energiae Solaris Sinica *34* (2013), No. 10, 1823–1828.

[6] Ma Yunhe, Jiang Shuguang, Teng Yuming, Cheng Bo: *Experimental studies on passive solar house heating in winter in the serve cold regions in Xinjiang.* Building Science *30* (2014) No. 8, 41–46.

[7] Wang Chun, Jiang Shu-guang, Huang Yu-wei, Duan Qi, Liu Yu-xi: *Experimental study on ventilation effect in system combined solar wall with basement in summer.* Architecture Technology *47* (2016), No. 7, 615–618.

[8] He Wei, Wang Chenchen, Ji Jie: *Study on the effect of Trombe Wall with Venetian blind structure on indoor temperature in different blade angle.* Acta Energiae Solaris Sinica *37* (2016), No. 37, 673–677.

[9] Wang Chun, Jiang Shuguang, Cheng Bo, Ma Yunhe, Duan Qi, Huang Yuwei: *Experimental study on heating of the system combined solar wall with basement in winter.* Acta Energiae Solaris Sinica *37* (2016), No. 3, 678–683.

[10] Fan Xin-jie: *Energy saving analysis based on survey data in rural areas for self-shading and sun space.* Building Energy & Environment *535*, (2016), No. 3, 71–74.

Received April 13, 2017

Acta Technica *62*, No. 1A/2017, 11–20

The damage effect of explosions on immersed tube cross-river tunnels

Yin Ni[1,2], Yonglai Zheng[1], Fang Li[1]

Abstract. Taking Shanghai Outer Ring Tunnel as an example, the safety of immersed tube cross-river tunnels under air defense loads is studied. Using the finite difference software FLAC, a model is built according to the coefficient of subgrade reaction derived from a dynamic triaxial test. The internal force distribution of a typical cross section in the main structure of tunnel under different working conditions is calculated. The joint opening of the immersed tube caused by longitudinal differential settlement under air defense loads is calculated, too. Results show that setting protective doors in a tunnel can significantly improve the blastproof performance of the immersed tube structure and keep the joint displacement of differential settlement within a controllable range.

Key words. Immersed tube tunnel, explosive effect, protective door, resistance coefficient, longitudinal settlement.

1. Introduction

At present, there are many lessons and theories about earthquake resistance and hazard reduction of cross-river tunnels at home and abroad. A vast majority of them focus on tunnels constructed with the advanced shield tunneling method today. But few are reported on the air defense of immersed tube tunnels. Cross-river tunnels, as key nodes of urban traffic trunks, used to be air defense evacuation exits and temporary shelters during wars. So they must be able to resist nuclear explosions in the wartime. Liu Ganbin et al. [1] carried out a numerical simulation on dynamic response of tunnels in soft soil under explosive loads and gave the dynamic response law of nodes in particular parts. Chen Bin et al. [2] studied the explosive shock wave load on a cross-river tunnel for metro. Lu Zhifang [3] analyzed dynamic response and damage of Yangtze River Tunnel under different explosive loads. Shi Xianwei [4] studied the structural calculation and analysis on an immersed tube cross-river tunnel from Yuzhu Wharf, Guangzhou to Changzhou Island and concluded that the greater difference between adjacent coefficients of subgrade reaction, the greater

[1]Department of Civil Engineering, Tongji University, Shanghai, 200092, China
[2]China State Construction Harbour Construction Co., LTD, Shanghai, 201300, China

negative bending moment peak. One of our research team members, Xiao Li et al. [5] examined the damage effect of a nuclear explosion on a cross-river shield tunnel and reported that setting protective doors in the shield tunnel can effectively prevent the effect of nuclear explosive shock wave on the structure of tunnel.

Different construction processes between immersed tube tunnel and shield tunnel also lead to different structural performances. The immersed tube tunnel adopts a reinforced concrete rectangular framework. There is multifarious equipment in the tunnel. It remains a controversy whether a protective airtight door needs to be set in the immersed tube tunnel. Therefore, it is necessary to study the damage effect of explosive load on immersed tube tunnels and identify the importance of protective airtight doors.

2. State of the art

Outer Ring Tunnel is the last single construction project along Shanghai outer ring. It is about 2000 m away from Wusong Port and 2880 m in length. Being the first cross-river tunnel constructed with immersed tube in Shanghai, Outer Ring Tunnel is composed of seven immersed tubes, each of which is equivalent to more than half of a soccer field. After drainage, leakage detection and other procedures, the immersed tubes are floated and transported to water surface and gradually sunk to desired positions. After tested, facilities on the end faces of segments are dismantled and assembled in water as a whole. Sand is filled between the tube bottom and riverbed by pressure to form foundations of segments. E7 and E6 segments are sunk into Pudong, while E1 to E5 segments are sunk into Puxi in proper order. Finally, E5 and E6 segments are jointed, to make the tunnel run-through as a whole [6].

E4 segment in the river is taken as a typical cross section, as shown in Fig. 1. E4 segment is a prefabricated immersed tube, whose cross section is 43 m wide and 9.55 m high. The lining of roof is 1.5 m thick. The side wall is 1.0 m thick. The floor is 1.5 m thick. The interior wall is 0.55 m thick. Roadway slabs are connected with the entire structure and filled with C30 concrete [6].

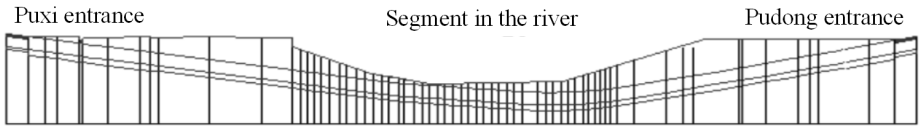

Fig. 1. Longitudinal section of outer ring tunnel

3. Methodology

Air defense loads can be divided into two working conditions, Grade-6 nuclear weapon and Grade-6 conventional weapon. For some of the parameters, we suppose as follows:

Suppose that all layers have the same soil parameters, i.e., the soil is a single soil

medium, whose properties are shown in Table 1.

Table 1. Properties of soil layers

Soil/Structure	Density (kg/m^3)	Elasticity modulus	Poisson's ratio	Bulk modulus	Shear modulus
Clayey silt	1860	3.471×10^7	0.30	2.892×10^7	1.335×10^7
Silty clay	1870	2.390×10^7	0.30	1.992×10^7	9.192×10^6
Mucky clay	1780	2.390×10^7	0.30	1.992×10^7	9.192×10^6
Backfill	1862	5.849×10^6	0.31	5.173×10^6	2.23×10^6
Huangpu River silt	1700	2.501×10^6	0.20	1.389×10^6	1.042×10^6

Under a nuclear explosion, when air shock wave propagates inside the tunnel, shock wave attenuation caused by energy loss incurred in the propagation process is ruled out. Meanwhile, it is supposed that the impact of tunnel shape transformation has little impact on shock wave parameters. Relevant factors can be neglected.

The impact of river water on shock wave in the propagation process is ruled out, i.e., it is believed that shock wave does not attenuate when propagating in water. When calculating the impact of conventional weapon, we rule out the impact of river water, too.

Under a nuclear explosion, given the short duration of shock wave, the internal air shock wave and external compression wave from soil are not applied to the structure simultaneously when calculating.

The overpressure of straight-in internal shock wave inside the structure is equal to the overpressure of ground shock wave ΔP_{m}. The overpressure of superimposed internal shock wave is three times as large as the overpressure of ground shock wave $3\Delta P_{\mathrm{m}}$ [7].

According to a dynamic triaxial test conducted by our team on undisturbed soil [5] and [8], the coefficient of subgrade reaction is calculated. The silty clay is $5130\,\mathrm{kN/m^3}$. The clayey silt is $4510\,\mathrm{kN/m^3}$. The silt and backfill is $2080\,\mathrm{kN/m^3}$.

For nuclear explosion, the waveform of compression wave in soil is simplified into a triangle of pressure rise time. The maximum pressure and pressure rise time can be calculated as

$$p_{\mathrm{h}} = [1 - \frac{h}{c_1 t_2}(1-\delta)]\Delta P_{\mathrm{m}}\,, \tag{1}$$

$$t_{0\mathrm{h}} = (\gamma - 1)\,\frac{h}{\nu_0}\,, \tag{2}$$

and

$$\gamma = \frac{\nu_0}{\nu_1}\,, \tag{3}$$

where p_{h} (MPa) is the pressure peak of compression wave. Symbol ΔP_{m} (MPa) is the overpressure peak of ground air shock wave and h (m) is the calculation depth of soil. When calculating roof, the thickness of covering soil is adopted. Symbol $t_{0\mathrm{h}}$

(s) is the pressure rise time of compression wave and t_2 (s) is the pressure drop time. Finally, δ is the residual strain ratio of soil, γ is the velocity ratio, ν_0 (m/s) is the initial pressure velocity of the soil and ν_1 (m/s) is the peak pressure velocity of the soil.

For the impact of an indirect hit of conventional weapon on the structure, we assume that under a Grade-6 air defense, with the increase of distance from charging point, explosive loads on different positions decrease. The resulting pressure peak of compression wave can be calculated as [9]

$$\Delta P_{\mathrm{m}} = 1.316 \left(\frac{L_{\mathrm{i}}}{\sqrt[3]{C}} \right)^{-3} + 0.369 \left(\frac{L_{\mathrm{i}}}{\sqrt[3]{C}} \right)^{-1.5}, \tag{4}$$

$$p_{\mathrm{h}} = \Delta P_{\mathrm{m}} \exp \left(-n_1 \sqrt[3]{\frac{h}{1000\tau_i}}, \right) \tag{5}$$

where ΔP_{m} (MPa) is the overpressure peak of ground shock wave at the projection point of slab center on the earth's surface. Symbol L_{i} denotes the horizontal distance from the charging center to calculation point, and C is the equivalent TNT load of conventional weapon. Finally, n_1 is the attenuation coefficient in soil and τ_i (s) is the duration of overpressure.

Equivalent static load method is used for calculation. According to resistance standards to Grade-6 nuclear explosion and Grade-6 conventional weapon, using a three-coefficient method, standard values are adopted for the roof equivalent static load, side wall equivalent static load and floor equivalent static load of the tunnel respectively [9].

4. Result analysis and discussion

4.1. Modeling

When protective air-tight doors are set on the entrances on both sides of the cross-river tunnel, a nuclear explosive shock wave acts on the external structure, known as external shock wave effect. If protective doors are not set in a timely manner, shock wave will rush into the tunnel from the entrances and produce a superimposed shock wave effect in the middle of tunnel (in the river). In Fig. 2, P_{roof} is the load of covering soil, P_{bottom} is the subgrade reaction, P_1 and P_2 are pressures from top and lateral soil, P_ν is the load of vehicle, P_{n1}, P_{n2} and P_{n3} are air defense loads on the roof, side wall and floor. Further, P_{in} is the internal shock wave load. Among them, pressures from covering soil and lateral soil, as well as gravity load are calculated using a soil mechanics approach.

Under an explosive load, standard values of the uniform equivalent loads on the roof, side wall and floor of the immersed tube can be calculated as

$$P_{\mathrm{n1}} = K_{\mathrm{d1}} \cdot K \cdot P_{\mathrm{h}}, \tag{6}$$

$$P_{\mathrm{n2}} = K_{\mathrm{d2}} \cdot \zeta \cdot P_{\mathrm{h}}\,, \tag{7}$$

$$P_{\mathrm{n3}} = K_{\mathrm{d3}} \cdot \eta \cdot P_{\mathrm{h}}\,, \tag{8}$$

where K_{d1}, K_{d2} and K_{d3} are dynamic coefficients of the roof, side wall and floor, K is the comprehensive reflection coefficient of roof, ζ stands for the pressure from lateral soil, and η is pressure from bottom soil. The specific values are shown in [9].

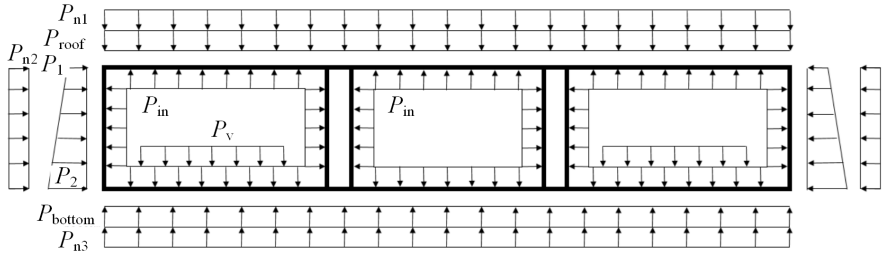

Fig. 2. Calculation model of E4 segment

Considering that E4 segment lies in the river and involves three working conditions, i.e., mean high water level, mean low water level and highest navigable water level, the water level elevation in its location can be divided into 1.02 m mean low water level (Huangpu River Elevation System, similarly hereinafter), 3.25 m means the high water level and 5.99 m is the highest navigable water level [10]. The most unfavorable conditions are adopted.

Using general finite element software FLAC5.0, the internal static force of plane strain is calculated. Using the Beam element structure in Struct module, the framework, roadway slab and internal partition of the tube are simulated. Beam elements of the rectangular framework are connected with stiff joints. The internal partition and framework are also connected with stiff joints. In FLAC5.0, beam elements can only add normal and tangential loads, so the loads are simplified into concentrated loads on nodes. Beam elements are 1.0 m wide, in order to reduce the calculation error. For ease of calculation, this rectangular tunnel is divided into 8 beam elements, which move in the horizontal restraint direction X and vertical restraint direction Y on the bottom left and right of the structure. The calculation model of FLAC is shown in Fig. 3.

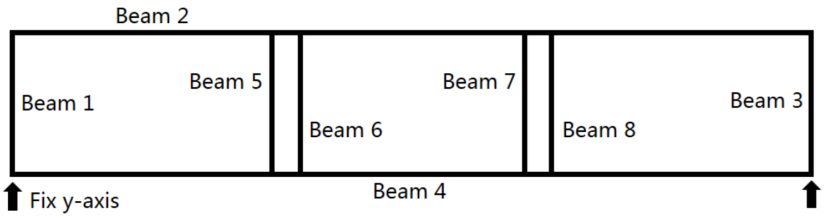

Fig. 3. Calculation model of FLAC

Beam 1 is the left wall in the left channel, beam 2 is the roof, beam 3 is the right wall in right channel, beam 4 is the floor, beam 5 is the right wall in left channel, beam 6 is the left wall in middle channel, beam 7 is the right wall in middle channel, and beam 8 is the left wall in the right channel.

4.2. Calculation results

Under a Grade-6 nuclear explosion, with protective doors, the internal force effects on cross section are depicted in Figs. 4 and 5.

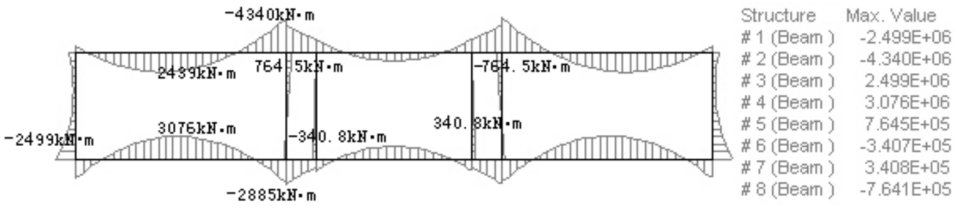

Fig. 4. Bending moment diagram (Grade-6, nuclear explosion, with protective doors

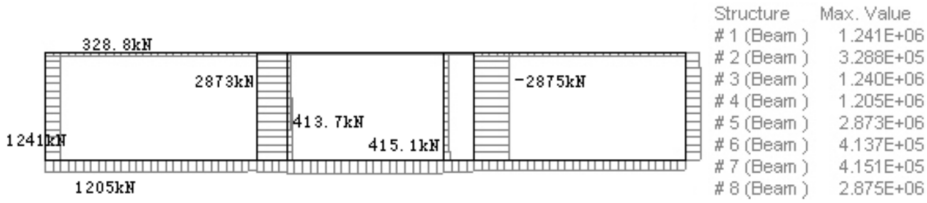

Fig. 5. Axial force diagram (Grade-6, nuclear explosion, with protective doors

Under a Grade-6 nuclear explosion, without protective doors, the internal force effects of superimposed shock wave on cross section are depicted in Figs. 6 and 7.

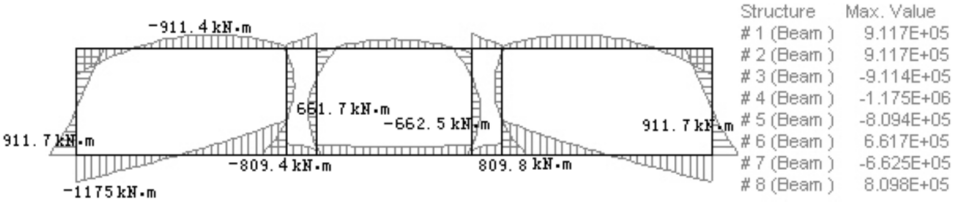

Fig. 6. Bending moment diagram (Grade-6, nuclear explosion, with protective doors open

4.3. Internal force analysis

Under the impact of a dynamic load, the strength of structural material is improved to a certain extent. When calculating reinforcement, the strength of structural material is adjusted [9], as shown in Table 2 below.

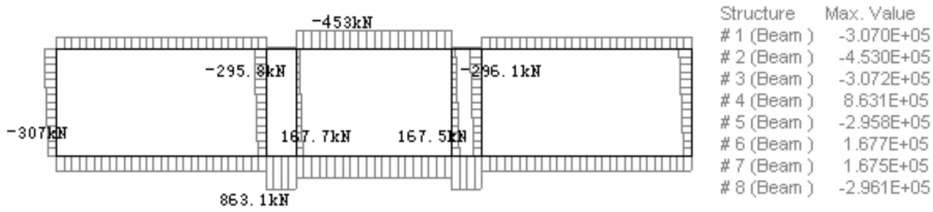

Fig. 7. Axial force diagram (Grade-6, nuclear explosion, with protective doors open

Table 2. Adjustment of material strength in dynamic calculation

Material	HPB235	HRB335	C30	C50
Strength before adjustment ((kN/m^2))	210	300	14.3	23.1
Strength after adjustment (kN/m^2)	315	405	19.305	31.185

Since the bending moment and axial force produced by an indirect hit of conventional weapon on the structure of an immersed tube tunnel with Grade-6 protection are far lower than the impact of nuclear explosion under the same conditions, in our study, when calculating reinforcement, we only calculate the effect of nuclear explosion. The calculation results are shown in Table 3. Under a Grade-6 nuclear explosion, with protective doors, all of the members of immersed tube satisfy requirements. Without protective doors, the right wall of left channel, left wall of right channel and left and right walls of middle channel do not meet the requirements for flexural capacity.

Table 3. Calculation results

Air defense grade	Member name	With protective doors	Without protective doors
Air defense grade	Roof (max positive bending moment)	Satisfied	Satisfied
	Roof (max negative bending moment)	Satisfied	Satisfied
	Right wall of right channel	Satisfied	Satisfied
	Floor (max positive bending moment)	Satisfied	Satisfied
	Floor (max negative bending moment)	Satisfied	Satisfied
	Right wall of left channel	Satisfied	Not satisfied
	Left wall of middle channel	Satisfied	Not satisfied
	Right wall of middle channel	Satisfied	Not satisfied
	Left wall of right channel	Satisfied	Not satisfied

4.4. Modeling calculation and analysis of longitudinal section

4.4.1. Modeling We consider differential settlement caused by Grade-6 nuclear explosion within 1600 m of the tunnel, with protective doors. Using the finite difference software FLAC, a longitudinal section model is built. Elastic models are adopted for the soil and tunnel structure. We make river water equivalent to hydrostatic pressures and load them to corresponding positions on the soil surface. Given that the existence of tunnel will not resist differential settlement under a dynamic weapon load, materials with the same properties as soil elements are used for the tunnel. The boundary conditions of model are: with the base fixed, move in the direction of Y and with left and right sides fixed, move in the direction of X.

Assume that protective doors are set on both ends of the tunnel. The shock wave load of Grade-6 nuclear explosion on the soil surface is 0.05 MPa and loaded on the model roof. Before loading, river water loads on corresponding positions of the model are calculated.

4.4.2. Calculation results The model is calculated using FLAC in two steps.

Step 1: to let the model reach an initial balance under acceleration of gravity, without a dynamic weapon load.

Step 2: to reset the displacement produced by the initial balance and add a weapon load, calculate until a balance is reached. Using detection points along the tunnel model, values of differential settlement at various points are recorded [11-12].

A curve fitting is conducted on values of differential settlement in different positions. The minimum radius of curvature is calculated by the fit curve of differential settlement. After that, the joint opening is calculated by the minimum radius of curvature. The fitting result is that the minimum radius of curvature is $\rho = 15.3$ km.

The horizontal opening of joint at the maximum radius of curvature of longitudinal settlement is calculated. Next relation is used to calculate the joint opening of immersed tube [11]:

$$\Delta x = \frac{Lh}{2\rho}\,, \tag{9}$$

where L is the length of a single segment. h is the depth of tunnel and Δx is the horizontal opening of joint. After calculation, the minimum radius of curvature of tunnel caused by differential settlement is 15.3 km. The segment joint opening is 32.7 mm.

4.4.3. Analysis of joint Since the deformability of GINA water-stop cannot be greater than the maximum allowable axial displacement of joint, which is 54.3 mm, provided by the tunnel official. It is concluded that the segment joint opening under a Grade-6 nuclear explosion, 32.7 mm, is not greater than the maximum allowable displacement.

So with the protective doors, even under Grade-6 nuclear explosion, the safety of the immersed tube structure is still guaranteed.

5. Conclusion

The damage effect of internal nuclear explosive shock wave on the main structure of cross-river tunnel. Without protective doors, under a Grade-6 air defense load, the right wall of left channel, left wall of right channel and left and right walls of middle channel do not meet the requirements for flexural capacity. While with protective doors, they all meet the requirements.

For the longitudinal structure of an immersed tube tunnel, under a Grade-6 nuclear explosive load, with protective doors, at the minimum radius of curvature of tunnel caused by differential settlement, the segment joint opening satisfies the allowable displacement of water-stop.

The impact of an indirect hit of conventional weapon on the main structure of tunnel is smaller than that of nuclear explosive shock wave.

With protective doors, nuclear explosion resistance of the immersed tube structure can be significantly increased.

References

[1] H. N. Dhakal, Z. Y. Zhang, N. Bennett, A. Lopez-Arraiza, F. J. Vallejo: *Effects of water immersion ageing on the mechanical properties of flax and jute fibre biocomposites evaluated by nanoindentation and flexural testing* . Journal of Composite Materials *48* (2014), No. 11, 1399–1406.

[2] AyŞe Öndürücü: *The effects of seawater immersion on the bearing strength of woven-glass–epoxy prepreg pin-loaded joints.* International Journal of Damage Mechanics *21* (2012), No. 2, 153–170.

[3] H. Gao, D. Carrick, C. Berry, B. E. Griffith, X. Luo: *Dynamic finite-strain modelling of the human left ventricle in health and disease using an immersed boundary-finite element method.* IMA Journal of Applied Mathematics *79* (2014), No. 5, 978–1010.

[4] S. Djili, F. Benmeddour, E. Moulin, J. Assaad, F. Boubenider: *Notch detection in copper tubes immersed in water by leaky compressional guided waves.* NDT & E International *54* (2013), 183–188.

[5] M. K. P. Kumar, K. S. Soorambail, S. B. Harisingh, A. D'costa, C. R. Chandra: *The effect of gamma radiation on the common carp (Cyprinus carpio): In vivo genotoxicity assessment with the micronucleus and comet assays.* Mutation Research/Genetic Toxicology and Environmental Mutagenesis *792* (2015), 19–25.

[6] Y. Zhu, S. Xiao, Y. Shi, Y. Yanga, Y. Wu: *A trilayer poly(vinylidene fluoride)/polyborate/poly(vinylidene fluoride) gel polymer electrolyte with good performance for lithium ion batteries.* Journal of Materials Chemistry A *1* (2013) 7790–7797.

[7] E. Lauer, X. Y. Hu, S. Hickel, N. A. Adams: *Numerical modelling and investigation of symmetric and asymmetric cavitation bubble dynamics.* Computers & Fluids *69* (2012), 1–19.

[8] A. M. A. Attia, A. R. Kulchitskiy: *Influence of the structure of water-in-fuel emulsion on diesel engine performance.* Fuel *116* (2014), 703–708.

[9] J. Tougaard, A. J. Wright, P. T. Madsen: *Cetacean noise criteria revisited in the light of proposed exposure limits for harbour porpoises.* Marine Pollution Bulletin *90* (2015), Nos. 1–2, 196–208.

[10] S. Pan, A. K. Kota, J. M. Mabry, A. Tuteja: *Superomniphobic surfaces for effec-*

tive chemical shielding. Journal of the American Chemical Society *135*, (2013), No. 2, 578–581.

[11] O. Antonov, L. Gilburd, S. Efimov, G. Bazalitski, V. Tz. Gurovich, Ya. E. Krasik: *Generation of extreme state of water by spherical wire array underwater electrical explosion*. AIP Physics of Plasmas *19* (2012), No. 10, paper 102702.

Received April 23, 2017

Acta Technica *62*, No. 1A/2017, 21–32

The industrial network system design based on PROFINET[1]

Yemin Cai[2], Zhendong Wang[2], Peiyi He[2], Zhuohao Lu[2], Jia Tang[2]

Abstract. With the development of Internet / Intranet technology, the traditional system has been unable to meet the requirements of modern industrial production and management. As a superior model to realize the integration of micro control and macro decision, the industrial network system based on PROFINET has been widely used in industrial process control. Based on the analysis of the layout of the plant and the communication needs, Bus and Ring topology structure was used, hierarchical network design model was designed. And the convergence layer network, access layer network, wireless access network and mobile AGV car terminal network were designed, the system fault treatment and late optimization program were put forward, factory network coverage, real-time monitoring of production data and field conditions were realized. The industrial Ethernet system based on PROFINET has good stability, reliability and expansibility. It improves the ability to withstand and solves the fault, meets the requirements of the production site, and it has a certain directive significance to other applications.

Key words. Industrial network, PROFINET, Ethernet, ring network redundancy.

1. Introduction

The Industrial network mainly meets the exchange of information between various levels of enterprise demands and it is the basic key system in process of the production, manufacture, packaging, etc. In the industrial field, the technology and equipment of commercial network could not be transplanted and reused if it needs to demand the real-time controlling of specific industrial process and the safety request of industrial production. Due to lacking of the international standard, every manufacturer forms an independent production and design according to their own standards of production in order seize market. So the products from different manufacturers cannot be compatible so that the equipment charge is hard to control.

[1]Foundation item: Research and industrialization of high speed precision robot and automatic production line for electronic device assembly (No. 2015BAF10B00).

[2]Engineering Training Center, Shanghai University of Engineering Science, Shanghai, 201620, China

It results in great obstacles for the development of industrial automation and the application of new technology.

In 2002, the PROFIBus International Organization (PI) launched an open and automatic Industrial Ethernet standard – PROFINET which is based on Ethernet. It uses the open IT standard. And it is compatible with the Ethernet TCP/IP standard, provides the real-time function, integrates with the existing field bus system, so as to protect the original investment. At present, the PROFINET standard has become a component of IEC 61784 and IEC 61158.

According to the new network architecture pushed out by SIEMENS PROFINET which instead of the original PROFINET has the three major advantages: open, standard, real time, the main solution framework was designed, the current industrial network design was analyzed mainly in the industrial 4 digital chemical plant backbone network for the application background, reflects the high-speed and real-time network demands under the industrial production. Virtual network VLAN, static routing, real time communication, wireless communication and redundant network core technology were designed, the system fault treatment and late optimization program were put forward, factory network coverage, real-time monitoring of production data and field conditions were realized. Therefore, it is a new method to design a hierarchical network based on PROFINET standard. Its theory and model is relatively simple, the evaluation is easily to realize. It can solve the problem that how to monitors industrial networks reliably from a macro perspective, which is the urgent need for the implementation of automation management and access to the Internet in the industrial field.

2. Methodology

2.1. The analysis of design requirements

According to the principle of industrial production rationalization, combined with the actual plant design, the plant area is analyzed by straight line manufacturing process. The first production line is controlled and managed 200 meters outside. The total length of the production line is 1800 m (300 m×6). In this range, the industrial network configuration mode and layout plan are given. And it should need to meet the following requirements:

(1). Integrated monitoring system to monitor the video server and PLC controller; Control center of the PLC control and production line AGV car I/O PLC devices to achieve real-time data communication, real-time data refresh time of 256 milliseconds; IP camera data and video server to achieve data communication.

(2).The convergence layer network and the access layer network realize the wired data communication, and the convergence layer uses the 1000 Mbit/s multi-mode optical fiber, and the access layer uses the 100 Mbit/s multi-mode optical fiber; Wireless overlay network in the full range of real-time seamless switching and data transmission, AP uses an omni-directional antenna and AP between the need to set roaming, and with the AGV car to achieve wireless data communication; From the bottom of the data transmission (AGV car) will be the video signal and control data

sub network isolation.

(3). To fully consider the redundancy of each network layer.

2.2. The design of topology structure

Network topology needs to be set according to the requirements of equipment units in the network which is the spatial structure of the transmission medium. Different network topology has different effects on the network transmission capacity. Network topology structure is composed of three basic topology structures that are Bus, Star and Ring. Blending of the three basic topology structures is completed in the practical project application.

Star topology structure. It refers to each site device is connected to a switch that presents a star distribution. It can be used in the field of high density of equipment, small coverage, and small space expansion, just like large car asked the control area, independent production machines or small automatic workshop. When other devices in the PROFINET network fails, it will not affect the entire network, only the switch failure will cause network communication failure.

Tree topology structure. It is formed by connecting several star topology structures together. It can be divided into several parts of the installation of complex equipment, to communicate as an independent device. Its level is very clear, the network transmission capacity is high and the data has a better security.

Bus topology structure. PROFINET network structure is similar to the Profibus bus structure, all communications equipment is a serial connection, the application of the switch is installed in the PROFINET network, to achieve PROFINET bus topology structure. Bus topology structure is realized by the switch switch which is close to the connecting terminal, it can be applied in the need to extend the structure of the bus system towel, also gives priority to the use of the best delivery systems, assembly lines and other equipment. In order to reduce the cable weight, the bus configuration can be selected. It is cabling saving, easy maintenance and maintain.

Ring topology structure. All sites are connected by an annular cable to form a ring topology structure. When the system has high availability of network components, it can be used to prevent the occurrence of a broken cable or a fault. In order to increase the effectiveness, Ring topology structure with redundancy can be selected. The advantages of ring topology in dealing with network component failures easily.

Therefore, the factory network can be divided into the aggregation layer network (including the control center, the production line main switch), the access layer network (to connect the wireless access point AP equipment), wireless coverage access network and mobile AGV car terminal network.

2.3. The design of topology structure

The internal network topology structure of the car adopts the Bus and Ring topology structures. It realizes the video data collection by IP camera, control data monitoring by PROFINET IO devices and uses SCALANCE W721 as a wireless

client and upper network (wireless access network covering layer) for wireless communications. It uses SCALANCE X310 as the car switches, IP camera, PROFINET IO devices and wireless client are connected via industrial Ethernet cable and switch.

However, considering the transmission distance of 5 GHz is lower than 2.4 GHz and the interference of the same frequency is small. According to the linear production line of the factory, the wireless coverage into the network and the need to meet the real-time transmission of video data and other specific circumstances, in order to avoid the same frequency interference, to ensure the transmission rate and relatively long-distance transmission, the program used 5 GHz band.

Using the PLC S7-1200 as the PROFINET I/O controller and the PROFINET I/O device, the PROFINET I/O controller is placed in the control center and the PROFINET I/O device is configured in each AGV car. Through the integrated monitoring system using the map software on the PROFINET I/O controller to operate, to achieve each AGV car control data monitoring and control, real-time communication data refresh time is set to 256 milliseconds.

Since five cars are in the lowest level of the network, and the small car wireless client has the same role. This layer switches can be divided in the same subnet; similarly, five IP cameras and five PROFINET I/O devices at the same time. As the network terminal, it is divided into the same subnet. According to the terminal equipment connected with the port must be in the same subnet, the gateway can get the switch ports. And five AGV cars were named AGV1, AGV2, AGV3, AGV4 and AGV5, as shown in Table 1. Now the wireless client is connected to port 2 of the switch, the IP camera is connected to port 3 of the switch, the PROFINET I/O device is connected to the switch of port, as shown in Table 2.

2.4. The design of wireless access network

Wireless access network layer is the main equipment of the wireless access point AP, W761 SCALANCE is selected. According to the technical requirements, an AP should be placed place, so as to complete the network coverage in the AGV car running track. Due to the lateral coverage of the AP omnidirectional antenna is circular, the AP should be set in the first production line and the first six production line tail in order to avoid dead ends. It is 19 AP totally. In the full range, real-time seamless video and data delivery ensure that the AGV car seamlessly switches in the high-speed mobile, the method that configure AP roaming is used to solve the technical requirements.

Table 1. VLAN division

VLAN ID Switch	AGV1's Switch	AGV2's Switch	AGV3's Switch	AGV4's Switch	AGV5's Switch
201	P1.3	P1.3	P1.3	P1.3	P1.3
202	P1.4	P1.4	P1.4	P1.4	P1.4
Note: This table is a single trunk VLAN trunk connection label settings, and the remaining trolley settings and this exactly the same.					

When VLAN is used for data isolation, the data in different VLAN needs to be transmitted at the same time on the trunk line. The VLAN connection of the switch to the switch (trunk trunk) must contain the VLAN tag. So the trunk connection should be to M for each VLAN ID, which is shown as Table 3.

Table 2. IP planning of mobile AGV car terminal network layer

	AGV1	AGV2	AGV3	AGV4	AGV5
Wireless client	192.168.25.1/21	192.168.25/21	192.168.25.3/21	192.168.25.4/21	192.168.25.5/21
IP camera	192.168.25.6/21	192.168.25.7/21	192.168.25.8/21	192.168.25.9/21	192.168.25.10/21
PROFINET I/O Device	192.168.25.11/21	192.168.25.12/21	192.168.25.13/21	192.168.25.14/21	192.168.25.15/21
P1.2	192.168.25.16/21	192.168.25.17/21	192.168.25.18/21	192.168.25.19/21	192.168.250/21
P1.3	192.168.251/21	192.168.252/21	192.168.253/21	192.168.254/21	192.168.255/21
P1.4	192.168.256/21	192.168.257/21	192.168.258/21	192.168.259/21	192.168.25.30/21

Note: Taking into account the number of IP needed for the upper layer equipment and ensure that the system can easily upgrade the network, and in order to facilitate the management of network equipment at all levels, The first 21 bits are selected as the primary network number. The rest of the layers are taken this method, the following will not repeat them.

Table 3. VLAN trunk connection settings

VLAN ID	P1.1	P1.2	P1.3	P1.4
1	U	-	-	-
201	-	M	U	-
202	-	M	-	U

Note: This table is a single trunk VLAN trunk connection label settings, and the remaining trolley settings and this exactly the same.

There are six main steps to build a wireless roaming network with multiple AP.

(1) Each AP set a different IP address to avoid the IP address conflict;

(2) Each AP sets the same SSID in the same data channel and sets the different SSID in the different data channel;

(3) Adjacent APs are placed in different frequency bands and are separated by more than 5 frequency bands to avoid mutual interference;

(4) The same encryption and authentication mode is set for each AP;

(5) Each AP sets the same password, and different AP in different data channels set different passwords;

(6) Each AP sets the same management channel.

The iPCF function is enabled on each AP. The AP are connected to their clients in turn in a fixed order. Each client takes about 2ms to transmit data. After

each client's communication, the polling interval. There is a short time slot, and a broadcast packet can be sent at this time, if necessary. Since there is no priority level for packets in the transmission buffer in the task request, the non-PNIO mode is used.

AP set from left to right is 1 to 19, which is shown as Table 4.

Table 4. AP roaming settings and wireless coverage Access network IP planning

AP	IP	SSID	Channel	Encryption	password
1	192.168.26.1/21	SiemensAPLine12	1	WPA2-PSK	SiemensCupLine1
2	192.168.26.2/21		6		
3	192.168.26.3/21		11		
4	192.168.26.4/21		1		
5	192.168.26.5/21	SiemensAPLine2	6		SiemensCupLine2
6	192.168.26.6/21		11		
7	192.168.26.7/21		1		
8	192.168.26.8/21	SiemensAPLine3	6		SiemensCupLine3
9	192.168.26.9/21		11		
10	192.168.26.10/21		1		
11	192.168.26.11/21	SiemensAPLine4	6		SiemensCupLine4
12	192.168.26.12/21		11		
13	192.168.26.13/21		1		
14	192.168.26.14/21	SiemensAPLine5	6		SiemensCupLine5
15	192.168.26.15/21		11		
16	192.168.26.16/21		1		
17	192.168.26.17/21	SiemensAPLine6	6		SiemensCupLine6
18	192.168.26.18/21		11		
19	192.168.26.19/21		1		

Note: Encryption Authentication Select the WPA2-PSK mode that is currently the most secure.

2.5. The design of access layer network

The access layer network mainly consists of 7 work switches and 3 redundant switches. 7 work switches are connected 2-3 wireless access points, and constitute a ring structure, to achieve single-loop redundancy. In order to make the access layer more stable and safe, and taking into account the cost, decided to add three redundant standby heat engine to form a ring, and three redundant switches with their own closest to a work switch connected to form Double ring redundancy. Double-loop redundancy can greatly reduce the network equipment failure and network

connection failure caused by the loss, when a single failure does not require staff to rescue, in a very short time (5-10 ms) to resume communication. The access layer network is connected through 100 Mbit/s multi-mode optical fiber, and the farthest transmission distance is 2000 m, which meets the requirement of dual-ring redundant transmission in the access layer of the scheme.

2.6. The design of convergence layer network

The convergence layer network consists of eight two-layer Switches and a three-layer Switch. The switches are connected with 1000 Mbit/s multimode fiber. The three-layer Switch is deployed in the control center as the last level of the entire network to the control center, distributing the data to the video server and the PROFINET I/O controller. Due to the ring protocol has many good characteristics such as the availability, high reliability, short recovery time, this solution meets the requirements of the related technology. At the same time, an increase of 2 Layer 2 switches to form a loop to achieve ring redundancy.

MRP can effectively guarantee the high availability of Association Network firewall in user network applications. It supports dual-system hot backup based on automatic detection and supports active load balancing, session protection and takeover, and active configuration synchronization. In a transparent, routing, mixed mode and other work load balancing, support up to 2 to 8 sets of equipment, and HRP in many ways not as good as MRP, so in the convergence layer of redundancy protocol selection, the choice of MRP protocol.

3. Result analysis and discussion

3.1. The analysis of feasibility

The design of the industrial network system based on PROFINET meets 13 technical requirements of the network, the sub network isolation uses VLAN technology. Network redundancy in the convergence layer using MRP redundancy protocol and in the access layer using a double loop structure. AVG car high speed mobile seamless switching using AP roaming technology. From the design and analysis of mobile AGV car terminal network, wireless coverage access network, access layer network and convergence layer network, many innovations are done to make the network program having more feasibility and innovation.

3.2. The economic analysis

The industrial network system based on PROFINET meets the technical requirements and ensures the availability of network systems under the premise of full account of the economy. Personnel cost budget related to the implementation, installation and maintenance of the industrial network project in order to achieve the balance between system performance and cost (as shown in Table 5).

Considering the transmission distance of 1000 Mbit/s multimode optical fiber

between the aggregation layer switches in the aggregation layer network, it is decided to add only two Layer 2 aggregation layers for redundancy to meet the requirements of Part A Switch to form a reliable ring network structure. Compared to every other switch to add a redundant device, greatly reducing the cost of equipment.

In the access layer network, taking full account of the access layer network as a link between the convergence layer network and the wireless coverage access network, in the case of higher importance in the system, choose to use 10 access layer switches Constitute a dual-ring network structure, in which seven access layer switches constitute the outer ring, used to connect the wireless AP, the remaining three constitute the inner ring, for the full realization of redundancy. In the original access to each AP access layer switch without a dual-ring redundancy, based on the reduction of nine switches and to achieve a double-loop redundancy.

Table 5. Hardware cost table

	Quantity (sets) / Length (m)
Wireless AP	19
Wireless client	5
IP camera	5
PLC	10
Layer 3 switches	1
Layer 2 switches	18
1000 MBit/s Multimode fiber	4000
100 MBit/s Multimode fiber	About 7500
Industrial Ethernet cable	About 400

3.3. The optimization of the system

When the plant area needs to expand the scope, you can use the atomic topology shown in Figure 1 to expand. Plant expansion is divided into horizontal and vertical two ways. Horizontal, at the end of the sixth line to continue to build production lines, consistent with the previous production line, this expansion plan is easy to achieve, directly in the corresponding network layer in accordance with the original design principles to add equipment, connection lines and configuration can be. Vertical expansion can be multiplied production line, with the original production line form U-shaped, this expansion in addition to the original topology to build again, the need to dock with the original network system.

The scheme is designed to ensure the feasibility of horizontal expansion and vertical expansion. In terms of hardware, the vertical expansion only need half of the original equipment; software, leaving enough IP addresses and VLAN number. It needs to expand the access layer, wireless overlay network layer and AGV, and expand beyond three times of the horizontal expansion, which needs to be extended uniformly.

As a result of using the ring redundancy technology, the network expansion and expansion of the need to expand the "loop" and "chain" operation, that is, the

original part of the original ring topology and other parts off, in accordance with the original design principles and methods section by section to add. And finally the original part of the ring on the top of the new network. Lateral expansion not only need to access the network layer and wireless coverage access network expansion, also need to aggre-layer network and AGV car expands exponentially. In practice, it is necessary to simultaneously expand and expand the horizontal and vertical, to build a stable, safe and reliable network system.

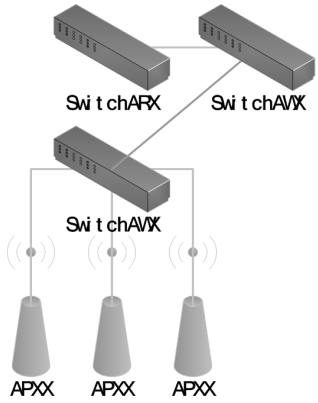

Fig. 1. Extended topological map

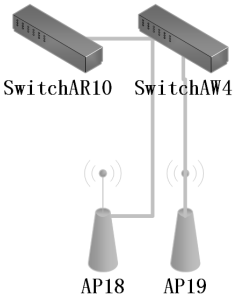

Fig. 2. Ring port part

4. Conclusion

As a strategic technology innovation, PROFINET provides a complete network solution for the automation communication field. The design of industrial network based on PROFINET is the accurate analysis and planning of the design object and it is an important means to make the traditional industrial production workshop covering network monitoring. It can realize remote control by combining the In-

ternet effectively and realize the network monitoring management of the industrial production line, production workshop, automated warehouse, intelligent workshop and so on. And it provides design ideas for the network architecture of industrial production line, assembly line and workshop.

The general design of SIEMENS PROFINET open standards based on industrial network was studied, the key technologies such as real-time industrial Ethernet was analyzed, the design principles and methods of industrial Ethernet were given, and the convergence layer network, access layer network, wireless access network and mobile AGV car terminal network are designed in detail. Through the analysis of the system performance and the solution of the factory in the all unexpected situations were quantified, the solution was put forward. The results show that the industrial system based on PROFINET has good innovation and practicability, good economic performance, and strong reliability of monitoring data communication. PROFINET bus communication provides a reliable guarantee for the complex system of large capacity data exchange. It will have a good application prospects. But there are still a lot of key technologies to be resolved, the positive research work will contribute to its rapid application, and produce good economic benefits.

References

[1] J. Wu, H. Qi, R. Wang: *Insight into industrial symbiosis and carbon metabolism from the evolution of iron and steel industrial network.* Journal of Cleaner Production *135* (2016), 251–262.

[2] A. Tischer, E. den Boer, I. D. Williams, A. Curran: *Industrial network design by improving construction logistics.* Proceedings of Institution of Civil Engineers: Waste and Resource Management *167* (2014), No. WR2, 82–94.

[3] T. Mahmoodi, V. Kulkarni, W. Kellerer, P. Mangan, F. Zeiger, S. Spirou, I. Askoxylakis, X. Vilajosana, H. J. Einsiedler, J. Quitek: *VirtuWind: virtual and programmable industrial network prototype deployed in operational wind park.* Transactions on Emerging Telecommunications Technologies *27* (2016), No. 9, 1281 to 1288.

[4] J. Wu, R. Wang, G. Pu, H. Qi: *Integrated assessment of exergy, energy and carbon dioxide emissions in an iron and steel industrial network.* Applied Energy *183* (2016), 430–444.

[5] A. Simboli, R. Taddeo, A. Morgante: *Analysing the development of industrial symbiosis in a motorcycle local industrial network: The role of contextual factors.* Journal of Cleaner Production *66* (2014), 372–383.

[6] M. H. Alizai, H. Wirtz, B. Kirchen, K. Wehrle: *Portable wireless-networking protocol evaluation.* Journal of Network and Computer Applications *36* (2013) No. 4, 1230–1242.

[7] M. R. Pasandideh, M. St-Hilaire: *Automatic planning of 3G UMTS all-IP release 4 networks with realistic traffic.* Computers & Operations Research *40* (2013), No. 8, 1991–2003.

[8] M. Mazaheri, J. S. Kavian, H. Sharif, H. F. Rashvand: *Low end-to-end delay fuzzy networking protocol for mobile wireless sensing.* Wireless Communications and Mobile Computing *16* (2016), No. 15, 2406–2418.

[9] Y. D. Lin, R. H. Hwang, G. Armitage, V. Eramo: *Guest editorial: Open source for networking: Protocol stacks.* IEEE Network *28* (2014), No. 2, 2–5.

[10] M. I. Sanchez, M. Gramaglia, C.J. Bernardos, A. de la Oliva, M. Calderon:

On the implementation, deployment and evaluation of a networking protocol for VANETs: The VARON case. Ad Hoc Networks *19*, (2014), 9–27.

[11] D. M. L.,Pacheco, T. T. Thai, E. Lochin, F. Arnal: *An IP-ERN architecture to enable hybrid E2E/ERN protocol and application to satellite networking.* Computer Networks *56* (2012), No. 11, 2700–2713.

[12] Q. Gao, W. Wang, J. J. Zhou: *Research progress for the interest control protocol of content-centric networking.* Sensors & Transducers Journal *154* (2013), No. 7, 87–93.

[13] J. Jang, J. Jung, Y. Cho, S. Choi, S. Y. Shin: *Design of a lightweight TCP/IP protocol stack with an event-driven scheduler.* Journal of Information Science and Engineering *28* (2012), No. 6, 1059–1071.

[14] H. D. Ngo, H. S. Yang: *Latency and traffic reduction for process-level network in smart substation based on high-availability seamless redundancy.* IEEE Transactions on Industrial Electronics *63* (2016), No. 4, 2181–2189.

[15] I. R. Altaha, J. M. Rhee, H. A. Pham: *Improvement of high-availability seamless redundancy (HSR) unicast traffic performance using enhanced port locking (EPL) approach.* IEICE Transactions on Information and Systems *98* (2015), No. 9, 1646–1656.

[16] A. M. Kroening: *Advances in ferrite redundancy switching for Ka-Band receiver applications.* IEEE Transactions on Microwave Theory and Techniques *64* (2016), No. 6, 1911–1917.

[17] O. Gerstel, C. Filsfils, T. Telkamp, M. Gunkel, M. Horneffer, V. Lopez, A. Mayoral: *Multi-layer capacity planning for IP-optical networks.* IEEE Communications Magazine *52* (2014), No. 1, 44–51.

[18] V. Gkamas, K. Christodoulopoulos, E. Varvarigos: *A joint multi-layer planning algorithm for IP over flexible optical networks.* Journal of Lightwave Technology *33* (20115 No. 14, 2965–2977.

[19] M. R. Pasandideh, M. St-Hilaire: *A local search heuristic to solve the planning problem of 3G UMTS all-IP release 4 networks with realistic traffic.* International Journal of Autonomous and Adaptive Communications Systems *7* (2014), Nos. 1–2, 1–20.

[20] O. M. Querin, V. M. Nicolás, C. Diáz-Goméz, M. M. Pascual: *Layout optimization of multi-material continuum structures with the isolines topology design method.* Engineering Optimization *47* (2015), No. 2, 221–237.

Received April 23, 2017

Acta Technica *62*, No. 1A/2017, 33–42

Predictive study on tunnel deformation based on LSSVM optimized by FOA

Jun Li[1,2], Zonglin Wang[1]

Abstract. As there are problems such as low precision and the failure of self-adaptive selection of parameters in prediction of tunnel deformation by using LSSVM, a prediction model of tunnel deformation based on Least squares support vector machine (LSSVM) optimized by FOA is proposed according to the advantages of global optimum and rapid convergence of the Fruit Flying Optimization Algorithm (FOA). The predictive study on tunnel deformation can be achieved through self-adaptive optimization of the penalty factor C and kernel function parameter g of LSSVM model. A tunnel of Guiyang-Guangzhou High-speed Rail was used as the object of study. The observation data of tunnel deformation from January 2009 to January 2015 was used as the object of study and predictive study on tunnel deformation was carried out by means of rolling prediction. As shown in the experimental result, according to the evaluation indexes of prediction time and the mean squared error of prediction (MSEP), FOA-LSSVM has higher prediction accuracy than LSSVM and BP; thus, the validity and reliability of predicting the tunnel deformation with FOA-LSSVM is verified.

Key words. FOA, LSSVM, tunnel deformation prediction, prediction accuracy, evaluation index.

1. Introduction

The amount and rate of tunnel deformation are not only the important reference indexes of tunnel construction progress and safety, but also dynamic information feedbacks of the ambient environment's influences on the whole tunnel. It is difficult to express tunnel deformation through the quantitative relation formula because it has complicated non-linear relationships with numerous random and indeterminate factors. At present, the deformation prediction methods mainly include the empirical method, theoretical analysis method and intelligent prediction method. The application condition and scope for the calculation formula deduced from the empirical method are limited and there is generally a large deviation between the

[1]School of Transportation Science and Engineering, Harbin Institute Of Technology, Harbin, 150090, China

[2]School of Building Engineering Technology, Heilongjiang Institute of Construction Technology, Harbin, 150050, China

calculating result and the measured value [1]. Numerous factors considered in practical engineering when using the theoretical analysis method largely increase the complexity in formula and thus enhance the difficulty in prediction [2]. Over the recent decades, many intelligent optimization methods have been applied in tunnel deformation prediction such as artificial neural network [3], artificial neural network [4], genetic algorithm [5] and wavelet analysis [6]. Although the above-mentioned methods are applied to some degree and some research achievements have been obtained accordingly, such algorithms need a large number of sample data of observed tunnel deformation amounts and it is rather difficult to acquire such data in reality. As for the weaknesses mentioned above, the Least Square Support Vector Machines (LSSVM) are widely applied to the study of issues with small sample data, because it can solve the tunnel deformation issues characterized by nonlinearity, few samples and high dimension.

In view of the weaknesses such as low precision and the failure of self-adaptive selection of parameters of the prediction method for LSSVM tunnel deformation amount, a tunnel deformation prediction method based on LSSVM optimized by FOA. The predictive study on tunnel deformation amount can be achieved by optimizing the penalty factor C and kernel function parameter g of LSSVM through FOA.

2. Methodology

The Fruit Fly Optimization Algorithm (FOA) is a brand-new swarm intelligence algorithm proposed by Pan Wenchao, who was enlightened by the fruit fly's foraging behavior. With the advantages of few control parameters and rapid convergence rate, the algorithm has been widely applied to the fields of engineering optimization and scientific research. The algorithm flow is shown below [1–2], [7]:

1. Set the *popsize* of fruit flies and the maximum *Iteration* of FOA; randomly initialize the location of fruit fly populations; the initialization results are denoted respectively with $X\_\,begin$ and $Y\_\,begin$.

2. Calculate the random optimization direction and distance of an individual fruit fly according to next two formulae

$$x_i = X\_begin + Value \times rand(1, N)\,, \tag{1}$$

$$y_i = Y\_begin + Value \times rand(1, N)\,. \tag{2}$$

In formulae (1) and (2), the symbol *Value* denotes the scouting distance of fruit fly; x_i and y_i signify the location of individual fruit fly in next moment.

3. Estimate the distance d_i between an individual fruit fly and the original point. Then, calculate the smell concentration s_i of individual fruit fly. Both variables are given as

$$d_i = \sqrt{x_i^2 + y_i^2}\,, \tag{3}$$

$$s_i = \frac{1}{d_i}\,. \tag{4}$$

4. The smell concentration s_i is substituted into the smell concentration decision function in the next formula to calculate the smell concentration of the current location of the individual fruit fly;

$$Smell_i = Function(s_i)\,. \tag{5}$$

5. Find out the optimum smell concentration value and optimum location in the fruit fly population; the optimum smell concentration is denoted as $Smell_{\mathrm{b}}$; the optimum location is denoted as x_{b} and y_{b}.

6. Keep and record the optimum location and optimum smell concentration of fruit fly; the optimum smell concentration *Smellbest*=$Smell_{\mathrm{b}}$; the initial position of fruit fly $X\_\,begin{=}x_{\mathrm{b}}$ and $Y\_\,begin{=}y_{\mathrm{b}}$; meanwhile, the fruit fly population searches for the optimum location.

7. Start the iterative optimization and repeat the iterative steps (2)–(5); meanwhile, judge whether the smell concentration is better than the iterative smell concentration of the previous generation; if so, carry out step (6).

2.1. LSSVM

The LSSVM put forward by Suykens can be converted into [3], [6–7]:

$$J(\omega,\xi) = \frac{1}{2}||\omega||^2 + C\sum_{i=1}^{N}\xi_k^2\,,$$

$$\text{s.t. } y_k = \phi(x_k)\omega^{\mathrm{T}} + b + \xi_k\,, \tag{6}$$

where $\xi_k \geq 0,\ k = 1,\, 2,\, \ldots,\, N$ and C is the penalty factor.

Using the lagrangian method, formula (6) can be converted into

$$L(\omega,b,\xi,\alpha) = \frac{1}{2}||\omega||^2 + C\sum_{i=1}^{N}\xi_k^2 -$$

$$-\sum_{i=1}^{N}\alpha_k[(\omega^{\mathrm{T}}\phi(x_k) + b + \xi_k) - y_k]\,. \tag{7}$$

In formula (7), $\alpha_k,\ k = 1,\, 2,\, \ldots,\, N$ denote the Lagrangian multipliers. Calculate now the partial derivatives of ω, b, ξ and α, and make them equal to zero. Then

$$\omega = \sum_{k=1}^{N}\alpha_k\phi(x_k) = 0\,,$$

$$\sum_{k=1}^{N} \alpha_k = 0\,,$$
$$\alpha_k = C\xi_k\,,$$

$$\omega^{\mathrm{T}}\phi(x_k) + b + \xi_k - y_k = 0\,. \tag{8}$$

According to the Mercer condition, the kernel function $k(x_i, x_j)$ is shown in formula

$$k(x_i, x_j) = \phi(x_i)\phi(x_j)\,. \tag{9}$$

As the RBF kernel function has the ability of nonlinear predictive diagnosis, it is used to achieve the tunnel deformation prediction and the formula is shown below [8, 9].

$$k(x_i, x_j) = \exp\left(-\frac{||x_i - x_j||^2}{2g^2}\right)\,. \tag{10}$$

Thus, the LSSVM tunnel deformation model is as follows:

$$f(x) = \sum_{i=1}^{m} \alpha_i \exp\left(-\frac{||x_i - x_j||^2}{2g^2}\right) + b\,. \tag{11}$$

In this paper, the penalty parameter C and the kernel function parameter g are used as the objects of optimization and FOA is used to optimize and acquire the optimal LSSVM model.

2.2. FOA-LSSVM tunnel deformation prediction model

Since parameters C and g need to be optimized in LSSVM, the optimized mathematical model is shown below:

$$Fitness = \{C, g\}. \tag{12}$$

After optimization in formula (12), the self-adaptive selection of parameters C and g is achieved in the condition of ensuring minimum error in tunnel deformation prediction. The fitness function can be defined. Suppose the practical amount of tunnel deformation in time t is $y(t)$ and the predicted amount of tunnel deformation is $\hat{y}(t)$, the difference value between the practical amount of tunnel deformation $y(t)$ and the predicted amount of tunnel deformation $\hat{y}(t)$ is formula [10–12]

$$e(t) = \hat{y}(t) - y(t)\,. \tag{13}$$

As for the nonlinear problems in tunnel deformation prediction, suppose the number of data samples of practical tunnel deformation is n, then use the kernel parameter and penalty parameter of LS-SVM optimized by FOA to minimize the quadratic sum of difference value between the practical amount of tunnel deformation and the predicted amount of tunnel deformation of LS-SVM; the fitness function is

shown in formula

$$\min Fitness(t) = \frac{1}{2n}\sum_{i=1}^{T} e^2(t)\,. \tag{14}$$

2.3. Algorithm steps

The algorithm steps of FOA-LSSVM-based tunnel deformation prediction are as follows:

Step 1: normalize the tunnel deformation data.

Step 2: set the maximum iteration (*maxgen*) and the population size (*popsize*) of FOA.

Step 3: input the constructed training samples into LSSVM; calculate the fitness function value of individual fruit fly according to the fitness function formula (14); look for individual fruit flies and the locations and optimum values of global optimum individual fruit fly.

Step 4: update the location and search direction of fruit fly.

Step 5: calculate and evaluate the fitness size and update the location and search direction of fruit fly.

Step 6: if *gen>maxgen*, preserve the optimal solution; on the contrary, if *gen=gen+1,* go to Step 4.

Step 7: achieve the tunnel deformation prediction according to the optimum parameters C and g corresponding to the optimum locations of fruit fly population; the flow chart is shown in Fig. 1:

3. Result analysis and discussion

3.1. Evaluation indexes

To verify the validity of the method, the MSE (mean square error) is used to evaluate the evaluation indexes of the result of tunnel deformation prediction. The MSE formula is shown below [13–17]

$$MSE = \sqrt{\frac{1}{K}\sum_{i=1}^{K}(x_i - \hat{x}_i)^2}\,. \tag{15}$$

In formula (15), x_i and y_i, respectively, signify the practical value of tunnel deformation and the predicated value of tunnel deformation.

3.2. Empirical analysis

To verify the validity of the algorithm in this paper, a tunnel of Guiyang-Guangzhou High-speed Rail was used as the object of study [18–19]. The observation data of tunnel deformation from January 2009 to January 2015 was used as the object of study and predictive study on tunnel deformation was carried out by

means of rolling prediction [20]. The FOA parameters are set as follows: the maximum iteration is 100; the popsize is 20. The prediction results are shown in Figs. 2, 3 and 4.

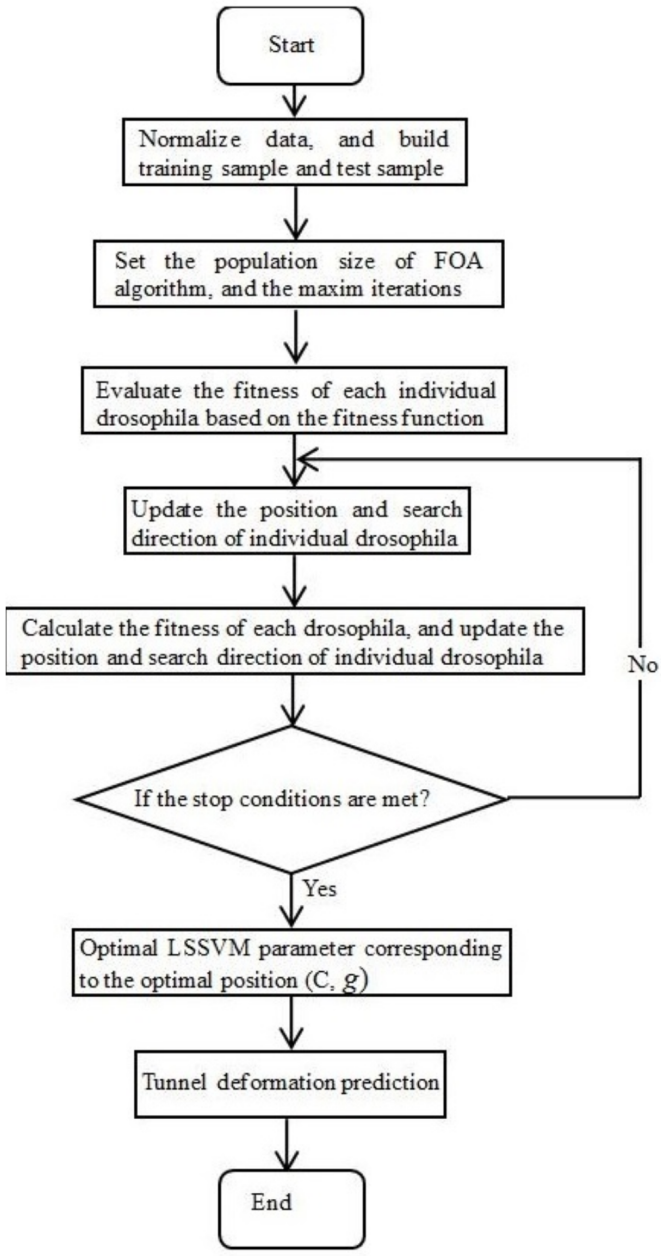

Fig. 1. Flow chart of FOA-LSSVM-based tunnel deformation prediction

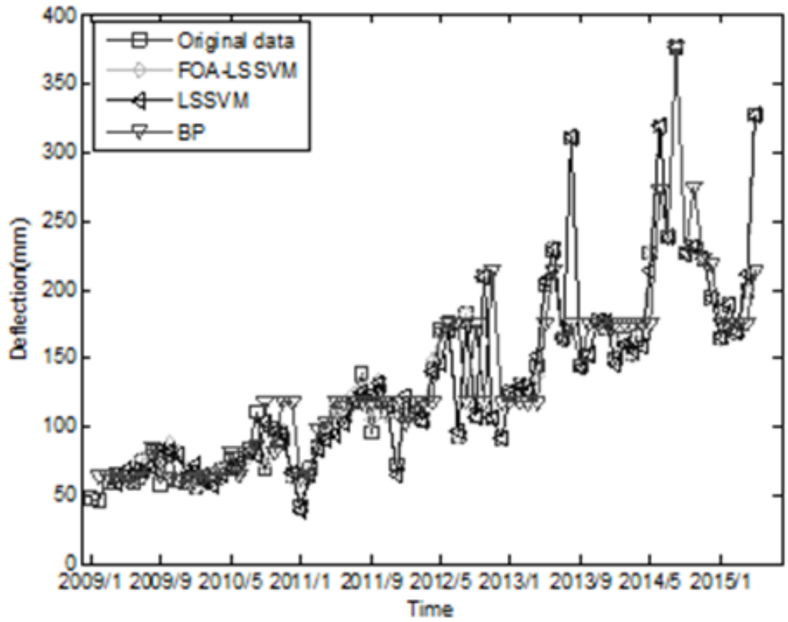

Fig. 2. Diagram of prediction results of FOA-LSSVM, LSSVM and BP algorithms

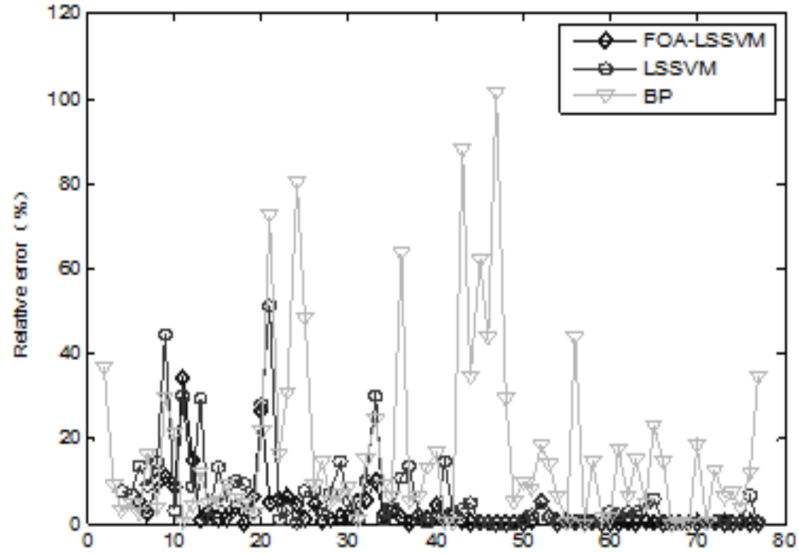

Fig. 3. Diagram of relative errors of prediction of FOA-LSSVM, LSSVM and BP algorithms

It can be seen from the prediction results in Figs. 2 and 3 that the FOA-LSSVM algorithm used in this paper is more precise than the LSSVM and BP algorithms

and its mean relative error in prediction is about 4 %. Figure 4 shows the fitness convergence curve of optimized LSSVM through FOA.

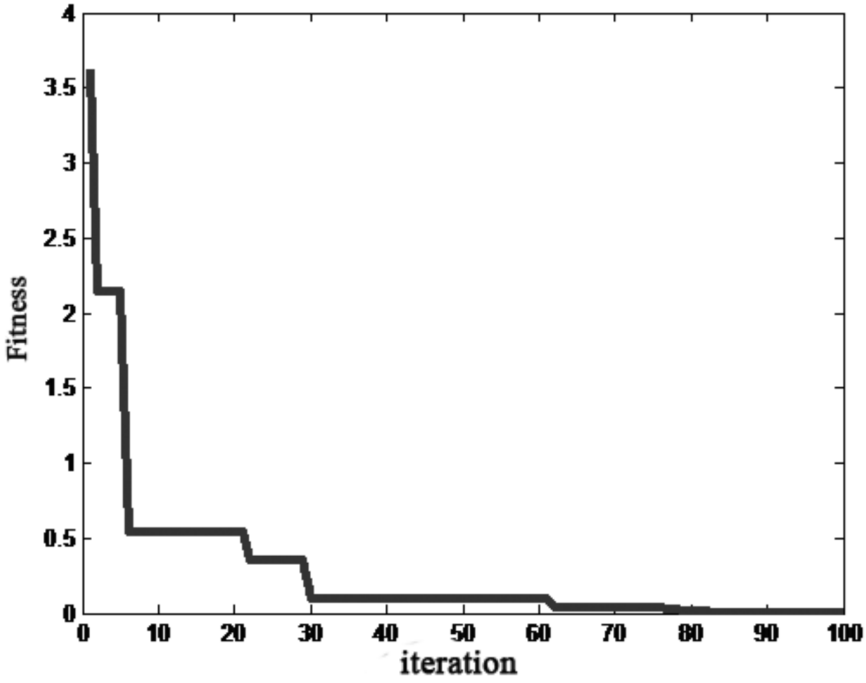

Fig. 4. Curve graph of fitness convergence of optimized LSSVM through FOA

To show the superiority of FOA-LSSVM algorithm, the prediction results of FOA-LSSVM algorithm, LSSVM algorithm [21] and BP [22] algorithm were compared and operated for 10 times; the comparative results are shown in Table 1.

Table 1. MSE comparison in prediction through FOA-LSSVM algorithm, LSSVM and BP algorithm

Times of operation	BP	LSSVM	FOA-LSSVM
1	0.0088	0.0060	0.0040
2	0.0072	0.0055	0.0046
3	0.0068	0.0050	0.0040
4	0.0084	0.0064	0.0042
5	0.0065	0.0056	0.0038
6	0.0074	0.0061	0.0043
7	0.0076	0.0056	0.0035
8	0.0064	0.0046	0.0042
9	0.0072	0.0076	0.0040
10	0.0067	0.0051	0.0047
Mean value	0.0072	0.0058	0.0041

From the comparative results of prediction MSE of FOA-LSSVM algorithm, LSSVM and BP in Table 1, it can be seen that the prediction effect of FOA-LSSVM algorithm is the best and is better than that of LSSVM and BP models; besides, the prediction effect of LSSVM is better than that of BP.

From the comparative results of prediction time of FOA-LSSVM algorithm, LSSVM and BP in Table 2, it can be seen that the prediction time of FOA-LSSVM algorithm is the shortest and is shorter than that of LSSVM and BP model; besides, the prediction time of LSSVM is shorter than that of BP.

Table 2. Comparison of prediction time of FOA-LSSVM, LSSVM and BP algorithms (unit/s)

Predictive step size	BP	LSSVM	FOA-LSSVM
Single step	111.40	97.36	37.21
3	97.60	89.22	34.25
5	86.33	74.22	32.18
7	79.45	65.80	31.27

4. Conclusion

As there are problems such as low precision and failure of self-adaptive selection of parameter in prediction of tunnel deformation by using LSSVM, a prediction method for tunnel deformation based on LSSVM optimized by FOA was proposed. The predictive study on tunnel deformation was achieved by using FOA to optimize the penalty factor C and kernel function parameter g of LSSVM. As shown in the experimental result, the prediction accuracy of FOA-LSSVM is higher than that of LSSVM and BP and the prediction time and MSEP of FOA-LSSVM are also more superior, so the validity and reliability of using FOA-LSSVM to predict tunnel deformation are verified. Therefore, this method can be popularized in other fields to solve other similar issues.

References

[1] W. Gu, Y. Lv, M. Hao: *Change detection method for remote sensing images based on an improved Markov random field.* Multimedia Tools and Applications (2015), doi:10.1007/s11042-015-2960-3.

[2] Y. Chen, W. Huang, Y. Lv: *Towards a face recognition method based on uncorrelated discriminant sparse preserving projection.* Multimedia Tools and Applications (2015), doi:10.1007/s11042-015-2882-0.

[3] D. Jiang, X. Ying, Y. Han, Z. Lv: *Collaborative multi-hop routing in cognitive wireless networks.* Wireless Personal Communications *86* (2016), No. 2, 901–923.

[4] Z. Lv, A. Tek, F. da Silva, C. Empereur-mot, M. Chavent, M. Baaden: *Game on, science-how video game technology may help biologists tackle visualization challenges.* PLoS ONE *8* (2013), No. 3, https://doi.org/10.1371/journal.pone.0057990.

[5] W. T. Pan: *A new fruit fly optimization algorithm: Taking the financial distress model as an example.* Knowledge-Based Systems *26* (2012), 69–74.

[6] H. Z. Li, S. Guo, Ch. J. Li, J. Q. Sun: *A hybrid annual power load forecasting model*

based on generalized regression neural network with fruit fly optimization algorithm. Knowledge-Based Systems *37* (2013), 378–387.

[7] L. Wang, X. L. Zheng, S. Y. Wang: *A novel binary fruit fly optimization algorithm for solving the multidimensional knapsack problem.* Knowledge-Based Systems *48* (2013), 17–23.

[8] X. L. Zheng, L. Wang, S. Y. Wang: *A novel fruit fly optimization algorithm for the semiconductor final testing scheduling problem.* Knowledge-Based Systems *57* (2014), 95–103.

[9] Y. Lin, J. Yang, Z. Lv, W. Wei, H. Song: *A self-assessment stereo capture model applicable to the internet of things.* Sensors *15* (2015), No. 8, 20925–20944.

[10] J. Yang, S. He, Y. Lin, Z. Lv: *Multimedia cloud transmission and storage system based on internet of things.* Multimedia Tools and Applications (2015), 1–16.

[11] G. Sheng, S. Dang, N. Hossain, X. Zhang: *Modeling of mobile communication systems by electromagnetic theory in the direct and single reflected propagation scenario.* Applications and Techniques in Information Security, Communications in Computer and Information Science, Springer, Berlin, Heidelberg *557* (2015).

[12] H. Li, H. S. Yang: *Fast and reliable image enhancement using fuzzy relaxation technique.* IEEE Transactions on Systems, Man, and Cybernetics *19* (1989), No. 5, 1276 to 1281.

[13] D. L. Peng, T. J. Wu: *A generalized image enhancement algorithm using fuzzy sets and its application.* Proceedings of the 1st International Conference on Machine Learning and Cybernetics, 4–5 November 2002, Beijing, China, IEEE Conference Publications, *2* 820–823.

[14] H. R. Tizhoosh, G. Krell, B. Michaelis: *On fuzzy enhancement of megavoltage images in radiation therapy.* Proceedings of 6th International Fuzzy Systems Conference, 55–55 July 1997, Barcelona, Spain, IEEE Conference Publications *3* 1398–1404.

[15] S. K. Pal, R. A. King: *Image enhancement using smoothing with fuzzy sets.* IEEE Transactions on Systems, Man, and Cybernetics *11* (1981), No. 7, 494–501.

[16] S. K. Pal, R. A. King: *On edge detection of X-ray images using fuzzy sets.* IEEE Transactions on Pattern Analysis and Machine Intelligence *5* (1983), No. 1, 69–77.

[17] J. J. Y. Wang, J. Z. Huang, Y. Sun, X. Gao: *Feature selection and multi-kernel learning for adaptive graph regularized nonnegative matrix factorization.* Expert Systems with Applications *42* (2015), No. 3, 1278–1286.

[18] J. Yang, S. He, Y. Lin, Z. Lv: *Multimedia cloud transmission and storage system based on internet of things.* Multimedia Tools and Applications (2015), 1–16.

[19] C. Guo, X. Liu, M. Jin, Z. Lv: *The research on optimization of auto supply chain network robust model under macroeconomic fluctuations.* Chaos, Solitons & Fractals *89* (2016), 105–114.

[20] X. Qu, X. Cao, D. Guo, C. Hu, Z. Chen: *Combined sparsifying transforms for compressed sensing MRI.* IET Digital Library *46* (2010), No. 2, 121–123.

[21] Y. M. Chen, X. J. Ye, F. Huang: *A novel method and fast algorithm for MR image reconstruction with significantly under-sampled data.* AIMS Inverse Problems and Imaging (IPI) *4* (2010), No. 2, 223–240.

[22] S. Ravishankar, Y. Bresler: *MR image reconstruction from highly undersampled k-space data by dictionary learning.* IEEE Transactions on Medical Imaging *30* (2011), No. 5, 1028–1041.

Received April 23, 2017

Acta Technica *62*, No. 1A/2017, 43–54

Active earth pressure with consideration of displacement effect of retaining wall[1]

Jicai Li[2,3], Bowen Yu[4], Jingbo Su[5]

Abstract. The existing problems of the calculation theory and method of earth pressure are analyzed and discussed. Based on the theory of soil arching, the stress state and the effect of principal stress rotation of backfill behind the wall are analyzed. Further, a new computation method for the earth pressure which considers the displacement effect of the retaining wall is obtained. The distribution of earth pressure of retaining wall is gained for the displacement mode of translation motion, rotation about the top and rotation about the bottom. And the change of the joint force and its position of earth pressure is analyzed along with the change of displacement value. Comparison is made among the results calculated by the proposed method, the other methods and the test observations.It can be demonstrated that the calculating results by the proposed method have better agreement with those of the experimental observations.

Key words. Displacement mode, theory of soil arching, distribution of earth pressure, active earth pressure, retaining wall.

1. Introduction

Retaining wall is one of the most widely-used retaining structures. Correspondingly, how to calculate earth pressure reasonably and accurately and to ensure its security and stability is an important topic for many scholars. The classical theory of earth pressure is widely used in many engineering designs. However, Terzaghi found the earth pressure behind the wall is not linear by different model experiments in 1943, what is more, the slip crack surface in classical theory is questioned by many

[1]Majority of the work presented in this paper was funded by the National Natural Science Foundation of China (Grant No. 51679081).

[2]Nanjing Hydraulic Research Institute, Nanjing, Jiangsu, 210029, China

[3]Nanjing R&D Tech Group co., LTD., Nanjing, Jiangsu, 211106, China

[4]School of Hydraulic Engineering, Dalian University of Technology, Dalian, Liaoning, 116024, China

[5]College of Harbour, Coastal and Offshore Engineering, Hohai University, Nanjing, Jiangsu, 210098, China

scholars [1], and the slip crack surface is a curved surface which was verified by many model and field experiment.

The earth pressure behind the wall has been proved to be nonlinear distribution by different model experiments by Fang and Ishibashi [2]. Also, it can be found that the earth pressure has different distributions for different displacement pattern and size. The earth pressure behind the retaining wall is closely related to the displacement effect of retaining wall. Many methods such as theoretical analysis [3], numerical simulation [4] and model experiment [5] are used to research the distribution of earth pressure behind the wall.

However, there are some insufficiencies about the research methods. First of all, the plain slip crack surface is used in many researches [6], the defect of the classical theory cannot be escaped. Although other researches [7], [8] partly consider that the slip crack surface is nonlinear, the slip crack surface was artificially supposed by simple curve equation. Secondly, there are some problems with the assumption of the trajectory and top surface of soil arch, and the non-uniform distribution and non-uniform change of compression stress in horizontal soil element do not considered, that cannot reflect the real situations. Finally, many studies [9] can only be used when the soil behind the wall reached fully active state, and that cannot consider the effect of the wall displacement pattern and the size of displacement for the size and distribution of earth pressure at the same time.

In this paper, the existing problems of the calculation theory and method of earth pressure are analyzed and discussed. A new computation method for the earth pressure which considers the displacement effect of the retaining wall is obtained by the theory of soil arching, the stress state and the effect of principal stress rotation of backfill behind the wall.

2. Methodology

2.1. Assumption of soil arching effect

If a retaining wall deforms outward, and the displacement is big enough, the soil behind the wall will be destroyed along the slip crack surface. The soil will be subjected to sheer stresses from slip surface and contact surface of soil and wall. At this time, the direction of principal stress will rotate and the track of minor primary stress is a bending curve. The track of minor principal stress is assumed as a circular arch in this paper. In any depth, the radius r of soil arch is

$$r = \frac{L}{(\cos\beta_{\mathrm{w}} - \cos\beta_{\mathrm{s}})}\,, \tag{1}$$

where L is the length of horizontal layer element, β is the angle between the third principal stress and horizontal direction, β_{w} is the angle between the third principal stress and the horizontal direction at the retaining wall, and β_{s} is the angle between the third principal stress and the horizontal direction at the slip crack surface.

The calculation model is shown in Fig. 1. The wall is a rigid body, its back is

vertical, and the soil behind the wall is homogeneous isotropic sandy soil with a horizontal surface. The height of the retaining wall is H, the horizontal direction is considered as the coordinate system x, the vertical direction is considered as the coordinate system y. In the model, the soil behind the wall is separated into slices with the number n, the upper surface of each layer is marked as i, the lower surface of each layer is marked as $i+1$, its length is marked as L_i, the angle between slip crack surface and horizontal direction is marked as α_i. The load-bearing of each slice is also shown in Fig. 2. φ is the angle of soil friction, δ is the angle of friction between wall and soil. The intersection spot of retaining wall and the slice is marked as D, the intersection spot of the slice and the slip crack surface is marked as E.

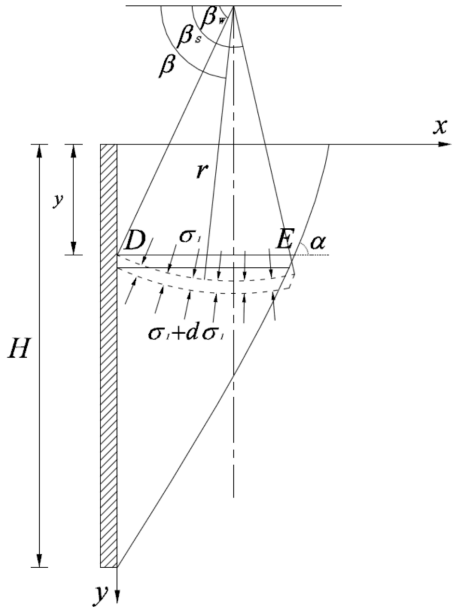

Fig. 1. Calculation model of active earth stress

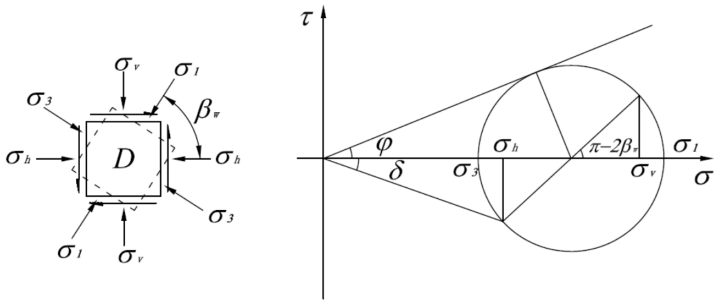

Fig. 2. Stress state at point D

As the wall deflects from soil to a certain extent, the soil behind the wall will reach the fully active condition. At this time, the soil will be forced by friction from the wall surface and the slip crack surface, and the principal stress rotation will happen, where the stress state is shown in Fig. 2 and Fig. 3.

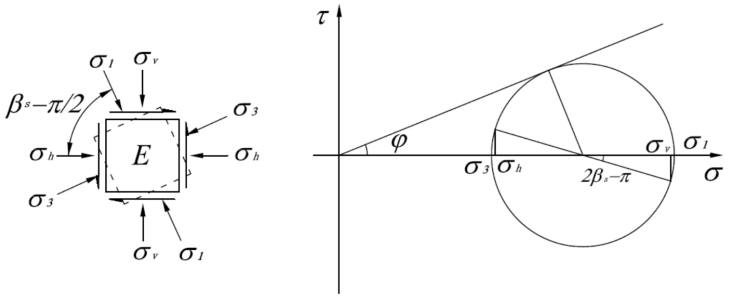

Fig. 3. Stress state at point E

For point D, the angle between the third principal stress and horizontal direction is

$$\beta_{\mathrm{w}} = \tan^{-1}\left[\frac{N-1\pm\sqrt{(N-1)^2-4N\tan^2\delta}}{2\tan\delta}\right]. \tag{2}$$

and for the point E we get

$$\beta_{\mathrm{s}} = \alpha + \frac{\pi}{4} - \frac{\varphi}{2}. \tag{3}$$

In the above formulas

$$N = \frac{\sigma_1}{\sigma_3} = \tan^2(\frac{\pi}{4}+\frac{\varphi}{2})$$

is the ratio between the major principal stress σ_1 and minor principal stress σ_3 and α is the angle between slip crack surface and horizontal direction.

From Eq. (3), if $\alpha > \varphi/2+\pi/4$, then $\beta_{\mathrm{s}} > \pi/2$, and we can see that the rotation directions of the principal stress at the slip crack surface and the wall surface are opposite. If $\alpha < \varphi/2+\pi/4$, then $\beta_{\mathrm{s}} < \pi/2$, and we can see that the rotation directions of the principal stress at the slip crack surface and the wall surface are the same. The rotation angles of the principal stress at the slip crack surface change with the depth. The change reflects the slide surface is nonlinear. That is to say, the slide surface is a curved surface with the changing angle α.

By the stress analysis, we know that the horizontal stress of point in each slice is

$$\sigma_{\mathrm{h}} = \sigma_1\cos^2\beta + \sigma_3\sin^2\beta, \tag{4}$$

the vertical stress is

$$\sigma_{\mathrm{v}} = \sigma_1\sin^2\beta + \sigma_3\cos^2\beta, \tag{5}$$

and the shear stress is

$$\tau = (\sigma_{\mathrm{h}} - \sigma_3)\tan\beta, \tag{6}$$

where β is the angle between the third principal stress and horizontal direction at the given point.

The length of each slice behind the wall can be obtained as

$$L = r(\cos\beta_{\mathrm{w}} - \cos\beta_{\mathrm{s}}). \tag{7}$$

For the differentiation element of each slice we can get the width of the differentiation element

$$\mathrm{d}L = r \cdot \sin\beta\,\mathrm{d}\beta\,. \tag{8}$$

Considering the principal stress rotation behind the wall, the average vertical force on each slice is obtained by the following formula

$$\overline{\sigma}_{\mathrm{v}} = \frac{1}{L}\int_{\beta_{\mathrm{w}}}^{\beta_{\mathrm{s}}} \sigma_v\,\mathrm{d}L = \frac{1}{L}\int_{\beta_{\mathrm{w}}}^{\beta_{\mathrm{s}}} \sigma_1\left(\sin^2\beta + \frac{\cos^2\beta}{N}\right)\cdot r\cdot\sin\beta\,\mathrm{d}\beta\,. \tag{9}$$

Substitution of Eq. (9) yields

$$\overline{\sigma}_{\mathrm{v}} = A\sigma_1\,, \tag{10}$$

where

$$A = \frac{1}{(\cos\beta_{\mathrm{w}} - \cos\beta_{\mathrm{s}})}\left[(\cos\beta_{\mathrm{w}} - \cos\beta_s) - \frac{1-1/N}{3}(\cos^3\beta_{\mathrm{w}} - \cos^3\beta_{\mathrm{s}})\right]. \tag{11}$$

In this way we can obtain the coefficient of active earth pressure

$$K = \frac{\sigma_{\mathrm{dh}}}{\overline{\sigma}_{\mathrm{v}}} = \frac{\cos^2\beta + \frac{\sin^2\beta}{N}}{A}\,. \tag{12}$$

2.2. The calculation method of active earth pressure

If the displacement of the wall away from the fill takes place, the load-bearing state of each slice is shown in Fig. 1. By the by the equilibrium condition, the vertical stress is

$$\overline{\sigma}_{\mathrm{v}i+1} = \frac{(L_i - \frac{B_i}{A_i}\Delta y)\overline{\sigma}_{\mathrm{v}i} + \Delta G}{L_{i+1} + \frac{B_{i+1}}{A_{i+1}}\Delta y}\,, \tag{13}$$

where

$$A_i = \frac{1}{(\cos\beta_{\mathrm{w}i} - \cos\beta_{\mathrm{s}i})}\left[(\cos\beta_{\mathrm{w}i} - \cos\beta_{\mathrm{s}i}) - \frac{1-1/N}{3}(\cos^3\beta_{\mathrm{w}i} - \cos^3\beta_{\mathrm{s}i})\right], \tag{14}$$

$$B_i = \frac{1}{2}(\cos^2\beta_{\mathrm{w}i} + \frac{\sin^2\beta_{\mathrm{s}i}}{N})\tan\delta + \frac{(1-1/N)\cos\varphi\cos(\alpha_i - \varphi)}{4\sin\varphi\sin\alpha_i}\,. \tag{15}$$

The active earth pressure in horizon against the retaining wall can be expressed as

$$p_{xi} = \sigma_{\mathrm{dh}} = \frac{\cos^2\beta + \frac{\sin^2\beta}{N}}{A}\overline{\sigma}_{\mathrm{v}i+1}\,. \tag{16}$$

The resultant force of active earth pressure at horizontal direction is

$$P_{xi} = \sum \frac{(p_{xi} + p_{xi+1})}{2} \Delta y, \tag{17}$$

and its location

$$h_{\mathrm{P}} = \frac{\sum 0.5(p_{xi} + p_{xi+1}) \cdot \Delta y(H - y_i - 0.5\Delta y)}{Q_x}, \tag{18}$$

where Q_x is the resultant force of horizontal earth pressure.

2.3. The displacement effect

It is very important for the size and distribution of active earth pressure whether the soil achieves the active state. In order to achieve fully active state of the soil, the friction angle of the interface between wall and soil must be fully working. The definition of active state is more strictly for the non-limit state of soil, the friction angle of the interface between wall and soil must be also fully working [10]. So the working state of the internal friction angle φ of the backfill and friction angle δ of the interface between wall and soil are related to the displacement of the backfill. By the analysis of the working state of φ and δ, the progressive failure process of the backfill can be simulated and the size and distribution of active earth pressure can be computed.

In this paper, we take the Chang's model to match the working state of φ and δ by φ_{m} and δ_{m} (where φ_{m} and δ_{m} are, respectively, the internal friction angle of the soil in the Chang's model and the friction angle of the contact surface on the wall in the Chang's model). The relationship between the friction angle and displacement is illustrated in Fig. 4.

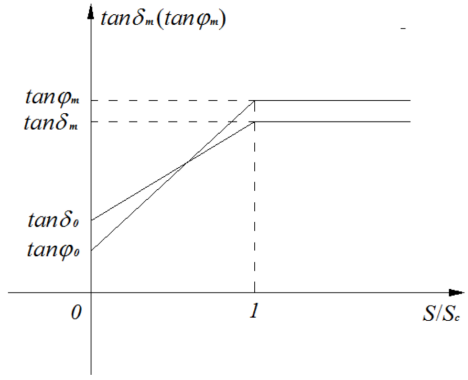

Fig. 4. Relationship between friction angle and displacement

While the retaining wall deforms outwards, the relationship between the friction

angle and displacement can be described as

$$\tan\varphi = \tan\varphi_0 + (\tan\varphi_\mathrm{m} - \tan\varphi_0)\frac{S}{S_\mathrm{c}}\,, \tag{19}$$

$$\tan\delta = \tan\delta_0 + (\tan\delta_\mathrm{m} - \tan\delta_0)\frac{S}{S_\mathrm{c}}\,, \tag{20}$$

where φ_0 and δ_0 are the initial values of internal friction angle of the backfill and friction angle of the interface between wall and soil respectively; its value may refer to Chang's thesis. Symbol S is the soil displacement of the calculation point, while S_c is the soil displacement of calculation point when the soil achieves fully active state.

According to the model test of Fang and Ishibashi, each point of the soil reaches active state needs the same displacement along the retaining wall. Furthermore, the displacement is independent of the wall displacement pattern. Thus, we assume that the translational displacement S_a is $0.0005H$ when the soil achieves active state, the rotation angles about the top and the bottom are respectively 0.0015 rad and 0.001 rad when the soil achieves active state.

In this paper, the Fang and Ishibashi's experiment is taken as the calculation example for the comparisons and analysis. In the experiment, the surface of the retaining wall is vertical, the height of the wall is 1 m, the backfill behind the retaining wall is sandy soil whose unit weight $\gamma = 15.4\,\mathrm{kN/m^3}$ and the internal friction angle $\varphi = 34°$. In the calculation, the friction angle between soil and wall $\delta = 2\varphi/3 = 22.67°$, the initial value of internal friction angle of the backfill $\varphi_0 = 9.69°$, the friction angle of the interface between wall and soil $\delta_0 = 4.16°$.

3. Result analysis and discussion

3.1. The slip crack surface

Different from the Coulomb theory, the angle is greater than the angle of the Coulomb's classical slip crack surface, and the width on the top of the slip crack surface is smaller for the displacement pattern of translational motion (T mode). For the displacement pattern of rotation about the bottom(RB mode), the angle between the slip crack surface and the horizontal direction decreases with the increasing depth by a smooth curved surface, the slip crack surface is steeper than the Coulomb's classical slip crack surface at the upper of the retaining wall and flatter than the Coulomb's classical slip crack surface at the bottom of the retaining wall. The width on the top of the slip crack surface is wider than that of the displacement pattern of translational motion, narrower than that of the Coulomb's theory. For the displacement pattern of rotation about the top(RT mode), at the upper of the retaining wall, the slip crack surface is a potential slip crack surface and it is flatter than the Coulomb's classical slip crack surface. At the lower of the retaining wall, the slip crack surface is steeper than the Coulomb's classical slip crack surface, the width on the top of the slip crack surface is wider than that of the displacement

pattern of translational motion, narrower than that of the Coulomb's theory. The shape of the slip crack surface is shown in Fig. 5.

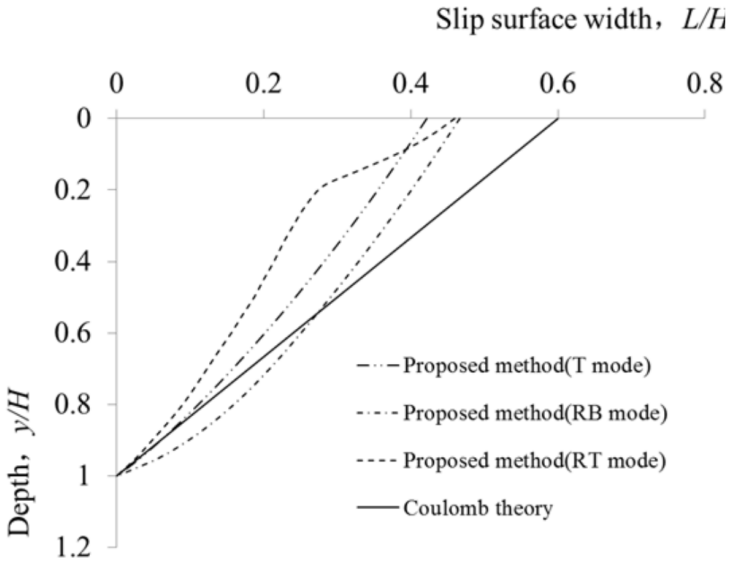

Fig. 5. Shape of slip crack surface

3.2. The earth pressure distribution

For the displacement pattern of translational motion (T mode), the active earth pressure increases with the increasing of depth at the upper and middle of the retaining wall, but the increasing rate decreases. The active earth pressure decreases with the increasing of depth at the bottom of the retaining wall. For the displacement pattern of rotation about the bottom(RB mode), the active earth pressure is same with that of T mode at the upper of the retaining wall because of the fully active state of the backfill; at the lower of the retaining wall, the backfill does not reach fully active state because of the smaller displacement, so the active earth pressure is bigger than that of T mode; at the bottom of the retaining wall, the active earth pressure is obviously larger than that of the Coulomb's theory. For the displacement pattern of rotation about the top (RT mode), the earth pressure is large because of the shear stress from the lower soil and the frictional force from the wall at the upper of the retaining wall; at the lower of the retaining wall, the active earth pressure increases firstly, then decreases with the increasing depth because of the fully active state of the backfill. Compared with the model test and Coulomb theory, the calculation method in this paper can reflect obviously the change rules of the active earth pressure, especially at the bottom of the wall, as is shown in Fig. 6.

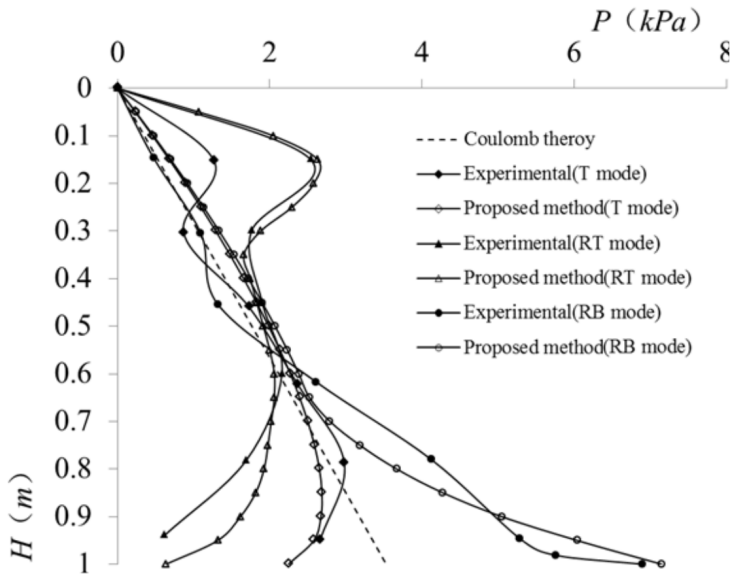

Fig. 6. Earth pressure distribution

3.3. The resultant force

The resultant force of active earth pressure decreases with the increasing of displacement and the decreasing rate decreases under different displacement of retaining wall. For the displacement pattern of translational motion (T mode), the location of the resultant force is higher than H/3 by Coulomb's theory, while the location of the resultant force of active earth pressure is about H/3 with the displacement pattern of rotation about the top (RT mode) and higher than H/3 with displacement pattern of rotation about the top (RT mode), as is shown in Fig. 7 and in Fig. 8.

4. Conclusion

In this paper, according to the analysis of the stress state and the effect of principal stress rotation of backfill behind the wall, the calculation method for active earth pressure which considers the effect of displacement of the retaining wall is established. Also, the obtained results of active earth pressure have good agreement with the test results.

The distribution curves of active earth pressure are nonlinear: for the T mode, the active earth pressure increases with the increasing of depth at the upper and middle of the retaining wall, the active earth pressure decreases with the increasing of depth at the bottom of the retaining wall; for the RB mode, the active earth pressure is same with that of T mode at the upper of the retaining wall, the active earth pressure is bigger than that of T mode or the Coulomb's theory at the lower of

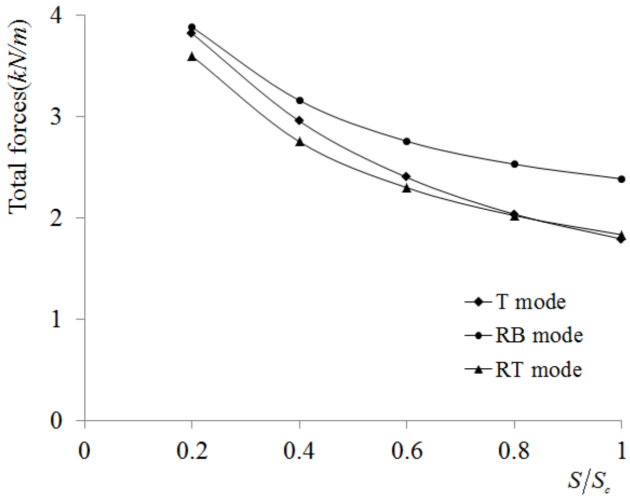

Fig. 7. Curve of the resultant force

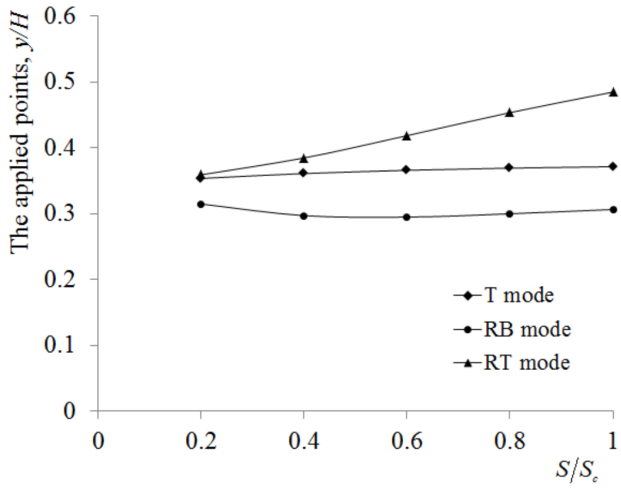

Fig. 8. Curve of the resultant force

the retaining wall; for the RT mode, the active earth pressure is large at the upper of the retaining wall, the active earth pressure increases firstly, then decreases with the increasing depth.

The resultant force of active earth pressure decreases with the increasing of displacement for three displacement modes: T mode, RB mode, and RT mode. For the T mode, the location of the resultant force of active earth pressure is higher than $H/3$ by Coulomb's theory; for the RB mode, the location of the resultant force of active earth pressure is about $H/3$; for the RT mode, the location of the resultant force of active earth pressure increases with the increasing displacement of rotation

and is higher than $H/3$.

References

[1] L. Chen: *Active earth pressure of retaining wall considering wall movement.* European Journal of Environmental and Civil Engineering *18* (2014), No. 8, 910–926.

[2] Y. S. Fang, I. Ishibashi: *Static earth pressures with various wall movements.* Journal of Geotechnical Engineering *112* (1986), No. 3, 317–333.

[3] M. H. Khosravi, T. Pipatpongsa, J. Takemura: *Theoretical analysis of earth pressure against rigid retaining walls under translation mode.* Soils and Foundations *56* (2016), No. 4, 664–675.

[4] O. Rahmouni, A. Mabrouki, D. Benmeddour, M. Mellas: *A numerical investigation into the behavior of geosynthetic-reinforced soil segmental retaining walls.* International Journal of Geotechnical Engineering *10* (2016), No. 5, 435–444.

[5] M. F. Chang: *Lateral earth pressures behind rotating walls.* Canadian Geotechnical Journal *34* (1997), No. 4, 498–509.

[6] P. Rao, Q. Chen, Y. Zhou, S. Nimbalkar: *Determination of active earth pressure on rigid retaining wall considering arching effect in cohesive backfill soil.* International Journal of Geomechanics *16* (2016) No. 3, 04015082.

[7] W. Kuihua, M. Shaojun, W. Wenbing: *Active earth pressure of cohesive soil backfill on retaining wall with curved sliding surface.* Journal Southwest Jiaotong University *46* (2011), No. 5, 732–738.

[8] E. Levenberg, N. Garg: *Estimating the coefficient of at-rest earth pressure in granular pavement layers.* Transportation Geotechnics *1* (2014), No. 1, 21–30.

[9] Y. T. Zhou, Q. S. Chen, F. Q. Chen, X. H. Xue, S. Basack: *Active earth pressure on translating rigid retaining structures considering soil arching effect.* European Journal of Environmental and Civil Engineering (2016), 1–17.

[10] M. A. Sherif, I. Ishibashi, C. D. Lee: *Earth pressures against rigid retaining walls.* Journal of the Geotechnical Engineering Division *108*, (1982), No. 5, 679–695.

Received April 23, 2017

Acta Technica *62*, No. 1A/2017, 55–66

Application of a fuzzy neural network based on particle swarm optimization in intermittent pumping[1]

Haibo Liang[2], Xiaodong Wang[2], Jie Mei[3], He Zhang[2], Weishi Chen[2], Guoliang Li[2]

Abstract. In the intermittent pumping, due to the complexity and uncertainty of oil production process, it is difficult to accurately determine the pumping running status, and pumping unit start-stop cannot match the downhole oil quantity change. To more effectively evaluate the pumping running status, this paper presents an improved fuzzy neural network evaluation model. The model uses particle swarm optimization to optimize the membership function and the final output layer connection weights of the fuzzy neural network, improving the fuzzy neural network parameter selection randomness, avoiding falling into local optimal solution and enhancing the accuracy and the convergence speed. By comparison, the improved model has higher accuracy and faster convergence rate. Through field application, it shows the evaluation results of the model are consistent with the actual situation, verifying the feasibility of the model.

Key words. Intermittent pumping, PSO, fuzzy neural network.

1. Introduction

In the oil field exploitation, beam pumping plays a decisive role in oil exploitation machinery because of its simple structure, reliability, practicability and handiness. But on account that beam pumping rated extraction capacity is greater than oil well's actual load and that there are different degrees of empty pumping , it makes electric motor light relatively and its power factor low, and makes pumping backlash increasing and energy waste [1]. If the motor can stop when it works lightly and the oil storing is less, and start up when the oil storing increases to the degree to

[1]The authors acknowledge the mega project of applied basic research in Sichuan province Research on safe drilling data mining and intelligent early warning technology (Grant: JY0049).

[2]Mechanic and Electronic Engineering, Southwest Petroleum University, Chengdu, 610500, China

[3]Petroleum Engineering Technology Research Institute, North China Oil and Gas Branch of Sinopec, Zhengzhou, 450009, China

which that the pumping can full pumping continuously, intermittent pumping can be realized, and thus it can save energy, reduce wear, and improve economic benefit. In intermittent pumping, evaluating the running status of pumping, such as accurate judgement of full pumping and empty pumping, is the key to determine the start-stop interval of pumping. However power supply of each well, weight and position of counterbalance, motor power and suspension center's load are different, and these factors are interconnected, which makes it difficult to have a clear criterion to judge the state of full and empty pumping. So how to use limited information to judge operation status of pumping is of practical significance for formulating reasonable intermittent pumping control plan.

At present, intelligent control for pumping has become a hot spot. Among that, neural networks control, fuzzy logic control and expert control are typical control methods. However due to the complexity, randomness and nonlinearity of oil extraction systems, there is not a unified approach so far.

Fuzzy neural network has been widely applied with good approximation ability of nonlinear function and learning capacity. The article proposed rule self-tuning RL fuzzy neural network, and has applied it to the intermittent pumping control with power-saving rate of 30 %. The article [2] proposed a simplified fuzzy neural network intelligent control program and has energy-saving result. The article [3] proposed self-adapting fuzzy control system and has applied it to the energy saving retrofit of pumping oil production successfully. However, it still exists randomness of fuzzy neural network's parameter selecting and local optimal solutions when modeling with fuzzy neural network.

In view of this, this paper improves fuzzy neural network using Particle Swarm Optimization algorithm through combinatorial optimization of center value and width value of membership function and the connection weights of final output layer of the fuzzy neural network. Particle Swarm Optimization algorithm improves fuzzy neural network's learning ability and generalization ability. Through using this for evaluating of operation state and being verified by the actual data, the modified method improves the evaluation model's accuracy and convergence rate.

2. Methodology

Fuzzy neural network is the combination of fuzzy logic and neural network, which has the advantages of reasoning process is easily understood, sample requirement is low, and stronger ability of self-learning. However, when modeling by fuzzy neural network, the relationship between learning ability and generalization ability of fuzzy nervous system is not direct ratio, only when the fuzzy neural network has moderate complexity, it has good generalization ability. Moreover, when parameters of the network front section arbitrarily selected, improper selection will result in the convergence speed of fuzzy neural network slower, and falling into the local optimum [4]. Thus, according to the performance requirements of model, select the best combination values of fuzzy neural network parameters.

In this paper, $T-S$ fuzzy neural network model is divided into five levels, namely input layer, fuzzification layer, fuzzy inference layer, normalization layer and defuzzi-

fication layer. The first layer and the second layer represent the predictor of fuzzy rules, namely the input space division of fuzzy systems; the left three parts represent the consequent of fuzzy rules, namely completing fuzzy inference rules of the system.

The input layer is the first layer in graph 1, and its nodes are the entrances of fuzzy information. The input layer transfers the information to the next layer, and each node represents input message $x_i,\ i = 1, 2, ..., n$, respectively. Therefore, the number of input layer nodes depends on the dimension of the input message, $N_1 = n$. There are three input quantities in this paper, namely current I of the pumping unit motor, differential value $\mathrm{d}I/\,\mathrm{d}t$ and integral value $\int I\,\mathrm{d}t$, so that $n = 3$. The second one is the fuzzification layer, where each node represents a language variable value. The layer is used to calculate the membership function of each input component which belongs to the fuzzy set of linguistic variables $\mu_{ij},\ i = 1, 2, ...n,\ j = 1, 2, ...m$. We select the Gaussian function as the membership function that is defined by the formula

$$\mu_{ij} = \exp\left[-\frac{(x_i - c_{ij})^2}{\sigma_{ij}^2}\right],\ i = 0, 1, 2, ..., n,\ j = 1, 2, ..., m\,. \tag{1}$$

Here, c_{ij} and σ_{ij} represent the center and width of the membership function in this equation, respectively. Symbol n is the dimension of input, m is the number of the fuzzy rules. In this article, we select $n = 3$ and $m = 5$. So the total number of nodes of this layer is $N_2 = n \cdot m = 15$.

The third is fuzzy inference layer, where each node represents a fuzzy rule. The layer is used to match premises of fuzzy rules and calculate fitness value of each rule. This will be normalized by the fourth layer that is the normalization layer. The normalized fitness value is calculated as follows:

$$\alpha_j = \frac{\alpha_j}{\sum_{i=1}^{m} \alpha_i},\ j = 1, 2, ..., m. \tag{2}$$

There are equal numbers of nodes between the third and fourth layers, that is, $N_3 = N_4 = \prod_{i=1}^{n} m$ ($n = 3$ and $m = 5$ in this paper), so there are equal node numbers between fuzzy inference and normalization layers, which is 125. The fifth is the output layer, also known as defuzzification layer, which realizes clear calculations in fuzzy neural network as shown in the following expression [5]:

$$y_i = \sum_{j=1}^{m} \omega_{\mathrm{ij}}\overline{\alpha_j},\ i = 1, 2, 3..., r. \tag{3}$$

Here, ω_{ij} represent the connecting weight between the ith output node and jth inference layer node. Symbol r is the number of nodes of the output layer. As there is only one output in this paper, $r = 1$.

By the above analysis, there are two kinds of learning parameters in Fuzzy neural network: one is the central value and width value of membership function, given by c_{ij} and σ_{ij}, respectively; another one is the output weight $omega_{ij}$ in the last layer.

First, the population of particles must be encoded and then the optimization for

central values and width values of membership function and the final output layer connection weights of the fuzzy neural network are conducted again and again. The optimization stops until it reaches the prescribed scope of mean square error function and outputs the optimal parameters.

The particle population is composed by n vectors of dimension D. The position vector X of the particle in the population represents the center value c_{ij}, the width value σij of the membership function of the fuzzy neural network, and final output layer connection weights ω_{ij}. Initialization of the particle swarm and updating the velocity and position of the particle is performed according to the following formulae

$$V_{is}^{t+1} = V_{is}^{t} + c_1 r_{1s}^{t} \left(P_{is}^{t} - X_{is}^{t}\right) + c_2 r_{2s}^{t} \left(P_{gs}^{t} - X_{is}^{t}\right) . \tag{4}$$

$$X_{is}^{t+1} = X_{is}^{t} + V_{is}^{t+1} . \tag{5}$$

Here, c_1 and c_2 are learning factors, r_{1s}, r_{2s} are uniform random numbers ranging from zero to one. Symbol V_{is}^{t} is the speed of sth dimension in tth iteration for particle i, X_{is}^{t} is the current position, P_{is}^{t} is the individual optimal position, and P_{gs}^{t} is the global optimal position of sth dimension in tth iterations for the entire population.

In this paper, the output mean square error of the fuzzy neural network is used as the fitness function of the particle swarm algorithm, and the output mean square error function of the fuzzy neural network is expressed as

$$SE = \frac{1}{2k} \sum_{i=1}^{k} \left(y_{di} - y_i\right)^2 , \tag{6}$$

where, y_{di} and y_i represent expected output and actual output, respectively, and K is the total number of the samples.

Parameter optimization of fuzzy neural network: the output mean square error of the fuzzy neural network is used as the fitness function of the particle swarm optimization algorithm. The maximum error is 0.005 and the maximum number of iterations is 800. When the error reaches the specified range or reaches the maximum number of iterations, the optimization stops and network model achieves the best.

3. Result analysis and discussion

Since the oil pumping control system has the characteristics of model uncertainty, highly nonlinear, and the system main equipment is placed underground, the measurable state variable are quite less. The most convenient, reliable and relatively low-cost method determining whether the pumping unit is empty or not is to detect current.

Therefore, the evaluation model established in this paper has three inputs and one output. The inputs include the current I, differential value $\mathrm{d}I/\,\mathrm{d}t$ and integral value $\int I\,\mathrm{d}t$ of motor of pumping unit, namely the load current, load changes, the load

accumulated. The output stands for the levels of pumping unit operating status, that are full pumping, half pumping and empty pumping and the corresponding values are 0,1,2. Table 1 shows input and output data of two representative wells.

Table 1. Data of two wells

time	A				B			
	I	$\mathrm{d}I/\mathrm{d}t$	$\int I\,\mathrm{d}t$	Output	I	$\mathrm{d}I/\mathrm{d}t$	$\int I\,\mathrm{d}t$	Output
1	24	0	1	0	31	0	1	0
2	25	1	2	0	32	2	2	0
3	29	4	4	0	32	0	4	0
4	31	2	7	0	34	2	4	0
5	34	3	9	0	35	1	7	0
6	34	0	12	0	35	0	8	0
7	34	0	14	0	35	0	10	0
.....	.....	.....	.....	.....	.....	.....	.....	.....
28	21	1	38	2	26	-1	35	1
29	19	-2	38	2	26	0	36	2
30	18	-1	38	2	25	-1	36	2
31	18	0	38	2	25	0	37	2
32	18	0	38	2	25	0	37	2

According to the data of Table 1, it can be seen the trends of current, current changes and current accumulation of motor of pumping unit, the running status of the pumping unit could be evaluated in turn.

1. Full pumping phase: After pumping starts, current has increased and current change will be larger and current accumulation will be small, these data show that pumping unit is in "full pumping" state. However, during the downtime to start, oil pump should be filled in a short time as oil flow from the pump back to the oil wells.

2. Stable full pumping phase: After pumping start-up, current I remains stable, current change $\mathrm{d}I/\mathrm{d}t$ is smaller.

3. Half pumping transitional phase: The current decreases slowly and the load of oil pumping reduces since the pump suction capacity is greater than the oil seepage ability of oil well.

4. Empty pumping phase: At oil production later period,the current stabilizes at a lesser extent, current change is small and current integration reaches the maximum, indicating the pumping unit to "empty pumping" [6].

3.1. Network training and evaluation model

1) Sample data: as Table 1 shows, input and output data of two representative wells being given, it is possible to select 32 sets of data in group A as the training sample data for training the model and another 32 sets of data in group B as the testing sample for model testing and inspection. Due to the large differences between the data, data normalization is done beforehand.

2) Network structure: according to the characteristics of current parameters, the first layer has three input variables and their fuzzy division numbers by the second layer are selected as 5, i.e., $m = 5$. Now, the second layer has 15 nodes, and the number of membership functions corresponds to 15. By the second section analysis, the number of nodes in the fuzzy inference layer is same as in the normalized layer and its value is 125. And output layer node number is 1, which can determine the topology of the fuzzy neural network based on PSO for the 3-15-125-125-1 type.

3) Determination of model parameters: the determination of model parameters is done through fuzzy neural network training process. Further parameters adjustment through continuous training of the model, actually the training process is a correction procedure for the parameters.

In this paper, the learning rate of the network is set as $\eta = 0.2$, the maximum number of iterations is set to 800, and the error is set to 0.005. 32 sets of sample data are input for specific training process of the model. First, enter a set of sample data namely data A, the output could be obtained after the gradual spread between the layers, and then calculate the change amount of neurons' weight in each layer of the data A, including $\Delta_{\mathrm{A}}\,\omega$, $\Delta_{\mathrm{A}}\,c$ and $\Delta_{\mathrm{A}}\,\sigma$. Second, repeat the first step process until completing the calculation of all the sample. According to $\Delta\omega = \sum \Delta_{\mathrm{A}}\,\omega$, $\Delta c = \sum \Delta_{\mathrm{A}}\,c$, $\Delta\sigma = \sum \Delta_{\mathrm{A}}\,\sigma$, the change of the connection weights of this round training are calculated, as $\Delta\omega$, Δc, $\Delta\sigma$. Again, according to the output mean square error, the center value and width value of the membership function of network with network connection weights can be adjusted through iteration. If the mean square error of the output is less than the present value or the maximum number of iterations is reached, the iteration stops; otherwise it continues. Thus, the fuzzy neural network evaluation model based on particle swarm optimization is established and it can be used to evaluate the running state of the pumping unit.

3.2. Comparative example simulation and evaluation results

1) Convergence speed comparison

The training for the traditional fuzzy neural network (called FNN) was done with the same sample data and consistent parameters, as the learning rate is $\eta = 0.2$, the maximum number of iterations is set to 800, error is set to 0.005. The FNN model reaches steady state after 583 iterations and the fuzzy neural network model based on particle swarm optimization (referred to the PSO-FNN) after 352 iterations is stabilized. The training error curves are shown in Fig. 1 and 2. Table 2 contains the performance analysis of two kinds of models. From the figures and the table, when the MSE objective value is 0.005, PSO-FNN model can meet the requirements after

352 iterations, which is less 231 iterations than the FNN's. Also the running time is shorter than the latter. Therefore, PSO-FNN model has the advantages of less iteration number and faster convergence speed.

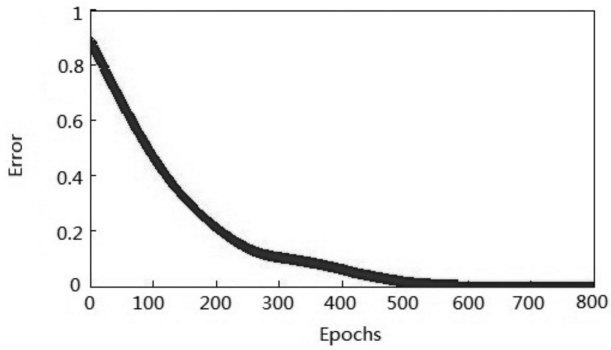

Fig. 1. Mean square error curve of FNN

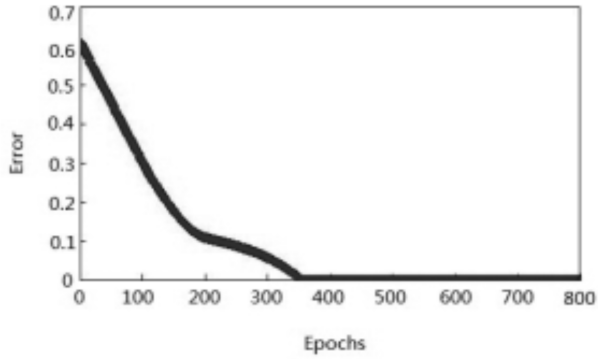

Fig. 2. Mean square error curve of PSO-FNN

Table 2. The performance analysis of two models

Performance	FNN	PSO-FNN
MSE	0.005	0.005
iterations	352	583
run time/s	23.6	37.3

The network is trained and tested by the normalized training sample and test sample data. Using the already trained fuzzy neural network, the model is tested by 32 sets of data of group B in Table 1. In contrast the model actual output to the expected output, the accuracy of the PSO-FNN model could be checked, furthermore, comparing with the output results of the FNN model. Figures 3 and 4 represent the test output results from the FNN model and PSO-FNN model,

respectively. Table 3 shows output average error comparison of test data of two models.

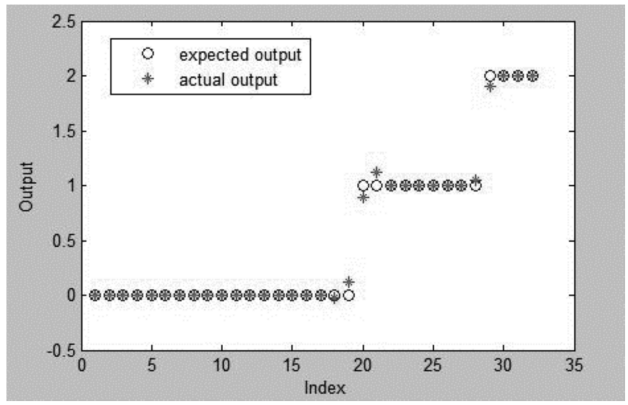

Fig. 3. FNN model test output diagram

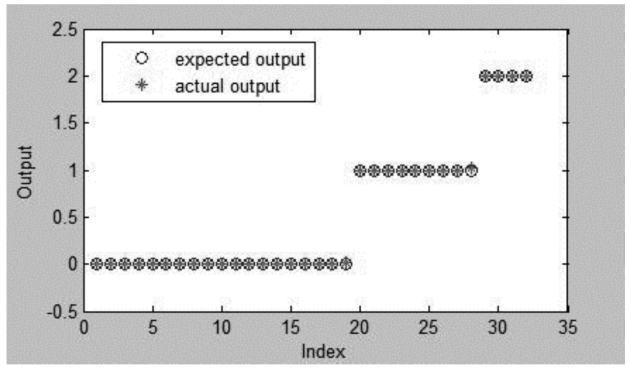

Fig. 4. PSO-FNN model test output diagram

Table 3. Comparison of average errors of two model test data

	FNN	PSO-FNN
Average error	0.0693	0.0083

Comparing the two methods by the above figures and tables, the PSO-FNN has better fitting degree since the actual output of it is very close to the expected output and average error of its test output is 0.0083 contrasting the FNN model's providing 0.0693. It is visible that PSO-FNN model is more accurate.

Comparative verification of the particular cases shows that the fuzzy neural network model based on PSO significantly improved on the convergence rate and accuracy of the evaluation results in contrast to the traditional fuzzy neural network model. The improved pumping state evaluation model has a strong self-learning

ability, good generalization ability and precision, so it will be more suitable for the pumping operating status evaluation.

3.3. Application of pumping unit operating state evaluation model

A field well is selected as the research object and its basic situation is as follows: pumping speed is $3.52\,\mathrm{min}^{-1}$, the length of stroke is 3 m and pump diameter is 28 mm. Data acquisition time is on 2016/3/9 15:00:23. A stroke of the current acquisition curve is shown in Fig. 5. The full part of the line represents the process of downstroke while the dotted part represents upstroke. The indicator diagram curve of the well is shown in Fig. 6.

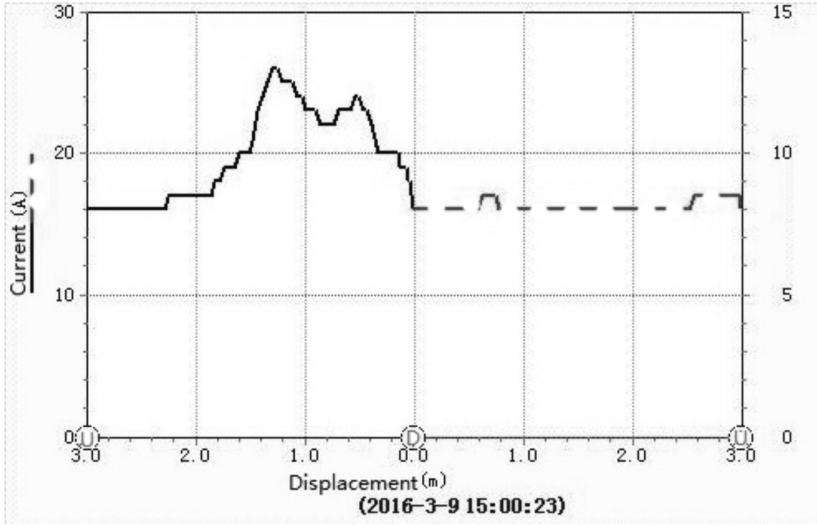

Fig. 5. Current curve in a stroke of the well

Figure 6 shows that the well has a "knife-type" indicator diagram that is typical characteristics for insufficient liquid supply of a well. Therefore, the well is currently in a state of insufficient supply. The results of the evaluation model are consistent with the actual situation. In addition, combined with the data and output evaluation results, the model not only can output the evaluation level, but also can detail evaluation results through analyzing data reflected in the level location. This would contribute to the analysis and accumulation of typical current parameters and provide more help to the decision makers.

According to Table 1, the current parameters of the downhole stroke is selected as the research object with extracting 20 sets of current values from it, then corresponding calculations including current differentiation and current integration allowed forming 20 groups of current data of the well's downhole stroke, as shown in Table 4. Then these current data, as the input of PSO-FNN model established in this paper, are used for pumping unit operation status evaluation and the model's output is shown in Figure 7. The figure shows that there are 16 sets of data in 20

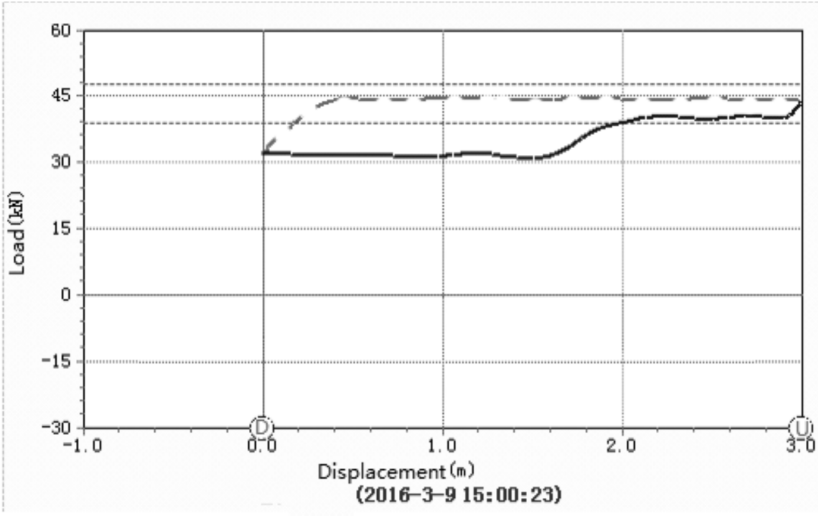

Fig. 6. Indicator diagram in a stroke of the well

groups output representing level 1 which stand for half pumping, while the remaining 4 sets represent level 0 standing for full pumping. Taking into account a certain chronological relationship among the 20 sets of data, the output results of the model can be evaluated according to the overall trend. Therefore, it can be judged that the operating state of the well pumping unit is half pumping, namely, liquid supply deficiencies and intermittent pumping measures need to be taken.

Table 4. Current parameters of the well

time	I	$\mathrm{d}I/\mathrm{d}t$	$\int I\,\mathrm{d}t$	time	I	$\mathrm{d}I/\mathrm{d}t$	$\int I\,\mathrm{d}t$
1	16	0	0	11	24	6	8
2	16	0	0	12	26	4	14
3	16	0	0	13	25	-2	19
4	16	0	0	14	23	-3	24
5	16	0	0	15	22	-2	28
6	17	2	0	16	23	2	32
7	17	0	1	17	24	2	36
8	17	0	1	18	21	-6	40
9	19	3	3	19	20	-1	42
10	20	2	5	20	17	-5	44

4. Conclusion

Improvement of fuzzy neural network uses PSO algorithm through combinatorial optimization of enter value and width value of membership function and the connection weights of final output layer of the fuzzy neural network, enhancing the learning ability and the generalization ability of fuzzy neural network. PSO-FNN model has

good generalization ability and has been improved both in the rate of convergence and the accuracy of evaluation results compared with traditional FNN model. And influences of some human factors may be avoided through this model's ability of evaluation and prediction, saving human and material resources and improving the intelligent degree of the running status evaluation of pumping unit. The PSO-FNN model has been applied to an oil well and verified feasibly of the model as evaluation results are consistent with the actual situation. At the same time, detailing evaluation results by the data location reflected in evaluating grade, contributes to analyzing and accumulating typical current parameters and providing arguments for qualitative and quantitative evaluation, which is of guiding significance of decision in the field.

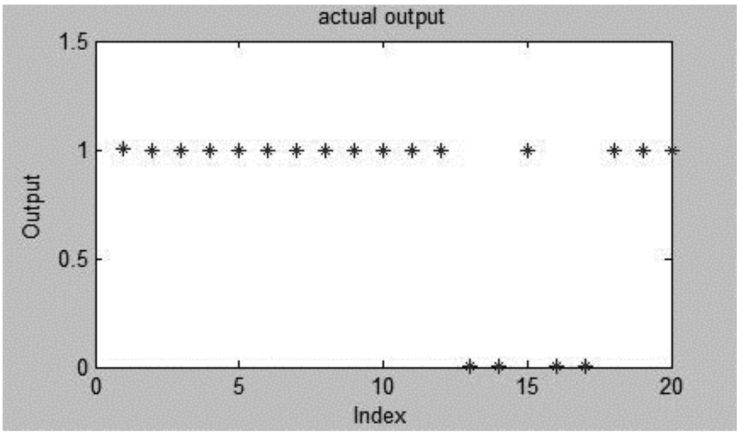

Fig. 7. PSO - FNN model output evaluation results

References

[1] B. Ding, Y. Zhang, L. Sun: *RL fuzzy neural etwork and its application to oil pumping control.* Control Engineering of China *9* (2002), No. 6, 57–59.

[2] W. Qi, X. Zhu, Y. Zhang: *A study of fuzzy neural network control of energy-saving of oil pump.* Proceedings of the CSEE *24* (2004), No. 6, 137–140.

[3] Ding Bao, Qi Wei-Gui, Wang Feng-Ping: *Research on an energy-saving software for pumping units based on FNN intelligent control.* Journal of Harbin Institute of Technology (New Series) *116* (2004), No. 3, 240–244.

[4] M. Xia, X. Liang, F. Han: *Water quality comprehensive assessment approach based on T-S fuzzy neural network and improved FCM algorithm.* Computers and Applied Chemistry *30* (2013), No. 10, 1197–1201.

[5] H. Sun, X. Zhang, A. Ning: *The application of fuzzy neural network based on PSO algorithm in speech recognition system.* Mathematics Practice and Theory *40* (2010), No. 6, 113–117.

[6] B. Ding, W. Qi, X. Zhu: *A study of energy-saving control of oil pump based on fuzzy neural network prediction.* Acta Electronica Sinica *32* (2004) No. 10, 1742–1745.

Received April 23, 2017

Acta Technica *62*, No. 1A/2017, 67–78

Analysis of rigid frame bridges with different high piers' dynamic behavior and seismic fragility

Min Xiang[1], Wenya Wang[1], Tian Li[1], Qinghua Ai[1]

Abstract. In order to study the seismic performance of different high pier bridges, the (106+200+106) m rigid frame bridge is taken as the engineering background. According to the RC pier of this bridge and the principle of same bearing capacity and pier-top's stiffness, two new types of high piers are optimal designed: one is CFS-1 pier, the other is CFS-2 pier. A finite element model is established by OpenSees to analyse seismic responses of three bridges with Incremental Dynamic Analysis method. IDA curves are drawn and the damage exceedance probability is calculated under different damage conditions. The dynamic response laws and vulnerability of rigid frame bridges at different levels peak ground acceleration with different structure form's high piers are obtained. CFS-1 and CFS-2 piers' seismic performance is better than RC pier. The results of this study could serve as reference and guidance for similar engineering design.

Key words. Double limb thin-walled high pier, concrete-filled steel high pier, double corrugated steel web, Incremental Dynamic Analysis, IDA curve, damage exceedance probability.

1. Introduction

In recent years, many long-span continuous rigid frame bridges with high piers are built in high seismic intensity area. Usually, the pier section forms are rectangular hollow pier and double limb thin-walled hollow pier [1]. And thin-walled hollow pier has a lot of characteristics, for instance, its complexity in structure, high axial compression ratio at the bottom of piers, and it has complex construction, multi-processes, long construction period, difficulty of control and so on. At the same time in bridge vibration, with the increase of pier height, the weight of high pier and higher mode shape becomes more and more significant for the seismic response of the whole structure. Therefore, the seismic design and analysis theory of the high pier bridges are quite different from that of middle and low pier bridges.

[1]School of Civil Engineering, Shijiazhuang Tiedao University, Shijiazhuang, 050043, China

In the foundation of referring to a large number of documents, the future development trends of long-span continuous rigid frame bridge with high pier are as follows:

- The weight of superstructure will be lighter.
- The span and the total length of superstructure will continue to increase.
- Many curved bridges will be built.
- The pier will be higher and higher.
- Some new types of pier and superstructure structures will continue to appear.
- New materials and composite structures will be applied to bridge completely and the durability will be fully reflected in structural design.
- The construction will be faster and more convenient and so on.

Based on the development trend of continuous rigid frame bridge with high piers, the (106+200+106) m long-span continuous rigid frame bridge is taken as the engineering background of this paper. The pier height of the main bridge is 166.405 m and 166.205 m and the pier section form is double limb rectangular hollow pier. The layout of the bridge is shown in Fig. 1. Its single limb section size is shown in Fig. 2.

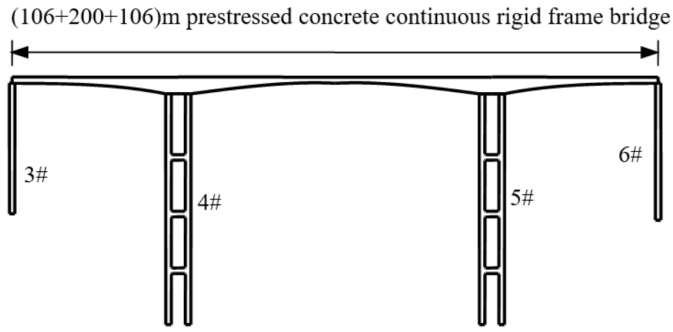

Fig. 1. Single limb section size

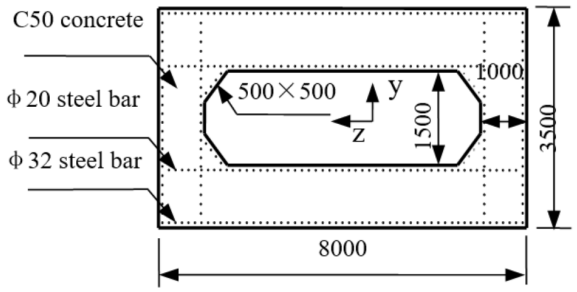

Fig. 2. Layout of main bridge (dimensions in mm)

Considering the convenience of high pier construction and advanced anti-corrosive techniques for steel members, the design life requirements can be met. According to the double limb rectangular hollow pier structure (RC pier) of this bridge and the principle of same bearing capacity and pier-top's stiffness, two new types of high piers are optimal designed in [2], as is shown in Figs. 3 and 4. Based on the research,

this paper explores the dynamic characteristics and the vulnerability of different high piers under different levels of ground motion of rigid frame bridges.

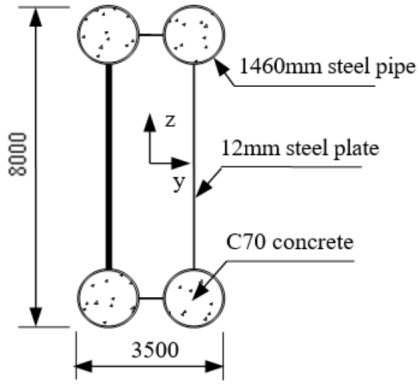

Fig. 3. CFS-1 pier section (dimensions in mm)

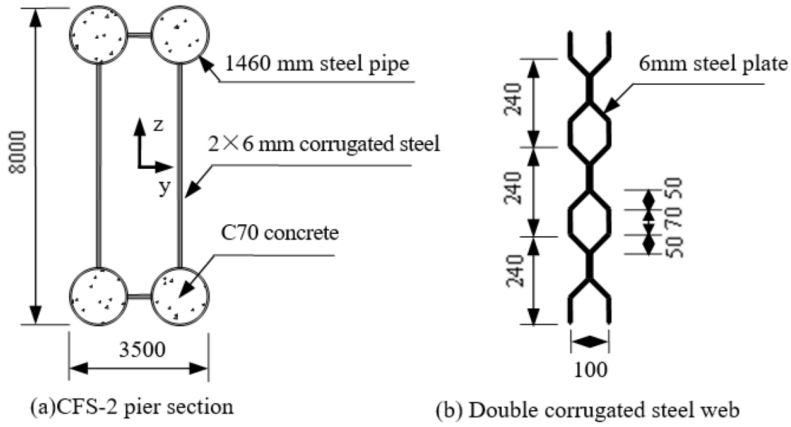

Fig. 4. CFS-2 pier section (dimensions in mm)

2. Methodology

2.1. Research on dynamic characteristics of bridges

According to double limb rectangular hollow pier (RC pier) and two new types of piers by optimal design, the dynamic analysis model of bridge is proposed. The dynamic characteristics of three continuous rigid frame bridges with different types of high piers are analyzed by multiple Ritz vector method. And the dynamic characteristics of the first 45 orders are analyzed. The cycle and mode characteristics of the first 5 orders are shown in Table 1.

Table 1. Dynamic characteristics of continuous rigid frame bridge with different high piers

Order number	RC pier		CFS-1pier		CFS-2pier	
	Cycle T/s	Characteristics of modes	Cycle T/s	Characteristics of modes	Cycle T/s	Characteristics of modes
1	5.725	Symmetrically horizontal bending of the main beam	11.620	Longitudinal floating of bridge	11.501	Longitudinal floating of bridge
2	5.042	Longitudinal floating of bridge	6.236	Symmetrically horizontal bending of the main beam	6.232	Symmetrically horizontal bending of the main beam
3	2.770	Counter-symmetrically horizontal bending of the main beam	2.480	Counter-symmetrically horizontal bending of the main beam	2.479	Counter-symmetrically horizontal bending of the main beam
4	1.420	Symmetrically horizontal bending of the main beam and high piers, the opposite direction	1.816	Symmetrically vertical bending of the main beam, inner longitudinal bending of high piers	1.804	Symmetrically vertical bending of the main beam, inner longitudinal bending of high piers
5	1.390	Symmetrically vertical bending of the main beam, inner longitudinal bending of high piers	1.636	Longitudinal bending of high pier in the same direction (4# pier)	1.620	Longitudinal bending of high pier in the same direction (4# pier)

2.2. Research on the seismic performance of bridges

By using the seismic record of PEER, three seismic waves that have similar geologic conditions and site types of the bridge site are selected for analysis [3–4]. The maximum value of three seismic waves is taken as the calculation result. Details of the seismic wave are shown in Table 2.

Table 2. Seismic waves

Year	Seismic event	Recording platform	PGA (g)
1992	Big Bear-01	Desert Hot Spring	0.225 26
1999	Chi-Chi, Taiwan	CHY025	0.159 22
1992	Landers	Desert Hot Spring	0.170 87

A finite element dynamic model is established to analyze seismic responses of bridge with Incremental Dynamic Analysis method [5–7] and the dynamic time-

history curve of the whole bridge is obtained.

Due to the high pier of research object, the maximum horizontal displacement of pier may occur at pier's top, pier's middle height or pier's other positions under earthquake. The pier's position of the largest displacement is found through comparative analysis. The peak ground acceleration of seismic wave is loaded from 0.1 g step by step to 1.2 g. Three different structure forms of high piers are RC pier, CFS-1 pier and CFS-2 pier. Their displacement time-history at pier's top and pier's middle height are shown in Fig. 5.

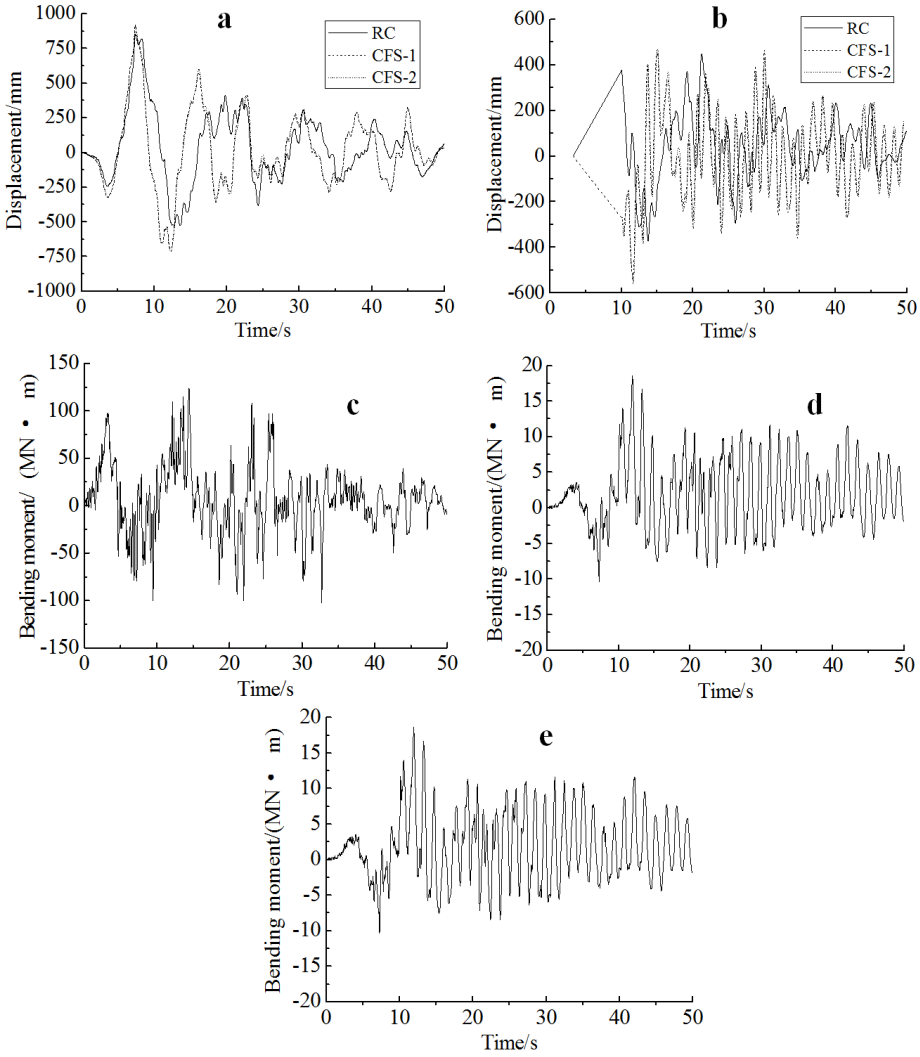

Fig. 5. Displacement time-history and bending moment time-history curves: **a**–PGA is 1.2 g at pier's top, **b**–PGA is 1.2 g at pier's middle height, **c**–PGA is 1.2 g (RC pier), **d**–PGA is 1.2 g (CFS-1 pier), **e**–PGA is 1.2 g (CFS-2 pier)

From the resultant figure, when the peak ground acceleration is small, the maximum displacement of pier's top and middle height of CFS-1 pier and CFS-2 pier is much larger than that of RC pier, while the maximum displacement of pier's top and middle height of CFS-1 pier are similar to those of CFS-2 pier. With the increase of the peak ground acceleration, the maximum displacement of pier's top and middle height increase gradually and their maximum displacements are close to the same.

In the case of the same peak ground acceleration, the moments that three types of high piers' reach maximum displacements of pier's top are different. The moments of maximum displacement of pier's middle height are also different. When the peak ground acceleration is different, the moment of reaching maximum displacement of pier's top is different for one type high pier and the time of maximum displacement of pier's middle height is also different. The displacement of pier's middle height lags behind the ground motion about a few seconds.

The peak ground acceleration of seismic wave is loaded from 0.1 g step by step to 1.2 g. The comparison of bending moment time-history of three types of piers' bottom is shown in Fig.. Three types of piers are double limb rectangular hollow pier(RC pier), concrete-filled steel tube high pier connected by steel plate (CFS-1 pier) and concrete-filled steel tube high pier connected by double corrugated steel web.

From the resultant figure it can be seen that in the case of the same peak ground acceleration, the moments when three types of high piers' reach maximum bending moment of pier's bottom are different. When the peak ground acceleration is different, the moment that maximum bending moment of pier's bottom is different for one type of high pier. At the same time, when the peak ground acceleration is same, the bending moment of pier's bottom of double limb thin-walled high pier is much larger than that of concrete-filled steel tube. And with the increase of the peak ground acceleration, the discrepancy is getting larger for their bending moment of pier's bottom.

3. Result analysis and discussion

Vulnerability is analyzed by IDA method and regression capability requirement method.

Under a given ground motion intensity, the conditional probability that the structural seismic demand D is equal to or greater than the conditional probability of seismic capacity C are as follows:

$$F_{\mathrm{r}} = P[D \geq C|IM]\,. \tag{1}$$

Earthquake intensity IM and earthquake demand D meet the relation

$$\ln D = b \cdot \ln(IM) + \ln a\,. \tag{2}$$

Logarithmic standard deviation of Structural seismic demand is

$$\beta_{D|IM} = \sqrt{\frac{\sum(\ln(d_i) - \ln(aIM_i^b))^2}{N-2}}. \tag{3}$$

Vulnerability function is given as

$$P[D \geq C|IM] = \Phi \cdot \frac{\ln \frac{D}{C}}{\sqrt{\beta_{D|IM}^2 + \beta_{\mathrm{c}}^2}}. \tag{4}$$

The vulnerability function is further deduced as follows:

$$P[D \geq C|IM] = \Phi\left(\frac{\ln(IM) - \frac{\ln C - \ln a}{b}}{\frac{\sqrt{\beta_{D|IM}^2 + \beta_c^2}}{b}}\right) \tag{5}$$

Symbol a is the IDA curve fitting coefficient, b is the IDA curve fitting coefficient, D_i is the ith earthquake demand peak, IM_i is the ith ground motion peak, and β_c is the structural seismic capacity logarithmic standard deviation.

3.1. Damage index

Select the appropriate control section to calculate the maximum curvature distribution of the RC pier and CFS pier along the high direction of the pier (as is shown in Fig. 6) for the seismic vulnerability analysis of the two types of piers [8–11].

The XRTACT software is used to establish the RC pier and CFS pier cross-section model to analyze the bending moment curvature, and the curvature values of different damage states are summarized in Table 3.

Table 3. Damage index corresponding to the curvature of piers m^{-1}

Damage status	RC pier	CFS pier
Slight Damage	0.000651	0.001014
Secondary Damage	0.000812	0.001582
Serious Damage	0.00371	0.00429
Collapse	0.01099	0.04776

It can be seen from Fig. 7 that under the action of seismic wave, the maximum curvature of CFS pier and RC pier is at the bottom of the pier. This means that the high-order vibration mode will affect the pier of the high pier, but the bottom of the pier is most likely to reach to the plastic stage. Therefore, the pier bottom section is selected as the control section for analysis. The damage state of the pier is divided: basic intact, slight damage, secondary damage, serious damage and collapse. The damage state of the pier is shown in Table 4.

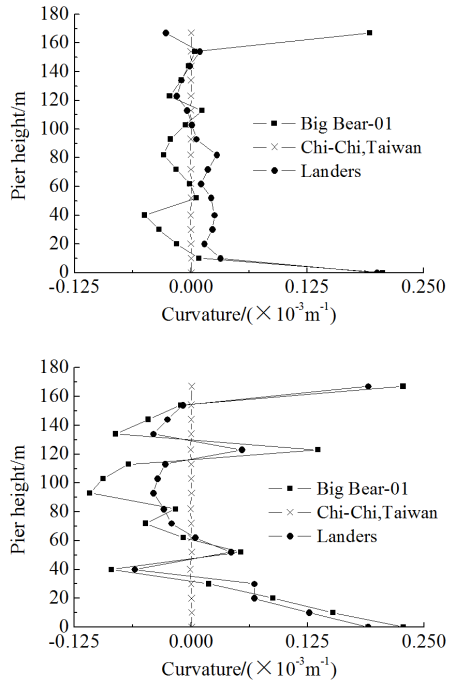

Fig. 6. Maximum curvature envelope of pier along the high direction of the pier: up–RC pier, bottom–CFS pier

Table 4. Pier damage status

Damage status	Damage description	Curvature range
Basically intact	Partial cracking of concrete	$\Phi \leq \Phi_1$
Slight damage	The lateral and longitudinal reinforcement for the first time to yield to the outer steel pipe	$\Phi_1 < \Phi \leq \Phi_y$
Secondary damage	The control section forms a plastic hinge and needs to be repaired	$\Phi_y < \Phi \leq \Phi_c$
Serious damage	Pier strength began to degenerate, difficult to repair	$\Phi_c < \Phi \leq \Phi_u$
Collapse	Core concrete crushed	$\Phi > \Phi_u$

Note: Φ_1 is the curvature of the first yielding of the inner or outer edge of the pipe; Φ_y is the equivalent yield curvature; Φ_c is the curvature at the ultimate bearing capacity; Φ_u is the ultimate curvature.

3.2. Vulnerability curve

The IDA method is used to analyze the RC pier, CFS-1 pier and CFS-2 pier. The IDA curve is drawn and fitted. The data of the regression analysis are obtained,

and the damage probability of the control section is calculated. Finally, get the vulnerability curve. The comparison of the vulnerability curves of three kinds of high-pier structures, RC pier, CFS-1 pier and CFS-2 pier, is shown in Fig. 7.

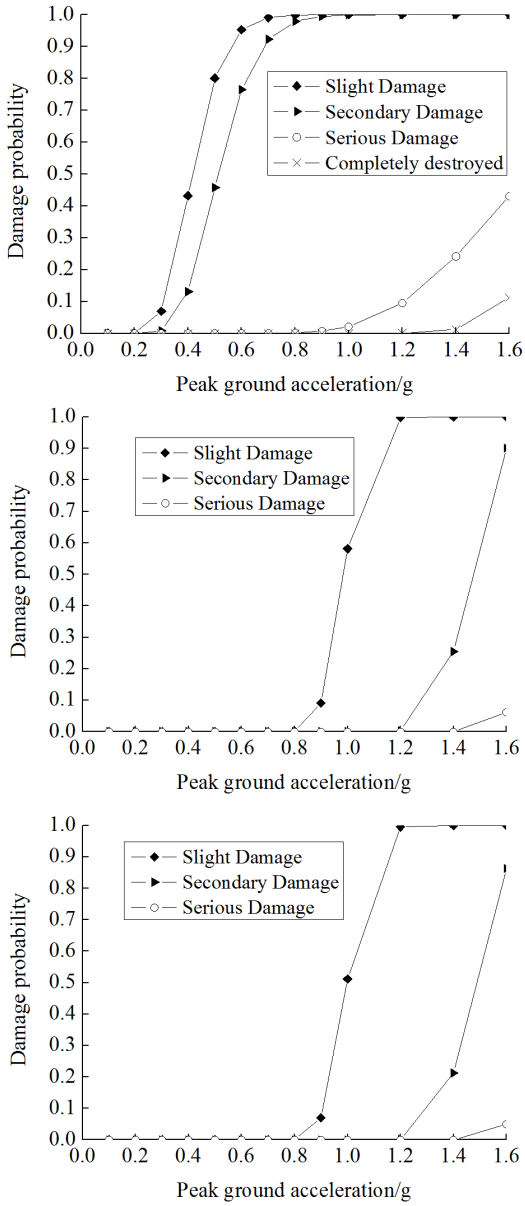

Fig. 7. Comparison of vulnerability curves of three kinds of high piers structures: up–RC pier vulnerability curves, medium–CFS-1-pier vulnerability curves, bottom–CFS-2-pier vulnerability curves

It can be seen from the comparison chart that when the ground motion is the same, the probability of slight damage of the RC pier is more than 90 % and the peak ground acceleration is 0.6 g. The peak ground acceleration of CFS-1 pier and CFS-2 pier is 1.2 g under the same damage probability. So when the peak ground acceleration value is between 0 and 1.2 g, RC-pier are more susceptible to occurred light damage. When the secondary damage probability is more than 90 %, the peak ground acceleration value of the RC pier is 0.7 g, while the peak ground acceleration value of CFS-1 pier and the CFS-2 pier is 1.6 g. So the seismic performance of CFS pier is better than the RC pier.

When the peak ground acceleration is 1.6 g, the secondary damage and serious damage probability of the CFS-2 pier are slightly smaller than those of the CFS-1 pier, so the contribution of double corrugated steel web is bigger than that of the ordinary steel plate.

4. Conclusion

Based on the analysis of dynamic characteristics, seismic response and vulnerability of three kinds of high-pier continuous rigid frame bridges, the following conclusions are given:

1. The dynamic characteristics of the first two orders of three different high-pier continuous rigid frame bridges are different,the cycle of the RC pier is much smaller than that of the CFS-1 pier and the CFS-2 pier. The natural vibration cycle of the other stages is not much difference. The first-order vibration mode of the RC pier is the symmetrically horizontal bending of the main beam, and the second-order mode is the longitudinal floating of bridge. And the first-order vibration mode of the CFS-1 pier and the CFS-2 pier is just the opposite.The seismic response of the RC piers is different from that of the CFS-1 pier and the CFS-2 piers, indicating that the seismic response of the different high-pier structures is different.

2. The value of the peak ground acceleration is loaded from 0.1 g step by step to 1.2 g. The maximum displacement of the pier top and the maximum bending moment of the pier bottom are increased. When the peak ground acceleration is the same, the maximum displacement of the pier top is different from the moment of the maximum bending moment.

3. When the ground motion is the same, although the maximum displacement of pier top of the CFS-1 pier and the CFS-2 pier is larger than that of RC pier, bending moment of the pier bottom is much smaller than the RC pier. It is indicating that the CFS-1 pier and the CFS-2 pier are more flexible than the RC pier.

4. As high piers, the flexibility of CFS-1 pier, CFS-2 pier and RC pier are better, so the probability of serious damage and collapse under the earthquake is small. However, under the same ground motion, the CFS-1 pier and CFS-2 pier are more secure than the rectangular hollow RC pier.

References

[1] Z. Zong, J. Xia, C. Xu: *Seismic study of high piers of large-span bridges: An overview and research development.* Journal of Southeast University (Natural Science Edition) *43* (2013), No. 2, 445–452.

[2] M. Xiang, W. Wang, Q. Ai: *Contrastive analysis on the seismic performance for new type of bridge pier based on different structure forms.* Journal of Railway Engineering Society (2016), No. 9, 62–69.

[3] D. Wang, M. Yue, X. Li, Z. Sun, H. Qu: *Selections of real ground motions in seismic history analysis for bridges with high columns.* China Civil Engineering Journal (2013), No. S1, 208–213.

[4] J. Liu, P. Long, R. Jiang, J. Xu: *Seismic analysis of bridges based on conditional simulation algorithm.* Engineering Mechanics (2013), No. 03, 282–288.

[5] G. Liao, B. Chen, S. Chen: *Response analysis of the high-piers and long-span rigid frame bridge subjected to varying spatial seismic excitation.* Journal of Sichuan University(Engineering Science Edition), (2011), No. 05, 27–31+44.

[6] Y. Zhan, R. Song, J. Hu, R. Zhao, T. Mu: *Research of bending properties of high pier made of concrete-filled steel tube laced columns.* Journal of Building Structures *34* (2013) No. S1, 240–245.

[7] Y.,Zhou, Y. Zhang, M. Ye, B. Liu: *Seismic performance of neotype column-slab high piers in double-column model of railway bridge.* Journal of Central South University(Science and Technology) (2013) No. 06, 2506–2514.

[8] K. Zheng, L. Chen, W. Zhuang, H. Ma, J. Zhang: *Bridge vulnerability analysis based on probabilistic seismic demand models.* Engineering Mechanics *30* (2013), No. 5, 165–171+187.

[9] L. Li, J. Huang, W. Wu, L. Wang: *Research on the seismic performance of bridge with high piers and long spans using incremental dynamic analysis.* Journal of Earthquake Engineering and Engineering Vibration (2012), No. 01, 117–123.

[10] J. Liu, Y. Liu, Q. Yan, Q. Han: *Performance-based seismic fragility analysis of CFST frame structures.* China Civil Engineering Journal (2010), No. 02, 39–47.

[11] C. Zhou, J. Chen, X. Zeng, B. Liu: *Evaluation of seismic vulnerability of reinforced concrete circular hollow high-piers.* Journal of Railway Engineering Society (2014), No. 11, 65–71.

Received April 23, 2017

Acta Technica *62*, No. 1A/2017, 79–90

Method and simulation of arterial coordination control based on the intensity of vehicle arrival time in connected-vehicle network[1]

Xiao-Hui Lin[2,3]

Abstract. The coordinated control of urban trunk roads played an important role in improving the capacity of urban network. In this paper, the optimization model of vehicle saturation under the condition of signal coordination control was put forward. Through the Vissim simulation analysis of the intersection of one road, the optimal allocation of signal coordination scheme was carried out. The results showed that the main traffic capacity had been significantly improved after optimization with obvious optimization effect, which had a very important reference for the improvement of urban traffic in our country.

Key words. Connected-vehicle network, arrival time, trunk coordination, Vissim simulation.

1. Introduction

With the development of economy, people are pursuing higher quality of life, and they are increasingly dependent on the freedom of the family car. The traffic jam and environmental pollution caused by this have a serious impact on the development of the city (Nellore et al., 2016) [1]. In recent years, China has carried out a wide range of infrastructure construction, but more and more traffic load makes the existing transportation infrastructure difficult to meet people's needs. The traffic congestion has become an important problem in the development of modern cities (Du T. et al., 2015) [2]. Traffic congestion makes cars in a low speed state for a long time, which can increase the amount of vehicle emissions and further deterioration of the urban environment, resulting in heavier urban air pollution. In addition, the traffic

[1]Funding: 2016 Guangdong Province Science and Technology Development Special Funds (Basic and Applied Basic Research), Project (2016A030313786).

[2]School of Civil Engineering and Transportation, South China University of Technology, Guangzhou, Guangdong, 455000, China

[3]College of Computer Engineering, Guangdong Communication Polytechnic, Guangzhou, Guangdong, 455000, China

congestion can cause the driver's mood become irritable, which seriously affects people's life and work. It is not conducive to social stability, and it also increases the probability of traffic accident to a certain extent (Jamshidnejad A. et al., 2016) [3]. Measures should be taken to reduce traffic congestion. On the one hand is to reduce the number of vehicles. On the other hand is to strengthen the construction of road traffic facilities, and improve urban traffic capacity. One of the most important factors that cause the congestion is the bottleneck of intersections.

At present, the traffic flow control of intersection is controlled by different color lights. At the same time, the traffic control system based on the connected-vehicle network greatly improves the coordinated control of urban traffic. All directions of the road vehicle signal can be collected and sent to the traffic control system (Haddad J. et al., 2016) [4]. Through the effective control of the traffic flow, it is possible to realize the smooth traffic around the network. Vissim simulation software can be used to simulate the network analysis, and objectively reflect the relevant parameters of the network data. In this paper, the Vissim software is used to optimize the coordination control of the vehicle at the intersection of the main road, and the travel time and delay value of the vehicle are taken as the evaluation indexes. According to the optimized scheme of coordinated control, the new signal scheme is simulated and analyzed. This has played a positive role in relieving the traffic pressure and solving the problem of traffic congestion.

2. State of the art

2.1. Current situation of urban traffic control

With the continuous development of human society, urban traffic load is also growing. Although our country has made great efforts to the construction of infrastructure, the increase in population and the increase in the number of vehicles have made the city traffic very congested. Traffic congestion not only seriously affects the normal operation of the city, but also causes serious inconvenience to people's daily travel (Chow A. F. et al., 2016) [5]. In order to solve the increasingly serious traffic congestion, people use scientific traffic control system to improve the existing urban road operation. In particular, the development of traffic signals has become one of the important signs of modern urbanization. The cost is less, and the traffic efficiency can also be improved rapidly. As early as more than 100 years ago, people began to carry out the study of traffic signals, but the first was just a simple way to control the entry and exit order of intersect vehicles (Kutadinata R. et al., 2016) [6]. With the continuous development of computer technology, people have made a breakthrough in the research of technology and mechanism of urban traffic signal control (Wan K. et al., 2016) [7]. In 1920s, the control of urban traffic flow had begun to be carried out through traffic lights, which were made out with lots of simulation and modeling to develop many traffic signal control systems, such as OPAC, SCATS, SCOOT, and SPOT.

In all kinds of traffic signal control systems, SCOOT is an optimization technique of green signal ratio- cycle-phase difference, which was a new adaptive control system

developed on the basis of the original TRANSYT system by the British Transport Research Institute in 1975 (Zhao S. et al., 2016) [8]. After a large number of field experiments, the system has a good application effect. In the following 20 years of development, there have been nearly 200 cities using the system. However, because the system is a centralized control model, it has some limitations in application. SCATS system is an adaptive control system developed by Australia in the 1970s, including three parts: graphical interface workstation, area control center and central monitoring system. It has the characteristics of large number, and flexible control, which has a wide range of applications in many cities of our country at present (Tao D. et al., 2014) [9]. The RHODES system was developed and implemented in the United States. It had a very significant effect at the beginning of the application, especially the effect of the traffic network was the most obvious (Kesten S. et al., 2016) [10].

The study of urban traffic control system in our country was relatively late. Until the 1970s, China began to develop and apply the traffic signal control of urban traffic trunk. After more than ten years of development, China had developed Microcomputer based arterial coordination control system based on computer. At present, China has developed dozens of traffic controllers (Sadraddini S. et al., 2016) [11]. NUTCS, China's first self-developed city traffic signal control system, is suitable for the actual traffic situation in our country, especially suitable for the traffic conditions that the density of road network is not high and the intersection space is very wide (Oskarbski J. et al., 2016) [12]. The system has the characteristics of on-line control, timing control and adaptive optimization, and the optimization of system is realized by taking into account the combination of parking times, traffic delays and congestion. However, the system also has a lot of problems. One is not fully considering the optimization of the target. The other is no comprehensive consideration of motor vehicle and non-motor vehicle control mode (Bie Y. et al., 2016) [13].

A typical traffic light control system is depicted in Fig. 1.

With the development of Internet technology, more and more applications of advanced GPS technology, sensor technology and wireless communication technology based on vehicle networking technology in the modern traffic control, vehicle networking technology can use road traffic information collection and utilization in the information platform, and realizes the coordinated management between people, road, vehicle and environment. Compared with the traditional traffic control system, the technology of vehicle networking pays more attention to the collection and processing of information, so it needs a high traffic information collection technology. The vehicle can be connected to the vehicle license plate number, owner information and other individual information, thereby accurately identify the identity of the vehicle. Once to construct a complete car networking, it can be a vehicle information acquisition is traveling on the road to the city collection network, so as to carry out data mining and analysis, control and optimization of traffic signal for the whole city, traffic control in the process of city operation, has a very important effect on the whole city traffic operation, improve the efficiency of city traffic, alleviate the traffic pressure in the city. Especially in the case of traffic accidents, can quickly understand the situation, timely traffic grooming, to avoid traffic jams. The

Fig. 1. Traffic light control system

application of RFID technology in the vehicle networking technology is also better to achieve the intelligent traffic management control, greatly enhance the level of traffic management. The application of vehicle networking technology in traffic control in our country is still in the initial stage, and there are still a lot of immature situations.

2.2. Basic theory of traffic flow

Traffic flow theory refers to the method system and model of traffic variation under the condition of certain time and space. Since it includes the relationship between human, road, vehicle and environment, the process of forming traffic flow is very complex (Xian C. et al., 2016) [14]. The parameters of traffic flow are traffic density, traffic flow and interval average velocity. Traffic refers to the number of traffic entities passing through a lane in a given period of time, which is a random

variable that will vary with time and place. The average velocity of an interval is the average speed of all vehicles traveling at a given time and length. Assume that there are n vehicles with the driving road length of L. The speed of the ith car is v_i, and the average speed of the interval is v. Then we can get:

$$v = \frac{1}{\frac{1}{n}\sum_1^n \frac{1}{v_i}} = \frac{nL}{\sum_l^n t_i}. \tag{1}$$

Traffic density refers to the number of vehicles passing through the road at the specified time, which can reflect the degree of closeness between vehicles on the road. According to the relationship between velocity and density, the relation model of velocity-density can be obtained:

$$v = v_{\mathrm{f}} - \frac{v_{\mathrm{f}}}{\rho_{\mathrm{j}}}\rho = v_{\mathrm{f}}\left(1 - \frac{\rho}{\rho_{\mathrm{j}}}\right). \tag{2}$$

If the speed is close to 0, we can use the 1961 Underwood index model:

$$v = v_{\mathrm{m}} \ln\left(\frac{\rho_{\mathrm{j}}}{\rho}\right). \tag{3}$$

When traffic is small, cars can run in both directions unblockedly, and the logarithmic model proposed by Green Bai can be used:

$$v = v_{\mathrm{m}} \mathrm{e}^{-\frac{\rho}{\rho_{\mathrm{m}}}}. \tag{4}$$

Here, the traffic free flow speed is v_{f}, the flow rate reaches the maximum when the speed is the critical speed v_{m}. Symbol ρ stands for the traffic density, the maximum flow of the optimal traffic density is ρ_{m}.

For the analysis of traffic flow, no matter what kind of mathematical statistical method is used, it will be random to some extent. Generally, there are two kinds of methods for statistical distribution: (1) using the continuous distribution as a tool to study the statistical characteristics of the time interval of the events occurring in the traffic flow; (2) using discrete distribution as a tool, it is necessary to achieve a certain period of time. In the calculation of the number of vehicles arriving in the interval, the discrete distribution can be used, which includes binomial distribution, negative binomial distribution and Poisson distribution (Yan F. et al., 2016) [15]. When using a continuous distribution to describe the distance between vehicles to reach, we need to select a specific distribution according to different occasions and the velocity distribution, and the commonly used distributions are the displaced negative exponential distribution, exponential distribution and so on.

3. Methodology

3.1. Signal coordination control

The quality of the main road traffic has a direct impact on the surrounding road traffic. This is mainly due to the large traffic flow on the main line, and it is also the traffic flow collecting and distributing center of multiple signal intersections. Under the influence of mixed traffic and other external interference factors, the simple traffic signal control is difficult to separate the traffic flow of human and non-motorized vehicles. In order to obtain more smooth communication and ensure traffic safety, it is necessary to reduce the speed of the vehicle through the intersection of each trunk. In the main road traffic flow control, we need to pay attention to the following points:

(1)–The traffic flow can show good continuity and reach the intersection as evenly as possible.

(2)–The peak and non-peak hours of urban traffic every day make the traffic flow change with time and show heterogeneity. Coordinate and control according to the characteristics of traffic flow in different periods.

(3)–Ensure the distance between the adjacent intersections. Only if the distance is long enough, the vehicle at the front intersection will reach the front intersection at random.

(4)–Give priority to the coordinated control of traffic flow on the main road of one-way traffic.

(5)–According to the type of the intersection of the main road, the system is chosen to control the system by the use of as little as possible phase.

In the process of arterial road coordinated control, it is necessary to understand the current situation of traffic flow, and then optimize the signal timing according to the relevant data. In the system, the longest intersection is the critical intersection. When the signal coordination is optimized, the key intersection is considered. The design flow of traffic signal coordination control is shown in Fig. 2.

Figure 3 is the time distance map that reflects the motion of the vehicle. The horizontal and vertical coordinates in the figure represent distance and time, respectively. Using the data of each intersection, we can draw a specific time distance map. The diagonal line in the graph represents the driving process line of the first vehicle in each cycle. Assuming a constant speed, according to the specific traffic flow at the intersection, the traffic lights are set. Assume that all vehicles through the intersection can avoid the red light stop.

The key of the scheme design is to determine and optimize the phase difference in the design of arterial system timing scheme. The most commonly used method is the maximum green wave method, and the specific way of thinking includes graphic method and numerical method. The graphic method is to use the color of the signal in the time-distance graph as the time function, so as to draw the coordination control chart of the signal lights. The synchronous or interactive coordinated control system is established in order to realize the repeated adjustment of broadband, and get the phase difference and the ideal green wave band. The optimal control of

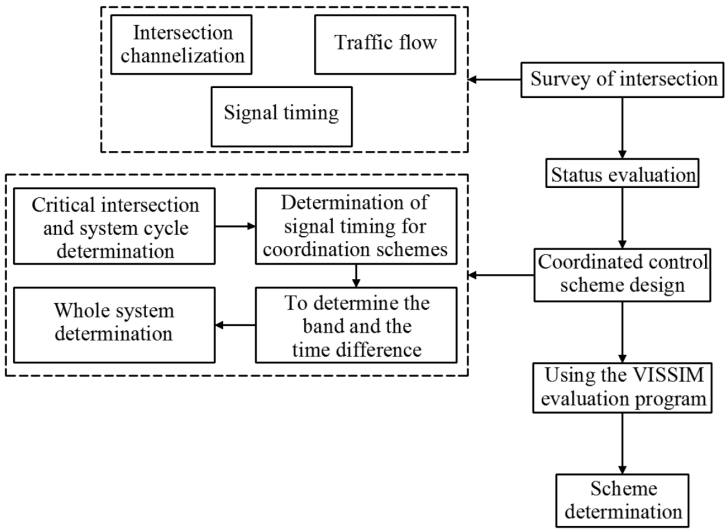

Fig. 2. Signal coordination control system design flow

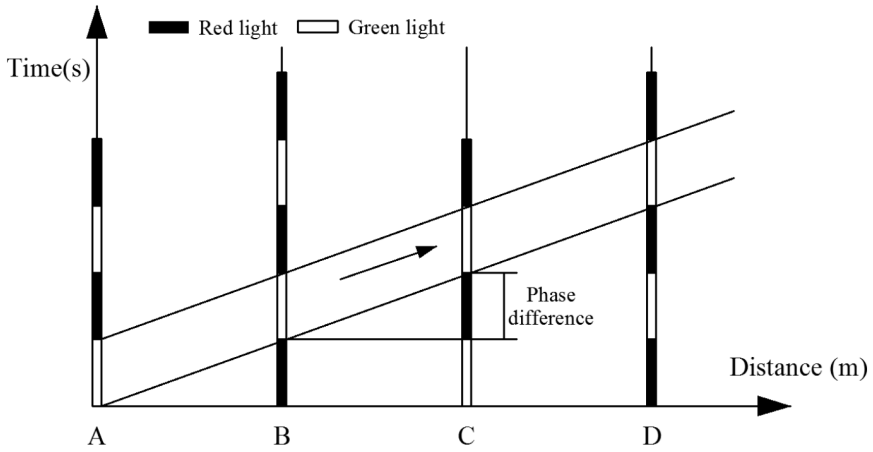

Fig. 3. Time distance graph of four adjacent intersections

the system by numerical solution is to find out the maximum diversion distance between the actual signal and the ideal selected signal of intersections, so as to find the optimal phase difference control scheme.

3.2. Coordinated optimization control of arterial signal

When the signal coordination optimization is carried out, the minimum delay method can be used to realize the minimized vehicles delay, so as to provide green band with enough wide for arterial vehicles. The main goal of arterial optimization is to minimize the total delay. The mathematical model is built by the relation-

ship between the delay and the phase difference. The optimal phase difference is determined by optimization. From the vehicle intensity, we should choose different formulas according to different saturations. When the saturation is more than 0.9, we can choose the Akcelik transient delay model. When it is less than 0.9, the Webster steady-state model can be chosen. Assume that the average delay time of each vehicle in the vehicle group is d, the cycle time is c, the green ratio is λ, and the saturation is x. When the saturation is less than 0.9, the formula of the Webster model is

$$d = \frac{c\,(1-\lambda)^2}{2\,(1-\lambda x)} + \frac{x^2}{2q\,(1-x)} - 0.65\left(\frac{c}{q^2}\right)^{\frac{1}{3}} x^{(2+5\lambda)}\,, \tag{5}$$

$$X_i = \frac{q_i}{CAP_i}\,. \tag{6}$$

When the saturation is greater than 0.9, the calculation formula of the Akcelik transient delay model is:

$$d = \left\{ \begin{array}{l} \frac{c\left(1-\frac{g}{c}\right)^2}{2\left(1-\left(\frac{g}{c}\right)x\right)} \cdots\cdots x < 1 \\ \frac{c-g}{2} \cdots\cdots x \geq 1 \end{array} \right\} + \frac{Q_0}{c}, \tag{7}$$

$$x_0 = 0.67 + \frac{s_g}{600}\,. \tag{8}$$

Here, the saturation flow rate of the lane is x_0, and the average queue length is Q_0 in the observation period. The traffic delay for the entrance road is d_{ij}, and the traffic volume in the road entrance is q_{ij}.

On this basis, the model is optimized, that is, the objective function is located at the intersection of the total delay value. Then we can get

$$D = \sum_i \sum_j d_{ij} q_{ij}\,. \tag{9}$$

The minimum delay is taken as the objective function and the constraint condition of the signal cycle length when calculating it with the saturation value is as follows

$$20n \leq C \leq 60n\,. \tag{10}$$

In order to realize that the cycle time of the intersection of the main road is the sum of the effective green time and the loss time of each phase, the following formula should be met

$$\sum_{i=1}^{n} g_i + L = C\,. \tag{11}$$

The objective function of the minimum delay is

$$\text{s.t.} \left\{ \begin{array}{l} 20n \leq C \leq 60n, \\ \sum_{i=1}^{n} gi + L = C. \end{array} \right. \tag{12}$$

After the model is determined, it is necessary to calculate the traffic capacity and the saturation of the intersection according to the actual situation of the intersection. The initial value of the delay is calculated according to the selected model, and the effective green time of the intersection is adjusted in accordance with the square reverse, so as to get the best effective green time and cycle time.

4. Result analysis and discussion

Arterial signal coordination control method based on optimization is used to carry out Vissim simulation and analysis of a traffic road intersection. A detector is arranged in each direction of each intersection to detect the traffic flow in different directions, and the obtained monitoring data is directly applied to the signal lamp in the direction. The main road is two-way with four lanes, a total of 1 km. The intersections of the study area are numbered 1, 2, 3, and 4, respectively. The optimization is carried out through the signal coordination scheme. The phase diagram of the intersection of the main road is shown in Fig. 4. In addition to the right turn phase in the No. 4 intersection, the right turn of other intersections is not controlled by the signal.

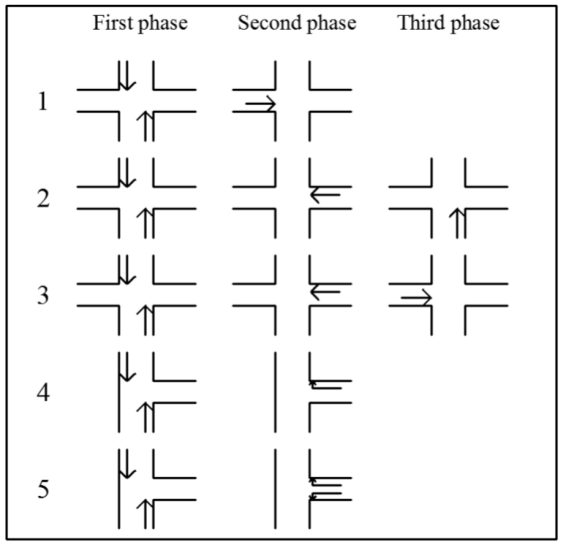

Fig. 4. Arterial intersection phase diagram

Based on the existing optimization scheme, the Vissim software is used to optimize the control scheme. Using this software, it can directly reflect the real-time situation of intersections, vehicles and roads in the road network, and record the change process of the related elements. After drawing a map, the plane graph of the intersection is set to be the simulation map. Then the road network is established, and the traffic structure is defined according to the network situation. A detector is set in the road network according to the path. The delay, travel time and queue

length are obtained by simulation. According to the simulation, we get the average value of the delay of the vehicles at the intersection of the main road, as shown in Table 1. It can be seen that the delay value of the east road of No. 2 intersection, the west and north road of No. 3 intersection is relatively large.

According to the simulation results of the current situation, the key traffic direction signal phase and traffic flow ratio of each intersection are determined, and the optimal signal period is calculated. After the optimization of the arterial road coordinated control simulation analysis, the simulation results are shown in Table 2.

Table 1. Road intersection signal timing (t/s)

Intersection number	1	2	3	4	5
Period (s)	85	120	130	100	95
Phase 1	55	50	55	70	60
Phase 2	20	25	35	20	25
Phase 3	-	30	25	-	-

Table 2. Comparison of delays of each entrance in the intersection

Intersection number	Present situation				After optimization			
	East	West	South	North	East	West	South	North
1	-	72	15	15	-	69	4	10
2	194	-	22	37	167	-	4	15
3	6	203	53	117	2	198	46	72
4	26	-	14	24	24	-	9	19
5	29	-	21	20	12	-	14	12

Through the simulation results, we can see that the travel time and delay of each intersection in the route are reduced compared with that before the optimization. The travel time of the intersection is reduced by 13 %, 23 %, 16 %, 21 %, and 46 %, respectively, and the delay value is reduced by 19 %, 26 %, 16 %, 19 % and 46 %, respectively. Thus, the optimization effect is obvious. The indicators based on the travel time and the average delay of vehicles can significantly improve the traffic conditions, and road traffic capacity has been greatly improved.

5. Conclusion

The problem of urban traffic congestion has become one of the most important factors that restrict the development of cities. The optimal control of traffic flow could effectively improve the urban traffic congestion. According to the saturation

of different models, different models were chosen for the optimal control of the main road signal. When the saturation was more than 0.9, we could choose the Akcelik transient delay model. When Webster was less than 0.9, the steady-state model could be chosen. In this paper, Vissim simulation software was used for the optimization control analysis of the intersection of a main road based on the traffic network. Through the analysis of the data of four intersections, the comparative analysis of the travel time and delay before and after optimization was carried out. It could be seen that after the optimization of each intersection, the travel time of the intersection was reduced by 13 %, 23 %, 16 %, 21 %, and 46 %, respectively, and the delay value was reduced by 19 %, 26 %, 16 %, 19 % and 46 %, respectively. Therefore, the traffic capacity of the intersection of the main road had been significantly improved by optimizing control. In the following research, the optimal control scheme can be applied to the intelligent traffic control system.

References

[1] K. Nellore, G. P. Hancke: *A survey on urban traffic management system using wireless sensor networks.* Sensors *16* (2016), No. 2, 157.

[2] T. Du, D. Yang, S. Peng, Y. Xiao: *A method for design of smoke control of urban traffic link tunnel (UTLT) using longitudinal ventilation.* Tunnelling and Underground Space Technology *48* (2015), 35–42.

[3] A. Jamshidnejad, I. Papamichail, M. Papageorgiou, B. de Schutter: *A model-predictive urban traffic control approach with a modified flow model and endpoint penalties.* 14th IFAC Symposium on Control in Transportation SystemsCTS, 18–20 May 2016, Istanbul, Turkey, IFAC-PapersOnLine *49* (2016), No. 3, 147–152.

[4] J. Haddad, M. Ramezani, N. Geroliminis: *Cooperative traffic control of a mixed network with two urban regions and a freeway.* Transportation Research Part B: Methodological *54* (2013), 17–36.

[5] A. H. F. Chow, R. Sha: *Performance analysis of centralized and distributed systems for urban traffic control.* Journal of the Transportation Research Board *2557* (2016), No. 7, 66–76.

[6] R. Kutadinata, W. Moase, C. Manzie, L. Zhang, T. Garoni: *Enhancing the performance of existing urban traffic light control through extremum-seeking.* Transportation Research Part C: Emerging Technologies *62* (2016) 1–20.

[7] K. Wan, N. Nguyen, V. Alagar: *Dependable traffic control strategies for urban and freeway networks.* Mobile Networks and Applications *21* (2016), No. 1, 98–126.

[8] S. Zhao, Y. Yu: *Effect of short-term regional traffic restriction on urban submicron particulate pollution.* Journal of Environmental Sciences, Available online (2016), Articles In Press.

[9] D. Tao, Y. Dong, S. Peng, Y. Xiao, F. Zhang: *Longitudinal ventilation for smoke control of urban traffic link tunnel: Hybrid field-network simulation.* Procedia Engineering *84* (2014), 586–594.

[10] A. S. Kesten, M. Ergün: *Retraction note: Efficiency analysis of the dynamic traffic control for an urban highway.* EURASIP Journal on Wireless Communications and Networking (2016), 185.

[11] S. Sadraddini, C. Belta: *A provably correct MPC approach to safety control of urban traffic networks.* American Control Conference (ACC), 6–8 July 2016, Boston, MA, USA, IEEE Conference Publications (2016), 1679–1684.

[12] J. Oskarbski, D. Kaszubowski: *Implementation of weigh-in-motion system in freight traffic management in urban areas.* Transportation Research Procedia *16* (2016), 449–463.

[13] Y. Bie, X. Wang, T. Z. Qiu: *Online method to impute missing loop detector data for urban freeway traffic control.* Journal of the Transportation Research Board *2593* (2016), No. 05, 37–46.

[14] C. Xian: *Integration management of urban traffic and regional traffic.* Jiangsu Science and Technology Information (2016), No. 29.

[15] F. Yan, F. Tian, Z. Shi: *Effects of iterative learning based signal control strategies on macroscopic fundamental diagrams of urban road networks.* International Journal of Modern Physics C *27* (2016), No. 04, paper 1650045.

Received April 23, 2017

Acta Technica *62*, No. 1A/2017, 91–98

New approach for detection of giant panda head in wild environment[1]

Donglin Wang[2], Jiaqi Huang[2], Bin Xie[2], Lei Yan[2]

Abstract. Video surveillance technology has been widely used for protection of pandas in wild environment, however, the automatic detection method of panda in the image was not efficient so far. So in this paper an improved approach of head detection of giant panda in the image was proposed. First image segmentation based on gray threshold was used to detect candidate region of giant panda in the image. Then a new kind of head region detection method was introduced, which was able to cluster giant panda head region of different sizes along the skeleton. Finally, standard data sets were used to train a fuzzy neural network for the detection of head region. The experiment results showed that the improved method was efficient and accurate to detect the head region of panda.

Key words. Panda head detection, skeleton extraction, k nearest neighbor (KNN) clustering, fuzzy neural network.

1. Introduction

A variety of images are captured in the video surveillance system for panda in the wild environment, but only the images with panda are necessary. At present, an abundance of algorithms in the human face detection are available, and their accuracy are more than 90 % for human detection. Viola et al. applied some algorithms, representations, and insights which are quite generic and may well have broader application in computer vision and image processing [1–3].

However, the animal face have more variation than human face [4–6], and animal face detection is more difficult than detecting human face. Some researchers proposed a cat head detection method, which well exploited the shape and texture information by extracting two kinds of patterns aligned by eyes and tips of ears [7–9].

[1]This research is supported by the Fundamental Research Funds for the Central Universities (NO.2015ZCQ-GX-03).

[2]Beijing Forestry University, Beijing, 100083, China

In the field of giant panda head detection, Chen et al. proposed two algorithms for giant panda head detection: 1) Detect panda facial region based on topology modelling; 2) Find the head region around the limb areas. Zhang et al. used haar of oriented gradient (HOOG) as their features and proposed two joint detection approaches to detect giant panda and other cat-like animal's head, which all have distinctive ears and frontal eyes [10].

In this paper, we proposed a new algorithm focused on the detection of giant panda's head, which firstly separated the background and the giant panda by segmentation of gray scale image, Secondly located its head from the binary image through the skeleton extraction technology. Thirdly based on the skeleton line or the surrounding region skeleton line, used two-stage KNN clustering method contrasted images in training set to detect the existence of giant panda's head in images. In the refining stage, a training set was established to detect the head based on fuzzy neural network. Our approach offers two advantages: 1) A rapid preliminary scanning, which due to fast threshold segmentation and a scan method based on skeleton line to reduce search region; 2) Fuzzy neural network promoted the accuracy after the two-stage KNN clustering method.

2. Methodology

The proposed algorithm is schematically depicted in Fig. 1.

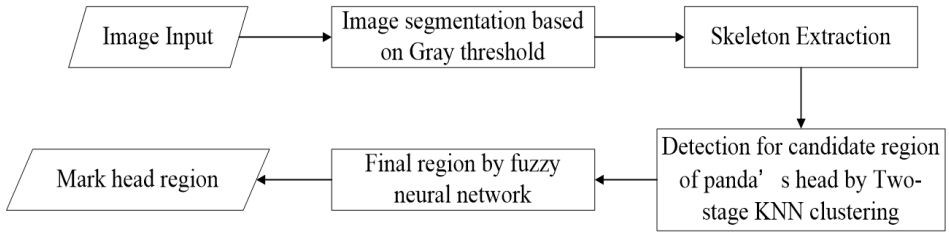

Fig. 1. Flow-chart of proposed algorithm

2.1. Image segmentation

For a giant panda image, its most prominent feature is the hair color. In addition to the region of mild change caused by stains, shadows and illumination changes, the giant panda body is mainly made up of pure black and pure white. Gray space is made of pure black, pure white and the different levels of gray between them, and interval of gray image is [0,255]. By converting RGB images into gray images, we could well describe its color feature. This study used a segmentation algorithm based on gray space, which first identified respectively the white and black areas in the body of the panda, and then separated it from the background.

According to the histograms of images, both the black hair and white hair of giant panda had a centralized gray value, and the value of images in database also

had a certain intersection with the black and white hair.

Threshold segmentation was applied to convert a gray image to binary image. As presented in formula (1), $f(x, y)$ is the original image. Grey value T was used as the threshold after being found out in the $f(x, y)$. The image was segmented into two parts: the gray value of the pixels that are greater than or equal to the threshold were set to 1, while the ones that were less than or equal to the threshold were set to 0. After the threshold operation, the image would be turned into a binary image $g(x, y)$.

$$g(x,y) = \begin{cases} 1 & f(x,y) \geq T \\ 0 & f(x,y) < T \end{cases} \tag{1}$$

Integrated the above properties, the preliminary segmentation of the panda region from the image could be completed. Experimental results are shown in Fig. 2. Once selected the panda region, we scanned for the head of the animal, which had the most obvious features.

Fig. 2. Results of segmentation: left pair–original images, right pair–segmented images

2.2. Skeleton extraction

In most cases, the panda's head could be found near the skeleton after the segmentation of the panda body region. There were two parts of the segmentation:

1) First, extract the skeleton from the separated region [6]. The result is presented in Fig. 3c. However, in some images in which the segmented region was relatively round and smooth, and the head was located near the edge of the selected region, instead of the skeleton. In this case, a second skeleton extraction method was needed

to complement the mentioned one.

2) As shown in Fig. 3d, we retained the largest white region, where the value was 1, in the binary image. Subtract the largest white region in its centroid location by an area in proportion p. In this paper, the value of p was 40 %. The computation formula of p is as follows:

$$p = 1 - \sqrt{\frac{\text{areaofpandaheads}}{\text{areaofwholepandabody}}}\,. \tag{2}$$

After that, we could get a ring region for the skeleton extraction. Synthesizing the two skeleton extraction methods, we could locate the giant panda head along the bone in different specific cases.

Since then, we adopted the two-stage KNN clustering method to locate the panda's head, comparing the images in training set. The Skeleton extraction method is implemented in the following:

Step 1: Use bwmorph function to extract the skeleton from the binary image, stored as S1.

Step 2: Calculate binary image in each region and locate the centroid of the largest white region.

Step 3: Subtract the largest white region in its centroid location by 30 % area of itself.

Step 4: In the new ring area, using bwmorph function to extract the skeleton, stored as S2.

Step 5: Get S as the superposition of S1 and S2.

Step 6: with the interval of 20 pixels, set the points on the bone S as the center of test blocks. The side length of various sizes blocks can be 50, 100, 150 and 200 pixels.

2.3. Two-stage KNN clustering method

After getting the blocks of various sizes of the image, they would be compressed to 50 ×50 pixels. A two-stage KNN clustering method was proposed to cluster the panda head. A Training set needed to be established, and the training images could be divided into several categories, such as head, head around images, the background, etc. The mean value of the compressed blocks were recorded as u whose computation formula is as follows:

$$u(x,y) = \frac{1}{8\times 8}\sum_{i=0,j=0}^{7,7} I(x+i, y+j)\,. \tag{3}$$

Here, I is the input block image and x and y are the coordinations of the pixel. Search for the K nearest training neighbors to the test pattern was based on distance measure with the feature u the number of each categories were recorded as $c1$, $c2$, $c3$. Furthermore, Euclidean distance was calculated by pixel block between the test block and the training sample, and denoted as d. Search for the $K/2$ nearest

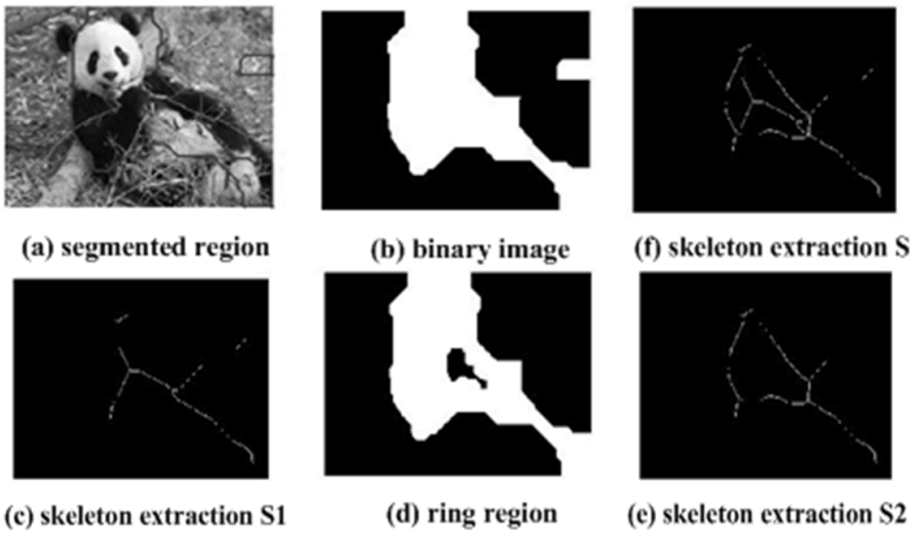

Fig. 3. Skeleton extraction result

training neighbors to the test pattern used the distance measure with the feature d. The values of distance of each category were recorded as $d1$, $d2$, $d3$. Formula (4) was used to calculate each confidence of categories

$$E = ci + 0.5 * di\,. \tag{4}$$

Here, E is the parameter used to determine whether the block was the head regions of giant pandas. After implementing two-stage KNN clustering method, multiple scale blocks close to the head regions were filtered. But most of the smaller blocks were within the border of faces, rather than included the whole face. So the blocks that were two levels smaller than the largest scale were unnecessary. For example, if the largest block was 200×200 pixels, so only two kinds of scales, 200×200 pixels and 150×150 pixels, would be adopted to detect the candidate head region, rather than other scales, such as 100×100 pixels and 50×50 pixels. The step of scale is 50×50 pixels is used in this research. They would be qualified as neural network input test images. Head candidate screening region diagram is shown in Fig. 4.

2.4. Detection

Although the areas of some candidate panda heads had been filtered, the accuracy was not high due to two reasons. First, the accuracy for KNN clustering method was not satisfactory. Second, there were too many outputs. In the next step, there should be a further recognition, in order to filter out unnecessary results, and to determine a final area of the head.

Fuzzy neural network identification methods were applied to some candidate panda images to identify the head zone. In the sample collecting stage, we built

up another training set to store the typical head samples of pandas in various poses including the background [11, 12]. The fuzzy neural network was implemented to filter the head of giant panda in various poses and angles from the background. The panda's head area after processing by the fuzzy neural network is depicted in Fig. 5.

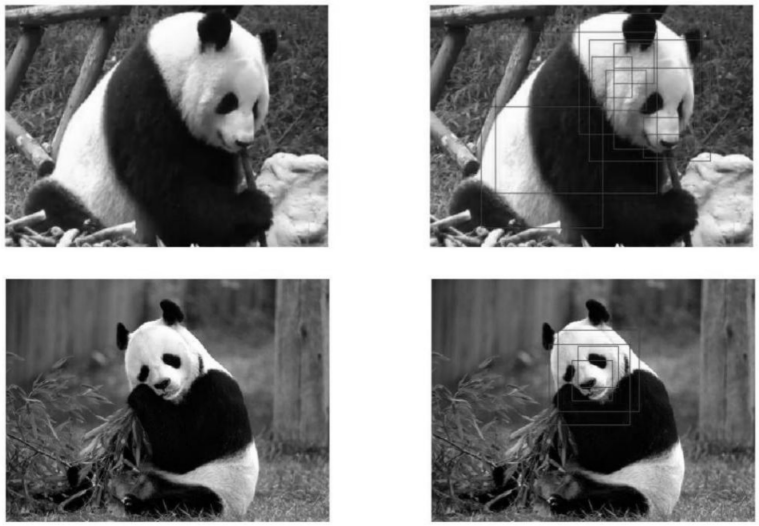

Fig. 4. Head candidate screening region diagram: left part–original images, right part–head candidate region

Fig. 5. Head area after fuzzy neural network

3. Result analysis and discussion

For all the output results of the identification of the giant panda head, they needed to be further integrated through the center position and figure block size, to determine a final head position and size. The giant pandas images in various cases were processed to test robustness of the algorithm. There were two items to evaluate:

1) Pose of the giant pandas, including looking front, side and down.

2) The distances of the giant pandas, it could be detected in different distances.

To measure the accuracy, 3000 wild giant panda images were collected. 2000 of them are frontal faces, and others are side face. Half of the images were taken over a long distance, and the other half were shot at close range. One thing to note is the images which were chosen were in the wild, so the backgrounds are almost close to green. The algorithm, for various cases of the giant panda heads, had very good detection effect. Short distance will make a positive influence in the detection effect. Fig. 6 shows the experimental results, and the giant panda head was boxed by red rectangular.

Fig. 6. The giant panda head region detection under different distances

4. Conclusion

In this paper a novel approach of detecting the head of panda in the images in wild environment was presented. The image segmentation method based on gray threshold was used to detect regions in the image that were candidate regions for giant pandas. The candidate regions of panda's head were detected by two stage KNN clustering method after extracting the skeleton of above result images. Finally, standard data sets are used to train a Fuzzy neural network for the detection of head area. The amount of experiments were conducted to prove the proposed algorithm

was useful and accurate. Furthermore, ongoing work aims to be able to detect pandas in different complicated environments.

References

[1] P. Viola, M. J. Jones: *Robust real-time face detection.* International Journal of Computer Vision *57* (2004), No. 2, 137–154.

[2] Y. Xia, B. Zhang, F. Coenen: *Face occlusion detection using deep convolutional neural networks.* International Journal of Pattern Recognition and Artificial Intelligence *30* (2016), No. 09, 1660010.

[3] Teng Sheng-Hua, Chen An-Jun, Yuan Jian-Hua, Yin Xue-Min, Wang Dong-Feng, Zou Mou-Yan: *An improved colorization algorithm for gray-scale image based on over-segmentation.* Journal of Electronics and Information Technology *28* (2006), No. 7, 409–410.

[4] Y. Huang: *Research on gray-level image segmentation in complex background.* Taiyuan University of Technology, Circuits and Systems, Globe Thesis (2008).

[5] Zhengzhou Li, Mei Liu, Huigai Wang, Yang Yang, Jin Chen, Gang Jin: *Gray-scale edge detection and image segmentation algorithm based on mean shift.* Telkomnika - Indonesian Journal of Electrical Engineering *11* (2013), No. 3, 1414–1421.

[6] A. C. Burton, E. Neilson, D. Moreira, A. Ladle, R. Steenweg, J. T. Fisher, E. Bayne, S. Boutin: *REVIEW: Wildlife camera trapping: a review and recommendations for linking surveys to ecological processes.* Journal of Applied Ecology *52* (2015) No. 3, 675–685.

[7] W. Zhang, J. Sun, X. Tang: *Cat head detection-how to effectively exploit shape and texture features.* 10th European Conference on Computer Vision, 12–18 October 2008, Marseille, France, Springer Berlin Heidelberg (2008), 802–816.

[8] J. Wall, G. Wittemyer, B. Klinkenberg, I. Douglas-Hamilton: *Novel opportunities for wildlife conservation and research with real-time monitoring.* Ecological Applications *24*, (2014), No. 4, 593–601.

[9] X. Zheng, M. A. Owen, Y. Nie, Y. Hu, R. R. Swaisgood, L. Yan, F. Wei: *Individual identification of wild giant pandas from camera trap photos – a systematic and hierarchical approach.* Journal of Zoology *300* (2016), No. 41, 247–256.

[10] W. Zhang, J. Sun, X. Tang: *From tiger to panda: animal head detection.* IEEE Transactions on Image Processing *20* (2011), No. 6, 1696–1708.

[11] H. Song, C. Miao, Roel, Z. Shen, F. Catthoor: *Implementation of fuzzy cognitive maps based on fuzzy neural network and application in prediction of time series.* IEEE Transactions on Fuzzy Systems *18* (2010), No. 2, 233–250.

[12] H. G. Jing: *Finger vein recognition based on feature points and subspace.* Ph.D. Thesis, Beijing Jiaotong University, China (2012).

Received April 23, 2017

Acta Technica *62*, No. 1A/2017, 99–108

Image processing and identification of lumber surface knots[1]

Jianhua Yang[2,3], Jiang Xiao[2], Wansi Fu[3], Jiawen Chen[3], Lei Yan[2], Shuangyong Wang[4]

Abstract. Surface knot defects seriously affect the quality and performance of lumber. In this paper, an image processing and recognition method was designed using the MATLAB image processing toolbox. Based on numerous prior experiments, two turning coordinate points of piecewise linear transformation were selected for this study and a surface recognition algorithm was put forward. Through defect image processing, morphological processing, feature extraction, the knots could been detected effectively and accurately, and the size and the location of the defects could also be calculated. The knot defects was identified by the following features: length over 0.5, eccentricity under 0.8, average under 180 gray, and gray variance over 30. The knots was detected automatically and positioned accurately using the algorithm. The detection and identification rate of knots was 88.97 %.

Key words. Lumber, surface knots, image processing, recognition algorithm.

1. Introduction

Lumber (as well as veneer, sawn-timber) surface defects (such as knots, cracks, and poles) will seriously affect the quality of lumber, change its normal performance, and result in ineffectiveness [1–3]. Among the numerous lumber surface defects, knots are the most common phenomenon and have the greatest impact on lumber quality.

Visual grading is one of the most important lumber grading systems in North America, in which lumber grading is completed by observing and measuring the lumber's superficial qualities or characteristics [4]. It is difficult to be classified artificially due to the limitations of visual grading, especially on the face of large

[1]This work is supported by the Fundamental Research Funds for Central Public Welfare Research Institutes project, China (No. CAFINT2015C14).

[2]School of Technology, Beijing Forestry University, Beijing, 100083, China

[3]Beijing Forestry Machinery Research Institute of State Forestry Administration, Beijing, 100029, China

[4]Research Institute of Wosod Industry, Chinese Academy of Forestry, Beijing, 100091, China

variations of the size and shape of defects. Furthermore, different experiences may cause inconsistent test results, so this grading method cannot meet the detection demands of rapid and continuous lumber production. Based on the computer image processing technology and mathematical morphology theory, this paper puts forward an automatic detection algorithm for knots on the surface of lumber. Also, MATLAB image processing tools are applied in the knot image test experiments to verify the image pre-processing methods.

2. Material and methods

2.1. Images of lumber

In the surface image recognition experiment, a group of 160 JPG format images taken by the digital camera with a resolution of 600×800 pixels were chosen as the test samples. Four of these images are shown in Fig. 1. Color information is removed. Through detection and recognition experiments on these images, the image processing algorithm was developed.

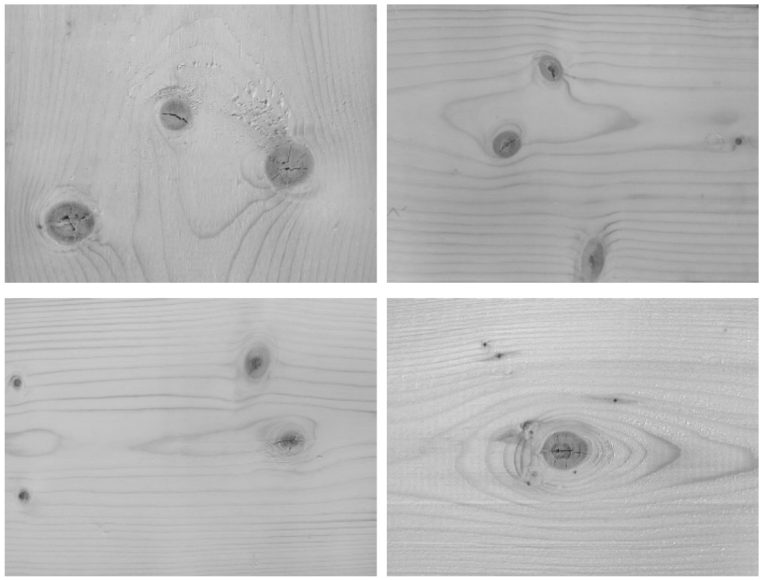

Fig. 1. Gray-scale images of knot defects

2.2. Methods

The image processing and recognition process for lumber surface knots focused on the surface image recognition algorithm. This algorithm consisted of five main steps: digital image pre-processing, image segmentation, morphological processing, feature extraction, and pattern recognition of lumber surface defects. The specific

algorithm flow is shown in Fig. 2.

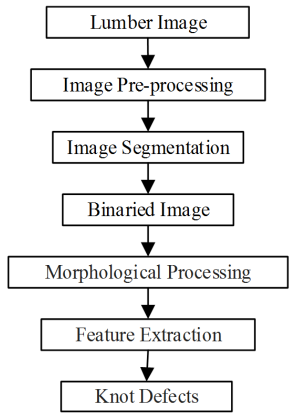

Fig. 2. Flowchart of the surface image recognition algorithm

2.2.1. Image pre-processing: This is an important step of the image processing technique [5]. Image pre-processing is used for image of the previous operation, and the image is usually represented by a matrix [6]. Image pre-processing includes image gray processing, gray-scale transformation, and image smoothing.

The process to convert a color image into a gray-scale image is called image gray processing. The purpose of this process is to reduce the difficulty of feature extraction. The color of the defect changes significantly compared with its surroundings, so that after the gray processing, the defect region still could be segmented effectively.

Gray-scale transformation is an important method of image enhancement, which can expand the dynamic ranges of the images, enhancing the contrast to make the images clearer, with more obvious features.

An image obtained in actual practice contains noise. The noise can be reduced through data processing. The main purpose of image smoothing is to reduce an image's noise [7]. This noise stems from lots of ways, including electromagnetic waves outside the system, high-frequency noise interference, thermal noise from within the system, and mechanical jitter noise interference.

2.2.2. Image segmentation: The image segmentation have practical significance in various fields [8]. Image segmentation is one of the most important steps leading to the analysis of processed image data, separating the target from the background [6, 9]. Gray-level thresholding is the simplest segmentation method, also the oldest one, but which is still widely used in simple applications. It is computationally inexpensive and fast [10, 11]. This step is extremely important, as it corresponds to the maximum loss of information [12]. Therefor, selecting an appropriate threshold is the key to image segmentation, which is suggested to be paid close attention to.

2.2.3. Morphological processing: Mathematical morphology is a nonlinear signal processing field which concerns the application of set theory to image analysis [13]. Morphology refers to the study of shapes and structures [14, 15]. Swelling and corrosion are two basic operations in mathematical morphology, based on which a variety of complex operations, such as opening and closing, can be composed [16].

2.2.4. Pattern recognition: Pattern recognition is the process of achieving the description, identification, classification, and interpretation of phenomena and things through processing and analysis of various forms of information of objects and phenomena (e.g., value, text, and the logical relationship). To put it simply, pattern recognition can help identify and classify a set of events or processes using a computer. This is an important part of information science and artificial intelligence.

Commonly used pattern recognition methods include the discriminant function method, the nearest neighbor method, the nonlinear mapping method, feature analysis, and the factor analysis method. In this study, the feature analysis method was adopted.

3. Results

3.1. Image pre-processing

Grayscale images are shown in Fig. 1. Color information has been removed. To highlight the gray range of the image of interest, the details of the other gray levels had to be removed. Piecewise linear transformation was considered as a relatively rational choice to achieve the gray-scale transformation. This transformation enhanced the contrast by stretching the gray level of the needed image detail, and unnecessary details of the grayscale were compressed.

The two turning points of the piecewise linear transformation were chosen here in as (0.35, 0.2) and (0.75, 0.9). The transformed images are shown in Fig. 4. It can be seen that the contrasts of these four images were enhanced significantly after transformation.

A median filter (5×5) and Gaussian filter (7×7, standard deviation 1.2) were combined to smooth the gray-scale image. Figure 4 shows that the surface texture became fuzzy and some glitches in the images were well suppressed.

3.2. Image segmentation

The thresholding method distinguishes between the object and the background by setting a threshold. Multiple experiments were performed to determine the appropriate binarization threshold, which was calculated according to the formula

$$V_{\mathrm{t}} = \frac{V_{\mathrm{m}} - V_{\mathrm{s}}}{V_{\mathrm{m}} + V_{\mathrm{s}}} \cdot V_{\mathrm{thresh}} \,, \tag{1}$$

where V_t is the binarization threshold used in this paper, V_m is the mean of the gray level, V_s is the standard deviation of the gray level, and V_{thresh} is the primary value of Otsu's method, which is one of the most commonly applied methods of image segmentation for selecting threshold automatically because of its simple calculation and ease of adaptation [17].

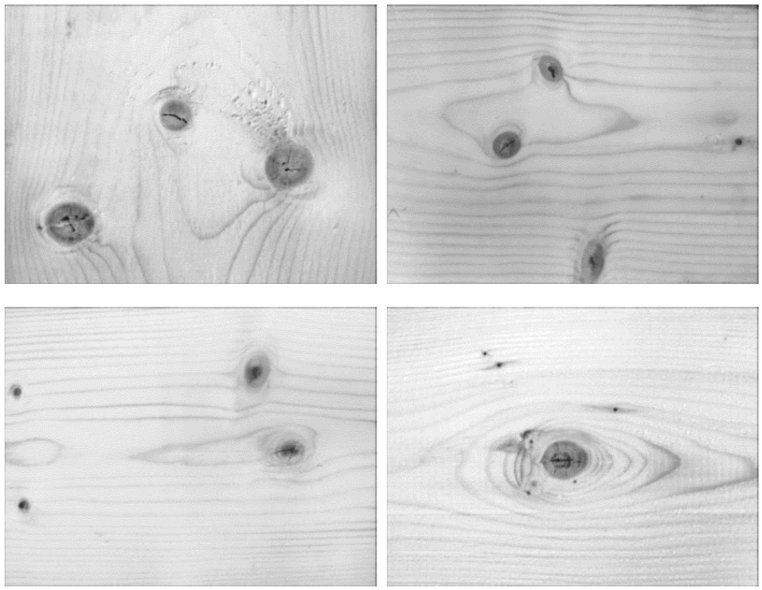

Fig. 3. Gray-scale transformed images

The method assumes that the image is composed of foreground and background classes, and then computes an optimal threshold value that minimizes the weighted within-class variances of these two classes. It has been mathematically proven that minimizing the within-class variance is the same as maximizing the between-class variance [17, 18]. The segmented binary image is shown in Fig. 5.

3.3. Morphological processing

In this paper, binary morphological image processing was carried out, which included the opening operation, closing operation, removal of isolated foreground pixels, and filling of single pixel holes. The processed images are shown in Fig. 6; the smaller isolated interference areas (normally, areas smaller than 8 pixels) were removed, and the edges of the foreground image became smoother. Figure 7 shows the suspected defect extractions from the images.

3.4. Feature extraction

The selection of the defect feature type and defect characteristic extraction algorithm were the key to building the defect pattern recognition system. By analyzing

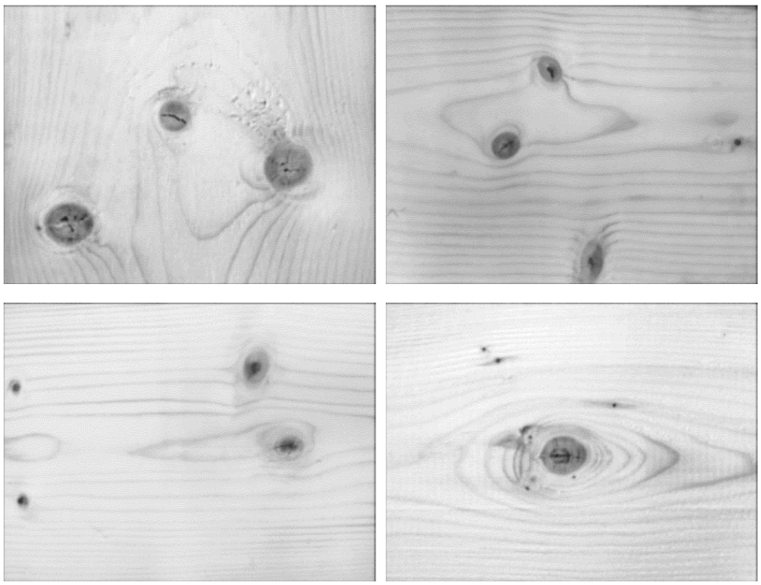

Fig. 4. Image smoothing

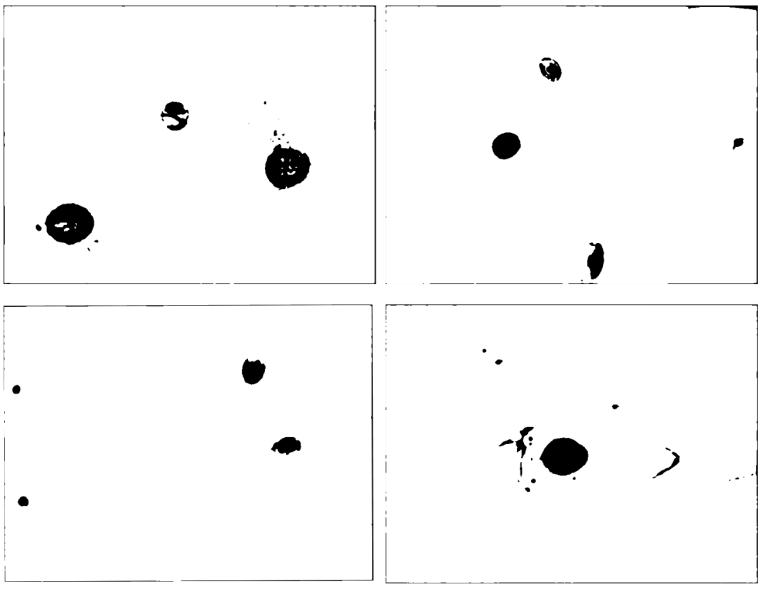

Fig. 5. Segmented images

the internal and external factors of the lumber images, four characteristics were selected as features to be extracted for lumber defects [19, 20]; these were the gray mean, the gray variance, the elongation of the defect contour, and the eccentricity.

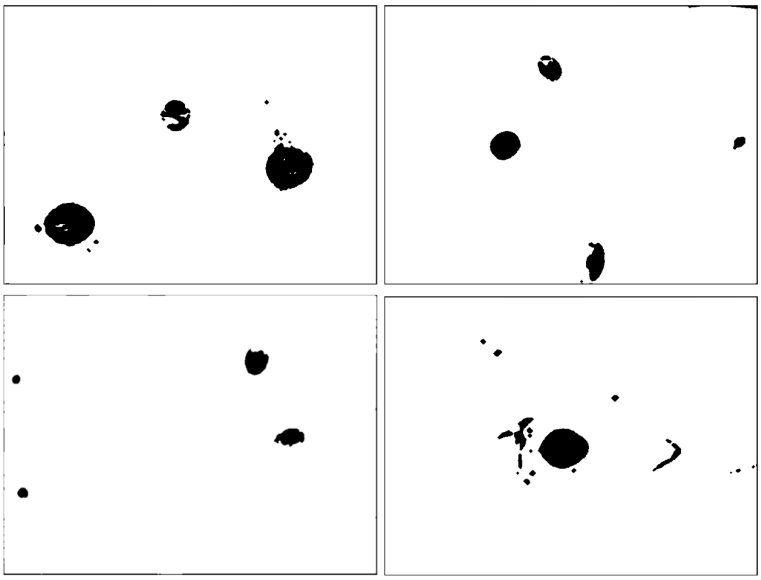

Fig. 6. Morphologically processed images

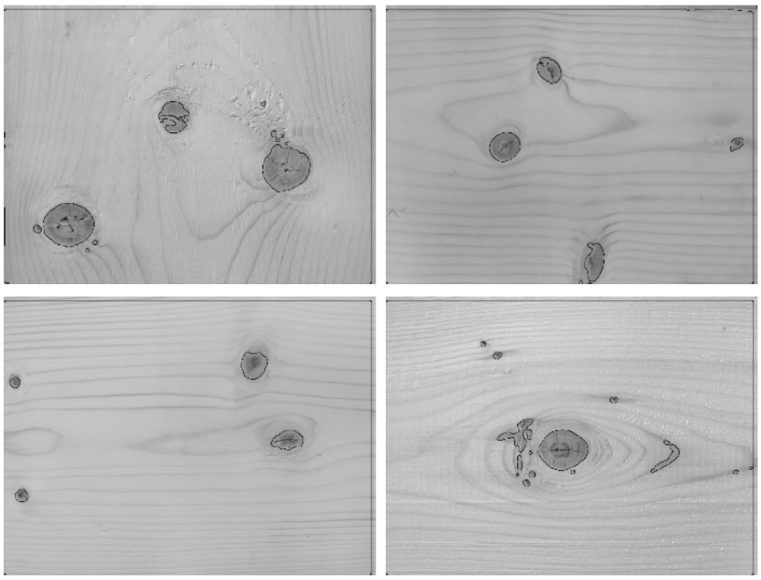

Fig. 7. Suspected defect extractions from images

The gray mean is used to distinguish the different types of defects, such as knots and poles; and the gray variance can reflect the changes in the gray value of the defect, which contributes to distinguishing the types of defects from similar gray means; finally both elongation and eccentricity primarily reflect the feature of the

defect's appearance. Here, MATLAB image processing tools were used to compute and analyze the characteristics of the target areas. Basic information about the characteristics, such as the area, centroid, major and minor axis length, eccentricity, gray mean, and gray variance, was extracted for pattern recognition. The size of the defect was reflected by the area, meanwhile the position of the defect was reflected by the centroid coordinates.

3.5. Pattern recognition

Through numbers of experiments based on 160 images and 255 knots (area larger than 30 pixels), knot defects could be identified if they had the following four basic features: length over 0.5, eccentricity under 0.8, average under 180 gray, and gray variance over 30.

The detection results can be seen in Table 1. The number of real knots was 136, of which 121 were detected correctly. The detection and identification rate of knots was 88.97 %, but 18 regions were wrongly identified as knots because their features met the parameters of algorithm for defining a knot. In addition, seven knots were undetected.

Table 1. Statistics of the detected results

Number of real knots	Number of knots detected	Number of knots correctly detected	Number of erroneously identified knots	Number of knots undetected
136	143	121	18	7

The primary factors affecting the accuracy of defect detection are as follows:

(1) The quality of the acquired lumber surface image. With a clearer and more strongly contrasted image, the detection and identification results significantly improved.

(2) The quality of the lumber, for example, sawing ineffectively, the surface glitches, and smoothness could greatly affect the quality of image.

(3) The difference between the knots and the surrounding wood, Detection performance improved with increasing differences.

4. Conclusion

(1) The aim of this knot detection project was to accurately detect the location and size of a knot on digital lumber images, with an emphasis on achieving efficient use of lumber. The image processing algorithms designed here could detect knots defects effectively and accurately; the size and the location of the defects could also be calculated.

(2) The consistency of the knot's color greatly influenced the recognition results. The sawing effect of lumber was also an important factor affecting the image quality. Using image processing technology to automatically detect and accurately position

the knot defects is significant for statistical analysis and controlling cutting work.

(3) Through statistical analysis of major defects of the lumber images, the entire lumber could be comprehensively evaluated. However, there are still some limitations to the current algorithm. And the software was designed only for circular knots. In the future, research will focus on other cases.

References

[1] J. X. Yin, X. W. Lou, M. L. Huang: *Application of grey histogram to wood surface defects' detection.* Journal of Zhejiang Forestry College (2008), No. 03, 272-276.

[2] X. B. Bai, Z. S. Wang: *Segmentation method of timber surface defects based on CV model and mathematical morphology.* Development & Innovation of Machinery & Electrical Products (2011), No. 05, 75–76+100.

[3] J. Yang, W. Zhang, W. Hu, W. Shang, W. Qu, inventors: *Image acquisition system for sawn timber surface defects and detection method.* China patent CN 102313747 B, 5 June 2013 (2013).

[4] W. Guo, H. Ren, Y. Yin, J. Jiang, C. Long: *Summary of visual grading on structural lumber in North America.* World Forestry Research (2007), No. 05, 57–62.

[5] G. Padmavathi, P. Subashini, M. M. Kumar, S. K. Thakur: *Comparison of filters used for underwater image pre-processing.* International Journal of Computer Science and Network Security *10* (2010), No. 1, 58–64.

[6] M. Sonka, V. Hlavac, R. Boyle: *Image processing, analysis, and machine vision.* 3rd edn. Nelson Engineering (2008), 114–162.

[7] P. Pouladzadeh: *An image processing and pattern analysis approach for food recognition.* Thesis, University of Ottawa, Ontario, Canada (2013), 14–22.

[8] M. Hanmandlu, O. P. Verma, S. Susan, V. K. Madasu: *Color segmentation by fuzzy co-clustering of chrominance color features.* Neurocomputing *120* (2013), 235–249.

[9] S. K. Sinha, P. W. Fieguth, M. A. Polak: *Intelligent system for condition monitoring of underground pipelines.* Computer-Aided Civil and Infrastructure Engineering *19* (2004), No. 1, 42–53.

[10] J. Cheng: *Automated detection and time lapse analysis of dendritic spines in laser scanning microscopy images.* Thesis, Northeastern University Shenyang, China, Electrical and Computer Engineering (2009), 60–65.

[11] D. Bajracharya: *Real time pattern recognition in digital video with applications to safety in construction sites.* Thesis, University of Nevada, Las Vegas, Computer Science (2013), 20–23.

[12] Y. Zhang: *A novel image processing platform development for preprocessing images with two-phase microstructures containing isolated particles.* Thesis, Wayne State University, Detroit, MI (2010), 4–9.

[13] N. P. Brouwer: *Image pre-processing to improve data matrix barcode read rates.* Thesis, University of New Hampshire, Electrical Engineering (2013), 24–26.

[14] K. Parvati, B. S. P. Rao, M. M. Das: *Image segmentation using gray-scale morphology and marker-controlled watershed transformation.* Discrete Dynamics in Nature and Society (2008), 307–318.

[15] B. Tang, J. Kong, X. Wang, G. Jiang, L. Chen: . *Steel strip surface defects detection based on mathematical morphology.* Journal of Iron and Steel Research *22* (2010), No. 10, 56–59.

[16] Q. Ruan: *Digital image processing using MATLAB.* Beijing, China: Publishing House of Electronics Industry (2005), 252–284.

[17] Y. Ramadevi, T. Sridevi, B. Poornima, B. Kalyani: *Segmentation and object recognition using edge detection techniques.* International Journal of Computer Science & Information Technology (IJCSIT) *2* (2010), No. 6, 153–161.

[18] N. Otsu: *A threshold selection method from gray-level histograms.* IEEE Transactions on Systems, Man, and Cybernetics *9* (1979), No. 1, 62–66.

[19] L. Li, J. Zhang: *Research on extraction method of image feature for wood surface defects.* Wood Processing Machinery *22* (2011), No. 02, 9–14.

[20] K. Wang, X. Ba: *The pattern recognition methods of wood surface defects.* Beijing, China: Publishing House of Science Press (2011), 62–65.

Received April 23, 2017

Acta Technica *62*, No. 1A/2017, 109–122

Piecewise affine modeling and explicit model predictive control for non-inverting buck-boost DC-DC converter[1]

Zhaozhun Zhong[2,5], Miao Guan[2], Xinpei Liu[3], Hongjing Zheng[4]

Abstract. An innovative EMPC (Explicit Model Predictive Control) method based on piecewise affine modeling is proposed for the non-inverting Buck-Boost DC-DC converter to overcome the control difficulties encountered in practice. Based on a piecewise affine model, the proposed EMPC method divides the state space into critical regions by multi-parametric programming and solves the traditional MPC optimal problem explicitly and fully off-line. As a result, the time-taking on-line iteration algorithm of MPC is replaced by a simple table lookup algorithm which greatly reduces the on-line computation time. Reliable control performance is achieved with respect to system constraints and hybrid dynamics. Compared with conventional controllers, the proposed EMPC method achieves better performance by accurate predictive model and coordinate control which is verified by simulation.

Key words. Piecewise affine modeling, explicit model predictive control, Buck-Boost DC-DC converter.

1. Introduction

DC-DC switched power converters are used to transform an unregulated DC voltage input to a regulated output DC voltage which have been widely studied and become a mature and well-established technology [1]. The Buck-Boost converter is

[1]This work was partially supported by National Natural Science Foundation of China (61304095), Natural Science Foundation of Jiangsu Province (BK20130317) and Jiangsu Planned Projects for Postdoctoral Research Funds (1302103B).

[2]School of Iron & Steel, Soochow University, Suzhou, Jiangsu, 215021, China

[3]School of Urban Rail Transportation, Soochow University, Suzhou, Jiangsu, 215021, China

[4]School of Computer Engineering, Suzhou Vocational University, Suzhou, Jiangsu, 215104, China

[5]Corresponding author

a combination of basic Buck and Boost DC converter topology which is successfully implemented in a wide range of electric power supply systems. This paper mainly focuses on the modeling and control problem of Buck-Boost converter. Most of conventional converters are regulated by simple analog controllers including a traditional PI (Proportional Integral) controller and a PWM (Pulse Width Modulation) unit [2]. Due to the inevitable dynamic of the analog PI regulator and PWM, conventional controllers are not suitable for high efficiencies demanding applications. In recent years, digital control strategies (such as H∞ methods, fuzzy control, nonlinear techniques, sliding mode control and so on), have emerged as an increasingly viable option for DC-DC converters with the fast development of the digital computational power [3].

The difficulty of the controller design for Buck-Boost converters stems from their hybrid and nonlinear nature, non-minimum phase behavior, the constraints of system states and so on. Among these modern control strategies, one research direction with significant potential is coordinated control using a MPC algorithm which have already been proposed in the DC-DC converter control [4, 5]. In the literature, MPC is regarded as an efficient control strategy based on the completely multivariable system framework [6]. In spite of its ability of optimal and constraint handling, the application of MPC strategy needs expensive on-line computation power and MPC is labeled as a technology for slow processes. Recently, EMPC is proposed to handle this problem [7, 8]. EMPC moves all the computations necessary for the implementation of MPC off-line using multi-parameter programming, while preserving all its other characteristics. Therefore, EMPC reduces on-line computation time and renders MPC suitable for fast systems such as switched power converters. For DC-DC power converters, EMPC has been studied in parallelized DC-DC converter [9] and electrical drives [10]. As for more complicated Buck-Boost converter, the application of EMPC strategies is still under investigation and more suitable model is needed.

A piecewise affine discrete-time modeling method, which is accurate and more adequate for EMPC paradigm to be applied, is proposed for non-inverting Buck-Boost DC-DC converter in this paper. Based on a piecewise affine discrete-time model, EMPC strategy is developed to reduce the on-line computation time and regulate the output voltage under system mismatches and disturbances. EMPC based on the piecewise affine model achieves more accurate and reliable performance compared with averaged model. As a result, the closed loop performance is improved and the complexity of controller is greatly reduced. Besides these benefits, the proposed EMPC respects all the constraints of the Buck-Boost system which is difficult to handle in the conventional control strategies.

2. Methodology

2.1. Circuit topology

An overview of the Buck-Boost DC-DC converter is given in this section to illustrate the background of the control problem. Fig. 1 depicts the circuit topology

and physical setup of the Buck-Boost converter where S_i are switches. while V_s and V_{rmo} represent the input and output voltages, respectively. Quantities D_i are the diodes and R_o is the load resistance. Symbols X_l and X_c are the inductance of the inductor and capacitance of the capacitor, respectively. Symbols R_l and R_c stand for the parasitic equivalent series resistances of the inductor and capacitor, respectively. Quantity T_s denotes the switching period and f_s is the corresponding switching frequency. Finally, d represents the duty cycle and $V_{\mathrm{o,ref}}$ denotes the reference value of the output voltage.

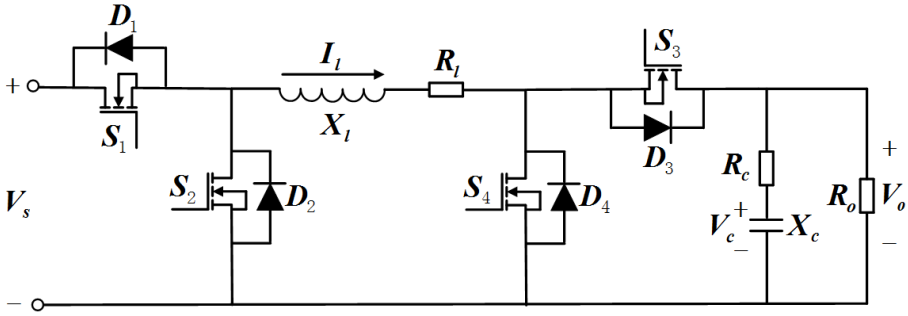

Fig. 1. Physical setup of Buck-Boost DC-DC converter

In Buck-Boost converters, couple transistors S_1 and S_2, (S_3 and S_4) work in a complementary manner, that is, when switch S_1 (S_3) is on, switch S_2 (S_4) must be off, and vice-versa. All of the switches are operated in a cyclic manner and duty cycle d is usually defined as $d = t_\mathrm{on}/T_\mathrm{s}$ where T_s is the switching period and t_on is the working time interval of S_1. The control objective is adjusting the duty cycle $d(k)$ to reach the output voltage reference. Buck-Boost DC-DC converter has two distinct dynamical modes: $[kT_\mathrm{s},\ kT_\mathrm{s} + d(k)T_\mathrm{s}]$ (Mode 1) and $[kT_\mathrm{s} + d(k)T_\mathrm{s},\ (k+1)T_\mathrm{s}]$ (Mode 2).

2.2. Mathematical model

To obtain a suitable numerical model for controller design, the parameters are normalized according to the base quantities: $R_\mathrm{b} = R_0$, $L_\mathrm{b} = R_\mathrm{b}/(2\pi f_\mathrm{s})$, $C_\mathrm{b} = 1/(2\pi f_\mathrm{s} R_\mathrm{b})$, $I_\mathrm{b}(k) = V_\mathrm{s}(k)/R_\mathrm{b}$, which simplifies the mathematical description of the system [4]. Mathematical model of the non-inverting Buck-Boost DC-DC converter can be derived by choosing $x(t) \in [i_\mathrm{l}(t), v_\mathrm{o}(t)]^\mathrm{T}$ as the state vector. By applying Kirchhoff's Voltage and Current Laws, we have the continuous time state space model for each mode.

Mode 1:

$$\dot{x}(t) = F_1 x(t) + g_1\,, \tag{1}$$

$$v_\mathrm{o} = \begin{bmatrix} 0 & 1 \end{bmatrix} x(t)\,. \tag{2}$$

Mode 2:

$$\dot{x}(t) = F_2 x(t) + g_2\,, \tag{3}$$

$$v_{\rm o} = \begin{bmatrix} 0 & 1 \end{bmatrix} x(t)\,. \tag{4}$$

where

$$F_1 = 2\pi f_{\rm s} \begin{bmatrix} -\frac{r_{\rm l}}{x_{\rm l}} & 0 \\ 0 & -\frac{1}{x_{\rm c}(r_{\rm o}+r_{\rm c})} \end{bmatrix},\ g_1 = \begin{bmatrix} \frac{1}{x_{\rm l}} \\ 0 \end{bmatrix},$$

$$F_2 = 2\pi f_{\rm s} \begin{bmatrix} -\frac{1}{x_{\rm l}} r_{\rm l} & -\frac{1}{x_{\rm l}} \\ -\frac{r_{\rm l} r_{\rm o} r_{\rm c}}{x_{\rm l}(r_{\rm o}+r_{\rm c})} + \frac{1}{x_{\rm c}} \left(\frac{r_{\rm o}^2}{(r_{\rm o}+r_{\rm c})^2} + \frac{r_{\rm c}}{r_{\rm o}+r_{\rm c}} \right) & -\frac{r_{\rm o} r_{rmc}}{x_{\rm l}(r_{\rm o}+r_{\rm c})} - \frac{1}{x_{\rm c} r_{\rm o}} \end{bmatrix},$$

$$g_2 = \begin{bmatrix} 0 \\ 0 \end{bmatrix}.$$

2.3. Piecewise affine modeling

Let us start from the normalized continuous state space model (1)–(4) and assume that the converter is either in mode 1 or mode 2 during the sampling period k, that is, either $d_k = d(k) = 1$ or $d_k = d(k) = 0$. Taking the switching period as the sampling period, the exact discrete-time state space update model is given as

$$x_{k+1} = F_{\rm d1} x_k + g_{\rm d1}\,,\ \text{for } d_k = 1\,, \tag{5}$$

$$x_{k+1} = F_{\rm d2} x_k + g_{\rm d2}\,,\ \text{for } d_k = 0\,. \tag{6}$$

Here $F_{{\rm d}i} = {\rm e}^{F_i T_{\rm s}},\ i = 1, 2$ and $g_{{\rm d}i} = \int_0^{T_{\rm s}} {\rm e}^{F_i}\,{\rm d}t \cdot g_i,\ i = 1, 2$. For the general case $0 \le d_k \le 1$, we employ the weighted discrete-time modeling method, that is, mode 1 and mode 2 are weighted with respect to their effective duration. And the resulting weighted discrete-time model is as follows:

$$x_{k+1} = (F_{\rm d1} x_k + g_{\rm d1})\, d_k + (F_{\rm d2} x_k + g_{\rm d2})\,(1 - d_k) =$$

$$= A_{\rm av} x_k + B_{\rm av} x_k d_k + C_{\rm av} d_k + D_{\rm av}\,. \tag{7}$$

However, due to existence of the multiple item $x_k d_k$, the state space model (7) is nonlinear. For high degree of accuracy, a piecewise affine approximation of the system dynamic is proposed, resulting in a piecewise affine system of the form:

$$x_{k+1} = A_i x_k + B_i d_k + f_i,\quad d_i \le d_k \le d_{i+1},\ i = 1, \cdots, I\,, \tag{8}$$

where d_i and d_{i+1} represent the lower and upper bound values of the duty cycle interval for which the ith approximation is valid, with $d_1 = 0$ and $d_I = 1$. Approximation is applied by choosing appropriate d_i for selected duty cycle intervals.

For each duty cycle interval, d_k in the nonlinear term $x_k d_k$ can be replaced by the constant median value of the interval, that is,

$$x_{k+1} = \left(A_{\text{av}} + B_{\text{av}} \frac{(d_i + d_{i+1}}{2} \right) x_k + C_{\text{av}} d_k + D_{\text{av}} ,$$

$$d_i \leq d_k \leq d_{i+1},\ i = 1, \cdots, I . \tag{9}$$

This achieves the piecewise affine system update model

$$A_i = A_{\text{av}} + B_{\text{av}} \frac{(d_i + d_{i+1}}{2},\ B_i = C_{\text{av}},\ f_i = D_{\text{av}} ,$$

$$d_i \leq d_k \leq d_{i+1}, ß = 1, \cdots, I , \tag{10}$$

where B_i and f_i can be determined by the steady-state operating point continuity constraints for the piecewise affine model consistently with the averaged model. To be specific, for the selected constant duty cycle d_i, the steady-state operating points calculated by the averaged model is as follows:

$$\bar{x}_{\text{av},i} = (I_2 - A_{\text{av}} - B_{\text{av}} d_i)^{-1} (C_{\text{av}} d_i + D_{\text{av}}) . \tag{11}$$

For the piecewise model, we have $\bar{x}_{\text{pwa},i,i} = (I_2 - A_i)^{-1} (B_i d_i + f_i)$ and $\bar{x}_{\text{pwa},i,i+1} = (I_2 - A_i)^{-1} (B_i d_{i+1} + f_i)$. The steady-state operating point continuity constraints are imposed by $\bar{x}_{\text{pwa},i,i} = \bar{x}_{\text{av},i}$ and $\bar{x}_{\text{pwa},i,i+1} = \bar{x}_{\text{av},i+1}$ which yields four equations for each piecewise approximation. Quantities B_i and f_i can be fully determined as

$$\begin{bmatrix} B_i \\ f_i \end{bmatrix} = M_i^{-1} \begin{bmatrix} \bar{x}_{\text{av},i} \\ \bar{x}_{\text{av},i+1} \end{bmatrix}, M_i = \begin{bmatrix} (I_2 - A_i)^{-1} \begin{bmatrix} d_i & 0 & 1 & 0 \\ 0 & d_i & 0 & 1 \end{bmatrix} \\ (I_2 - A_i)^{-1} \begin{bmatrix} d_{i+1} & 0 & 1 & 0 \\ 0 & d_{i+1} & 0 & 1 \end{bmatrix} \end{bmatrix} . \tag{12}$$

As a result, a piecewise affine model is completely defined and is continuous across its boundaries. The approximation accuracy is determined by the duty cycle intervals.

2.4. EMPC based on multi-parametric programming: a brief review

A brief review of EMPC based on multi-parametric programming is given in this section [8]. Consider a discrete-time MIMO LTI (Linear Time-Invariant) system of the regular form:

$$\begin{cases} x(k+1) = Ax(k) + Bu(k), \\ y(k) = Cx(k), \end{cases} \tag{13}$$

while subjecting to the constraints $x_{\min} \leq x(k) \leq x_{\max}$, $y_{\min} \leq y(k) \leq y_{\max}$, $u_{\min} \leq u(k) \leq u_{\max}$. In the literature, for system (13), MPC solves the following

optimization problem:

$$\min_{U \triangleq \{u_k, \cdots, u_{k+N_{\mathrm{u}}-1}\}} J$$

where

$$J = \left\{ J\left(U, x(k)\right) = x_{k+N_{\mathrm{p}}}^{'} P x_{k+N_{\mathrm{p}}} + \sum_{j=0}^{N_{\mathrm{p}}-1} \left[x_{k+j}^{'} Q x_{k+j} + u_{k+j}^{'} R u_{k+j} \right] \right\}. \quad (14)$$

The idea of MPC is the construction of an optimal control input sequence $U^* = \left\{u_k^*, u_{k+1}^*, \cdots, u_{k+N_{\mathrm{u}}-1}^*\right\}$, which minimizes the cost function J in (14) with respect to the state, output and input constraints (13). And MPC employs the receding horizon control principle, only the first step of the control input U^* (i.e., $u^*(k)$) is taken into the system at the time instant k. As for $k+1$, the whole procedure will be repeated once again. In this paper, we adopt a recently proposed EMPC strategy based on multi-parametric programming which is able to move all the computations of MPC off-line [11]. To be specific, EMPC utilizes multi-parametric programming to systematically subdivide the space X of parameters x_k into critical regions (CRs). For each CR, the optimal solution is an affine function of x_k. Once the critical region CR_0 has been defined, the rest of the space $\mathrm{CR}^{\mathrm{rest}} \triangleq X \backslash \mathrm{CR}_0$ can be explored and new critical regions will be generated by an iterative algorithm which partition $\mathrm{CR}^{\mathrm{rest}}$ recursively [7, 8]. As a result, state space X are divided into critical regions, and in each region, the optimal solution is an affine function of x_k which is calculated off-line. EMPC is extremely suitable for the piecewise affine discrete-time model of the Buck-Boost converter.

3. Result analysis and discussion

3.1. EMPC controller design

Non-inverting Buck-Boost DC-DC converter is taken as an example to the implementation of EMPC strategies. And the parameters are given as follows: $x_{\mathrm{l}} = 2.5133$, $x_{\mathrm{c}} = 50.2655$, $r_{\mathrm{c}} = 0.005$, $r_{\mathrm{l}} = 0.025$, $r_{\mathrm{o}} = 1$, $i_{l,\max} = 10$, $v_{\mathrm{s}} = 1$, $v_{\mathrm{o,ref}} = 0.75$, $v_{\mathrm{o,max}} = 2$. Piecewise affine discrete-time model can easily be derived from the parameters by choosing appropriate duty cycle intervals. The control objectives are to minimize the output voltage error $v_{\mathrm{o,err}} = v_{\mathrm{o}} - v_{\mathrm{o,ref}}$ with respect to the constraints. Additionally, we introduce the difference of two consecutive duty cycles $\Delta d(k) = d(k) - d(k-1)$. Define the penalty matrix $Q = diag(q_1, q_2)$ and the vector $\varepsilon(k) = [v_{\mathrm{o,err}}(k), \Delta d(k)]$. The performance index function is given as

$$J = \sum_{l=0}^{N-1} \varepsilon^{\mathrm{T}}(k) Q \varepsilon(k). \quad (15)$$

Based on the piecewise affine discrete-time linear model and the performance index function (15), piecewise affine EMPC controllers can be designed according to

the standard design procedure.

3.2. Simulation result analysis and discussion

Dynamic simulations using Matlab were carried out to evaluate the performance of the proposed EMPC strategy based on piecewise affine model. For the sake of comparison, we also report simulation results of the conventional PI algorithm which employs output feedback and EMPC based on averaged model. As far as the characteristics of the Buck-Boost converter system are concerned, we choose prediction horizon $N = 5$ for EMPC. Weight matrix is selected as $Q = diag(1, 5)$. And the constraints are chosen as $0 \leq d \leq 1$, $|\Delta d| \leq 0.2$. The duty cycle interval is selected as: $[0, 0.3]$, $[0.3, 0.7]$ and $[0.7, 1]$.

Simulation results of the Buck-Boost converter are given in Figs. 2–6, where the results of EMPC based on piecewise affine model (represent by PEMPC) are drawn in solid lines, EMPC based on averaged model (represent by EMPC) are drawn in dashed dot lines, PID controllers in dashed lines. The polyhedral partition of PEMPC are shown in Fig. 2. For each critical region, the optimal control law is an affine function of the states and the previous control input. Once the critical region of the state is determined, the optimal feedback control law is directly calculated. As a result, the online calculation time will be greatly reduced compared with traditional MPC approach.

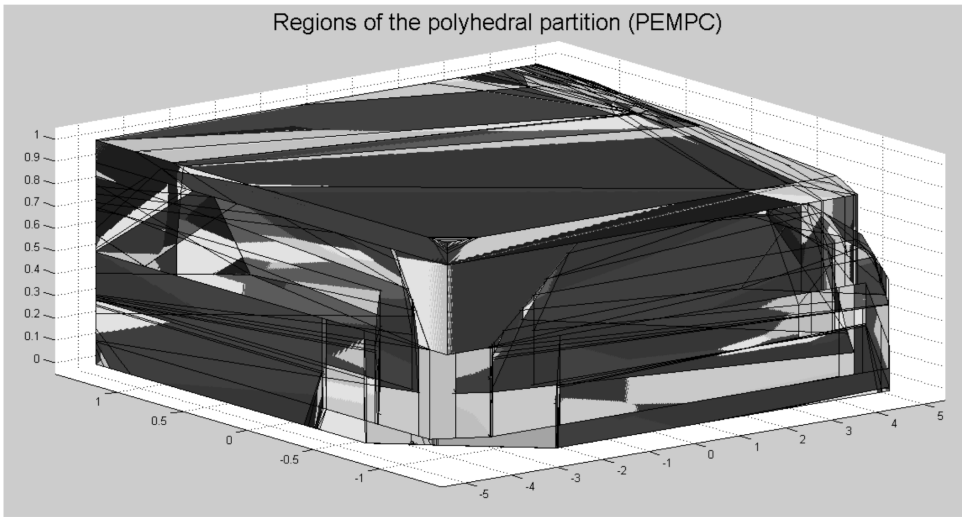

Fig. 2. Regions of the polyhedral partition calculated based on piecewise affine model

Figs. 3–4 give the closed-loop responses during startup with output voltage reference $v_{\text{oref}} = 0.4\,\text{p.u.}$ under PI, EMPC and PEMPC controllers. As we can see from the trajectories, EMPC has a steady state error caused by inaccurate averaged model which is overcomed by PEMPC. PEMPC controller derives the output voltage to the reference quickly and with small overshot whereas the PI controller reacts

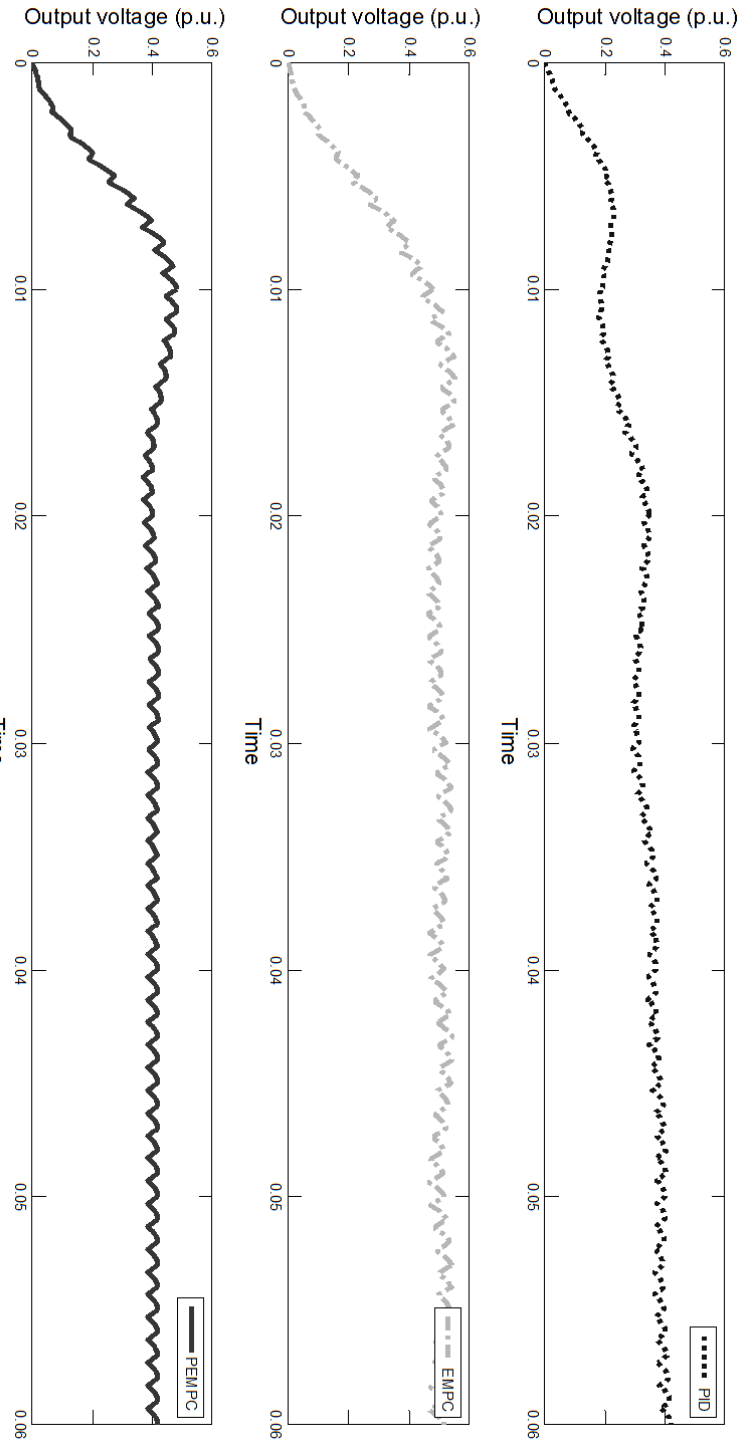

Fig. 3. Output voltage responses during startup

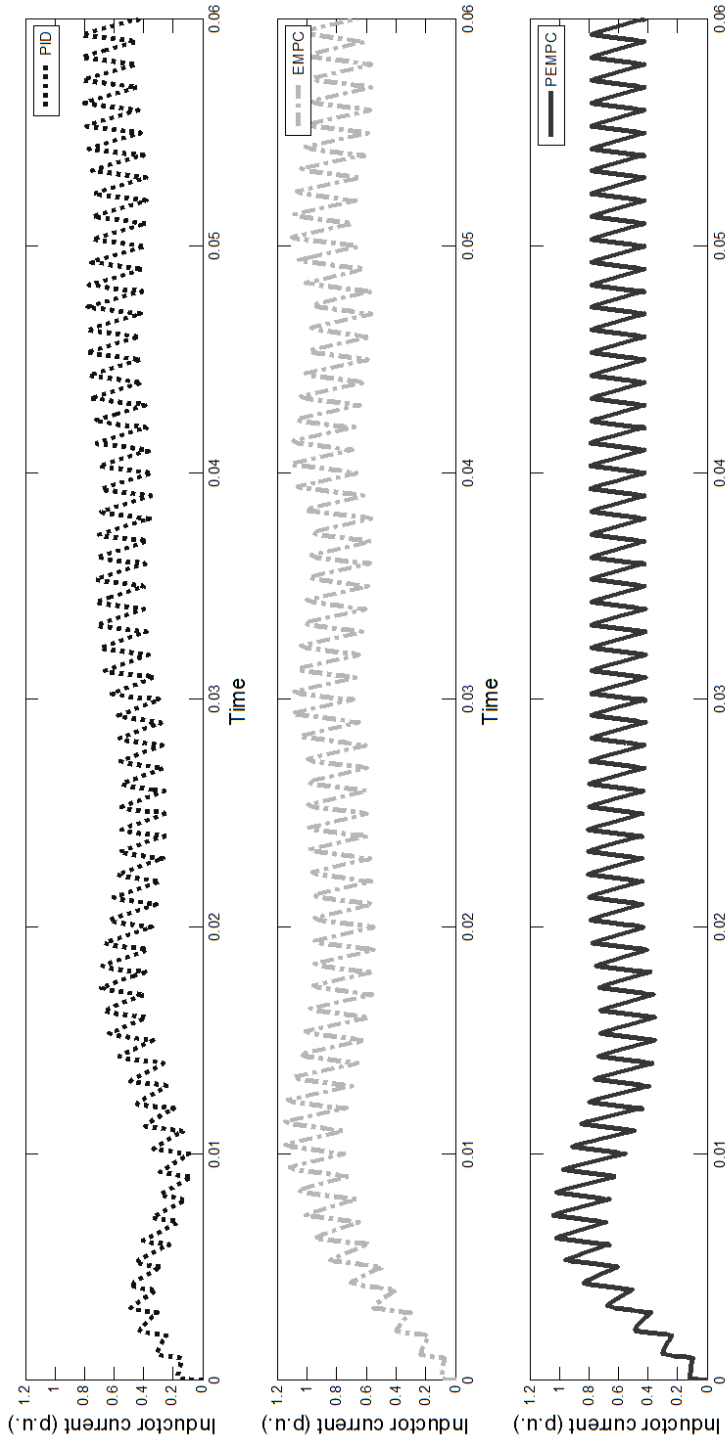

Fig. 4. Inductor current responses during startup

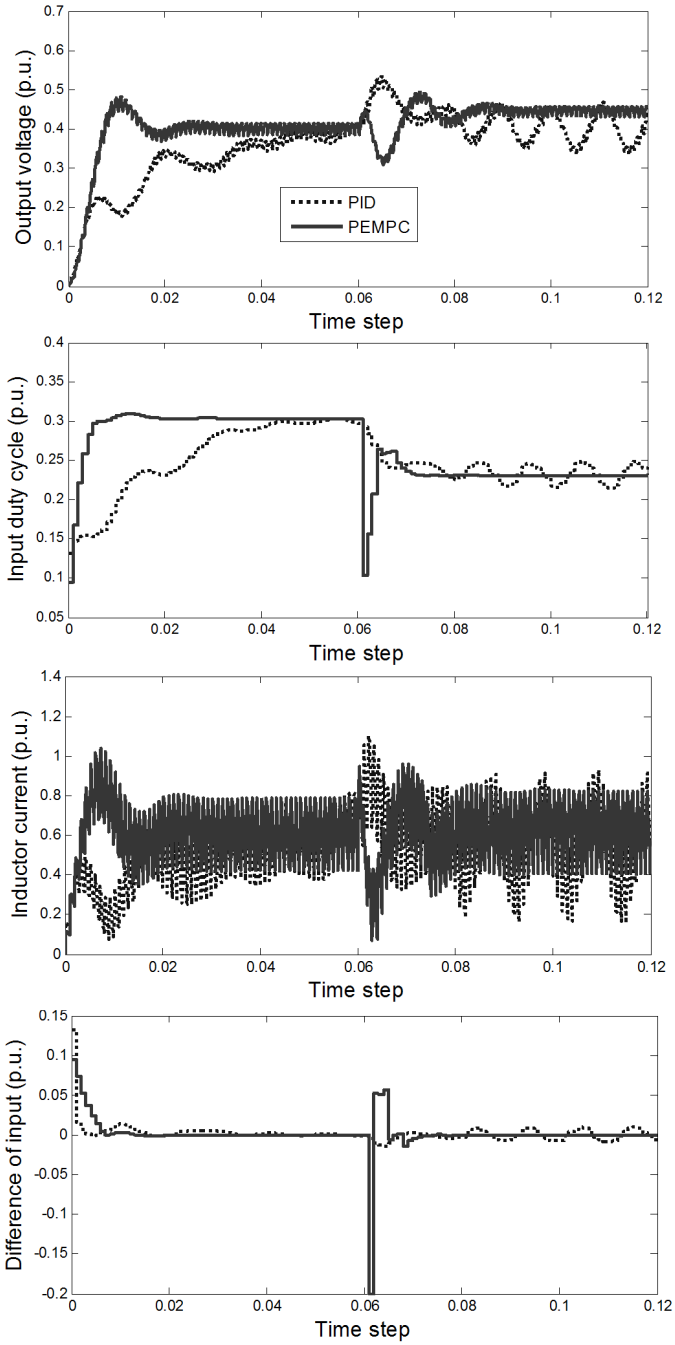

Fig. 5. Closed-loop responses to the step-up change in the input voltage active for $t \geq 0.06\,\mathrm{s}$

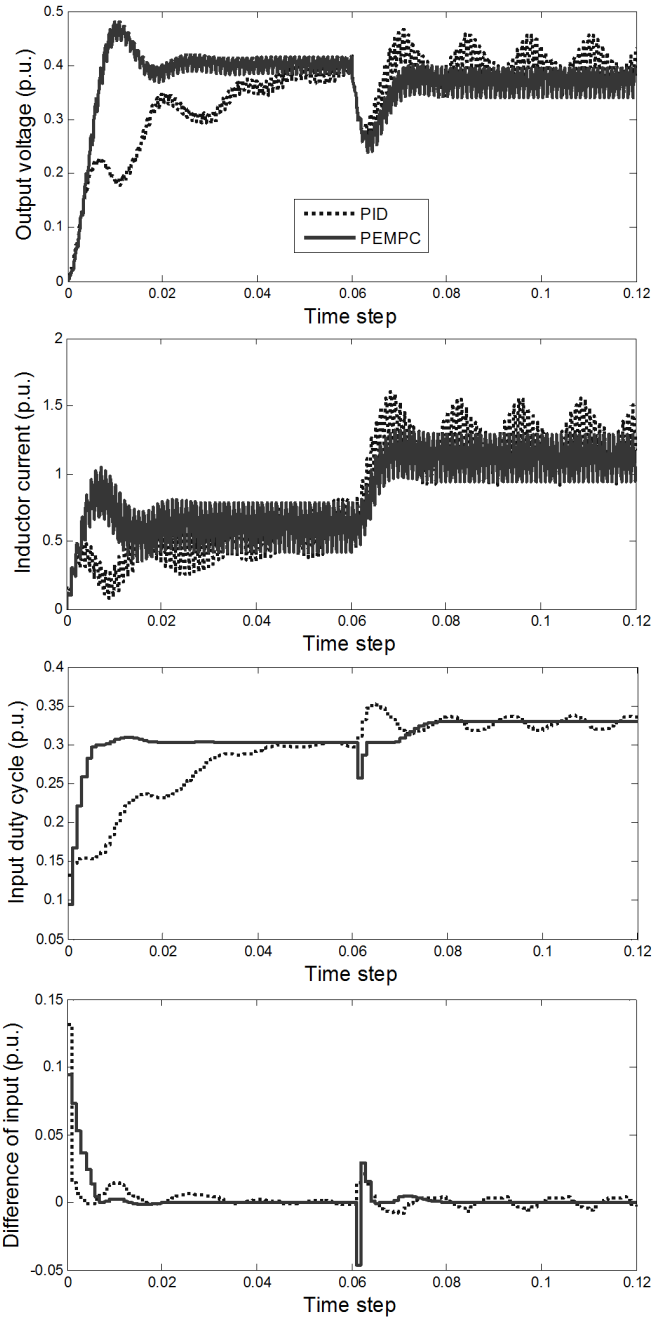

Fig. 6. Closed-loop responses to the step-down change in the load resistor active for $t \geq 0.06\,\mathrm{s}$

slowly and results in big overshot. Closed-loop responses to several typical kinds of disturbances, which are frequently encountered in practice, are also analyzed. Since the input voltage source of Buck-Boost converter is unregulated, the variations in the input voltage is frequently encountered. Therefore, a step-up change in the input voltage from 1 p.u. to 1.4 p.u. after start up is simulated and the closed-loop responses are given in Fig. 5. Both PEMPC and PI controllers can derive the output voltage to the reference, however PEMPC provides less deviations in output voltage and inductor current. The output load may vary dramatically, so the variation in the load resistor is also investigated. Fig. 6 gives the closed-loop responses to the step-down change in the load resistor from 1 p.u. to 0.5 p.u. after start up. Trajectories of the system output and states show the effectiveness of PEMPC controller compared with traditional PI controller.

As we can see from the simulation results, EMPC based on piecewise affine model improves the closed-loop performance systematically and the controller is easy to tune by adjusting the weight matrices.

4. Conclusion

An innovative non-inverting Buck-Boost DC-DC converter control based on EMPC was investigated in this paper to overcome the control difficulties encountered in practice. A piecewise affine model is derived to model the hybrid and nonlinear system dynamic precisely. The traditional MPC optimal controller is transformed into a table lookup algorithm and the online computation is greatly reduced. As a result, Buck-Boost converter system could be precisely modeled and coordinately controlled by proposed EMPC. EMPC strategy investigated in this paper solves the control problem of high switching frequency converters systematically. It could be extended to converters with higher switching frequency and more complicated topology to get better control performances compared with existing ones.

However, in order to apply this scheme to industry practice, a major and important work to be done is realization of the algorithm in the embedded system which has limited computation power and hardware resources.

References

[1] G. Villar-Piqué, H. J. Bergveld, E. Alarcon: *Survey and benchmark of fully integrated switching power converters: Switched-capacitor versus inductive approach.* IEEE Transactions on Power Electronics *28* (2013), No. 9, 4156–4167.

[2] J. Alvarez-Ramirez, I. Cervantes, G. Espinosa-Perez, P. Maya, A. Morales: *A stable design of PI control for DC-DC converters with an RHS zero.* IEEE Transactions on Circuits and Systems I: Fundamental Theory and Applications *48* (2001), No. 1, 103–106.

[3] G. Gavagsaz-Roghayeh, M. Phattanasak, J. P. Martin, S. Pierfederici, B. Nahid-Mobarakeh, B. Davat: *Generalisation of an averaged model approach to estimate the period-doubling bifurcation onset in power converters.* IET Power Electronics *9* (2016), No. 5, 997–988.

[4] T. Geyer, G. Papafotiou, R. Frasca, M. Morari: *Constrained optimal control of*

the step-down DC-DC converter. IEEE Transactions on Power Electronics *23* (2008), No. 5, 2454–2464.

[5] C. Vlad, P. Rodriguez-Ayerbe, E. Godoy, P. Lefranc: *Advanced control laws of DC-DC converters based on piecewise affine modelling. Application to a step-down converter*. IET Power Electronics *7* (2014), No. 6, 1482–1498.

[6] J. B. Rawlings: *Tutorial overview of model predictive control*. IEEE Control Systems *20*, (2000), No. 3, 38–52.

[7] A. Bemporad, M. Morari, V. Dua, E. N. Pistikopoulos: *The explicit linear quadratic regulator for constrained systems*. Automatica *38* (2002), No. 1, 3–20.

[8] F. Bayat, T. A. Johansen: *Multi-resolution explicit model predictive control: Delta-model formulation and approximation*. IEEE Transactions on Automatic Control *58* (2013), No. 11, 2979–2984.

[9] A. G. Beccuti, M. Kvasnica, G. Papafotiou, M. Morari: *A decentralized explicit predictive control paradigm for parallelized DC-DC circuits*. IEEE Transactions on Control Systems Technology *21* (2013), No. 1, 136–148.

[10] S. Mariethoz, A. Domahidi, M. Morari: *High-bandwidth explicit model predictive control of electrical drives*. IEEE Transactions on Industry Applications *48* (2012), No. 6, 1980–1992.

[11] M. A. Mohammadkhani, F. Bayat, A. A. Jalali: *Design of explicit model predictive control for constrained linear systems with disturbances*. International Journal of Control, Automation and Systems *12* (2014), No. 2, 294–301.

Received April 23, 2017

Acta Technica *62*, No. 1A/2017, 123–134

Robust H_∞ rotating consensus control for second-order multi-agent systems with uncertainty and time-varying delay in three-dimensional space[1]

Ping Li[2], Kaiyu Qin[2]

Abstract. The robust delay-dependent H_∞ control problems for rotating consensus of second-order multi-agent systems is studied, which is subject to uncertainty, external disturbances and time-varying delay in three-dimensional space. First, a rotating consensus is defined in three-dimensional space. Then a distributed control protocol based on state feedback of neighbors is designed. In the next place, a sufficient delay-dependent condition in terms of the matrix inequalities is derived to make all agents asymptotically reach rotating consensus with the desired H_∞ performance index. Furthermore, an algorithm is elaborately designed to get a feasible solution to this condition. Finally, simulation results are provided to illustrate the effectiveness of our theoretical results and algorithms.

Key words. Multi-agent systems, rotating consensus, H_∞ control, uncertainty, time-varying delay.

1. Introduction

As a special case of the consensus problems, the rotating consensus is used to describe a class of collective circular motions such as the motion of celestial bodies, flocks of birds flying around a closed circuit course and schools of fish swimming along an approximately circular orbit, which can find important potential applications in formation flight of satellites around the earth, spacecraft docking, circular mobile sensor networks, etc. However, most of existing results cannot be straightly applied to imitate or explain such motions and rare results are derived to generate such motions. In [1], Sepulchre et al. formulated a new rotating formation control problem

[1]This work was supported by the Specialized Research Fund for the Doctoral Program of Higher Education of China under Grants No. 20130185110023.

[2]School of Astronautics and Aeronautics, University of Electronic Science and Technology of China, Chengdu, 611731, China

according to application of autonomous underwater vehicles to collect oceanographic measurements. In [2] and in [3], Lin et al. investigated collective rotating motions of second-order multi-agent systems on a plane and in three dimensional space, respectively. In [4], Yang et al. studied distributed rotating consensus in networks of second-order agents using only local position information in three-dimensional space. In [5], distributed composite rotating consensus problem was investigated for second-order multi-agent systems, where all agents move in a nested circular orbit.

As a typical networked system, multi-agent systems often contain disturbances, uncertainties and time-delay in practical applications. Moreover, the existence of these facts might destroy the convergence properties of the systems. Therefore, it is significant to investigate robust consensus problems of multi-agent systems, which reflect the effects of these facts on their behavior. In the past decade, some interesting results have been obtained for robust consensus problems in [6–9]. However, these results cannot be straight applied to robust delay-dependent H_∞ control problems for rotating consensus [10]. So far, only the author of this paper studied distributed robust H_∞ rotating consensus control problems for directed networks of second-order agents with mixed uncertainties and time-delay in [10], but we only considered constant time delay, rotating consensus on a plane, and we only obtained the sufficient conditions that the parameters of control protocols should be satisfied, but their calculation method was not directly given in [10]. Therefore, this paper will further study robust delay-dependent H_∞ control problems for rotating consensus of second-order multi-agent systems with uncertainty and time-varying delay in three-dimensional space.

2. State of the art

Consider a multi-agent system consisting of n second-order agents. Each agent is regarded as a node in a graph $\mathcal{G}$. Suppose that the ith agent

$$s_i,\ (i \in I_{\mathrm{g}},\, I_{\mathrm{g}} = \{1,\, 2 \cdots,\, n\})$$

has the dynamics as follows:

$$\begin{aligned} \dot{r}_i(t) &= v_i(t), \\ \dot{v}_i(t) &= u_i(t) + w_i(t), \end{aligned} \tag{1}$$

where $r_i\,(t)$, $v_i\,(t)$ denote the position and velocity state of the ith agent s_i, $u_i\,(t)$ denote the control input or control protocol of the ith agent, and $w_i\,(t) \in \mathcal{L}_2\,[0, \infty)$ denotes the external disturbances of the ith agent. Finally, $r_i\,(t)$, $v_i\,(t)$, $u_i\,(t)$, $w_i\,(t) \in \mathcal{R}^3$.

In this paper, our main objective is to design a distributed protocol to make all agents reach rotating consensus while satisfying the desired H_∞ disturbance attenuation index. It is called that all agents reach rotating consensus if all agents reach consensus and surround a common point with a desired constant angular velocity $\omega \in \mathcal{R}$ on a plane, whose normal is a specified unit vector $\mathrm{i}_\omega \in \mathcal{R}^3$. The

rotating consensus can be defined as follows

Definition 1.[3]: The multi-agent system (1) reaches rotating consensus, if and only if the states of agents satisfy

$$\begin{aligned}
&\lim_{t\to+\infty} \mathrm{i}_{\omega}^{\mathrm{T}} v_i(t) = 0,\\
&\lim_{t\to+\infty} (\dot{v}_i(t) - \omega R_{\omega} v_i(t)) = 0,\\
&\lim_{t\to+\infty} (v_i(t) - v_k(t)) = 0,\\
&\lim_{t\to+\infty} (c_i(t) - c_k(t)) = 0
\end{aligned} \tag{2}$$

for $\forall i, j \in I_{\mathrm{g}}$, where ω denotes the desired constant angular velocity, $c_i\,(t) = r_i\,(t) + \omega^{-1} R_{\omega} v_i\,(t)$

$$R_{\omega} = R_{\omega 0}^{\mathrm{T}} R_{i_{\omega}}\,(\pi/2)\, R_{\omega 0} R_{i_{\omega}}\,(\pi/2) = \begin{bmatrix} 0 & -1 & 0 \\ 1 & 0 & 0 \\ 0 & 0 & 1 \end{bmatrix}.$$

3. Methodology

In this section, we will solve H_{∞} control problem for rotating consensus of multi-agent systems with parameter uncertainties and time-delay in three-dimensional space. Firstly, we will design a distributed control protocol. Then, we will deduce the rule and algorithm for designing state feedback matrix $\boldsymbol{K}$.

3.1. Protocol design

Based on the state feedback of neighbors, the distributed control protocol we used is given as

$$u_i(t) = u_{i1}(t) + u_{i2}(t) \tag{3}$$

for all $i \in I_{\mathrm{g}}$, where

$$\begin{aligned}
u_{i1}(t) &= \omega R_{\omega} v_i(t),\\
u_{i2}(t) &= (\boldsymbol{I}_3 + \Delta \boldsymbol{B}(t))[\boldsymbol{K}_{\mathrm{v}} \textstyle\sum_{s_k \in N_i} a_{ik}(v_k(t - d(t)) - v_i(t - d(t))] + \\
&\quad + \boldsymbol{K}_{\mathrm{c}} \textstyle\sum_{s_k \in N_i} a_{ik}(c_k(t - d(t)) - c_i(t - d(t))).
\end{aligned}$$

In the protocol, $\boldsymbol{K}_{\mathrm{v}}$ and $\boldsymbol{K}_{\mathrm{v}}$ are the state feedback matrices, ω denotes the desired constant angular velocity, $d\,(t)$ $(0 < d\,(t) \leq \tau,\ \left|\dot{d}\,(t)\right| < \mu)$ denotes the time-varying delay, N_i denotes the set of neighbors of agent s_i and $\Delta \boldsymbol{B}\,(t)$ is a matrix-valued function representing time-varying parameter uncertainties. The parameter uncertainties are assumed to be norm-bounded and $\Delta \boldsymbol{B}\,(t) = \boldsymbol{G} \boldsymbol{F}\,(t)\, \boldsymbol{E}$, where $\boldsymbol{G}$ and $\boldsymbol{E}$

are known constant matrices with appropriate dimensions and $\boldsymbol{F}(t)$ is an unknown matrix function with Lebesgue measurable elements satisfying $\boldsymbol{F}^{\mathrm{T}}(t)\boldsymbol{F}(t) \leq \boldsymbol{I}$ for all $t \geq 0$.

Define the output functions $z_i(t)$, which is computed from the average of the relative states of all agents as follows:

$$z_i(t) = [z_{i1}^{\mathrm{T}}(t),\, z_{i2}^{\mathrm{T}}(t)]^{\mathrm{T}} \in \mathcal{R}^6, \qquad i \in I_{\mathrm{g}}, \tag{4}$$

where $z_{i1}(t) = v_i(t) - \frac{1}{n}\sum_{j=1}^{n} v_j(t)$ and $z_{i1}(t) = c_i(t) - \frac{1}{n}\sum_{j=1}^{n} c_j(t)$.

Therefore, it is clear that the rotating consensus of the system (1) can be reached if and only if the states of agent satisfy

$$\begin{aligned} &\lim_{t\to+\infty} z_i(t) = 0 \\ &\lim_{t\to+\infty} [\dot{v}_i(t) - \omega R_\omega v_i(t)] = 0 \end{aligned} \tag{5}$$

for all $i \in I_{\mathrm{g}}$.

Denote

$$\begin{aligned} &\xi(t) = [\xi_1^{\mathrm{T}}(t), \cdots, \xi_n^{\mathrm{T}}(t)]^{\mathrm{T}}, && \xi_i(t) = [v_i^{\mathrm{T}}(t), c_i^{T}(t)]^{\mathrm{T}}, \\ &w(t) = [w_1^{\mathrm{T}}(t), \cdots, w_n^{\mathrm{T}}(t)]^{\mathrm{T}}, && z(t) = [z_1^{\mathrm{T}}(t), \cdots, z_n^{\mathrm{T}}(t)]^{\mathrm{T}}, \\ &\boldsymbol{A} = \begin{bmatrix} \omega R_\omega & \boldsymbol{0}_3 \\ \boldsymbol{0}_3 & \boldsymbol{0}_3 \end{bmatrix}, && \boldsymbol{B}_1 = \boldsymbol{B}_2 = \begin{bmatrix} \boldsymbol{I}_3 \\ \omega^{-1} R_\omega \end{bmatrix}, \\ &\boldsymbol{K} = [\boldsymbol{K}_v, \boldsymbol{K}_c], && \Delta\boldsymbol{B}_1(t) = \boldsymbol{B}_1 \Delta\boldsymbol{B}(t), \\ &\boldsymbol{C} = [C_{ij}]_{i,j=1}^{n}, && C_{ij} = \begin{cases} \frac{n-1}{n}, & i = j, \\ -\frac{1}{n}, & i \neq j. \end{cases} \end{aligned}$$

By using the protocol (3), the closed-loop dynamics of the system (1) can be written as

$$\begin{aligned} &\dot{\xi}(t) = (\boldsymbol{I}_n \otimes \boldsymbol{A})\xi(t) - \boldsymbol{L} \otimes [(\boldsymbol{B}_1 + \Delta\boldsymbol{B}_1(t))\boldsymbol{K}]\xi(t - d(t)) + (\boldsymbol{I}_n \otimes \boldsymbol{B}_2)w(t), \\ &z(t) = (\boldsymbol{C} \otimes \boldsymbol{I}_6)\xi(t), \qquad 0 < d(t) \leq \tau, \quad \dot{d}(t) \leq \mu, \end{aligned} \tag{6}$$

where $\otimes$ denotes the Kronecker product and $\boldsymbol{L}$ is the Laplacian matrix of graph $\mathcal{G}$.

According to robust control theory, the attenuating ability of consensus performance for multi-agent system (1) against external disturbances can be quantitatively measured by the H_∞ norm of the closed-loop transfer function matrix $\boldsymbol{T}_{wz}(s)$ from the external disturbance $w(t)$ to the controlled output $z(t)$, we design a distributed

state feedback protocol $u_i(t)$ such that

$$\| \boldsymbol{T}_{wz}(s) \|_\infty < \gamma \tag{7}$$

holds for prescribed H_∞ disturbance attenuation index γ.

3.2. Some necessary lemmas

Lemma 1. [8]: Assume that the interaction graph $\mathcal{G}$ is connected. For a given $\gamma > 0$, the closed-loop system (6) reaches consensus with the desired H_∞ disturbance attenuation index $\gamma\,(\boldsymbol{T}_{wz}(s)_\infty < \gamma)$, if and only if the following $n-1$ systems are simultaneously asymptotically stable with $\boldsymbol{T}_{\hat{w}\hat{z}}(s)_\infty < \gamma$ for $i = 1, 2, \cdots, n-1$.

$$\begin{aligned} \dot{\hat{\delta}}_i(t) &= A\hat{\delta}_i(t) - \lambda_i(\boldsymbol{B}_1 + \Delta\boldsymbol{B}_1(t))\boldsymbol{K}\hat{\delta}_i(t - d(t)) + \boldsymbol{B}_2\hat{w}_i(t), \\ \hat{z}_i(t) &= \hat{\delta}_i t), \quad 0 < d(t) \le \tau,\ \dot{d}(t) \le \mu, \end{aligned} \tag{8}$$

where λ_i, $(i = 1, 2, n-1)$ are positive eigenvalues of the Laplacian matrix $\boldsymbol{L}$, and $\hat{\delta}_i(t)$, $\hat{w}_i(t)$, $\hat{z}_i(t) \in \mathcal{R}^6$.

Lemma 2. (Schur complement formula) [6]: For a given symmetric matrix $\boldsymbol{S}$ with the form $\boldsymbol{S} = [S_{ij}]$, $S_{11} \in \mathcal{R}^{r\times r}$, $S_{12} \in \mathcal{R}^{r\times(n-r)}$ or $S_{22} \in \mathcal{R}^{(n-r)\times(n-r)}$, then $S < 0$ if and only if $S_{11} < 0$, $S_{22} - S_{21}S_{11}^{-1}S_{12} < 0$ or $S_{22} < 0$, $S_{11} - S_{12}S_{22}^{-1}S_{21} < 0$.

Consider a nominal time delay system as follows:

$$\begin{aligned} \dot{x}_{(t)} &= \boldsymbol{A}x(t) + \boldsymbol{A}_d x(t - d(t)) + \boldsymbol{B}_w w(t), \\ z(t) &= \boldsymbol{C}x(t), \quad 0 < d(t) \le \tau,\ \dot{d}(t) \le \mu. \end{aligned} \tag{9}$$

A bounded real lemma (BRL) will be introduced in the following part.

Lemma 3. (BRL) [12]: For a given $\gamma, \tau, \mu > 0$, the nominal time delay system (9) is asymptotically stable with $\boldsymbol{C}_{wz}(s)_\infty < \gamma$, if there exist positive definite matrices $\boldsymbol{P}$, $\boldsymbol{Q}$, $\boldsymbol{R}$, $\boldsymbol{S}$ and matrices $\boldsymbol{M}_1$, $\boldsymbol{M}_2$, $\boldsymbol{N}_1$, $\boldsymbol{N}_2$ with appropriate dimensions such that

$$\boldsymbol{\Gamma} = \begin{bmatrix} \boldsymbol{\Gamma}_{11} & \boldsymbol{\Gamma}_{12} & -\boldsymbol{M}_1 & \boldsymbol{P}\boldsymbol{B}_w & \tau A^T\boldsymbol{S} & \tau\boldsymbol{M}_1 & \tau\boldsymbol{N}_1 \\ * & \boldsymbol{\Gamma}_{22} & -\boldsymbol{M}_2 & 0 & \tau\boldsymbol{A}_d^{\boldsymbol{T}}\boldsymbol{S} & \tau\boldsymbol{M}_2 & \tau\boldsymbol{N}_2 \\ * & * & -\boldsymbol{R} & 0 & 0 & 0 & 0 \\ & * & * & -\gamma^2\boldsymbol{I} & \tau\boldsymbol{B}_w^{\mathrm{T}}\boldsymbol{S} & 0 & 0 \\ * & * & * & * & -\tau\boldsymbol{S} & 0 & 0 \\ * & * & * & * & * & -\boldsymbol{S} & 0 \\ * & * & * & * & * & * & -\boldsymbol{S} \end{bmatrix} < 0 \tag{10}$$

where

$$\begin{aligned} \boldsymbol{\Gamma}_{11} &= \boldsymbol{P}\boldsymbol{A} + \boldsymbol{A}^{\mathrm{T}}\boldsymbol{P} + \boldsymbol{Q} + \boldsymbol{R} + \boldsymbol{N}_1 + \boldsymbol{N}_1^{\mathrm{T}} + \boldsymbol{C}^{\mathrm{T}}\boldsymbol{C}, \\ \boldsymbol{\Gamma}_{12} &= \boldsymbol{P}\boldsymbol{A}_d + \boldsymbol{M}_1 - \boldsymbol{N}_1 + \boldsymbol{N}_2^{\mathrm{T}}, \\ \boldsymbol{\Gamma}_{12} &= (\mu - 1)\boldsymbol{Q} + \boldsymbol{M}_2 + \boldsymbol{M}_2^{\mathrm{T}} - \boldsymbol{N}_2 - \boldsymbol{N}_2^{\mathrm{T}}. \end{aligned}$$

3.3. Condition of robust H_∞ rotating consensus

Theorem 1. Assume that the interaction graph $\mathcal{G}$ is connected. For given positive constants τ, μ and γ, by distributed protocol (3), multi-agent system (1) can reach rotating consensus while satisfying desired H_∞ disturbance attenuation index, if there exist positive definite matrices $\boldsymbol{Q}$, $\boldsymbol{R}$, $\boldsymbol{S}$, $\boldsymbol{T}$, $\boldsymbol{X} \in \mathcal{R}^{6\times 6}$, matrices $\boldsymbol{M}_1$, $\boldsymbol{M}_2$, $\boldsymbol{N}_1$, $\boldsymbol{N}_2 \in \mathcal{R}^{6\times 6}$, $\boldsymbol{Y} \in \mathcal{R}^{3\times 6}$ and a positive scalar ε such that

$$\boldsymbol{\Phi}_i = \begin{bmatrix} \boldsymbol{\Phi}_{i0} & \boldsymbol{\Pi}_{i1}^{\mathrm{T}} & \boldsymbol{\Pi}_2^{\mathrm{T}} & \boldsymbol{H}^{\mathrm{T}} \\ * & -\boldsymbol{T} + \varepsilon\lambda_i^2\tau^2\boldsymbol{B}_1\boldsymbol{G}\boldsymbol{G}^{\mathrm{T}}\boldsymbol{B}_1^{\mathrm{T}} & 0 & 0 \\ * & * & -\boldsymbol{X}\boldsymbol{T}^{-1}\boldsymbol{X} & 0 \\ * & * & * & -\varepsilon\boldsymbol{I} \end{bmatrix} < 0 \tag{11}$$

is satisfied for $i = 1$ and $n-1$, where

$$\boldsymbol{\Phi}_{i0} = \begin{bmatrix} \boldsymbol{\Phi}_{i11} & \boldsymbol{\Phi}_{i12} & -\boldsymbol{M}_1 & \boldsymbol{B}_2 & 0 & \tau\boldsymbol{M}_1 & \tau\boldsymbol{N}_1 & \boldsymbol{X} \\ * & \boldsymbol{\Phi}_{22} & -\boldsymbol{M}_2 & 0 & 0 & \tau\boldsymbol{M}_2 & \tau\boldsymbol{N}_2 & 0 \\ * & * & -\boldsymbol{R} & 0 & 0 & 0 & 0 & 0 \\ * & * & * & -\gamma^2\boldsymbol{I} & 0 & 0 & 0 & 0 \\ * & * & * & * & -\tau\boldsymbol{S} & 0 & 0 & 0 \\ * & * & * & * & * & -\tau\boldsymbol{S} & 0 & 0 \\ * & * & * & * & * & * & -\tau\boldsymbol{S} & 0 \\ * & * & * & * & * & * & * & -\boldsymbol{I} \end{bmatrix},$$

$$\boldsymbol{\Phi}_{i11} = \boldsymbol{A}\boldsymbol{X} + \boldsymbol{X}\boldsymbol{A}^{\mathrm{T}} + \boldsymbol{Q} + \boldsymbol{R} + \boldsymbol{N}_1 + \boldsymbol{N}_1^{\mathrm{T}} + \varepsilon\lambda_i^2\boldsymbol{B}_1\boldsymbol{G}\boldsymbol{G}^{\mathrm{T}}\boldsymbol{B}_1^{\mathrm{T}},$$

$$\boldsymbol{\Phi}_{i12} = -\lambda_i\boldsymbol{B}_1\boldsymbol{Y} + \boldsymbol{M}_1 - \boldsymbol{N}_1 + \boldsymbol{N}_2^{\mathrm{T}},$$

$$\boldsymbol{\Phi}_{22} = (\mu-1)\boldsymbol{Q} + \boldsymbol{M}_2 + \boldsymbol{M}_2^{\mathrm{T}} - \boldsymbol{N}_2 - \boldsymbol{N}_2^{\mathrm{T}},$$

$$\boldsymbol{\Pi}_{i1} = [\tau\boldsymbol{A}\boldsymbol{X} + \varepsilon\lambda_i^2\tau\boldsymbol{B}_1\boldsymbol{G}\boldsymbol{G}^{\mathrm{T}}\boldsymbol{B}_1^{\mathrm{T}}, -\lambda_i\tau\boldsymbol{B}_1\boldsymbol{Y}, 0, \tau\boldsymbol{B}_2, 0, 0, 0, 0],$$

$$\boldsymbol{\Pi}_2 = [0, 0, 0, 0, \boldsymbol{S}, 0, 0, 0],$$

$$H = [0, \boldsymbol{E}\boldsymbol{Y}, 0, 0, 0, 0, 0, 0].$$

Proof: According to Lemma 3, the subsystem (11) is asymptotically stable with $\boldsymbol{T}_{\hat{w}\hat{z}}(s)_\infty < \gamma$, if there exist positive definite matrices $\boldsymbol{P}$, $\boldsymbol{Q}$, $\boldsymbol{R}$, $\boldsymbol{S}$ and matrices $\boldsymbol{M}_1$, $\boldsymbol{M}_2$, $\boldsymbol{N}_1$, $\boldsymbol{N}_2$ with appropriate dimensions such that

$$\begin{bmatrix} \boldsymbol{\Gamma}_{11} & \boldsymbol{\Gamma}_{i12} & -\boldsymbol{M}_1 & \boldsymbol{P}\boldsymbol{B}_2 & \tau\boldsymbol{A}^{\mathrm{T}}\boldsymbol{S} & \tau\boldsymbol{M}_1 & \tau\boldsymbol{N}_1 \\ * & \boldsymbol{\Gamma}_{22} & -\boldsymbol{M}_2 & 0 & -\lambda_i\tau(\boldsymbol{B}_d\boldsymbol{K})^{\mathrm{T}}\boldsymbol{S} & \tau\boldsymbol{M}_2 & \tau\boldsymbol{N}_2 \\ * & * & -\boldsymbol{R} & 0 & 0 & 0 & 0 \\ * & * & * & -\gamma^2\boldsymbol{I} & \tau\boldsymbol{B}_2^{\mathrm{T}}\boldsymbol{S} & 0 & 0 \\ * & * & * & * & -\tau\boldsymbol{S} & 0 & 0 \\ * & * & * & * & * & -S & 0 \\ * & * & * & * & * & * & -\boldsymbol{S} \end{bmatrix} \triangleq \boldsymbol{\Gamma}_i < 0, \quad (12)$$

where

$$\boldsymbol{B}_d = \boldsymbol{B}_1 + \Delta\boldsymbol{B}_1(t)\,,$$
$$\boldsymbol{\Gamma}_{11} = \boldsymbol{P}\boldsymbol{A} + \boldsymbol{A}^{\mathrm{T}}\boldsymbol{P} + \boldsymbol{Q} + \boldsymbol{R} + \boldsymbol{N}_1 + \boldsymbol{N}_1^{\mathrm{T}} + \boldsymbol{I}\,,$$
$$\boldsymbol{\Gamma}_{i12} = -\lambda_i\boldsymbol{P}\boldsymbol{B}_d\boldsymbol{K} + \boldsymbol{M}_1 - \boldsymbol{N}_1 + \boldsymbol{N}_2^{\mathrm{T}}\,,$$
$$\boldsymbol{\Gamma}_{22} = (\mu - 1)\,\boldsymbol{Q} + \boldsymbol{M}_2 + \boldsymbol{M}_2^{\mathrm{T}} - \boldsymbol{N}_2 + \boldsymbol{N}_2^{\mathrm{T}}\,.$$

Due to the convex property of linear matrix inequality (LMI) of $\boldsymbol{\Gamma}_i$, $\boldsymbol{\Gamma}_i < 0$ for all $i = 1, 2, n-1$ if and only if $\boldsymbol{\Gamma}_1 < 0$ and $\boldsymbol{\Gamma}_{n-1} < 0$, which is associated with the smallest eigenvalues λ_1 and the largest eigenvalues λ_{n-1}, respectively.

Pre- and post-multiplying the inequality (12) with

$$\mathrm{diag}\left\{\boldsymbol{P}^{-1}, \boldsymbol{P}^{-1}, \boldsymbol{P}^{-1}, \boldsymbol{I}, \boldsymbol{P}^{-1}, \boldsymbol{P}^{-1}, \boldsymbol{P}^{-1}\right\}$$

and applying the variable changes $\boldsymbol{X} = \boldsymbol{P}^{-1}$, $\hat{*} = \boldsymbol{P}^{-1} * \boldsymbol{P}^{-1}$, where $*$ denotes $\boldsymbol{Q}, \boldsymbol{R}, \boldsymbol{S}, \boldsymbol{M}_1, \boldsymbol{M}_2, \boldsymbol{N}_1, \boldsymbol{N}_2$, the inequality (12) is congruent to $\hat{\boldsymbol{\Gamma}}_{i0} + \hat{\boldsymbol{\Gamma}}_{i1} + \hat{\boldsymbol{\Gamma}}_{i1}^{\mathrm{T}} < 0$. On one hand, $\hat{\boldsymbol{\Gamma}}_{i1}$ can be rewritten as $\hat{\boldsymbol{\Gamma}}_{i1} = \hat{\boldsymbol{\Pi}}_{i1}^{\mathrm{T}}\boldsymbol{X}^{-1}\hat{\boldsymbol{\Pi}}_2$, where $\hat{\boldsymbol{\Pi}}_2 = \left[0, 0, 0, 0, \hat{\boldsymbol{S}}, 0, 0\right]$ and $\hat{\boldsymbol{\Pi}}_{i1} = [\tau\boldsymbol{A}\boldsymbol{X}, -\lambda_i\tau\boldsymbol{B}_d\boldsymbol{K}\boldsymbol{X}, 0, \tau\boldsymbol{B}_2, 0, 0, 0]$. On the other hand, according to square inequality, it is easy to construct the following inequality:

$$\hat{\boldsymbol{\Pi}}_{i1}^{\mathrm{T}}\boldsymbol{X}^{-1}\hat{\boldsymbol{\Pi}}_2 + (\hat{\boldsymbol{\Pi}}_{i1}^{\mathrm{T}}\boldsymbol{X}^{-1}\hat{\boldsymbol{\Pi}}_2)^{\mathrm{T}} \leq \hat{\boldsymbol{\Pi}}_{i1}^{\mathrm{T}}\boldsymbol{T}^{-1}\hat{\boldsymbol{\Pi}}_{i1} + \hat{\boldsymbol{\Pi}}_2^{\mathrm{T}}\boldsymbol{X}^{-1}\boldsymbol{T}\boldsymbol{X}^{-1}\hat{\boldsymbol{\Pi}}_2\,,$$

where $\boldsymbol{T}$ is any symmetric positive definite matrix with appropriate dimensions. Therefore, $\hat{\boldsymbol{\Gamma}}_{i0} + \hat{\boldsymbol{\Pi}}_{i1}^{\mathrm{T}}\boldsymbol{T}^{-1}\hat{\boldsymbol{\Pi}}_{i1} + \hat{\boldsymbol{\Pi}}_2^{\mathrm{T}}\boldsymbol{X}^{-1}\mathrm{T}\boldsymbol{X}^{-1} < 0$ implies that $\hat{\boldsymbol{\Gamma}}_i < 0$. Then, defining $\boldsymbol{Y} = \boldsymbol{K}\boldsymbol{X}$ and applying Lemma 2 (Schur complement formula) on $\hat{\boldsymbol{\Gamma}}_{i0} + \hat{\boldsymbol{\Pi}}_{i1}^{\mathrm{T}}\boldsymbol{T}^{-1}\hat{\boldsymbol{\Pi}}_{i1} + \hat{\boldsymbol{\Pi}}_2^{\mathrm{T}}\boldsymbol{X}^{-1}\boldsymbol{T}\boldsymbol{X}^{-1} < 0$, we obtain the matrix inequality condition

$$\bar{\boldsymbol{\Phi}}_i = \begin{bmatrix} \bar{\boldsymbol{\Phi}}_{i0} & \bar{\boldsymbol{\Pi}}_{i1}^{\mathrm{T}} & \bar{\boldsymbol{\Pi}}_2^{\mathrm{T}} \\ * & -\boldsymbol{T} & 0 \\ * & * & -\boldsymbol{X}\boldsymbol{T}^{-1}\boldsymbol{X}\,, \end{bmatrix} < 0 \quad (13)$$

where

$$\bar{\boldsymbol{\Pi}}_{i1} = [\tau\boldsymbol{A}\boldsymbol{X}, -\lambda_i\boldsymbol{B}_d\boldsymbol{K}\boldsymbol{X}, 0, \tau\boldsymbol{B}_2, 0, 0, 0, 0],$$
$$\bar{\boldsymbol{\Pi}}_2 = [0, 0, 0, 0, \hat{\boldsymbol{S}}, 0, 0, 0]$$
,

$$\bar{\boldsymbol{\Pi}}_{i0} = \begin{bmatrix} \bar{\boldsymbol{\Pi}}_{11} & \bar{\boldsymbol{\Pi}}_{i12} & -\hat{\boldsymbol{M}}_1 & \boldsymbol{B}_2 & 0 & \tau\hat{\boldsymbol{M}}_1 & \tau\hat{\boldsymbol{N}}_1 & \boldsymbol{X} \\ * & \boldsymbol{\Pi}_{22} & -\hat{\boldsymbol{M}}_2 & 0 & 0 & \tau\hat{\boldsymbol{M}}_2 & \tau\hat{\boldsymbol{N}}_2 & 0 \\ * & * & -\hat{\boldsymbol{R}} & 0 & 0 & 0 & 0 & 0 \\ * & * & * & -\gamma^2\boldsymbol{I} & 0 & 0 & 0 & 0 \\ * & * & * & * & -\tau\hat{\boldsymbol{S}} & 0 & 0 & 0 \\ * & * & * & * & * & -\hat{\boldsymbol{S}} & 0 & 0 \\ * & * & * & * & * & * & -\hat{\boldsymbol{S}} & 0 \\ * & * & * & * & * & * & * & -\boldsymbol{I} \end{bmatrix},$$

$$\bar{\boldsymbol{\Pi}}_{11} = \boldsymbol{A}\boldsymbol{X} + \boldsymbol{X}\boldsymbol{A}^{\mathrm{T}} + \hat{\boldsymbol{Q}} + \hat{\boldsymbol{R}} + \hat{\boldsymbol{N}}_1 + \hat{\boldsymbol{N}}_1^{\mathrm{T}},$$

$$\bar{\boldsymbol{\Pi}}_{i12} = -\lambda_i\boldsymbol{B}_d\boldsymbol{Y} + \hat{\boldsymbol{M}}_1 - \hat{\boldsymbol{N}}_1 + \hat{\boldsymbol{N}}_2^{\mathrm{T}},$$

$$\bar{\boldsymbol{\Pi}}_{22} = (\mu-1)\hat{\boldsymbol{Q}} + \hat{\boldsymbol{M}}_2 + \hat{\boldsymbol{M}}_2^{\mathrm{T}} - \hat{\boldsymbol{N}}_1 - \hat{\boldsymbol{N}}_1^{\mathrm{T}}.$$

Note that $\boldsymbol{B}_d = \boldsymbol{B}_1 + \Delta\boldsymbol{B}_1(t) = \boldsymbol{B}_1 + \boldsymbol{B}_1\boldsymbol{G}\boldsymbol{F}(t)\boldsymbol{E}$. Define

$$\begin{aligned} \boldsymbol{J}_i &\triangleq [-\lambda_i(\boldsymbol{B}_1\boldsymbol{G})^{\mathrm{T}}, 0, 0, 0, 0, 0, 0, 0, -\lambda_i\tau(\boldsymbol{B}_1\boldsymbol{G})^{\mathrm{T}}, 0]^{\mathrm{T}}, \\ \boldsymbol{H} &\triangleq [0, \boldsymbol{E}\boldsymbol{Y}, 0, 0, 0, 0, 0, 0, 0, 0]. \end{aligned}$$

Now we can obtain $\bar{\boldsymbol{\Phi}}_i = \hat{\boldsymbol{\Phi}}_i + \boldsymbol{J}_i\boldsymbol{F}(t)\boldsymbol{H} + \boldsymbol{H}^{\mathrm{T}}\boldsymbol{F}^{\mathrm{T}}(t)\boldsymbol{J}_i^{\mathrm{T}}$, where $\hat{\boldsymbol{\Phi}}_i$ is constructed through replacing $\boldsymbol{B}_d$ term in $\bar{\boldsymbol{\Phi}}_i$ with $\boldsymbol{B}_1$. Note that $\boldsymbol{F}^{\mathrm{T}}(t)\boldsymbol{F}(t) \leq \boldsymbol{I}$, so that there exists an $\varepsilon > 0$ such that $\hat{\boldsymbol{\Phi}}_i + \varepsilon\boldsymbol{J}_i\boldsymbol{J}_i^{\mathrm{T}} + \varepsilon^{-1}\boldsymbol{H}^T\boldsymbol{H} < 0$ guaranteeing $\bar{\boldsymbol{\Phi}}_i < 0$. Therefore, applying Lemma 2 on $\hat{\boldsymbol{\Phi}}_i + \varepsilon\boldsymbol{J}_i\boldsymbol{J}_i^{\mathrm{T}} + \varepsilon^{-1}\boldsymbol{H}^{\mathrm{T}}\boldsymbol{H} < 0$ and using the definitions $* \triangleq \hat{*}$, where $*$ denotes $\boldsymbol{Q}, \boldsymbol{R}, \boldsymbol{S}, \boldsymbol{M}_1, \boldsymbol{M}_2, N_1, \boldsymbol{N}_2$, we can obtain that $\boldsymbol{\Phi}_i < 0$ (see (11)) and $\boldsymbol{K} = \boldsymbol{Y}\boldsymbol{X}^{-1}$.

On the basis of the above analysis, if $\boldsymbol{\Phi}_1 < 0$, $\boldsymbol{\Phi}_{n-1} < 0$ and $\boldsymbol{K} = \boldsymbol{Y}\boldsymbol{X}^{-1}$, the subsystems (9) are simultaneously asymptotically stable with $\boldsymbol{T}_{\hat{w}\hat{z}}(s)_\infty < \gamma$. Then, by Lemma 1, the multi-agent system (1) reaches rotating consensus while satisfying desired H_∞ disturbance with attenuation index γ. This completes the proof.

3.4. Algorithm for robust H_∞ rotating consensus

Because the matrix inequality condition (11) is not in the form of LMI, we cannot directly use the LMI method to solve the matrix inequality (11). But we can turn this problem into the LMI optimization problem by the cone-complementary linearization algorithm [13]. First, we define a new variable $\boldsymbol{U} = \boldsymbol{U}^{\mathrm{T}} > 0$ such that $\boldsymbol{U} \leq \boldsymbol{X}\boldsymbol{T}^{-1}\boldsymbol{X}$. It is easy to derive that $\boldsymbol{U}^{-1} - \boldsymbol{X}^{-1}\boldsymbol{T}\boldsymbol{X}^{-1} \geq 0$. Furthermore, by defining $\bar{\boldsymbol{X}} \triangleq \boldsymbol{X}^{-1}$, $\bar{\boldsymbol{T}} \triangleq \boldsymbol{T}^{-1}$, $\bar{\boldsymbol{U}} \triangleq \boldsymbol{U}^{-1}$, and using Lemma 2, we can turn the condition (11) into

$$\begin{bmatrix} \boldsymbol{\Phi}_{i0} & \boldsymbol{\Pi}_{i1}^{\mathrm{T}} & \boldsymbol{\Pi}_2^{\mathrm{T}} & \boldsymbol{H}^{\mathrm{T}} \\ * & -\boldsymbol{T} + \varepsilon\lambda_i^2\tau^4\boldsymbol{B}_1\boldsymbol{G}\boldsymbol{G}^{\mathrm{T}}\boldsymbol{B}_1^{\mathrm{T}} & 0 & 0 \\ * & * & \boldsymbol{U} & 0 \\ * & * & * & -\varepsilon\boldsymbol{I} \end{bmatrix} < 0 \tag{14}$$

and

$$\begin{bmatrix} \bar{\boldsymbol{U}} & \bar{\boldsymbol{X}} \\ \bar{\boldsymbol{X}} & \bar{\boldsymbol{T}} \end{bmatrix} \geq 0, \begin{bmatrix} \bar{\boldsymbol{X}} & \boldsymbol{I} \\ \boldsymbol{I} & \boldsymbol{X} \end{bmatrix} \geq 0, \begin{bmatrix} \bar{\boldsymbol{T}} & \boldsymbol{I} \\ \boldsymbol{I} & \boldsymbol{T} \end{bmatrix} \geq 0, \begin{bmatrix} \bar{U} & \boldsymbol{I} \\ \boldsymbol{I} & \boldsymbol{U} \end{bmatrix} \geq 0. \tag{15}$$

Then, we may solve the following optimization problem and find a feasible solution satisfying $\boldsymbol{U} \leq \boldsymbol{X}\boldsymbol{T}^{-1}\boldsymbol{X}$:

$$\begin{array}{ll} \min & \text{Trace}(\bar{\boldsymbol{X}}\boldsymbol{X} + \bar{\boldsymbol{T}}\boldsymbol{T} + \bar{\boldsymbol{U}}\boldsymbol{U}) \\ \text{s.t.} & (14), (15). \end{array} \tag{16}$$

In conclusion, in order to solve matrix inequality condition (11), an algorithm is designed as follows:

Algorithm 1:

Step 1. Solve the LMIs (14) and (15) for given positive scalar constants τ, μ and γ. There exists a feasible solution set $\{\bar{\boldsymbol{X}}_0, \boldsymbol{X}_0, \bar{\boldsymbol{T}}_0, \boldsymbol{T}_0, \bar{\boldsymbol{U}}_0, \boldsymbol{U}_0,\}$ and set $k = 0$.

Step 2. Solve the following optimization problem for the variables

$$\begin{array}{ll} & \{\bar{\boldsymbol{X}}, \boldsymbol{X}, \bar{\boldsymbol{T}}, \boldsymbol{T}, \bar{\boldsymbol{U}}, \boldsymbol{U}\}, \\ \min & \text{Trace}(\bar{\boldsymbol{X}}_k\boldsymbol{X} + \bar{\boldsymbol{T}}_k\boldsymbol{T} + \bar{\boldsymbol{U}}_k\boldsymbol{U} + \bar{\boldsymbol{X}}\boldsymbol{X}_k + \bar{\boldsymbol{T}}\boldsymbol{T}_k + \bar{\boldsymbol{U}}\boldsymbol{U}_k), \\ \text{s.t.} & (14),\ (15) \end{array} \tag{17}$$

and set $\bar{\boldsymbol{X}}_{k+1} = \bar{\boldsymbol{X}}$, $\boldsymbol{X}_{k+1} = \boldsymbol{X}$, $\bar{\boldsymbol{T}}_{k+1} = \bar{\boldsymbol{T}}$, $\boldsymbol{T}_{k+1} = \boldsymbol{T}$, $\bar{\boldsymbol{U}}_{k+1} = \bar{\boldsymbol{U}}$, $\boldsymbol{U}_{k+1} = \boldsymbol{U}$.

Step 3. If $\boldsymbol{U} \leq \boldsymbol{X}\boldsymbol{T}^{-1}\boldsymbol{X}$ for the above solution set, then save the current $\boldsymbol{X}$, $\boldsymbol{Y}$ and exit. Otherwise, set $k = k + 1$, go to step 2 and repeat the optimization for a prescribed maximum iterative number $k_{\max}$ until finding a feasible solution satisfying $\boldsymbol{U} \leq \boldsymbol{X}\boldsymbol{T}^{-1}\boldsymbol{X}$. If such a solution does not exist, then exit.

If a feasible solution set is found by Algorithm 1 for the given disturbance attenuation index γ, delay parameter τ and μ by distributed protocol (3), the multi-agent system (1) can reach rotating consensus with the desired H_∞ disturbance attenuation index γ and the feedback matrix can be constructed by $\boldsymbol{K} = [\boldsymbol{K}_v\ \boldsymbol{K}_c] = \boldsymbol{Y}\boldsymbol{X}^{-1}$.

4. Result analysis and discussion

To illustrate the obtained theoretical results and optimization algorithms, numerical simulations will be given in this section. Figure 1 shows a communication topology for the multi-agent system (1) when $n = 4$.

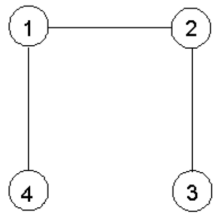

Fig. 1. Communication topology of four-agent system

Suppose that the weight of each edge is 1, the desired angular velocity $\omega = 1$ and the normal vector of the desired rotating plane $\mathrm{i}_\omega = \begin{bmatrix} -0.5 & -0.5 & 0.5\sqrt{2} \end{bmatrix}^{\mathrm{T}}$.In order to clearly reflect the effect of external disturbances to the rotating consensus performance, we first assume the external disturbance

$$w(t) = [0.4, 0.1, 0.9, 0.2, 0, 0.4, -0.5, -0.3, -0.8, -0.5, -0.3, -1.3]^{\mathrm{T}}$$

where $\varepsilon(t) = \begin{cases} 1 & 0 \le t \le 1 \\ 0 & \text{otherwise} \end{cases}$.

Secondly, we suppose that the parameter uncertainty matrix $\Delta \boldsymbol{B}(t) = \boldsymbol{G}\boldsymbol{F}(t)\boldsymbol{E}$, where $\boldsymbol{G} = [0.02, 0.01, 0; 0.01, 0.02, 0; 0, 0, 0.01]$, $\boldsymbol{F}(t) = \mathrm{diag}\{\sin 10t, \sin 20t, \cos 20t\}$ and $\boldsymbol{E} = \boldsymbol{I}_3$. At last, we presume that the initial state of the multi-agent system is taken as $\xi(t=0) = 1_4 \otimes \left[v_0^{\mathrm{T}}, c_0^{\mathrm{T}}\right]^{\mathrm{T}}$, where $v_0 = R_{\omega 0}^{\mathrm{T}}[0, -1, 0]^{\mathrm{T}}$ and $c_0 = [0, 0, 0]^{\mathrm{T}}$.

Suppose that the H_∞ performance index $\gamma = 0.8$ and the delay $d(t) = 0.1 \sin t$ (so $\tau = \mu = 0.1$). By Theorem 1 and Algorithm 1, we can figure out the feedback matrix $\boldsymbol{K}$ as follows:

$$\begin{bmatrix} 1.4296 & 0.9149 & -0.6213 & 0.1279 & 0.2114 & 0.8991 \\ 0.2846 & 1.4329 & -1.0665 & -0.9176 & 0.1322 & 0.1044 \\ -1.0628 & -0.6188 & 2.0203 & 0.1012 & 0.8966 & -0.2231 \end{bmatrix}.$$

On one hand, Fig. 2 shows the position trajectories of all agents. It is clear that all agents reach an agreement on their positions while surrounding a common point c with a desired angular velocity ω on a plane perpendicular to the vector i_ω.

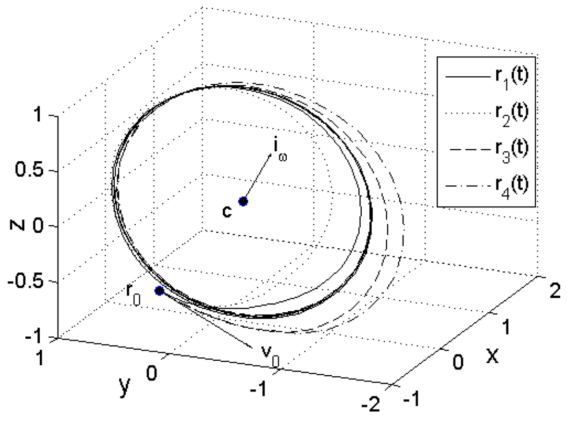

Fig. 2. Position trajectories of all agents

On the other hand, Fig. 3 shows the energy relation of the controlled output and external disturbance. Obviously, the rotating consensus of the multi-agent system is achieved with the H_∞ disturbance attenuation index.

Therefore, using the distributed protocol (3) and calculating the feedback ma-

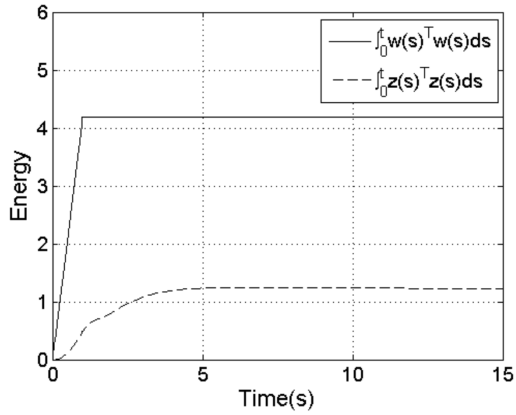

Fig. 3. Energy trajectories of the controlled output $z(t)$ and external disturbance $w(t)$

trix $\boldsymbol{K}$ by Theorem 1 and Algorithm 1, the multi-agent system can reach rotating consensus while satisfying the desired H_∞ disturbance attenuation index. So we validate the effectiveness of the proposed protocol and demonstrate the correctness of Theorem 1 and Algorithm 1.

5. Conclusion

In this paper, robust delay-dependent H_∞ control problems are studied for rotating consensus of second-order multi-agent systems with parameter uncertainties, external disturbances and time-varying delay in three-dimensional space. Firstly, a rotating consensus is defined in three-dimensional space. Based on state feedback of neighbors, a distributed control protocol is designed. Then a sufficient delay-dependent condition in terms of the matrix inequalities is derived to make all agents asymptotically reach rotating consensus with the desired H_∞ performance index. Furthermore, an algorithm is elaborately designed to get feasible solution to this condition. The main contributions of this paper are as follows: First, the influence of parameter uncertainty, external disturbances and time-varying delay on rotating consensus are considered at the same time; Second, a delay-dependent control condition is derived, whose complexity is lower because the system is decoupled; Third, an algorithm is proposed for calculating parameters of control protocol.

References

[1] R. Sepulchre, D. A. Paley, N. E. Leonard: *Stabilization of planar collective motion with limited communication.* IEEE Transactions on Automatic Control *53* (2008), No. 3, 706–719.

[2] P. Lin, Y. M. Jia: *Distributed rotating formation control of multi-agent systems.* Sys-

tems & Control Letters *59* (2010), No. 10, 587–595.

[3] P. Lin, K. Y. Qin, Z. K. Li, W. Ren: *Collective rotating motions of second-order multi-agent systems in three-dimensional space.* Systems & Control Letters *60* (2011), No. 6, 365–372.

[4] T. Yang, Y. H. Jin: *Multi-agent rotating consensus without relative velocity measurements in three-dimensional space.* International Journal of Robust and Nonlinear Control *23* (2013), No. 5, 473–482.

[5] P. Lin, W. T. Lu, Y. D. Song: *Collective composite-rotating consensus of multi-agent systems.* Commun. Chinese Physics B *23* (2014), No. 4, 040503.

[6] P. Lin, Y. M. Jia: *Robust H_∞ consensus analysis of a class of second-order multi-agent systems with uncertainty.* IET Control Theory & Applications *4* (2010) No. 3, 487–498.

[7] Z. K. Li, Z. S. Duan, G. R. Chen: *On H_∞ and H_2 performance regions of multi-agent systems.* Automatica *47* (2011), No. 4, 797–803.

[8] Y. Liu, Y. M. Jia: *H_∞ consensus control for multi-agent systems with linear coupling dynamics and communication delays.* International Journal of Systems Science *43* (2012), No. 1, 50–62.

[9] Y. B. Hu, P. Li, J. Lam: *On the synthesis of H_∞ consensus for multi-agent systems.* IMA Journal of Mathematical Control and Information *32* (2015), No. 3, 591–607.

[10] P. Li, K. Y. Qin, M. J. Shi: *Distributed robust rotating consensus control for directed networks of second-order agents with mixed uncertainties and time-delay.* Neurocomputing *148*, (2015), 332–339.

[11] R. H. Battin: *An introduction to the mathematics and methods of astrodynamics.* Published by American Institute of Aeronautics and Astronautics, AIAA Education Series (1999).

[12] H. Yazici, R. Guclu, I. B. Kucukdemiral, M. N. A. Parlakci: *Robust delay-dependent H_∞ control for uncertain structural systems with actuator delay.* Journal of Dynamic Systems, Measurement, and Control (ASME) *134* (2012), No. 3, 031013.

[13] L. el Ghaoui, F. Oustry, M. A. Rami: *A cone complementarity linearization algorithm for static output-feedback and related problems.* IEEE Transactions on Automatic Control *42* (1997), No. 8, 1171–1176.

Received April 23, 2017

Acta Technica *62*, No. 1A/2017, 135–144

Application of quasi Monte Carlo polymerization re-sampling particle filter algorithm in airborne passive location[1]

Hongping Pu[2], Kaiyu Qin[2]

Abstract. Aiming at the problems that the the performance of the airborne passive location filter is poor and the noise is small, a method of Quasi Monte Carlo polymerization re-sampling particle filter algorithm is proposed in this paper, and which is applied to the airborne passive location. Weighted aggregation of similar particles in the discrete space is carried out, so as to make the particles in a reasonable space distribution, and also effectively suppress the degradation of the particles. Then the Quasi Monte Carlo technique is used to move the heavily sampled particles to the high likelihood region to optimize the distribution characteristics of the particles, and improve the accuracy of the filter. Finally, the simulation analysis of several algorithms is carried out in three conditions. The results show that the application of the Quasi Monte Carlo polymerization re-sampling particle filter algorithm in airborne passive location can improve the filtering precision and positioning efficiency.

Key words. Airborne passive location, quasi Monte Carlo, aggregated re-sampling particle filter.

1. Introduction

In the information warfare, because the airborne location radar has many problems [1], the research scholars have to search for the new airborne positioning technology at home and abroad, so that the passive location technology has been widely concerned [2]. Passive location technology has very important significance for the modern information warfare because of its low weight, wide range of positioning and strong concealment [3]. Passive tracking algorithm has become the core of passive location technology in recent years, because it cannot get the distance between the

[1]This work was supported by the Specialized Research Fund for the Doctoral Program of Higher Education of China under Grants No. 20130185110023.

[2]School of Astronautics and Aeronautics, University of Electronic Science and Technology of China, Chengdu, 611731, China

observation station and the signal transmitting point, so it needs to calculate the distance by the positioning algorithm [4]. In general, the distance measurement formula of the single observer passive location system is a very difficult nonlinear equation, at the same time, it has a large error in the position information, based on this, which must be processed by the observation equation of the passive location system. Compared with the traditional positioning and tracking algorithm, the single observer passive location is more difficult to be processed because of its own characteristics [5]. Because the observability performance of the system is weak, the equation is difficult to be solved, and the error is big, it also can appear the filter efficiency low and other problems, so the passive tracking algorithm has become the core of the research of the airborne positioning technology in recent years.

In recent years, the particle filter (PF) algorithm is applied to the nonlinear filtering problem, the probability distribution of random variables is calculated by a large number of random samples and their corresponding assignment. However, due to the poor performance of the airborne passive location, the initial errors and the co-variance of which are large. The standard particle filter algorithm is prone to degradation and impoverishment and other issues, which will lead to the poor filtering performance. In this regard, Klaas proposed a higher efficiency of the Gauss particle filter algorithm [6]. The core idea of which is to make the post probability distribution of airborne location state information approach to the Gauss distribution, and take the Quasi Monte Carlo integral to reduce the mean and co-variance of the sample. Gauss particle filter algorithm has no re-sampling, so the filter performance can be improved. However, in the use of single station passive location system, the noise is small, so it is easy to make data samples appear aggregation condition, so as to reduce the accuracy of positioning estimation. Based on this, Moradkhani proposed the Quasi Monte Carlo (QMC) algorithm and the Quasi Monte Carlo Goss particle filter (QMCGPF) algorithm, and the estimation accuracy could be obtained by using the Monte Carlo samples randomly generated in the sample space [7]. But because the operation rate is proportional to the number of the sample particles, so the speed of the operation of the system will be greatly decreased with the increase of the number of the samples.

Based on this, a method of Quasi Monte Carlo polymerization re-sampling particle filter algorithm is proposed in this paper, and which is applied to the airborne passive location. Weighted aggregation of similar particles in the discrete space is carried out, so that the particles are in a reasonable space distribution, so as to effectively suppress the degradation of the particles; The Quasi Monte Carlo technique is used to move the heavily sampled particles into the high likelihood region to optimize the distribution characteristics of the particles, so as to improve the accuracy of the filter. Finally, a variety of algorithms are simulated and analyzed.

2. State of the art

The airborne passive location system is quite different from the ground fixed position system, because its measurement is carried out under the coordinate system of the body, so it is necessary to convert the data measured by the airborne posi-

tioning system to the data of the ground fixed coordinate system. First of all, the body coordinate system is defined, it is assumed that the body centroid is the origin of the airborne passive location coordinate system, and the flight direction of the aircraft is the Y' axis, the direction which is perpendicular to the direction of the Y' axis is the Z' axis. Transformation of the coordinate system is shown in Fig. 1.

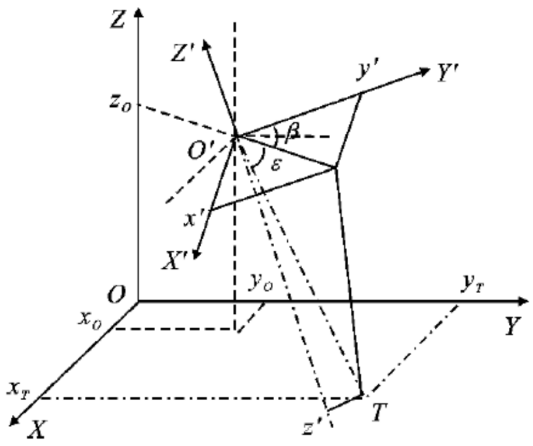

Fig. 1. Observer and object in three-dimensional geometry

The state vector and attitude information of the body at time T_k can be obtained by GPS and airborne navigation equipment. The relative state vector of the airborne passive location and the passive location in the body coordinate system is

$$X_{0k} = [x_{\mathrm{T}k},\, y_{\mathrm{T}k},\, z_{\mathrm{T}k},\, \dot{x}_{\mathrm{T}k},\, \dot{y}_{\mathrm{T}k},\, \dot{z}_{\mathrm{T}k}]^{\mathrm{T}} \,.$$

Here, $x_{\mathrm{T}k}$, $y_{\mathrm{T}k}$, $z_{\mathrm{T}k}$ is the target position in the XYZ coordinate system and $\dot{x}_{\mathrm{T}k}$, $\dot{y}_{\mathrm{T}k}$, $\dot{z}_{\mathrm{T}k}$ is the target position in the $X'Y'Z'$ coordinate system.

Based on the above assumptions, the coordinate conversion of the position vector can be considered as:

$$\left[x_k^{'},\, y_k^{'},\, z_k^{'}\right]^{\mathrm{T}} = A_k \left[x_{\mathrm{T}k} - x_{0k},\, y_{\mathrm{T}k} - y_{0k},\, -z_{0k}\right]^{\mathrm{T}} \,. \tag{1}$$

Here, A_k represents the matrix of the ground coordinate system and body coordinate system transformation [8], and x_{0k}, y_{0k}, z_{0k} is the position of point $0'$ in the XYZ coordinate system. Vector $\left[x_k^{'},\, y_k^{'},\, z_k^{'}\right]$ is speed. In the same way, the speed loss between the two systems can be expressed in the formula (1).

The state equation and observation equation are established in the following way:

$$X_{Tk+1} = f\left(X_{Tk}, w_k\right) = \Phi_k X_{Tk} + G_k w_k \,, \tag{2}$$

$$Z_k = \left[\beta_k, \varepsilon_k, \dot{\beta}_k, \dot{\varepsilon}_k, \dot{f}_{dk}\right]^{\mathrm{T}} + v_k \,. \tag{3}$$

In the equation, the state transition matrix is represented by

$$\Phi_k = \begin{bmatrix} I_2 & TI_2 \\ 0 & I_2 \end{bmatrix}, \quad G_k = \begin{bmatrix} T^2 I_2/2 \\ TI_2 \end{bmatrix} .$$

The process noise is expressed by w_k, and the observation noise is expressed by v_k. The process noise and observation noise are independent of each other, and the Gauss noise is of zero mean; $E\left[w_i, w_j^{\mathrm{T}}\right] = O_k\delta_{ij}$, $E\left[v_i, v_j^T\right] = R_k\delta_{ij}$, the measurement period is expressed by T, and the 2-order unit matrix is expressed by I_2. Symbols X_{Tk+1} and X_{Tk} are $k+1$th and kth time state vectors, and Z_k is kth time observation vector. Symbols β_k and ε_k are target bear in the XYZ coordinates in the kth time while $\dot{\beta}_k$ and $\dot{\varepsilon}_k$ represent target bear in the $X'Y'Z'$ coordinates in the kth time. Finally, $\dot{f}_{dk}$ is frequency offset in $k-1$th and kth time instants.

Based on the principles of particle kinematics, the following equations are used to express the observed variables:

$$\beta_k = \arctan\left(x_k^{'}/y_k^{'}\right) , \tag{4}$$

$$\varepsilon_k = \arctan\left(z_k^{'}/\left(x_k^{'2} + y_k^{'2}\right)^{1/2} , \right) \tag{5}$$

$$\dot{\beta}_k = \left(y_k^{'}\dot{x}_k^{'} - x_k^{'}\dot{y}_k^{'}\right) / \left(x_k^{'2} + y_k^{'2}\right) , \tag{6}$$

$$\begin{aligned} \dot{\varepsilon}_k = &\left[-x_k^{'}z_k^{'}\dot{x}_k^{'} - y_k^{'}z_k^{'}\dot{y}_k^{'} + \left(x_k^{'2} + y_k^{'2}\right)\dot{z}_k^{'}\right] / \\ &/ \left[\left(x_k^{'2} + y_k^{'2}\right)^{1/2}\left(x_k^{'2} + y_k^{'2} + z_k^{'2}\right)\right] . , \end{aligned} \tag{7}$$

where $\dot{x}_k^{'}$, $\dot{y}_k^{'}$, $\dot{z}_k^{'}$ are changes of the velocity components. When a relative radial velocity appears between the observation station and the aircraft radio frequency, the Doppler frequency will be received by the observation station $f = f_T + f_d$. The value of f_T (frequency of aircraft RF) is set to a constant amount, then f_d is used to represent the Doppler frequency, and the formula is as follows

$$\begin{aligned} f_{dk} = &-f_T(\dot{x}_k^{'}\sin\beta_k\cos\varepsilon_k + \dot{y}_k^{'}\cos\beta_k\cos\varepsilon_k + \\ &+ \dot{z}_k^{'}\sin\varepsilon_k)/c \,. \end{aligned} \tag{8}$$

The Doppler frequency change rate of the can be obtained:

$$\begin{aligned} \dot{f}_{dk} = &-f_T(\ddot{x}_k^{'}\sin\beta_k\cos\varepsilon_k + \ddot{y}_k^{'}\cos\beta_k\cos\varepsilon_k + \\ &+ \ddot{z}_k^{'}\sin\varepsilon_k + r_k\left(\dot{\beta}_k\cos\varepsilon_k\right)^2 + r_k\dot{\varepsilon}_k^2)/c \,. \end{aligned} \tag{9}$$

In this expression, symbol c represents the propagation velocity of electromag-

netic wave, while $\ddot{x}_k^{'}$, $\ddot{y}_k^{'}$, $\ddot{z}_k^{'}$ is the vector of acceleration.

When a relatively large maneuver is generated from the observation station and the aircraft, the acceleration term in (9) can be ignored, so that

$$\dot{f}_{dk} = -f_T \left[r_k \left(\dot{\beta}_k \cos \varepsilon_k \right)^2 + r_k \dot{\varepsilon}_k^2 \right] / c \,. \tag{10}$$

3. METHODOLOGY

3.1. Thompson-Taylor algorithm

As a new algorithm, Thompson-Taylor algorithm is mainly used in the generation of random samples [9]. The basic principle of the algorithm is to deal with the random number of samples which are similar to that of m samples by centralized processing, and then to get a new random sample of the m samples. Its advantage consists in the fact that it will not be too dependent on the distribution of the state space of the sample, which is not necessary to be similar to Gauss approximation. Its process is as follows:

Step one: a random sample x^i is extracted from the sample set $\left\{x^i\right\}_{i=1}^N$, and the adjacent m samples $\left\{x_1^i, x_2^i, \cdots, x_m^i\right\}$ (including x^i) are obtained by smooth operation, and the average value of the m samples is $\bar{x}^i$.

Step two: a random number set is obtained:

$$\{u_i\}_{i=1}^m \sim U\left(\frac{1}{m} - \sqrt{\frac{3m-3}{m^2}}, \frac{1}{m} + \sqrt{\frac{3m-3}{m^2}} \right) . \tag{11}$$

Step three: new random sample is generated:

$$z^i = \bar{x}^i + u_i \left(x_k^i - \bar{x}^i \right), k = 1, 2, \cdots, m \,. \tag{12}$$

Thompson-Taylor algorithm can generate a more uniform random sample distribution, and keep the the same mean and variance of the sample set, although it is not for the particle filter algorithm, but the method can be used to make the particle filter sample diversity to be met.

3.2. Quasi Monte Carlo re-sampling particle filter

Because the operation of the Quasi Monte Carlo Goss particle filter algorithm has a positive correlation with the number of Quasi Monte Carlo samples [10], so the decrease of the number of Quasi Monte Carlo samples can improve the computing speed, so as to obtain a new algorithm, that is, the Quasi Monte Carlo aggregated re-sampling particle filter algorithm [11]. Its core idea is: the weighted aggregation of the similar particles in the state space is carried out, the boundary conditions is set as the average forecast in the space of the center of the polymer particle, and the Quasi Monte Carlo re-sampling is carried out in the space. In this process, the Quasi

Monte Carlo sampling is carried out in the neighborhood of the aggregated particles, and the steps of the Quasi Monte Carlo re-sampling particle filter prediction sampling space are omitted, so that the diversity of the sample is improved, and the filtering precision and the positioning accuracy are improved, too [12].

Initialization: The initial relative distance $\hat{r}_0 = -\lambda \dot{f}_{d0} / \left(\dot{\varepsilon}_0^2 + \dot{\beta}_0^2 \cos^2 \varepsilon_0\right)$ obtained by the initial observation is combined with the azimuth angle and pitching angle to obtain the observed object. Based on the estimation $\left[\hat{x}_0^{'}, \hat{y}_0^{'}, \hat{z}_0^{'}\right]$ of the position vector of the body coordinate system and the $\hat{X}_{O0}$, the two-dimensional position vector estimation $\left[\hat{x}_{T0}^{'}, \hat{y}_{T0}^{'}\right]^T$ of the observed object in the ground coordinate system is obtained, so as to get the initial state $\hat{X}_{T0}$, the initial error co-variance matrix $\hat{P}_0$ is calculated based on the initial observation error.

Quasi Monte Carlo sampling: Based on the example of the HALTON sequence, the method that can generate the Gauss point is given, so as to generate N Gauss points which obey the $P\left(x_{k-1}\right)$:

$$\left\{x_{k-1}^{(i)}\right\}_{i=1}^{N} \sim N\left(x_{k-1}; \bar{x}_{k-1}, \hat{P}_{k-1}\right) . \tag{13}$$

The particle set $\left\{x_{k|k-1}^{(i)}\right\}_{i=1}^{N}$ is predicted at the k moments according to the state equation,and the mean and co-variance of the $\left\{x_{k|k-1}^{(i)}\right\}_{i=1}^{N}$ are estimated, that is:

$$\bar{x}_{\,k|k-1} = \frac{1}{N} \sum_{i=1}^{N} x_{k|k-1}^{(i)} , \tag{14}$$

$$\hat{P}_{k|k-1} = \frac{1}{N} \sum_{i=1}^{N} \left(x_{k|k-1}^{(i)} - \bar{x}_{\,k|k-1}\right) \left(x_{k|k-1}^{(i)} - x^{\,k|k-1}\right)^{\mathrm{T}} . \tag{15}$$

According to the importance density $q\left(x_k \,|z_{1,k}\,\right)$, the quasi Gauss sample $\left\{x_k^{(i)}\right\}_{i=1}^{N}$ is extracted by the Quasi Monte Carlo sampling.

According to the observed value Z_{k}, the weight value $\omega_k^{(i)}$ of each particle is calculated and its normalization processing is carried out, that is

$$\omega_k^{(i)} = P\left(z_k \left| x_k^{(i)} \right.\right) N\left(x_k^{(i)}; \bar{x}_{\,k|k-1}, \hat{P}_{k|k-1}\right) / q\left(x_k \,|z_{1,k}\,\right) \omega_k^{(i)} = \omega_k^{(i)} / \sum_{i=1}^{N} \omega_k^{(i)} . \tag{16}$$

The state of the target and the posterior distribution after the K moments are estimated:

$$\bar{x}_k = \sum_{i=1}^{N} \omega_k^{(i)} x_k^{(i)}, \quad \hat{P}_k = \sum_{i=1}^{N} \omega_k^{(i)} \left(x_k^{(i)} - \bar{x}_k\right) \left(x_k^{(i)} - \bar{x}_k\right)^{\mathrm{T}} . \tag{17}$$

Particle aggregation: the number of particles $\#N_{ki}^2,\ i = 1, 2, \cdots, m$ in each grid set $\#G_{ki}^2$ is recorded, among them

$$\#N_{k1}^2 + \#N_{k2}^2 + \cdots + \#N_{km}^2 = N.$$

. Then the particles in each grid are focused, so as to get the m polymer particles $\left\{\left(x_k^{t_i}, \omega_k^{t_i}\right)\right\}_{i=1}^{m}$.

Quasi Monte Carlo particle aggregation re-sampling: A four dimensional random Quasi Monte Carlo sequence $\{u_i\}_{i=1}^{N-m}$ is truncated by the particle, so as to get m sub-sequences with the length of $\#N_{ki}^2 - 1$, then:

$$x_k^{t_i}(j) = x_k^{t_i} + \left(x_k^{t_i} - \bar{x}_k\right) \times u_j\,. \tag{18}$$

Based on the above formula, $\#N_{ki}^2 - 1$ Quasi Monte Carlo sampling particle $\left\{\left(x_k^{t_i}(j), \omega_k^{t_i}(j)\right)\right\}_{j=1}^{\#N_{ki}^2-1}$ is obtained. Finally, the average weight of all the particles in the grid is solved, and the formula is as follows:

$$\omega_k^{t_i}(j) = \omega_k^{t_i} / \#N_{ki}^2\,. \tag{19}$$

4. Result analysis and discussion

In this paper, three sets of experiments are set up, under different observation conditions of the Quasi Monte Carlo re-sampling particle filter algorithm. The comparison of the performance of the particle filter algorithm, Gauss particle filter algorithm and the Quasi Monte Carlo Goss particle filter algorithm is carried out. Among them, the particle filter algorithm uses re-sampling, the simulation parameters are set as follows: it is assumed that in the ground coordinates, the starting position of the machine is (0,2.0 km), the navigation speed of the aircraft is (20 m/s, 0, 0), the accuracy of airborne equipment is $\sigma_{x_0} = \sigma_{y_0} = 20\,\text{m}$, $\sigma_{z_0} = 8\,\text{m}$; the initial position of the signal receiving station is (160 km, 160 km), the absolute velocity is (-15 m/s, 15 m/s). The measurement accuracy of the three groups is summarized in the following table:

experiment 1	$\sigma_\beta = \sigma_\varepsilon = 1.64 \times 10^{-3}$ rad	$\sigma_{\dot{f}_d} = 1$ Hz	$\sigma_{\dot{\beta}} = \sigma_{\dot{\varepsilon}} = 0.1 \times 10^{-3}$ rad/s
experiment 2	$\sigma_\beta = \sigma_\varepsilon = 28.4 \times 10^{-3}$ rad	$\sigma_{\dot{f}_d} = 2$ Hz	$\sigma_{\dot{\beta}} = \sigma_{\dot{\varepsilon}} = 0.2 \times 10^{-3}$ rad/s
experiment 3	$\sigma_\beta = \sigma_\varepsilon = 35.7 \times 10^{-3}$ rad	$\sigma_{\dot{f}_d} = 4$ Hz	$\sigma_{\dot{\beta}} = \sigma_{\dot{\varepsilon}} = 0.3 \times 10^{-3}$ rad/s

In the three groups of experiments, $\sigma_{f_T} = 10\,\text{MHz}$, the sample period is 1 s, the number of observations is 100, and the number of selected particles $N = 400$. The performance index of each algorithm adopts the relative distance error E_{rr}, and the degradation degree of the particle is expressed by the mean effective particle number

N_{eff}, that is:

$$E_{\text{rr}} = \frac{\left(x_{\text{ture}}^2 - \hat{x}\right)^2 + \left(y_{\text{ture}}^2 - \hat{y}\right)^2}{\left(x_{\text{ture}}^2 + y_{\text{ture}}^2\right)^2} \times 100\,\%\,, \tag{20}$$

$$N_{\text{eff},k} = 1/\sum_{i=1}^{N}\left(\omega_k^i\right)^2\,, \quad N_{\text{eff}} = \frac{1}{100}\sum_{k=1}^{100} N_{\text{eff},k}\,. \tag{21}$$

The simulation results are shown in Figs. 2, 3 and 4.

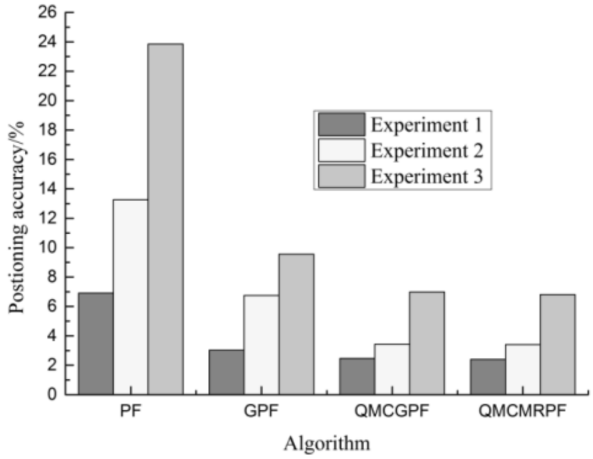

Fig. 2. Comparison of positioning accuracy in different observation accuracy

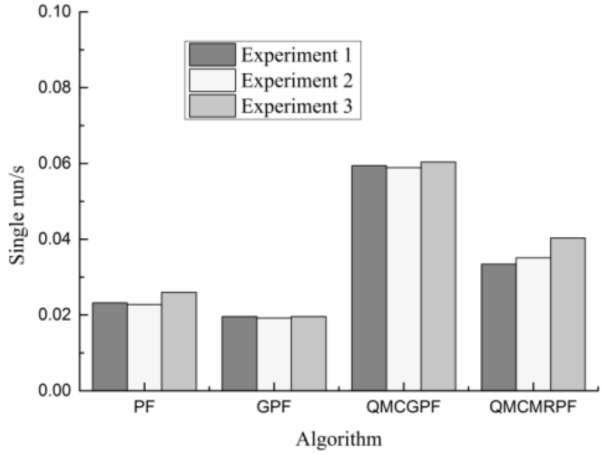

Fig. 3. Comparison of single operation time in different observation accuracy

From Figs. 2–4, it can be drawn that the observation accuracy is proportional to the positioning accuracy of the algorithm. The positioning accuracy of particle

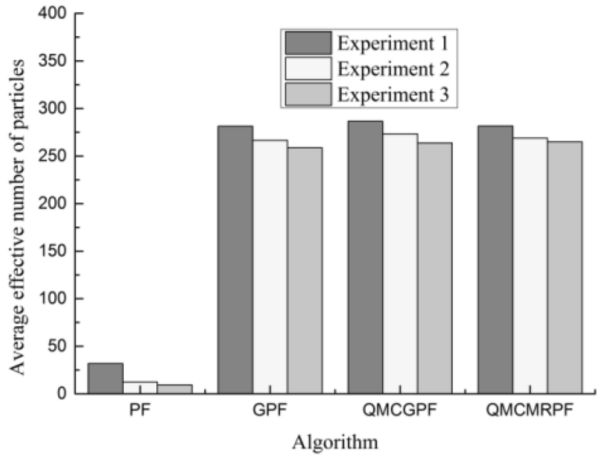

Fig. 4. Comparison of average effective number of particles in different observation accuracy

filter algorithm is approximate to a certain value, and will continue to maintain convergence. In addition, from the number of the average effective particle, it can seen that the particle filter algorithm exhibits serious particle degeneracy and impoverishment, while the Gauss particle filtering algorithm does not exhibit the phenomenon of impoverishment because of the Gauss distribution. The main reason is that Gauss's assumption is established, at the same time, the Gauss particle filter algorithm obtains the samples from the continuous distribution of the state space, and the Gauss interference of each sample is also carried out, so as to increase the diversity of particles, and avoid the emergence of the phenomenon of dilution, which shows that Gaussian particle filter algorithm is obviously superior to the particle filter algorithm. Quasi Monte Carlo Goss particle filter algorithm uses the Quasi Monte Carlo sampling on the basis of the Gaussian particle filter algorithm, so that the sample distribution in the state space is more uniform, so as to further improve the precision of estimation. Therefore, under the same conditions, the accuracy of the Quasi Monte Carlo Goss particle filter algorithm is much higher than that of the Gauss particle filter algorithm. In addition, the Quasi Monte Carl Goss particle filter algorithm improves the positioning accuracy, and the operation time of this algorithm is significantly improved.

5. Conclusion

In this paper, Quasi Monte Carlo aggregated re-sampling particle filter algorithm based on the airborne passive location method is proposed, and the following conclusions are obtained:

Through the simulation and analysis of a variety of filtering algorithms, Gaussian particle filter algorithm cannot appear phenomenon of impoverishment because of

its Gaussian distribution, the main reason is that the Gauss particle filter algorithm carries out the Gauss interference for each sample, so as to increase the diversity of particles, and avoid the emergence of the phenomenon of dilution, so it can be known that the Gauss particle filter algorithm is significantly better than the particle filter algorithm. At the same time, Quasi Monte Carlo Goss particle filter algorithm uses the Quasi Monte Carlo sampling on the basis of the Gaussian particle filter algorithm, so that the sample distribution of the state space is more uniform, so as to further improve the precision of estimation.

References

[1] X. Liu, S. Jiao, X. Lan: *Quasi-Monte-Carlo merging resampling particle filter for passive location.* Journal of Xidian University *39* (2012), No. 05, 154–160.

[2] L. Zhao, P. Ma, X. Su: *A fast quasi-Monte Carlo-based particle filter algorithm.* Acta Automatica Sinica *36* (2010), No. 09, 1351–1356.

[3] T. Hayat, T. Javed, M. Sajid: *Quasi-Monte-Carlo article filter fault prognosis algorithm based on GRNN.* Journal of Convergence Information Technology *7* (2012), No. 7, 96–103.

[4] X. Fu, Y. Jia: *An improvement on resampling algorithm of particle filters.* IEEE Transactions on Signal Processing *58* (2010), No. 10, 5414–5420.

[5] Q. Li, H. B. Ji, H. Guo: *Research and hardware implementation of Quasi-Monte-Carlo Gaussian particle filter.* Journal of Electronics & Information Technology *32* (2010), No. 07, 1737–1741.

[6] F. Lindsten, T. B. Schön, L. Svensson: *A non-degenerate Rao-Blackwellised particle filter for estimating static parameters in dynamical models.* IFAC Proceedings Volumes *45* (2012) No. 16, 1149–1154.

[7] H. Moradkhan, C. M. Dechant, S. Sorooshian: *Evolution of ensemble data assimilation for uncertainty quantification using the particle filter-Markov chain Monte Carlo method.* Journal Water Resources Research *48* (2012), No. 12, 502–502.

[8] X. Wang, M. Xu, H. Wang, Y. Wu, H. Shi: *Combination of interacting multiple models with the particle filter for three-dimensional target tracking in underwater wireless sensor networks.* Mathematical Problems in Engineering (2012), No. 11, 939–955.

[9] Q. Wen, J. Gao, K. Luby-Phelps: *Multiple interacting subcellular structure tracking by sequential Monte Carlo method.* Proc. IEEE International Conference on Bioinformatics and Biomedicine (BIBM), 2–4 Nov. 2007, Silicon Valley, USA, 437–442.

[10] H. Wang: *Improved quasi monte carlo particle filter algorithm based on GRNN.* Proc. IEEE International Conference on Communication Technology (ICCT), 9–11 Nov. 2012, Chengdu, China, 257–261.

[11] G. G. Rigatos: *Extended Kalman and Particle Filtering for sensor fusion in motion control of mobile robots.* Mathematics and Computers in Simulation *81* (2010), No. 3, 590–607.

[12] M. K. Pitt, R. dos Santos Silva, P. Giordani, R. Kohn : *On some properties of Markov chain Monte Carlo simulation methods based on the particle filter.* Journal of Econometrics *171* (2012), No. 2, 134–151.

Received April 23, 2017

Acta Technica *62* No. 1A/2017, 145–156

The application of graphics creativity in product design

Weiqi Cai[1]

Abstract. The development of society has led people to pay more and more attention to the quality of life and the details of the use of products. The application of graphic creativity in the product design makes the product can better meet people's needs. In order to make the relevant theories and technologies of graphic creativity in the product design further improved, the basic concepts of graphic creativity were summarized, and the influence of graphic creativity on product design was expounded. On this basis, the relationship between the graphic creativity and the product design popularity was analyzed by fuzzy evaluation method. The results show that graphic creativity can enhance the relevant characteristics of the product itself and can better meet people's needs, which can provide theoretical basis and scientific support for the development of product design industry in China.

Key words. Graphic creativity, product design, fuzzy evaluation, creative life, correlation analysis.

1. Introduction

After the reform and opening up, people's living standards have been a qualitative leap, under the leadership of the party, people's life has changed from the period that the food and clothing are difficult to be solved to the period that most people are comparatively well-off at present. Nowadays, people's life is changed, which is no longer as before that they are easy to be satisfied, and they have more pursuits. This is not only reflected in people who dare to pursue their own ideals, dreams and the "Chinese dream", but also in some small details, people become more demanding. For the product, the former people paid attention to the quality, and the appearance request of the products was relatively low, the practicability was the highest. However, now, the requirements of the peoples on the product are not only practicality and durability, the appearance requirements are also improved. Today's products should be not only good-looking but also creative, which can attract people's attention, and furthermore, they also need to combine with the functions. In order to make a breakthrough, simply relying on the colors and simple appearance

[1]East China University of Technology, Nanchang, Jiangxi, 330000, China

of lines is not enough. So in this case, the design field introduces the concept of graphic design creativity.

The word "graph" in the graphic creative design is not just the so-called simple graphic or image, but also the abstract symbol in the plane media. Here, the "graphics" earliest originated in Latin and Greek, and then, it was directly translated by English. Its implication is to use specific visual graphics, graphics and special symbols to express a particular concept or meaning to the world, which contains author's intention [1]. Then, the characteristics of the graphic creativity are that its expression is very intuitive, because when people is perceiving this world, they firstly use their eyes, and the graphics can directly transfer the information, so as to give the most intuitive visual effects. In addition, the graphic creativity is usually derived from life but higher than life, and the ultimate goal of the combination of graphic creativity and products is to serve the human, so that people can enjoy the visual effects brought by the appearance of this product, at the same time, it does not affect the practical function of the product itself. Graphic creativity does not appear in modern times. In ancient times, people already had the latent consciousness of the graphic creativity, but it was not conceptualized and developed as a discipline [2]. Then, the image of Sphinx in ancient Egypt is a representative of the image of creativity, which embodies the authority of the Pharaoh and ancient Egyptian people's supreme respect to him. In addition, in fairy tales, people will also add the elements of graphic creativity, such as Medusa's image in the fairy tales. Medusa's hair is a state that a lot of snake wrap around each other, and the meaning is also derived from the background of the fairy tale, then, in the fairy tale, Pinocchio's nose will grow longer when lying, which are also typical examples. All of these graphic ideas leave us a deep impression, because although they originate from the life, they have their own unique creativity and thinking, which makes people feel refresh and hard to forget. In fact, in the absence of learning the concept of graphic creativity, the graphic ideas are already integrated into people's lives. Therefore, the graphic design can give the product a brand new look [3].

In order to explore the application of graphic creativity in the actual product design, in the paper, the related basic concepts of the graphic creativity in the second section was introduced; and the automatic synthesis holographic method of graphic creativity in the third section was studied, furthermore, the influence of graphic creativity on product popularity was analyzed by fuzzy evaluation method. And in the fourth section, the customer was interviewed and the data was analyzed. The results show that graphic creativity can enhance the popularity of the products, and the use of the actual products can enhance the value and sales of products.

2. State of the art

2.1. The influence of Chinese culture on figure creativity

If Chinese characters' expansion to graphic creativity is from the content and scope to the training methods, what the Chinese paintings bring to the creative graphics is the update in the frame of the picture.

Not only graphic creativity, the concept of the whole modern designs originated from the modern design teaching units established by Weimar, Germany in 1919-Bauhaus school. The design school of Bauhaus is the pioneer of modern design art, and a large number of modern design theories are from the Bauhaus, such as point and line surface composition theory and the golden section theory. This design theory surly has a guiding significance for the creative design of the graphics, so which should be accurately grasped. But in the actual design process, especially when we are dealing with the traditional content of the subject matter, it can be found that the proportion of graphic appearance can be very coordinated, and the layout can also be arranged orderly, but at the same time, there is little "gas", so that the entire graphics or pictures are not consistent with the design theme. This is indeed a need to solve, and it is necessary to study the problem. In the research of traditional Chinese painting art, it can be seen that the unique aesthetic characteristics of the traditional Chinese painting and calligraphy art are equally applicable to graphic creative design, furthermore, the graphic design can be better after combining with Western theories [4].

Western aesthetics focus on point, surface, line and golden section (the beauty of mathematics), and then, there are many modern Western composition laws, taking into account the above rules, it can be found that the Western people focus on the mathematics of the rationality and design. This is very good, because it is very strict, but it also appears to be little mechanical, which cannot express the unique temperament of traditional themes. The fundamental principle of Chinese traditional painting and calligraphy art for distinguishing and judging the artistic level of the painting is to see whether the creator can fully achieve the requirements of the "Six Laws" [5]. "Six Laws" was first from the Southern Qi Dynasty Xiehe's Ancient Paintings Records. The Ancient Paintings Records said: the six laws include artistic conception, the two bone method with the pen, the pictographic shape, the conformity to type in applying colors, the business location and the writing of the shift mode. Although Xiehe did not explain the content of "Six Laws" more concretely, while because it involved the basic art problems of Chinese paintings, the basic framework of Chinese painting theory was initially established, which had a profound and lasting effect, and it also had an important position on the development history of Chinese painting. Moreover, the artistic conception is like this: gas is the carrier of the essence of everything, and is "the essence of life", which originated in the substance. The concept of gas contains Chinese understanding of the nature. Rhyme is the gas to inspire all things in the cosmos, the rhyme and cadence. The vivid is the state of the artistic conception that should be presented, which is dynamic rather static. At this point, it is more flexible and natural than the Western theory of composition. After using the golden section method to split the picture, the "real" elements of the point, line and plane are put into the sub-lattice units. And the Chinese aesthetics not only focuses on "real", but also pays more attention to "virtual", in addition, it also concerns about the blank space among entities. Then, while painting the mountains and lakes, characters and buildings, the movement of the artistic conception is concerned [6].

During the Olympic Games in Beijing, our Olympic logo vividly embodied this

feature, as shown in the Fig. 1.

Fig. 1. Graphic creativity in the use of products

2.2. The design idea and creative method of graphic creativity in product design

Creativity is the core of graphic design. In the practice of graphic creative design, the creative thinking is a result that is mainly based on the image thinking, it combines with intuitive thinking, logical thinking, divergent thinking and aggregation thinking and other forms of comprehensive application. Among them, the image thinking is the most important part of the human brain in image processing, which can be divided into association and imagination, both of two are also the basic ways and sources of our visual graphic design. First of all, through association and imagination, people have a perceptual image, and then, some specific images are obtained by rational thinking reasoning and judgment according to combine with some inspiration, this is a simple process of graphic creativity.

The associative method is used to think the thing from one thing to another. Starting from the around things, the pink spring is thought, and the lying falcon, and fighters and so on also can be thought, so that the imagination and creativity can be stimulated by this thinking method. Besides, the creativity starts from the life, so it is necessary to learn to observe things around.

Association and imagination is an inexhaustible motive force of graphic creativity. In real life, in addition to those inherent things in nature, all tools, such as archi-

tecture, art and so on, are created through association and imagination methods. We are very familiar with the Sydney Opera House's shape design, it is composed of three groups of huge white shell pieces, of which there are several spacious concert halls that are provided for people, someone say that it is like a huge white shell on the surface of water, while someone say that it is like a sail raised at sea. However, talking about its design, there is a little-known little story. Designer Joan Uzon was a little-known designer in Denmark, he gained the Pulitzer Architecture Award in 2003 because of his design of Sydney Opera House. However, his inspiration was not as people thought which was from shells or sails, but from a bunch of orange peel of the designers who conveniently peeled and placed it on the table. Thus, it can be seen that the association and imagination is so powerful. Similarly, Newton also discovered the gravitation because of a fall of the apple.

The material selection of the product is also part of the product design, which can also be practical and ingenious. Previous people only concerned about the practical durability, but ignored whether the product was environmentally friendly, whether it was easy to clean such these problems. Sometimes, the materials of the product will make the appearance of this product a new look. For example, in recent years, the popular paper sofa, which uses the characteristics of the paper products that after layer folding, it can have a strong bearing capacity, and in addition, it can also be deformed and elongated randomly, and can be used as a table, anyhow, it has many functions, such as the environmental protection, besides, it does not account for local. And this is also adhering to the people-oriented design concept.

3. Methodology

3.1. Graphic creativity and synthetic holographic product design

The product design is not just the 2D graphic design, but the three-dimensional design. Compared with ordinary products, the appearance of the graphic design products will be more special, innovative, and there will also be a big difference. After the completion of the design, model product testing generally takes a long time, during this period, if it cannot be done well because of various reasons, we will allow the factory to modify, which will take a lot of time. Therefore, if we can adjust the model ourselves, it will be a great help to the whole design, which can also reduce a lot of time. Then, the synthetic holographic computer technology can be used to solve this problem better.

Synthetic holography can realize dynamic three-dimensional display of large field of view, extended depth of field, full color (or true color), which is an important technique for realizing holographic display. However, the traditional synthetic holographic technique is complicated, and it has many human intervention factors and long production cycle, which hinders the quality of the synthetic hologram and limits its application prospect. With the development of computer technology and optoelectronic technology, and in view of the disadvantages of the traditional synthetic holography, the computer graphics technology, photoelectric technology and com-

puter automatic control technology were introduced into the synthetic holography process. According to the use of computer graphics design software, the previous film camera or digital camera was replaced to obtain two-dimensional parallax picture, and then the liquid crystal spatial light modulator and the automation device of the main hologram recording constructed by automatic partition servo system were used to replace the traditional manual intervention, so that the entire process was completed automatically under the control of the computer, which optimized the recording process of the synthetic holography.

The recording of the synthetic hologram was finished in two steps. Firstly, a series of two-dimensional images with parallax were recorded on the same master hologram step by step. And each picture occupied a slit position on the master hologram, then, the image reproduction and rainbow hologram recording optical path of the master hologram was used to record the composite hologram of white light reproduction, as shown in Fig. 2.

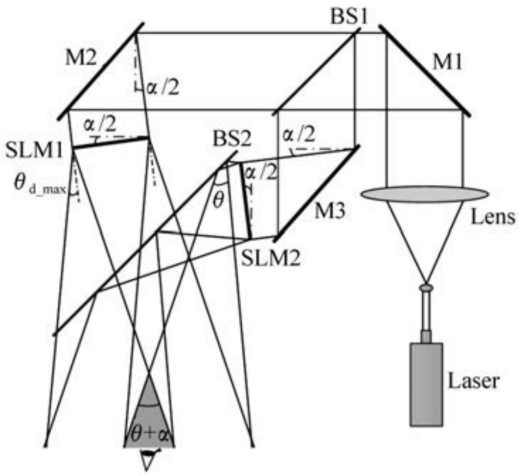

Fig. 2. Main holographic optical path

These two-dimensional pictures were orderly put into the system software platform, as shown in Fig. 3, and then, starting from the automatic monitoring program, the system automatically changed pages, and refreshed the two-dimensional pictures on the spatial light modulator orderly, at the same time, the slit was moved to a predetermined position, and the exposure time of each hologram was controlled. In the experiment, the slit width was 5 mm, the main hologram was divided into four interval exposures, and the static time was 6 s, moreover, the exposure time depended on the interference intensity of the recording plane and the sensitivity of the recording material, and the whole recording time did not exceed 20 min, then, a three-dimensional image was generated.

The application of this technology can better analyze the product structure and product color, etc., which has a very big help for the graphic creative product design.

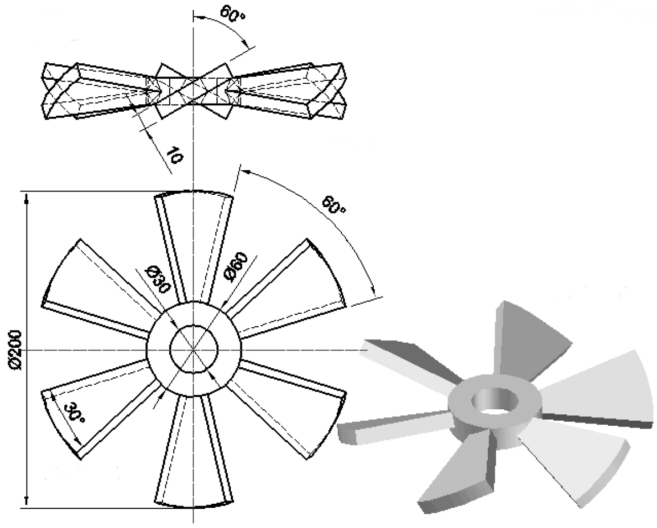

Fig. 3. 3D image of product

3.2. Research on the relationship between product popularity and graphic creativity design based on fuzzy evaluation method

The fuzzy evaluation method is a concrete application method of fuzzy mathematics, and it has a good effect on the multi-factors and multi-level complex problems. The fuzzy method is closer to the thinking habits in the evaluation process. Therefore, in this paper the fuzzy evaluation method was selected to evaluate the relationship between product popularity and graphic creativity, and then the multi-level evaluation model was adopted.

There are many factors for the popular products: product availability, aesthetics, durability and so on. This article built the index system only from the consumer's favorite degree of the products. According to the discussion, it was determined that the evaluation of each index was divided into four grades, and the evaluation scale set was V = very relevant, good, general, and poor = 0.9, 0.7, 0.4, 0.2. The evaluation matrix R' was determined. R' was a fuzzy relation, where each element r_{ij} was the membership degree of each index U_i to the evaluation scale V_j. Symbol V_1 denotes the first evaluation scale. In Table 1, N represents an evaluation of the index U_i, and N_i represents that the evaluation object F already reached the V_i level of the evaluation scale set.

Table 1. U_i score results

Opinion scale	V_1	V_2	...	V_n
Index U_i	N_1	N_2	...	N_n

As a result, the membership function was defined as:

$$r_{ij} = \frac{N_j}{\sum_{i=1}^{n} n_s}\,. \tag{1}$$

There is a comprehensive evaluation to the four indicators A, B, C, D, and then, the vector B was calculated and comprehensively evaluated as follows

$$B_i = W_i \circ R_i\,, \tag{2}$$

where $i = A, B, C, D$, and the symbol $\circ$ is defined as the compositional operation represented by the Zade operator $(\wedge, \vee)$.

Then any evaluation vector $B = (b_{ij})$ satisfies the relation.

$$bij = \vee k[W_{ik} \wedge r_{kj}]\,. \tag{3}$$

Here, W_i is the second level index weight, which is a 1×4 order weight vector, R_i is the 4×4 level single factor evaluation matrix of the evaluation object F obtained by second level index evaluation, therefore, B_i is the 1×4 resultant matrix of the first level comprehensive evaluation.

1. Second level comprehensive evaluation

The evaluation matrix R was determined. Then the four indicators A, B, C, D were respectively regarded as a single element, then, the B_i $(i = A, B, C, D)$ was regarded as a single factor evaluation of R, so the 4×4 level judgment matrix was obtained.

$$R = \begin{bmatrix} BA \\ BB \\ BC \\ BD \end{bmatrix}\,. \tag{4}$$

According to the calculated second-level evaluation result, the vector B was obtained.

2. Calculating the comprehensive evaluation value P.

$$P = B \bullet VT\,. \tag{5}$$

Quantity P not only made full use of the information brought by the secondary evaluation vector B, but also combined with the grade evaluation parameter of the evaluation scale V, so according to the size of P value, the order of evaluation objects was optimally arranged, and the information was provided for decision making.

The consumers who participate in the experiment were divided into three groups, and they were composed of three age groups, namely, 10–20 years old, 20–35 years old, 35–45 years old, men and women were in half, and there were 10 people in each group. The experimental method is as follows. Three groups of people scored the ten products that did not carry out graphic design and the ten same types of products that the graphs were already designed, and the score was 0∼10, then, the evaluation data were tested and analyzed.

Experimental process is shown in Fig. 4.

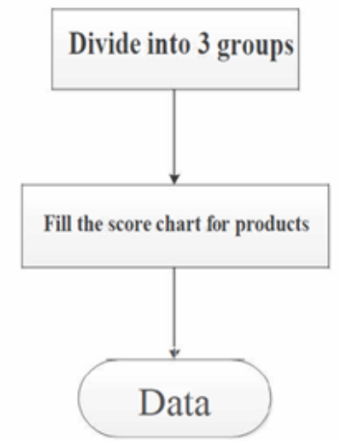

Fig. 4. Flow chart of survey

4. Result analysis and discussion

As can be seen from Table 2, in the questionnaire survey of consumers in three groups of different age stages, the total average score of the appearance of common products was lower than the average score of products designed by graphs. Among them, 10 to 35-year-old crowd had a high evaluation to the graphic creative design products, which proved that young people prefer the products with new appearance design, while the elders pay more attention on product quality. The voting results are depicted in Fig. 5.

Table 1. U_i score results

Content	Average of the common products	Average of the products designed by graphs
10∼20 years old	5	8
20∼35 years old	6	9
35∼45 years old	4	8
Total average	15	23

There was one more time of a total vote, at this time, the groups were not divided, and there was a voting test for the 30 consumers to their favorite products in the two groups of products. Finally, as can be seen from the results that the products after the graphic design have higher votes than the ordinary products.

Finally, according to the survey results of a consumer questionnaire, the fuzzy evaluation method was used to calculate the correlation between the graphic creative

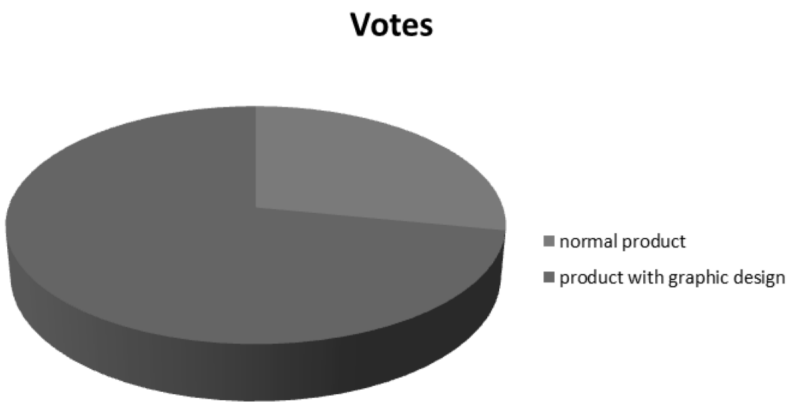

Fig. 5. Voting results

design and the popularity, then, according to the relevant calculation method in Section 3, the result of $B_{\mathrm{b}} = (0.78, 0.62, 0.1, 0.02)$ was obtained. Based on the standard of the evaluation scale set, V = very relevant, good, general, bad = 0.9, 0.7, 0.4, 0.2, it can be concluded that the graphic creative design is closely related to the popularity of the products.

5. Conclusion

With the development of society, the improvement of economic level has made people's quality of life higher and higher, people have begun to pay more attention to the details of the use of the product. In order to further arouse people's desire for the purchase of products, and better promote the further development of the design industry in the present age, graphic creativity began to be used in product design and provided a positive impact on the development of the design industry. In order to further analyze the influence of graphic creativity on the development of the design industry in China, through the reading and summary of relevant information, the related concepts of graphic creativity were recognized in this paper; on this basis, the influence of Chinese culture on graphic creativity and how to carry on the graphic creativity design were expounded; at the end of the study, the importance of graphic design industry in product design was further determined by using fuzzy comprehensive evaluation analysis and questionnaire. The results show that the product which uses graphic creativity design is more popular in the consumer crowd, which proves that the graphic creative design has a high correlation with the popularity of the product. The purpose of this study is to provide some driving force and positive influence for the development of the design industry in China.

References

[1] Q. Y. Wang, L. Tian: *A systematic approach for 3D VRML model-based assembly in Web-based product design.* International Journal of Advanced Manufacturing Technology *33* (2007), Nos. 7–8, 819–836.

[2] C. Stones, T. Cassidy: *Comparing synthesis strategies of novice graphic designers using digital and traditional design tools.* Design Studies *28* (2007), No. 1, 59–72.

[3] K. Mullet, D. Sano: *Designing visual interfaces: communication oriented techniques.* Book, Prentice-Hall, Upper Saddle River, NJ, USA (1995).

[4] G. Swanson: *Graphic design education as a liberal art: Design and knowledge in the university and the "Real World".* Design Issues *10* (1994), No. 1, 53–63.

[5] L. Wang, W. Shen, H. Xie, J. Neelamkavil, A. Pardasani: *Collaborative conceptual design—state of the art and future trends.* Computer-Aided Design *34* (2002), No. 13, 981–996.

[6] P. Schenk: *The role of drawing in the graphic design process.* Design Studies *12* (1991), No. 3, 168–181.

Received May 22, 2017

Acta Technica *62* No. 1A/2017, 157–166

Integration of information security and network data mining technology in the era of big data

Lu Li[1]

Abstract. The purpose of this paper is to apply data mining technology to effectively analyze and process these data and find valuable information that can help the decision and understanding. In the paper, privacy preserving algorithm to data mining is studied, and the methods of classification of privacy preserving algorithm for existing data mining are introduced. In addition, the existing algorithms are summarized from the perspective of data processing technology, and the algorithm is evaluated and analyzed with the given criteria. Moreover, a privacy preserving mining algorithm for frequent patterns based on the increase of noise is put forward, which solves two key problems: the noise increase and transaction noise in the way of the noise generated. At last, an experiment is designed to verify the effectiveness of privacy preserving algorithm facing frequent pattern mining proposed by this paper. And in the same experimental platform, the time and space efficiency of privacy preserving based on frequent pattern mining in data cleaning are compared. The experimental results and comparative analysis show that the the privacy preserving system has good performance. In conclusion, the effectiveness of the system is verified and it can be used in the protection of information security.

Key words. Data mining, privacy preserving, frequent pattern mining.

1. Introduction

Various privacy preserving techniques are gradually applied to various branches of data mining, including classification, clustering, association rule mining and so on. A lot of ways to protect the sensitive information have been put forward. But no matter which way is used to protect the privacy, it will produce different degrees of damage to the quality of data [1]. As a result, in the privacy preserving, we must consider the impact of mining results. To ensure the correctness and effectiveness of the mining results is the ultimate goal of the mining, and the privacy preserving is the needs of the data provider [2], which should be considered.

This paper introduces several classification standards of privacy preserving algorithm for data mining. In addition, from the point of view of data processing

[1]Nanjing Audit University Jinshen College, Jiangsu Nanjing 210000, China

technology, the typical algorithms of data mining privacy preserving are introduced in detail, the advantages and disadvantages of each algorithm are analyzed, and the evaluation standard of privacy preserving algorithm for data mining is put forward. What is more, the privacy preserving algorithm for frequent pattern mining is discussed with great attention. On this basis, the method for increasing the noise is introduced into the frequent pattern mining privacy preserving, noise data generation is illustrated in details, and the experimental verification is carried out. The experimental results showed that this algorithm can effectively improve the efficiency of privacy preserving algorithm for frequent pattern model mining.

2. Materials and methods

First of all, the classification of privacy preserving algorithms for data mining is introduced, and then, from the data processing technology, the privacy preserving algorithm facing data mining of the current typical collective data set is analyzed.

2.1. Privacy preserving techniques and algorithm analysis for data mining

The existing privacy preserving algorithms for data mining can be classified from the aspects of data distribution, data processing technology, data mining algorithm, privacy preserving object and so on angles.

According to the different data storage methods, the data set used for data mining can be divided into centralized data and distributed data. The distributed data can be divided into two levels: horizontal distribution and vertical distribution. The horizontal distribution refers to the distribution of data in different sites in accordance with records, and the vertical distribution indicates the distribution of data n different sites according to the properties [3]. The privacy preserving algorithm based on data mining can be classified according to the different data storage methods. In this paper, the studied algorithm is the centralized data privacy preserving algorithm.

The privacy preserving algorithm based on data mining can also be classified according to different data processing methods, such as data cleaning, data conversion, data block, data encryption, data anonymity and so on.

Different privacy preserving algorithms are suitable for different data mining tasks. For instance, some privacy preserving algorithms are suitable for classification, some are suitable for clustering, while some are generally suitable for both classification and clustering [4]. The privacy preserving algorithm based on data mining can be classified according to the application problems.

According to the privacy preserving objects, privacy preserving algorithms for data mining can be divided into the following two categories. One category is the objects of privacy preserving with the sensitive data in the data source, the other is the objects of privacy preserving with the implied sensitive knowledge in the data source.

2.2. Data mining privacy preserving based on data cleaning

Based on the idea of data cleaning, Oliveria and so on scholars proposed a series of privacy preserving association rule mining algorithms. The SWA algorithm realizes the purpose of privacy preserving by deleting some data. Specifically, the solution of the problem can be described as follows: if there are the two sides of cooperation A and B [5]. A has the transaction data set, and B desires to mine the association rules. The problem is that if A doesn't want B to dig out some rules, then A needs to implement a number of techniques, and the preserved rules are called sensitive rules.

The SWA algorithm involves three basic concepts: sensitive rules, sensitive models and sensitive transactions. Sensitive rules refer to a collection of association rules that are necessary to be hidden in the original data set. Sensitive patterns can also be called sensitive frequent item sets, which refer to all of the frequent item sets set mined out from it, supporting the frequent item sets of the sensitive rules. Sensitive transactions are transaction records that contain sensitive patterns in the original database [6].

2.3. Data mining privacy preserving based on data encryption

Medical researchers may not have the expertise to analyze the data, and its software and hardware facilities are not complete. For a large number of medical data, they can only not analyze or looking for professionals to analyze. No analysis of data will result in a waste of data resources, and professional analysis has a potential security problem. Using increasing noise method or data cleaning method, it will reduce the accuracy of results, so these two kinds of methods are not suitable for medical data sets. The reason is that the medical field has a high requirement on security of data and accuracy of results. While the use of data encryption method can just avoid this problem.

In this paper, a data set encryption algorithm is proposed to protect the privacy information. Medical data can be generally divided into digital data, character data, time data, and image data these four kinds. As a result, it is possible to make encryption of data of different types by defining a set of reversible conversion rules. Symbol f1 refers to the conversion function of digital data, f2 indicates the conversion function of character data, f3 suggests the conversion function of time data, and f4 represents the conversion function of image data. Then, the new table is built according to the old table structure by using the conversion rules, and then the content of the old table is converted into the new table according to the transformation rule, and the new data set is generated. Medical research institutions only transfer the encrypted data set for the data analysis professionals. The data analysis professionals make data mining of the encrypted data table, and then the mined results are returned back to the medical scientific research institutions. Medical research institutions only need to convert the results into the initial stage in accordance with reverse conversion, and then they can get the meaningful results.

2.4. Privacy preserving algorithm for frequent pattern mining

The knowledge discovered by data mining can be used not only for derivation of sensitive information from non-sensitive information, but the knowledge itself may be the sensitive information related to national security, business secrets, personal privacy and so on. If data mining technology is abused by some malicious users, it will pose a threat to privacy and information security in the data sharing.

Based on some existing research ideas, this paper focuses on how to protect the hidden knowledge information in the original data set. The basic research idea is: before the release of the data set, in advance, make change processing of the original data set, so as to prevent the leakage of these sensitive knowledge. However, transforming the original data set will inevitably distort some non-sensitive information, and the true extent of them will be influenced. Thus, it will make misleading for the data receiver, especially for some important non-sensitive information. The purpose of this paper is to reduce the side effects of the knowledge information as much as possible in the change processing of the original data set, and focus on the privacy preserving in the mining of frequent patterns.

As a basic research in data mining, frequent pattern mining has its application value in data mining, such as association rule mining, feature extraction, data classification and clustering. At the same time, frequent pattern itself is an effective means of knowledge expression. The objective for studying the frequent pattern privacy preserving is, without disclosing sensitive patterns, to preserve non-sensitive patterns as much as possible in the data retention, especially some non-sensitive patterns containing important information. And it aims at improving the usability of the data set, which can identify the non-sensitive patterns containing important information by using frequent pattern mining.

Figure 1 shows the flow of processing the original data set to get the result data set.

The original data set contains all the frequent patterns, and the result data set contains only non-sensitive patterns.

First of all, the frequent pattern mining is carried out in the original data set to get the corresponding set of frequent pattern mining. Data owners, through the analysis, determine which contains sensitive information in the frequent pattern mining (called sensitive pattern or private pattern). Then, according to the frequent pattern mining (some of which are frequent patterns that have been identified as sensitive pattern by data owners), apply the privacy preserving algorithm to process the original data set and get a new results data set. As a result, when the results data set is mined, it will not lead to the leakage of the sensitive pattern in the original data set. That is to say, even if the attackers do data mining on the results data set, they cannot find the sensitive patterns in the original data set. At the same time, taking into account the increase of the usability of the data set, it also requires reducing the impact of data change on those non sensitive patterns in the original data set as much as possible, especially some non-sensitive patterns containing important information, so as to improve the usability of the results data set.

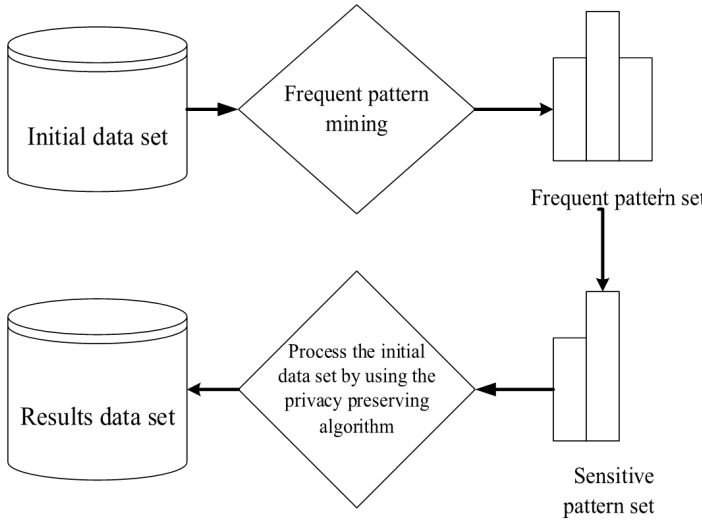

Fig. 1. Schematic diagram of privacy preserving flow in frequent pattern mining

In order to solve the problem of privacy preserving algorithm for frequent pattern mining based on data mining, this paper takes the method of increasing noise to transform the original data set, so as to realize the preserving of sensitive patterns. That is, by increasing some transaction records to the original data set D, to obtain the results data set D'.

Because the transaction mode support equals to the number of transactions containing patterns divided by the total number of transactions, it is necessary to hide the sensitive patterns in the results data set D'. That is, to reduce the support of the sensitive pattern to be less than the specified support threshold. The following two ways can be applied: one is to reduce the number of transactions containing sensitive pattern. The preserving of sensitive patterns based on data cleaning is, by deleting sensitive items in the transaction containing sensitive patterns, to reduce the number of transactions that contain sensitive patterns, thereby reducing the support of sensitive patterns in D'. The second is to increase the total number of transactions. That is to say, increasing noise transactions in the original data set, to reduce the support of sensitive patterns, so as to hide the sensitive patterns.

The basic idea of increasing noise sensitive mode preserving is shown below in Fig. 2.

Firstly, the original data set is performed with frequent pattern mining, obtaining the sensitive pattern set and release mode set. According to the above pattern set, appropriate noise transaction is generated. Then, the original data set and noise data are fused to produce the final results data set D'. Among them, the principle of increasing the noise transaction should be: to reduce the support of sensitive patterns in the sensitive pattern set and to reduce the support of the release pattern in the release pattern set.

In this paper, the core problems that the noise increasing method need to solve

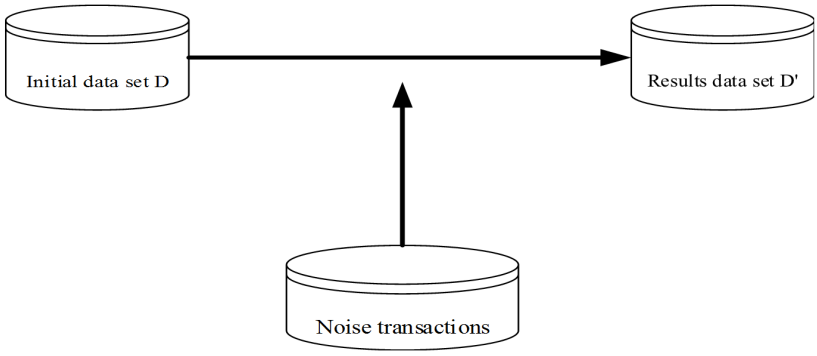

Fig. 2. Increased noise sensitive mode preserving

are summed up in two aspects. One is to increase the number of noise transactions, and the other is to generate the noise transaction, that is, which is included in the noise transactions. The idea to solve the problem of this article is: through the support of sensitive pattern and privacy preserving threshold set in advance, to calculate the number of noise transactions needed to increase, and to generate the noise transactions through the decomposition of the existing non-sensitive patterns.

3. Results

In this chapter, we design and implement a privacy preserving mining algorithm for frequent pattern mining, which is used to verify the effectiveness and performance of the new privacy preserving algorithm based on increased noise designed in the paper. And the privacy preserving algorithm for frequent pattern mining based on data cleaning on the same platform is realized, the privacy preserving algorithm for frequent pattern mining based on noise increase is compared in a number of indicators, and the conclusion is given.

3.1. Experimental flow framework of privacy preserving for frequent pattern mining

The first stage is to preprocess the original data set, convert the data in the original data set for the form that the frequent pattern mining needs, and then apply the typical frequent pattern mining algorithm, according to the given support threshold, to find all the frequent patterns (frequent item sets), and then randomly select sensitive pattern set and released pattern set.

The second stage is, based on the results of the first stage (sensitive pattern set and released pattern set), to apply the privacy preserving algorithm for mining frequent patterns in the original data set. That is, to apply the privacy preserving algorithm for frequent patterns based on data cleaning and the privacy preserving algorithm for frequent pattern based on noise increase for the processing, and get the final results data set.

The third stage is to verify the results. For the results data set generated in

the second stage, frequent pattern mining algorithm is used to obtain the frequent patterns in D'. It also verifies whether the sensitive patterns in the first stage is hidden, that is, to verify the effectiveness of privacy preserving algorithm in the second stage.

Specific experimental environment is:

Hardware: Microsoft: IBMX86, CPU Intel T5750 2.00G, Memory: 2G

Software: operating system: Windows XP SP2, developing language is JAVA

Data: the data set in the experiment is generated by IBM data generator according to different parameter configuration dynamics.

3.2. Experimental results analysis

We compare the effectiveness and efficiency of the two algorithms through two groups of experiments. In the experiment, in a given minimum support threshold, we first of all use the frequent pattern mining algorithm to get all the frequent patterns in the original data set. And then, from the mining results, we randomly choose 15 frequent patterns to constitute a sensitive pattern set, and take the rest non-sensitive patterns as the release pattern set.

In the first set of experiments, we use the support error to measure the effectiveness of the two algorithms. The support error α is defined as

$$\alpha = \sum_{i=1}^{k} \frac{\mathrm{SUP}_{\mathrm{D}'}(\mathrm{P}_i) - \mathrm{SUP}_{\mathrm{D}}(\mathrm{P}_i)}{\mathrm{SUP}_{\mathrm{D}}(\mathrm{P}_i)} \,. \tag{1}$$

Here, P_i refers to the pattern in the release pattern, $\mathrm{SUP}_{\mathrm{D}'}(\mathrm{P}_i)$ indicates the support of the pattern P_i in the results data set D', and $\mathrm{SUP}_{\mathrm{D}}(\mathrm{P}_i)$ suggests the support of the pattern P_i in the original data set. From the definition of support error α, the greater the value of α, the greater the impact of the algorithm on the results data set. In the case of initial data set not changing (the number of transactions in the data set is 10 thousand), we gradually increase the privacy preserving threshold to compare the effectiveness of the two algorithms. The experimental results are shown in Fig. 3.

In this set of experiments, we set the minimum support threshold of frequent pattern mining as 2 %, the original data set keeps unchanged, and the privacy preserving threshold is gradually increased from 10 % to 30 %. It can be seen from the figure that, for the preserving algorithm of sensitive pattern based on data cleaning, a smaller threshold means to protect the privacy of sensitive pattern in a higher degree. That is to say, more sensitive transactions are processed. In consequence, the support degree error is higher. And when the privacy preserving threshold increases gradually, since that the impact of the results data set on the original data set is smaller, the support error of two algorithms is gradually approaching.

In the second set of experiments, we compare the efficiency of the two algorithms by increasing the size of the original data set in the case of the same threshold. The experimental results are shown in Fig. 4.

In this set of experiments, we set the threshold of privacy preserving as 20 %, and

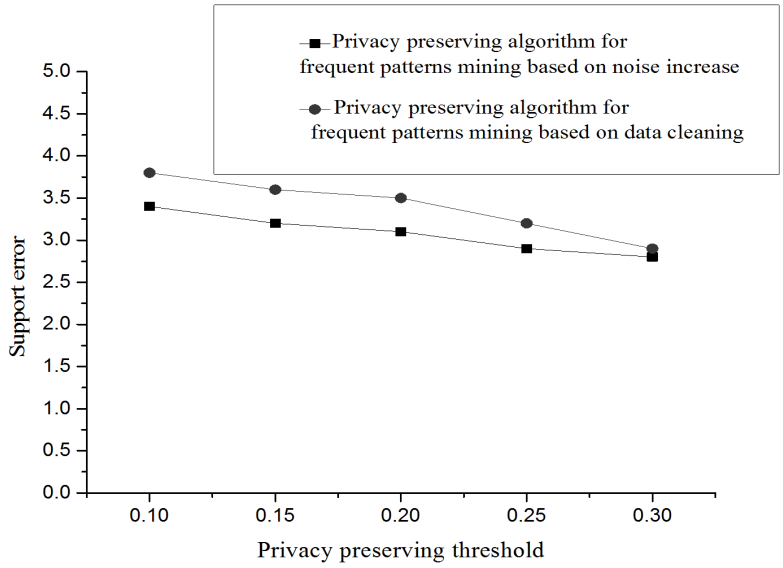

Fig. 3. Comparison of support error under different privacy preserving threshold

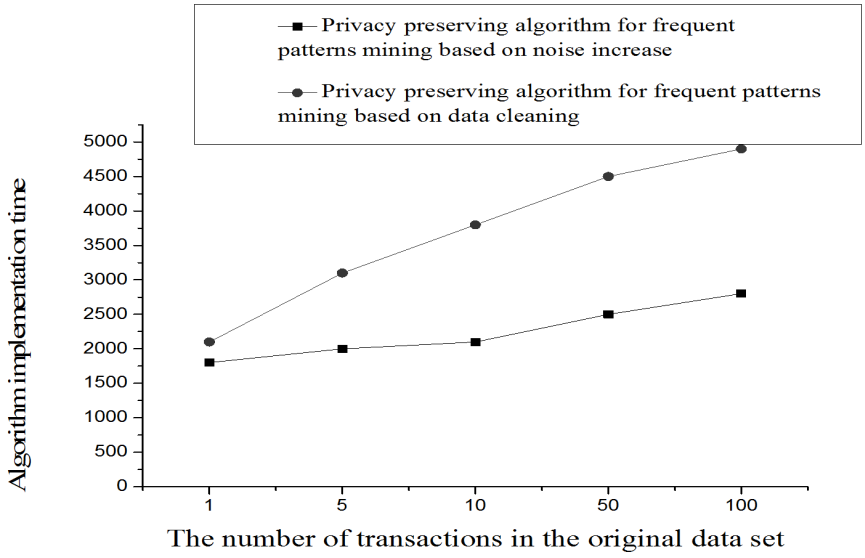

Fig. 4. Comparison of algorithm execution time under different original data sets

the minimum support threshold of frequent pattern mining as 1.5 %, but the initial data set is gradually increasing. As can be seen from the figure that, when the original data set is the same, the implementation time of privacy preserving algorithm for frequent patterns mining based on noise increase is less than that of the privacy preserving algorithm for frequent patterns mining based on data cleaning. With the gradual increasing of the original data set, the algorithm implementation time of

privacy preserving algorithm for frequent patterns mining based on data cleaning is much greater than that of privacy preserving algorithm for frequent patterns mining based on noise increase.

From the above two experiments, in different experimental conditions, the privacy preserving algorithm for frequent patterns mining based on noise increase, from effectiveness, complexity and scalability, is superior to privacy preserving algorithm for frequent patterns mining based on data cleaning.

4. Conclusion

As a large number of private data or enterprise data are widely collected and analyzed, the application of data mining technology in these data containing sensitive information may be a threat to the privacy of individuals or businesses. Therefore, it is very meaningful to study how to deal with privacy preserving for the data sets applied in different fields of data mining. Based on the existing privacy preserving algorithm for frequent pattern mining based on data cleaning, a privacy preserving algorithm for frequent pattern mining is proposed. Compared with the method of hiding the sensitive patterns by deleting the sensitive items, the algorithm proposed in this paper can achieve the hiding of sensitive patterns by increasing the noise transactions. In addition, we design and implement the privacy preserving experiments for frequent pattern mining, and validate the effectiveness and performance of privacy preserving algorithm for frequent pattern mining based on the noise increase through experiments.

References

[1] Y. C. Chiu, S. Chen, G. J. Wu, Y. H. Lin: *Three-dimensional computer-aided human factors engineering analysis of a grafting robot.* Journal of Agricultural Safety & Health *18* (2012), No. 3, 181–194.

[2] Z. Li, X. G. Han, J. Sheng, S. J. Ma: *Virtual reality for improving balance in patients after stroke: A systematic review and meta-analysis.* Clinical rehabilitation *30* (2016), No. 5, 432–440.

[3] Y. Huang, Q. Huang, S. Ali, X. Zhai, X. Bi, R. Liu: *Rehabilitation using virtual reality technology: A bibliometric analysis, 1996—2015.* Scientometrics *109* (2016), No. 3, 1547–1559.

[4] S. Strangio, P. Palestri, M. Lanuzza, F. Crupi, D. Esseni, L. Selmi: *Assessment of InAs/AlGaSb tunnel-FET virtual technology platform for low-power digital circuits.* IEEE Transactions on Electron Devices *63* (2016), No. 7, 2749–2756.

[5] Y. Chao-Gan, Z. Yu-Feng: *DPARSF: A MATLAB toolbox for "pipeline" data analysis of resting-state fMRI.* Frontiers in Systems Neuroscience *4* (2010), No. 13, 13.

[6] J. A. Chen, M. S. Tutwiler, S. J. Metcalf, A. Kamarainen, T. Grotzer, C. Dede: *A multi-user virtual environment to support students' self-efficacy and interest in science: A latent growth model analysis.* Learning and Instruction *41* (2016), 11–22.

Received May 22, 2017

Acta Technica *62* No. 1A/2017, 167–178

Analysis of the evaluation system of energy enterprises based on KPI evaluation system

Bo Yu[1]

Abstract. Performance evaluation is an important mean to improve the efficiency of enterprise managements. In the energy industry, the application of performance appraisal system is still in the initial stage. In order to better enhance the performance management of energy enterprises, the application of performance appraisal system in China was introduced in this paper firstly, then A company was taken as an example, and the actual application of the performance evaluation system of energy enterprises was analyzed through the method of factor analysis model. Finally, the data obtained from factor analysis was analyzed and the conclusions were drawn. The result shows that the performance evaluation system of a company is not satisfactory, and the company's performance evaluation index is seriously inconsistent with the actual operation of the enterprise. According to the research results, the problems of energy enterprise assessment systems in this paper were summarized and relevant suggestions were put forward, so as to provide some references for the improvement of the performance evaluation of energy enterprises.

Key words. KPI, energy enterprise, performance evaluation, factor analysis.

1. Introduction

The rapid development of the market economy has brought unprecedented opportunities for enterprises in all sectors of our country. Under such an era background, the effectiveness of enterprise managements is very important for the long-term development of enterprises. And the assessment system of employees directly affects the efficiency of the whole enterprise management. At present, the energy sector is one of the sunrise industries in China. The development of energy enterprises is still in the initial stage, and how to do a good job of staff assessments is crucial. There are some errors in the assessment of staffs for many energy companies, for example, the strategic target is not clear, the assessment index is unreasonable, the assessment method is not proper and the feedback efficiency of the assessment result is

[1]Department of Economic Management, Xijing University, 1 Xijing Road, Xi'an Shaanxi, 710123, China

low. The assessment system and assessment management of most energy enterprises become a mere formality, which is of no benefits to the development of enterprises.

Assessment system is the basis of the staff incentive mechanism, and it is the most important part of human resource managements in energy enterprises. At the same time, the assessment system bears the primary responsibility for feedbacks on the information of employees' achievements. From this point of view, the evaluation system provides not only a bridge for communications between enterprises and employees, but also a reference for employees to continuously improve their work results. The fairness of the assessment system determines the overall development of the enterprise to a great extent. Performance appraisal system is the most widely used staff assessment system, which is an evaluation system that consists of a set of independent and interrelated evaluation indicators which can express the requirements of the evaluation. This assessment system can be used to conduct a more rational and comprehensive assessment of individual employees' work abilities through specific methods.

In the energy industry, the enterprise's human resource management departments have set up the corresponding performance appraisal system for staff assessments, but the application effect of performance appraisal system in most enterprises is not ideal. The application of performance appraisal system in our country is late, and many human managers still lack some experiences in the effective application of performance appraisals. In recent years, many enterprises begin to pay more attentions to the construction and design of performance systems. Enterprises in various industries have made great efforts in the selection of KPI indicators and the setting of weights. However, in the process of building performance evaluation systems, most enterprises draw on the experience of foreign related achievements and experiences, which is different from China's market economy and the development environment of enterprises, thus leading to the little effect of performance appraisal works in enterprises, and this phenomenon is reflected in the energy enterprises, which is particularly prominent.

Based on this, the selection of the performance evaluation index system and the optimization of the assessment system were analyzed and studied through the construction of factor analysis model in this paper.

2. State of the art

The concept of performance appraisal originated earlier in foreign countries, but our country had the form of performance appraisal since ancient times. At present, domestic and foreign scholars have conducted a lot of researches on performance appraisal systems, which not only includes the design of performance systems, the determination of evaluation indexes and the feedback validity of performance appraisals, but also makes a great deal of researches on the application of performance appraisal systems.

Wang put forward that performance management could be divided into two main aspects: peripherals and tasks. At the same time, he also made a detailed study on the model construction of performance managements (Wang et al. 2013) [1].

Under the background of international economic developments, Liu used the factor analysis method to determine the indexes and factors of enterprise performance evaluations, and the related factors that affected enterprise performance appraisals were also clarified and analyzed (Liu et al. 2014) [2]. He pointed out that the market structures, capital statuses, enterprise operating costs and enterprise profits would affect the performance of enterprises to varying degrees. Kosonen made a qualitative analysis of the effectiveness of enterprise performance managements. He studied the relationship between the two companies from the perspective of the impact of corporate reputations and corporate performances. The results show that the two are positively related (Kosonen et al. 2015) [3].

The above researches are the qualitative analysis of the concept, index and influencing factor of performance managements, which lacks the concrete analysis of the whole construction of the assessment system and the evaluation effect. At the same time, these studies have not put forward practical application performance evaluation systems from the point of view of practical applications of performance appraisal systems. Therefore, the construction of a targeted performance appraisal system is of great significance. In addition, scholars at home and abroad have done a lot of researches on enterprise performance managements. Rialland put forward a balanced scorecard approach. He believed that market shares, target customers, labor productivities and schedule completion rates should be included in the performance appraisal system (Rialland et al. 2014) [4]. Tian proposed to establish a strategy-oriented performance appraisal system, which mainly includes the intelligent behavior evaluation system, performance index evaluation system, potential evaluation and assessment system and so on (Tian et al. 2013) [5]. Piscesa believed that the development strategy of the performance management should be enterprise-oriented, and based on this, horizontal and vertical index system could be constructed, at the same time, the performance management system should include three aspects: behavior appraisal, performance evaluation and potential evaluation (Piscesa et al. 2017) [6]. Lavy believed that corporate strategies could serve as the main direction of performance managements (Lavy et al. 2014) [7]. However, it is very important to decompose the strategic performance management index and do the index decomposition and dynamic evaluation. Therefore, in view of the shortcomings of the existing research, a factor analysis model was proposed in this paper to analyze and study the existing performance appraisal system of energy enterprises. The factor analysis model can qualitatively analyze the indexes of the existing KPI evaluation system in the energy enterprises on the basis of previous studies, at the same time, the factor analysis model can also measure the rationality of the indexes through the score of each index factor, so as to provide a certain reference for the enterprise to adjust and select the assessment index reasonably.

The rest of the paper is organized as follows. In the third part, the research object and the concrete content of the factor analysis model construction were elaborated; In the fourth part, the specific data of the factor analysis model was obtained, and the data results were analyzed. In the last part, the paper was summarized and the relevant conclusion was given.

3. Methodology

In this paper, energy company A was selected as the object of study, and the KPI assessment system of energy enterprises was analyzed and researched through the construction of factor analysis model.

Company A is a subsidiary of the Energy Corporation of China in Shanxi province, and it is established in the mid-90s of the last Century, which is mainly engaged in coal washing and power generation. Enterprise achieves rapid developments under the leaderships of the head offices and their own technological advantages. At present, the company has accounted for 60 % of the market share in coal washing and power generation industries of Shanxi province. In order to make sustainable developments in the energy industry, it has introduced a more advanced human resource management system and formulated a more systematic performance appraisal system. Table 1 is the main content of the performance appraisal system adopted by A company.

Table 1. Performance appraisal system of company A based on KPI

Category	Content
Hypothetical premise	It is assumed that all necessary actions will be taken to achieve a predetermined goal
Purpose of examination	Taking the strategy as the center, and the design and application of the index system serve for the enterprise's strategic goal
Index generation	Within the enterprise, the strategic objectives are decomposed from top to bottom
Source of indicators	Based on strategic objectives and competitive requirements of value-added work outputs of enterprises
Composition and function of indexes	Through the combination of finance and non-finance, it reflects the principle of paying attention to short-term benefits and taking long-term developments into account. The index itself not only conveys the result, but also delivers the process of producing the result

In the process of performance appraisals, managers of A enterprise found that there were some problems in the assessment. Department staffs thought that management scores were biased, and managers were beginning to show negative emotions about their workload. They thought their work pressure and work task were heavy, and there was no time to fill out a large number of examination forms and documents. After two years, through this performance appraisal system, A company

had not obtained the more ideal results, so enterprise managers believed that performance appraisal system had not played its proper role. From the feedback of the performance appraisal, the author hopes to analyze the performance appraisal system of enterprises through the factor analysis, so as to find out the existing problems in performance appraisals and ultimately improve the performance evaluation results and experiences for reference of other energy enterprises.

Mascia believed that factor analysis referred to the study of statistical techniques for extracting common factors from variable groups (Mascia et al. 2016) [8]. This method of analysis was proposed by British psychologists. In the study of student achievements and other contents, psychologists found that students had good results in all subjects, so the level of achievements was good, so that they put forward the existence of common factors. From this life example, it can be seen that factor analysis is the method of finding common influence factors in different influencing factors. Figure 1 is the general idea of factor analysis of the performance appraisal system of A enterprise.

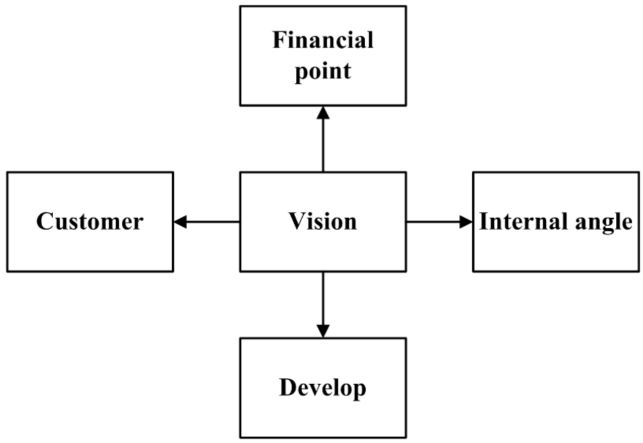

Fig. 1. Analysis thinking of evaluation factors of A company

Horta considered that factor analysis method could effectively reduce the complexity of computation and realize the best analysis of things through the assumption of variable relations (Horta et al. 2014) [9]. Tong believed that the methods of factor analysis included exploratory and confirmatory. The former does not have the hypothesis, while the latter assumes the presupposition as the basis of analysis (Tong et al. 2015) [10]. Liu thought there were many kinds of factor analysis methods. These methods are approximate analysis methods based on correlation coefficient matrixes (Liu et al. 2014) [11]. Edokpia believed that principal component analysis was a typical example of factor analysis (Edokpia et al. 2013) [12]. Veronesi believed that the main advantage of confirmatory factor analysis was that it could analyze and study the details of the theoretical model (Veronesi et al. 2015) [13]. Therefore, there are many different factor items in the analysis of validity and validation, and there are some hierarchical and progressive relations among these items. Gail-

lard considered that measurement model was one of the main application models of confirmatory factor analysis (Gaillard et al. 2016) [14]. The main reason why the paper chooses the factor analysis model to analyze the performance evaluation system of energy enterprises is that the business scope involved in energy enterprises is more specific and its business line is clear, and this kind of enterprise category is not complicated. These facts are good for factor selections and classifications of factor analysis models. At the same time, the actual operation of energy enterprises is conducive to the construction and analysis of the factor model.

In factor analysis, the number of factors needs to be specified by the analyst, while the number of factors specified is different and the result is different. In principal component analysis, the number of ingredients is certain, and there are several variables, in which there are several principal components. Compared with principal component analysis, factor analysis can help to explain factors by using the rotational technology, and it has more advantages in interpretation. Generally speaking, when searching for potential factors and explaining these factors, they are more inclined to use factor analysis, and it can help to explain better with the aid of rotational technology. If we want to change the existing variables into a few new variables for subsequent analysis, the principal component analysis can be used. Of course, this can be done with factor scores. So this distinction is not absolute.

The factor analysis method is used to construct the performance appraisal system of A energy enterprise, as follows:

Firstly, the assessment teams are established, including members of the group of human resource experts, evaluation experts and other staffs. Generally speaking, the difference between the object and purpose of the examination determines the basis for the selection of the examination experts.

Secondly, according to the related evaluation systems for factor analysis, judgment and choice, the corresponding comparison for each factor is obtained by experts of, and there will be a more specific score. Allen considers that the factor judgment of enterprise assessment systems is mainly based on the correlation of factor variables (Allen et al. 2013) [15]. Generally speaking, factor analysis should firstly be compared and divided into groups. Each group of variables represents the corresponding factor structure, and the common factor and the random variable are determined according to the structure of the factors. At the same time, we must construct the linear model of the index according to the formula

$$X = AF + \varepsilon\,, \tag{1}$$

where A is a linear coefficient, F is a common factor and ε is a random variable.

Thirdly, the result of factor comparison is compared and the score of each factor is calculated according to the following formula

$$D_{i\mathrm{R}} = \sum_{i=1}^{n}\sum_{j=i}^{n} a_{ij}\,. \tag{2}$$

Here, $D_{i\mathrm{R}}$ is the factor evaluation value and a_{ij} is the factor value.

Fourthly, the average value of factor evaluation is obtained according to the formula

$$P_i = \sum_{R=1}^{L} \frac{D_{i\mathrm{R}}}{L}\,, \tag{3}$$

where P_i is the average value of the factors and L is their value.

Fifthly, the results of the calculation of comprehensive statistics and the weights of the assessment index are calculated according to the formula

$$W_i = \frac{P_i}{\sum_{i=1}^{n} P_i}\,. \tag{4}$$

Sixthly, according to the contrast of the above calculation results and the existing assessment systems of each factor index, the problems and advantages of the performance appraisal system are found.

4. Result analysis and discussion

By using the method of factor analysis model, the performance evaluation system of A company was analyzed and studied. The results are listed in Table 1.

The indicators and weights of employees' performance appraisal of energy company A are shown in Table 2. One of the examined staffs was taken as an example, the performance evaluation indexes of each grade of KPI were calculated as follows:

Financial performance index $= 90 \times 0.3 + 100 \times 0.15 + 96 \times 0.15 + 96 \times 0.4 = 95$.

Operating efficiency index $= 95 \times 0.22 + 85 \times 0.5 + 88 \times 0.28 = 88$.

Competitive capability index $= 90 \times 0.42 + 90 \times 0.42 + 95 \times 0.16 = 91$.

Service quality index $= 95 \times 0.34 + 96 \times 0.33 + 95 \times 0.33 = 95$.

Social contribution index $= 92 \times 0.5 + 95 \times 0.12 + 90 \times 0.38 = 92$.

Capability index $= 90 \times 0.32 + 94 \times 0.68 = 93$.

The performance evaluation index score of the second-class KPI index was calculated as follows:

Financial performance index $= 90 \times 0.3 + 96 \times 0.15 + 95 \times 0.15 + 95 \times 0.4 = 94$.

Operating efficiency index $= 95 \times 0.22 + 95 \times 0.5 + 88 \times 0.28 = 93$.

Competitive capability index $= 90 \times 0.42 + 92 \times 0.42 + 95 \times 0.16 = 92$.

Service quality index $= 92 \times 0.34 + 95 \times 0.33 + 90 \times 0.33 = 92$.

Social contribution index $= 95 \times 0.5 + 90 \times 0.12 + 85 \times 0.38 = 91$.

Capability index $= 88 \times 0.32 + 90 \times 0.68 = 89$.

According to the weight of employee evaluation indexes of A enterprise, the factor function $M_i = \sum_{n=1}^{2} A_n F_n$ was applied to make the factor analysis and sorting to get two main factors. The specific contents are shown in Table 3. From the data in Table 3, it can be seen that the corporate social contribution index and the capacity index are more reasonable, and the differences between the financial performance and operational efficiency index, competition ability index and service quality index of main factors are larger. Its rationality is not ideal, and these indicators need to make some appropriate adjustments.

Table 2. Indicators and weights of employee performances in A company

The first-class KPI index	The second-class KPI index	Self-evaluation score	Assessment team score	Departmental colleague score
Financial performance index	Net assets income	90	90	86
	Turnover of total assets	100	96	95
	Sales growth rate	96	95	95
	Rate of profit growth	96	95	96
Operating efficiency index	Utilization ratio of cost	95	95	86
	Delivery accuracy	85	95	86
	Logistics management cost rate	88	88	88
Competitive capability index	Timely rate of information feedback	90	90	95
	Contribution rate of new products	90	92	95
	Technology input rate	95	95	90
Service quality index	Customer acquisition rate	95	92	90
	Customer satisfaction	96	95	92
	Customer retention rate	95	90	95
Social contribution	Rate of total assets	92	95	95
	Public participation rate	95	90	92
	Ecological efficiency	90	85	86
Capability index	Labor discipline	90	88	90
	Work efficiency	94	90	90

Table 4 is the final factor analysis score of employee performance evaluation in A company. Figure 2 is a comparison of employee factor scores in A company. The data shows that the result of factor analysis of employee performance appraisal of A company has great difference, at the same time; there is the stratification in the evaluation of performance indexes of the enterprise staffs.

Table 3. Coefficients of factor scores

Original index	Main factor 1	Main factor 2
Financial performance index	0.887	-0.106
Operating efficiency index	0.924	0.199
Competitive capability index	0.862	0.238
Service quality index	0.885	0.410
Social contribution index	0.649	0.906
Capability index	0.629	0.950

Table 4. Comprehensive factor score of staff performance evaluations in A company

Staff code	Composite score	Score of main factor 1	Score of main factor 2
1	3.460	4.542	2.189
2	3.413	4.452	2.269
3	1.485	2.548	-1.334
4	1.916	2.742	0.352
5	-2.140	-3.113	-0.201
6	-2.405	-2.597	-3.651

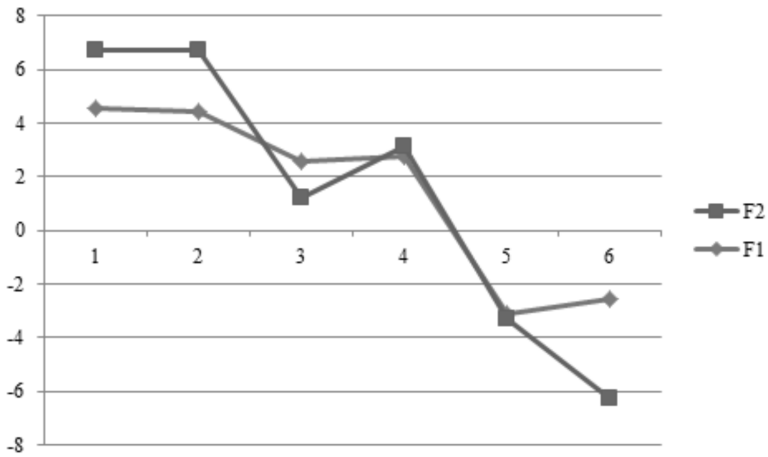

Fig. 2. Comparative analysis of employee factor scores

Thus, the performance evaluation system of A enterprise lacks a certain degree of scientificalness, and at the same time, the choice of the enterprise performance

evaluation indicators is inconsistent with the actual operating environment of the enterprise. Therefore, the author puts forward the following suggestions to adjust and improve the KPI performance appraisal system of energy enterprises: First of all, the energy enterprises should start from the actual situation to make the popularization of cultural knowledge of performance managements in the enterprise, so they to need not only actively communicate with all levels of the organization, but also implement the unified and fair performance management to all employees; Secondly, from the point of view of enterprise management systems, it is necessary to establish the interview system and complaint system of performance appraisals, so as to strengthen the layered communication of internal performance managements; Finally, the introduction of information management systems of enterprise performance appraisal systems can help employees to better understand and accept the performance management, so as to make researches reasonably choose the corresponding performance evaluation index and enhance the overall effect of enterprise performance managements.

5. Conclusion

In order to improve the performance appraisal system and enhance the effect of the enterprise performance management, in this paper, company A was taken as an example on the basis of the construction of the factor model, and the performance appraisal system of energy enterprises was analyzed, and the existing problems of performance appraisals of the enterprise were put forward. Finally, the main conclusions were drawn as follows:

(1) The social contribution index and capability index of this enterprise are more reasonable, and the differences between the other assessment indexes are greater, and their rationality is not ideal. These indexes need to be adjusted appropriately.

(2) The results of factor analysis of performance appraisals of employees in A enterprise have great differences, at the same time; there is a stratification in the evaluation of performance indexes of the enterprise staffs.

(3) The performance appraisal system of A enterprise is not scientific enough, and the choice of the enterprise's performance evaluation index does not accord with the actual operating environment of the enterprise.

To sum up, the existing performance appraisal system of energy enterprises has the problem that the index selection is inconsistent with the actual operation. The method of factor analysis used in this paper is helpful to make clear the direction of the reasonable index of performance appraisals. However, because there are still some differences among the energy companies, the research of this paper still has some reference values, but there are some shortcomings too. The author believes that energy companies can improve the effectiveness of performance managements from perspectives of system managements and performance cultures.

References

[1] W. Wang: *Design of performance assessment system of human resource operation of logistics enterprises based on KPI.* Logistics Technology *4* (2013), No. 01, 11–19.

[2] X. Liu, X. N. Zhu: *Study on assessment method of logistic service performance based on KPI.* Railway Transport and Economy (2014), No. 09.

[3] D. Kosonen: *Plant operation performance assessment in O&M Brownfield cases.* Aalto University Library, Finland (2015).

[4] A. Rialland, D. A. Nesheim, J. A. Norbeck, Ø. J. Rødseth: *Performance-based ship management contracts using the shipping KPI standard.* WMU Journal of Maritime Affairs (JoMA) *13* (2014), No. 2, 191–206.

[5] H. X. Tian, R. H. Fan, Y. R. Jia : *Design and establishment on clinical departments performance assessment index system in a hospital in Shanxi province.* Soft Science of Health (2013), No. 05.

[6] B. Piscesa, M. M. Attard, A. K. Samani, S. Tangaramvong: *Plasticity constitutive model for stress-strain relationship of confined concrete.* ACI Structural Journal *114* (2017), No. 02, 361–371.

[7] S. Lavy, J. A. Garcia, P. Scinto, M. K. Dixit: *Key performance indicators for facility performance assessment: Simulation of core indicators.* Journal Construction Management and Economics *32* (2014), No. 12, 1183–1204.

[8] M. Mascia, S. Hu, K. Han, A. Sun, R. North, J. D. Lees-Miller: *A holistic approach for performance assessment of personal rapid transit.* Research in Transportation Business & Management *18* (2016), 70–76.

[9] I. M. Horta, A. S. Camanho: *Competitive positioning and performance assessment in the construction industry.* Expert Systems with Applications *41* (2014), No. 4, 974 to 983.

[10] G. L. Tong: *The innovation of the company's assessment system based on the Balanced Scorecard and KPI theory.* Technological Development of Enterprise, (2015), No–ID. 20150889474, 7413.

[11] L. Q. Liu: *CRM-based researches and designing of KPI system in university library management.* Journal of Shijiazhuang Vocational Technology Institute (2014), No. 06.

[12] R. O. Edokpia, P. C. Oparah: *Maintenance and availability study of a manufacturing company: Case study of a flour mill company.* Advanced Materials Research *824* (2013), Chapter 8, 584–594.

[13] M. Veronesi, A. Visioli: *Deterministic performance assessment and retuning of industrial controllers based on routine operating data: applications.* Processes *3* (2015), No. 1, 113–137.

[14] P. Gaillard: *Rational solutions to the KPI equation and multi rogue waves.* Annals of Physics *367* (2016), 1–5.

[15] V. Allen: *Home improvement.* Journal of Obstetrics & Gynaecology Canada *35* (2013), No. 1, 11–13.

Received May 22, 2017

Acta Technica *62* No. 1A/2017, 179–190

Design and key technology of coal mine safety monitoring system based on analytic hierarchy process (AHP)[1]

Gao Xiaoxu[2,3]

Abstract. The paper aims at analyzing the causes for coal mine safety accidents dishonesty and verifying the applicability of coal mine safety monitoring system. The analytic hierarchy process (AHP) is used to establish the dishonesty model of gas explosion. In addition, combined with the current situation of coal mine safety monitoring system and the development trend of wireless sensor network technology, the design scheme of coal mine comprehensive monitoring system based on wireless sensor network technology is put forward. What is more, on the basis of theoretical research, based on CC2430/CC2431 node design, the safety monitoring system in a wireless sensor network is achieved, and the test of the system in the simulated mine is carried out. The test results showed that when the layout distance of wireless nodes is 10 m, it meets the communications needs of the system. In conclusion, the coal mine safety monitoring system is of great significance in reducing coal mine accidents, which has good performance and applicability.

Key words. Analytic hierarchy process, wireless sensor, coal mine safety, monitoring system
.

1. Introduction

Coal is the foundation of our national economy and social development. Our country belongs to the country poor in oil but rich in coal. At present, the coal energy accounts for about 73 % of energy production and consumption in China. Moreover, for a long time in the future, the status of coal as the major energy will not change. As a result, the coal still is a basic industry related to sustainable development of national economy, and this situation will not change in the long historical period. Safety is very important for coal production. At present, the

[1]The study was Supported by National Natural Science Foundation of China (51504183).

[2]School of Energy Science and Engineering, Xi'an University of Science and Technology, Xi'an Shaanxi 710054, China

[3]Key Laboratory of Western Mine & Hazard Prevention, China Ministry of Education, Xi'an Shaanxi 710054, China

production of coal mine in our country is mainly using the method of well drilling, and the production environment is complex, so it is essential to ensure the safe production of coal mine [1]. After years of development, the security situation of China's coal industry has been significantly improved. However, the underground casualty accident is still very serious, and major accidents occurred sometimes, which has become a "bottleneck" problem that constraints the development of China's coal industry.

Since that China's coal seam conditions and geological structure are complex, spontaneous combustion, high gas, coal and gas outburst coal seam are various. As a result, it resulted in the complex safety problems in the production of coal mine. In addition, with the increase of mining depth and development of high yield and high efficiency coal mine, it put forward many new security technology problems for the safety production of coal mine in China. Therefore, it is an inevitable trend of loss of historical development and the urgent problem in the coal industry safety needed to be solved to take scientific, systematic, and complete measures to change the coal security situation in our country and the backwardness, and to strengthen the research and application of the safety management and safety science and technology. In addition, it is quite urgent to effectively prevent and control all kinds of accidents, and reduce the casualties and economic loss caused by all kinds of accidents.

From the causes of coal mine accidents in China in recent years, in China's coal mine accidents, the vast majority are caused by responsibility accidents. In consequence, to simply improve the coal mine safety control technology is not enough to solve the present situation of mining accidents in our country [2]. Instead, only by comprehensively and systematically analyzing coal mine accident causes, finding the root cause of coal mine accidents, establishing effective accident model, and taking effective measures and countermeasures from two aspects of technology and management, can we effectively prevent and reduce the occurrence of coal mine accidents and the hazards brought about. This paper starts from research on the dishonesty factors resulting in all kinds of typical coal mine safety accidents, and uses AHP method to construct the coal mine safety accidents dishonesty model. In addition, we make a systematic analysis of the causes of coal mine safety accidents by the importance degree of influence of various dishonesty factors on the accidents. What is more, on this basis, for the existing problems of coal mine safety monitoring system, according to the development trend of wireless sensor network technology, we put forward the solution for the coal mine safety monitoring system based on wireless sensor network.

2. Methodology

According to statistics of the State Administration of Work Safety, in the past five years, gas accidents accounted for a half of the coal mine safety accidents with more than 10 people died. And the gas explosion accident accounted for the first in all gas accidents. As a result, this paper only selects the representative top 45 gas explosion typical coal mine safety accident with high occurrence percentage and frequency for the analysis.

2.1. Accident cause statistics

First of all, according to the necessary conditions of the controllable gas explosion, we make a classification statistics of the direct causes of the 45 accidents: the fire source causing the occurrence of accidents and the reason of the gas concentration overrun, and the data in Table 1 are obtained.

Table 1. Statistical analysis of gas explosion accident

Necessary conditions for gas explosion	Reasons	Frequency
Source of fire	Electric spark	17
	Blasting spark	17
	Others	11
Gas concentration overrun	Ventilation system	27
	Mined out area	6
	Others	12

2.2. Establishment of the hierarchy model of dishonesty factors

Through the investigation report of the 45 cases of heavy gas explosion accidents, we can see that these accidents are all the responsibility accidents, so they can be attributed to the personnel dishonesty factors and the equipment dishonesty factors. For the personnel dishonesty factors, they include managers' dishonesty and staff dishonesty.

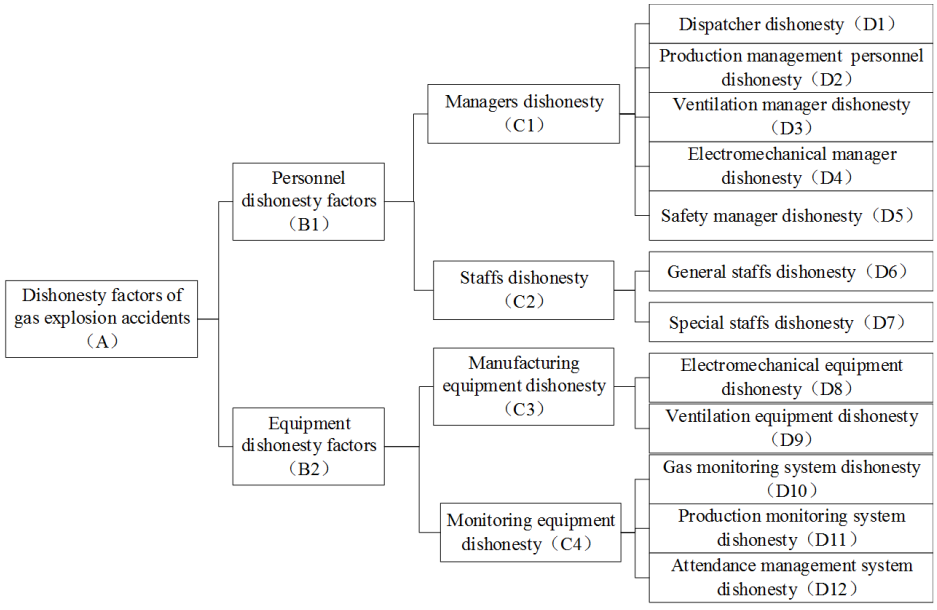

Fig. 1. Hierarchy structure model of dishonest factors in gas explosion accident

For equipment dishonesty factors, they include the production equipment dishonesty and monitoring equipment dishonesty. Through the dishonesty analysis of the gas accident, the dishonest factors in the gas accident are decomposed into several sub factors, and the hierarchical structure model is constructed according to the relationship among these factors, as shown in Fig. 1.

2.3. Construction of judgment matrix

The analytic hierarchy process uses 1∼9 scaling to assign the importance degree of various factors, and the value of each factor we get is the number for them appearing in the accident. In consequence, the differences between various factors are used as the basis for determining 1∼9 scaling. Set the difference of each factor value to be $a_x = u_i - u_j,\ x = 1, 2, ..., n$, where n indicates the number of lower indicators [3]. And for the lower level indicators u_i and u_j corresponding to the higher level indicators, the meaning of corresponding 1∼9 scales are shown in Table 2. According to the meaning of scales in Table 2, the comparison judgment matrix under different criteria can be obtained.

Table 2. Meaning of 1∼9 scaling

Scaling	Difference (a_x)	Meaning
1	0∼4	It represents that u_i and u_j have the same importance.
3	6∼9	u_i is slightly more important than u_j
5	11∼14	u_i is more important than u_j
7	16∼19	u_i is quite important than u_j
9	above 20	u_i is extremely important than u_j
2,4,6,8	5,10,15,20	The adjacent intermediate values of above judgments
1,1/2,1/3,...,1/9	The negative values	The importance ratio of u_i to u_j is a_{ij}, then the importance ratio of u_j to u_i is $1/a_{ij}$

According to Table 2, we can obtain the judgment matrix W between managers and the subordinate personnel in the form

$$W = \begin{bmatrix} C_1 & D_1 & D_2 & D_3 & D_4 & D_5 \\ D_1 & 1 & 9 & 1 & 1/5 & 1/7 \\ D_2 & 1/9 & 1 & 5 & 3 & 2 \\ D_3 & 1 & 1/5 & 1 & 1/5 & 1/7 \\ D_4 & 5 & 1/3 & 5 & 1 & 1/2 \\ D_5 & 7 & 1/2 & 7 & 2 & 1 \end{bmatrix}$$

The vector of characteristics values of the matrix is $W = (0.0426, 0.4285, 0.05, 0.1823, 0.2965)$.

Matrix W refers to the weights of four kinds of personnel dishonesty, including dispatcher, production managers, ventilation managers, electromechanical managers, and safety managers. Similarly, we can get the various judgment matrices under other criteria. We calculate and obtain the comprehensive weights of various dishonesty factors, and thus get the dishonesty model of gas accidents.

According to the dishonesty model of gas accidents, the weight of personnel dishonesty accounted for 0.9, while the weight of equipment dishonesty is only 0.1 [4]. And in the staffs' dishonesty, what accounted for the larger weight are the special personnel dishonesty, production management personnel dishonesty and safety management personnel dishonesty.

3. Result analysis and discussion

In view of defects and shortcomings in the coal mine safety monitoring and control system, and underground dishonesty factors, we put forward the coal mine safety monitoring system based on wireless communication technology and the multimedia wireless sensor network technology. It is composed of sensing and detecting system, security information network and communication system, security management information system, safety warning decision and decision support system, and rescue information support system, as shown in Fig. 2.

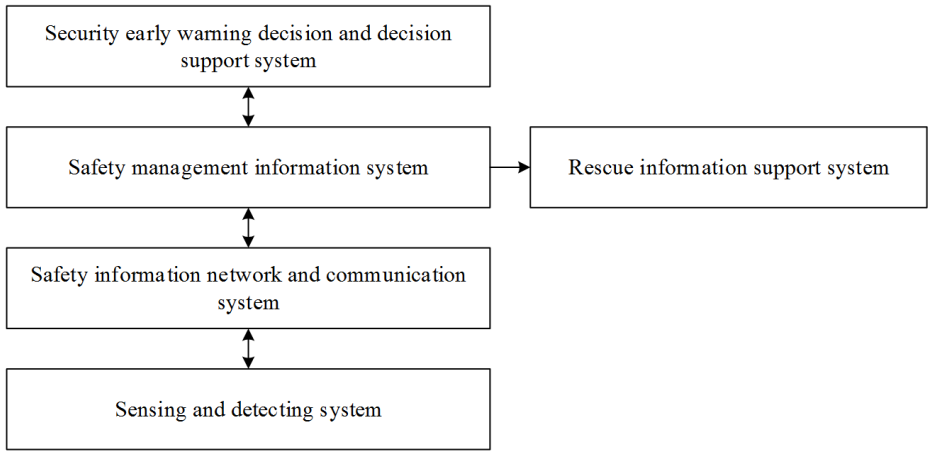

Fig. 2. Structure of coal mine safety monitoring system

3.1. Sensing and detection system

Sensing and detection system is the bottom support system of a coal mine safety comprehensive monitoring system. It is composed of a large number of sensors underground and wireless sensor network nodes, to realize the collection of underground basic data, and to upload it to the upper system for processing. Sensor is the terminal equipment for underground data acquisition, which can acquire the

underground environment and equipment data. In accordance with the needs of underground production safety monitoring, sensors usually include environmental sensors, equipment sensors, video sensors, audio sensors and vital signs sensors.

Each sensor is connected with the underground wireless sensor network nodes through the interface. Each underground sensor node has the function of calculation, storage, and wireless communication, with embedded operating system inside. According to the monitoring needs, write the monitoring program [5]. Each sensor node has the intelligent interface identification function. It can automatically identify the connected sensor types and models, and automatically call the corresponding monitoring program to drive the sensor to work.

3.2. Safety information network and communication system

The system is mainly used for data transmission of safety monitoring system. Wireless sensor network (WSN) is a network composed of a large number of micro mobile sensor nodes, which can monitor, perceive and collect environmental information, process the data and transmit to the monitoring center. It combines sensor technology, remote control technology, embedded computing technology, distributed information processing technology and wireless communication technology. It can be widely used in coal mine harmful gas monitoring, moving target tracking, environmental state changes monitoring and so on.

The underground wireless sensor network is composed of three parts: wireless gateway, wireless sensor node and sensor. The gateway is the connection and conversion equipment between wireless sensor networks and wired LAN, with computing and storage capacity. It is the data export of wireless sensor network, responsible for data transmission acquired by wireless sensor network to the wired network, and transmission of the control command to the wireless sensor network.

The overall structure of the integrated monitoring system of mine is shown in Fig. 3. The system is mainly composed of integrated ground control station, intrinsically safe network intelligent substation, flameproof and intrinsically safe network switches, intrinsically safe network video server, intrinsically safe mobile communication base station, intrinsically safe network camera, cable or coaxial cable, wireless sensor network convergence device, sensor nodes and so on. The system is interconnected with the local area network and the Coal Mining Group Corporation (Bureau) wide area network [6].

3.3. Safety management information system

The safety management information system is used to deal with the state data of the environment, equipment, personnel, vehicles and so on acquired underground, and to issue various control commands according to the needs of safety control. Mine information is the dynamic and active information that is closely related to spatial location information. The safety monitoring information with location information is meaningful. And the coal mine safety monitoring information is dispersing in positions and unified in types. The data content collected by different monitoring

systems has different types and the forms are dispersing, necessary for effective integration. Only in this way can it provide complete, comprehensive and unified safety information for coal mine safety managers [3]. Therefore, based on the coal mine geographic information system (GIS), the platform of safety management information system is constructed which organically integrates various monitoring information systems.

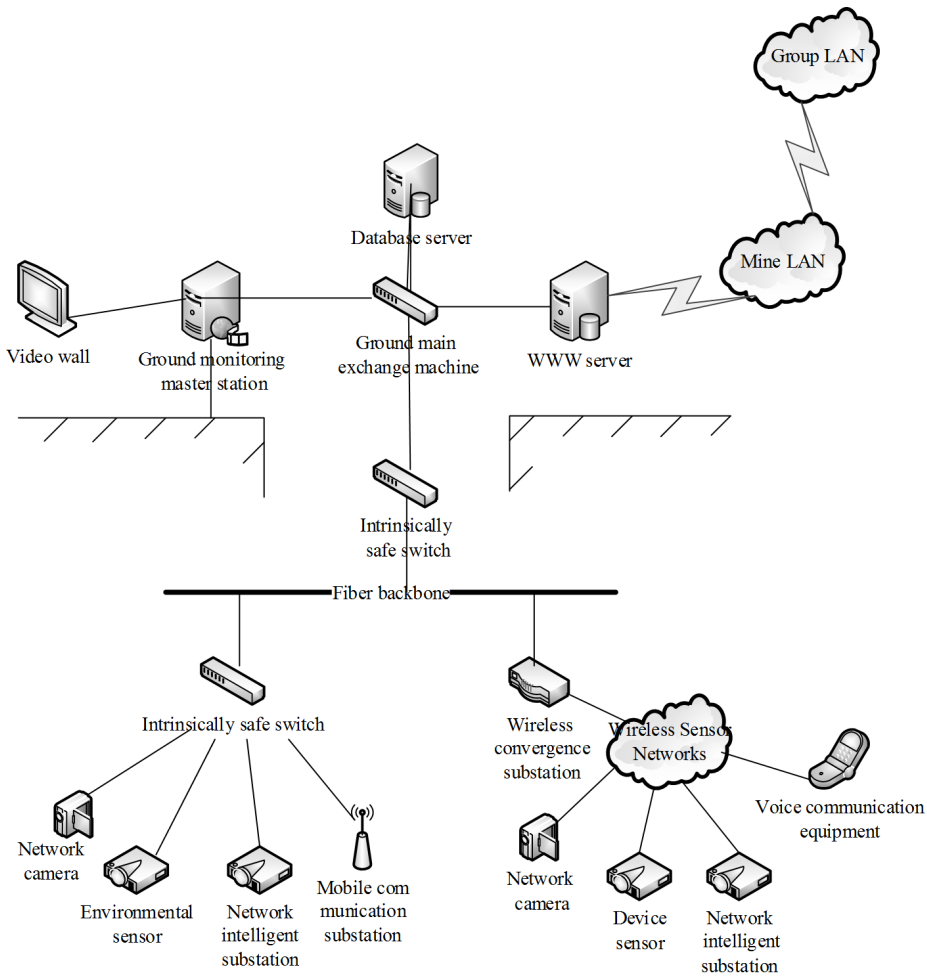

Fig. 3. The overall structure of the system

3.4. Security early warning decision and decision support system

Safety early warning decision and decision support system, based on coal mine safety production needs, combined with geological conditions of coal mines, establishes a variety of security early warning models and realizes the online identification of security risks. The system is able to in time identify the major hazard sources that may be of high risk, to send out early warning signals, and to start early warning response action plan according to the environment, equipment and production data. At the same time, it can be used to evaluate the changing process of the hazard degree of high risk source in real time, and to continuously change the level of the early warning, so as to adapt to the complex coal mine production environment. The decision support system shall carry out uninterrupted continuous monitoring on all kinds of underground dangerous source. According to the enterprise development, the critical value or the critical environmental parameters Approved by industry authorities make a dynamic monitoring of the dangerous source. As long as there is a danger source reaching the set value, enterprises have entered into early warning management period.

3.5. Rescue information support system

The rescue information security system can extract the information needed by the rescue from the security information management system after the occurrence of the mine disaster, which can be used for rescue decision makers to facilitate the timely rescue. Rescue information security system can extract the number of personnel underground and distribution information when the accidents occur from the underground personnel positioning system. In addition, it can extract various environmental data from underground mine environment information system when the accidents occur. Moreover, it can extract the state of various equipment information from the equipment information system when accidents occur. At last, it can extract underground geological data, distribution of roadway information from the underground GIS system. Rescue information security system, based on the extracted information, can use virtual reality technology to generate three-dimensional tunnels real map information and simulate the effect graph of underground mine accidents. What is more, it can analyze the possible personnel moving track and distribution after the mine accidents occurred, and based on virtual reality technology, simulate the effects of various rescue scheme, so as to determine the best rescue plan.

3.6. Data analysis

The beacon node of the wireless sensor network node of the system uses the CC2430 node, the unknown node uses the CC2431 node, and the sink node uses the C51RF-CC2431-ZDK network expansion board. The software development environment of CC2430/CC2431 node is composed of IAR Embedded Workbench and C51RF-CC2431-ZDK emulator. PC control software is running on the PC control computer, and making data exchange with the sink node through the RS232 inter-

face. It is mainly responsible for the deployment of nodes in the wireless sensor network, network data receiving, storage and graphical display.

In order to verify the change of network signal of the coal mine safety monitoring system based on wireless sensor network with the distance, we design the experiments that the underground signal intensity changes with the distance. First of all, according to the wireless sensor network test platform constructed, the acquisition and test of the RSSI value between the nodes with the distance in the tunnel is carried out. The two nodes are deployed in the underground roadway and the transportation lane, one is the transmitter, and the other is the receiving end. Continuously change the distance between the nodes and record the RSSI value of the communication between the two nodes.

The results of the experiments are shown in Figs. 4 and 5.

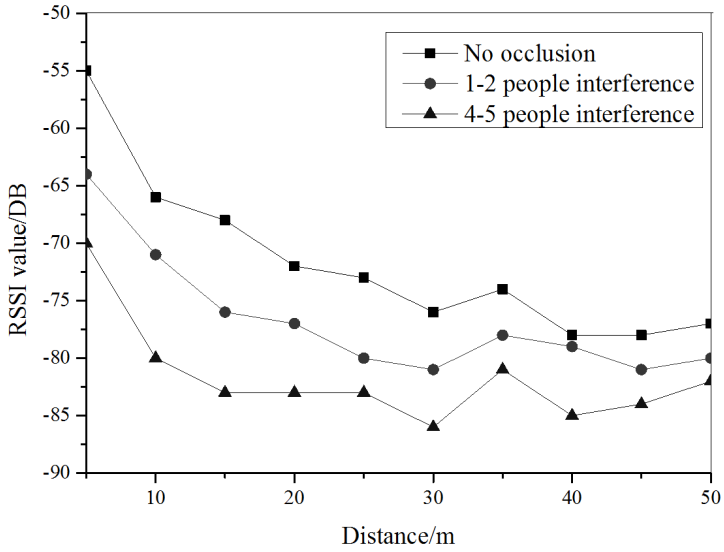

Fig. 4. RSSI test data in main lane

As can be seen from the results, with the increase of distance between the transmitter node and the receiving end node, the change of distance will result in that the RSSI values between nodes produce greater change. The closer the two nodes distance, the stronger the received signal strength, and the greater the RSSI value; the farther the distance, the weaker the received signal strength, and the smaller the RSSI value. In the case of the same distance, with the narrowing of the tunnel width, the attenuation degree of wireless signal is increasing, and the narrower the roadway is, the smaller the RSSI value received in the same distance will be. Because the width of the roadway is larger than the width of the lane, the signal attenuation in the traffic lane is worse than that in the lane. When there is no barrier between the nodes, the change of RSSI value with the distance is relatively smooth; when the nodes are shielded, the change curve of RSSI value with the distance is relatively fast, and with the increase of disturbance, the degree of signal attenuation increases.

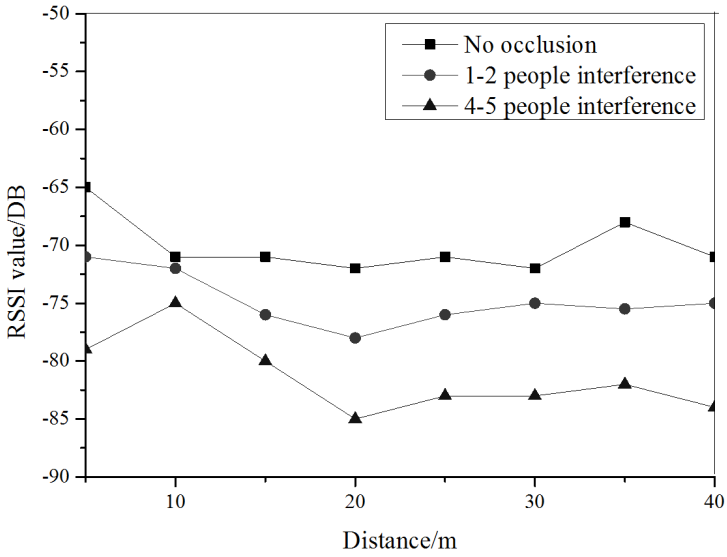

Fig. 5. RSSI test data in the transport lane

The experimental results showed that when the distance between nodes is 10 m, the intensity of the signal meets the needs of the system

4. Conclusion

According to the present situation of coal mine accidents in our country, this paper analyses the causes of the typical coal mine safety accidents from the perspective of dishonesty by the statistics and analysis of the typical coal mine safety accidents in recent years. Using AHP method, we establish the dishonesty model of the typical gas explosion accidents. In addition, on this basis, in view of the existing problems of coal mine safety monitoring system, combining with the development trend of wireless sensor network technology, we put forward the solution of coal mine safety monitoring system based on wireless sensor network. It is composed of five parts: a sensing and detection system, security information network and communication system, safety management information system, safety early warning decision and decision support system, and rescue information support system. The experimental results showed that when the distance between the nodes is 10 m, the signal strength of the underground wireless network meets the needs of system data transmission.

References

[1] T. L. Saaty: *Decision making with the analytic hierarchy process.* International Journal of Services Sciences *1* (2008), No. 1, 83–98.

[2] O. S. Vaidya, S. Kumar: *Analytic hierarchy process: An overview of applications.* European Journal of Operational Research *169* (2006), No. 1, 1–29.

[3] G. Sun, H. Zhou, K. Sun: *Coal mine safety evaluation method based on incomplete labeled data stream classification.* Open Cybernetics & Systemics Journal *8* (2014), No. 1, 918–923.

[4] D. Mondal, P. N. S. Roy, PP. K. Behera: *Use of correlation fractal dimension signatures for understanding the overlying strata dynamics in longwall coal mines.* International Journal of Rock Mechanics and Mining Sciences *91* (2017), 210–221.

[5] S. Han, H. Chen, R. Long, H. Qi, X. Cui: *Evaluation of the derivative environment in coal mine safety production systems: Case study in China.* Journal of Cleaner Production *134* (2017), 377–387.

[6] L. Xin, Z. T. Wang, G. Wang, W. Nie, G. Zhou, W. M. Cheng, J. Xie: *Technological aspects for underground coal gasification in steeply inclined thin coal seams at Zhongliangshan coal mine in China.* Fuel *191* (2017) 486–494.

Received May 22, 2017

Acta Technica *62* No. 1A/2017, 191–200

Optimization scheme of computer network reliability

Weilong Zhang[2], Tao Yu[2]

Abstract. With the rapid development of computer network technology, computer networks rise gradually, and penetrated into all aspects of the national economy. Whether it is political and economic or commercial, etc., each domain is inseparable from the computer network. Based on this, the application of computer network reliability optimization scheme was studied. In this paper, firstly, the computer network was briefly introduced, and then the application of computer network model planning in computer network processing was studied, finally, the optimization design of computer network reliability was carried out and the actual test was carried out. The results show that the reliability factors of computer network reliability analysis are more comprehensive, and the establishment of computer network reliability index system is more objective and realistic.

Key words. Computer network, reliability, optimization, network processing.

1. Introduction

The concept of computer network reliability was proposed in the 1970s. Due to the rapid development of communication technology, optical fiber technology and computer Internet technology, the function of network is becoming more and more important, and the research on the reliability of computer network is deepening. With the beginning of the process of social information, computer network users continue to increase, the computer network connection area and network connection scale also expands rapidly. As the computer network is widely used in business, banking, transportation, communications and other important areas, the computer network function is huge and the complexity of the structure is proportional. In view of this situation, in this paper, we study the optimization of computer network reliability. Computer network is an important foundation of research. So in this paper, firstly, computer network standards and types were studied, then programming model of computer network was analyzed, some results were obtained, finally, the computer network reliability optimization design was studied in detail, and the

[1]Chongqing College of Electronic Engineering, 401331, Chongqing, China
[2]Hebei Vocational College of Labour Relations, Shijiazhuang, 050002, Hebei, China

experiment was carried out. It is shown that the computer network link cost model and the computer network reliability model can meet the actual demand. It can accurately describe the state of the computer network and it has a good application prospect.

2. State of the art

In foreign countries, the earliest research on computer network reliability began with Professor Lee's research on telecom switching networks. The failure of computer network components greatly reduces the total transmission capacity of the telecommunication switching network, which causes call congestion, and the telecommunications exchange network area is significantly paralyzed. Professor Li defines call congestion as a link failure for a telecommunications switching network, and he first presents a reliability measure of a computer network based on connectivity [1]. In 1968, the world's first computer network Arpanet was born in the United States, which led to a lot of research on the reliability of computer networks. During this period, it is primarily a network connection. The connectivity of a computer network is required as a standard reliability requirement: As long as the computer network links, or as long as the communication between the computer network users need to connect, or computer network node failure, the computer network is in the process of work [2]. Wilkov, AHC, Baggal and other well-known scholars have given some connection based on the standard computer network reliability measures. Computer network reliability optimization design is firstly proposed by Boesch, which mainly involves the computer network reliability optimization and other issues about the improvement of the computer network topology. In the process of discussing these two problems, the calculation of the reliability of computer network is inseparable. On the calculation of computer network reliability, Satyanarayana, Baggal and other well-known scholars have given some specific algorithms [3]. After the 1980s, the rapid development of computer technology makes the computer network become an important component of the main communication channels and public life of industry, commerce, banking, telecommunications, postal service, transportation, energy, military, national security and so on. Under the background of the great development, the actual situation of the international computer network reliability index system and computer network is changing [4]. At present, the research on the reliability of computer network hardware has made great progress and it has gradually formed a relatively complete theoretical system. The research emphasis is gradually turning to the evaluation of the reliability of network management software and computer network reliability index system [5]. The research on the reliability of computer network in China is nearly 20 years later than that in the world. In addition, due to the ideological understanding, organization and management, manpower, material resources, financial resources and other factors, there are few researches on the reliability of computer network. The computer network reliability optimization design is a very popular research field at present. Therefore, it is feasible to study the relevant theories and techniques of computer network reliability, and it has theoretical and practical value.

3. Methodology

3.1. Introduction to computer networks

A computer network can be connected to each other through a communication link, an interactive device, and a related network protocol. It can perform complex network system specific functions, belongs to a number of different geographically distributed computers. The so-called independence indicates that any computer can not completely control the other computers in the network, they are independent of each other, and each computer is free to access the information resources that exist on the computer network [6]. Computer network is a kind of component in essence, which can provide mobile path for the communication between computers. The computer network can be composed of two parts: the user resource subnet and the communication subnet [7]. The subnet of the user resource can provide and process the relevant resource information to the computer network. The communication subnet can be responsible for the transmission of information in the computer network. The computer network itself has inherent structure and specific functions. The computer network is relatively large in the geographical distribution of the computer, and the computer network computer is independent of each other; The communication of computer network can be carried out through the network of communication facilities, and the communication facilities are composed of two parts, namely, the communication link and the switching equipment [8]. Computer network realizes information exchange and coordination through communication facilities. Interoperability is a higher level of requirement in computer network applications. It requires a command mechanism to support process interoperability between heterogeneous computer systems in an interconnected network environment while collaborating with application-related integration. Figure 1 is the actual operation of the computer network.

Fig. 1. Computer network

The computer network is generally composed of three parts. The first is the user device, which includes the user terminal, the server; the second part is the transmission of switching equipment, including communication lines and routers. The third

part is the network software, which consists of network management software and application software. Computer network is a structural framework of computer network, which represents the physical configuration of all kinds of hardware facilities in computer network. The structure of computer network is one of the most important factors that affect the reliability of computer network. Well-running computer network structure design should be carried out in accordance with the following five requirements, as seen in Table 1.

Table 1. Topological structure of computer network

Construction requirements	Computer network topology must meet the communication needs of all users to achieve the computer network planning, design, construction, operation of the expected objectives
	Computer network topology can adapt to the communication environment between buildings and buildings
	Computer network topology can facilitate the construction of computer network construction
Compatibility requirements	According to the actual requirements, the media can be selected to the appropriate computer network link
	With open planning, design benchmark, as far as possible with most manufacturers of network products and equipment compatible

The user terminal is a direct user oriented operating equipment, and its reliability is very important. It is one of the important factors of computer network reliability [9]. Routine maintenance during computer network operation is a reliable basis for ensuring that the user terminal is reliable. The higher the ability of user terminals, the better the network reliability, for example, the installation of two NIC connected to different LAN segments is more reliable. Server is the information hub and service provider of computer network [10]. It usually includes a database server, and a variety of application servers, including e-mail server, event server, Web server, and so on. These sub servers can directly affect the reliability of computer network operating efficiency. In general, the server's error resilience is associated with the response time and its reliability. While improving the reliability of each sub server, the server should be related to the dual switch system, when the server uses two servers, one as a host, and the other as a backup machine. Although this will increase the cost of the computer network, the corresponding computer network reliability is also improved.

3.2. Computer network model planning

The computer network topology is the problem of computer network planning, and it also affects the reliability of computer network. The practice shows that the different levels of computer networks must have different network topologies; otherwise it is impossible to improve the reliability of computer networks. The interconnection network topology is the main connection between components in the

computer network, which can be represented by Fig. 2, so graph theory is the most powerful mathematical tool to study the performance of the internet. First, people use diameter and connectivity to measure the effectiveness and fault tolerance of computer networks. With the deep research and analysis of computer network topology, computer network designers have proposed many new concepts of network and graphics theory, such as fault-tolerant diameter and width Diameter, limit connectivity, edge connectivity and fault tolerance. These parameters can measure the reliability and fault tolerance of computer networks more accurately. This provides a scientific basis for computer network planning and design. The following describes the impact of several commonly used computer network topologies on the computer network reliability.

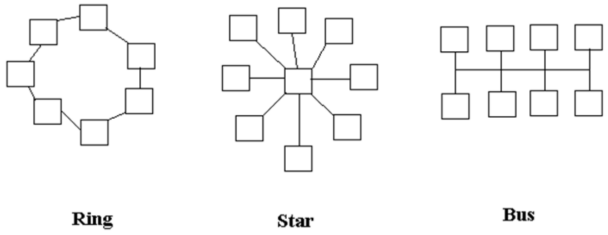

Fig. 2. Topological structures of computer networks

The bus topology itself is a link diagram of the network topology. The links between any two points in the link are unique, and they are often used for point-to-point networks or local area networks. Bus all nodes of the LAN are directly connected to the bus via a network card and are used as a general purpose transmission medium. The structure is simple, easy to implement and easy to expand. However, since all nodes in the computer network can only send or receive information through the bus transmission medium, Therefore, there may be two or more nodes using the bus to send information at the same time, leading to transmission conflict, resulting in transmission failure. The star topology of the network topology, most of the LAN systems which are based on the computer exchange center use the star topology network topology. Ring network structure is simple and easy to achieve the central node and then control the entire network communication. Any two nodes communicate through the central node. Therefore, it is easy to manage the computer network, any non-central node failure does not affect other node communication, but the network topology node is prone to failure. Pyramid network has excellent fault tolerance and effective performance, and it is applied by a lot of parallel computing, network computing, image processing, pattern recognition and intelligent systems and other network system. Various structures are shown in Fig. 2.

3.3. Optimal design of computer network reliability

Improving the fault tolerance of network system is the most effective way to improve the reliability of computer network. The general operation flow of fault-tolerant design of computer networks is to find the most common fault points by re-

dundancy and strengthen them, and the aim is to minimize the duration of computer network failure. In order to avoid data loss or problems caused by various faults, and even computer network failure, we must take a variety of redundancy measures to enhance the fault-tolerant ability of computer networks. In reality, many factors that affect the computer network's fault tolerance, including the degree of data link redundancy of the computer network components, how the computer network central hub equipment fault tolerance, how does the computer network backbone and the server be fault tolerant. Multilayer network architecture of computer network can most effectively use network layer service functions, such as network traffic segmentation, load sharing, and common network problems caused by fault recovery and incorrect configuration or equipment failure. In addition, the multi-layer network architecture of the computer network can also isolate the associated network faults well and support all frequently seen network protocols. The multi-level model of computer network makes it more convenient to transplant the computer network, for it preserves the various network addressing schemes, and has better compatibility with the previous computer networks. There are three layers of multilayer network structure in computer network. The multi-layer network structure of the computer network is shown in Fig. 3, which shows the design of the computer network.

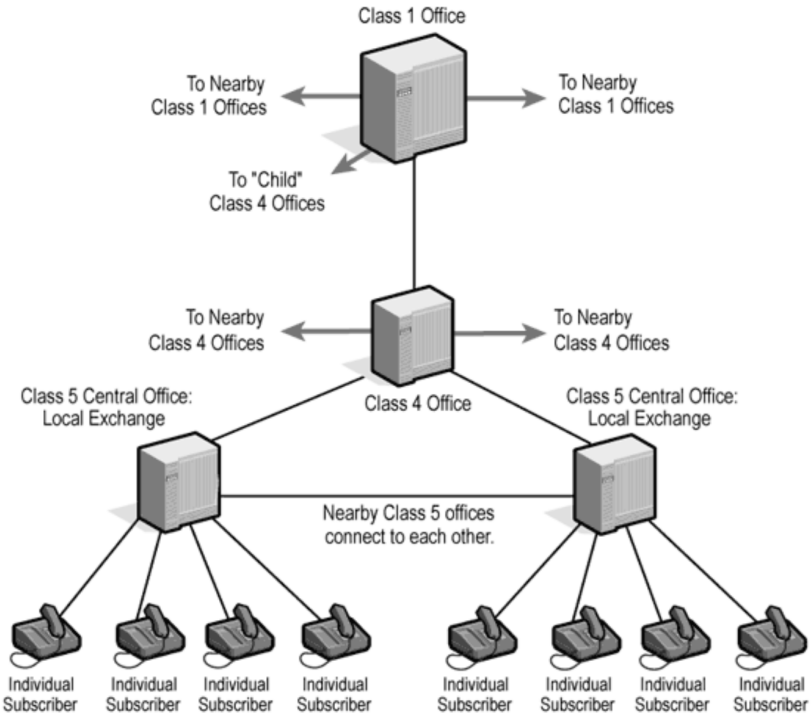

Fig. 3. Multi-layer network structure of computer network

In theory, improving the reliability of computer-related components and improving additional redundant components are the two main ways to improve the reliabil-

ity of computer networks. Under the premise of satisfying the expected function of the computer network, adopting the redundant technology (increasing the number of spare links) can improve the reliability of local fragmentation of the computer network; On the other hand, the construction cost of the computer network has also increased. The reliability matrix of the computer network link is as follows:

$$R_0 = \begin{bmatrix} r_{11} & \ldots & r_{1n} \\ \ldots & \ldots & \ldots \\ r_{m1} & \ldots & r_{mn} \end{bmatrix} \tag{1}$$

Due to the low reliability and cost of each computer network link, the number of links in the computer network is small, so the reliability of computer network is high, which is in line with the actual demand.

4. Result analysis and discussion

In this paper, E1, E2, E3, E4, E5, five different computer network reliability index systems are evaluated. The training time of neural network learning algorithm is 600 times, the accuracy of neural network training error is $g = 0.030$, neural network input node $M = 5$ output node $n = 5$, the first layer neural network neuron threshold is $B = Ml2 = 2.5$, and the neuron threshold of the second layer neural network is 5.8. The reliability index and weight of computer network are shown in Table 2. In the table: the letter R indicates the user's complaint rate of the whole network service quality and the letter E indicates the failure rate of the computer network system software.

Table 2. Computer network reliability index system and its weight tab

Index	E_1	E_2	E_3	E_4	E_5	
R_1	0.022	0.024	0.018	0.068	0.084	0.10
R_2	0.013	0.018	0.019	0.017	0.024	0.10
R_3	0.965	0.995	0.896	0.963	0.936	0.20

In this paper, we use Matlab and its neural network toolbox function to write a specific neural network learning algorithm program, and use the program to train the neural network training samples for 600 times. When the precision of neural network training error is 0.03, the simulation curve is shown in Fig. 4.

The simulation results are shown in the figure, and the second layer output of the neural network evaluation model is 0.96, 0.97, 0.93, 0.67, and 0.92. The results of computer network reliability index system are as follows: E_4, E_2, E_1, E_3, E_5.

5. Conclusion

The problem of computer network reliability optimization design is extremely difficult. Genetic algorithms such as genetic algorithms and neural networks provide

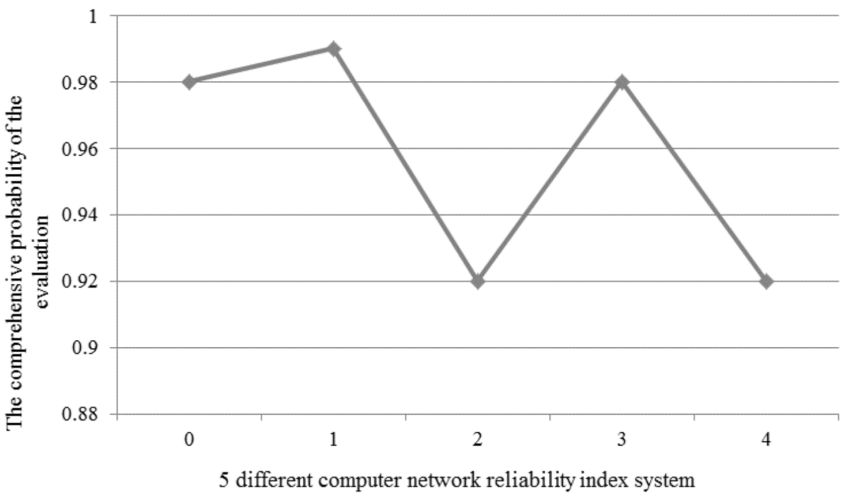

Fig. 4. Graph of reliability index system of computer network

a new way of thinking to solve these problems. Based on the analysis of the factors that affect the reliability of computer network, in this paper, the application of computer network reliability optimization scheme was studied, the computer network was briefly introduced, and then the application of computer network model planning in computer network processing was studied, finally, the reliability design of computer network was studied and the actual test was carried out. Neural network and other intelligent algorithms provide a new way of thinking to solve these problems. This paper solves the problem of computer network reliability optimization design, and provides some theoretical basis for computer network designers and constructors. The shortcomings of the thesis are mainly that the simulation program is running slowly, and the application of nested structure, recursive structure and Matlab neural network toolbox function is used in the program. This takes up a lot of memory and operation time. It is necessary to prepare a more effective simulation program in the future.

References

[1] M. Papadrakakis, N. D. Lagaros: *Reliability-based structural optimization using neural networks and Monte Carlo simulation.* Computer Methods in Applied Mechanics and Engineering *191* (2002), No. 32, 3491–3507.

[2] W. Kuo, V. R. Prasad: *An annotated overview of system-reliability optimization.* IEEE Transactions on Reliability *49* (2000), No. 2, 176–187.

[3] J. S. Kong, D. M. Frangopol: *Life-cycle reliability-based maintenance cost optimization of deteriorating structures with emphasis on bridges.* Journal of Structural Engineering *129* (2003), No. 6, 818–828.

[4] B. Koo, M. Fischer: *Feasibility study of 4D CAD in commercial construction.* Journal of Construction Engineering and Management *126* (2000), No. 4, 251–260.

[5] B. A. G. Bossink, H. J. H. Brouwers: *Construction waste: Quantification and*

source evaluation. Journal of Construction Engineering and Management *122* (1996), No. 1, 55–60.

[6] H. J. Wang, J. P. Zhang, K. W. Chau, M. Anson: *4D dynamic management for construction planning and resource utilization.* Automation in Construction *13* (2004), No. 5, 575–589.

[7] V. Carr, J. H. M. Tah: *A fuzzy approach to construction project risk assessment and analysis: Construction project risk management system.* Advances in Engineering Software *32* (2001), Nos. 10–11, 847–857.

[8] P. E. D. Love: *Influence of project type and procurement method on rework costs in building construction projects.* Journal of Construction Engineering and Management *128* (2002), No. 1, 18–29.

[9] D. Baloi, A. D. F. Price: *Modelling global risk factors affecting construction cost performance.* International Journal of Project Management *21* (2003), No. 4, 261–269.

[10] T. Ahonen, A. Hadid, M. Pietikainen: *Face description with local binary patterns: Application to face recognition.* IEEE Transactions on Pattern Analysis and Machine Intelligence *28*, (2006), No. 12, 2037–2041.

Received May 22, 2017

Acta Technica *62* No. 1A/2017, 201–214

Research on performance detection system and damage identification method based on civil engineering structure

Lin Zhi-xiong[1], Zou Wen-ping[1,3], Zheng Bin[2]

Abstract. The paper is devoted to studying the application of structural health monitoring of large civil engineering structures. In this paper, an artificial neural network (ANN) method for structural damage identification based on structural dynamic response statistical characteristics is put forward. In addition, a model experiment of structural damage identification for a set of model beams with two ends consolidation is carried out. The model beam is made of aluminum alloy profile, and the thin-walled box girder with flange is simulated. The experimental results show that the trained neural network can accurately identify the structural damage location and degree. Based on the above work, we conclude that the system verifies the validity and reliability of the structural damage identification artificial neural network method based on statistical properties of structural dynamic response.

Key words. Civil engineering, structural dynamic response, damage identification, neural network.

1. Introduction

With the constant appearance of high-rise buildings, large span space structure, large bridges and other important buildings and higher and higher safe and comfortable requirements of civil engineering structure application, the health monitoring system for large civil engineering structures has become a hot research topic in the field of civil engineering [1–2]. The research on the structural health monitoring system of civil engineering has important theoretical significance and engineering value. Although the structural health monitoring of civil engineering has made great progress, and tried on parts of the structures, strictly speaking, at present, it has not

[1]Fujian Agriculture and Forestry University, College of Transportation and Civil Engineering, Fuzhou 350108, Fujian, China
[2]Jinshan College of Fujian Agriculture and Forestry University, Fuzhou, Fujian, 350002, China
[3]Corresponding author

established a long-term health monitoring system that can fully meet the needs of structure monitoring in the world. This is because that the civil engineering structures and infrastructures have large volume, long span, wide distribution area, and long life cycle. The stability, durability and distribution range of long-term health monitoring system based on traditional sensor cannot well meet the actual needs of the project. In addition, the theory methods that can effectively use structure real-time monitoring data for structural damage identification and safety assessment need further studies [3]. At present, the application of artificial intelligence technology represented by artificial neural network in structural damage identification has become the trend of civil engineering structural health monitoring.

2. Materials and methods

In the experimental verification of structural damage identification method of artificial neural network based on structural dynamic responses statistical properties, various damage samples of consolidation beam obtained through model experiments, partial damage samples are used to train the neural network, and the other parts are applied to test the neural network. In this paper, the single damage condition and double damage condition are considered.

2.1. Design of damage location and damage degree

For making the neural network identify the damage in the structure correctly, it needs a comprehensive structural damage sample and considers the limitation of experimental conditions. The complexity and cost of experiment cannot increase the damage samples without limitation, which needs to consider the representative damage sample that is easy to appear. In addition, in order to make up for the training samples, other damage samples are obtained through the finite element numerical simulation method. On the condition of not seriously increasing neural network training burden, the method of combining damage sample obtained from model experiment and that obtained from finite element numerical simulation is used for neural network training. Due to the single structure of the actual engineering, it is impossible to obtain all the damaged samples of the actual structure needed by the trained neural network, but to obtain enough damage samples by finite element numerical simulation method. As a result, this method of model experiment and numerical simulation to obtain damage samples is more close to the method of structural damage identification artificial neural network, which is applied in the damage identification of actual civil engineering structures.

In order to facilitate the damage location, the beam model at the two ends is divided into 12 units from left to right, as shown in Fig. 1. In the middle part of a beam, the gap is opened to indicate the damage of the beam, and the gaps in different depth represent the damage in different degrees. At the time of damage identification, the results show that there is a crack in the beam, which causes the reduction degree of rigidity of the section.

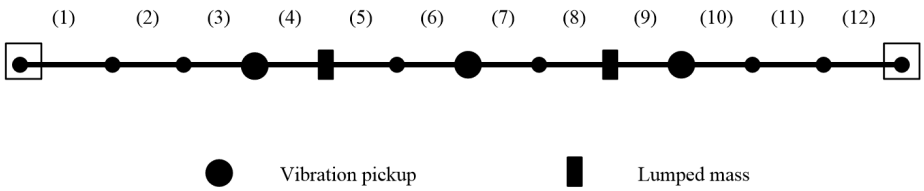

Fig. 1. Finite element model and element partition of consolidation beam

2.2. Single damage samples and multi-damage samples

In the single damage cases, considering the symmetry of the structure, we only simulate 10 damage samples on the left half beam as the damage samples for neural network training, respectively the damages in different degrees appeared in 1, 3, 4, 6 section of beam, as shown in Table 1. At the same time, the other 5 damage conditions are simulated as test samples of the neural network, as shown in Table 2.

Table 1. Neural network training samples for single damage identification in model experiment

No.	Damage units	Damage degree
S-1	1	14.5 %
S-2	1	29.3 %
S-3	1	43.7 %
S-5	4	14.5 %
S-6	4	29.3 %
S-7	6	14.5 %
S-8	6	37.9 %
S-9	6	43.7 %
S-10	6	59.1 %

Table 2. Neural network training samples for single damage identification in model experiment

No.	Damage units	Damage degree
ST-1	1	37.9 %
ST-2	3	14.5 %
ST-3	4	37.9 %
ST-4	5	14.5 %
ST-5	6	29.3 %

In the case of double damage, 25 damage samples are simulated as the training samples of the neural network, as shown in Table 3. Two damage location were near left pedestal and 1/4 of right ends, 1/4 of left span and near the mid-span, 1/4 of left span and near right support, 1/4 of left span and the mid-span, between 1/4 of left

span and the mid-span, near the left support and the mid-span. The above double damage locations basically contain the positions may be prone to two damages. At the same time, 10 damage samples are simulated as test samples of neural network, as shown in Table 4.

Table 3. Neural network training samples for double damage identification in model experiment

No.	Damage units	Damage degree	Damage units	Damage degree
M-1	1	43.7 %	10	14.5 %
M-2	1	43.7 %	10	37.9 %
M-3	1	43.7 %	10	43.7 %
M-4	1	43.7 %	10	59.1 %
M-5	3	29.3 %	7	14.5 %
M-6	3	29.3 %	7	37.9 %
M-7	3	37.9 %	7	37.9 %
M-8	3	37.9 %	7	43.7 %
M-9	3	43.7 %	7	59.1 %
M-10	3	59.1 %	7	59.1 %
M-11	4	37.9 %	11	14.5 %
M-12	4	43.7 %	11	29.3 %
M-13	4	59.1 %	11	37.9 %
M-14	4	59.1 %	11	43.7 %
M-15	4	59.1 %	11	59.1 %
M-16	5	14.5 %	8	14.5 %
M-17	5	14.5 %	8	37.9 %
M-18	5	29.3 %	8	37.9 %
M-19	5	37.9 %	8	37.9 %
M-20	5	43.7 %	8	43.7 %
M-21	5	59.1 %	8	43.7 %
M-22	5	59.1 %	8	59.1 %
M-23	6	59.1 %	2	14.5 %
M-24	6	59.1 %	2	37.9 %
M-25	6	59.1 %	2	59.1 %

2.3. Finite element model updating

In addition to the structural damage samples obtained from the model experiment, the damage samples simulated by using finite element method is used to do the neural network training. Usually in the finite element numerical simulation of damage, we generally represent that damage occurs in the damage units by reducing the stiffness of a unit. And in the corresponding experiment verifications, the method used is to cut parts of the entire damage unit to simulate the damage [4] or continuously cut a series of gaps in the damage units. As a result, the gap covered

the entire unit length to simulate the decrease of stiffness at the unit [5]. But these two methods have some defects. The actual civil engineering structure damage is not a regional structural stiffness degree decline, while in most cases, it is the structure stiffness reduction near the cracks caused by one or several cracks. In consequence, a crack should be used to simulate the damage in the experiment [6–7].

Table 4. Neural network test samples for double damage detection in model experiment

No.	Damage units	Damage degree	Damage units	Damage degree
MT-1	1	43.7 %	10	29.3 %
MT-2	1	59.1 %	10	59.1 %
MT-3	3	29.3 %	7	29.3 %
MT-4	3	37.9 %	7	59.1 %
MT-5	4	37.9 %	11	29.3 %
MT-6	4	43.7 %	11	37.9 %
MT-7	5	14.5 %	8	29.3 %
MT-8	5	37.9 %	8	43.7 %
MT-9	6	59.1 %	2	29.3 %
MT-10	6	59.1 %	2	43.7 %

In this paper, a crack in the bottom of the beam is used to simulate the damage, so, on the contrary, it is more demanding for the finite element model. The finite element method of reducing the stiffness of a unit to simulate the structural damage has a great error with the experimental method of cutting a crack to simulate the damage. In consequence, in the finite element numerical simulation process, it is necessary to adopt special methods to reduce this error. The method of damage location refinement unit by using the finite element model is adopted in this paper. It ensures that the structure damage caused by the reduction of refined element stiffness is consistent with the damage caused by cutting the crack. It can be proved by the comparison of structure natural frequency by finite element method and model experiment method.

The discrete finite element model, due to various uncertainties, there is always some errors with the actual structure. In order to make the finite element model accurately simulate the dynamic response after the structure damage, it is necessary to refine the finite element model. Therefore, in this paper, according to the natural frequency of the structure obtained in the model experiment, the initial model of structure finite element is updated. Table 5 shows the first two order natural frequencies of the structure before and after the damage obtained by the updated finite element model and experiment. It can be seen from the table that, the first order natural frequency of the updated finite element model before and after the structural damage is quite consistent with the natural frequencies obtained from the experiments. And the second order finite element method natural frequencies before the damage is also quite consistent with the results of experimental methods. Only the results of the two methods after the second order natural frequencies are slightly different. The results show that the updated refined finite element model can ac-

curately describe the basic characteristics of the beam model, which is suitable to simulate the dynamic response after the structure damage.

Table 5. The first two natural frequencies of the beam at the two ends of the beam before and after damage

Finite element simulation	First order frequency (Hz)		Second order frequency (Hz)	
	No damage	After damage	No damage	After damage
Finite element simulation	37.12	33.93	99.45	88.91
Model experiment	37.11	33.45	99.12	77.51

2.4. Analysis of natural frequency of damage consolidation beam model

Before the neural network training, according to the consolidation beam dynamic response of the vibration absorber, we make a natural frequency analysis of the structure. What is more, we observe the relationship between the change of the natural frequency and the structure damage, so as to compare the performance with the structure natural frequency change and structure dynamic response statistical feature as damage index.

The natural frequency of the structure is one of the important damage indexes in the damage identification method based on the vibration. The larger damage in the structure has obvious influence on the natural frequency of the structure, and the influence of the thin crack damage on the natural frequency of the structure needs to be analyzed by the specific analysis of dynamic response of the structure. The natural vibration frequency of the structure under the condition of single damage and multi-damage is analyzed. In the case of single damage, the damage in unit 6 is taken as an example. Figure 2 shows the first order natural frequency of the structure when different degrees of damage occur within the unit 6 of the beam element model. It can be seen from Figure 2 that, when the damage is small, the natural frequency of the structure did not change. Only when the degree of structural damage reached the maximum damage considered in the model experiment will the natural frequency of the structure decreased slightly.

In the case of double damage, the damage occurred in unit 5 and unit 8 is taken as the examples to illustrate. Table 6 shows the first order natural frequency of the structure with different degrees of damages in unit 5 and unit 8. It can be seen from Table 6 that, when the two damages were small, the natural frequency of the structure did not change. Even when the degree of structural damage reached the maximum damage considered in the model experiment will the decrease range of the natural frequency of the structure be very small, only about 5 %. In order to further study the impacts of damage degree on the natural frequency of the structure, the cracks of unit 5 and unit 8 are continuing to be cut deeper, until the section stiffness decreased more than 90 %. The natural frequencies of structure corresponding to the damage of the part are shown in the second part of table 6. As can be seen from the table, only when the damage degree is more than 80 % the natural frequency of the structure will significantly change.

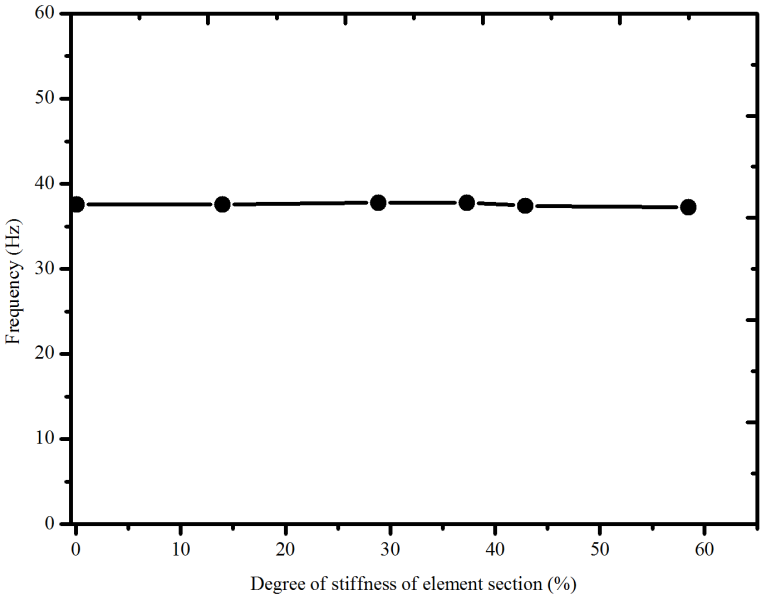

Fig. 2. Relationship between the natural frequency and the damage degree in single damage condition

Table 6. The first order natural frequencies of the structure under different damage degrees in multi damage condition

Damage level	Unit 5 damage level	Unit 8 damage level	Natural frequency(Hz)
0	0	0	37.60
1	14.5 %	14.5 %	37.48
2	14.5 %	29.3 %	37.35
3	14.5 %	37.9 %	37.60
4	29.3 %	37.9 %	37.48
5	37.9 %	37.9 %	37.48
6	37.9 %	43.7 %	37.35
7	43.7 %	43.7 %	36.25
8	59.1 %	37.9 %	35.89
9	59.1 %	59.1 %	35.52
10	71.6 %	59.1 %	35.16
11	71.6 %	81.3 %	34.06
12	81.3 %	81.3 %	33.33
13	88.7 %	81.3 %	32.35
14	88.7 %	93.9 %	30.64

The damage samples of both ends of the specimen consolidation beam obtained through model experiments are used. Combining with damage samples of finite

element numerical simulation, the joint training of artificial neural network is carried out. As a result, the corresponding relationship between structural dynamic response statistical characteristics and structural damage location and degree. In addition, the test samples are used for testing and evaluating the validity evaluation of structural damage identification method of artificial neural network.

2.5. Single damage condition

In single damage cases, the input vector of the neural network to identify the damage contained six items: variation of the midspan and two 1/4 points displacement variance, variation of the midspan and left 1/4 points displacement covariance, and variation of the midspan and right 1/4 points displacement covariance variation; the output vectors contained two items: damage location and damage degree. Therefore, there are 6 nodes in the input layer of the neural network, and there are 2 nodes in the output layer. The number of hidden layers and that of hidden layer nodes are obtained through the test and training. There are 25 damage samples of training neural network, of which there are 10 damage samples obtained from the model experiment, and the other 15 samples are obtained by the finite element method. The neural network is trained as a single hidden layer structure, and the hidden layer is 23 nodes. The test results of the neural network are shown in Table 7. As can be seen from Table 7, the damage location of all the single damage can be accurately identified, and the identification relative error of the damage degree is not more than 4 %, meeting the accuracy requirements of civil engineering.

Table 7. Single damage condition identification results

No.	Actual damage		Identification results		
	Damage units	Damage degree	Damage units	Damage degree	Damage degree identification relative error
1	1	37.90 %	1	39.35 %	3.84 %
2	3	14.50 %	3	14.58 %	0.57 %
3	4	37.90 %	4	38.87 %	2.56 %
4	5	14.50 %	5	14.06 %	-3.04 %
5	6	29.30 %	6	28.40 %	-3.09 %

2.6. Double damage condition

The test results of the double damage identification neural network are shown in Figs. 3–10. As can be seen from Figs. 3–10, the damage location of two damages in all test samples can be correctly identified, most of the damage degree can be accurately identified, and only a small part of the damage degree identification has large relative errors, the maximum relative error of 12.24 %. Observing the details of damage identification in Figs. 3–10, it can be found that, the units with relative

large error in the damage identification results are basically near the supporting place. This is because that the structure dynamic response near the supporting is vulnerable to be influenced by supporting conditions, and three measuring points on the beam consolidation near the supporting are far away. The structure response statistical characteristics obtained by vibration pickup are difficult to reflect the changes of the structure, so the relative error of identification results is large.

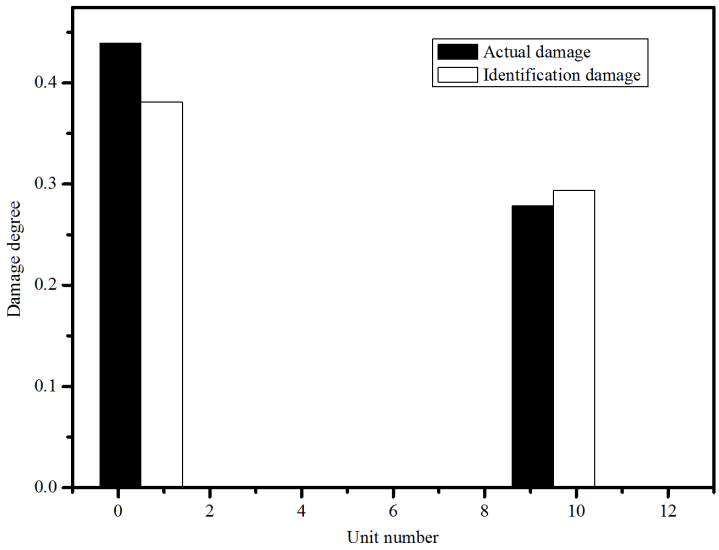

Fig. 3. Test results of neural network with double damage identification–sample 1

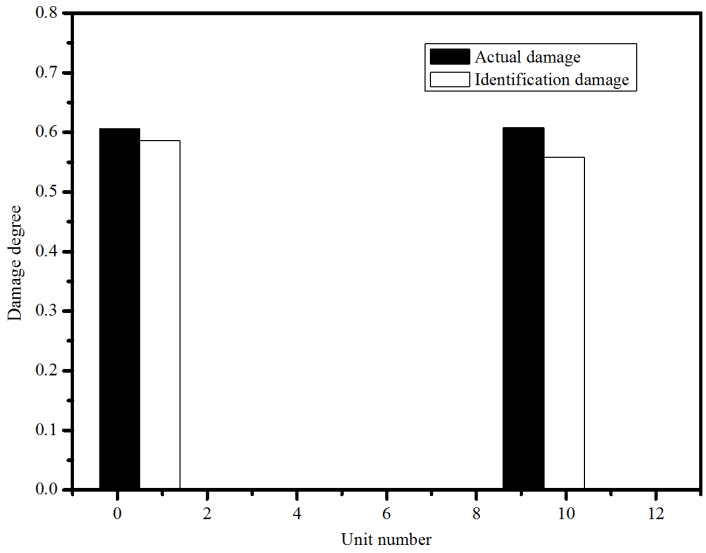

Fig. 4. Test results of neural network with double damage identification–sample 2

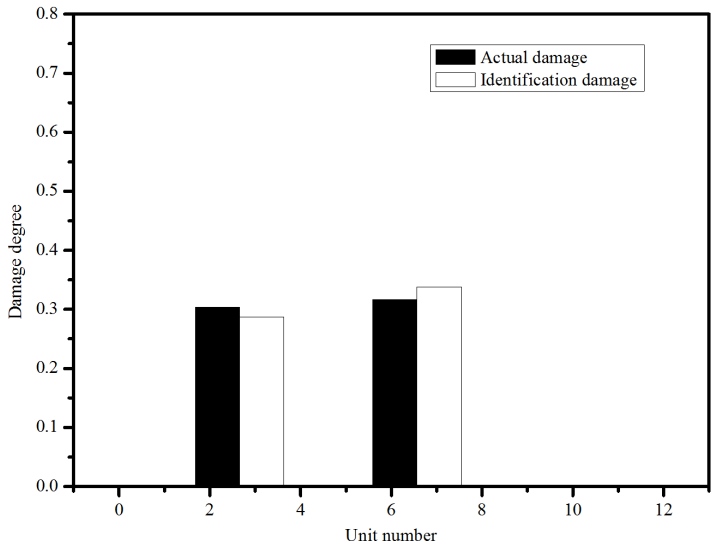

Fig. 5. Test results of neural network with double damage identification–sample 3

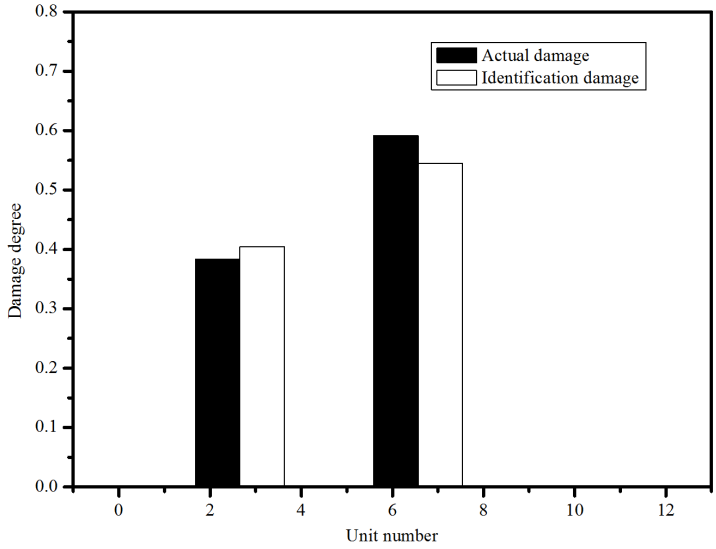

Fig. 6. Test results of neural network with double damage identification–sample 4

In addition, it is found that the damage degree identification results with large relative error are the cases with great damage degrees. This is because the larger damage degree is located in the edge of the damage state space, and it is easy to have a large error. It can be seen from Figs. 3–10 that, the damage degree identification relative error of damage units located in the measurement points are generally smaller than that located in the non-measurement points. Moreover, for the middle damage, the damage degree identification relative error is relatively smaller than

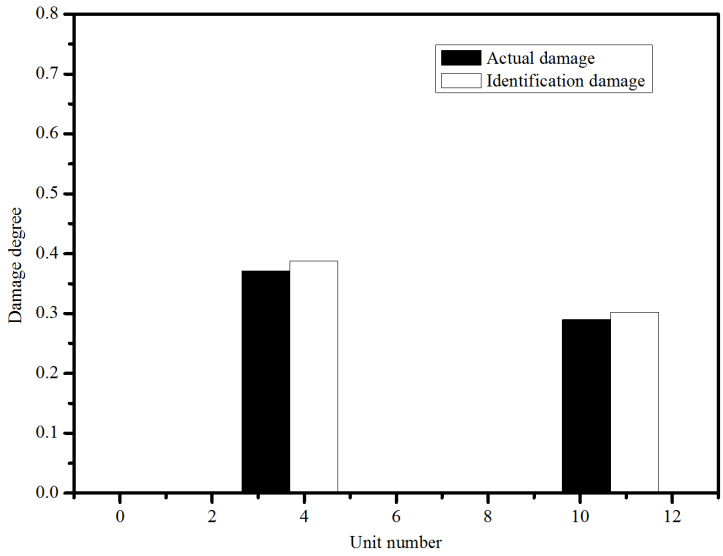

Fig. 7. Test results of neural network with double damage identification–sample 5

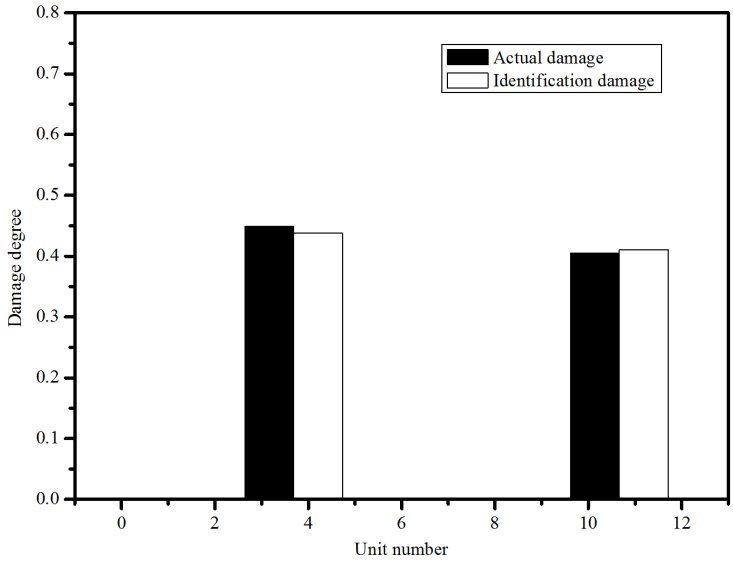

Fig. 8. Test results of neural network with double damage identification–sample 6

that of serious damage degree.

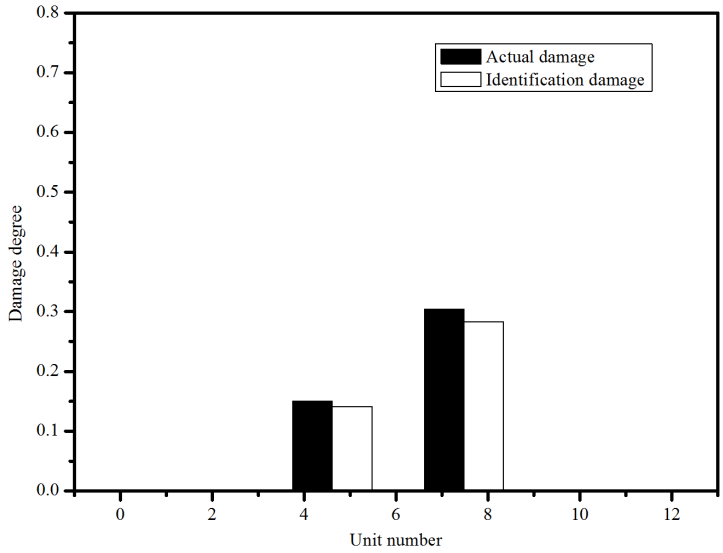

Fig. 9. Test results of neural network with double damage identification– sample 7

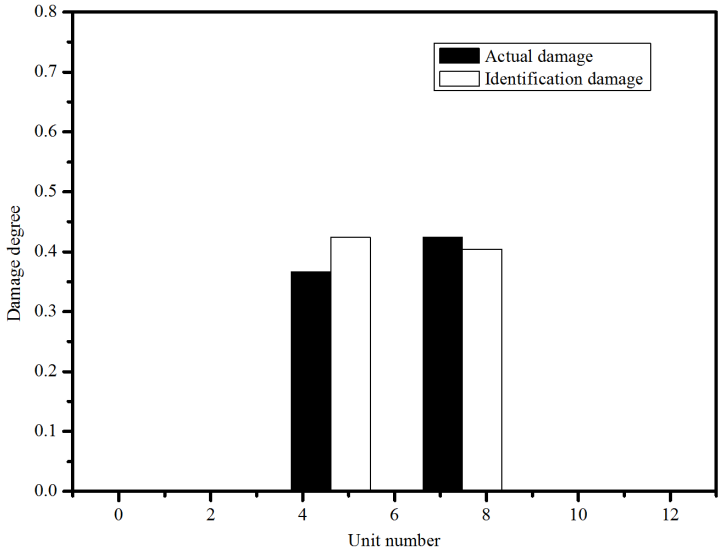

Fig. 10. Test results of neural network with double damage identification–sample 8

3. Conclusion

In this paper, the dynamic response of the structure of beam with two ends is obtained by the model experiment under the condition of white noise excitation, and its variance is taken as the input vector of neural network. In the bottom of the model beam, cracks are cut and used to simulate the damage occurred in the structure. Cracks in different locations with different degrees represent various

damages. The model is used to obtain different damage samples, and the neural network used in damage identification is trained and tested. Through the analysis of identification results of the well trained neural network in single damage cases and multiple damages, it is obtained that, from the actual measurement results of the vibration pickup model experiment, it can be seen that the structural dynamic displacement response statistical characteristics are quite sensitive to the damages in the structure. For the double damage cases in the consolidation beam model, the neural network can accurately identify the locations of two damages, and it can correctly identify the most damage degrees. The other small part of the damage identification error is large, and the maximum identification relative error is 12.24 %. From the double damage identification results, it also can be seen that, the damages near the measuring points and the damage degree is the middle can be accurately identified. While the damages far away from the measuring points and the damage degree is relatively great have large damage degree identification relative error. In this paper, the artificial neural network (ANN) method based on the statistical characteristics of structural dynamic response is effective and reliable. The method can be applied to practical civil engineering structures.

References

[1] H. N. Li, L. Ren, Z. G. Jia, T. H. Yi, D. S. Li: *State-of-the-art in structural health monitoring of large and complex civil infrastructures.* Journal of Civil Structural Health Monitoring *6* (2016), No. 1, 3–16.

[2] H. N. Li, D. S. Li, L. Ren, T. H. Yi, Z. G. Jia, K. P. Li: *Structural health monitoring of innovative civil engineering structures in Mainland China.* Structural Monitoring and Maintenance *3* (2016), No. 1, 1–32.

[3] G. Gautier, J. M. Mencik, R. Serra: *A finite element-based subspace fitting approach for structure identification and damage localization.* Mechanical Systems and Signal Processing *58–59* (2015), 143–159.

[4] J. Zhi, L. Zhao, J. Zhang, Z. Liu: *A numerical method for simulating the microscopic damage evolution in composites under uniaxial transverse tension.* Applied Composite Materials *23* (2016), No. 3, 255–269.

[5] L. Brely, F. Bosia, N. Pugno: *A hierarchical lattice spring model to simulate the mechanics of 2-d materials-based composites.* Frontiers in Materials *2* (2015), No. 51.

[6] J. Zhi, L. Zhao, J. Zhang, Z. Liu: *A numerical method for simulating the microscopic damage evolution in composites under uniaxial transverse tension.* Applied Composite Materials *23* (2016), No. 3, 255–269.

[7] C. Zhang, N. Li, W. Wang, W. K. Binienda, H. Fang: *Progressive damage simulation of triaxially braided composite using a 3d meso-scale finite element model.* Composite Structures *125* (2015), 104–116.

Received May 22, 2017

Acta Technica *62* No. 1A/2017, 215–224

Application research of virtual reality technology in environmental art design[1]

Wang Zhanjun[2]

Abstract. With the advent of the information age, a great many of modern means of science and technology have changed people 's lives. With regard to environmental art design, the computer technology and virtual reality technology emerging in large numbers has broke the conventional mode of environmental art design and accelerated the environmental art design plan based on virtual reality technology and its application. This paper introduces virtual reality technology and its practical application and probes into the profound impact brought by virtual reality technology in the specific design process of environmental art design so as to provide some inspirations on ideas of environmental art design. The paper suggest the designers to lower the cost of the project design to a certain extent, avoid artificial design error, improve quality and efficiency of environmental art design, and most importantly enhance the resource utilization rate of the environment art design projects and then improve the economical benefits of substantial project in operation process, In addition, it is worthwhile to promote such technology in relative industries.

Key words. Virtual reality technology, environmental art design, application research.

1. Introduction

At present, information technology is rapidly developing and at the same time all sorts of multimedia technologies are coming forth, which brings new development impetus for practical work. In the market under increasingly fierce competition, it has become common concern for experts and scholars in this field to study how to enhance the level of modern environmental art design. In the past, environmental art design schemes were often ceased under limitations from expenditure, site, and other factors. Therefore, the integration of virtual technology technology and environmental art design is put forward for the purpose of improving efficiency

[1]This work was supported by Philosophy and social science research project in Shanxi Province 2015 "Research on innovation value and development trend of Digital technology in the restoration of ancient buildings in Shanxi", Project No. 2015262.

[2]Taiyuan University, Taiyuan, Shanxi, 030032, China

and economy of environmental art design. In the actual application of virtual reality technology in the design process, technical features such as multi-sensation, interaction and imagination of the technology can make up for the deficiencies in conventional environmental art design.

2. State of the art

Virtual reality technology is essentially a collection of a series of advanced technologies, including multimedia technology, computer network technology and simulation technology and so on. Based on those kinds of technologies, a more realistic three-dimensional virtual environment is created and under the support of hardware devices, building of multi-dimensional information space is realized. Thus, a visualized virtual environment is presented to specific industries (Fig. 1) [1–6]

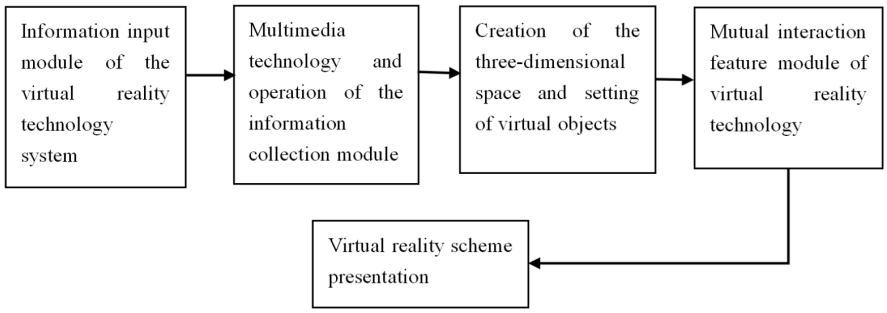

Fig. 1. Visualized virtual environment is presented to specific industries

It is clearly shown in Fig. 1 that, the virtual reality technology is completed step by step under guidance of the requirements designated by customers and different virtual scenes need to be realized by different technology means. In general, application of the overwhelming majority of virtual reality technologies requires an information input module of the virtual reality system. Besides, by means of multimedia technology and through specific operation of the information collection module, a foundation for the virtual environment is laid for the purpose of creation of the three-dimensional space and setting of the specific virtual objects in later period to make the virtual environment more real. Most importantly, it is the operation of mutual inductance feature module in virtual technology allows the interactive experience process between human and the environment in actual application of the virtual reality technology. Finally, the virtual reality scheme is presented to the audience by means of multimedia technology and computer technology etc. Table 2 compares the Traditional Expression Method and VR Technology.

3. Methodology

Scene creation in application of virtual reality technology is to build a realistic simulated environment mainly by computer technology and based on modern high-

tech hardware and software product so as to create a visualized three-dimensional scene. In addition, a series of means is used to arouse vision, hearing, touching and other senses of the audience in the live environment, thus, the audience may think they are in a realistic environment [7–8]. Specifically speaking, the main features of virtual reality technology include the following aspects:

3.1. Multi-sensation feature of virtual reality technology

Under normal conditions, we perceive things usually by the abilities such as visual impression, touching or hearing, however, under operation of the virtual reality technology, the most ideal outcome is to use the sensory abilities of human that can be aroused so as to reach the objective of panoramic view or overall consideration [9–10]. But with the existing technical level, the ideal virtual reality technology fails to reach such peak state and requires further development of multi-sensation feature.

3.2. Interaction feature of virtual reality technology

The interaction feature of virtual reality technology is mainly reflected in its interactive effect, that is to say, within the simulated technical environment, human can interact with the virtual scene and objects. Although such interaction is a specific manifestation of the appreciable scene, it presents extremely high technical practice value and can predicate all the possible outcomes in the real environment.

3.3. Imagination feature of virtual reality technology

To put it simply, imagination feature of virtual reality technology is the conception of the virtual environment to meet people's need of exploring the scene that does not exist in the objective world. In spite of the obvious imagination feature of such technology, the scene imagined often comes from people's perception and imagination of the unknown world. Thus, the imagination of virtual reality technology is realized with the aid of operation of assistive technological means. Table 2 contains the application advantages of VR Technology in Environmental art design.

4. Exploration of practical application of the virtual reality technology

The virtual reality technology can not only manifest the condition of environmental art design intuitively but also help increase the accuracy of environmental art design budget so as to enhance the interaction between the two sides in the design process. In addition, virtual reality technology changes the situation where traditional environmental art design is limited by expression of thinking thus makes environmental art design more dynamic [6].

Table 1. Comparison of Traditional Expression Method and VR Technology

	Type performance	Color	Dynamic	Interaction	Information
2D plan	Single plane	single	-	-	-
3D renderings	Three-dimensional	Rich	-	-	-
Animation	Three-dimensional	Rich	dynamic	-	-
VR system	Three-dimensional	Rich	dynamic	real time	Can be checked

Table 2. Application advantages of VR Technology in Environmental Art Design

VR	Basic characteristics	Application advantages
Immersion	People can immerse themselves in the environment created by the computer system	Increase the dimension of architects' exploration space degree
Interactivity	People can interact with the virtual information environment through interactive devices	Form a dynamic experience, to ensure continuous thinking
Conception	From the qualitative and qualitative environment to get emotional and rational knowledge, so as to deepen the concept and germination of new ideas	In the process of roaming to deepen the understanding of space, produce more design inspiration

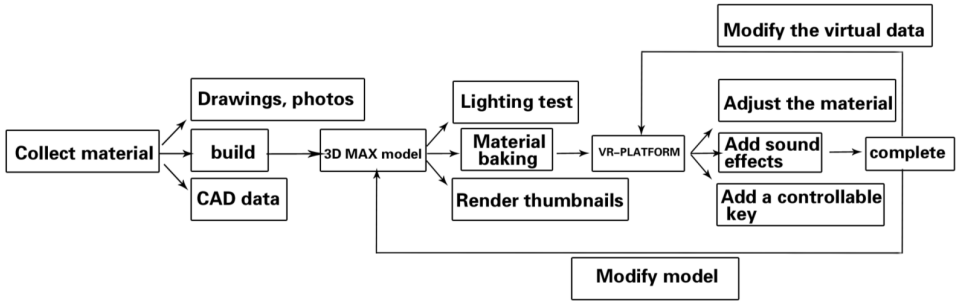

Fig. 2. VR technology in the actual modeling of the flow chart

4.1. VR technology in the actual modeling of the flow chart

On the whole, various kinds of advanced technologies are needed to highlight its embedded value in China's architectural design and environmental design fields, among which, the environmental art design philosophy is to present design schemes with high value at the lowest cost. In the practical process, all feasible measures can be taken to improve quality and efficiency of environmental art design to break through development bottlenecks in environmental art design industry [11–14].

From the point of view of objective analysis, some practical problems that cause unreality of environmental design would occur in the process of application of virtual

reality technology in environmental art design, however, it is decided by the technical features of the technology. Even so, the application of virtual reality technology brings much stronger technical support to environmental art design in that under its effect, expectations on environmental art design schemes are realized and conceptualized colors are given to environmental art design, which is the artistic level beyond reach of substantial project design [15–17].

Table 3. Original data of indexes influencing environmental art design

	X1	X2	X3	X4	X5	X6	X7	X8	X9
X1	1	0.6567	0.7202	-0.3036	0.6551	0.7256	0.6226	0.6515	-0.5633
X2	0.6567	1	0.7235	-0.1762	0.6565	0.7631	0.6436	0.6636	-0.5612
X3	0.7202	0.7235	1	-0.1405	0.5175	0.625	0.5665	0.5705	-0.5567
X4	-0.3036	-0.1762	-0.1405	1	-0.2402	-0.0272	-0.0343	0.0562	0.4363
X5	0.6551	0.6565	0.5175	-0.2402	1	0.7036	0.4434	0.6163	-0.7406
X6	0.7256	0.7631	0.625	-0.0272	0.7036	1	0.4566	0.4753	-0.6605
X7	0.6226	0.6436	0.5665	-0.0343	0.4434	0.4566	1	0.6866	-0.753
X8	0.6515	0.6636	0.5705	0.0562	0.6163	0.4753	0.6666	1	-0.6061
X9	-0.5633	-0.5612	-0.5567	0.4363	-0.7406	-0.6605	-0.753	-0.6061	1

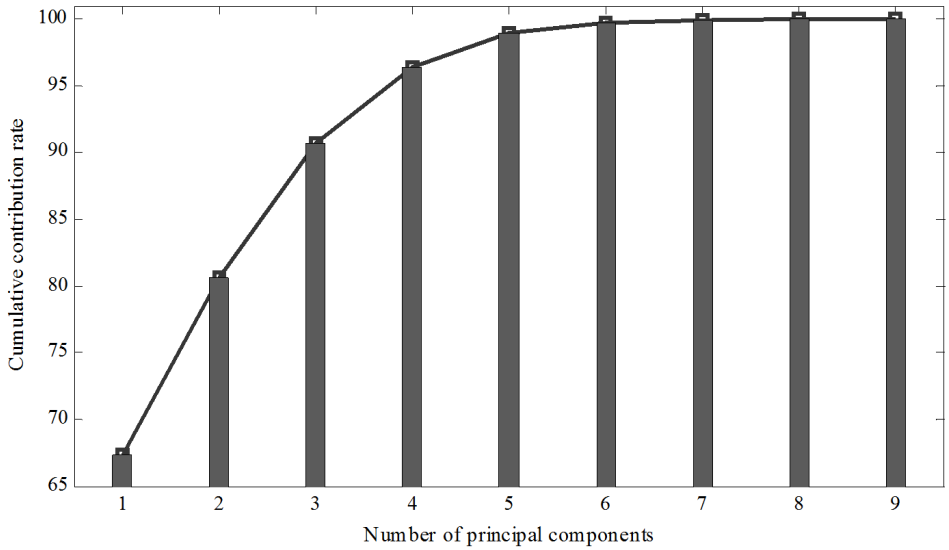

Fig. 3. Results of the cumulative contribution rate along with the number of principal components

4.2. Connection between virtual reality technology and environmental art design

Virtual reality technology needs to break limitations from space and even time. Under such technical support, environmental art design can expand into any physical

environment that can be realized by imagination. With powerful and unconstrained artistic ideas, content of environmental art design scheme is further adjusted to develop higher artistic value or practical value. In essence, there are inextricable professional relations between virtual reality technology and environmental art design for they both involve in creation of specific environment. Thus, application of virtual reality technology into environmental art design gives prominence to advantages of virtual reality technology. On this ground, much more outstanding outcomes can be gained through application of virtual reality technology into environmental art design [18–19]. On a smaller scale, environmental art design project is the large-scale fusion display engineering, which is aimed at stimulating various human experience with the dynamic atmosphere created by high-tech scenes so as to get a more intuitive and specific understanding of the conception of environmental design.

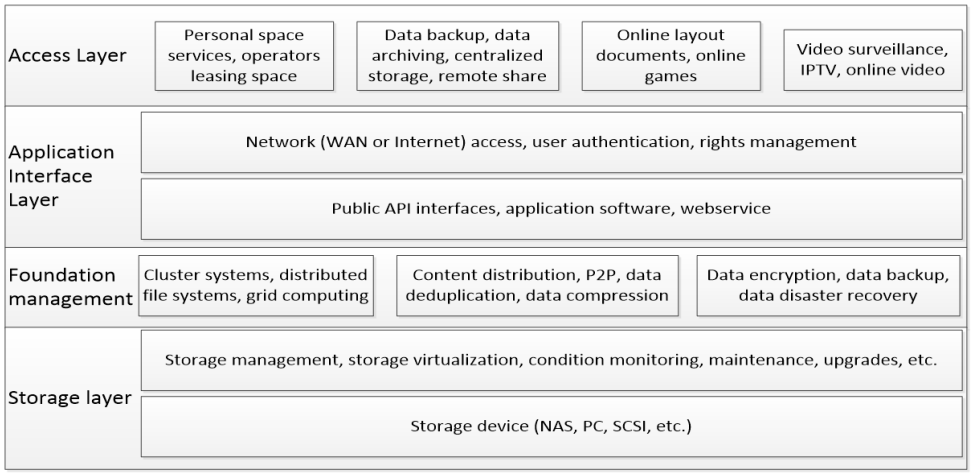

Fig. 4. Model of virtual reality technology and environmental art design structure

5. Result analysis and discussion

It is found out in practice that, the actual application of virtual reality technology has profound impacts on environmental art design for it can not only make up for the deficiencies and push limitations in space design conception of conventional environmental art design, but also avoid many potential problems in actual operation, such as coordination between human and the environment and design of the dynamic environment. What is more, under the strong support of virtual reality technology, the cost of previous repetitive design is saved in that only the computer technology and multimedia technology are used in creation of the virtue space for realization of overall environment design. On this ground, practical application of virtual reality technology improves to a certain extent the economic and social benefits of project construction.

5.1. Advent of virtual reality technology makes up for the deficiencies

In the past, environmental art design in conventional form used to be limited by space factors, for example, if the design scheme went beyond the specific spatial range, high incompatibility would occur and cause failure of the environmental art design. But at present, that situation can be completely avoided by application of the virtual reality technology, under the support of which, environmental art design breaks through limitations from spatial range and even time. The independent art design space created thereby is of certain realistic value and enables the audience personally on the scene to enjoy the unique connotations of environmental art design. The virtual reality system is characterized with multi-sensation, immersion, interaction and imagination, and it is the virtual reality technology that brings the audience into a simulated real environment true to nature. The application of virtual reality technology is a new mode of practice for human to realize visualized operation and interaction of the complex data via computer. Compared with traditional man-machine interface and the popular windows operation, the virtual reality technology has a qualitative leap in technological thoughts and presents unprecedented real effects.

5.2. The application of virtual reality technology can effectively avoid potential problems

In view of the special technical requirements of environmental art design, integration of multiple knowledge systems is required to complete the design scheme. If any technical oversight is found, the entire environmental art design scheme may be overthrown. It is shown in the practice process that application of virtual reality technology can effectively avoid potential problems in environmental art design schemes. On a smaller scale, the three-dimensional modeling technology in the virtual reality system is to represent the abstract statistical data or concept in forms, curves and legends. On average, the virtual reality system can be divided into the foreground simulation presentation and background technological processing, which jointly complete construction of the simulation system model. As a matter of fact, the virtual reality system itself is an integration of a series of technologies and plays the biggest role of every single module by orderly operation of simulation system platform so as to realize virtual reality of a certain scene. As thus, application of the virtual reality technology integrates advantages of the simulation system, multimedia technology system, and avoids the previous problems in design efficiency. In addition, practical application of the virtual reality technology can effectively avert information asymmetry effect among all departments in the environmental art design process. In short, formulation of the environmental art design scheme requires integration of the knowledge systems of all professionals, that is to say, if the key points of environmental art design are laid on the unified design platform, information exchange can be improved, which also avoids design errors. At the present, scientific integration operation has been realized in many industry fields for the purpose of improving industrial benefits. During the actual simulation operation, scene setting

is completed with the aid of projector equipment and physical programming model. In addition, through combined utilization of the database system and relevant technologies, various kinds of information resources, geographical location resources, and media stockpile resources are input in the core system so as to invoke different types of the information resources. Thus, actual effects of application of the virtual reality technology in field of environmental art design are fully manifested.

The most important function of the virtual reality technology adopted in environmental art design process is mainly reflected in its interaction, which is different from implementation of large-scale fusion display project alone. In the man-machine virtual environment, the experiencer can interact and communicate with the central system via some of the simulation function modules of the system, thus, the high-tech fusion performance of the interactive three-dimensional environment model is realized. In this way, once any unreasonable and inconsistent problems occurs in the environmental art design scheme, it is reflected by the virtual scene, which is good for the technical designer to adjust or revise the design scheme so as to avoid problems in actual environmental construction. Besides, other unwanted troubles including waste of resources are avoided to some extent. Figure 5 depicts a typical example—scene division modeling.

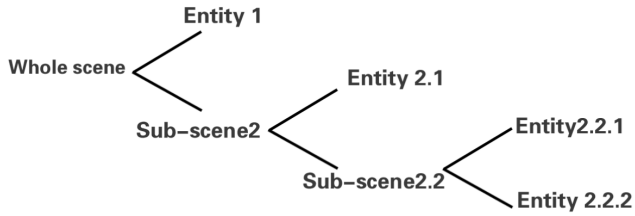

Fig. 5. Scene division modeling

6. Conclusion

From the past experience, the virtual reality technology has been widely used in many practical projects such as architecture engineering design, environmental art design and simulation operation platform and shown outstanding advantages. Via computer software, the virtual reality technology can build framework of the three-dimensional simulation model within a remarkably short period of time, which greatly reduces the design period of substantial project. Meanwhile, if any adjustment is to be made during the design process, it is not necessary to overthrow the design content and redesign objects, which usually take place in the conventional environmental design but only to revise the part to be adjusted in the design scheme via the corresponding design software. Thus, we can lower the cost of the project design to a certain extent, avoid artificial design error, improve quality and efficiency of environmental art design, and most importantly enhance the resource utilization rate of the environment art design projects and then improve the economic benefits

of substantial project in operation process.

The integrated application of electronic information technology and other modern technologies has brought new experience to human and vivid virtual real scene has offered us better multiple sensory feelings. The practical application of virtual reality technology in the field of environmental art design makes up the deficiencies of conventional environmental art design, effectively avoids the potential problems in actual operation, and improves the economic benefits of substantial project construction. Therefore, it is worthwhile to promote such technology in relative industries.

References

[1] A. Z. Sampaio, O. P. Martins: *The application of virtual reality technology in the construction of bridge: The cantilever and incremental launching methods.* Automation in Construction *37* (2014), 58–67.

[2] A. Bargelis, A. Baltrušaitis: *Applications of virtual reality technologies in design and development of engineering products and processes.* Mechanika *19* (2013), No. 4, 473–477.

[3] Z. Li: *Application and design of virtual reality technology in railway maintenance training.* International Journal of Technology Management (2013), No. 04, 42–44.

[4] L. P. Berg, J. M. Vance: *Industry use of virtual reality in product design and manufacturing: A survey.* Virtual Reality *21* (2017), 1–17.

[5] J. P. Dickey, T. R. Eger, R. J. Frayne, G. P. Delgado, X. Ji: *Research using virtual reality: Mobile machinery safety in the 21st century.* Minerals *3* (2013), No. 2, 145–164.

[6] J. Chen, P. Mitrouchev, S. Coquillart, F. Quaine: *Disassembly task evaluation by muscle fatigue estimation in a virtual reality environment.* The International Journal of Advanced Manufacturing Technology *88* (2017), No. 5, 1523–1533.

[7] R. P. Fernández, V. Alonso: *Virtual reality in a shipbuilding environment.* Advances in Engineering Software *81* (2015), 30–40.

[8] V. Chulvi, E. Mulet, F. Felip, C. García-García: *The effect of information and communication technologies on creativity in collaborative design.* Research in Engineering Design *28* (2017), No. 1, 7–23.

[9] R. I. García-Betances, M. T. Arredondo Waldmeyer, G. Fico, M. F. Cabrera-Umpiérrez: *A succinct overview of virtual reality technology use in Alzheimer's disease.* Frontiers in Aging Neuroscience (2015), No. 7, 80.

[10] R. J. Menzies, S. J. Rogers, A. M. Phillips, E. Chiarovano, C. de Waele, F. A. J. Verstraten, H. MacDougall: *An objective measure for the visual fidelity of virtual reality and the risks of falls in a virtual environment.* Virtual Reality *20*, (2016), No. 3, 173–181.

[11] W. Xiong, Q. H. Wang, Z. D. Huang, Z. J. Xu: *Disassembly task evaluation by muscle fatigue estimation in a virtual reality environment.* International Journal of Advanced Manufacturing Technology *85* (2016), No. 5, 955–969.

[12] F. Sun, Z. Zhang, D. Liao, T. Chen, J. Zhou: *A lightweight and cross-platform Web3D system for casting process based on virtual reality technology using WebGL.* International Journal of Advanced Manufacturing Technology *80* (2015), No. 5, 801 to 816.

[13] N. Vaughan, V. N. Dubey, T. W. Wainwright, R. G. Middleton: *A review of virtual reality based training simulators for orthopaedic surgery.* Medical Engineering & Physics *38* (2016), No. 2, 59–71.

[14] F. Ferrise, S. Graziosi, M. Bordegoni: *Prototyping strategies for multisensory product experience engineering.* Journal of Intelligent Manufacturing (2015), 1–13.

[15] G. Lorenzo, A. Lledó, J. Pomares, R. Roig: *Design and application of an immersive virtual reality system to enhance emotional skills for children with autism spectrum disorders.* Computers & Education *98* (2016), 192–205.

[16] T. P. Antunes, A. S. Oliveira, T. B. Crocetta, J. Y. Antão, R. T. Barbosa, R. Guarnieri, T. Massetti, C. B. Monteiro, L. C. Abreu: *Computer classes and games in virtual reality environment to reduce loneliness among students of an elderly reference center: Study protocol for a randomised cross-over design.* Medicine (Baltimore) *96* (2017), No. 10, e5954.

[17] D. Yelshyna, M. F. Gago, E. Bicho, V. Fernandes, N. F. Gago, L. Costa, H. Silva, M. L. Rodrigues, L. Rocha, N. Sousa: *Compensatory postural adjustments in Parkinson's disease assessed via a virtual reality environment.* Behavioural Brain Research *296* (2016), 384–392.

[18] J. Peng, L. Xu, Y. Shao: *Research on the virtual reality of vibration characteristics in vehicle cabin based on neural networks.* Neural Computing and Applications (2016), 1–8.

[19] P. Parijat, T. E. Lockhart, J. Liu: *TEffects of perturbation-based slip training using a virtual reality environment on slip-induced falls.* Annals of Biomedical Engineering *43* (2015), No. 4, 958–967.

Received May 22, 2017

Acta Technica *62* No. 1A/2017, 225–236

Application research on an extended fractional lower-order cyclic music algorithm in radio frequency narrow band signal time delay estimation in wireless positioning

Hongping Pu[1], Kaiyu Qin[1]

Abstract. In view of the problems of wireless location technology for the smooth transmission of signals in the steady state and DOA estimation, this paper proposed an extended fractional lower order cyclic MUSIC algorithm which is based on the extended helical circular array algorithm. The principle is that the spiral and conjugate are jointly related. In view of the error estimation of the intermediate frequency difference in the original MUSIC algorithm, the method of MUSIC frequency detection time delay estimation based on frequency difference compensation is proposed. The advantage of high resolution of the original MUSIC algorithm was fully played, and at the same time the accuracy of the estimation of the time difference was improved, which made up for the deficiencies of the original MUSIC algorithm. In the simulation experiment, it is concluded that the improved algorithm is better than the traditional algorithm. This paper not only provides a new idea for wireless positioning technology, but also promotes the development of the wireless industry.

Key words. Fractional lower order cyclic MUSIC algorithm, wireless positioning, radio frequency narrow band signal, time delay estimation.

1. Introduction

Estimation of time difference is the most important point in wireless location technology. It has characteristics of high positioning accuracy, long effective time, small external interference, and small probability of being found; therefore, it has been widely used in a variety of engineering [1, 2]. The main reason for the existed estimation error of time difference is that two receivers are actually independent. The two independent receivers cannot cooperate with each other; therefore, amplitude

[1]School of Astronautics and Aeronautics, University of Electronic Science and Technology of China, Chengdu 611731, China

cannot match each other as well. This error will cause a serious deviation of the signal on both sides, so as to affect the time difference estimation of the positioning signal. This effect has not been considered in the existing algorithms [1–4]. In view of the existing problems of time difference estimation, this paper presents an extension of fractional lower order cyclic MUSIC algorithm by using the method of frequency difference detection to compensate the time difference. Therefore, the advantage of high resolution of the common MUSIC algorithm can play a full role in improving the accuracy of the estimation of the time difference [5].

2. State of the art

Using statistics to establish mathematical model, and the tool is the stable distribution of α. The stable distribution method of α is based on the concept of limit distribution. This new distribution is more popular. This distribution will become more stable if the constraint of this kind of distribution law is enlarged in a certain way. Based on this, the paper thought under the constraint of limit distribution, it is very suitable for many situations. When under some specific circumstances, even if it is beyond the constraints, it still can be used.

Gauss distribution is a kind of special distribution mode, which is approximately the same as the above mentioned distribution of α [6]. When the α distribution is specifically required, Gauss distribution will be produced. Obviously, the range of Gauss distribution is narrower. But the two are not much different in terms of stability. According to the research on Gauss distribution, it can be deduced to the α stable distribution, which is absolutely applicable. Therefore, the random variables are arranged and input into a certain system according to the α stable distribution. The results are identical to the original input variables in their own nature. The α stable distribution has a very important role in the processing of positioning signals. It will be the focus of the next step. Because the distribution of the noise signal generated in this distribution mode is very similar to that of the actual operation, it can be a good way to simulate the generation and propagation of noise generated in the process as well as to set and save the relevant data to record more details of all kinds of noise signals.

In recent years, as an important part of signal processing, time delay estimation method has been widely used in radar, sonar, wireless communication and other fields [7]. Based on the classical estimation method of time delay, due to the limitation of signal bandwidth, the estimation accuracy will decrease obviously when the signal source distance is close, therefore, it is impossible to separate similar signals, which cannot meet the needs of practical applications in many fields. In order to solve the problem of delay estimation in close distance signal source, Schmidt and other scholars [8] have proposed time domain frequency domain estimation methods based on subspace, however, these methods have special requirements for the array flow patterns, and the time delay estimation problem is transformed into a sinusoidal parameter estimation problem. Pallas and Hasan [9–10] have proposed time delay estimation methods with high resolution, however, these methods are only suitable for wideband or flat spectrum signals, and these methods do not take into account

the influence of intermediate frequency deviation on the estimation accuracy.

The envelope extraction method based on Hilbert transform which can eliminate the deviation directly without the estimation of intermediate frequency deviation has been introduced in literature [11]. There are many methods to estimate the intermediate frequency deviation, such as square frequency doubling method, frequency domain correlation method and so on. A circular MUSIC algorithm based on uniform circular array has been proposed in literature, which is called B-Cyclic-MUSIC algorithm; although the B-Cyclic-MUSIC algorithm can well estimate the azimuth and elevation angle of the incoming signal, the algorithm is not a robust algorithm, that is, the algorithm is effective only in the Gauss noise conditions, while the performance of the algorithm will be degraded when there is impulsive noise in the environment. Based on this, this paper proposed the UCA-FLOCC-MUSIC algorithm based on uniform circular array. The proposed method can not only suppress the noise and interference of a stable distribution, but also be effective in Gauss noise condition, which is a robust DOA estimation algorithm with high resolution.

3. Methodology

3.1. Fractional lower order cyclic correlation and fractional lower order conjugate cyclic correlation

When the array is a uniform matrix, the rank of the matrix is M. When the position signal is incident into the array, the bandwidth of the signal is narrow band, and its rank is L. The distance between the array elements in each matrix is K_a, and the remaining signals are not in accordance with the predetermined frequency to disturb signals circularly. The complex envelope signals of the output signal of the first k element can be expressed as

$$x_k(t) = \sum_{m=1}^{K_a} A_{km} s_m(t) + n_k(t),\ k = 1, 2, \cdots, m\,. \tag{1}$$

In the formula, the response of the first k array elements of the M signal can be expressed as A_{km}, $S_m(t)$ is the signal, independent and identically distributed complex noise can be expressed as $n_k(t)$. The observed signal vector may be expressed by the matrix equation

$$X(t) = A(\theta)S(t) + N(t)\,. \tag{2}$$

Here, the observed signal vector is expressed as $X(t) = [x_1(t), \cdots, x_m(t)]^{\mathrm{T}}$, and specified cycle frequency is the incident signal vector of ε, which can be expressed as $S(t) = [s_1(t), s_2(t), \cdots, s_{K_a}(t)]^{\mathrm{T}}$. When $K_a < L$, $A(\theta) = \{A_{km}\}_{M\times K_a} = [a(\theta_1),\ a(\theta_2), \cdots,\ a(\theta_{K_a})]$. Besides, $a(\theta_m) = \left[1, \mathrm{e}^{-j\omega_m}, \cdots, \mathrm{e}^{-\mathrm{j}(M-1)\omega_m}\right]^{\mathrm{T}}$, $\omega_m = 2\pi\frac{d}{\lambda}\sin(\theta_m)$, the incidence angle is θ_m, d is the distance, λ is the wavelength. Interference and noise vectors received by the array can be expressed as $N(t) = [n_1(t), n_2(t), \cdots, n_M(t)]^{\mathrm{T}}$, and the noise obeys the stable distribution of α.

The correlation is described by the following two equations:

$$R_{XX}^{P}(\varepsilon;\tau)=\left\langle X(t+\tau/2)\left[X^{H}(t-\tau/2)\right]^{\langle p-1\rangle}\mathrm{e}^{-\mathrm{j}2\pi\varepsilon t}\right\rangle_{t}, \tag{3}$$

where H is used as the conjugate transpose. Symbol ε is used as the cyclic frequency, and p is the order of fractional lower order cyclic statistics. Then fractional lower order cyclic correlation matrix and element of (i,k) are given by the following equation.

$$R_{X_iX_k}^{P}(\varepsilon;\tau)=\left\langle x_t(t+\tau/2)\left[x_k^{*}(t-\tau/2)\right]^{\langle p-1\rangle}\mathrm{e}^{-\mathrm{j}2\pi\varepsilon t}\right\rangle_{t}. \tag{4}$$

3.2. Frequency detection time delay estimation model

The positioning signal received at the receiving end is expressed as $x(n)$ and$y(n)$, and the duration time of the positioning signal is $s(n)$. The radio frequency of the positioning signal of the narrow band is T_r, the time difference between the two ends of the signal is t_0, and f_s expresses signal sampling rate. When the frequency error is 0, then the model of time difference can be expressed as

$$\begin{cases} x(n)=s(n)+w_1(n), \\ y(n)=\beta s(n-D_t)+w_2(n). \end{cases} \tag{5}$$

In the formula, we use $w_1(n)$ and $w_2(n)$ to indicate noise which is unrelated with signal source, and discrete time delay of $x(n)$ and $y(n)$ is $D_t=t_0f_s$. We use β to the express signal attenuation factor. $n=0,1,\cdots,K_r-1$ and $K_r=T_rf_s$ are sampling points of the signal. Complement and illustrate the above equations to obtain the equation

$$R_{xy}(m)=\sum_{n=0}^{N-1}x(n)y(n+m), \tag{6}$$

where $S(k)$ and $W_1(k)$ are assumed to be the result of the transformation of the signal $s(n)$, and the noise $w_1(n)$, and the mutual power spectrum density is $x_p(k)=DFT(R_{xy}(m))$. According to the above density relationship, the density can be expressed by XY:

$$x_p(k)=X(k)Y^{*}(k). \tag{7}$$

In the formula (7),

$$X(k)=DFT\left[s(n)+w_1(n)\right]=S(k)+W_1(k), \tag{8}$$

$$Y^{*}(k)=DFT^{*}\left[\lambda s(n-D_t)+w_2(n)\right]=\lambda S^{*}(k)\mathrm{e}^{\mathrm{j}2\pi kD_t/N}+W_2^{*}(k). \tag{9}$$

The above formula is substituted uniformly.

$$x_p(k)=\lambda\left|S(k)\right|^{2}\mathrm{e}^{\mathrm{j}2\pi kD_t/N}+W(k),\ k=0,1,\cdots,N-1 \tag{10}$$

Based on $W(k) = \lambda S^*(k)\mathrm{e}^{\mathrm{j}2\pi kD_t/N}W_1(k) + S(k)W_2^*(k) + W_1(k)W_2^*(k)$, time difference estimation problem can be transformed into a spectral wave frequency estimation. The above equation is also converted similarly:

$$X_p = \lambda \wedge S + W \tag{11}$$

In the formula

$$X = \left[\begin{array}{cccc} X(0) & X(1) & \cdots & X(n-1) \end{array} \right]^T \tag{12}$$

$$\wedge = diag \left(\begin{array}{cccc} 1 & \mathrm{e}^{\mathrm{j}\omega} & \cdots & \mathrm{e}^{\mathrm{j}(N-1)\omega} \end{array} \right). \tag{13}$$

In the formula, $\omega = 2\pi D_t/N$, In order to optimize the test efficiency of the new algorithm and the estimation accuracy of the time difference, the above data X_p an be segmented, so as to divide the whole data into $L = N - M + 1$ submatrix.

For positioning signal in such a narrow band in transmitter, when the pulse signal is concentrated in a range of frequency, the value of L will not be very large. The estimated value $\hat{\omega}_1$ of angular frequency is obtained by constructing spatial spectral function; thus, the time delay value is obtained as

$$\hat{D}_t = \hat{t}_0 f_s = -\hat{\omega}_1 N/(2\pi). \tag{14}$$

3.3. Time delay estimation method based on envelope extraction

The literature mentioned a method using Hilbert transformation to directly eliminate the difference produced by all the intermediate frequency instead of estimating again. The positioning signal model based on this kind of conversion is

$$\begin{cases} x(n) = a(n)\cos(\omega_0 n + \varphi_1(n)) + w_1(n) \\ y(n) = a(n - D_t)\cos((\omega_0 + \Delta\omega_0)n + \varphi_2(n)) + w_2(n). \end{cases} \tag{15}$$

In formula (15), $a(n)$ is the signal amplitude, $\varphi_1(n)$ and $\varphi_2(n)$ are the initial phases. We can see that the acquisition of time delayD_t is actually through $a(n)$ and $a(n - D_t)$, then we can offset the error value of the intermediate frequency after we obtain D_t.

The following formula can be used in practical use:

$$\hat{a}(n) = \sqrt{x^2(n) + H^2[x(n)]}, \tag{16}$$

$$\hat{a}(n - D_t) = \sqrt{y^2(n) + H^2[y(n)]}. \tag{17}$$

Here, H [] represents the transformation of Hilbert. By summing up all the above formula we can be found that this transformation will have a huge impact on the noise. Moreover, this impact can make the algorithm have a great effect on the accuracy of the estimation of time difference.

3.4. Time delay estimation method based on frequency difference compensation

When the above solutions are unable to reasonably eliminate the error caused by the intermediate frequency, we can first calculate and estimate the error values, and then make up for the signal. The value we make up for is the above estimation value. Set the estimation value of intermediate difference Δf_0 as $\Delta\hat{f}_0$, we compensate for the received signal $x(n)$:

$$x_0(n) = x(n)\mathrm{e}^{\mathrm{j}2\pi n\Delta\hat{f}_0/f_s}\,. \tag{18}$$

In the same way, the estimated value $\hat{\omega}_t = -2\pi\hat{D}_t/N$ of the angular frequency is obtained by using the MUSIC algorithm, then the corresponding time delay estimation is $\hat{D}_t = -\hat{\omega}_t N/(2\pi)$. We assume that the error value of intermediate frequency is $\Delta f = \Delta\hat{f}_0 - \Delta f_0$, and then the corresponding experimental estimation error will be

$$\varepsilon_t(k) = \frac{N^2}{2\pi f_s}\frac{d^2\varphi(k)}{dk^2}\Delta f\,. \tag{19}$$

4. Result analysis and discussion

4.1. Robustness analysis

In this paper, simulation experiments are used to verify the performance and robustness of the algorithm. The above three algorithms are brought into the simulation experiment, and the experimental ontology is the uniform array of $M = 8$. The incident signal selects a narrow band signal with the same power, and all the noise distribution adopt stable distribution of α. The preset cycle frequency of the incident signal is $\varepsilon = f_b$, and the frequency of the interference signal is 4.2 MHz. For the collection of the incident signal, the selected time frequency is 30 MHz. Among the obtained results, finally we get the pros and cons of the three algorithms based on the comparison of angular resolution.

Simulation experiment 1: in this paper, the interference shielding ability of the noise in the algorithm is affected by the low order fractional matrix P. The choice of SOI is 10 degrees and 20 degrees, and the initial angle of the interference information is 50 degrees. The noise in this experiment is consistent with the stable distribution of α, and the value α of this experiment is 1.4. The generalized noise-signal ratio is respectively set to 10 dB, 15 dB and 20 dB. The number of snapshot of signals is 1000. 500 cycles of Monte Carlo Simulation is carried out in each experiment.

Figure 1 shows the curve of the mean square error changed with the fractional lower order moment P. From Fig. 1 we can detect that under different signal and noise ratio conditions, when $1 < p < \alpha$, the root mean square error of the algorithm is relatively small. Apparently, when $p = 2$, the algorithm in this paper is reduced to EX-Cyclic-MUSIC algorithm. That is to say, EX-Cyclic-MUSIC is the special case of this algorithm.

Simulation experiment 2: the effect of the snapshots used in this paper to verify the signal on algorithm. Different from experiment 1, the generalized noise-signal ratio is set to 10,dB, and the value of P will be changed to 1.2. Figure 2 is a diagram of the relationship between the RMS error and the number of signal snapshots. In this experiment, the three algorithms are using the cycle data. Cycle itself is periodic, so circulation of signal itself can be reflected only when numerical value of signal snapshots is large. Through analysis of the following figure, when the numerical value of snapshots is identical, the root mean square error of the improved algorithm is obviously smaller than that of the other two algorithms, which proved that the improved algorithm has better performance than other algorithms. With the increase of the number of snapshots, the gap between the three becomes smaller, until basically coincident.

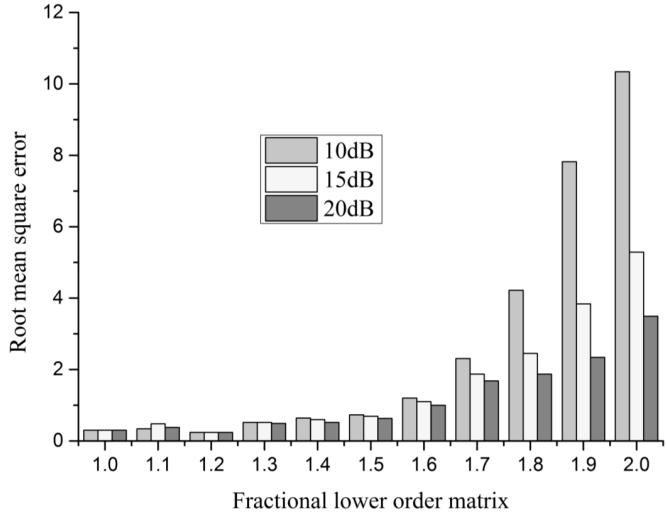

Fig. 1. RMSE of DOA estimates versus p

4.2. Time difference estimation analysis

The time difference estimation methods are compared with the simulation experiment. These three methods are MUSIC method without compensating for frequency difference, the MUSIC method with compensating for frequency difference and the method for estimating time difference by using envelope extraction. In the experiment, the acquisition time and frequency of the incident signal is 50 MHz, and the incident signal adopts modulation signal. The carrier frequency of the signal itself is 10.7 MHz. The time of acquisition of each incident signal is 20 μs. The generalized noise-signal ratio is 10 dB.

When the bandwidth of the signal is not the same, the error produced by intermediate frequency increases from 0.5 to 2.5. The signal bandwidth is 4–10 MHz every 2 minutes. 100 cycles of Monte Carlo Simulation are carried out in each experiment.

From Figs. 3–6, we can come up with the corresponding conclusion that when

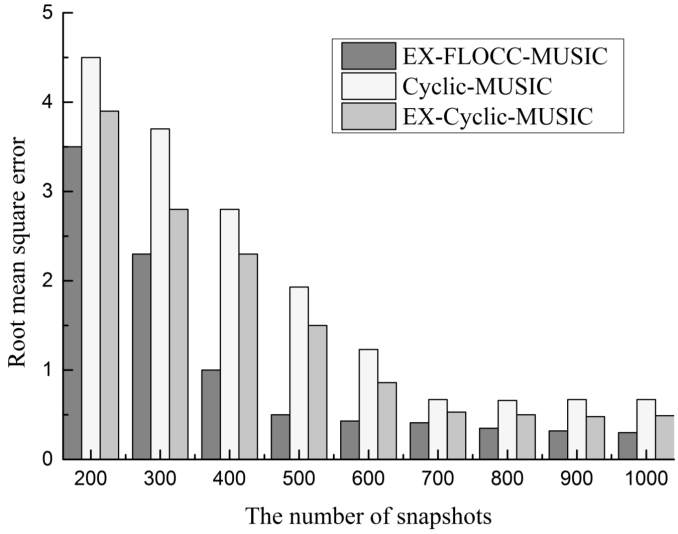

Fig. 2. RMSE of DOA estimates versus number of snapshots

the error of the intermediate frequency remains unchanged, due to the existence of error, the first estimation method can produce very large error in the estimation of time difference. The third estimation method can eliminate the error, which will not affect the accuracy of the final value. The second estimation method proposed in this paper can not only ensure the accuracy of the final results, but also produce the corresponding compensation value with the constant change of the bandwidth. Compared with the other two time difference estimation methods, this scheme achieves better results with better accuracy. When conditions are changed, it can timely generate corresponding changes, which is more suitable for the use of the current positioning systems.

5. Conclusion

This paper mainly studied how to reduce the error of the time delay estimation accuracy of radio frequency narrow band signal caused by the intermediate frequency deviation. Therefore, this paper proposed an extended fractional lower order cyclic MUSIC algorithm. The conclusions drawn are as follows:

This paper combined fractional lower order cycle and fitting spectrum correlation signal subspace, and put forward a new algorithm of MUSIC time delay estimation based on frequency difference compensation. This algorithm retains the advantages of the traditional algorithm, and it also improves the defects of the traditional algorithm. For example, it can better distinguish the angle of impulse noise, and it has good anti-interference performance. Experimental results showed that the new algorithm of MUSIC time delay estimation can effectively reduce the workload and improve the running speed. It has high precision and strong adaptability, and it is

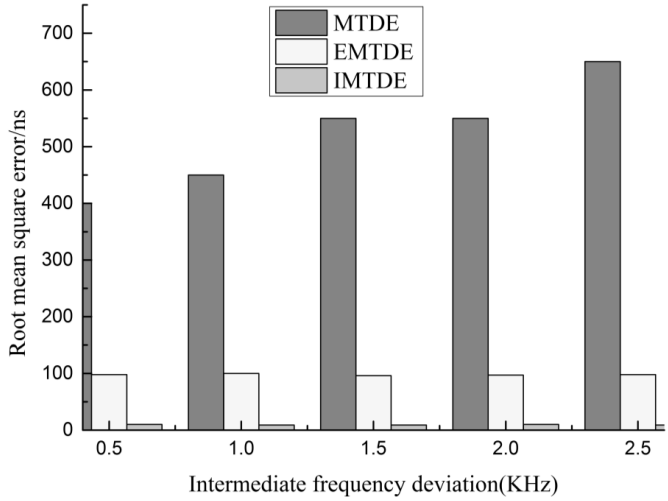

Fig. 3. Root mean square error versus intermediate frequency deviation, 10 kHz wide signal band

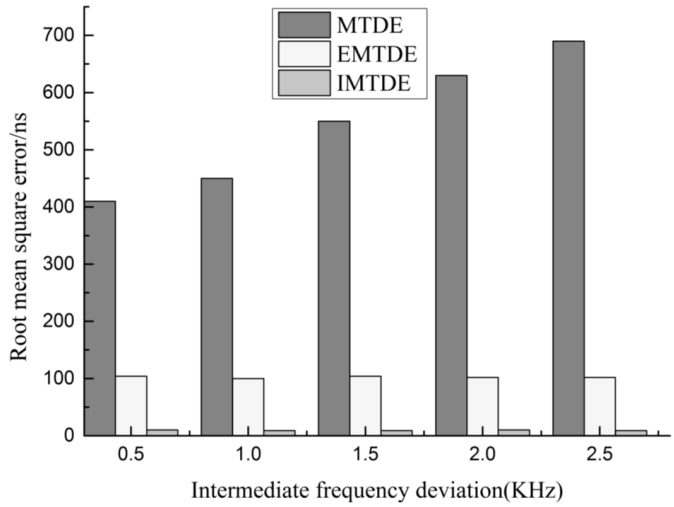

Fig. 4. Root mean square error versus intermediate frequency deviation, 8 kHz wide signal band

of great application value.

In order to solve the problem of similar signal source and time delay estimation, this paper made a comparison between the time delay estimation model and the MUSIC algorithm estimation model, and proposed an extended fractional lower order cyclic MUSIC algorithm based on frequency difference compensation. This method has high resolution and good performance in time delay estimation. Compared with the traditional algorithm, the algorithm is more adaptable and suitable for various time delay estimation conditions.

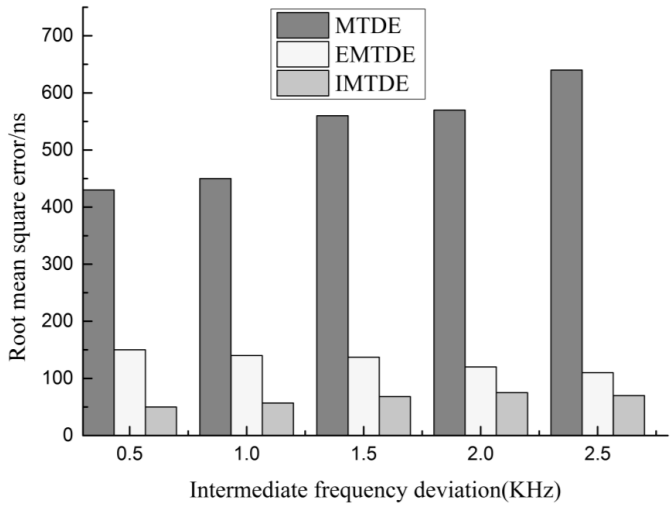

Fig. 5. Root mean square error versus intermediate frequency deviation, 6 kHz wide signal band

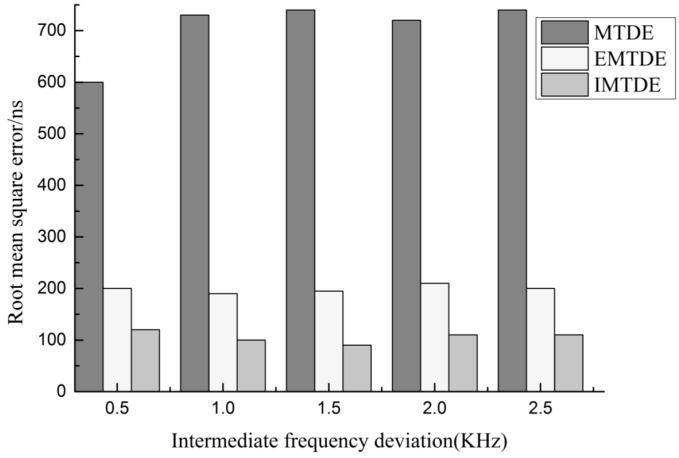

Fig. 6. Root mean square error versus intermediate frequency deviation, 4 kHz wide signal band

An extension of the fractional lower order cyclic MUSIC algorithm proposed in this paper is not comprehensive enough. This paper only focus on the deviation of intermediate frequency in time delay estimation, and there is still much research space for the analysis of other influencing factors. In the further study, we should focus on the new time delay estimation method when multiple factors coexist.

References

[1] R. Cabot: *A note on the application of the Hilbert transform to time delay estimation.* IEEE Transactions on Acoustics, Speech, and Signal Processing *29* (1981), No. 3, 607 to 609.

[2] Z. Cheng, T. T. Tjhung: *A new time delay estimator based on ETDE.* IEEE Transactions on Signal Processing *51* (2003), No. 7, 1859–1869.

[3] H. C. So: *Fractional lower-order moment based adaptive algorithms for time delay estimation in impulsive noise.* Proc. Midwest Symposium on Circuits and Systems, 8–11 August 1999, Las Cruces, NM, USA, IEEE Conference Publications *2* (1999), 985–988.

[4] G. Fong, W. A. Gardner, S. V. Schell: *An algorithm for improved signal-selective time-difference estimation for cyclostationary signals.* IEEE Signal Processing Letters *1* (1994), No. 2, 38–40.

[5] Y. G. Yang, X. T. Huang, Z. M. Zhou: *A new method of direction finding for cyclostationary signal sources with uniform circular array.* Proc. IEEE International Conference on Signal Processing Proceedings, 31 Aug.–4 Sept. 2004, Beijing, China, IEEE Conference Publications *1* (2004), 431–434.

[6] M. Shao, C. L. Nikias: *Signal processing with fractional lower order moments: Stable processes and their applications.* Proceedings of the IEEE *81* (1993), No. 7, 986–1010.

[7] S. R. Shaw, C. R. Laughman: *A Kalman-filter spectral envelope preprocessor.* IEEE Transactions on Instrumentation and Measurement *56* (2007), No. 5, 2010–2017.

[8] A. Quazi: *An overview on the time delay estimate in active and passive systems for target localization.* IEEE Transactions on Acoustics, Speech, and Signal Processing *29* (1981), No. 3, 527–533.

[9] Z. Q. Hou, Z. D. Wu: *A new method for high resolution estimation of time delay.* Proc. IEEE International Conference on Acoustics, Speech, and Signal Processing, 3–5 May 1982, Paris, France, IEEE Conference Publications *7* (1982), 420–423.

[10] M. A. Pallas, G. Jourdain: *Active high resolution time delay estimation for large BT signals.* IEEE Transactions on Signal Processing *39*, (1991), No. 4, 781–788.

[11] F. X. Ge, D. Shen, Y. Peng, V. O. K. Li: *Super-resolution time delay estimation in multipath environments.* IEEE Transactions on Circuits and Systems I: Regular Papers *154* (2007), No. 9, 1977–1986.

Received May 22, 2017

Acta Technica *62* No. 1A/2017, 237–246

Preliminary exploration of escape slide[1]

Gang Hou[1], Xiaoqi Niu[1,3], Liyang Zhu[2]

Abstract. Using escape stairs is conventional way to escape from the fire building. But using the stairs as an escape path has many shortcomings, and in some conditions escape stairs cannot be used to escape in reality. Using ropes and other emergency tools to escape from balconies or windows is very dangerous. Escape slide, a new indoor fire escape facility, is put forward with the conventional design method and the function design method. The problems of structure, fireproof, lighting, ventilation, lighting, setting place, the exit of escape slide and alarm linkage are discussed. The advantages and disadvantages of escape slide are analyzed. Less occupation space, no energy consumption, fast escaping speed, safe use, easy protection are the advantages of the escape structure. Escape slide is an escape structure having research value and worth to popularize, and this structure is a supplement to the evacuation staircase.

Key words. Slide, escape, fire, construction.

1. Introduction

In modern buildings, the fire spreads quickly. When the fire starts, the evacuation time is very short. The escape route is used to determine the probability of survival. Staircase and elevator are two forms to solve perpendicular traffic problems mainly in buildings. In case of fire state, the elevator is forced to land on the first floor and cannot be used as an escape. Using staircase is the only way to escape. As a means of escape, staircase has many advantages. But it has many disadvantages, too. Staircase has strong ability to convey flow, but it occupies a large floor area at the same time; for the individual conveying speed it is not fast; relying on walking, people consume a lot of physical strength to evacuate; staircase cost is increased for the dual application of normal and fire status; all materials must comply with fire resistance requirements if the fire resistance requirement is necessary despite the large volume of stairwell; due to the large volume of stairwell, high capacity smoke device and large amount of lighting is necessary for large volume of stairwell. Is there other form of escape way beside the escape stairs? The fire development

[1]Institute of Civil Engineering, Anyang Normal University, Anyang, Henan, 455000, China
[2]Anyang Municipal Design and Research Institute Co., Ltd., Anyang, Henan, 455000, China
[3]Corresponding author

characteristic is depicted in Fig. 1.

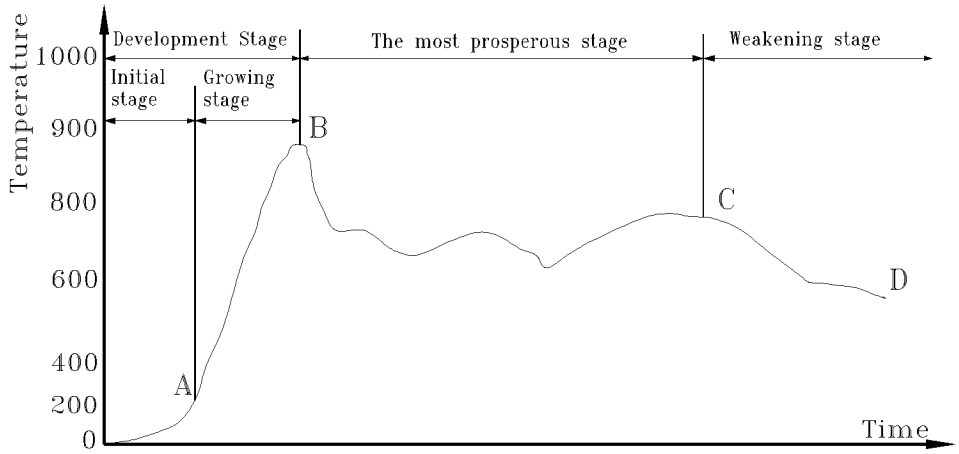

Fig. 1. Fire development law

Slide way is often disposed at mountain tourist attractions as recreation facility. People enjoy the scenery, and experience the joy of speeding down at the same time. Can we build a escape slide in the building construction as a form of escape? Parameters of commonly used staircases in high-rise buildings are listed in Table 1.

Table 1. Evacuation time in high buildings through the stairs in different number of layers and in different number of cases (the stair width being 1.1 m)

Number of layers	Evacuation time (min)		
	240 people per layer	120 people per layer	60 people per layer
50	131	66	33
40	105	52	26
30	78	39	20
20	51	25	13
10	38	19	9

2. State of the art

How to escape has been the focus of research, when the building or structure is on fire. Mathematical simulation method and other methods were used to study the fire escape by a lot of scholars. He Yijing used buildEXODUS to simulate the time of evacuation of high-rise dormitories [1]. Xie Haiming used three-bit simulation technology to make the fire evacuation drill more visualizable [2]. The smoke spread speed, temperature, the CO concentration, variation of visibility and evacuation behavior characteristic of indoor personnel in the high-rise building fire scene were simulated by Wang Hairong using FDS and Pathfinder [3]. Software simulation

was used to select the best escape route by He Peichong and Jiang Huixian [4][5]. Liu Yunxiang wrote programs named firesim to study the rule of fire [6]. Through simulation analysis, Weng Tao pointed out that the efficiency of orderly evacuation was much higher than that of evacuation together. Ran Haichao found the values of the actual evacuation might exceed the design values using the method of software simulation also [7]. Hou Lei pointed out through simulation that increase of exits can greatly reduce casualties [8]. Through the statistical analysis, Shi Xingjun also pointed out that lack of evacuation stairs and evacuation export blocked was the main reason for the increase in the number of fire victims [9]. Zhang Hao provided another way to escape from fire except regular evacuation channel, including rope, ladder, slide and air cushion [10]. Zhang Ruihua proposed a rescue apparatus for high-rise buildings, which can convert kinetic energy into electrical energy and then convert into heat by resistance [11]. Lin Li designed a slow-down escape device, which was simple in structure and could be used in reciprocating [12]. Zhang Rui put forward an expandable fire escape passage made by hinge, connecting rod and soft package material which was folded up in normal times and deployed automatically by water pressure and springs [13]. No matter software simulation or statistical analysis of historical data reveals the situation that often appears, that cannot use conventional escape routes to escape. While using the ropes, ladders, and other outdoor escape devices is very dangerous. It is lack of new type of escape facility in the room, though there are some inventions, but the practicality is poor. It is necessary to seek a reliable new indoor escape facility.

3. Methodology

3.1. The design of escape

The idea of the proposed slide is depicted in Fig. 2.

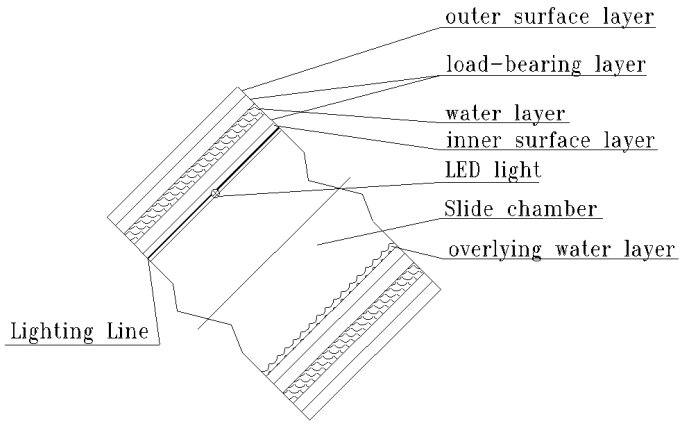

Fig. 2. Lengthwise profile of the slide

The escape slide is a circular or similar circular cavity structure. In the middle of the cavity there is a personnel evacuation channel. The slide wall is composed of a variety of materials. The walls of the slide are required the exhibit some properties such as load-bearing, refractory or lighter weight.

The slide wall is divided into intermediate structural layer (i.e., the load-bearing layer), inner surface layer and outer surface layer.

As for the load of slide, the structural layer is required to have a certain carrying capacity. Strong-bearing capacity materials can be used like steel and reinforced concrete. Outer layer of the slide is required to enhance the fire resistance and to have a certain aesthetic requirements. Outer layer may be a single layer of material or a composite material.

Table 2 presents the temperature of the main rib in the beam and the thickness of the protective layer under the action of fire temperature and Fig. 3 shows the relationship between the temperature of the main rib in the beam and the thickness of the protective layer.

Table 1. The relationship between the temperature of the main rib in the beam and the thickness of the protective layer under the action of fire temperature

Thickness of protective layer of main reinforcement (cm)	Temperature of main reinforcement heated up for different times (°)									
	15 min	30 min	45 min	60 min	75 min	90 min	105 min	140 min	175 min	210 min
1	245	390	480	540	590	620				
2	165	270	350	410	460	490	530			
3	135	210	290	350	400	440		510		
4	105	175	270	270	310	340			500	

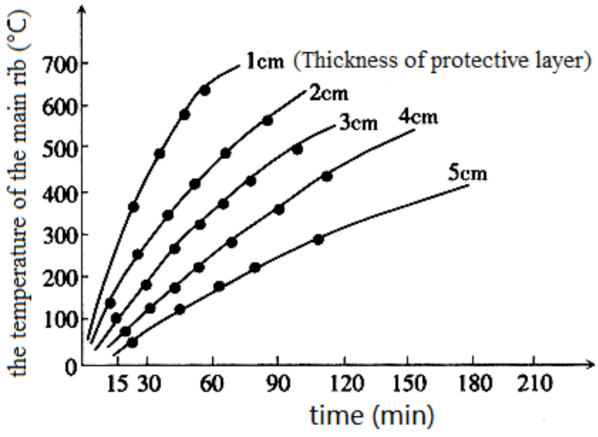

Fig. 3. The relationship between the temperature of the main rib in the beam and the thickness of the protective layer

The inner surface layer is required to conceal electrical lines and to installation of lighting fixtures. Further requirements of inner surface layer are a smooth surface on lower part and certain roughness on both sides. The inner surface layer is often required to use a variety of materials to meet the requirements. In hot regions, a method can reduce decline friction and reduce the friction damage to people and the burning sensation when sliding down which is forming a overlying water layer by turn on the water from the top of slide [1]. Figure 4 shows the cross section of the slide.

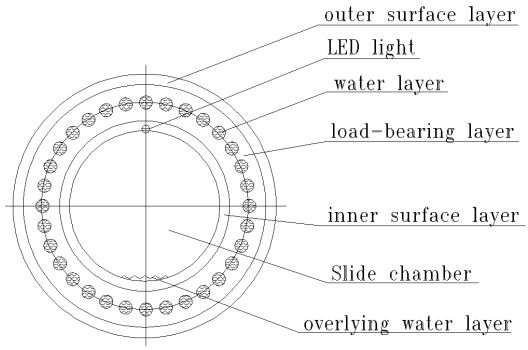

Fig. 4. Cross profile of the slide

Slide should be set to an inlet and an outlet; the middle should not be set to an opening. Normal closed door is set at opening of slide. Inlet door can be set to automatically lock, usually in the locked state, can automatically open fire, and should be able to manually open. Outlet door should open when people slid down, and it does not affect personnel slipping, automatically shut down after staff through.

Set the water layer in the wall is possible to improve the fire resistance. The water layer may be made of a plurality of tubular cavities, or other shape. Water is flowing in the time of fire; constantly take the heat to ensure that the internal slide at lower temperatures.

When the fire broke out, sending fresh air into the slide by the pressurized air supply system would positive pressure state in the slide chamber.

It is unnecessary to identify by eyes, because people in the chute is completely passive. The only thing to do for people is stepping on both sides of the slide by feet to control the rate of decline in the slide. Therefore, the chute cannot even install lighting, but in order to alleviate human stress, fear of emotions, low luminance lighting is appropriate. LED lights can be embedded in the upper chamber slide and supply pipeline embedded in the slide wall. Since LED lamp consumes very little electricity, power supply can also be powered by batteries.

By buried cable fixed temperature detector in the slide wall, the door of the slide opening will be closed when temperature in slide chamber in order to prevent overheating wounding. Cable fixed temperature detectors embedded wiring should adopt spiral, which rounded in the tube wall. In the top of the slide should be set smoke detector to detect whether there is smoke fleeing slide, and close the slide if necessary.

3.2. Possible use of premises and the use of forms

In the case of arrangement of the slide does not affect the perception, setting slide may be a good choice in the large space like tall plants. Slide can be made a spiral or a long slope or other curve, just paying attention to coordination with the chamber. Long slippery slope is more comfortable.

Layout method is similar to an outdoor staircase. We can use a long curve slope, and can use folded arrangement. Exhumation arrangement is a straight slope joins a chicane, and then joined a straight slope in the opposite direction, followed by a sharp turn and so forth. This arrangement requires less flat position, but the corner slide is relatively uncomfortable.

Because of the sharp turn, small radius of rotation makes people feel dizzy, but the position of plane occupied is small. On the contrary, large radius of rotation gives people a feeling of comfort, but the position of plane occupied is large. The slide can be constructed around some regions or rooms, such as shafts.

3.3. Some notes

A direct ground slide is ideal. But there are some benefits segmentation settings. Segmentation settings can avoid prolonged friction burning sensation or skin rubs; also can avoid entire slide can not be used for the smoke caused by fleeing into the slide; and people can also change the way of escape in the segment of slide, such as the slide change into the stairs or the stairs change into the slide. It is suitable for refuge floors to segment. Antechamber should be set at segment if the segment is not at refuge floor.

The position near the inlet of slide should ensure the safety for where people waiting in turn to access the slide. An antechamber of sufficient area should be set for people waiting to enter the chute. Where should have positive pressure air in antechamber on fire.

Though it is temporary safe for people evacuated to refuge floor or roof, to leave the building on fire is necessary for more security. The inlet of slide should be set at refuge floor and roof, so that people can be transferred along the slide to the ground.

The slide need combine with automatic fire alarm and linkage system. Cable type fixed temperature detectors installed in the inner wall of slide and smoke detectors installed in the top of the slide will transmit fire alarm signal to the control panel. In case of fire, the host command to open the chute entrance door, and to turn on the water in order to form overlying water layer, and to feed water pressure to flow in the water layer, and to light the lamp in the slide, and to send fresh air in the slide.

4. Result analysis and discussion

4.1. The disadvantages of escape slide

As a channel, the biggest problem is, that slide cannot fuse coordinately with other interior space which divided into rectangular space for its shape which presents an oblique curve. While the space occupied by the slide may be little, the space up and under the slide cannot be used suitably. The space of a straight slide occupied is small, while its projection area in the plane is large. Its application is limited and few people study it for this reason. The cavity shape of slide is depicted in Fig. 5.

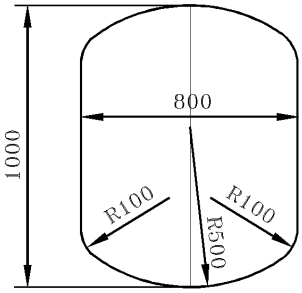

Fig. 5. Cavity shape of slide

Though the transport speed of slide using by single person is quick, fewer personal can use it synchronously. The slide has not a high efficiency as the stairs when a large number of people need evacuate. Table 3 contains the capacity comparison of down-stairways with different widths.

Table 3. Capacity comparison table of down-stairways with different widths [13]

Down-stairways width (m)	2.0	2.5	3.0	3.5
Practical traffic capacity (person/h)	8064	10080	12096	14112
Maximum traffic capacity (person/h)	8400	10500	12600	14700

Sliding to the ground directly from a certain height is or sliding from a high plane to a much lower plane suitable by the slide. Therefore exit cannot be set up every floor as the stairwell.

4.2. The advantages of escape slide

The angle of slide is generally between 20 degrees to 50 degrees [14]. People slide down in the escape slide just need a space which higher than person's head [15]. If people use the prone position, the slide can be made slimmer [16–17]. Small space structure can reduce the cost, for it need fewer building material, and need smaller-scale smoke control systems and lighting systems [18].

For a healthy adult it is not a difficult thing, evacuation from a higher floor by the stairs to the ground, but for the infirm and the disabled people this action is

difficult [19]. The momentum of decline comes from the weight of the human body in escape slide, it do not consume physical fitness [20].

For individual evacuee, who slides down along the escape slide will faster than the other who walks down the stairs.

Bumps, grazes, or even stampedes are often occurred when people are escaped down the stairs who will inevitably have to panic. The things will not happen escaping from the slide. Such an environment will help to eliminate fear, where the light is dim, and the body close to the chute, and field of view is limited to a narrow space.

Staircase design requirements to be considered when peacetime and fire-time, but the slide design requirements emergency use only for the only use of fire-time.

The slide is actually a pipe erected. Because of the small space volume, we can easily take some protective measures to improve its fire resistance. The same measures are difficult to achieve on the staircase. We can add a refractory material layer in the pipe wall of the escape slide and can add an integument of refractory materials on the outer surface of the slide, even can add a layer of water in the pipe wall, in which heat can be taken away by flow water so as to greatly improve the fire resistance. When we need to design a fire escape through the channel, the slide is most appropriate.

5. Conclusion

In order to find out a new way to escape from fire building in addition to the fire escape staircases, an escape slide is put out mainly through the method of function design in this paper, and a comprehensive analysis of its security is carried out including heat insulation, fire resistance, prevention of scratch damage, smoke prevention, air supply, lighting and fire alarm. Escape slide is a novel fire escape facility, which can enrich the means of escape, improve the building fire safety, and reduce casualties caused by fire. The use of it is more comfortable, and the elderly, children can use. It has good fire resistance and safety, and it can be widely used in industrial and civil buildings. It also has certain limitations, such as the relationship with the other building spaces is not easy to be deal with, and the exits cannot be set up each floor, and cannot be use by more people at the same time. The structure is particularly suitable for use in large space buildings and outdoor spaces. When being used in the reentry design and rotation design, it can also be used in other occasions. The deficiencies of the evacuation stairs are made up by this structure, which plays a complementary role and has broad application prospects.

References

[1] Y. J. He, J. Zeng, Z. H. Wang, M. D. Fu, X. Z. Zhang: *Numerical simulation of high-rise dormitoryand the psychological behavior duringthe fire evacuation.* Fire Science and Technology *32* (2013), No. 01, 15–18.

[2] H. M. Xie, Z. Liu: *Research on home fire escape system based on virtual reality.* Jour-

nal of System Simulation *24* (2012), No. 01, 108–111.

[3] H. Wang, Q. Chen, Y. Yu, Z. Yuan, J. Yan, D. Liang: *Study on simulation and escape behavior of high-rise building fire.* Acta Scientiarum Naturalium Universitatis Sunyatseni *53* (2014), No. 03, 151–154.

[4] P. C. He, X. G. Chen, X. Y. Wu, Y. Wang: *Simulation research of intelligent directing system for occupant evacuation in fire.* Fire Science and Technology *29* (2010), No. 09, 804–806.

[5] H. X. Jiang, G. F. Lin, L. H. Jiang, D. C. Huang: *Analysis and application of evacuation path inside buildings geared to campus fire.* Journal of System Simulation *25* (2013), No. 09, 2171–2176.

[6] Y. Liu, X. Yuan, C. Dou, F. Xu: *Research of fire risk factor evaluation in FDS field simulation.* Computer Measurement & Control *21* (2013), No. 04, 993–995.

[7] T. Weng, L. H. Hu: *Simulation on human evacuation efficiency of two different strategies in large commercial constructions.* Journal of Safety Science and Technology *8* (2012), No. 8, 157–162.

[8] L. Hou, J. G. Liu, X. Pan, Q. Guo, B. H. Wang: *Simulation of pedestrian evacuation based on Jilin fire.* Acta Physica Sinica *63* (2014), No. 17, 178902.

[9] X. J. Shi, S. P. Zhang: *Investigation of fire evacuation in guesthouse.* Fire Science and Technology *23* (2004), No. 01, 89–91.

[10] H. Zhang, H. W. Li, J. B. Shen: *New escaping method during building fire-outdoor emergency evacuation.* Building Science *24*, (2008), No. 01, 850–852.

[11] R. H. Zhang, H. C. Chen, S. L. Liu: *Design of rescue apparatus for high-rise buildings.* Machinery Design & Manufacture *67* (2011), No. 12, 24–25.

[12] L. Lin, X. S. Ran, H. B. Wei, D. H. Ye: *Study on fire escape device for high-rise building creative design.* Packaging Engineering *30* (2010), No. 24, 29–31.

[13] A. Dicembre, S. Ricci: *Railway traffic on high density urban corridors: capacity, signaling and timetable.* Journal of Rail Transport Planning & Management *1* (2011), No. 2, 59–68.

[14] Y. H. Zhang: *Research on the structure of Wuhan Yantze river tunnel escape chute.* Industrial Safety and Environmental Protection *37* (2011), No. 7, 55–56.

[15] X. M. Li, B. Z. Ren, X. H. Liu: *Study on fire prevention and escape safety countermeasures of urban high-rise buildings.* China Safety Science Journal *19* (2009), No. 8, 61–66.

[16] Z. H. Yang, X. Z. Wang, Y. Gao, X. H. Zhang, X. Y. Wang, J. E. Mei: *A domino-rope for evacuation tools from high-rise buildings.* Journal of Xi'an University of Architecture & Technology (Natural Science Edition), *37* (2005), No. 4, 546–551.

[17] R. Zhang, X. Chi, X. L. Wang, P. J. Yuan: *Research on expandable fire escape passage.* Fire Science and Technology *31* (2012), No. 1, 57–60.

[18] H. Y. Liu, G. F. Liang: *Discussion on the technical characteristics of home fires escape equipments.* Fire Science and Technology *30* (2011), No. 05, 425–428.

[19] Q. Zhu, M. Hu, W. Xu, H. Lin, Z. Du, Y. Zhang, F. Zhang: *3D building information model for facilitating dynamic analysis of indoor fire emergency.* Geomatics and Information Science of Wuhan University *39* (2013), No. 7, 762–766 + 872.

[20] H. C. Ran, L. H. Sun: *Research on Chinese modern commercial buildings fire protection design parameters.* China Safety Science Journal *24* (2014), No. 4, 33–37.

Received May 22, 2017

Acta Technica *62* No. 1A/2017, 247–258

Natural frequency of PC composite simple supported beam with corrugated steel webs

Li Rongjian[1], Liu Xia[1]

Abstract. The prestressed corrugated sheet steel exhibits a good performance and has been widely used in the construction of bridges and other similar structures. But the performance of the prestressed corrugated sheet metal is easily affected by external conditions, especially if its frequency of self-oscillation decreases the life span. So this paper presents a combination of corrugated steel web PC simply-supported box girder, the natural frequency of vibration research of corrugated steel belly PC combination of simply supported box girder structure natural frequency and dynamic characteristics analysis of corrugated steel web PC combination simply supported box beam shear lag effect of corrugated steel web PC combination of simply supported box girder shear effect and the coupling effect of the two is the influence of three important factors, which greatly influenced by the shear effect, prestress tension and steel anchor beam position is affected, a greater influence on the steel beam section.

Key words. Corrugated steel web, PC composite, simply supported box girder, natural frequency.

1. Introduction

With the development of economy and society, the prestressed concrete box girder has been widely used because of its strong anti-bending and twisting performance. At the same time, because of the increasing span of prestressed concrete box girder, the proportion of the beam's self-weight load increases, which makes the prestressing force consume most of the internal forces generated by the self-weight of the load beam, resulting in its economy becoming lower and lower. Therefore, in order to reduce the weight of prestressed concrete box girder, both in the choice of materials or structural design have been a high degree of attention. The simple composite box girder with corrugated steel web can optimize the web structure while reducing the dead weight of the girder, and it replaces the internal prestressing with the external prestressing force, so as to achieve the purpose of reducing the weight of the

[1]Chongqing Vocational Institute of Engineering, Chongqing, 400037, China

structure. However, due to the influence and limitation of the external environment, the mechanical properties of simply supported PC box girder with corrugated steel webs will affect its performance. Therefore, the mechanical properties of simply supported PC box girder with corrugated steel webs have become the research focus and direction of researchers at home and abroad in recent years. Some scholars have studied the mechanical behavior of trapezoidal corrugated steel web girders under fatigue loading, which provides a reliable basis for judging the fatigue life of corrugated steel web girder [1]. Later, some scholars have put forward the research on the seismic performance and torsional resistance of corrugated steel web girders, and some results are obtained [2]. Some scholars have combined the characteristics of the steel beam with corrugated steel web, and considered the effect of shear deformation. The formulas for calculating the deflection of steel web with corrugated steel web under the action of concentrated force are given. This has been helpful for subsequent in-depth studies [3]. In order to optimize the structure of corrugated steel web girders and to reduce the weight of the steel girders, some scholars have studied the effect of prestressed steel web girder accordion, and concluded that the accordion effect can help the corrugated steel web steel [4].With the research on the mechanical properties of steel webs with corrugated steel webs, many scholars have shifted their research points from static mechanics to the study of the dynamic properties of steel webs with corrugated steel webs. Some scholars have proposed the study of natural frequencies of steel webs with corrugated steel webs, this reduces the external influences of corrugated steel webs and improves their overall performance [5].Some scholars have put forward the in vitro dynamic factors of the natural frequency of steel webs with corrugated steel webs, which provides a new research direction for the study of steel webs with corrugated steel webs. Because the study of corrugated steel web steel girder is relatively late in China, the main research is focused on the study of static mechanics, and the research of dynamics is still in need of further study.

Based on the current research and development of PC composite simply supported box girders with corrugated steel webs, this paper will study the natural frequency of simply supported PC box girder with corrugated steel webs.In the second part, the development and future prospect of PC combined simple box girder with corrugated steel web will be summarized.In the third part, the structure and advantages of simply supported PC box girder with corrugated steel web are expounded, and the factors affecting the natural frequency of simply supported PC box girder with corrugated steel webs are discussed. In the fourth part, the experimental data of the factors affecting the natural frequency of simply supported PC box girder with corrugated steel web are analyzed. Finally, the process and results of the study on natural frequency of simply supported PC box girder with corrugated steel web are summarized in the fifth part.

2. State of the art

The prestressed concrete box girder has been widely used in the construction of bridges and other structures before the concrete composite box girders with corru-

gated steel webs are widely used. However, due to the shortcomings of the longer the weight of the beams, it makes a lot of scholars to improve the research of concrete box girder. A French engineer in the initial study of concrete box girder proposed the use of flat steel plate instead of the idea of concrete webs. As a result of the high stress of the steel plate, the prestress in the concrete slab will be consumed, and the web will need to be thickened to prevent the web from bending. The final result is not ideal [6]. French company Campenon Bernard proposed a further idea that the using corrugated steel plate replaces flat steel. In this scenario, the corrugated steel plate replaces the original flat steel plate and can be extended along the bridge, resulting in a more reasonable structure of the corrugated PC composite bridge. Its concrete definition is that the corrugated web panel PC composite box beam is a thin steel plate to replace the traditional concrete box beam thicker web, and the steel plate is bent into a certain corrugated shape, forming a new, structural force. A more reasonable box girder structure greatly improves the bridge's ability to leap [7]. Then the Japanese introduced the technology, and carried out a lot of research. With the application of PC box girder with corrugated web, the researchers have found that external factors affect its mechanical characteristics and even affect the safety and service life of corrugated PC composite box girder. Therefore, the mechanics characteristics of PC box girder with corrugated webs are studied and some achievements have been obtained. However, there are still few researches on the dynamics of PC composite box girders with corrugated steel webs, which requires further study. Figure 1 is the corrugated steel web PC composite simple box girder bridge construction site map.

3. Methodology

3.1. Structure and advantages of PC composite simply supported box beam with corrugated steel web

The corrugated web panel PC structure is a simple box beam structure in the concrete between the upper and lower plate by the steel web instead of concrete thick web, and the steel web in the bridge is a vertical fold shape, which is the accordion effect [8]. Although this form is simple, it does not substantially bear the axial forces, which avoids the problem of prestress loss due to web restraints when using flat steel plates, and it does not have to be otherwise thickened to avoid the thickness of the steel web buckling deformation of steel plate. In addition, the interaction between the corrugated steel web and concrete roof and floor is the combination of the two. Its main function is to resist the longitudinal shear force between the corrugated steel web and concrete roof and floor [9]. The connection between corrugated steel web and concrete roof and floor is usually made by shear connectors. The design of connection key is directly related to the bearing capacity of the whole structure and its safety. Prefabrication of corrugated webs is usually done by means of high-strength bolts or by field welding [10]. The connection between the corrugated steel web and the concrete roof and floor is usually of two kinds. One is a non-embedded connection, that is, welding the steel plate at the upper and lower ends

of the corrugated steel plate, and the steel plate is provided with welding shear nails to help the corrugated steel plate and the concrete plate to be joined together. The second connection is an in-line connection, which involves perforating the corrugated steel plate through the rebar and then welding the longitudinal reinforcement at the upper and lower ends of the steel plate and finally into the concrete [11]. In addition, it was also derived from other connection methods. Here is not a repeat. As shown in Figure 2 is a wave plate and concrete plate connected to the common schematic.

Fig. 1. Two snaps of a bridge constructed with simply supported PC beams with corrugated steel webs

The merits of the structure of the box-girder structure with the corrugated web-shaped PC simply embodying the box girder are firstly manifested in the condition that the weight of the box girder is reduced to a great extent and the load proportion of the bridge girder is reduced. The prestress loss is greatly reduced. Secondly, the effect of prestressing force on the concrete box girder and concrete box girder with plane steel web is improved significantly by its organ effect, and the efficiency of prestressed concrete box girder with prestressed concrete box girders is significantly

improved, which greatly increased the span capacity of the bridge. And it makes the corrugated rigid web PC combination simply box beam has more extensive application fields [12].

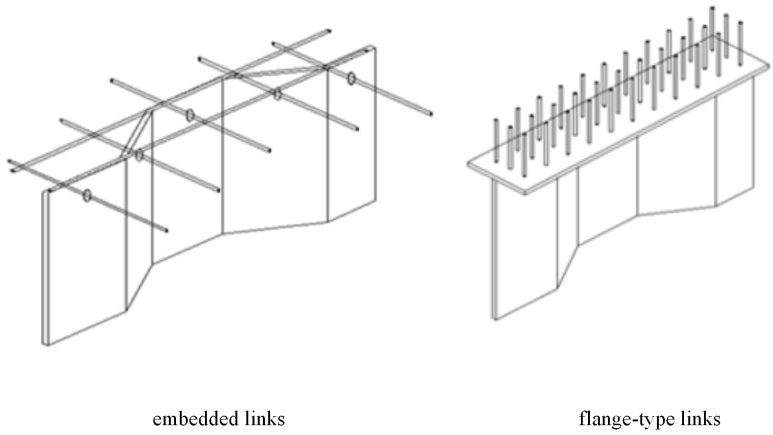

Fig. 2. Schematic diagram of common connections for corrugated steel plates and concrete slabs

3.2. Free vibration equation of PC box girder with corrugated steel webs

The free vibration equation of the PC box girder with corrugated steel webs is based on the structural and mechanical properties of the PC box girder with corrugated steel webs. It is also based on the basic assumptions of the energy law. First of all, because of the special structure of corrugated steel PC box girder, its bending resistance in the longitudinal direction of the bridge is almost negligible, and the cross section of the PC box girder of the corrugated steel web is subject to the "pseudo-section assumption" [13]. Second, Fig. 3 is a corrugated steel box PC box girder diagram. The symbols b, ζb and b_1 in the figure are, respectively, 1/2 of the width of the box girder of the corrugated steel PC box girder, the width of the cantilever plate and the width of the flat section of the vane in the box. Symbols hu, h_{b} are the distances from the center of the upper wing and the lower wing to the mandrel. When calculating the strain energy of the upper and lower wings, only the longitudinal strain of the concrete wing plate εx and the shear strain of the cross-section plane γ_{xy} are taken into account, and the vertical strain, lateral strain and shear strain outside the plate plane are neglected, that is to say, $\varepsilon_y = \varepsilon_z = \gamma_{xz} = \gamma_{yz} = 0$. Finally, the corrugated steel web PC box girder and the concrete vane are connected tightly, without slip condition. When the PC box girder bridge with corrugated steel webs is subjected to free bending vibration, the vertical and horizontal dynamic displacement functions can be introduced to describe the

displacement mode because of the influence of shear lag effect:

$$W = W(x,t)\ , \tag{1}$$

$$U(x,y,z,t) = h_{\mathrm{i}}\left[\varphi(x,t) + \left(1 - y^{-3}\right)\xi(x,t)\right]\ , \tag{2}$$

$$\bar{Y} = \begin{cases} y/b, 0 \le y \le b\,, \\ (b + \zeta b - y)/\zeta b, b \le y \le b + \zeta b\,. \end{cases} \tag{3}$$

In the formula, $\varphi(x,t)$ and $\xi(x,t)$ are the angular displacement and the maximum longitudinal displacement difference function of the box girder section due to bending deformation when the PC box girder bridge with free corrugated steel web is vibrated. Then the natural frequency of the PC box girder with corrugated steel web is obtained by using the eigenvalue equation of the free bending vibration equation of the PC web girder with corrugated steel webs according to the actual boundary condition.

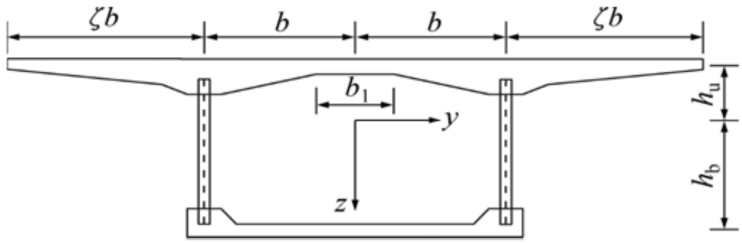

Fig. 3. Sectional view of the PC box girder with corrugated steel webs

3.3. Influencing factors of natural frequency of PC composite simple supported beam with corrugated steel webs

Corrugated steel web PC composite simple box girder is mainly used in the construction of bridges. In the course of the use of the bridge, the dynamic load and wind force of the vehicle, the ground motion of the earthquake, and the individual dynamic loads of the individual population arise because the bridge structure will vibrate because of the influence of external forces.And this vibration can increase the internal forces calculated in accordance with the static force and the possibility of causing local structural fatigue damage. Seriously, it would even destroy the bridge completely [14]. Therefore, the structural vibration of the bridge is an important factor affecting the safety of the bridge. The vibration of bridge structure is a cyclical process in which the deformation energy and kinetic energy of the structural system are transformed with each other due to the input of external force and the friction loss. How much structural system by external force input is the sensitivity of the system and its inherent natural frequency and the frequency of the input effect, that is, the degree of resonance is closely related. So it is necessary to understand and determine the natural frequency and dynamic characteristics of PC simply supported

box girder with corrugated steel webs.

The solution of the bending vibration equation of PC simply supported box girder with corrugated steel web can be obtained by the governing differential equations and natural boundary conditions for bending vibration are obtained from equations (1–3) above. The shear lag effect of simply supported PC box girder with corrugated steel web can be seen. The shear effect and the coupling effect of PC composite simple box girder with corrugated steel webs are the three important factors affecting the natural frequency of simply supported PC box girder with corrugated steel webs. And in the process of solving the low-order bending vibration frequency solution, the influence coefficient of the shear lag is much smaller than 1, and the influence coefficient of the coupling effect is also very small. Therefore, the influence of the two factors on the natural frequency of PC composite simple box girder with corrugated steel web is small, and the effect of shearing effect of corrugated steel web PC composite simple box girder is not negligible, otherwise it will cause wrong result. Besides prestressed concrete box girder structure with corrugated steel web, the external prestressing influences the natural frequency of simply supported PC box girder with corrugated steel webs, and its dynamic characteristics are more significant than that of prestressed concrete box girder [15]. Therefore, the study on the natural frequency of PC simple box girder with corrugated steel web is carried out by external prestressing. The prestressed external prestressed concrete box girder with corrugated steel web is PC - type. Both ends of the prestressing force exert a pair of prestressing force, the eccentricity is e. According to the natural vibration equation of corrugated steel web PC combined simple box girder, the bending differential equation of PC simply supported box girder with corrugated steel web under external prestressing force can be obtained as:

$$EI\frac{\partial^4 y}{\partial x^4} + \frac{\partial^2 (N_1 y)}{\partial x^2} - \frac{\partial^2 M}{\partial x^2} + m\frac{\partial^2 y}{\partial t^2} = 0\,. \tag{4}$$

In the formula, y is the vibration displacement, EI is the bending rigidity of the beam, m is the mass per unit length of the beam, M is the bending moment of the external prestressing force to the beam. Beam bending moment caused by external prestress $M = N_1 e + N - 2x$, among them, N_1 and N_2 are the components in the horizontal and vertical directions of the predecessor N_p. That is, $N_1 = N_\mathrm{p}\cos\theta$ and $N_2 = N_\mathrm{p}\sin\theta$. According to the vibration of the beam in the process, the external prestressing is constantly changing, so we can put

$$N_1 = N_\mathrm{p}^0 + \Delta N_1\,, \tag{5}$$

$$N_2 = N_\mathrm{p}^0 + \Delta N_2\,, \tag{6}$$

$$M = N_1 e + N_2 x = (N_1^0 + \Delta N_1)e + (N_2^0 + \Delta N_2)x\,. \tag{7}$$

Substituting equations (5–7) into equation (4), we obtain

$$EI\frac{\partial^4 y}{\partial x^4} + \frac{\partial^2}{\partial x^2}\left[(N_1^0 + \Delta N_1)y\right] -$$

$$-\frac{\partial^2}{\partial x^2}\left[(N_1^0 + \Delta N_1)e + (N_2^0 + \Delta N_2)x\right] + m\frac{\partial^2 y}{\partial t^2} = 0\,. \tag{8}$$

Due to vibration displacement $y \leq e$, so $\Delta N_1 y \leq \Delta N_1 e$. Thus, $\Delta N_1 y$ can be ignored and also, since N_{p}^0 is the effective prestress of external prestressing tendons, the value is constant. So its second derivative with respect to x is equal to 0, which provides

$$EI\frac{\partial^4 y}{\partial x^4} + N_1^0\frac{\partial^2 y}{\partial x^2} - e\frac{\partial^2 \Delta N_1}{\partial x^2} - \frac{\partial^2 \Delta N_2}{\partial x^2}x + m\frac{\partial^2 y}{\partial t^2} = 0\,. \tag{9}$$

The influence of external prestressing on the natural frequency of PC composite simple box girder with corrugated steel web is mainly manifested in three aspects: prestressed beam tension, anchorage position of steel beam, steel cross-sectional area. After that, the three aspects of corrugated steel web PC combined simple box girder are compared.

4. Result analysis and discussion

In this paper, the experimental data of prestressed beam tension, anchorage position of steel beam and cross section of steel beam are analyzed for three factors affecting the natural frequency of PC combined simple box girder with corrugated steel web. Table 1 presents is the impact of prestressed beam tension on the natural frequency of pc composite simple supported beam with corrugated steel webs. In the experiment, the anchorage position of the prestressed steel beam is $6h/12$ (h being the beam section height), the cross-sectional area of the prestressed steel beam being $A = 1.4 \times 10^{-4}\,\mathrm{m}^2$. It can be seen from the data in the table that the prestress of prestressed PC simply supported box girder with prestressed corrugated steel web is slightly increased.This is in accordance with the results of theoretical calculation and finite element experimental results of the natural frequencies of the simply supported PC box girder with corrugated steel webs under different prestressing tendons. This also shows that prestressed beam tension on the corrugated steel web PC composite simple box girder of the natural frequency of the impact is relatively small.

Table 1. Impact of pre-stressed beam tension on the natural frequency of PCcomposite simple supported beam with corrugated steel webs

Prestressed beam tension (kN)	Theoretical value (Hz)	Finite element value (Hz)	Error (%)
50	31.8471	32.0841	0.73
80	31.8495	32.0843	0.72
110	31.8519	32.0845	0.71
140	31.8542	32.0847	0.71

Table 2 shows the influence of anchorage location of steel beam on natural frequency of PC composite simply supported box girder with corrugated steel webs. In the experiment, the prestressing force of prestressed steel beam of prestressed steel box with corrugated steel PC composite simple box girder is $F = 50\,\mathrm{kN}$, the cross - sectional area being $A = 1.4 \times 10^{-4}\,\mathrm{m}^2$. It can be seen from the experimental data in the table that the natural frequency of prestressed PC steel box girder with corrugated steel web is reduced with the increase of anchorage position. And the theoretical calculated values of the box girder at different prestressed anchor positions are in accordance with the calculated values of the finite element method. That is to say, the anchoring position of the steel beam has little effect on the natural frequency of the PC combined simple box girder with corrugated steel webs.

Table 2. Effect of anchorage location of steel beam on natural frequency of simply supported PC box girder with corrugated steel webs

Anchorage position of steel	Theoretical value (Hz)	Finite element value (Hz)	Error (%)
$3h/12$	31.8481	32.0935	0.72
$4h/12$	31.8445	32.0902	0.71
$5h/12$	31.8503	32.0871	0.73
$6h/12$	31.8570	32.0841	0.73

Table 3 presents the influence of cross sectional area of steel bundle on natural frequency of pc composite simple supported box girder with corrugated steel webs. In the experiment, the tensile force of the prestressed steel beam is $F = 50\,\mathrm{kN}$, the anchoring position is $6h/12$, $A = 1.4 \times 10^{-4}\,\mathrm{m}^2$. It can be seen from the experimental data in the table that the natural frequency of prestressed steel PC composite simple box girder with the corrugated steel web will increase with the increase of the cross-sectional area of prestressing beam. The theoretical value of the natural frequency of the box girder with different cross-sectional area of the prestressed steel beam is in accordance with the calculated value of the finite element experimentally. This also shows that the steel beam cross-sectional area of the corrugated steel web PC composite simple-support box girder self-oscillation frequency has a certain impact.

Table 2. Influence of cross-sectional area of steel beam on natural frequency of simply supported PC box girder with corrugated steel webs

Sectional area of steel	Theoretical value (Hz)	Finite element value (Hz)	Error (%)
A	31.8473	32.0843	0.75
$2A$	31.9435	32.2060	0.83
$3A$	32.0363	32.3049	0.84
$4A$	32.1263	32.3843	0.81

5. Conclusion

Prestressed wave steel plate PC combined with simply supported box girder is better than concrete box girder in structure and material weight. It has been widely used in bridge and other construction. However, due to the structural characteristics of corrugated steel belly PC combined with simply supported box girder and the influence of external conditions, the safety of its use is reduced and its service life is affected. The mechanical properties of simply supported box girder with corrugated steel belly PC are studied. This paper presents a study on the natural frequency of simply supported PC box girder with corrugated steel sheet. In this paper, the development and advantages of corrugated steel sheet abutment PC combined box girder are expounded, and the influence factors of the natural frequency of bellows composite box girder with corrugated steel plate are studied. The experimental results show that the effect of shearing effect on the natural frequency of the PC box girder with corrugated steel plate is more significant. In the external stress, the prestressing force and the anchoring position of the steel beam have little effect on the natural frequency of composite pc box girder with corrugated steel plate. The influence of the steel beam cross section on the natural frequency of the composite box girder with corrugated steel sheet is greater, and the natural frequency of the composite box girder increases with the increase of the sectional area.

References

[1] Y. Noda, K. Ohtoi: *A calculation of sectional deformation for PC box girder bridge with steel web.* Doboku Gakkai Ronbunshu *46*(2000), No. 641, 29–37.

[2] S. Shetty, V. Lehtinen, A. Dasgupta, V. Halkola, T. Reinikainen: *Fatigue of chip scale package interconnects due to cyclic bending.* Journal of Electronic Packaging *123* (2000), No. 3, 302–308.

[3] G. Kiymaz, E. Coşkun, C. Coşgun, E. Seçkin: *Transverse load carrying capacity of sinusoidally corrugated steel web beams with web openings.* Steel & Composite Structures *10* (2010), No. 1, 69–85.

[4] H. K. Kim, M. J. Lee, S. P. Chang: *Non-linear shape-finding analysis of a self-anchored suspension bridge.* Engineering Structures *24* (2002), No. 12, 1547–1559.

[5] E. Spacone, F. C. Filippou, F. F. Taucer: *Fibre beam-column model for non-linear analysis of R/C frames: Part I. Formulation.* Earthquake engineering and structural dynamics *25* (1996), No. TOC 7, 711–726.

[6] M. E. A. H. Eldib: *Shear buckling strength and design of curved corrugated steel webs for bridges.* Journal of Constructional Steel Research *65* (2009), No. 12, 2129–2139.

[7] S. A. Edalati, Y. Yadollahi, I. Pakar, A. Emadi, M. Bayat: *Numerical study on the performance of corrugated steel shear walls.* Wind and Structures *19* (2014), No. 4, 405–420.

[8] J. Brozzetti: *Design development of steel-concrete composite bridges in France.* Journal of Sound and Vibration *55* (2000), Nos. 1–3, 229–243.

[9] B. M. Ayyub, Y. G. Sohn, H. Saadatmanesh: *Prestressed composite girders. II: Analytical study for negative moment.* Journal of Structural Engineering (United States) *118* (1992), No. 10, 2763–2783.

[10] J. F. Bariant, T. Utsunomiya, E.,Watanabe: *Elasto-plastic analysis of PC girder with corrugated steel web by an efficient beam theory.* Doboku Gakkai Ronbunshuu A *62*, (2006), No. 2, 393–404.

[11] J. T. Kim, J. H. Park, D. S. Hong, W. S. Park: *Hybrid health monitoring of prestressed concrete girder bridges by sequential vibration-impedance approaches.* Engineering Structures *32* (2010), No. 1, 115–128.

[12] F. Emami, M. Mofid: *On the hysteretic behavior of trapezoidally corrugated steel shear walls.* Structural Design of Tall & Special Buildings *23* (2014), No. TOC 2, 94–104.

[13] K. Shitou, A. Nakazono, N. Suzuki, H. Asai: *Experimental research on shear behavior of corrugated steel web bridge.* Doboku Gakkai Ronbunshuu A *64* (2008), No. 2, 223–234.

[14] F. K. Schaefer, P. J.,Schaefer, J. Brossmann, R. E. Hilgert, M. Heller, T. Jahnke: *Experimental and clinical evaluation of acromioclavicular joint structures with new scan orientations in MRI.* European Radiology *16* (2006), No. 7, 1488–1493.

[15] M. Kano, E. Watanabe: *A study on distribution of shearing force in prestressed concrete box girders with corrugated steel webs.* Kou Kouzou Rombunshuu *12* (2005), No. 48, 1–9.

Received May 22, 2017

Acta Technica *62* No. 1A/2017, 259–268

Engineering management informationization based on computer information network technology

Shijun Wang[1]

Abstract. In order to make the computer information network technology to better serve the project and effectively develop innovation and project management technology, this paper made a research for project management informationization technology based on computer information network. In this paper, C/S three-layer structure was adopted, and the specific requirements of project management was taken as the breakthrough point, the overall framework of the system and the function modules of each part were designed. The results show that the system is applied to the practice of project management, which can effectively save the production cost and achieve the comprehensive management of the time limit, safety and other indicators. Therefore, it is believed that the research in this paper can be used as a reference for the engineering management of computer information network technology.

Key words. Computer, information technology, project management.

1. Introduction

Engineering management information of computer information network technology refers to the computer network, the realization of engineering management information, under the operation of the related system, the project in all aspects of information input, memory, editing and output can be achieved, so as to realize the guiding role of network technology of computer information network in engineering management.

Yin Juan said: "In the computer information network technology project management information, the way of information transmission is the flow of information, the media is a computer network, obviously, this is a very low cost management mode, the communication is not affected by the limit of time and space, it is convenient, safe and secure at the same time [1]."

Ye Guowen put forward: "The engineering management information system

[1]School of Architecture and Engineering, Kunming University of Science and Technology, 650093, China

based on the computer information network technology can keep the sensitivity to the environment at any time, and can make the response actively when the environment changes." Engineering management information can make the project management system with the external environment to build an effective information communication bridge. Flexible means of communication can ensure that the project management project to a variety of categories of resources can be fully used [2]. Haifeng realized that information engineering and management of computer information network technology can achieve the maximization of resource utilization, which can realize the complementary advantages of resources [3]. Because in the project management information system of computer network technology, the project management organization is not limited by space boundaries, they can break the boundaries of the existing departments, integration of resources in the internal and external organizations, so as to make project management more adapt to the needs of the development of the market economy.

In Sheng Xiaoqing's view, "the traditional project management has the limitation in the aspect of data statistics, and the performance is obvious lag. The engineering management information system of computer information network technology can make up for this defect; it can quickly integrate data information through the computer network [4]. This will ultimately achieve the optimization of all aspects of project management, such as cost minimization, quality optimization." In the face of the wave of information, the project management needs to develop its own information management system, to ensure the optimization of the project management effect. Based on the relevant theory, the paper designed the engineering management information system based on the computer information network technology. Using the system dynamic control module, the related project management content was optimized. Based on information technology and related means, and the various elements of the project management to consider, put forward the improvement of the system and the project management module. In the second section, the paper briefly analyzed the development status of engineering management information based on computer information network technology; in the third section, the design and analysis of the project management information system based on computer information network technology was designed and analyzed; in the fourth section, the practical effect of the system was analyzed. Finally, the research process and the results were summarized in the fifth section.

2. State of the art

In project management, the information transmission through the computer network system to each have the same right to know the management, the information transmission has good quality, and it gets to the managers at the same time, so decision-making can be effectively carried out smoothly when we discuss in common [5]. Ni Weihua also said that, in particular, the computer information network technology project management information system through the sub project tracking, coding and other engineering projects for classification and guidance. This achieves the overall control of the project schedule, manpower and procurement and other

aspects [6].

In reality, the development of engineering management information of computer information network technology is not optimistic, in order to achieve the comprehensive development project management information system of computer network based on the technology, there are many issues need to be overcome.

Firstly, the project is widely distributed, not every project has good communication conditions, for example, the remote location that wants to connect with the project management information system of computer network based on technology can only rely on dial-up, and cannot achieve a comprehensive project management information. Secondly, Qi Anbang put forward, at present, our country is in the big environment of engineering management information technology based on computer information network, lacking of a good and orderly development [7]. This means that in all walks of life, a unified standard of information has not formed yet; the result is that each industry need to according to their own actual situation to develop its own software engineering management information system, and increase development costs. Moreover, each industry's information software cannot carry out the information exchange between each other, for the project management information system, it is unfavorable to realize the comprehensive information management.

Thirdly, Liu Erlie pointed out that the project management information system based on computer information network technology, it is difficult to carry out quantitative investment return analysis [8]. The state provides legal protection to the interests of electronic documents, but companies tend to exclude the electronic documents in the core interests involved, so a lot of development benefit managers are not optimistic about the information system engineering management, so as to slow down the pace of the popularity of project management information system [9].

3. Methodology

3.1. Database technology

Database technology plays an important role in the process of engineering management information. This technique is based on the database as the research object, storage, editing, deletion and management of the data. Database system is developed based on database technology [10, 11]. The database system based on computer network technology can realize the integration and utilization of a large number of data conveniently and quickly. At the same time, for users, they can access the database system to obtain an effective data resources. Developed in the database system based on database management system, the system aims at the building, updating and querying data, it is between the user and the operating system, and its nature is software for the management of data [12].

In order to achieve the purpose of optimization algorithms library, database management system designed in this paper is mainly aimed at the project integration management, according to strict standards, advanced information technology, providing relevant resources of information engineering management allows users to find easily, enables the system to be standardized [13]. The system can achieve the

optimal allocation of resources; through the optimization algorithm library it can accurately calculate the project cost, schedule, and so on.

In addition, the system supports the network collaborative work, therefore, in the system the user can operate this system at the same time, it is helpful for improving work efficiency, and ensure the consistency of the data information. Based on this database management system, it can be used for engineering management in the design of the construction project. Figure 1 is the construction plan of the construction process [14].

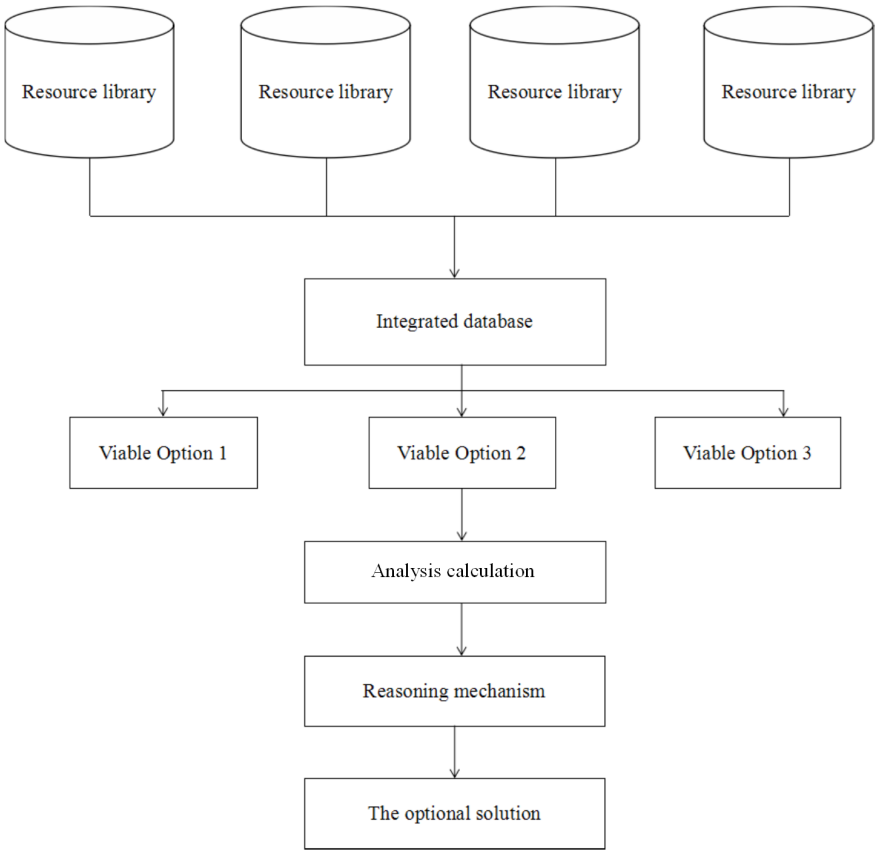

Fig. 1. Generating process of engineering construction plan

3.2. Engineering management information system architecture

Project management information related to the various business organizations, in different times, all kinds of engineering management information system construction is different, lack of interactivity between them, and even the technical standards are not consistent, the types of production is also a wide variety, so realizing the integration of engineering management information system is bound to face a lot

of challenges, the cost of the development will be too high [15]. Considering all aspects, it is not necessary to build a special integration scheme. We can build an integrated public platform, which can maximize the use of existing different types of engineering management information systems, saving capital while achieving the efficient operation of the system. We are using the SARI four tiers structure, including services and applications, resources and infrastructure in four areas.

Service layer is an important part of the whole system. It provides information for the application system interface, at the same time, the user can timely and effective communicate between the organization and partners. The function of the service layer is to rely on the high level of public service platform. In this platform, it can be used for remote applications, such as knowledge management, office automation, and so on. The service enterprise bus is also an important part of the service layer. It is mainly responsible for the interface integration of the application layer system, as shown in Fig. 2.

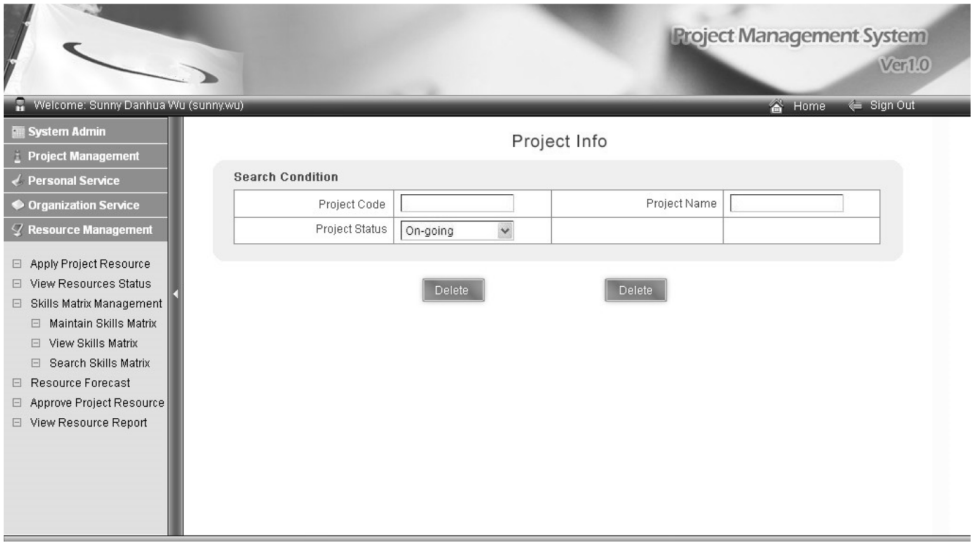

Fig. 2. Management interface of application system

Application layer plays an important role in the flexible operation of the whole system. The structure of the system is relatively loose, but it can be used in the system, so it can be regarded as a collection of application system. Application layer ensures that the system can be operated in accordance with the specific business of the specific disposal, the expansion of the system of flexible space.

The main business of the resource layer is the macro control of the data in the project management, the database operation interface as shown in Fig. 3. In particular, it is in charge of maintaining the good operation of the database, it carries on the dynamic maintenance to the data warehouse, guarantees the database storage, the memory, the extraction function validity. Among them, there is a very close relationship between the operation of the database and the management of the data warehouse. Resource layer must focus on the two things; they will achieve the

logical interoperability and resource sharing.

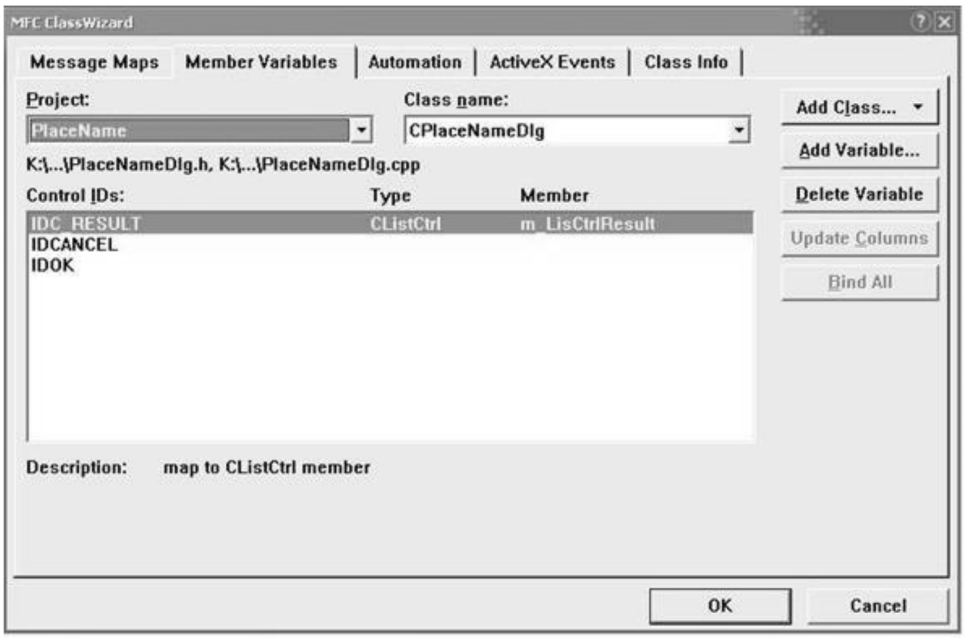

Fig. 3. Database operation interface

The infrastructure layer is the structure layer which provides the foundation support for the other structures in the engineering management information system. Infrastructure layer has two aspects, one is the network; one is the public equipment. The network also involves the wireless network and wired network, some special network is also included, as it is also related to the network and is closely related to the various types of equipment, whether the hardware or software equipment are contained in it. With the development of IP technology, the sharing platform of infrastructure can make communication equipment, automatic recognition and other devices can no longer rely on a specific network to carry out data transmission between each other. Therefore, these devices do not have to be a specialized system of monopoly, but in a wide variety of information systems for information transmission and business support.

4. Result analysis and discussion

4.1. General structure analysis

The advantages of the four layers structure of SARI is very obvious, it can realize the information resource sharing, let the global project management as the starting point, the spirit of integration and sharing ideas of all kinds of business within the system provide support and diversified services. Generally speaking, the advantages

of the SARI four layers structure are shown in three aspects, such as service unification, data sharing and application integration, as shown in Table 1. The integration of these benefits depends on the level of infrastructure, in the past it is just a simple interconnection, and now through the unified planning of the infrastructure to achieve network integration based on IP protocol, simplifies the network, so as to improve the efficiency of communication.

The advantages of SARI 4-layer structure are:

- Service unification
- Data sharing
- Application integration

Firstly, The unity of service, the unified service can simplify the communication channel, which is helpful to maintain the communication efficiency of the organization, in all kinds of applications, we must through the browser interface, which is the unity of all kinds of application system interface after the operation of the effect, thus, cross organizational interaction can be in an orderly and efficient state.

Secondly, data sharing, SARI four layers structure is the establishment of a unified mechanism of data storage and data backup mechanism and data disaster recovery mechanism, on the one hand, it is the logic of the database resources, on the other hand, the network resources and the network associated with the basic design of hardware, such as the physical focus. So the data can be shared.

Thirdly, application integration, on the one hand it is based on data integration. On one hand, it is based on message integration. The consequence of the application integration is that the system can maintain its independence while ensuring the effective interaction between the systems.

Generally speaking, SARI four layers structure can effectively provide services for engineering management information. In the actual operation process, it is needed to improve the dispersion mode into the mode of coexistence of dispersion and concentration. There is a need to improve the business process, in order to provide a unified service, independent business processes must be established, its premise is that it will be related to the application of information technology to organize the integration of the organization. Similarly, project managers also need to form a unified standard for systems integration, in order to regulate the technical standards among the various organizations, such as its own standards, it is needed to establish a network protocol, the storage standard selection criteria, software and hardware equipment specification interface standard and so on. In general standards, the selection of the norms of national standards, organizational standards, and so on, for the establishment of a single standard system, the above two aspects are indispensable.

In addition, the implementation of SARI four layers structure of the information system project management also cannot do without a unified technical support system, unified technical support system can be said to be a prerequisite for the realization of the four layers structure of SARI information system project management, such as the construction and maintenance of infrastructure. Unified technical support system is responsible for regular training of users; it is also responsible for the maintenance of infrastructure related to all kinds of hardware facilities, software

facilities and network and guarantee the stability of the network system. Unified technical support system also includes the construction team, training of information technology related personnel, strengthen the management of human resources within the team, so that every member of the team can play their own a bit, can share resources, has technology innovation; At the same time, we also need to train a team of lecturers to provide the support of human resources for regular customer training.

4.2. Application effect analysis

System is based on information technology as a means; each database is established in the project management, for example: the construction process, the construction of the library, and so on. In the concrete construction process, production personnel can use different databases for different permutations and combinations, by comparing the pros and cons of each of the different programs to achieve the best use of resources to maximize the use of the program, in order to achieve the comprehensive management of the system in terms of cost, schedule, construction period, quality and safety, and other aspects. The system provides managers with a network diagram that can automatically generate construction time scales, the network diagram is not fixed, rigid, it can according to the needs of users for different time periods of access to provide needs for users, a variety of construction network plans for the development of the project at different stages, and these pictures will not be restricted by the format, it is convenient to change the construction plan, compared with the traditional method, it can save a large part of the drawings, and achieve a fundamental resource saving. The system can provide great convenience for flexible adjustment of construction plan, it can carry on macro statistics to the resources on the whole, carry on the overall plan to the field material, and use the database to carry on the computation and the analysis to the field material storage area, so it can assist the construction of the general planning of the timely adjustment.

The ultimate goal of the system platform is to provide computer technical support for the project management decision makers, the system platform has achieved the national engineering construction standard strictly, it can take control of the process, strictly abide by the safety and quality management system, it has achieved the progress of effective tracking, and the project management information in the progress of the project, cost, quality, safety, and the full range of construction requirements. System in the process of information management platform and engineering management information management platform, it has met the national standards and regional standards, has provided data support to the engineering management information system. The majority of the project managers, owners, and design units of all users are able to achieve smoothly communication on the platform of the system; it can ensure the equivalence of information. Among various departments, they not only maintain their independence and flexibility, but also through the system platform to carry out effective circulation of information, it saves time greatly, it can be said that the system is worth promoting.

The development of engineering management system based on integration and

decentralization has played a good role in the practical application of a certain project. In fact, it greatly saves the production cost of the project, because in the initial project construction, through the system various construction schemes are compared to select the most realistic quality program. In the process of construction, it is also able to use the system platform to carry out the adjustment of the plan, and ensure the progress of the project. Making use of the database to make the production organizer according to the field condition, the corresponding countermeasures are introduced, this maximized the subjective initiative, and finally realized the plan to shorten the construction period by 25 %, through the organization of production, so that the direct cost reduced by 10 %, the indirect cost reduced by 20 %, see Fig. 4. The project is currently listed as a national demonstration project.

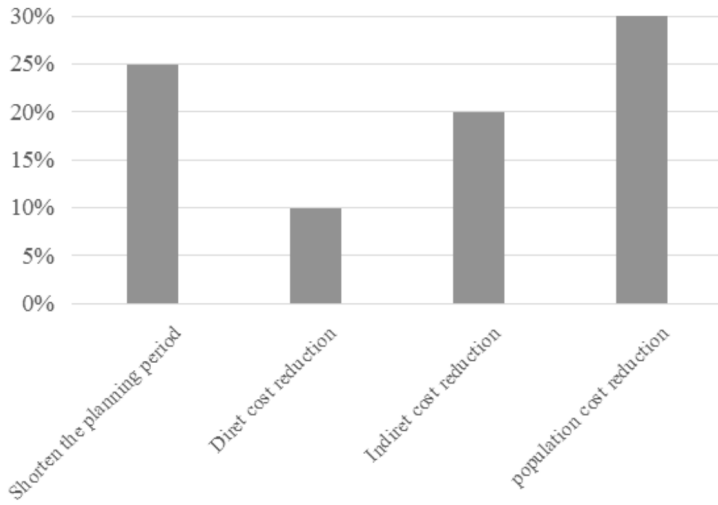

Fig. 4. The effectiveness of the system platform

5. Conclusion

In summary, in this paper, the theory of computer network technology was analyzed, combined with China's current situation of the development of information engineering and management of computer information based on network technology, the feasible plan of project management information system based on the technology of computer information network was put forward. Considering the limitations of the traditional C/S structure, in this paper, the four layers structure of SARI based on computer information network technology engineering management information system was adopted. The system is related to the interface, data and so on, it can provide effective technical support for project management. It is a combination of integration and decentralization, in which the integrated management information system is to save Inter Organizational and Inter Organizational communication costs

to provide an important resource support. Integrated project management information system of computer network technology has a long way to go, so in this paper the present situation of the whole project management cannot be made a qualitative leap, therefore, the future work will focus on deepening the integration of the project management information system based on computer information network technology, so that the computer information technology can provide better service for the project management.

References

[1] M. F. Porter: *An algorithm for suffix stripping.* Program *14* (1980), No. 3, 130–137.

[2] M. L. Markus, D. Robey: *Information technology and organizational change: Causal structure in theory and research.* Management science *34* (1988), No. 5, 583–598.

[3] S. Hochstein, M. Ahissar: *View from the top: Hierarchies and reverse hierarchies in the visual system.* Neuron *36* (2002), No. 5, 791–804.

[4] A. M. Burley, W. Mattli: *Europe before the Court: A political theory of legal integration.* International Organization *47* (1993), No. 1, 41–76.

[5] D. Heesom, L. Mahdjoubi: *Trends of 4D CAD applications for construction planning.* Construction Management and Economics *22* (2004), No. 2, 171–182.

[6] O. Kapliński: *Development and usefulness of planning techniques and decision-making foundations on the example of construction enterprises in Poland.* Technological and economic development of economy *14* (2008), No. 4, 492–502.

[7] H. J. Wang, J. P. Zhang, K. W. Chau,M. Anson: *4D dynamic management for construction planning and resource utilization.* Automation in Construction *13* (2004), No. 5, 575–589.

[8] S. L. Zhang, U. Smith: *Self-aligned silicides for Ohmic contacts in complementary metal-oxide-semiconductor technology: TiSi 2, CoSi 2, and NiSi.* Journal of Vacuum Science Technology *22* (2004), No. 4, 1361–1370.

[9] D. E. Lumley: *Business and technology challenges for 4D seismic reservoir monitoring.* The Leading Edge *23* (2004), No. 11, 1166–1168.

[10] H. Mei, F. Chen, Y. D. Feng, J. Jang: *ABC: An architecture based, component oriented approach to software development.* Journal of Software *14*, (2003), No. 04, 721–732.

[11] S. Liu, Y. X. Liu, F. Zhang, N. Jing: *A dynamic web services selection algorithm with QoS global optimal in web services composition.* Ruan Jian Xue Bao (Journal of Software) *18* (2007), No. 3, 646–656.

[12] Q. Sun, J. Liu, S. Li, J. J. Sun: *Internet of things: Summarize on concepts, architecture and key technology problem.* Beijing University of Posts and Telecommunications *33* (2010), No. 3, 1–9.

[13] K. Yue, X. L. Wang, A. Y. Zhou: *Underlying techniques for web services: A survey.* Journal of software *15* (2004), No. 3, 428–442.

[14] G. Chen, R. Lu, Z. Jin: *Constructing virtual domain ontologies based on domain knowledge reuse.* Journal of Software *14* (2003), No. 3, 350–355.

[15] J. Li, Y. Jing, X. Xiao, X. Wang: *A trust model based on similarity-weighted recommendation for P 2 P environments.* Ruan Jian Xue Bao(Journal of Software) *18* (2007), No. 1, 157–167.

Received May 22, 2017

Acta Technica *62* No. 1A/2017, 269–278

Industrial product graphic design based on visual communication concept

Fei He[1]

Abstract. The development of multimedia information technology and design concept in today's society has made the graphic design to go beyond the scope of the plane to the development of modern science and technology. In view of this, graphic design of industrial products based on visual communication concept was studied. First of all, the application searches graphic design sequence and fuzzy comprehensive evaluation of industrial products. Industrial product graphic design in Guangdong Province was analyzed. The results show that the concept of visual communication is helpful to the expression of industrial product graphic design, and the imagery and association of the audience needs to be taken into account in the design process. This also reveals that Message transmission can be a body of communication, it is possible to communicate between individuals.

Key words. Visual communication, industrial product graphic design.

1. Introduction

With the rapid development of science and technology and people's daily art life, the original printing art design has no longer adapt to the continuous development of the society and the world of human life. Visual communication design emerged. Visual communication design refers to that visual graphic design information is communicated to every person in the society through a variety of media, including aesthetics, design, history, religion, psychology, physics, sociology and literature, which is a new, highly integrated discipline [1]. Visual communication and visual culture have become increasingly important in the role of the image. Image narrative can span the obstacles of language and characters, and it is more likely to attract people's attention. As a result, visual communication design will be a potential and developmental specialty under this trend [2].

Researchers at home and abroad believe that visualization is the trend of the future. Visual communication and visual culture have become increasingly important

[1]School of Art and Design, Jingdezhen Ceramic Institute, Jiangxi, 333403, China

in the role of the image. Image narrative can span the obstacles of language and characters, and it is more likely to attract people's attention. As a result, visual communication design will be a potential and developmental specialty under this trend [3].

In addition, because visual communication design (especially commercial design part) is closely related to marketing, planning and advertising. The concept of visual communication began to be applied to industrial product graphic design. Therefore, the plane-based visual communication design can express and present the design theme with the aid of more and more expression means and concepts of plane and transcendental plane as well as visual and transcendental vision, which is the purpose of this paper [4]. In the information age, in the face of technology change rapidly, knowledge and update, as the visual communication design of the workers and educators, visual communication design is a practical attempt and reflective discussion. Design techniques are updated in a timely manner, the design concept is continuously improved, which is an inevitable choice in the sense of achieving the design realm of extension, transboundary, interaction and experience under the global integration [5].

The remainder of this paper is organized as follows. In the second chapter, the connotation of visual communication design and related concepts of industrial product graphic design based on visual communication are briefly introduced. In Chapter 3, the research methods are introduced. Through the way of looking for industrial products graphic design sequence, fuzzy comprehensive evaluation of industrial product graphic design effect, graphic design of industrial products based on visual communication is analyzed. In Chapter 4, industrial product graphic design based on the concept of visual communication is analyzed by associative analysis. Image based on Visual Communication Industrial graphic design is analyzed. Finally, industrial product graphic design based on the concept of visual communication is evaluated and analyzed. Chapter 5 is the conclusion.

2. State of the art

2.1. Discussion on the connotation of visual communication design

Visual communication design includes: font design, logo design, poster design, advertising design, printing design, corporate identity design, packaging design, brand promotion design, fashion design and so on [6]. In general, the design of visual communication is to transform ideas into images, to make effective use of image to convey the impression of others.

Visual communication design is defined as: a sense of beauty is captured through the words, symbols and modeling. Expressing images, ideas, and attempts are captured to achieve communication and persuasion effect. Communicating design is an intellectual, technical, and creative activity that is not only to create the image, but also must have the analysis, organization and presentation of visual solutions, to solve the problem of communication [7]. Therefore, the definition of visual commu-

nication design can be summarized as follows:

(a) Analysis, organizational visual elements (text, symbols and modeling) create a visual aesthetic solution.

(b) The information is communicated correctly and persuasively in order to achieve the effect of communication and persuasion [8].

Based on the design function of visual communication, abstract shapes, bodies, colors and ideas, or figurative things are imaged by design. Through various visual media such as posters, packaging, newspapers and magazines and books, ideas are clearly communicated to the aspirations of the object in mind [9].

Based on the principle of visual communication design, the general performance is to create more innovative forms or expression techniques to enrich the public's visual enjoyment, and to satisfy people's new psychological, such as unity and change, symmetry and balance, contrast and reconcile, proportion and scale, rhythm and prosodic [10].

Based on the application of visual communication design, visual communication design is the design of the transmission and communication of visual information. Its involved fields include: corporate identification another, commercial marketing, advertising design, environmental landscape and personal image and so on. Good visual communication design not only can promote the goods and promotional activities, but also can enhance the people's aesthetic and lifestyle [11].

2.2. Industrial product graphic design based on visual communication concept

With the change of design environment, industrial product graphic design or visual communication design appellations have a certain meaning, in the future design industry, a broader definition of the industry will appear, visual communication design contains more comprehensive information, covering all walks of life , so that the design can go deep into every field. Designer Haruya said that design is not a skill, but the ability to capture the essence of things and insight. Therefore, the designer's main task is not to design practice, but to maintain the sensitivity of the community. According to the changes of the times, resources in the design field are carried out a reasonable configuration [12].

The new approach of the development of industrial product graphic design is to make rational allocation of different media resources in order to promote the development of graphic design of industrial products [13]. The main development trend of graphic design based on visual communication is the evolution process of information integration and information transmission to the visual translator. Whether it is the traditional graphic design or modern visual communication based on the concept of visual communication design needs to rely on design functions to achieve. No matter how the new media technology develops, it will become the development space of the industrial product graphic design, it is the extension of the visual communication carrier, and it will also provide more possibilities for the graphic design reproduction to further enhance the social value of the graphic design [14]. The following is a visual communication design works related pictures (see Fig. 1).

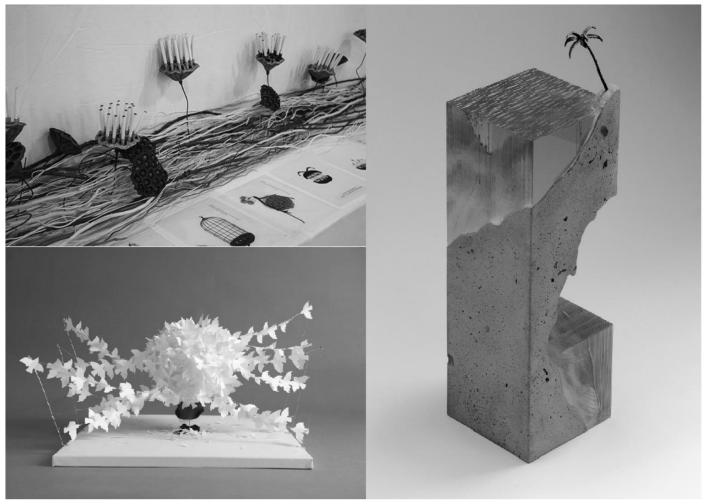

Fig. 1. Visual communication design works

3. Methodology

The design flow of industrial products based on the concept of visual communication is: firstly, the unification and change, symmetry and balance, contrast and harmony, proportion and scale, rhythm and rhythm and other related to visual communication design knowledge is stored in different knowledge base according to their different structure forms. The basic information base of industrial products was improved and the corresponding graphic design style was searched according to the industrial product type. Then the design style was combined with the concept of visual communication, and then the fine adjustment was made according to the characteristics of industrial products. Therefore, industrial product graphic design system structure based on visual communication concept is shown in Fig. 2.

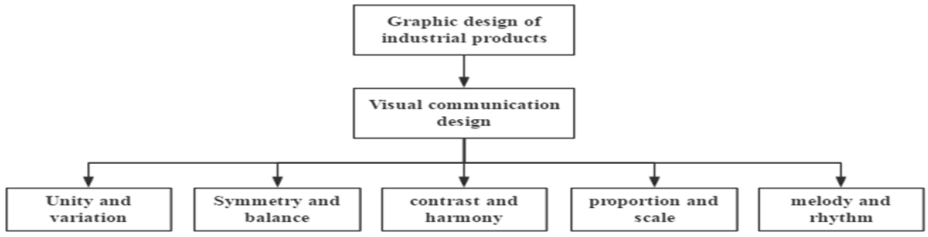

Fig. 2. Framework model of industrial product graphic design based on visual transmission

Graphic design of industrial products based on visual communication starts from the business requirements of industrial products. The elements and contents of the graphic design are determined. Therefore, the design sequence in the graphic

design of industrial products based on visual communication plays a certain role in the effect of the finished product. Graphic design of industrial products based on visual communication is divided into a number of design patterns. First of all, the results of color and association analysis of industrial product graphic design based on visual communication are sorted out. With the results of the analysis, each color and association have their corresponding flat transmission effects. According to the demand of the graphic design goals, image color and other sequences are designed and acquired, the corresponding design is generated, graphic design tasks are carried out.

In addition, this paper applies the method of fuzzy comprehensive evaluation to quantify and comprehensive evaluate the factors (uniform and change, symmetry and balance, contrast and harmony, proportion and scale, rhythm and rhythm) involved in industrial product graphic design based on visual communication concept, which helps the visual communication of industrial product graphic design to obtain accurate evaluation information. Here, a set can be used to represent and then perform a quantitative analysis: (r means the influencing factors of visual communication design, v means evaluation factors of visual communication design)

$$R = \begin{pmatrix} r_{11} & \cdots & r_{1n} \\ \vdots & \ddots & \vdots \\ r_{m1} & \cdots & r_{mn} \end{pmatrix}, \tag{1}$$

$$V = (v_1, v_2, v_3, \ldots). \tag{2}$$

Graphical design of industrial products based on visual communication can be expressed by decomposition of logic function. Each decomposition is uniquely determined by a set of sub-functions. In this way, as long as the sub-function is known, the logical function can be determined. The sub functions and decomposition of logical functions are defined as follows: (x means the explanatory factors of visual communication design)

$$f_{\mathrm{c}} = f(x_1, x_2, \cdots x_{i-1}, c, x_{i+1}, \cdots, x_n). \tag{3}$$

4. Result analysis and discussion

4.1. Association analysis of industrial product graphic design based on visual communication concept

In the expression of visual communication design emotions, in addition to the instinct level and behavior level, there is a very important emotional element, that is, Lenovo, especially color association. Lenovo is the link of thinking people, but also the main way to transfer and think of human emotions. Positive and conscious association can promote people's thinking, to help people sublimate knowledge of things. In general, there are two main ways to use association in visual communication design. One is to allow viewers to imagine the specific physical, and the other

is to allow the viewer to imagine the abstract emotion or idea directly. Therefore, association reasoning and imagination are carried out in the visual communication design, the audience's habit of thinking and understanding of color and other factors should be fully taken into account and meet. In the visual communication industry graphic design, the things and abstract emotions that can be associated with a variety of colors are in Table 1.

Table 1. A variety of colors can be associated with things and abstract emotional classification

Colour	Specific things	Abstract emotions
white	Facial tissues, bride, doctor	Nature, purity, peace
red	Apple, blood, sun, pepper	Warm, unrestrained, dazzling
Orange	Wu Zi, the flame, the sun	Dazzling, warm, vibrant
yellow	Oranges, tigers, bees	Sweet, warm, fresh
green	Grass, trees, forest	Nature, freshness, health, peace
blue	Sea, sky	Melancholy, steady, rational
black	Hair, black, eyes	Mystery, darkness, despair, death
purple	Grapes, Li Zi, purple roses	Mysterious, noble, dream

From the table above, in the design of industrial products based on the concept of visual communication, the characteristics and functions of industrial products need to be fit, the appropriate lines and patterns are selected, which constitute a harmonious plane to stimulate the audience positive emotions and other positive associations, in addition, the color of the mix also has important significance.

4.2. Imagery analysis based on visual communication industrial graphic design

Visual communication of industrial graphic design is required to achieve the communication effect that when the audience looks at the design work, the judgment, preferences and attitudes should be consistent with the original intention of the designers. One of the ultimate goals of visual communication is to make design works resonate in the hearts of people. The communication between the designer and the audience is realized, which gives the audience a sense of heart and emotional dependence. The three-dimensional color image is composed of hue, lightness and chroma three properties, and can be expressed by color solid. Therefore, in the visual communication of industrial graphic design, in the expression of color images and their feelings, cold and warm, strong and weak, likes and dislikes are the three elements of feelings, which constitute a three-dimensional color scheme for visual communication design. The results of the image survey are shown in Table 2.

Table 2. Three kinds of color image can be used in visual communication design

Image type	Specific images
Evaluation image	beautiful - ugly, elegant - vulgar, favorite - disgusted, natural - tweaking, close - alienated, balanced - messy, clean – dirty, valuable–worthless
Active image	warm - cool, eye-catching - muddy alone, gorgeous - simple, lively - quiet, male - female, stable - restless, trendy - classical, active dial - steady, casual - formal, sweet - bitter, fresh - stale
Power image	hearty - tough, tough - soft, young - aged, brisk - thick, bright - dark, powerful - weak, nervous - relaxation, sharp - slow, romantic - rational, natural - artificial

4.3. Fuzzy evaluation of industrial product graphic design based on visual communication concept

In this experiment, the industrial product designs of a number of enterprises in Guangdong Province are used as a research sample. Graphic design effects are divided into five levels. At this time, the fuzzy relation between the evaluation factor set and the evaluation set can be expressed by the evaluation matrix, the evaluation factor set = (unity and change, symmetry and balance, contrast and harmony, proportion and scale, rhythm and rhythm), the evaluation level set = (the ultimate expression of the theme of the industrial industry, the better expression of the theme of industrial products, part of the expression of the theme of industrial products, very little expression of the theme of industrial products, deviation from industrial products). The fuzzy evaluation form of industrial product graphic design based on visual communication concept is the contents of Table 3 and the statistical analysis of the expression of industrial products based on the concept of visual communication is shown in Fig. 3.

From the chart in Fig. 3, in the result of fuzzy evaluation of graphic design of industrial products based on the concept of visual communication, the proportion of ultimate expression of the industrial industry theme reached 50 %. Especially in the evaluation of unity and change, symmetry and equilibrium, in the comparison and harmonization, proportion and scale evaluation, the ultimate expression of the theme of the industrial industry reached more than 30 %. In general, in the graphic design of industrial products based on visual communication concept, 70 % industrial enterprises in the ultimate express the industrial industry theme in the unity and change, theme of change, symmetry and balance. 80% above can express the design of industrial product theme. Only 10 % of industrial products deviate from the industrial product design in proportion and scale, rhythm and rhythm. It can be seen that the design method based on visual communication can improve the unity and change, symmetry and balance, contrast and harmonization, proportion and scale, rhythm and rhythm of industrial product graphic design. In addition, the actual characteristics of industrial products need to be fit. Imagery and association are incorporated into the visual communication design, so as to design and improve the turnover of industrial products plan.

Table 3. Fuzzy evaluation of industrial product plane design based on visual communication concept

Evaluation factors Unification and change		Evaluation level				
		Ultimate expression of the theme of the industrial industry	Better expression of the theme of industrial products	Part of the expression of the theme of industrial products	Very little expression of the theme of industrial products	Deviation from industrial products
Symmetry and equilibrium	0.11	0.5	0.2	0.2	0.1	0
Contrast and harmony	0.13	0.5	0.2	0.1	0.2	0
Scale and scale	0.16	0.3	0.2	0.4	0.2	0
Rhymes and rhythms	0.18	0.4	0.3	0.2	0.1	0
Evaluation factors	0.20	0.4	0.3	0.1	0.2	0.1

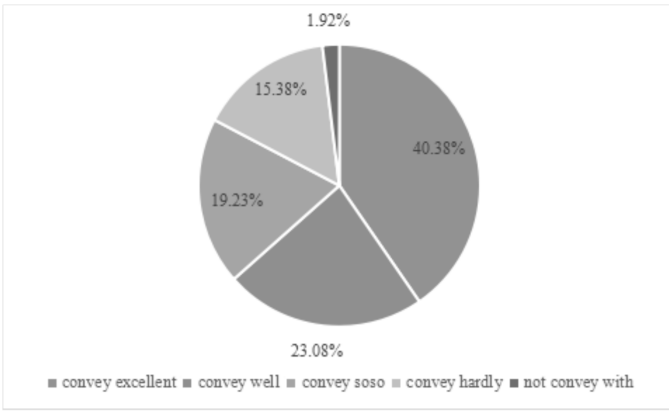

Fig. 3. Statistical analysis of the expression of industrial products based on the concept of visual communication

5. Conclusion

The characteristics of the era of productivity determines the characteristics of the design, modern multimedia technology is a kind of ubiquitous power. The emergence of digital multimedia challenges and enriches the traditional visual communication. Modern graphic design is extended. Visual communication transforms from plane and static of the shape to dynamic and comprehensive, from a single media to the

media, from the two-dimensional plane to three-dimensional and space, from the traditional printing design products to the communication of virtual information image. Based on the concept of visual communication design, design method based on visual communication concept is gradually widely used.

The research and analysis of industrial product plane design based on visual communication concept was completed in three steps. Firstly, the image and association in industrial product graphic design based on visual communication were analyzed. The design was carried out according to different industrial product characteristics and audience psychology. Finally, the industrial enterprises in Guangdong Province were used as samples. The graphic design of industrial products based on visual communication was evaluated in a fuzzy way. The results show that the design based on the concept of visual communication can improve unity and change, symmetry and balance, contrast and harmony, proportion and scale, rhythm and rhythm of elements in industrial plane. In addition, imagery and audience association needs to be considered in visual communication.

References

[1] M. van der Schaar, N. S. Shankar: *Cross-layer wireless multimedia transmission: challenges, principles, and new paradigms.* IEEE Wireless Communications *12* (2005), No. 4, 50–58.

[2] R. Wood, J. Ashfield: *The use of the interactive whiteboard for creative teaching and learning in literacy and mathematics: A case study.* British Journal of Educational Technology *39* (2008), No. 1, 84–96.

[3] E. Kasten, S. Wüst, W. Behrens-Baumann, B. A. Sabel: *Computer-based training for the treatment of partial blindness.* Nature medicine *4* (1998), No. 9, 1083–1087.

[4] D. Forlenza: *Computer-based training.* Professional Safety *40* (1995), No. 5, 28–29.

[5] C. Södergård, M. Aaltonen, S. Hagman, M. Hiirsalmi, T. Järvinen, E. Kaasinen, T. Kinnunen, J. Kolari, J. Kunnas, A. Tammela: *Integrated multimedia publishing: Combining TV and newspaper content on personal channels.* Computer Networks *31* (1999), Nos. 11–16, 1111–1128.

[6] P. R. Panda, N. D. Dutt, A. Nicolau, F. Catthoor, A. Vandecappelle, E. Brockmeyer, C. Kulkarni, E. de Greef: *Data memory organization and optimizations in application-specific systems.* IEEE Design & Test of Computers *18* (2001), No. 3, 56–68.

[7] F. Catthoor, K. Danckaert, S. Wuytack, N. D. Dutt: *Code transformations for data transfer and storage exploration preprocessing in multimedia processors.* IEEE Design & Test of Computers *18* (2001), No. 3, 70–82.

[8] M. F. Jacome, G. de Veciana: *Design challenges for new application specific processors.* IEEE Design & Test of Computers *17* (2000), No. 2, 40–50.

[9] I. Lee, S. Kim, H. Lee, B. Kwon, S. Lee, K. Cho: *Optimal beam steering for maximal visual quality over a multimedia broadcasting system.* IEEE Transactions on Broadcasting *62* (2016), No. 1, 35–45.

[10] F. G. H. Yap, H. H. Yen: *A survey on sensor coverage and visual data capturing/processing/communication in wireless visual sensor networks.* Sensors (Basel) *14*, (2014), No. 2, 3506–3527.

[11] A. Hadjidj, M. Souil, A. Bouabdallah, Y. Challal, H. Owen: *Wireless sensor networks for rehabilitation applications: Challenges and opportunities.* Journal of Network and Computer Applications *36* (2013), No. 1, 1–15.

[12] F. C. R. Estrada, L. S. Davis: *Improving visual communication of science through the incorporation of graphic design theories and practices into science communication.* Science Communication *37* (2015), No. 1, 140–148.

[13] M. P. Cook: *Visual representations in science education: The influence of prior knowledge and cognitive load theory on instructional design principles.* Science Education *90* (2006), No. TOC. 6, 1073–1091.

[14] Y. A. U. Rehman, M. Tariq, T. Sato: *A novel energy efficient object detection and image transmission approach for wireless multimedia sensor networks.* IEEE Sensors Journal *16* (2016), No. 15, 5942–5949.

Received May 22, 2017

Acta Technica *62* No. 1A/2017, 279–288

The redesign of brand visual identity in the information age[1]

Wenyan Zhao[1]

Abstract. To deal with the change of modern brand visual identity coming up with the information age, this paper studied the basic theory of brand visual identity design in the internet era. And combined with the specific brand of the case, the visual image recognition was researched, analyzed and summarized. After that, the traditional brand redesign was discussed. This paper focused on the new strategy of visual identity. From the point of view of design management, the change of brand design in the information age was summarized. And the improvement of the brand image design space, which consists the creative points of the paper, was explored. As the result, it is found that the Internet platform provides a wide opportunity for the brand in product design, marketing and communication design. And the use of systematic way of thinking can enhance the image of the traditional brand in all aspects.

Key words. Information age, brand image, visual identity, design strategy, redesign.

1. Introduction

The technology of the Internet has brought a new vision for the life of all mankind. The great changes have been made in various fields, such as science, economy and so on. In the traditional sense, as a relative concept to the rapidity and innovation of the Internet, "Brand" needs to maintain its long-term, classic, so as to create the corresponding value. In the Internet era, the visual identity of the modern brand also has a new development space, which needs to make a brand new culture. Some of the new Internet brands, such as Amazon, Facebook, Tencent, Baidu and so on, are springing up, bringing a new visual identity. And some of the traditional brands, such as Chanel, SIEMENS, BMW, Audi, Coca-Cola and so on, have also used the Internet technology. By using its transcendence, revolutionary technology value and concept value, the brand image is successfully re designed. At present, many scholars at home and abroad have paid great attention to the research of Internet information technology. In the study, they have summarized Internet's help to brand image design, and discussed the redesign of the visual identity of the brand in the

[1]School of Art and Design, Jingdezhen Ceramic Institute, Jingdezhen, 333001, China

information age.

In Crilly's article, a complete framework for the formation of product vision is discussed. The corresponding understanding of aesthetics, semantics and notation in design is emphasized. The effects of incidental emotional and behavioral reactions are discussed, and the effects of these reactions in the design process are analyzed. The advent of the Internet era has brought about a change in the way people interact, which has been discussed in this paper [1]. Van and others have explained the corporate image design, defined the corporate image, and explained the basic principles of corporate identity management. With the development trend of the Internet age, the redesign of corporate brand image is analyzed and discussed [2]. Orth and others have realized the expected response of consumers by selecting and modifying the visual image of the brand. In this paper, seven key types of packaging design are listed, and the influence factors of the packaging design are discussed. The author believes that mature brand image design should be refined and natural [3]. Keller and others have proposed that, in the past decades, the brand had been increasingly recognized as one of the most valuable intangible assets. Therefore, it is necessary to make a corresponding exploration of its image management. From the academic point of view, the problems of brand positioning, integration and asset measurement are studied in the paper. Through the study of the brand image design in the Internet age, the role of brand in the enterprise competition is explored [4]. In Park and others article, the brand image design of online products is studied. Electronic brand personality is an important factor in the business enterprise to obtain a unique identity. In this paper, the four main dimensions of the visual properties of the online leather brand are studied by constructing a feasible objective, and the influence, restriction and future prospect of brand visual identity redesign are given in the information age [5].

In this paper, based on the great background of the information age, combined with the previous research results, the basic theory of brand design in information age is studied. And combined with the specific brand of the case, the visual image recognition is researched, analyzed and summarized. In the second part of this paper, the impact of the Internet information age on the redesign of visual brand image is generally introduced, which lays the foundation for the analysis of the text. In the third part, the strategy of the visual image redesign of the brand in the information age is analyzed and explored. In the fourth part, combined with the successful case of corporate brand redesign, taking Yantai apple as the analysis object, the feasibility of the brand design and related issues are analyzed. In the fifth part, the summary of the whole paper is made. Through the combination of theory and case method, this paper hopes to provide valuable suggestions for the redesign of the brand visual identity image in the development trend of the new era.

2. State of the art

In this part, a concrete analysis of the influence of the technology change and the behavior pattern of the Internet information age to the brand's visual identity design will be made. The so-called brand is the specified name, mark, term or the

combination of the design elements, to identify the product of one or more categories [6]. In the representation of these symbols, this one or a class of products will be different from other products and services. Figure 1 contains a number of famous brand image designs.

Fig. 1. Examples of famous brands

A complete brand needs to have a wealth of meaning to support its value, so that it will have a long lasting appeal. The famous scholar Philip Kloet has proposed that a complete brand image design should include six meanings [7], as shown in Fig. 2.

These six meanings are: it can give people the impression, bring the benefit, express the practical value and the value of the function, carry on the enterprise culture, give people the psychological set, and reflect the target consumer groups. These aspects must be considered in the traditional brand design. Among them, the impression given by the physical properties is the most closely related elements to the audience layer. It is directly expressed as the product design form, which is the ultimate outcome that the designer should show to both the buyers and merchants. At the same time, the other five elements should be internalized and contributed to the visual design. They shoulder the spiritual parts of the whole brand visual forms. Obviously, there has been a long history for the participants of the field to attach the six meaning to high attention. But the coming of the informative age has opened a new way for brand design. This part will introduce the brand design

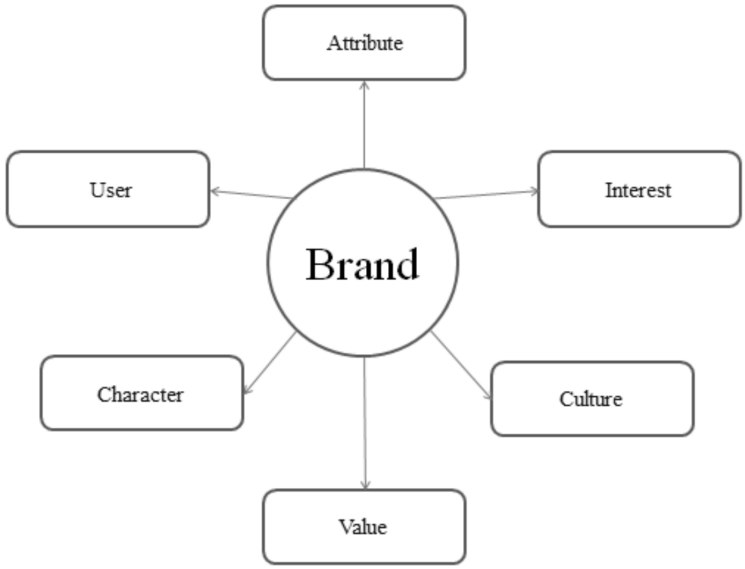

Fig. 2. Six meanings of brand

method after the "Net".

2.1. Ideas and methods of product development

In the traditional sense, product development mainly refers to the original made by technical personnel or the introduction, improvement, or the combination of the two. And then after market research, products will be put into the production stage, and finally put into the market. According to the user's feedback on the product, after collecting the relevant information, the developer will cycle the improvement. This process is relatively long and easy to lose customers, resulting in huge economic losses. The way of information technology can shorten the production cycle, so that the enterprise brand has timeliness, information feedback is in time, and the product individuation is obvious [8].

2.2. Ideas and methods of brand communication

The traditional brand media is mainly advertising, print etc. However, these industries have received a huge impact in the Internet age. In order to provide better service and more reasonable products, and meet the needs of users more accurately, through the network technology, the Internet brand and the traditional brand can use the network resources to make the corresponding improvement to the brand image design as well as the communication way [9].

2.3. Ideas and methods of brand marketing

The main way of traditional brand marketing is store sales, which has a long history, and has the characteristic of stability. However, online business marketing is now in vogue. In addition to physical stores, the electricity suppliers also occupy the majority of marketing. In brand design, this marketing approach should be taken into account. Combined with the store sales, and combined with the characteristics of online and offline, the marketing ideas with the times and the vanguard can be developed [10].

2.4. Ideas and methods of brand service

Traditional brand store sales methods make the service model more stereotypes, mainly including one to one service and self-service. Internet brand users are more emphasis on user experience, taking the user as the center, which has characteristics of interactive, low cost, and high efficiency. Therefore, in the traditional brand image design, the service's innovation and improvement can be considered [11].

2.5. Changes in design and style

Under the impact of the information age, the brand image design has a new style and form of expression. First of all, a significant change is the change of the brand image from the plane to the three-dimensional [12]. As early as 2011, Valentino began to run the digital museum. Users could experience the design world of Valentino by the information technology. With a little click, the history of a design work and other relevant information could be understood. In addition, the design style from the realism to the flat change was also a major bright spot [13]. Because people's Internet mobile devices have different requirements with the traditional media, the flat design can be more easily spread by the information platform, which is also consistent with the trend of the development of art.

3. Methodology

Based on the theory of brand design, a strategic study on the redesign of the traditional brand image in information age is carried out. The traditional brand has a long history and culture, and in people's minds, the brand image has a profound memory. In the development of the moment, the traditional brand also has a complex structure. Enterprise strength is strong, the product category is also various, and the industry is usually larger [14]. However, the Internet technology has brought a different opportunity and crisis to the traditional brand. Therefore, the traditional brand needs to face the trend of this technology, and plan their brand culture and image redesigns by drawing on the experience of the Internet brand image design.

3.1. The common thinking path of the traditional brand image redesign in the information age

A technology can bring about a universal direction and strategy for a time. In the trend of information technology, the development of the Internet makes the traditional brands with a common characteristic in the aspect of image redesign, summarized in Table 1.

Table 1. Four common features

Uniqueness	The so-called unique is that the brand culture, brand related products, as well as the brand's promotional culture are unique. In these three, the most important is the brand culture, which is the core of product originality. In the era of information, the brand needs to register trademarks, select the independent domain name with the brand characteristics, and protect their own website and other ways to ensure their uniqueness.
Interactive quality	Interactivity is the interaction between the enterprise and the related users. This interaction is not simply the interaction between the purchase and sale of the process, which needs to remove all communication barriers between consumers. In this process, independence and creativity are the most important.
Timeliness	Timeliness not only refers to the timeliness of product information updates, but also includes the use of product information in the timeliness of feedback. Product information mainly needs to include the technical information of the product as well as the updating information of the product. Social information and product information are closely related, which has important significance to the adaptability of the product. These two must be in a timely manner through a variety of media and consumer interaction, to enhance the user's sense of participation.
Diversity	In this category, the diversity is mainly the diversity of brand expression. Usually, the brand's cultural expression will make people think of the brand's Logo, store display and website design, etc. However, the brand's publicity should also have diversity, which can use VR technology, or simple animation technology to achieve a sense of immersive user experience.

3.2. The product design strategy of the traditional brand image redesign in the information age

Product is the core competitiveness of enterprises, and also the basis for the survival of corporate brands, and brand is able to enhance the user's awareness and understanding of the product. Traditional brands usually have a guarantee of product quality. After a long history of the test, it has a wide range of influence, forming its own family characteristics [15]. Therefore, the traditional brand image design should learn from each other, and hold their own inherent advantages of consumer groups and family characteristics, constantly adding new design elements.

First of all, the traditional brand image redesign should ensure the quality of the product. Secondly, in the innovative design, the traditional brand should consider the needs of the current customer, and conduct in-depth investigation in terms of technology, color, appearance, emotion, material, function, experience and environ-

mental protection, and so on to reflect the personality of the brand. In addition, the information technology should be used to collect user feedback in a timely manner and make an analysis. On this basis, the user's demands can be understood, so as to improve product design and service provision.

3.3. The product communication strategy of the traditional brand image redesign in the information age

In the design process of the brand visual identity, the design of the product is the core of the brand. But how can the product be popular, and get a wide range of consumer support, more communication strategies are required. In this paper, combined with the characteristics of the technology and thinking of the information age, in the process of brand image redesign, the product communication strategy is summarized in Table 2.

Table 1. Four common features

Complementary communication tools	The information age has brought the multimedia communication mode, which can deepen the user's memory of the brand through the diversification of the communication channels, so as to effectively improve product awareness and consumer groups to brand recognition. The traditional brand has a good line, which can double the integration of online and offline resources, and continue to carry forward the traditional media print, television and other advantages. At the same time, it can use the website, social platform for online communication, so as to make the brand's publicity more interactive and durable, and establish a long-term relationship with consumers.
Consistency of communication information	Internet era has brought a lot of opportunities for traditional brands, making the traditional brand have a wide range of choices in the media. However, regardless of the choice of platform for publicity, the consistency and accuracy of the information determine the effectiveness of brand communication. The design of the brand image not only has the aesthetic feeling, but also should reflect the brand philosophy. Flat visual communication style should take into account the times and lasting, so as to be in the hearts of the people, to deepen the core values of the brand to convey the values.
Use design to tell the story of the brand	Brand story is a big advantage in the spread of traditional brands. A long history makes the traditional brand in the process of growing up with more cultural heritage. When a proper narrative has been widely disseminated, the brand image will be able to have affinity and persuasion, to stimulate the emotional identity. The spread of the story of the brand can use print ads to integrate into the film and television design.
The scene of the real and virtual experience	Technology has made it possible to make all sorts of illusions. In the use of virtual scenes to provide customers with relevant experience, the brand can break through time and space constraints, and make people feel more intimate services and more personalized brand culture expression, so as to reduce the user's time cost, and enhance the user experience.

4. Result analysis and discussion

In this part, taking Yantai apple as an example, a case study is made on the visual recognition image redesign of the traditional brand in the information age. Yantai apple is the most representative brand of Shandong province, has been walking in the forefront of brand design for many years. According to the enterprise's own strategic planning, the core content of the product is to do a good job of brand totem design and the corresponding protection.

In the variety of culture, Yantai Apple has reached the international leading level. For a long time, Yantai has continued to quote and develop excellent varieties at home and abroad, and has established a nursery stock breeding base with high level, so as to actively update and transform the old orchard. According to the relevant regulations, the use of the trademark of Yantai Apple should have a certain size and reach the standard of non-pollution businesses. Before using the trademark, first of all, businesses need to apply to the Apple Association of Yantai city. After a series of strict on-site inspection, the relevant departments will review and approve, and finally, a contract will be signed and submitted to the State Administration for Industry and Commerce Trademark Office for the record. This series of measures are able to effectively guarantee the quality of Yantai apple, and also can ensure the quality of Apple's trademark in Yantai.

In the new strategic plan, Yantai Apple has designed and released a new brand image, as shown in Fig. 3.

Fig. 3. Brands of Yantai apple

The first logo on the map is the new brand image of Yantai apple, the later five pattern are the brand value. Yantai Apple launches a new slogan "China's first apple, Yantai apple", using a sense of historical narrative way to increase the charm of the brand image. Thumb Apple's shape design is with a cartoon effect, which can make people remember. The thumb in the cultural context is the first meaning, which is just in line with Apple's image. Different brand graphics have different content, including the first in history, the first brand value, the world class natural conditions, planting level priority, and sweet and sour taste, expanding the amount of information about the brand image.

In this case, the company use a series of new brands. It can be an outbreak because that traditionally a single icon can be the only choice for the companies. With the six pictures, the Yantai Apple shows a dynamic trend. Six different apples refer to different characteristics of the commodity so as to make the brand's publicity more interactive and durable, and establish a long-term relationship with consumers. When a proper narrative has been widely disseminated, the brand image will be able to have affinity and persuasion, to stimulate the emotional identity. The form of various pictures is similar to telling a story so that the icon turns to be more

persuasive.

5. Conclusion

With information technology as the background, how to redesign the visual identity of the brand in the Internet environment was discussed in this paper, which focused on the new strategies to make brand design. Based on this background and concept, the basic theory of brand design in the information age was studied. And combined with the specific brand of the case, the visual image recognition was researched, analyzed and summarized. Through the case study, it is found that the Internet platform provides a wide opportunity for the brand in product design, marketing and communication design. And the use of systematic way of thinking can enhance the image of the traditional brand in all aspects. Taking Yantai apple as an example, the present situation was investigated and analyzed. It is considered that in Shandong's agricultural brand, Yantai Apple has forward-looking brand awareness. Yantai Apple brand image redesign has enhanced the level of the brand, and enriched the content of the brand culture, which is worth learning. Before the icon revolution, the Yantai Apple is usually ignored by people, though it is widely sold and promoted. Few people would pay attention to the brand. However, with the new brands, the special form is thus attractive and both the history and culture of the products are obvious exhibited. Therefore, the paper showed that the coming of the informative age has opened a new way for brand design, and the strategies mentioned could be lighting suggestions. By the limitation of space, this paper still has the problem of lack of refinement in theory and case analysis. But through the combination of theory and case, this paper has provided valuable suggestions for the redesign of the brand visual identity image in the development trend of the new era.

References

[1] N. Crilly, J. Moultrie, P. J. Clarkson: *Seeing things: Consumer response to the visual domain in product design.* Design studies *25* (2004), No. 6, 547–577.

[2] C. B. M. van Riel, J. M. T. Balmer: *Corporate identity: The concept, its measurement and management.* European Journal of Marketing *31* (1997), Nos. 5–6, 340–355.

[3] U. R. Orth, K. Malkewitz, Chair: *Holistic package design and consumer brand impressions.* Journal of Marketing *72* (2008), No. 3, 64–81.

[4] K. L. Keller, D. R. Lehmann: *Brands and branding: Research findings and future priorities.* Marketing Science *25* (2006), No. 9, 740–746.

[5] S. Park, D. Choi, J. Kim: *Visualizing e-brand personality: Exploratory studies on visual attributes and e-brand personalities in Korea.* International Journal of Human–Computer Interaction *19* (2005), No. 1, 7–34.

[6] T. M. Karjalainen, D. Snelders: *Designing visual recognition for the brand.* Journal of Product Innovation Management *27* (2010), No.TOC. 1, 6–22.

[7] C. A. Boudreaux, S. E. Palmer: *A charming little Cabernet: Effects of wine label design on purchase intent and brand personality.* International Journal of Wine Business Research *19* (2007), No. 3, 170–186.

[8] R. Abratt, T. N. Mofokeng: *Development and management of corporate image in South Africa.* European Journal of Marketing *35* (2001), Nos. 3–4, 368–386.

[9] K. Lim, A. O'Cass: *Consumer brand classifications: An assessment of culture-of-origin versus country-of-origin.* Journal of Product & Brand Management *10* (2001), No. 2, 120–136.

[10] C. Ranscombe, B. Hicks, G. Mullineux, B. Singh: *Visually decomposing vehicle images: Exploring the influence of different aesthetic features on consumer perception of brand.* Design Studies *33*, (2012), No. 4, 319–341.

[11] P. V. Henderson, J. A. Cote, S. M. Leong, B. Schmitt: *Building strong brands in Asia: Selecting the visual components of image to maximize brand strength.* International Journal of Research in Marketing *20* (2003), No. 4, 297–313.

[12] D. M. Frías, M. A. Rodriguez, J. A. Castañeda: *Internet vs. travel agencies on pre-visit destination image formation: An information processing view.* Tourism Management *29* (2008), No. 1, 163–179.

[13] S. T. E. Wang: *The influence of visual packaging design on perceived food product quality, value, and brand preference.* International Journal of Retail & Distribution Management *41* (2013), No. 10, 805–816.

[14] R. A. Shang, Y. C. Chen, H. J. Liao: *The value of participation in virtual consumer communities on brand loyalty.* Internet Research *16* (2006), No. 4, 398–418.

[15] B. Merrilees, M. L. Fry: *Corporate branding: A framework for e-retailers.* Corporate Reputation Review *5* (2002), Nos. 2–3, 213–225.

Received May 22, 2017

Acta Technica *62* No. 1A/2017, 289–300

Research and application of virtual reality technology in the restoration of ancient buildings in Huizhou[1]

Jing Dong[1]

Abstract. This paper introduces the concept of virtual reality technology, current situation and future development trend, and the ancient buildings in Huizhou as an example, a detailed description of the specific process of virtual reality technology in the restoration of ancient buildings in the ancient buildings, including basic data collection, collation, 3D modeling, lighting, rendering and baking processing process and system debugging process, analysis of the specific application of virtual reality technology in the architectural restoration of the particular school of ancient, to provide some references to provide a theoretical basis and reference for the research and application of virtual reality technology in the restoration of ancient buildings in the implementation of virtual reality technology in the application of the restoration of ancient buildings in the city, in order to better promote the construction of and development.

Key words. Virtual reality technology, Huizhou architecture, VR rendering, 3DMAX.

1. Introduction

Virtual reality technology is a hot research topic at present. Virtual reality technology can realize the three-dimensional visual environment, auditory effects, three-dimensional, friendly interaction, and many other functions, so that the past exists only in the two-dimensional plane of the object can be presented in three-dimensional form, at present, virtual reality technology has been applied in many fields such as architectural design, industrial design, communication, aerospace and so on.

Based on the principle of virtual reality technology and the starting point, J. Wang explored the application of virtual reality technology in the visual and urban planning, it provides a real, objective and effective reference value for the user to provide the user with a real, objective and effective design, and it provides a lot of reference for applying the virtual reality technology in the field of urban planning

[1]School of Liberal Arts, Xi'an University of Finance and Economics, 710100, China

[1]. X. Yu pointed out that the virtual reality technology can not only be used in the traditional manufacturing industry, but also has a great application value in disaster protection engineering, for example, in the emergency drill, it is not needed to put a lot of manpower and material resources to imitate the disaster scene, it can be through the virtual scene to do some man-made accidents, this not only can save costs, but also can ensure personnel safety to the greatest degree [2]. Through the analysis of the application of computer network technology in the ancient Greek theater restoration project, C. J. Liu points out that virtual reality technology can not only realize the restoration of monuments, but also can achieve its permanent preservation and resource sharing, virtual reality technology can make quick access to the information industry of Archaeology and Museology Era [3]. D. L. Jia and others proposed the application of virtual reality technology in geographical science, which can meet the development needs of digital city technology from 2D GIS to 3D virtual reality visualization, such as high-definition Google maps street view is the application of 3D visualization map currently which is used most widely, is most famous, and has most of the audience [4]. H. U. Feng-Lian pointed out the application of virtual reality technology in mechanical manufacturing industry, it can greatly shorten the equipment manufacturing time, simplify the manufacturing process, ensure the accuracy of parts manufacturing, installation, shorten the design cycle, and improve the reaction ability of the market [5].

In this paper, the definition of virtual reality technology, the specific operation process in the restoration work of ancient architecture, and the realization of the algorithm are introduced, taking the Huizhou architecture as the research object. The restoration of ancient buildings was implemented successfully, a certain reference value for the restoration of ancient buildings in the virtual reality technology was provided, and a new case for the virtual reality technology in the field of architectural design was provided.

2. State of the art

2.1. Virtual reality technology

Virtual reality is an advanced intelligent human computer interaction technology based on the characteristics of immersion, interactivity and imagination. It uses the computer software modeling, the plane two-dimensional drawings three-dimensional, simulation, and finally generates a realistic 3D virtual 3D scene model. Experience person use certain devices, such as VR glasses, to achieve real-time interaction with the scene model, and generate the same feedback as the real world, this makes people no longer on the scene only two-dimensional sense, but a three-dimensional, realistic. Virtual reality technology is widely used in communication, architectural design, urban planning, network games, product simulation and other fields. As shown in Fig. 1, it is the application of virtual reality technology in the interior design. The application of virtual reality technology in the restoration work of ancient architecture cannot destroy the original building site, but also restore the real ancient buildings. This will not only give people an immersive sense of reality,

but also can store the history of building information stored in the computer, through the transmission of the mobile network, so that people can also travel to the building within the building [6].

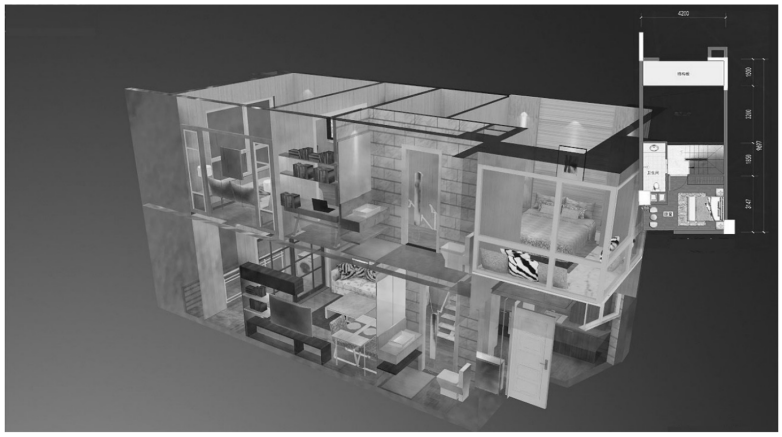

Fig. 1. Application of virtual reality technology in interior design

2.2. The process analysis of computer virtual reality technology in the digital restoration of ancient buildings

In the use of virtual reality technology for restoration of ancient buildings, the first work should be done to restore the work of the project, this need to collect information and data collection, and draw the plan. The parties involved in the restoration work of ancient buildings are designed and repaired on the basis of the ancient architectural sites, the repair work of ancient buildings need to meet the needs of history, aesthetics and other aspects in line with the historical appearance, in the early stage, historians also should strengthen communication with other historians to ensure the scientific nature and rationality of the design scheme. The preliminary planning work includes: Engineering surveying, ancient photo shoot, graphic drawing, ancient building repair technique to determine the repair, software selection, computer configuration setting, restoration of ancient buildings display and display device, virtual ancient architecture of the size, resolution, clarity and other factors.

The construction of ancient architecture determines the difficulty of restoration work. The building process of the 3D model of the ancient building is the process of restoring the ancient building system by using the virtual reality technology. Through the data collection and sorting of project planning work, this stage bases on its basis, using model to make software, for example, the establishment by using models of 3DMAX and other ancient buildings. After the completion of the ancient architecture model, the complex model needs to be optimized and designed, which is used for real time rendering, scene rendering, image rendering, and so on. And this need to control the distance between the elevation model, scheduling model in architecture, scene and other equipment to ensure the appearance of the scene, the

density of the important scene can be cut, in order to reduce the memory, and reduce the system pressure. After completing the above steps, it needs to make the scene map, light and baking process. This step has the significance that ancient buildings through the wind and rain erosion, wall color, pattern and detail components are incomplete and damaged to different extent, scene mapping, processing and baking processing effect are the results of using modeling software, this can realize the construction model in the natural light under the shadow processing and daylight effect, can map the form of virtual interactive software, and can get a better sense of reality and the improvement of the art. Ancient architecture 3D model establishment, rendering and baking all completed, followed by archaeologists, architects and other professionals to make corrective recommendations, according to historical data, determining the architectural style, details and other factors, to ensure the authenticity and artistry of ancient building model, adjusting the rectification, finally getting the draft of the restored model.

Virtual roaming refers to the establishment of a virtual character model, importing virtual environment, users can interact through the module, through the mouse, keyboard or other control keys, to move the virtual character in the virtual change of the upper and lower, this establishment of this step can be used by the user to obtain a more intuitive, three-dimensional experience of the building.

The latter part of the virtual reality technology is to test, adjust and improve the system. The main purpose of the system testing is to test the stability of the model, the compatibility of the system, and the requirements of the equipment configuration, the ability to successfully transplant to other equipment and run the test. The main contents include: the operation model of computer detection test of different hardware configurations, inviting users to try different education model, operating model under different operating platform, and crossing the three categories of the above test. Through testing, we can find problems, solve problems, and ensure that people with different levels of education can easily operate the model to achieve virtual roaming.

2.3. The characteristics of Huizhou ancient architecture

Huizhou architecture is an important part of China's architectural style, Huizhou culture is one of the three major regional cultures in china, Huizhou people pay attention to the attitude of no mountain and water cannot form a home. Therefore, Huizhou architectures emphasize the integration of the living environment and the natural ecological environment and ecology, being situated at the foot of a hill and beside a stream becomes a typical feature of Huizhou architectures.

3. Methodology

3.1. Realization process of virtual reality technology

As shown in Fig. 2, it is the process of achieving the virtual reality technology of building. According to Fig. 2, in the whole process of the realization of building

a virtual reality, aerial photography, the photography and other modes should be used to collect building, the image data can be obtained through the photography scene in the city side of the building; the recognition of buildings can be realized by aerial image technology, and it can be separated from the surrounding trees and other natural environment; by collecting the data of buildings, after the aerial image edge information extraction of three-dimensional 3D information and building body, we can start the construction of three-dimensional model building by using the three-dimensional information. In the use of virtual technology to restore ancient buildings, urban planning applications, usually require the building to rebuild the model as close to reality as possible, with a sense of reality, and therefore it needs to map the model information. Map baking technology is the key to the restoration design of ancient architecture, so in the specific modeling process, we should pay special attention to it. Because of the large scale of ancient buildings, more details, with a large number of data, so in order to meet the requirements of the virtual reality repair work, it is necessary to deal with the data processing, detail planning and so on; secondly, the model should be classified and corrected in order to achieve the effect of real recovery.

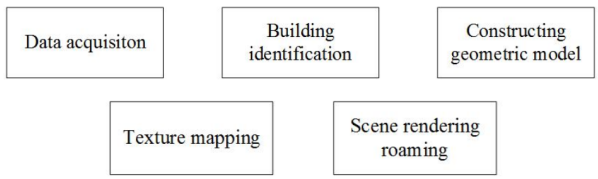

Fig. 2. Realization process of building virtual reality

3.2. Collection of data on restoration of ancient buildings

The sampling point set collected in the collection of data of buildings through aerial photography, ground photography and many other ways is called point cloud $p_i = (x_i, y_i, z_i)^t$. Supposing that the n data points which describe an elevation of the building model are $p_i = (x_i, y_i, z_i)^t$, $1 \leq i \leq n$, and the bounding set $x_{\min} \leq x \leq x_{\max}$, $y_{\min} \leq y \leq y_{\max}$ of the entire point set after traversing all data points can be obtained. In the formula, $x_{\min}$ and $x_{\max}$ are the minimum and maximum values of the point cloud coordinate x, respectively; similarly, $y_{\min}$ and $y_{\max}$ are the minimum and maximum of the point cloud coordinate y. Then the length of the grid element can be calculated, and the formula is

$$\text{size} = \sqrt[3]{(x_{\max} - x_{\min})(y_{\max} - y_{\min})(z_{\max} - z_{\min})/n} \tag{1}$$

The number of grid cells in the three directions x, y, z are, respectively:

$$\begin{aligned} x_{\text{res}} &= \left[\tfrac{x_{\max}-x_{\min}}{\text{size}}\right] + 1, \\ y_{\text{res}} &= \left[\tfrac{y_{\max}-y_{\min}}{\text{size}}\right] + 1, \\ z_{\text{res}} &= \left[\tfrac{z_{\max}-z_{\min}}{\text{size}}\right] + 1, \end{aligned} \tag{2}$$

Each data point in cloud p_i is put into a grid cell (u, v, w), among them:

$$\begin{aligned} u &= \left[\tfrac{x_i-x_{\min}}{\text{size}}\right] + 1, \\ v &= \left[\tfrac{y_i-y_{\min}}{\text{size}}\right] + 1, \\ w &= \left[\tfrac{z_i-z_{\min}}{\text{size}}\right] + 1. \end{aligned} \tag{3}$$

As far as there are duplicate points p_i in the cloud, p_i can be ignored.

Suppose that the plane S represents a plane with a boundary and there is a field which is homeomorphic with open disk $D^2 = \left\{x \in R^2 | \, \|x\| < 1\right\}$, in which, R is the unit circumference. At the same time, there is a field on the boundary point of plane S, which is homeomorphic with half circular disc $D^2 \cap H_+^2$ in which the half space $H_+^2 = \left\{(x, y) \in R^2 | x \geq 0\right\}$ and R in the formula is the unit circumference. The set of all boundary points constitutes the boundary of the plane S.

The complete least square plane fitting point set $N(p)$ is used to establish a local plane coordinate system OXY is established in the fitting plane, and the projection $\bar{p}'$ of $\bar{p}$ in the plane is taken as the origin O, where

$$\bar{p} = \frac{1}{k} \sum_{i=1}^{k} p_i \, .$$

The X axis and Y axis are the feature vectors e_1 and e_2, which correspond to the maximum and secondary eigenvalues of scatter matrix S, respectively.

Each point $p_i, \ 1 \leq i \leq k$ in $N(p)$ is projected onto the fitting plane, then the coordinates of the projection $p_i^{'}$ in the local plane coordinate system are, respectively

$$S = \sum_{i=1}^{m} (p_i - \bar{p})(p_i - \bar{p})^{\mathrm{T}} \, . \tag{4}$$

$$\begin{aligned} x_i^{'} &= e_1^{'}(p_i - \bar{p}), \\ y_i^{'} &= e_2^{'}(p_i - \bar{p}). \end{aligned} \tag{5}$$

Then, the origin of the local plane coordinate system is translated to the projection p' of the point p, so that a new local plane coordinate system $O'X'Y'$ is obtained, the polar coordinates (r_i, α_i), of each projection point are calculated $0° \leq \alpha_i \leq 360°$ and all projection point are sorted according to the order of angles from small to large. The maximum difference β between the two adjacent α_i is found, and the

boundary probabilities of point p_i can be expressed by the following formula:

$$\text{angle}\Pr(p_i) = \min\left(\frac{\beta - 2\pi/k}{\pi - 2\pi/k}, 1.0\right). \tag{6}$$

The formula for the boundary probability value of point p_i on the basis of the half disk metric algorithm is

$$\text{halfdisk}\Pr(p_i) = \min\left(\frac{3\pi\,\|\bar{p}' - p'\|}{4\bar{r}}, 1.0\right), \tag{7}$$

in which,

$$\bar{r} = \frac{1}{k}\sum_{i=1}^{k} r_i$$

and the distance between the barycenter and the center of half circular disc with the radius of $\bar{r}'$ is

$$\frac{4\bar{r}}{3\pi}$$

.

The boundary probability value of p_i is determined as follows by shape measurement method: the scatter matrix S of $N(p_i)$ describes the three-dimensional shape of the approaching $N(p_i)$ and its shape can be determined by three eigenvalues. According to the characteristic values $\lambda_1 \geq \lambda_2 \geq \lambda_3 \geq 0$ and their eigenvectors e_1, e_2, e_3, the scatter matrix S can be expressed as $S = \lambda_1 e_1 e_1^{\mathrm{T}} + \lambda_2 e_2 e_2^{\mathrm{T}} + \lambda_3 e_3 e_3^{\mathrm{T}}$. The three eigenvalues are normalized to form a judgment vector

$$(\lambda_1', \lambda_2', \lambda_3'),\ lambda_i' = \frac{\sqrt{\lambda_i}}{\sqrt{\lambda_1} + \sqrt{\lambda_2} + \sqrt{\lambda_3}}, i = 1, 2, 3\,.$$

Therefore, the probability formula of the point p_i belonging to the boundary point can be expressed as:

$$\text{shape}\Pr(p_i) = \min\left(\frac{(\lambda_1' - \lambda_2')(\lambda_2' - \lambda_3')}{1/9}, 1.0\right). \tag{8}$$

The classification is carried out on the basis of Table 1.

Table 1. Judgment vector of characteristic points

Characteristic value	Judgment vector
Interior point	$\lambda_1' \approx \lambda_2' \gg \lambda_3'$
Corner or noise point	$\lambda_1' \approx \lambda_2' \approx \lambda_3' \approx 1/3$
Points on a straight line	$\lambda_1' \approx 1,\ \lambda_2' \approx \lambda_3' \approx 0$
Boundary points	$\lambda_1' \gg \lambda_2' \gg \lambda_3'$

Based on the above three calculation methods, the probability that the calculated

point p_i belongs to the boundary points is

$$\Pr(p_i) = \frac{1}{3}(\text{angle}\Pr(p_i) + \text{halfdisk}\Pr(p_i) + \text{shape}\Pr(p_i)) . \tag{9}$$

Point cloud is used as the vertex set V of $G = (V, E)$ and the local adjacency relation of the points in the point cloud set is taken as the boundary point set E of the planar graph G, so the weight formula of the boundary line (p_i, p_j) of a planar graph is

$$w(p_i, p_j) = \frac{\Pr(p_i) + \Pr(p_j)}{2 * d(p_i, p_j)} , \tag{10}$$

where, $d(p_i, p_j)$ is the Euclidean distance between the two points.

The weight of an arbitrary section of a planar graph G is defined as $w(C) = \sum_{(u,v)\in C} w(u, v)$, and the closed curve with the largest weight is the largest circle.

The perfect matching value M of a planar graph is a subset of its set of edges, and each vertex of the planar graph has only one associated boundary line that belongs to M. The weight of perfect matching M is defined as $w(M) = \sum_{(u,v)\in M} w(u, v)$, and the perfect matching with the maximum weight is called the maximum perfect matching.

3.3. Calculation of the vector of point cloud data

Set plane equation as $ax + by + cz + d = 0$, $a^2 + b^2 + c^2 = 1$, normal vector is defined as $n = (a, b, c)'$, fitting point cloud data set as $\{p_1, p_2, \cdots, p_k\}$. Among $p_i = (x_i, y_i, z_i)'$ the least square method is used to calculate the distance between the surface point and point of the surface

$$E(a, b, c, d) = \sum_{i=1}^{k} (ax_i + by_i + cz_i + d)^2 . \tag{11}$$

Formula (11) meets the minimum value $\frac{\partial E}{\partial d} = 2\sum_{i=1}^{k}(ax_i + by_i + cz_i + d) = 0$, hence $d = -(a\bar{x} + b\bar{y} + c\bar{z})$. Let $\bar{u} = \frac{1}{k}\sum_{i=1}^{k} u_i$. From formula (10) we obtain

$$E(a, b, c, d) = \sum_{i=1}^{k} [a(x_i - \bar{x}) + b(y_i - \bar{y}) + c(z_i - \bar{z})]^2 = |U_n|^2 . \tag{12}$$

Here,

$$U = \begin{pmatrix} x_1 - \bar{x} & y_1 - \bar{y} & z_1 - \bar{z} \\ \cdots & \cdots & \cdots \\ x_k - \bar{x} & y_k - \bar{y} & z_k - \bar{z} \end{pmatrix} .$$

.

The minimum singular value U corresponds to the unit vector $n = (a, b, c)'$.

4. Result analysis and discussion

According to the third section of the image point cloud acquisition and location, the location of the plane map stitching algorithm, in this chapter, we designed a virtual reality restoration system based on the image of the ancient buildings. The system uses the C++ Visual language programming, combines with 3DMAX, Photoshop and Unity3D software combination, finally the program is applied to the restoration process of ancient architecture in Huizhou and achieved good results.

Huizhou ancient building restoration processes are as follows: First, collecting data of drawing plane graphics, as shown in the figure, according to the model plane and aerial data, as shown in figure, the map is a map rendering effect, the final completion of the map. It can be seen that the use of virtual reality technology to restore ancient buildings can achieve very good visual effect.

Figures 3 and 4 show the use of computer virtual reality technology. Virtual reality technology through the interaction of the way, you can simulate the restoration of ancient buildings, and it does not produce any two damages. Virtual reality technology in the record of the cultural heritage monomer at the same time, you can also save the surrounding environment together. The application of virtual reality technology, makes the building is no longer alone in a fixed place, and you can share in the computer equipment through the mobile network, so that people do not have to go personally, you can feel the magnificent grand buildings. The emergence and application of virtual reality technology can be stored and spread in a digital way. Virtual reality technology is the technical guidance and support after the ancient restoration work, it plays a decisive role.

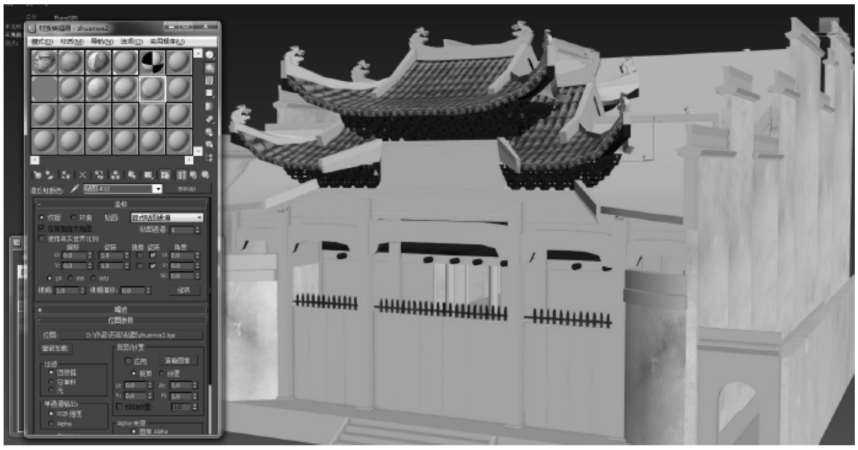

Fig. 3. Map processing

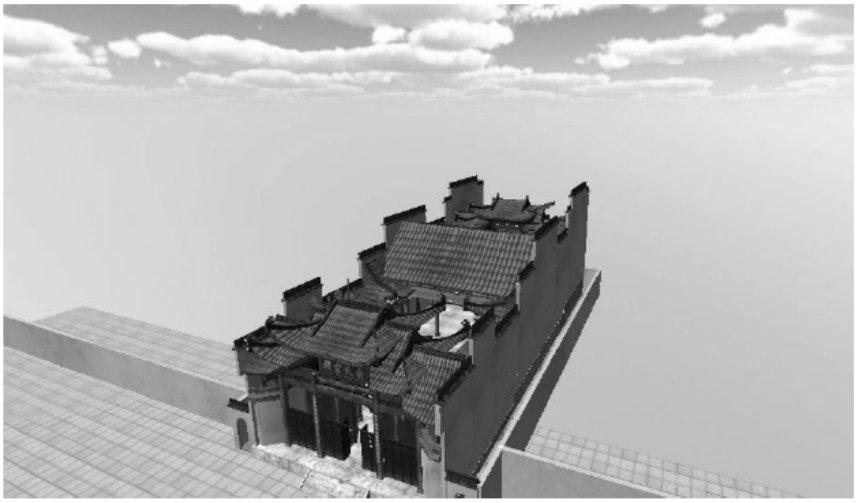

Fig. 4. Final effect charts

5. Conclusion

In this paper, the concept, current situation and future development trend of virtual reality technology were introduced, the application of virtual reality technology in the restoration work of ancient buildings was introduced, and the description of the virtual reality technology in the restoration of ancient buildings of the specific process was described carefully, the basic data collection, arrangement, the establishment of three-dimensional model, the model of light and shadow, rendering, baking, and the system debugging process were introduced. After introducing the basic algorithm of modeling, this paper took the Huizhou architecture as the research object, and the Huizhou architecture of the repair process. It is proved by an example that the application of virtual reality technology in the restoration of ancient buildings, it provided some reference suggestions for the application of virtual reality technology in the restoration of ancient buildings, and provided some technical support for the future research and application of virtual technology in the restoration of ancient buildings.

With the development of virtual reality technology, the rising and the extensive use of virtual reality technology, using virtual reality technology to demonstrate the performance of architectural design and housing design have become more and more popular among the people. The rapid development and experience of VR technology in architectural design also provide a lot of reference opinions to the restoration of ancient buildings, and reduces the design risk. However, the virtual reality technology in our country is still in the beginning of the stage of research, restoration of ancient buildings now needs to put energetic research to get more and better applications. This paper studied conditions and equipment constraints, only the Huizhou architecture is the appearance of a general repair, Huizhou architecture constructions are exquisite, many details of the decoration processing are not repaired, and

we look forward to having further studies.

References

[1] J. Wang: *Research on application of virtual reality technology in competitive sports.* Procedia Engineering *29* (2012), 3659–3662.

[2] X. Yu: *Research and practice on application of virtual reality technology in virtual estate exhibition.* Procedia Engineering *15* (2011), 1245-1250.

[3] C. J. Liu: *Research on application and development of competitive sports simulation based on virtual reality technology.* Advanced Materials Research *179–180* (2011), 1063–1068.

[4] G. Peng, G. Wang, W. Li, H. Yu: *A desktop virtual reality-based interactive modular fixture configuration design system.* Computer-Aided Design *42* (2010), No. 5, 432–444.

[5] R. Moreno: *Does the modality principle hold for different media? A test of the method-affects-learning hypothesis.* Journal of Computer Assisted Learning *22* (2006), No. 3, 149–158.

[6] C. Z. He: *The application of computer virtual reality technology in ancient buildings digital restoration.* Journal of Guangxi University for Nationalities (Natural Science Edition) (2013), No. 02, 15.

Received May 22, 2017

Acta Technica *62* No. 1A/2017, 301–312

The influence of bearing stiffness and gear helix angle on the vibration noise of reducer[1]

Xiaorong Zhou[2], Lidong Huang[2], Hua Zhang[2]

Abstract. With the rapid development of China's current mechanical technology, the traditional reducer has been difficult to adapt to the requirements of the development in the times because its vibration noise was too large. The effect of bearing stiffness and gear helix angle on the vibration and noise of the gear reducer was studied in this paper. The meaning of the vibration and noise of the gear reduce was introduced firstly, and then the application of the bearing stiffness and the diagnosis of the spiral angle of the gear were conducted expedition in this paper. Finally, the research process of bearing stiffness and gear helix angle on the vibration and noise of gear reducer was studied in detail. The experimental results showed that the effect of bearing stiffness and gear helix angle on the vibration and noise of gear reducer had the advantage of reducing noise, which can be used to reduce noise.

Key words. Reducer vibration, bearing stiffness, gear spiral angle, noise reduction.

1. Introduction

With a large number of applications of large scale integrated bearing and gear, the mechanical structure was developing in two directions. Study on the noise reduction of vibration and noise reduction by using modern mechanical technology was one of the key problems that need to be solved in real life [1]. According to statistics, the reliability of the reducer part determined whether the whole hybrid system was reliable in the bearing and gear, so the demand for the reliability of the reducer was more urgent. And the noise was one of the important factors that affected the stability of the reducer, and a series of problems in the vibration noise have been paid more and more attention [2]. The noise caused by the vibration of industrial facilities will not only cause noise pollution in residential areas, but also affected

[1]This work is supported by Science and technology planning project of Hunan science and Technology Department (NO.2011FJ3005) "A Technical Study on the Precision Forming Technology of Automatic Globoidal Cam".

[2]Hunan Mechanical and Electrical Polytechnic, 410151, China

the stability of the operating equipment and operator comfort. Therefore, the noise reduction of speed reducer was concerned by people widely. The development of the bearing was introduced firstly, and then the application of the bearing stiffness and the spiral angle diagnosis of the gear was conducted expedition in this paper. Finally, the research process of bearing stiffness and gear helix angle on the vibration and noise of gear reducer was studied in detail [3]. The experimental results showed that the effect of bearing stiffness and gear helix angle on the vibration and noise of gear reducer had the advantage of reducing noise, which can be used to reduce noise.

2. State of the art

Many foreign experts have long been concerned about the bearing stiffness and the spiral angle of the gear on the vibration noise of the gear reducer [4]. Berkowitz proposed the concept of the noise reduction of the bearing reducer firstly in 1962, which opened the prelude of the research on the noise reduction of the simulation speed reducer [5]. Navid demonstrated that the value of the part of the linear reluctance bearing can be solved in 1979, and the simulation of the vibration of the bearing reducer was developed [6]. Researchers have been working to address all component values to determine the speed reducer vibration area and related components since 1980s. The simulation of bearing reducer vibration developed to more direction since then. For large-scale integrated bearings, Salama proposed a network based decomposition of network level reducer vibration noise reduction method in 1984 and the condition was that the network between the associated nodes was controllable and pull all the associated nodes. Because the method was based on the KCL equation, the computation was large and the noise reduction was slow with its limited application. The development of artificial intelligence information processing technology provided a reliable tool to solve the problem of vibration and noise reduction. Gear system had the advantages of high efficiency, compact structure and stable transmission ratio, which was used in various industrial fields widely. The gear box shell can generate vibration and radiated noise in the process of transmission due to the inevitable meshing stiffness and error excitation. Domestic and foreign scholars have conducted a lot of research. Kevin Gerner and others used the method of sound and solid coupling to analyze the sound radiation of the simple gear box structure under the excitation of time varying stiffness. Researches on vibration and noise radiation of gearbox were analyzed by using FEM/BEM method, and they made a comparison with the test results, which demonstrated the effectiveness of the FEM/BEM method. The main excitation components and prediction methods of the vibration noise of the reducer were analyzed by Kevin and Jim, and the vibration and noise reduction method were proposed from the aspects of the geometry of the gear and the stiffness of the gear box. Lin Tengjiao conducted the comprehensive consideration of the internal excitation of the gear system and analyzed the dynamic characteristics of the marine gear box under the rated conditions. Sairui Connor believed on reducer noise radiation was not only affected by the meshing performance of gears, but also had a certain relationship with

the inherent characteristics of box, and the experiment analyzed the influence of gear reducer noise radiation. The dynamic response of the gear box was analyzed by Kylie in the method of finite element, and the influence of different bearing connection form and stiffness on the dynamic response was analyzed in the analysis model. The FEM/BEM method was used to calculate the vibration and noise of the gear box and the dynamic characteristics of the dynamic characteristic of the transmission system were considered synthetically. The influence of the bearing support stiffness and the helical angle of the gear on the dynamic excitation and vibration noise of the gear reducer were analyzed. The front end and the top of the bevel gear reducer were weakened obviously, especially at the top of the noise reduction. However, the noise on both sides increased due to the helical gear produced axial excitation.

3. Methodology

3.1. Reducer vibration noise wave changing

The vibration noise of reducer was analyzed, and the result of the decomposition function and the coefficient of the vibration noise of the gear reducer were observed in this paper. We knew that the vibration and noise of the complex periodic reducer can be decomposed into sine function and Fourier series as well as the Fu Liye transform corresponding to the Fu Liye series coefficient. Similarly, noise reducer vibration wave of vibration and noise signal can also be expressed as a set of tree structure. Coefficient of vibration and noise wave transformation of reducer corresponded coefficient of vibration noise of gear reducer. Multi scale decomposition was based on multi-resolution analysis theory and the length of the decomposition coefficient was smaller (by half the ratio) with the larger scale decomposition. We also found that the low frequency coefficient of the vibration noise of the gear reducer was similar to the low frequency coefficients of the original reducer vibration noise wave signal. However, it was noted that the value and length of the low frequency coefficient are not the same as the original reducer's vibration and reconstruction of the reducer vibration noise wave signal. The decomposition process of the vibration and noise of the gear reducer was as follows: Specific process can be designed for high pass filter and low pass filter to obtain high frequency coefficients and low frequency coefficients, and the length of each decomposition of the data halved. Speed reducer vibration and noise wave transform were used to increase the sampling frequency for the inverse of the decomposition process. And zero was inserted in each of the two numbers in order to make a convolution with the conjugate filter, and finally the sum of the convolution results was obtained. We often used the coefficient of each layer to rebuild the gear reducer noise wave signal (noting that although the number of coefficients was smaller than the original gear vibration noise signal, but after the length was same in the reconstruction), and it viewed time of each band domain selectively in the application so as to determine the frequency range of shock component. We regarded it as a reducer vibration noise signal through a series of different types of filters in order to obtain the gear reducer noise wave signals of different frequency range, and the gearbox vibration noise signal was decomposed

into wave reducer vibration noise wave decomposition and used coefficients of each layer to the reconstruction of gearbox vibration noise wave signal. The important applications of noise reduction and noise reduction were two important applications in the analysis of vibration and noise. The original reducer vibration noise wave signal can be decomposed into a series of approximate components and detail components by using the analysis of vibration and noise. Reducer vibration noise signal noise concentrated in the reducer vibration noise signal of the details of the signal mainly. Speed reducer vibration noise wave reconstruction can be used to smooth gear vibration noise signal after the use of a specific threshold to deal with the details of the component. The commonly used functions of reducer vibration noise wave can be used to deal with the engineering drawings of bearings. Its process was as follows: The engineering image processing of two-dimensional bearing was consistent with the one dimensional vibration and noise wave signal processing, but some formulas were not the same. The basis function formula was as follows in the engineering image of two dimensional bearing:

$$f[x,y] = \cos\left[\frac{(2x+1)u\pi}{16}\right]\cos\left[\frac{(2y+1)v\pi}{16}\right]. \tag{1}$$

In the formula, x and y refer to the pixel in the spatial domain (corresponding to one dimensional time domain) coordinates, and u and v are the coordinates in the basis function frequency domain. The basis function formula was based on the 8×8 block and value range of x, y, u, v is $\langle 0 - 7\rangle$. The low frequency information was concentrated in the upper left corner of the matrix, and the high frequency information was concentrated on the lower right corner after the vibration of the bearing of the project image was transformed by the reducer. The direct current component was in the [0,0], and the basis function of [0,0] was a cosine function of the 1.5 period in one direction and was a constant in the other direction. The basis function of [1,0] was similar to [0,1], but the direction was rotated by 90 degrees. The used transform basis function is depicted in Fig. 1.

Compression can be achieved by discarding some of the smaller elements of the 64 spectrum (spectrum) after the reducer vibration noise wave transform, which made it possible to achieve compression and that information can be kept as large as possible. The engineering drawing of the upper bearing showed contrast ratio of using different number of frequency domain amplitude (frequency spectrum) from the original bearing engineering image d reconstruction of the bearing engineering image. It can be seen from the bearing of the engineering drawing c that even if the high frequency amplitude (spectrum) of the total 3/4 was discarded, it can be obtained by using the following formula to obtain the spectrum of the original bearing image: the low frequency amplitude (frequency spectrum) result. In addition, the error seemed to be random and can be considered as random noise. Then the appropriate threshold was selected, reconstruction can achieve the purpose of eliminating noise after the reducer vibration noise wave decomposition.

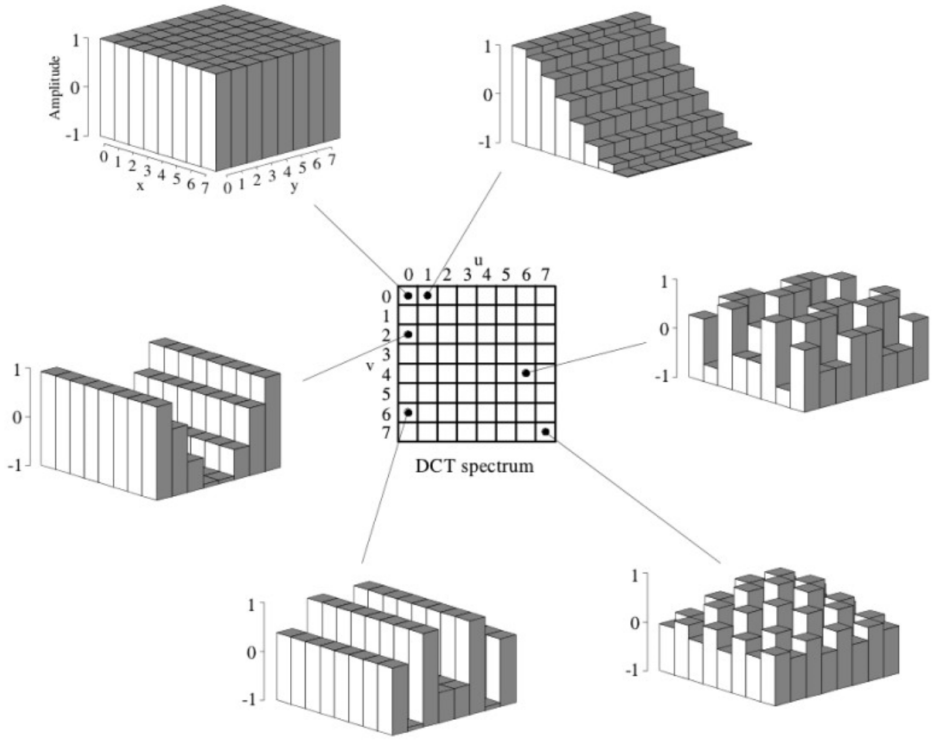

Fig. 1. Transform basis functions used

3.2. Investigation on the application of the bearing stiffness and the diagnosis of the spiral angle of the gear

The relationship between manufacturing industry and its main gear were studied and the data was collected from the angle of bearing and gear in this paper. We used the way of WeChat survey to conduct questionnaire issued to let management who were responsible for the sales of bearings and familiar with the situation in the enterprise investigated fill in the questionnaires. A total of 250 questionnaires were issued with online 100 and 150 copies of the site. 135 valid questionnaires were recovered and the effective questionnaire recovery rate was 54 %. Among them, the field release questionnaires recovered 82, accounting for 59.74 % and online payment of 53 copies of the questionnaire recovered, accounting for 40.26 %. The data were tested by double sample T, and the two had no significant difference ($p > 0.05$), which could be combined together to analyze the data. The specific way was shown in Table 1 and bearing manufacturing in kind was shown in Fig. 2.

We can find other manufacturing companies to provide the same service (reverse score) with A (previously selected by the manufacturing firm), and then find other inspectors instead of A.

Table 1. Business people who fill out their features

Feature		Frequency	Percentage (%)
Industry	Machinery manufacturing	24	17.8
	Electronic Product Manufacturing	25	18.5
	Food processing industry	14	10.4
	Other	72	53.3
Company size	100 or less	25	18.5
	100–499	25	18.5
	499 or more	85	63
Working year	1	4	3
	5 or more	102	75.5

Fig. 2. Bearing manufacturing physical map

Although this will bring loss to our company, but it was difficult to find a distributor that can bring us so low as A company bearing stiffness and gear helix angle rate. At the time of the survey, we asked the manufacturer representative to point out the extent to which they agree or disagree with these statements (1 = disagree; 2 = does not agree; 3 = has no opinion; 4 = agrees; 5 = extremely agrees). The measurement results were analyzed by the factor analysis and then the scores of the two factors were added together

$$\text{InterptPD} = \text{DP}_\text{d} + \text{DP}_\text{s}\,, \tag{2}$$

$$\text{AsymPD} = \text{DP}_\text{d} - \text{DP}_\text{s}\,. \tag{3}$$

We can calculate the specific values by these two formulae. These are listed was in Table 2.

Table 2. Multiple hierarchical regression analysis results: the standard line posture

Model	DP_d	DP_s	InterptPD	AsymPD
JPlan	0.165	−0.017	0.024	0.118
JSolve	249	0.057	0.061	306

The above data showed that the stiffness and the spiral angle of the gear had a significant positive impact on the bearing manufacturers to solve the problem. There was a clear negative impact on the speculative behavior of the bearing manufacturers that are perceived by the bearing manufacturers. However, the impact of the joint development plan for the bearing manufacturer and the bearing manufacturer was not obvious. The interdependence between the bearing manufacturer and the bearing demand had no significant impact on the use of relationship governance for bearing manufacturers. But the bearing manufacturer was more dependent on the non-symmetry, which had a significant negative impact. The relationship marketing orientation has no obvious influence on the speculative behavior of the bearing manufacturers' perceptions. There was a positive interaction between the bearing manufacturer and the bearing manufacturer to make plans and to solve the problem. That was to say, bearing manufacturers often make plans with bearing consumers.

3.3. Study on the influence of bearing stiffness and gear helix angle on the vibration and noise of gear reducer

We used the method of extracting the effective points in Fig. 3 when extracting the characteristics of the bearing stiffness and the helix angle of the gear. Altogether 6 characteristic values were extracted from the waveform of the vibration noise of the output response reducer: The frequency response of voltage amplitude corresponding to the frequency of 10 kHz was 1 V. The frequency response of voltage amplitude corresponding to the frequency of 20 kHz was 3 V, and the frequency response of voltage amplitude corresponding to the frequency of 30 kHz was 5 V. The frequency response of voltage amplitude corresponding to the frequency of 40 kHz was 10 V and the frequency response of voltage amplitude corresponding to the frequency of 50 kHz was 20 V. The frequency response of voltage amplitude corresponding to the frequency of 60 kHz was 10 V and the frequency response of voltage amplitude corresponding to the frequency of 70 kHz was 5 V. The frequency response of voltage amplitude corresponding to the frequency of 80 kHz was 3 V and the frequency response of voltage amplitude corresponding to the frequency of 90 kHz was 1 V.

The 9 sampling points can describe the zigzag curve bearing frequency output and can also distinguish between zigzag curve when other components changing. Structure sample set was as follows: As was shown in the figure, the resistance and capacitance of the bearing are measured to be 2 % and 5 % respectively. The output frequency response was normal when changing in this range. The allowable variation tolerance of current was 50 %–70 % and tolerance range of voltage U allowed variation was 40 %–80 %.

According to the above settings, I or U changed in the scope of: small, normal, partial. Symbols L, N, M were used to represent them. Sample data is shown in

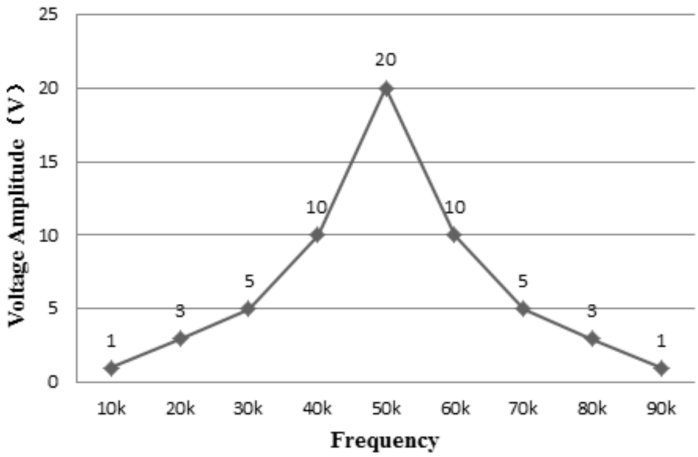

Fig. 3. Output sampling frequency response diagram

Table 3 and Table 4 according to the stiffness of each bearing element and the spiral angle of the gear.

Table 3. The first group pickup

L	N	M
0.02	0.95	0.12
0.03	0.84	0.15
0.04	0.93	0.14

Table 4. The second group pickup

L	N	M
0.08	0.95	0.11
0.05	0.85	0.19
0.06	0.94	0.09

Each of the first or second sets of changes in the component correspond bearing frequency response curve of output sampling time and was considered as the reducer noise input changes. The representation method was used by network output status: 0 (stiffness and gear helix angle) 1 (normal) represented. If both L and M are 1, the bearing component is normal.

The classical two layer perceptron was used to simulate the bearing stiffness and the diagnosis and location of the helical angle of the gear. The formula was as follows:

$$y = g\left(\sum_{i=1}^{n}(K_i F_i - \theta)\right). \tag{4}$$

Among them, K_i is the weight and F_i is the input. Symbol θ represents the limit value and $g(x)$ is the transfer function.

4. Result analysis and discussion

We used the heuristic method to improve the vibration noise of the gear reducer in order to improve the training intensity of the network. That is to say, the method was adding momentum correction. The training sample sequence was input to the gearbox vibration noise network and the mean square error (MSE) was set to 0.011. The double layer perceptron has been spread and the learning speed was 0.5 after several adjustments. Momentum factor 0 network achieved the expected value after 30215 training adjustment. The relationship between the mean square error and the training times of the multi-layer perceptron network was shown in figure. The first 70 local relations between mean square error and training times are shown in Figs. 4 and 5.

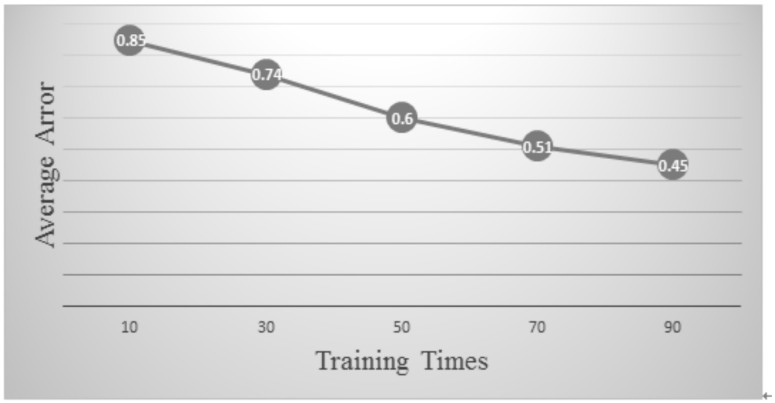

Fig. 4. Average error of the relationship between training times

It can be seen that the average accuracy of partial bearing stiffness and gear helix angle were not stable, but the average accuracy of bearing stiffness and gear spiral angle were stable, which showed that the effect of the stiffness and the helix angle of the gear on the vibration and noise of the gear reducer had the advantage of a certain degree and can be used to reduce the noise of large scale reducer.

5. Conclusion

Bearing and gear, as the representatives of the precision parts, occupied an increasingly important position in modern industrial manufacturing in the modern mechanical manufacturing industry. And the large number of precision parts made it often appear to affect the noise of reducer, so it was necessary to reduce the noise of the reducer by the appropriate method. We used bearing tolerances in order to obtain the bearing on the sample in this paper. Bearing tolerance, as a statistical

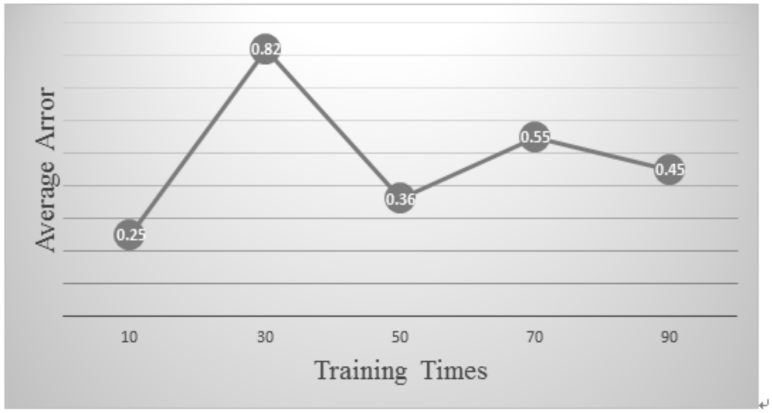

Fig. 5. Average error of the relationship between local training times

analysis of the random response signal and was attached to the nominal bearing, can only be obtained through the simple operation of training and test samples, which can reduce the computational complexity greatly. Firstly, the meaning of the vibration noise of the gear reducer was introduced and then the application of the bearing stiffness and the diagnosis of the helical angle of the gear were investigated in this paper. Finally, the research process of bearing stiffness and gear helix angle on the vibration and noise of gear reducer were studied in detail. The experimental results showed that the effect of bearing stiffness and gear helix angle on the vibration and noise of gear reducer had the advantage of reducing noise, which can be used to reduce noise. And this method was simple and effective and it can solve the problem of high stiffness and high gear helix angle. However, there were still some deficiencies in the research process due to the limitation of my ability and time. For example, the results of this study may not be suitable for other types of bearing stiffness and spiral angle of the gear due to the bearing stiffness and the type of gear helix angle more, which also needed to be explored and studied further.

References

[1] M. T. Khabou, N. Bouchaala, F. Chaari, T. Fakhfakh, M. Haddar: *Study of a spur gear dynamic behavior in transient regime.* Mechanical Systems and Signal Processing *25* (2011), No. 8, 3089–3101.

[2] L. Walha, T. Fakhfakh, M. Haddar: *Nonlinear dynamics of a two-stage gear system with mesh stiffness fluctuation, bearing flexibility and backlash.* Mechanism and Machine Theory *44* (2009), No. 5, 1058–1069.

[3] P. Velex, S. Baud: *Static and dynamic tooth loading in spur and helical geared systems—experiments and model validation.* Journal of Mechanical Design *124* (2002), No. 2, 334–346.

[4] M. Amabili, A. Fregolent: *A method to identify modal parameters and gear errors by vibrations of a spur gear pair.* Journal of Sound and Vibration *214* (1998), No. 1, 339–357.

[5] E. Mucchi, G. Dalpiaz, A. Rivola: *Elastodynamic analysis of a gear pump. Part II:*

Meshing phenomena and simulation results. Mechanical Systems and Signal Processing *24* (2010), No. 7, 2180–2197.

[6] Y. Wang, W. J. Zhang: *Stochastic vibration model of gear transmission systems considering speed-dependent random errors.* Nonlinear Dynamics *17* (1998), No. 2, 187–203.

Received May 22, 2017

Acta Technica *62* No. 1A/2017, 313–320

Railway signal simulation system based on microcomputer interlocking

Xiong Sheng Wu[1]

Abstract. With the rapid development of railway transportation industry, the higher demand for railway signal control is put forward. In recent years, the rapid development of computer technology and the continuous enhancement of reliability have laid the foundation for the development and application of microcomputer interlocking system. The microcomputer interlocking system is gradually replacing the electric interlocking system used by many stations. Based on this, the railway signal simulation system based on microcomputer interlocking was studied in this paper. The microcomputer interlocking system was introduced in this paper. Then, the control system design of microcomputer interlocking was studied. Then, the simulation system of railway signal based on microcomputer interlocking was studied and debugged. The actual test results show that the signal serial port is working properly, and the signal is consistent with the relay action and interlock table information, which shows that the system is stable and will be applied in a large number of railway stations in the future.

Key words. Railway signal, simulation system, microcomputer interlocking, control system.

1. Introduction

China is the most populous country in the world, and the annual railway ride rate is the highest in the world. With the gradual development of social economy, people's demand for railway transportation safety is improving. In this case, the railway sector has begun to implement the reform and revision of railway signal control system. Nowadays, the computer interlocking simulation system has gradually replaced the traditional relay centralized control system, and has been applied in a large number of railway stations. Therefore, the research on the railway signal simulation system based on microcomputer interlocking has important practical significance for the development of green ecological building and environment-friendly society. In view of this situation, the railway signal simulation system based on microcomputer interlocking is studied deeply in this paper. The microcomputer interlocking system is the important foundation of the research, and so the microcomputer interlocking system is firstly interpreted. Then, the design of the computer

[1]Liuzhou Railway Vocational Technical College, Liuzhou, 545616, China

interlocking control system is analyzed, and some results are obtained. Finally, the railway signal simulation system based on microcomputer interlocking is studied in detail. The test results show that, compared with the interlock table, it is found that the signal of the system is consistent with the relay action and interlocking table information, indicating that the whole system function is good, and the module is working properly.

2. State of the art

In 1978, the world's first microcomputer interlocking devices appeared in Sweden (Dong et al. 2010) [1]. National computer interlocking technology is developing rapidly. Sweden is one of the first countries in the world to develop and apply microcomputer interlocking. Its development is divided into three stages (Wang et al. 2004) [2]. In the first generation of products, the relay control signals, steering, and tracking relay were used. In the second generation of products and signal, the fault safety non-contact circuit was adopted. The tracking relay was still the main contact. At present, the third generation products were all electronic control circuits. Contactless functional block was adopted track relay. In 1985, Halsburg station first used this product (Akita et al. 1985) [3]. In 1979, West Germany decided to develop computer interlocking. In 1983, West Germany commissioned SIEMENS and AGE to develop. In December 1985, Munich developed the first set of computer interlocking devices, and used it at Walter's station (Wang et al. 2006) [4]. The computer interlocking device developed by SIEMENS, Lorenz and AGE three companies was basically of three levels. The difference was that the connection between computer systems was determined by the number of outdoor signal devices and the use of hardware and its fail safe solutions (Ning et al. 2011) [5]. The three levels were: the first level was to preprocess the input and output of the computer, the order of the keyboard input and the individual operating commands. The instruction level was promoted to the next level and displayed in the working state of the interlock logic, so as to display the location and status of the outdoor signal equipment. The second level was the interlocking logic level, and the interlock logic program ran according to the operating conditions. The third level task was to connect and control signals, and carry out polling and track inspection equipment. British SS solid state interlocking system was a distributed structure. The whole system can be divided into several parts: the control and supervision subsystem, the interlocking subsystem, the data path module and the terminal processing device. There were following features in the design: In order to avoid confusion when using the new system, the traditional control panel was still used. Centralized interlocking control mode was used. The interlocking function of each station was concentrated in the control center, and each station was equipped with a terminal processing device, such as a driving signal machine and a switch machine. In the control center, the interlocking function was dispersed. The monitoring object was divided into several regions along the line, and each region was assigned a microcomputer for interlocking. The interlocking device adopted three-fold structure, and the majority voting function was realized by software. In addition to the track circuit, the signal

and switch control relays were fully electronic.

3. Methodology

3.1. Overview of microcomputer interlocking systems

Railway signal is an important technical means for railway transportation department to ensure traffic safety, improve transport efficiency, and realize automation of transportation management and automatic control of train operation (Chandra et al. 1991) [6]. According to its application, railway signal system can be divided into station signal control system, marshalling station shunting control system, interval signal control system, railway driving control system and automatic train control system. The station signal control system is one of the important control systems in the field of railway transportation (Wang et al. 2006) [7]. It is based on the station signal, voting, segmentation control. The main function of the station signal system is to eliminate or weaken the safety hidden trouble of the station, ensure the traffic safety, provide the transportation efficiency, and manage the modern information scientifically through the identification of the technical means (Roanes et al. 2011) [8]. The system is a security system, and the output fault of any part of the system will be safely guided. On the other hand, the station signal control system consists of indoor control equipment (outdoor station equipment personnel signal lights, polling stations, parts), as well as communication lines and other hardware devices and circuits (Yang et al. 2006) [9]. These specific rules, the relationship between lights, switches, cross sections, as well as the relationship between constraints, are called interlocking, and the realization of such interlocking devices called interlocking devices, and a device that implements this interlocking is called an interlocking device (Turner et al. 1987) [10]. It can be seen that the core of the station signal control system is interlocked. Therefore, the station signal control system is the realization of interlocking system, also known as the station interlocking system. Figure 1 depicts the actual situation of railway signals.

Fig. 1. Railway signal

From the technical point of view, the station interlocking system has been carried out in the process of mechanical interlock and electrical interlock phase, and now it has been turned on the electronic lock. In the application of the railway station interlocking system in China, according to the difference of the concentration of the scheduling signal and the interlocking control, it can be divided into non-centralized interlocking system and centralized interlocking system. The non-centralized interlocking system is not perfect in identifying, eliminating and mitigating the technical measures that endanger traffic safety, which is only for busy and unreliable stations. A centralized interlocking system is an interlocking system that focuses on the signal floor, which is used to control signals and voting systems. The interlocking mechanisms are also concentrated in the signal architecture (Verma et al. 1985) [11]. At present, the widely used centralized interlocking system is realized by the relay interlocking logic, which is also known as the power centralized interlocking system (Geng et al. 2008) [12]. Electrical control is used to centrally control and monitor station rutting, traffic lights, sections and sections, and to achieve linkage control among them, as shown in Fig. 2.

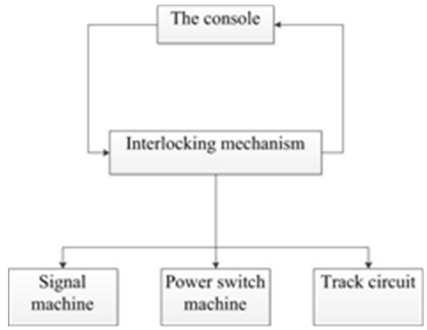

Fig. 2. Microcomputer interlocking system control

3.2. Design of microcomputer interlocking control system

In a computer interlocking system, a computer control system is used to monitor and control the transportation and production processes of a railway station. It works in the field of railway transport production, and is directly connected with the station signal equipment (Tian et al. 2005) [13]. Therefore, unlike the traditional information processing computer system, the computer itself has a series of features to suit its use. Real time refers to the characteristics of an industrial control computer that must respond to external events within a limited period of time. Industrial control computer can be driven simultaneously. The industrial control computer can respond to an interrupt request within a certain period of all detected scan events (Cribbens et al. 1978) [14]. These changes are usually not very fast, and even if they do not respond immediately, events will not be affected or damaged. The retention time is very short in the inspection process, needing a computer to respond immediately. As the source of the interrupt request, the computer can respond immediately when the event occurs.

The standardization and serialization of an industrial control computer is the use of the recommended standard bus and the preferred industrial control machine, which not only increases the probability of success, but also enhances the benefits of mass production by low price and high performance. At the same time, the low-level repeated development should be avoided, and the system design, manufacturing and debugging, and open cycle should be shortened. In order to ensure the industrial control computer system can lay a good foundation for the long time work in the field of railway transportation production, a series of technical measures must be adopted to improve its reliability (Jianrui et al. 1998) [15]. Modularization means that: in accordance with the implementation of the function, the industrial control computer system' each part is divided into a number of modules, which are produced by computer manufacturers. In the design and manufacture of industrial control computer system, these modules can be used directly. These modules can be used as building blocks in the form of building blocks. With the increase of the size of the system or the increase of the required system function, the industrial control computer system may need to be transformed into the distributed control system, which requires that the industrial control of the computer system should have reliable and simple communication capabilities, and can constitute a LAN capacity. Specific advantages are shown in Table 1.

Table 1. Advantages of computer interlocking system

Advantage	Summary
Strong real-time	An industrial control computer has the ability to respond to external events in a given time.
Full process input and output capability	In addition to CPU, RAM and ROM, a wealth of input devices and output devices, as well as perfect external equipment should also be equipped.
Full process input and output capability	The industrial control computer has the basic part of an ordinary computer.
Standardization and serialization	The standardization and seriation of the industrial control computer is to use the national recommended standard bus and the industrial control machine.
High reliability	Industrial control computer system must be able to work in the environment of railway transportation production for a long time.
Strong communication and networking capabilities	The industrial control computer system must have the reliable and simple communication ability and the ability of the local area network.

3.3. 3 Research on railway signal simulation system based on microcomputer interlocking

Interlocking railway signal system is an important part of interlocking software, and usually with the following characteristics: one is the multi functionality. Because

the interlocking process is in accordance with the design of the road control process, different structures have different station modules. As long as the base station data is modified into an interlocking program, and different data tables are provided, different modes of control can be realized. Therefore, the interlocking procedure is general. In the use of this generic standard structure, it is not necessary to design each specific route program. Because of the program's information sharing, if the program has some defects, then the defects can be easily exposed in the process of debugging and in the simulation of road control process, which can be corrected in time to improve the reliability and security of the program. The second feature is the convenience of the design, production, and maintenance of interlocking systems. For different sites, interlocks are common. The third one is that the station is easily to be easy rebuilt and expanded. The general computer control system is the same, and the modular structure is also adopted in the computer interlocking software design. Interlocking program is based on the process of completing the function, which can be divided into different modules to prepare. These modules are a whole, are relatively independent. The modular software architecture makes the system easy to expand and update.

The software of railway signal simulation system based on microcomputer interlocking can realize the following functions: man-machine interface information processing function. Business information processing: the transaction can be run properly to form an effective order operation, and the corresponding representation should be shown on the screen to let the waiter to confirm their operations. Information processing: the status of the field signal equipment can be displayed on the screen in real time, so that the staff can monitor the use of the equipment at any time. The basic interlocking control functions can complete the interlock function. By clicking the mouse in the track section, the trajectory occupation can be simulated to achieve the normal way to unlock, manual unlock, and abnormal unlock, as well as the manual voting, 64D relay semi-automatic block function, and so on. The control function: the control circuit of the field equipment is driven according to the control commands generated by the interlocking software. Input control: the scene, signal, and voting status information of the track circuit are collected in real time to provide data for the interlock operation.

4. Result analysis and discussion

In this paper, the railway signal simulation system based on microcomputer interlocking is tested. Firstly, the control panel of the switch is connected with the microprocessor interface board and the signal control panel through the cable. Secondly, in order to facilitate the software debugging, the network interface and PC are used. Finally through the RS-422/RS-232 converter, the interlocking center of the RS-422 serial port is connected to the PC serial port. The purpose of using the NFS root file system is to connect the microprocessor interface board and PC through the network cable, which is easy to debug the system software. The RS-422/RS-232 converter is connected through the microprocessor interface board and PC to verify that the serial port is working normally. For the test condition of the signal control

board and the board, the action can be directly determined by the control panel. So after the connection is complete, the debug circuit can be tested on the whole system.

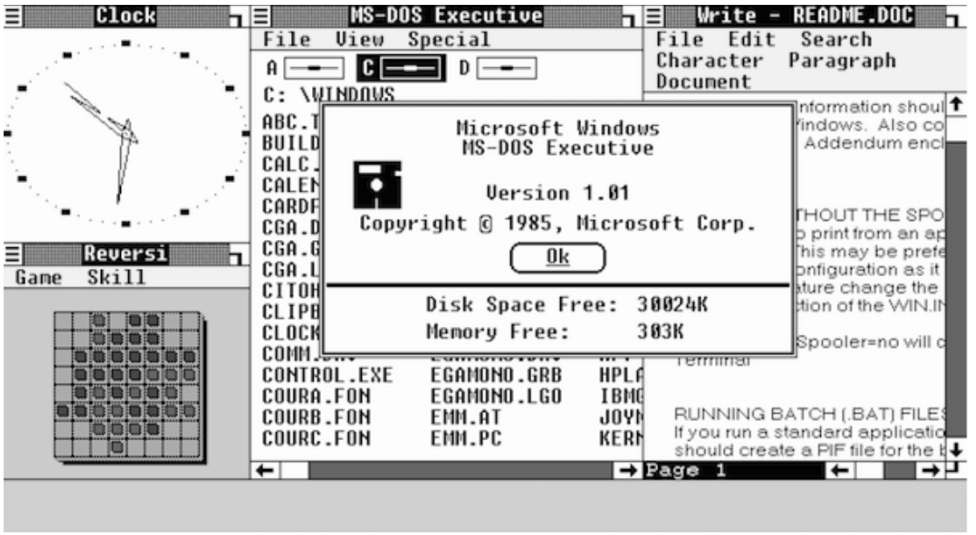

Fig. 3. Debugging process of railway signal simulation system based on microcomputer interlocking

Finally, the signal control board, the switch control panel and the serial port module are debugged. Simulation system can be called in the simulation of the whole process of the PC system, as shown in Fig. 3. The host program is running, the start and end buttons are clicked to observe the signal and relay action. Compared with the interlock table, it is found that the signal is consistent with the relay action and interlock table information, indicating that the whole system function is good, and the module is working properly.

5. Conclusion

The microcomputer interlocking analog signal control system is the future development direction of railway station signal control. Its application has obvious advantages. Through the design and development of the corresponding PLC software, the signal control operation can be realized, and the system design can make appropriate changes according to the different railway station conditions. It is found that its performance is good after evaluation. The microcomputer interlocking system was firstly introduced in this paper. Then, the design of microcomputer interlocking control system was studied. And the simulation system of railway signal based on microcomputer interlocking was studied and debugged. However, at present, the research of computer interlocking signal control system is still at the primary stage, and a lot of professional knowledge is not known to the public. Therefore, the combination of hardware and software can be used to achieve the control of the station

signal. With the continuous deepening of scientific research, it is believed that in the near future, all of the domestic railway station signal control system can achieve computer interlocking simulation control. Due to the limited time and ability, there are some deficiencies in this paper. For example, due to the uneven development of railway in various regions, the results of this study may not be suitable for other areas, thus needing further study.

References

[1] H. Dong, B. Ning, B. Cai: *Automatic train control system development and simulation for high-speed railways.* IEEE Circuits and Systems Magazine *10* (2010), No. 2, 6–18.

[2] Y. H. Wang, H. X. Liu, B. F. Xie, X. M. Zhang: *Study and realization of automatic test simulation system of computer interlocking software.* China Railway Science (2004), No. 2.

[3] K. Akita, T. Watanabe, H. Nakamura, I. Okumura: *Computerized interlocking system for railway signaling control: SMILE.* IEEE Transactions on Industry Applications *IA-21* (1985), No. 3, 826–834.

[4] X. Wang, T. Tang, Y. Huang: *Design and realization of interlocking station of urban railway transportation train operation control simulation platform.* Journal of System Simulation (2006), No. 12, 3407–3410.

[5] B. Ning, T. Tang, H. Dong, D. Wen, D. Liu, S. Gao, J. Wang: *An introduction to parallel control and management for high-speed railway systems.* IEEE Transactions on Intelligent Transportation Systems *12* (2011), No. 4, 1473–1483.

[6] V. Chandra, M. R. Verma: *A fail-safe interlocking system for railways.* Journal IEEE Design & Test *8* (1991), No. 1, 58–66.

[7] X. Wang, T. Tang: *Design and realization of train operation control system onboard MMI based on UML.* Journal of System Simulation (2006), No. 2, 338–342,361.

[8] E. Roanes-Lozano, A. Hernando, J. A. Alonso, L. M. Laita: *A logic approach to decision taking in a railway interlocking system using MAPLE.* Mathematics and Computers in Simulation *82* (2011), No. 1, 15–28.

[9] J. Yang J, M. Li: *Research on railway unterlocking software modeling based on UML and Petri net.* Computer Engineering (2006), No. 11.

[10] D. B. Turner, R. D. Burns, H. Hecht: *Designing micro-based systems for fail-safe travel: For reliable control of railroads, aircraft, and space vehicles, designers are harnessing the power of the microprocessor.* IEEE Spectrum *24*, (1987), No. 2, 58–63.

[11] M. R. Verma, V. Chandra: *The design and development of a fail safe interlocking system using microprocessors for Indian Railways.* Proc. IEEE Region 10 International Conference TENCON'89, 22–24 November 1989, Bombay, India, IEEE Conference Publications (1989), 511–514.

[12] G. Zhu: *Realization of k-steps pervasion search algorithm in generating the interlock route.* Microcomputer Information (2008), No. 21.

[13] T. Y. Shi: *A general framework of information system of high-speed passenger railways.* Journal of Transportation Systems Engineering and Information Technology (2005), No. 1.

[14] A. H. Cribbens, M. J. Furniss, H. A. Ryland: *An experimental application of microprocessors to railway signalling.* Electronics and Power *24* (1987), No. 3, 209–214.

[15] Z. Yang, J. Xi, J. Miao, Y. Yong, Q. Sun: *A research on simulation system of train running and organization.* Journal of the China Railway Society (1998), No. 6.

Received May 22, 2017

Acta Technica *62* No. 1A/2017, 321–330

Research and application of ASP technology in dynamic web page design

Hu Rongqun[1], Li Wenying[1]

Abstract. With the rapid development of modern network technology, dynamic web page has become the mainstream in today's web production of electronic commerce enterprises. In view of this, the characteristics and performance of dynamic web page design based on ASP technology were studied in this paper. The characteristics and performance of the dynamic web pages in ASP technology were analyzed by improving the access performance of the large dynamic web database, the decision diagram, the types of the data packet structure, the logical functions and the functions of the page. The results show that under the support of ASP technology the decision diagrams can express the database information clearly at the same time, which provides flexible and fast information exchanges, secondly, the efficiency of data paging is improved obviously and the database is greater, and the effects are more obvious.

Key words. ASP technology, dynamic web page design, application.

1. Introduction

With the in-depth application of Internet and the development of ASP technology and database technology, on the one hand, people in the world wide web are urgent to access and release a large amount of information, and most of these information exist in database; On the other hand, rich and colorful multimedia information and a large number of multi-format data cannot get solution through traditional database technology. Therefore, the combination of ASP technology and database technology is the inevitable trend of the development of computer network technology and it is also the key point of the Internet applications [1].

ASP script on the server execution and it can be spread to the user's browser just through the ASP implementation results in the generation of the conventional HTML code, which can avoid the loss of writing program annihilated by the others, and it also can guarantee the safety of the source code. Third, it has higher execution efficiency [2]. ASP can connect with SQL server, Oracle, Access, VFP and other database, and it uses some special techniques of collections of objects such as ADO,

[1]Nanchang Institute of Technology, Nanchang, Jiangxi, 330044, China

and they are used in the same process on the server, so it can deal with the page requests of customers faster and more effectively [3].

The remainder of this paper is organized as follows. The second chapter briefly introduces the ASP dynamic server page technology and related knowledge of background database of ASP (Dynamic Server Page Technology) dynamic web page. The third chapter introduces the research methods through the improvement of the access performance of large dynamic web database, the decision diagram, the data packet structure type, the logical function, the paging function and so on. In the fourth chapter, based on the analysis results of the sample data, the performance of dynamic web page design based on ASP technology is studied and analyzed. The fifth chapter is the conclusion.

2. State of the art

2.1. ASP dynamic server page technology

ASP technology (active server pages technology) is a kind of open scripting environment developed by the Microsoft that runs on the server side, and it closely connects with script development and improves the flexibility of programming, which reduces the difficulty of development [4]. The code is interpreted at one end of the server, and the contact server is responsible for all the script processing, and it generates standard web contents to the browsers [5]. So there is no specific requirement for the client browser and the source code will not be transmitted to the other browsers, which makes the technology have a wider application prospects [6].

ASP file is a plain text format, so you do not need to compile and you can directly run it on the server, so ASP application is analyzed in the Web server, and the browsers only receive and process pure HTML flow. In the entire process, the browser completely does not distinguish HTML and ASP pages, and it does not know how to deal with the ASP server, but the ASP program is transparent for the browsers. Strictly speaking, people should not say "dynamic pages" and "static pages", because the "dynamic state" and "static state" are actually collection terms that are related to the concepts of the database, so the correct statements are "dynamic web site" and "static web site", and the page belongs to a single term, so we can say that this page is dynamic or static, which means whether it has a real-time link with the database.

2.2. ASP (Dynamic Server Page Technology) dynamic web page background database

Formal dynamic web sites must have database service support in the background. The so-called "database (Date Base) base" refers to the record data files that are stored according to a certain format. In daily life, personal address book, company accounts thin, customer lists, the details of check and performance are database. They have not only fixed format but also characteristics, and they can be recorded with tabular forms. Because the database has the advantages of automation man-

agement, rapid query and statistics and it strengthens the original keyword to carry on the data processing, storage and sampling, so as to ensure the integrity of reference of the dynamic web database, which is stored on the server side, and from the beginning of the compilers, it is helpful to achieve the updating, inserting and deleting function of dynamic web page design based on ASP technology.

Background database of ASP dynamic web page uses SQL Server database management system. The database management system closely integrates the network service, and due to complicated operation of SQL Server and Microsoft's web server IIS, the users do not need complex operation and they can directly use the ODBC or ADO data driver provided by SQL Server, and through the browser they can obtain information provided by SQL server. Secondly, we can use the network environment effectively, so that all the database query actions are focused on the server, and it can effectively reduce the network traffic. Figure 1 shows typical applications of dynamic pages.

Fig. 1. Application of dynamic pages

3. Methodology

Regardless of the distance of the database server, the database administrator can use SQL enterprise managers to manage all the servers in a central location, which will greatly reduce the cost of multiple servers, and it can maintain the dynamic backup of the database at the same time, and it still has the ability to provide numbers, which allows users to update or read the database content to cope with the requirements of the task of oriented programs. In addition, distributed transaction processing of Server SQL allows the workstation to access data on several SQL Server servers at the same time, and it also allows developers to design distributed applications. According to the analysis above, ASP technology in the key technologies of dynamic website mainly includes: display technology of paging of ASP development process, query technology in dynamic web database query process, optimization strategies of dynamic web database access based on dynamic web database and the analysis technique of data packets, and the relation schema is

depicted in Fig. 2.

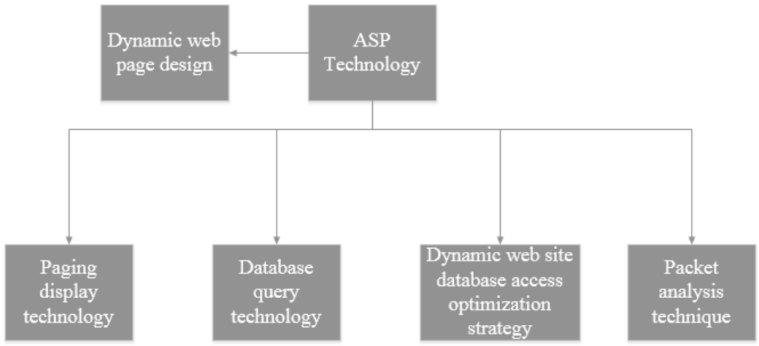

Fig. 2. Frame of dynamic web page design analysis

The traditional C/S structure is generally divided into the client and the server, but with the rapid popularization of Internet, the calculation whose center part is the computer network has been got attention, and two-layer C/S structure has low efficiency and it is difficult to maintain, and the security is poor, which cannot meet the actual needs, so the extension of two-layer C/S structure is the three-layer C/S: the client is used to provide a visual interface for the users, which is mainly responsible for information representation and data collection; application servers usually make responses to the user's requests and carry out certain application logic, which is a bridge of connecting the client and the database volatility; the database server in the operation carries out database management system, which realizes the definition, maintenance, access, update and management of data and responses the requests of application server of data. The three-layer C/S structure has high efficient, and it is easy to maintain and it is very flexible.Based on dynamic web design of ASP, it has the following basic characteristics: first one is the interaction, the page will make changes and responses according to the user's requirements and selection dynamically, and the real-time exchange of data is made too, and the browser, as a client, become a bridge of the dynamic exchanges, and the interaction of dynamic web page will be the development trend in the future. Secondly, it can make automatic updating, which means that it does not need to update the document manually, and it will automatically generate a new page, so that you can greatly save the workload. Third, it will appear different pages when different people visit the same website at the same time.

One of the key problems of carrying out effective on-line man-machine interaction on the dynamic web page is to improve the access performance of the large-scale dynamic web database, which means to reduce the searching time of large amounts of data to meet the complex interaction. Therefore, for the server, the optimization of database access has become an important tool to improve its efficiency. Through the optimization of a variety of query processing options, the most appropriate query strategy can be selected. At present, the research tool of optimization of database

access mainly depends on the query optimization theory of relational database. However, in the query optimization problems such as discovery of knowledge, online interactive services and complex multimedia objects, the optimization strategy cannot meet the requirements of the application.

Based on ASP technology of dynamic web page design, electronic commerce website is taken as an example, this type of website can realize the interaction between users and the database, so as to determine a best choice of products or services. The process of selection is a kind of decision. The decision table can be used to express the selection process easily. Multi-level selection efficiency of decision table method is low and it is not intuitive, so it needs to be converted into a structured approach based on graphics. Decision trees and decision graphs are effective ways to solve the problem.

The decomposition of the database information of the dynamic web pages based on ASP technology can be expressed by the decomposition of the logic function of variable, and the decomposition can be determined by a set of sub function factors. In this way, as long as the sub function is known, the logical function can be determined. The sub function and decomposition of the logical function are defined as follows (x means Factor decomposition of Web Design Based on ASP)

$$f_{\mathrm{c}} = f(x_1, x_2, \cdots x_{i-1}, c, x_{i+1}, \cdots, x_n)\,. \tag{1}$$

The decision diagram is a graph based on data structure mention above, which is directed as a cyclic graph connecting the vertex set and edge set, and each non-terminal vertex is marked by the variable x (x represents the decision variable). The decision diagram expresses the logical structure of the database access. From the root node, users can ask questions, so as to find their interest by going along a path of the web page browsing, and if the users' answer leads to the determination of specific contents of the products, which indicates that the completion of a final decision is made.

The optimization of database access can be achieved on the basis of the decision diagrams, and its essence is to choose appropriate decision variables to reduce the size of decision graph (number of minimization), so as to speed up the query speed and improve the utilization rate of memory at the same time. The formula used is: (a means the rate)

$$H(A) = -\sum_{i=1}^{n} p(a_1) \log 2p(a_i)\,. \tag{2}$$

The conditional probability formula is

$$H(A|B) = -\sum_{i=1}^{n}\sum_{j=1}^{m} p(a_i, b_j) \log 2p(a_i|b_j)\,. \tag{3}$$

According to the above conclusion, firstly, the optimization strategy of decision diagram of database access is carried out according to the following steps:

1. For the given database information, the truth table of the logical function is obtained according to the method described above.

2. The decision diagram is made (each vertex is determined by the current minimum value of the variable basin) through the equation selection variables.

3. A query sequence is formed in accordance with decision graphs.

Secondly, for the dynamic web database based on ASP technology, in this paper, the function of the page display is studied by creating a stored program in the database. The main parameters stored include the following parameters.

1. The current page.

2. The number of records that are set at the current definition of each page, which can be used to modify the number of pages in the page program based on the needs of it. Of course, if the scalability of the program is not considered, each page that has N records can also be directly provided;

3. An output parameter that is derived from the database and records the total number in the current table.

4. Result analysis and discussion

4.1. Decision diagram analysis of dynamic network design based on ASP technology

The benefit of decision diagrams is that it can provide concise and flexible expression and human-computer interaction of dynamic web database information based on ASP technology, especially in the application of online shopping. The classification of database can be in line with people's decision thinking better, and customers can buy goods through the visual navigation of the decision diagram. This paper believes that the method which is constructed by using information theory can be applied to the dynamic e-commerce web page based on ASP, and it also can be widely applied in logic design, computer aided medical diagnosis, artificial intelligence and other related decision-making problems (see Table 1). The first column in the table represents the event set and the second column represents the browsing feature of the product of users, and the third column is the logical function.

Table 1. Analysis of decision graph

S	X$\|x_1 \ldots x_n$	f
S1	1 0 ... 1	1
S2	0 2 ... 2	2
...	...	...
SK	2 3 ... 2	7

The decomposition of ASP technology is shown in the above table. Because these factors can be divided into the speed, redundancy and so on, people can analyze the technology by studying such few factors.

This helps to test the technical efficiency of ASP. On the other hand, SQL Server is allowed to deal with a single distributed processing, and the number of different

server data is updated, which still can maintain the integrity and consistency of the data. If the workstation or any server is invalid, all the changes on the server will be canceled automatically, and the state will be restored to the former state.

4.2. Analysis of the page display of ASP technology in the dynamic web page design

In order to test the new method above, this paper chooses the database tables with different size, and it respectively takes old paging method and the new method that is previously proposed for paging, then we record the time displaying in each page, and the test data and test results are recorded in Table 2.

Table 2. Time spent on the web page from request to display (s)

Data on the page	Traditional paging method	Improved paging method
100	0.5	0.4
500	0.7	0.5
1000	1	0.8
2000	2	1
5000	4	1.5
10000	7	2

From the test results, we can clearly know that the paging speed significantly increases, and the larger the data table is, the more obvious the effects will be when using this paging method. In the dynamic web page based on ASP technology, the new paging method returns only one page of record each time and forms a set of records, in addition, the client can use two-dimensional array to store data without traditional Vernier method that uses rs.next to output Recordset record, and the speed of read has been improved and the database does not use temporary tables, which greatly improves the speed of dump records. Third, using a rolling cursor, and the cursor can complete the positioning only after two operations, and its speed is also greatly improved. In addition, in the processing of tree structure and database operations, you can also use a number of methods to further improve the speed. So ASP technology is widely used in dynamic web page design, and because the ASP technology has driven force and the oriented-object, therefore, the formation of dynamic web page in this design pattern can make data analysis for the browsing preferences of users and other information, which has important significance on creating composite browsing preferences of dynamic pages

4.3. Packet analysis of dynamic web page based on ASP technology

The steps of capture research and analysis of network data packet are as follows: open the form to realize the initialization and automatically obtain the IP address of the machine. If there are multiple cards that can be respectively regarded as objects of getting data packets, then you should bind the Socket, and the local area network captured can get data packet interacted by the local network adapter and

the captured data packets are listed in the form of a list. The contents have elapsed the passing time of data packets, the protocol, source IP, destination IP, source port, and destination port and packet length. The details of the package are listed in Table 3.

Table 3. Details about data packet

Type of information	Value
Start time	2015-7-18 15:55:39
Source address	220.181.131.239.80
Destination address	192.168.0.121:15849
Protocol type	Top
Survival time	47
Version information	4
Header size	20
Message length	40
Priority	Routine
Delay	Normal Delay
Throughput	Normal throughput
Reliability	14319
Check sum	1AF2

In the generation process of actual dynamic page, it is necessary to make treatment after collecting the data packets, like cleaning dirty data or adding incomplete data, to ensure the integrity and consistency of data structure, and the host log and network data packets need the respective unification with log format. We can conclude that current Web database technology mainly achieve the seamless connection between Web and database through the expansion of servers or clients.And ASP is a very ideal tool of making dynamic web pages and web database development in the B/S mode established by the Microsoft, in addition to providing all the features of CGI and ISAPI, there are many significant advantages: first, ASP technology can make operation easily and it uses a simple foot language, and it combines with HTML code, so that it is easy to write and it shortens the development time of dynamic web page, and it supports almost all of the scripting languages. Therefore, the production of ASP file is very simple and you can use any plain text editor, and in writing ASP application, you just need to enclose the script of special markers of ASP without compiling or connection, so you can directly execute on the servers, forming a dynamic web page. Secondly, the security is good and the ASP source code does not leak. Users only need to use the browser to explain the conventional HTML code, and you can browse the web page designed by ASP.

5. Conclusion

This paper discusses the advantages of ASP application in dynamic web page design and expounds the method of making remote maintenance by using ASP technology in the development of dynamic web page. In the display of dynamic web page, it provides a new method: in dynamic web query, the new methods of fuzzy query and multi-keyword query are put forward to guarantee that they can still find the reasonable results in the course of the input of uncertain keywords; in the optimization of access of dynamic web page, constructing decision graph is proposed as a new method.With the help of the concepts of Shannon's information theory, the method can effectively realize the optimal access to dynamic web pages.

The application research of ASP technology in dynamic web page design is divided into two steps. After obtaining the sample data, first of all, the injury data of soccer players are classified and analyzed combined with the details of dynamic web page design (including decision diagrams, paging technology, conditional probability of factors analysis) of ASP (active server pages), and the data packets got in the process of the formation and storage of dynamic pages are analyzed systematically. From the analysis what can be obtained is that the dynamic web site can form the user's page efficiently and rapidly with the new paging method; in addition, in the process of acquiring data packets, it needs protocols between different network layers and the message should be studied and analyzed to obtain the key information for dynamic web page, so thee dynamic web page design based on ASP involves various network protocols, types of data structure, machine language and so on, and it is also an advanced web page with multi-directions that contains computer languages, algorithms and protocols.

References

[1] L. D. Paulson: *Building rich web applications with Ajax.* Computer *38* (2005), No. 10, 14–17.

[2] Y. T. Sung, K. E. Chang, S K. Chiou, H. T. Hou: *The design and application of a web-based self- and peer-assessment system.* Computers & Education *45* (2005), No. 2, 187–202.

[3] M. Eirinaki, M. Vazirgiannis: *Web mining for web personalization.* Journal ACM Transactions on Internet Technology *3* (2003), No. 1, 1–27.

[4] L. T. Lv, J. H. Wan, H. F, Zhou: *Research of not refurbishing and updating data method in AJAX web application.* Application Research of Computers (2006), No. 11, 199–200,223.

[5] C. Greenhow, B. Robelia, J. E. Hughes: *Learning, teaching, and scholarship in a digital age: Web 2.0 and classroom research: What path should we take now?.* Journal Educational Researcher *38* (2009), No. 4, 246–259.

[6] Consumer e-shopping acceptance: Antecedents in a technology acceptance model. Journal of Business Research *62* (2009) 565–571.

Received May 22, 2017

Acta Technica *62* No. 1A/2017, 331–340

Application of 3D printing technology in the production of modern complex structure sculpture[1]

Maomao Liu[1]

Abstract. The development of the information age has brought the digital technology to the artistic creation. 3D printing is usually achieved by the use of digital technology printer, often used in mold manufacturing, industrial design and other fields to be used in the manufacture of models. In view of this, the music teaching mode based on the computer platform was studied and analyzed in this paper. Firstly, the sequential methods and fuzzy comprehensive evaluation methods in the production of modern complex structure sculpture based on 3D printing technology were analyzed. Then the 3D printing was compared with the traditional printing, and the sculpture production process of 3D technology was analyzed. The results show that the 3D printing technology is helpful to the sculpture creation writer who can design the sculpture which is more in line with the modern aesthetics.

Key words. 3D printing technology, modern complex structure, sculpture, production.

1. Introduction

In the history of mankind, the development and progress of science and technology will always affect and even change the field of art. Since modern times, the rapid development of science and technology and the expression of the forms and creative means of art are also constantly enriched and improved. A series of industrial revolutions in modern history have promoted the rapid development of computer and network communication technology, and the computer and the network have become an indispensable part of human life [1]. Computer technology has been involved in almost all areas of human production and life, which has brought great changes to not only the society, but also the field of art, and it has also brought new art forms and creative means to the field of art. Digital art is a new art form that is produced by the application of computer technology in the field of art [2].

Digital art has been integrated into and even replaced some of the traditional art design techniques. Among them, applications of the three-dimensional modeling

[1]School of Ceramic Art, Jingdezhen Ceramic Institute, Jingdezhen, 333001, China

design in three-dimensional video effects, three-dimensional games and animation show a wealth of artistic expression, which has brought opportunities for the sculpture art to enter a virtual space [3]. Art creators use 3D printing technology to realize the reproduction and simulation of the sculpture material, texture and space in the virtual space [4]. In addition, by increasing the contrasts of backgrounds, space environments, sounds, animations and other effects, the digital technology brings us new visual experiences and feelings, which cannot be achieved if we only depend on the traditional technology [5].

The remainder of this paper is organized as follows. In the second chapter, the author briefly introduced the requirement analysis and the related content of the 3D printing technology in the creation of the modern complex structure sculpture. The third chapter introduced the research method, sequence analysis and fuzzy comprehensive evaluation of the 3D printing technology in the production and application of modern complex structures. In the fourth chapter, the 3D printing technology and the traditional printing technology were compared, and then the production process of modern complex structure sculpture based on 3D printing technology was analyzed. Finally, the fuzzy comprehensive evaluation and analysis of the modern complex structure sculpture products based on 3D printing technology were made. The fifth chapter was the conclusion.

2. State of the art

2.1. The demand analysis of 3D printing technology in the creation of modern complex structure sculptures

From the rigorous mathematical logic of the computer, human beings have calculated the points, lines and surfaces that conform to the human aesthetics, which is changed actively, and it can change them within the scope of their ability too [6]. For example, scientists have invented three-dimensional digital software based on mathematical principles [7], so the most complex computing programs have been become the most basic visual elements, so as to meet their own aesthetic rules. The digital technology based on computer can achieve the traditional aesthetic principles in the virtual space [8].

The needs of sculpture creations of 3D printing technology are shown in the following two aspects: firstly, in the usual practice of sculpture creation. By using the three-dimensional model of computer sculpture, it can be marked at any time on the model, so as to get a clear structural analysis, and it can continue to withdraw and move forward at the same time, which is the function that the traditional sculpture cannot achieve [9]. Secondly, in some large-scale sculpture creations, it needs to enlarge the model according to the small draft [101]. In the real world, there are some errors in the data of the scanning model, which cannot reach the precision requirement of large-scale projects. But in the model of the software, its data is very accurate, which can be guaranteed by the proportion of size, so as to enlarge the accuracy of the size [11].

2.2. The creation method of 3D printing technology in the creation of modern complex structure sculptures

In the digital age, the virtual space of the computer is more likely to be appreciated by people. Under normal circumstances, due to the environments, spaces, locations and other restrictions, people cannot be based on their own needs to make specific multi-angle observations. Virtual simulation technology based on the computer can solve this problem, and in this virtual space, people can experience the visual experience they want [12]. The performance of virtual creations means that we can use three-dimensional computer software to easily simulate the objective world in the virtual world, which even can not only reproduce the complex structure of the ancient Greek, but also present the simple structure of the industrial structure. Computer has opened the window with special significance for art, which makes the art form enter another space level, showing the true reproduction of material of the space [13], see Fig. 1.

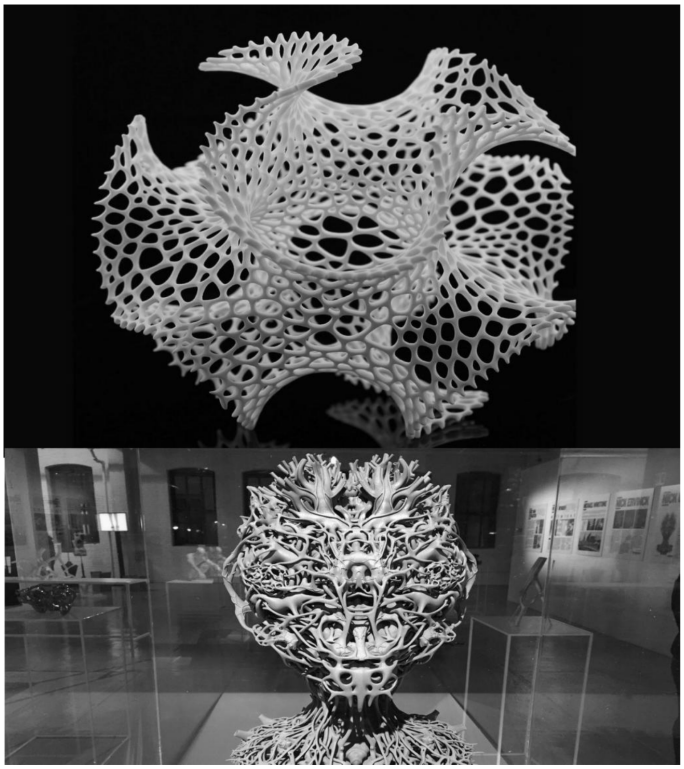

Fig. 1. Creation of the modern complex structure using 3D printing technology

The creative thinking and the thinking of software influence each other, so that the artistic creation activities can get a higher level [14]. The efficient performance means that in order to preserve the authentic social life of ancient times, the artists use reproduction to obtain the preservation of works of art, which is the earliest

way to implement a simple and unaffected hand copy. Hand-copied things will be different from the original object, which is caused by the manual labor error and the shape and material of the object.

3. Methodology

3D digital sculpture is regarded as a new discipline with science and art, and it has a broad space for development. At present, with the rapid development of science and technology, the plastic material and equipment have been improved, so the sculpture community has been formed from three-dimensional engraving software to 3D fast-printing equipment, which is a complete industrial chain. The production processes of the modern complex structure sculpture of 3D printing technology are: firstly, the design of the modern complex structure sculpture will obtain the unity and change, the symmetry and balance, the contrast and harmony, the proportion and scale, the rhythm and cadence and other design knowledge. According to their different structure forms, they will be put in different knowledge bases, and the basic information database of the complex structure will be perfected, and according to the type of the product structure, we will search its corresponding structure design styles. Then the design style is combined with 3D printing technology, and then according to the characteristics of sculptures we will make fine adjustments. Therefore, the design block diagram of the modern complex structure of the 3D printing technology is as follows (see Fig. 2):

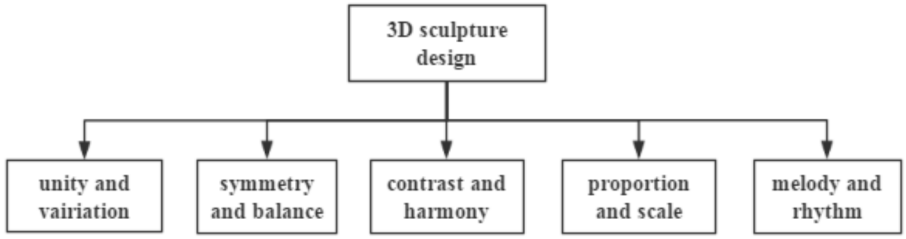

Fig. 2. Design block diagram of the modern complex structure of the 3D printing technology

Due to the design of modern complex structure sculpture works, we start from the production business requirements to determine the elements and contents of the sculpture structure design. Therefore, the design sequences of the modern complex structure sculpture works have certain influences on the effects of the finished products. Sculpture works of modern complex structure are divided into a number of design patterns. First of all, we will finish the results of the design of the color of the complex structure and the three-dimensional structure, then based on the results of the analysis, each color and space structure have their own corresponding conveying effects. According to the requirements of the design goal of the sculpture, we can obtain the visual effects of the image, colors, structures and other sequences, so as to get the corresponding designs and carry out the 3D print tasks.

Digital technology has been introduced into the process of sculpture by some artists; however, most of the researches and attempts at present are to combine the 3D scanning technology with the 3D printing technology or the digital engraving technology and 3D printing technology. And the studies on the comprehensive utilization of the three are still relatively rare, especially in the recreation of the sculpture digital model. In order to combine the three kinds of digital technologies, the key lies in how to convert the 3D model data acquired by 3D scanning to the model data that can be used to meet the needs of digital engraving technology.

In addition, this paper applies the method of fuzzy comprehensive evaluation to make quantitative evaluations on the comprehensive factors (unity and change, symmetry and balance, contrast and harmony, proportion and scale, rhythm and cadence) that are involved in the modern sculpture works of 3D printing. In order to obtain the accurate evaluation information of the modern complex structure sculpture of 3D printing. Here, we can use a set to show the representation, and then we carry out the quantitative analysis: (r means every factor of 3D printing technology)

$$R = \begin{pmatrix} r_{11} & \cdots & r_{1n} \\ \vdots & \ddots & \vdots \\ r_{m1} & \cdots & r_{mn} \end{pmatrix}. \tag{1}$$

Among them, the most representative is 3D printing technology, which extends the creation means of sculptures to the three-dimensional virtual space of the computer. So the creation of sculptures and the sculpture art break away from the limits of materials, and the 3D modeling in virtual space enters the real world, which is shown by the solid material. Among them, the modern digital graphic design is based on the visual communication can be expressed by the decomposition of the logic function, and each decomposition is determined by a set of sub function factors. In this way, as long as the sub function is known, the logical function can be determined. The sub function and decomposition of the logical function are defined as follows: (x means the evaluation factor)

$$f_{\mathrm{c}} = f(x_1, x_2, \cdots x - i - 1, c, x_{i+1}, \cdots, x_n). \tag{2}$$

4. Result analysis and discussion

4.1. Comparison of 3D printing technology and traditional printing technology

In this experiment, the sculpture manufacturer in Guangdong Province was taken as the study sample, and the comparative study on the design of the complex structure of the three-dimensional space of the traditional print design and 3D printing technology was made. The contents of the score included the color, the balance, the symmetry of the structure and the novelty, and the color and balance had 20 points, the symmetry and novelty of the structure had 40 points, and the results are shown in Table 1.

Table 1. Comparison of 3D printing technology and traditional printing technology

	Sub item	Total score	Grade
Sculpture design of 3D printing technology	Color and balance	40	34.7
	Symmetry of structure	30	24.9
	Novelty	30	23.6
	Total score	100	83.8
Graphic design of traditional printing technology	Color and balance	40	31.3
	Symmetry of structure	30	24.6
	Novelty	30	22 5
	Total score	100	78.4

Through the above table, the comprehensive score of 3D printing technology products was higher than the graphic design products of traditional print technology. This showed that compared with the traditional plane printing technology, 3D printing technology had better display effects, and the combination of 3D technology and digital art included not only the visual and auditory art, static and dynamic model art, but also the 3D art and graphic art, and the 3D printing technology included the points of traditional plane printing technology. More and more artists begin to use the computer to make virtual sculpture, and the sculptor can not only design the shape of sculpture by using the computer software, but also simulate the space environment of the sculptures, so as to get better display effects.

4.2. Production of modern complex structure sculpture based on 3D printing technology

The first step of 3D printing process is to use the 3D modeling software, such as AutoCAD, ProE and other computer vector modeling software or reverse engineering reconstruction software to make digital editing on the targeted products, so as to print the "original manuscript". Subsequent use of the same 3D printer driver which is regarded as the layered slice software will be built into a number of 3D digital models with the thin layer, and the thickness of each layer depends on the properties of the spraying materials and 3D printing precision, which usually is in ten micrometers to hundreds of micrometers. After the completion of the preparation work, it will enter the printing process, and according to the different characteristics of the printing products, it can choose different printings. After the completion of the printing, it also needs to print out the 3D model for post processing. The production processes of modern complex structure sculpture based on 3D printing technology are shown in Table 2.

This is what we call the software thinking, which affects the creative thinking of

the artist in a certain extent. This effect produces two interactive processes: the active exploration of the creator; the new thinking of the creator brought by the software. The performance of interactive creations is to generate a variety of other shapes by using the digital computing of the software, and the sculptor will refer to this style, which can bring inspiration to the creators and stimulate the creative and active creations. Secondly, in the use of computers for sculpture creations, it will produce many unexpected and good art forms, and these form are usually in the scopes of thinking that are unimaginable for the sculptor.

Table 2. Production process of modern complex structure sculpture based on 3D printing technology

Data acquisition and processing of the sculpture model	Scanning sculpture model
	Point data processing
Processing 3D model scan data	Using 3D technology to obtain low modulus
	Mapping model
	Two sculpture creation
3D technology will produce sculpture works	Model slice
	Print model

4.3. Fuzzy evaluation of the modern complex structure sculpture products of 3D printing technology

In this experiment, we took the modern complex structure sculpture products in Guangdong Province as the research sample, and the effects of complex structure sculpture were divided into five levels. At this time, the evaluation factors and the fuzzy relations between the set of comments can be represented by using the evaluation matrix, and the evaluation factors set = (unity and change, symmetry and balance, contrast and harmony, proportion and scale, rhythm and cadence). The evaluation grade set = (the ultimate expression of the modern digital theme, the better expression of the modern digital theme, a part of the expression of the modern digital theme, less expression of the modern digital theme, far away from the modern digital theme), and the fuzzy evaluation form of the modern complex structure sculpture products of 3D printing technology is shown in Table 3.

Since we knew that it is the kind of duplication precisely that makes the ancient art become more primitive and unique. Because the digital technology itself has the function of data storage and saving, so it is convenient for the creators to observe the previous model in the creation of the similar art works, and through the adjustment and modification, people can accelerate the work efficiency of the creator. The following figure is the creation of the modern complex structure of 3D printing technology. So digital sculpture and traditional sculpture follow the principle of common aesthetics, and it is very important to introduce the former to the latter [15].In the information age, the computer technology gives infinite possibilities to

the art and makes its creation and expression forms have diversified tends. In the art of sculpture, the three-dimensional digital software technology is involved, so that the sculpture with a new face is shown in front of everyone

Table 3. fuzzy evaluation form of the modern complex structure sculpture products of 3D printing technology

Evaluation factors		Evaluation level				
		Ultimate expression of the modern digital theme	Better expression of the modern digital theme	Part of the expression of the modern digital theme	Less expression of the modern digital theme	Far away from the modern digital theme
Unification and change	0.11	0.5	0.2	0.2	0.1	0
Symmetry and equilibrium	0.13	0.5	0.2	0.1	0.2	0
Contrast and harmony	0.16	0.3	0.2	0.4	0.2	0
Proportion and scale	0.18	0.4	0.3	0.2	0.1	0
Rhymes and rhythms	0.20	0.4	0.3	0.1	0.2	0.1

From Fig. 3, in the fuzzy evaluation results of the modern complex structure sculpture product of the 3D printing technology, the ratio of the ultimate expression of the theme of the modern digital reached 50 %, especially in the unity and change and the symmetry and balance. In contrast and harmony and scale and scale evaluation, the ultimate expression of the theme of the modern digital reached more than 30 %. Overall, in modern complex structure sculpture products of 3D printing technology, 70 % of the 3D printing products in the symmetry and balance, unity and change had the ultimate expression of modern digital theme, and the design that can express the theme of modern digital theme was more than 80 %, and only 10 % of the modern digital graphic design in the scale and rhythm deviated from the modern digital theme. Thus, 3D printing technology was helpful to improve the unity and change, symmetry and balance, contrast and harmony, scale and rhythm of the modern digital complex structure sculpture products.

5. Conclusion

The sculpture is the use of different plastic materials through the method of carving, so as to create the artistic image that has a sense of volume, and it also can be seen and touched, which can map some social phenomenon or express the aesthetic and emotion of individual artists. Digital sculpture is a small branch of digital art.

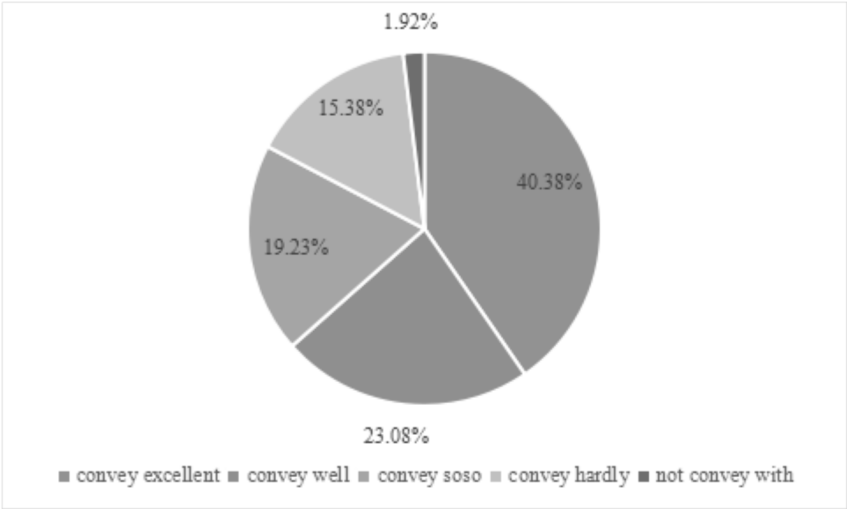

Fig. 3. Effect statistics of the modern complex structure sculpture product of 3D printing technology

Digital sculpture is the combination of 3D printing technology and traditional engraving art, which uses computers for artistic creation. Digital sculpture, as a newly emerging subject of art and science, has wide development spaces and application fields.

The research on the application of 3D printing technology in the production of modern complex structure sculpture was divided into three steps. Firstly, the sequential methods and fuzzy comprehensive evaluation methods in the production of modern complex structure sculpture based on 3D printing technology were analyzed. Then the 3D printing was compared with the traditional printing, and the sculpture production process of 3D technology was analyzed. From the experiment what can be obtained was that the 3D printing technology fitted the actual characteristics of the modern digital technology, which was conducive to bringing new thinking inspirations for complex sculpture designs, and it could inspire the creation of the sculptor.

References

[1] M. M. Tseng, J. Jiao, M. E. Merchant: *Design for mass customization.* CIRP Annals - Manufacturing Technology *45* (1996), No. 1, 153–156.

[2] J. Dumas, J. Hergel, S, Lefebvre: *Bridging the gap: Automated steady scaffoldings for 3D printing.* Journal ACM Transactions on Graphics (TOG) *33* (2014), No. 4, 98.

[3] C. B. Highley, C. B. Rodell, J. A. Burdick: *Direct 3D printing of shear-thinning hydrogels into self-healing hydrogels.* Advanced Materials *27* (2015), No. TOC 34, 5075 to 5079.

[4] B. C. Gross, J. L. Erkal, S. Y. Lockwood, C. Chen, D. M. Spence: *Evaluation*

of 3D printing and its potential impact on biotechnology and the chemical sciences. Analytical Chemistry *86* (2014), No. 7, 3240–3253.

[5] V. L. Colvin: *The potential environmental impact of engineered nanomaterials.* Nature Biotechnology *21* (2003), No. 10, 1166–1170.

[6] S. H. Ahn, K. T. Lee, H. J. Kim, R. Wu, J. S. Kim, S. H. Song: *Smart soft composite: An integrated 3D soft morphing structure using bend-twist coupling of anisotropic materials.* International Journal of Precision Engineering and Manufacturing *13* (2012), No. 4, 631–634.

[7] S. J. Hollister: *Porous scaffold design for tissue engineering.* Nature materials *4* (2005), No. 7, 518–524.

[8] J. F. Xing, M. L. Zheng, X. M. Duan: *Two-photon polymerization microfabrication of hydrogels: An advanced 3D printing technology for tissue engineering and drug delivery.* Chemical Society Reviews *44* (2015), No. 15, 5031–5039.

[9] C. Wu, W. Fan, Y. Zhou, Y. Luo, M. Gelinsky, J. Chang, Y. Xiao: *3D-printing of highly uniform $CaSiO_3$ ceramic scaffolds: preparation, characterization and in vivo osteogenesis.* Journal of Materials Chemistry *22*, (2012), No. 24, 12288–12295.

[10] B. Sanz-Izquierdo, E. A. Parker: *3D printing technique for fabrication of frequency selective structures for built environment.* Electronics Letters *49* (2013), No. 18, 1117–1118.

[11] F. J. O. Varum, H. A. Merchant, A. W. Basit: *Oral modified-release formulations in motion: The relationship between gastrointestinal transit and drug absorption.* International Journal of Pharmaceutics *395* (2010), Nos. 1–2, 26–36.

[12] L. Ouyang, R. Yao, X. Chen, J. Na, W. Sun: *3D printing of HEK 293FT cell-laden hydrogel into macroporous constructs with high cell viability and normal biological functions.* Biofabrication *7* (2015), No. 1, 015010.

[13] S. D. Laycock, G. D. Bell, D. B. Mortimore, M. K. Greco, N. Corps, I. Finkle: *Combining X-ray micro-CT technology and 3D printing for the digital preservation and study of a 19th century Cantonese chess piece with intricate internal structure.* Journal on Computing and Cultural Heritage *5* (2012), No. 4, 13.

[14] T. Billiet, E. Gevaert, T. De Schryver, M. Cornelissen, P. Dubruel: *The 3D printing of gelatin methacrylamide cell-laden tissue-engineered constructs with high cell viability.* Biomaterials *35* (2014), No. 1, 49–62.

[15] W. S Tan, C. K. Chua, T. H. Chong, A. G. Fane, A. Jia: *3D printing by selective laser sintering of polypropylene feed channel spacers for spiral wound membrane modules for the water industry.* Virtual and Physical Prototyping *11* (2016), No. 3, 151–158.

Received May 22, 2017

Acta Technica *62* No. 1A/2017, 341–350

Application of X optical intelligent detection technology in the field of electronic production

Hou Yan[1]

Abstract. With the rapid development of information technology, the application of electronic technology is more and more extensive, rapid detection of electronic production needs of the field has become increasingly strong. Based on this, research on the application of X optical intelligent detection technology in the field of electronic production was carried out. In this paper, the electronic production in the field of traditional security model was introduced firstly, and then the principles and characteristics of application of X intelligent detection technology in electronic production in the field were discussed, finally the application of X intelligent detection technology in electronic production in the field was introduced. The test results show that the application of X optical intelligent detection technology in the field of electronic production is more realistic and reasonable. It has a broad application prospects, can provide researchers with a new way of thinking.

Key words. X light, intelligent detection technology, electronic production, security model.

1. Introduction

With the rapid development of X technology, the application of X based optical technology is more and more extensive, but this makes it necessary for people to quickly and effectively detect electronic products. Especially in the last century in nineties, the rapid development of technology has greatly accelerated the pace of social information. However, the openness of technology also provides convenience for the technical application. Therefore, it becomes a big problem to be solved in the field of electronic production for the application of X optical intelligent detection technology in the field of electronic production. Based on this, we have carried out research on the application of X optical intelligent detection technology in the field of electronic production. In this paper, the electronic production in the field of traditional security model was introduced firstly, and then the principles and characteristics of application of X intelligent detection technology in electronic production

[1]College of Electrical Engineering, Henan University of Technology, 450001, China

in the field were discussed, and finally the application of X intelligent detection technology in electronic production in the field was introduced. The test results show that the application of X intelligent detection technology in electronic production in the field are more realistic and reasonable, it can better meet the requirements of electronic engineering optimization, so this method has very strong practical value. There is strong evidence that some X light can recognize and respond to stimuli [1]. Research shows that X light can reflect timely after stimulating the signal [2]. In this paper, an effective exponential model is established to prove the application of X in computer [3]. In this paper, we mainly study the construction process of the specific substance detection in the field of electronic production [4]. In this paper, the detection method can be used to detect the biological virus derived from the base [5].

2. State of the art

Optoelectronic information technology is a kind of high technology, which combines optical technology, electronic technology, computer technology and material technology. Photoelectric detection technology is the most important part of optoelectronic information technology. The characters conclude high precision, fast speed, non-contact, high bandwidth and large information capacity, high efficiency of information, high degree of automation. Technology is one of the most important means and methods to promote the development of information science and technology. It is widely used in industry, agriculture, military, aerospace, and everyday life, including light conversion technology, optical information acquisition and optical information measurement technology, optical processing technology measurement information, image detection technology, optical scanning detection technology, optical fiber sensing detection technology and system. X ray technology has been widely used in the national economy, national defense, scientific research and other fields, it has become an important technical support for the new technological revolution and information society. Optical detection technology and electronic technology achieve a variety of products, the combination of detection is the leading science in twenty-first Century, and the whole technology development has played a huge role in promoting the development. Because it covers a large number of science and technology, so its development has led to the development of much science and technology, and in the process of communication and development, a huge photoelectric detection industry is formed. Many foreign scholars and experts have been particularly concerned with the research of analog electronic circuit testing and fault diagnosis. In 1962, Berkowitz first proposed the concept of analog electronic circuit to solve the problem, and opened the research of analog electronic circuit fault diagnosis. In 1979, Navid demonstrated sufficient conditions for the solution of the linear resistive element, which laid a theoretical foundation for the fault diagnosis of analog electronic circuits. In eighties, researchers from the actual situation of the fault, the focus of all parts of the solution will be transferred to the diagnostic part of the value of the parts to determine the fault area or failure parts. During this period, the typical method is the method of fault element delimitation and node failure. From

then on, analog electronic circuit fault diagnosis develops towards the direction of more practical multiple faults. For large integrated electronic circuits, Salama, who first proposed the network level network decomposition diagnosis method in 1984. However, the method requires that all the nodes in the network are reachable, and all the related nodes are removed. The tear of the electronic circuit is destructive and is not allowed in the actual diagnosis. Since then, many scholars have perfected and complemented this approach. However, most of the KCL equations are based on the large amount of calculation, slow diagnosis, application is very limited. Intelligent information processing technology continues to develop and in-depth, and solve the traditional diagnostic methods of analog electronic circuits in the component tolerances and nonlinear, electronic circuit diagnosis and other problems to provide a powerful tool. Since nineties of last century, neural network, expert system, fuzzy theory has been used to simulate the fault diagnosis of electronic circuits. Expert system fault diagnosis method is mainly reflected in the following points: analog electronic circuit fault and the relationship between the symptoms is easy to express through the intuitive and modular rules. The expert system based on production rules allows to add, delete or modify some rules to ensure the real-time and effectiveness of the diagnostic system. To a certain extent, it solves the problem of uncertainty, and can give the conclusion of the human language habit and has the appropriate explanation. In this paper, the detection of electronic products is accomplished by generating a detector [6]. In this paper, there are two main methods of detection, respectively, on behalf of the two models. The research of this paper is of high accuracy. Single electron detection method has high accuracy. At present, the use rate of electronic products in our country is greatly increased, and there is a great demand for electronic testing methods. This report describes some of the characteristics of the monitoring system, explores some of the basic model. Detection of mine construction is difficult to fully describe the soft tissue sometimes. Some experimental results show that the detection of computer is especially difficult to control, but it can be overcome by special methods. The current detection of electronic products mainly focuses on several aspects. This paper is mainly about the characteristics of some special light on electronic production.

3. Methodology

3.1. Security model in the traditional field of electronic production

A security model for the field of electronics production is used to describe the core part of the security environment in the system environment. The basic components of the security model in the field of electronic production are: entity and access control. Entities are further divided into subject and object. All of the electronic security products, no matter how complex, they can be abstracted from the basic model of security in the field of electronic production, it follow some basic principles and basic, join the I & A subsystem and audit subsystem in the object access on the basic constitute of electronic products, the traditional security model, as shown

in Fig. 1.

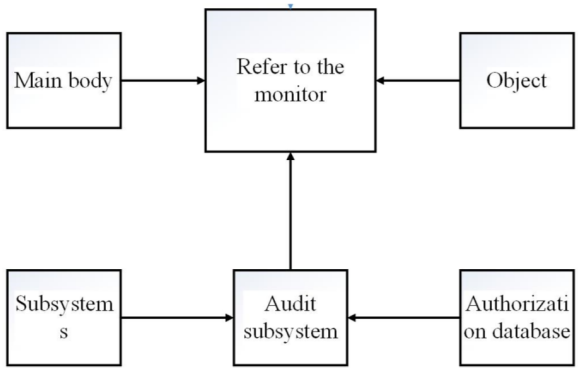

Fig. 1. Traditional security model

Among them, the control monitor is also known as a security kernel, is the main body. The control monitor is primarily used to control the subject's only way to access the object when it makes a request to access the object. The control monitor has two main functions: the first is a comparison function used to calculate and evaluate the access request issued by the main one. When the subject issues an access request, the control monitor will refer to the authorization database to determine whether to accept or reject the received request; the second is the authorization function to control the change to the authorization database. Control monitor not only controls the subject how to access the object engine, but also controls the change of access rules. In addition, the security kernel, identification and verification system (I & A) can identify and verify the subject and object. Audit subsystem, the need to monitor the activities of the control monitor, it can determine whether the control monitor operating normally; the need to store the access control rules, which indicates that the access is acceptable or object or deny the authorized database. By adding the subject, object and the I & A, based on safety kernel, three parts enhanced audit and authorization database, security model security of electronic production areas have stronger. Among them, the security kernel and enhance the components to each other trust each other. The traditional security model in the field of electronic production defines the interaction between entities and entities and controls the rules to achieve confidentiality, integrity and availability of security objectives. Figure 2 is the actual application of X light in the field of electronic production.

3.2. Research on the principle and characteristics of the application of X optical intelligent detection technology in the field of electronic production

According to Stefan-Boltzmann's Law, any object whose temperature is higher than the absolute zero exhibits X - ray radiation and the radiated power W is proportional to its absolute temperature T of the four power. In the case of electronic equipment in the work of the normal circumstances, each component will pass a cer-

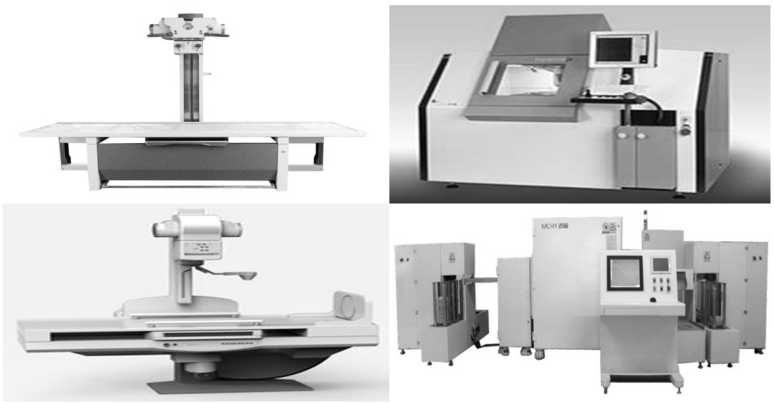

Fig. 2. X-ray in the field of electronic production of the actual application

tain current, and consume a certain amount of power, to achieve thermal balance; there is a clear working temperature. When the temperature of the component exceeds the ambient temperature, there will be three kinds of heating processes: conduction, convection and radiation, in which the heat radiation is expressed as X - ray radiation. The power of dissipation and the power of the radiation or the absolute temperature of the object are proportional to the two. Measuring the temperature of the radiating element can provide all the information which is required to determine the thermal and thermal stress characteristics of the element. Thermal interactions in electronic devices are very complex. The electronic components only heat when the temperature is higher than the ambient temperature. Due to the heat conduction, convection, radiation, X - ray radiation components may be much more complex, the surface temperature range of the component must be measured using X - ray equipment.

Resistance is the power element. In electronic equipment, a large number of resistive elements form the main source of X - ray radiation. Through its own dissipation of 20 % of the resistance of the heat, the remaining 80 % of the heat from the lead ends (each 40 %) by conduction away, So the heat distribution of the measured X - ray shows that the center temperature is the highest, and the direction of the gradual descent toward the two ends. So when the resistance itself is defective, or turns off, welding, heat distribution symmetry change of semiconductor devices is very sensitive to the temperature component, the higher the temperature, the X radiation emission contains non coherent radiation and compound radiation of two. The center of the transistor temperature is the highest, gradually reduced to the surrounding. The shell temperature of the transistor increases linearly with the increase of power consumption. The same type of different transistors have different emissivity, different surface temperature, different lead length and good substrate to substrate welding quality, but also the temperature of the device has an impact on it. The general power of 5∼10 minutes can rough measurement of transistor temperature, accurate measurement needs power 0.5 h to reach thermal equilibrium. Before reaching the peak temperature of second, the transistor can be

used to measure the peak value of the X - ray measurement device, which can be used to measure the peak temperature of the X - ray radiation. Integrated circuits in scale and large scale integrated circuits, it has complex internal structure, a number of resistance and semiconductor devices, the resulting in X - ray radiation is also more complex. The power consumption of IC is different from that of the actual working state, and the temperature of the integrated circuit package of different models is sometimes significantly different. From the testing point of view, the thermal distribution of the integrated circuit is mainly concentrated in the middle, and the temperature of each component of the same type of integrated circuit under the same operating conditions is high because of the difference between the packages.

3.3. Application of X optical intelligent detection technology in the field of electronic production

Electronic equipment design, including electrical design, component selection, product design, and many of these problems are related to heat, the thermal design of equipment must be considered. X ray technology can be used to solve many conventional detection technology which is cannot find the hidden dangers, while these problems lead to premature failure of equipment, it mainly due to the circuit design of the circuit design, according to the equipment reliability requirements, the assignment of each component of the working load of the size allows the working temperature. If the component is fully loaded or overloaded, premature failure may occur, and the heat sink must be fitted with a larger load of components, all of which must be considered by the designer at the design stage.

Once the design is completed, the designer must check the rationality of his design, using X ray detection technology can quickly provide all the components of the working temperature, help the designers to check the change, help us eliminate the hidden dangers in the radar design repository backup board, we found that although we use the same number of printing plates and the same component manufacturers in the same types of power supply, there still some big difference in temperature difference and individual temperature, especially the integrated circuit, complete function, high temperature is bound to shorten the service life of the components. In order to optimize the design, the assembly must be screened to remove more power consumption components, namely, the overheated. This work with the traditional detection is very troublesome, and is difficult to do, but with X ray detection is very easy to design the circuit, so product designers need design the circuit board, layout of all elements and connections.

With the miniaturization of product requirements, more and more intensive components will come out, designers often view things only from an aesthetic angle, when the component neatly, the individual space constraints, the radiator may not be used, finally the following questions will appear: Large components, high temperature and heat radiation will affect the power consumption of adjacent components in a low way, so the load and temperature of these parts is increased; Because the power consumption of the component is not installed in the radiator, the heat radiation is not very good, and the component life is shortened greatly. Using X ray technology can help designers to change the design to achieve the best calculation method,

calculation of stress components are comprised by components of the calculation of current and power, and then according to the ambient temperature, the size of the internal components of the working temperature is calculated. This method is not accurate enough. Other methods of direct temperature measurement are cumbersome, not only subject to many limitations, but also do not work. In addition, due to the limited data available at the measurement point, sometimes severe points are missed. X ray detection technology without any restrictions and any risk, we can quickly get the temperature information of all parts, can accurately measure the actual surface temperature, it can be used to calculate the stress components, provide accurate thermal parameters, which is a valuable tool for stress analysis.

We assume that the variation range of I or U of the electronic circuit is small, normal and large, and the symbol L, N, M, is used. Therefore, according to the failure mode of each component, the sample data is specific as shown in Table 1 and Table 2.

Table 1. The first group pickup

L	N	M
0.02	0.95	0.12
0.03	0.84	0.15
0.04	0.93	0.14

Table 2. The second group pickup

L	N	M
0.08	0.95	0.11
0.05	0.85	0.19
0.06	0.94	0.09

According to each value of the first or second group of each component, the corresponding circuit frequency response curve is sampled once, and as a neural network input. Network output status uses two states: 0 (fault) 1 (normal). If both L and M are equal to 1, the component is normal.

Fault diagnosis and location of analogue circuits based on classical two- layer perceptron. BP algorithm is used in the sigmoid transfer function, the output layer neurons using linear transfer function. Set up

$$y = g\left(\sum_{i=1}^{n}\left(K_i F_i - \theta\right)\right). \tag{1}$$

Here, K_i is the weight and F_i is the input. Symbol θ is the limit value and $g(x)$ is the transfer function.

4. Result analysis and discussion

When the index system is set up, we need to reestablish the weight of each index. First invite experts to score, and then sort the results. Second, the sort after the results of the 22 comparisons has a distribution of an index of scale. The relative weight of the index and calculation of the weight of the index, of course, here the object is a qualitative indicator. We invited six experts scoring; six were mentor, off campus tutor, electronic Chief Engineer, electronic engineering project chief engineer, electronic engineering project manager, and electronic engineering technology person in charge. They all have professional theoretical knowledge and rich experience in electronic engineering operation, they have a profound understanding of the various types of viruses, so I chose six experts to explore the importance of indicators. Figure 3 is the results of the two items.

The test results show that the application of X intelligent detection technology in electronic production in the field of are more realistic and reasonable, it can better meet the requirements of electronic engineering optimization, so this method has very strong practical value.

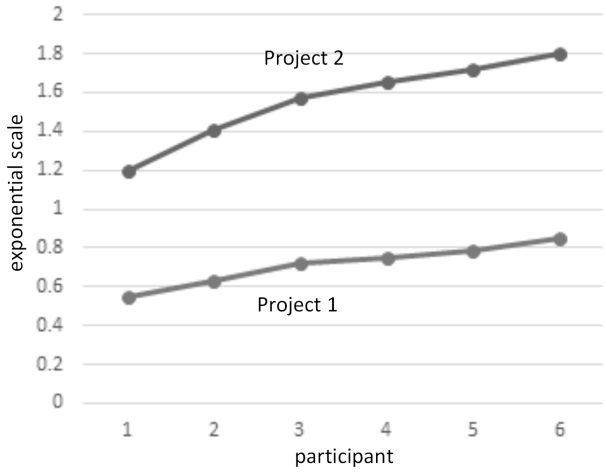

Fig. 3. Results of two projects scoring

5. Conclusion

X optical intelligent detection technology in the field of electronic production has a very important practical significance; it has become one of the new ways to get rid of the current field of electronic production detection difficulties. Based on this, we have carried out research on the application of X optical intelligent detection technology in the field of electronic production. In this paper, the electronic production in the field of traditional security model was introduces firstly, and then the principles and characteristics of application of X intelligent detection technology in

electronic production field were discussed, and finally the application of X intelligent detection technology in electronic production in the field was introduced. The test results show that the application of X optical intelligent detection technology in the field of electronic production is more realistic and reasonable. In a word, we have made an encouraging step in the field of application of X optical intelligent detection technology in the field of electronic production, and have found a new way to detect the current dilemma. In the future, we will further expand the research and application in order to eventually build a strong, powerful testing system. Due to the limitation of time and my ability, there are some deficiencies in the research of this paper. For example, due to uneven development between regions, the various regions of the X optical intelligent detection technology application development level is not the same, the results of this study may not be suitable for other regions. In addition, the object of this study does not address the poor basis of the electronic industry, for this type also need to be further explored and studied.

References

[1] W. Ehrfeld, H. Lehr: *Deep X-ray lithography for the production of three-dimensional microstructures from metals, polymers and ceramics.* Radiation Physics and Chemistry *45* (1995), No. 3, 349–365.

[2] R. Hanke, T. Fuchs, N. Uhlmann: *X-ray based methods for non-destructive testing and material characterization.* Nuclear Instruments and Methods in Physics Research Section A: Accelerators, Spectrometers, Detectors and Associated Equipment *591* (2008), No. 1, 14–18.

[3] G. Acciani, G. Brunetti, G. Fornarelli: *Application of neural networks in optical inspection and classification of solder joints in surface mount technology.* IEEE Transactions on Industrial Informatics *2* (2006), No. 3, 200–209.

[4] C. K. Malek, V. Saile: *Applications of LIGA technology to precision manufacturing of high-aspect-ratio micro-components and -systems: A review.* Microelectronics Journal *35* (2004), No. 2, 131–143.

[5] A. D. Wilson, M. Baietto: *Applications and advances in electronic-nose technologies.* Sensors *9* (2009), No. 7, 5099–5148.

[6] M. Gerard, A. Chaubey, B. D. Malhotra: *Application of conducting polymers to biosensors.* Biosensors and Bioelectronics *17* (2002), No. 7, 345–359.

Received May 22, 2017

Acta Technica *62* No. 1A/2017, 351–360

Web image retrieval based on cloud computing model

Zhifang Zhang[1]

Abstract. As Internet technology has been popularized in people's lives; network data grow at an explosive rate and there is growing demand from users, it is increasingly difficult to obtain demand information from massive data. Since computer and server architecture in distributed computing systems can hardly meet actual demand in the case of the surge in data volume, enterprises and individuals have to overcome many obstacles in the process of obtaining data by using computers. How to build high-performance distributed applications has become a key concern of the vast majority of scholars. For image retrieval, web image retrieval based on cloud computing models has been researched, which has markedly improved the efficiency of retrieval. IBM Almaden Research Center developed the QBIC system for image retrieval in the 1990s and used it for commercial search. It has diverse query features, including color, texture, and silhouette, and enables automatic segmentation of image objects [1]. The QBIC system has a relatively rich set of interfaces that can be interfaced with multiple applications. Virage, Inc. has developed a content-based image search engine that is similar to QBIC and supports retrieval of color, texture, and silhouette features. In addition, this engine can effectively combine image features, so that users can change the query mode by giving different weights in tune with actual demand.

Key words. Cloud computing, WEB, image retrieval.

1. Introduction

As Internet technology has been popularized in people's lives; network data grow at an explosive rate and there is growing demand from users, it is increasingly difficult to obtain demand information from massive data. Since computer and server architecture in distributed computing systems can hardly meet actual demand in the case of the surge in data volume, enterprises and individuals have to overcome many obstacles in the process of obtaining data by using computers. How to build high-performance distributed applications has become a key concern of the vast majority of scholars. For image retrieval, web image retrieval based on cloud computing models has been researched, which has markedly improved the efficiency of retrieval. IBM Almaden Research Center developed the QBIC system for image retrieval in

[1]Ordos Vocational College, Inner Mongolia Ordos, 017009, China

the 1990s and used it for commercial search. It has diverse query features, including color, texture, and silhouette, and enables automatic segmentation of image objects [1]. The QBIC system has a relatively rich set of interfaces that can be interfaced with multiple applications. Virage, Inc., has developed a content-based image search engine that is similar to QBIC and supports retrieval of color, texture, and silhouette features. In addition, this engine can effectively combine image features, so that users can change the query mode by giving different weights in tune with actual demand.

TinEye is a reverse image search engine. Users can find out where an image came from only by inputting the image in the software. Compared to traditional image search software, TinEye is more accurate. It can only retrieve images that have been indexed in the database, and cannot retrieve unindexed images, which means the search will return no results. ImageRover can use themes as a clue for browsing, and is equipped with the traditional keyword search function, which means to search relevant content by entering keywords in the search bar. In addition to precise search, the system is also capable of fuzzy searching, which is to look for contents similar to keywords in the webpage [2].

2. Materials and methods

2.1. Overview

Cloud computing is a new information resource processing model that relies on back-end computer capabilities. It connects many end-users to the system by interface means which are different from traditional ones, thereby achieving multiple resource retrieval functions [3]. Users can use this model via the Internet, which can reduce costs of background operations and maintenance. Moreover, suppliers only need to install a unified set of hardware and software systems and develop a network environment that is suitable for all users. In this case, many users can use this platform.

Hadoop is a distributed system foundation framework. When using Hadoop, users are freed from needing to understand all those underlying details, so it is practical and promotional [4]. At present, many companies use Hadoop as the foundation to support the building of their computer platforms. The core components include HDFS, Map Reduce and HBase. HDFS frame structure is shown in Fig. 1.

An HDFS uses a structural model of master/slave. In general, an HDFS contains a single Namenode and a number of Datanodes, in which Namenode acts as central server. It manages the file system's namespace and users' access through the client. Datanodes are generally used in conjunction with node significance, with the effect of managing its own node storage. The primary role of Datanodes is to serve read and write requests from the clients on the file system, and also perform block creation and deletion through unified scheduling. As per HDFS frame structure shown in Fig. 1, an HDFS contains a single Namenode and a number of Datanodes [5].

Map Reduce. Research has found that most abstracted operations can be transformed into Map Reduce. Map Reduce can be divided into two parts: Map and Reduce, in which Map is responsible for decomposing Input into Key/Value, and

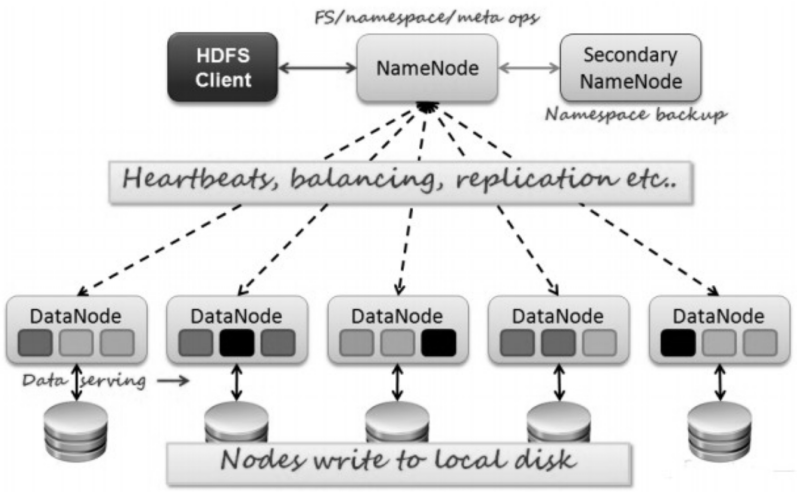

Fig. 1. HDFS frame structure

then synthesizing and outputting the Key/Value obtained through Reduce. Map and Reduce can be run in the cluster, and the results will be stored in the distributed file system. The system algorithm is mainly edited by the programmer who assigns corresponding functions according to actual needs. The Map Reduce framework is shown in Fig. 2.

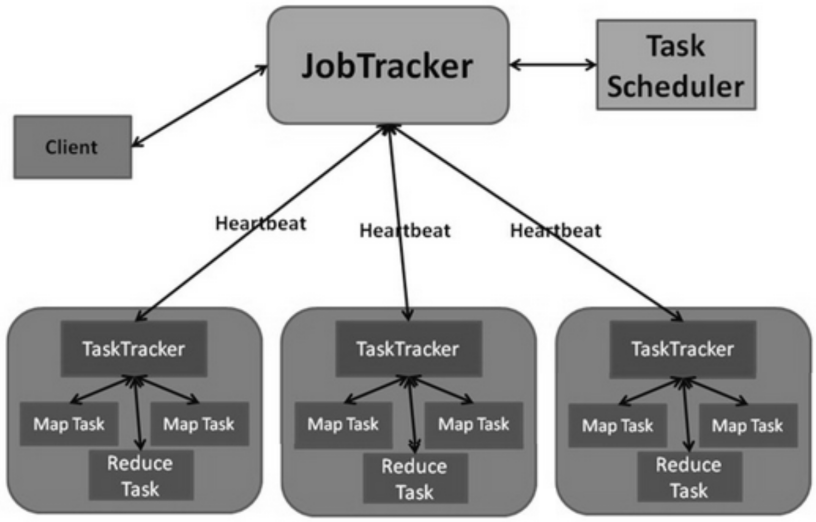

Fig. 2. Diagram of the Map/Reduce framework

Fig. 2 shows that Map Reduce often breaks data down into number of independent modules in the operation. First of all, Map processes these independent modules,

sorts the output of the processed data, and feeds back the results to Reduce. In the Map Reduce operation, input and output are stored in the file system, and task scheduling and monitoring are carried out by the whole frame. The task system that fails in system running is automatically reexecuted.

HBase is an open-source, distributed database that differs from traditional databases [6]. HBase uses a data model very similar to that of Bigtable. In the data storage process, each data row has a sortable key and an arbitrary number of columns. The table is stored sparsely, and users can make different definitions of it. In the visit process, HBase is random and can store large user data in coordination with the system in real time.

2.2. Content-based image retrieval

The image retrieval process is to find image features quickly, timely and effectively, and to find objects with similar characteristics. Retrieval characteristics include image characteristics, shape and texture, among others [7].

Color is an important feature for image retrieval, and is currently the most common bases to retrieve images. Color is the most widely used underlying visual feature. Compared to visual features of other attributes, color has the least reliance on image rotation, translation and size changes, and makes image retrieval relatively simple in the system retrieval process, so it is a retrieval way that is easy to implement [8].

Shape is another important feature for image retrieval. The shape feature provides a high-level visual retrieval way, which is an advanced retrieval method developed on the traditional retrieval methods, and can further find the semantics of images during the retrieval process. Firstly, we need to combine the bottom-level features with high-level features, and express the features by using advanced algorithms. It is hard to obtain the shape of an object. Therefore, it is difficult to retrieve images based on the shape feature in applications and this retrieval method is suitable for images that are easily recognizable.

Texture feature. Texture is one of the basic characteristics of an image, and an important basis for visual presentation. It can effectively reflect the surface features of an object. Texture is independent of color, brightness and other characteristics of an image. The essence is the distribution of pixels in the image space. Pixels are distributed either densely or loosely. The basic components that make up texture are called primitives. Texture features mainly include directions, linearity, roughness, etc. These can be used as an important basis for texture retrieval [9].

2.3. Feature matching

Objects identical or similar to the matching image are found during image retrieval. Currently there are two types of feature matching: exact match and similar match. Exact matching mainly means that the image is exactly the same as the reference object. In this case, the two images are basically a copy of the same object. In addition, we can also set a threshold. If the image falls within the specified

range, it indicates a similar match. In other words, the search image is similar to the reference image. Through using image content as a retrieval basis, image matching can be done by a corresponding measurement strategy after retrieving the image feature, which is to determine the similarity between the retrieval image and the feature vector distances in the database. The image feature can be converted to any number of eigenvectors, e.g., n-dimensional feature vectors in images A, B, and C, d refers to the distance on the basis of which the following axiom constraints are satisfied [10]:

$$d(A,A) = d(B,B) = 0\,, \tag{1}$$

$$d(A,B) \geq d(A,A) = 0\,, \tag{2}$$

$$d(A,B) \geq d(B,A)\,, \tag{3}$$

$$d(A,C) \leq d(A,B) + d(B,C)\,, \tag{4}$$

The algorithm used in the actual image retrieval process does not completely meet the above four axioms, but generally meets one or several of them. In view of this, image feature matching can be conducted. At present, common image feature matching algorithms include the Minkowski distance, the Manhattan distance, the Euclidean distance, and the Mahalanobis distance, respectively given by [11]

$$d(A,C) \leq d(A,B) + d(B,C)\,, \tag{5}$$

$$d(X,Y) = \sum_{i=1}^{n} |x_i - y_i|\ , \tag{6}$$

$$d(X,Y) = \left(\sum_{i=1}^{n} w(x_i - y_i)^2 \right)^{\frac{1}{2}}\ , \tag{7}$$

$$d(X,Y) = \sum_{i=0}^{n} \sum_{j=0}^{n} (x_i - y_i) \cdot a_{ij}(x_j - y_j),\ a_{ij} \in A\,, \tag{8}$$

where A in (8) denotes the covariance matrix. Symbol w refers to the weight and α refers to the attribute value.

3. Results

As previously mentioned, cloud computing platform and images serve as the basis. In this paper, a set of image retrieval systems are designed on the basis of cloud computing platforms. The system supports retrieval of image input information, and retrieves similar or same images in webpage.

3.1. Needs analysis of image retrieval system

The traditional image retrieval system based on cloud computing platforms fails to use images to retrieve input information [12]. The current image retrieval system is built upon the traditional database, which has a limited image storage capacity and thus can hardly adapt to needs of retrieving massive image information. The traditional retrieval method can retrieve some simple images intelligently, while many images are intricate at present, so the traditional image retrieval cannot meet the actual demand.

Focusing on the above problems, the system needs to meet the following demands in the design: the system is built upon efficient databases and can store images efficiently. It has large storage capacity and can meet the future needs. Moreover, it is scalable to some extent. When the capacity or function cannot meet the demand, users can increase its functionality and capacity; users can quickly retrieve the required image through the image retrieval system, which is faster and more accurate than traditional retrieval systems. The system can provide users with a more convenient, user-friendly retrieval mode, and users can master the retrieval function through basic learning. The system can provide users with a good interactive interface, through which users can retrieve images efficiently.

3.2. Overall design

In combination with the needs analysis, subsystems like image retrieval, feature extraction, cloud computing and user interaction are set up when designing the web image retrieval system based on cloud computing models. The structure of web image retrieval system based on cloud computing model is shown in Fig. 3.

As shown in Fig. 3, image retrieval is the central module of the whole system and has an important effect on the system image retrieval results [13]. The image retrieval module can realize image analysis and processing, and extract features from the image. The control input feature extraction module mainly provides platform support for image retrieval and feature extraction and enhances the system's operation efficiency. The user interaction module is responsible for providing users with a scientific interactive interface, through which users can achieve their own needs and view the test results on the terminal display interface. The IQL engine module is responsible for interpreting the statement.

3.3. Module functions

Feature extraction subsystem module. Feature extraction needs to be based on the database generation subsystem, which is a core of the whole system. It is responsible for preprocessing the image information collected to get a clearer image, extract the feature of the processed image and store the feature values acquired in a specific database. On this basis the feature extraction process is realized. Image preprocessing is to preprocess an image. The image processing process consists of rotation, translation, zooming and mirroring. It also provides a basis for later image

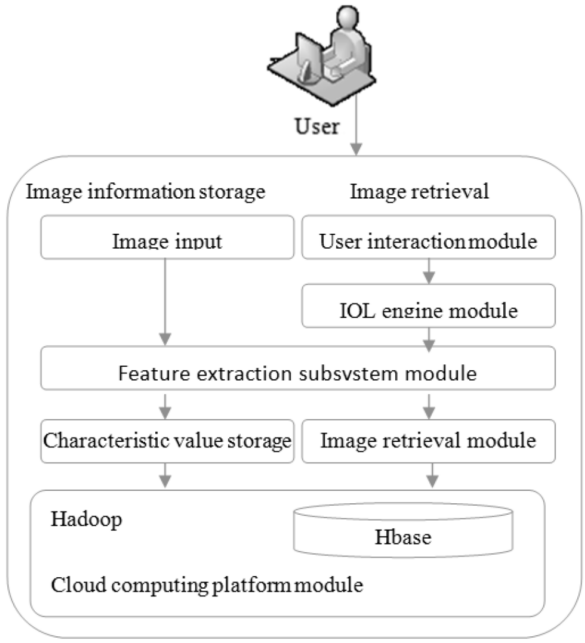

Fig. 3. Structure diagram of web image retrieval system based on cloud computing models

segmentation, such as sharpening and blurring the image, removing the image noise. A diagram of image preprocessing functions is shown in Fig. 4.

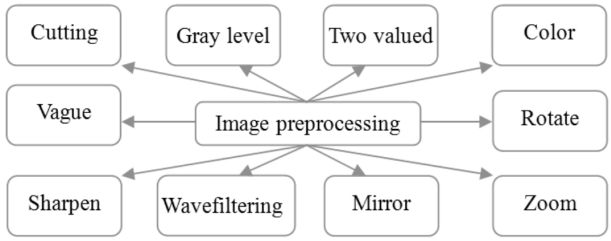

Fig. 4. Image preprocessing process

Image extraction is to extract a key factor from the image, and use the factor as an index of image retrieval. Key factors encompass color, texture, shape and other characteristics, which are the focus of this paper. The image retrieval submodule is a core module of the entire system. It is responsible for retrieving images that resemble the target image from the database. In the retrieval process, the feature is extracted from the target image according to the extraction function, and then it judges whether single or multiple query is used to retrieve images. The appropriate interface is selected in tune with the actual situation, and the image feature is matched with the feature database to object a distance value close to the

target image feature value and sort in ascending order to display the image to the user through the display terminal [14].

3.4. Module functions

Cloud computing platform module. Cloud computing platform module is the basis of establishing this system. In this paper, Hadoop is taken as a basis to quickly build the cloud computing platform through HDFS. The Hadoop system has high stability and builds the system operating platform together with Ubuntu. The cloud computing platform framework for image retrieval is shown in Fig. 5.

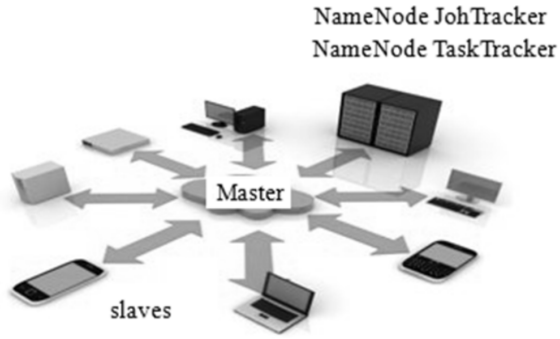

Fig. 5. The cloud computing platform framework for image retrieval

It can be seen from Fig. 5 that the cloud computing model assigns tasks to server nodes via a master node. On the basis of building the framework, the image retrieval process can be realized by combining subsystems such as user interaction and IQL engine module. In combination with the needs analysis, subsystems like image retrieval, feature extraction, cloud computing and user interaction are set up when designing the web image retrieval system based on cloud computing models [15]. Image retrieval is the central module of the whole system and has an important effect on the system image retrieval results. The image retrieval module can realize image analysis and processing, and extract features from the image. The control input feature extraction module mainly provides platform support for image retrieval and feature extraction and enhances the system's operation efficiency.

4. Conclusion

Cloud computing is a new information resource processing model that relies on back-end computer capabilities. It connects many end-users to the system by interface means which are different from traditional ones, thereby achieving multiple resource retrieval functions. The image retrieval process is to find image features quickly, timely and effectively, and to find objects with similar characteristics. Retrieval characteristics include image characteristics, shape and texture, among others. Color is an important feature for image retrieval, and is currently the most

common bases to retrieve images. Shape is another important feature for image retrieval. The shape feature provides a high-level visual retrieval way, which is an advanced retrieval method developed on the traditional retrieval methods, and can further find the semantics of images during the retrieval process. Texture is one of the basic characteristics of an image, and an important basis for visual presentation. It can effectively reflect the surface features of an object. Texture is independent of color, brightness and other characteristics of an image. Objects identical or similar to the matching image are found during image retrieval. Currently there are two types of feature matching: exact match and similar match. In combination with the needs analysis, subsystems like image retrieval, feature extraction, cloud computing and user interaction are set up when designing the web image retrieval system based on cloud computing models.

References

[1] A. Q. H. Al-Neami: *Measurement of trace elements association with diabetes mellitus based on atomic absorption spectrophotometers.* Advances in Life Science and Technology *24* (2014), No. 2, 21–27.

[2] M. Z. Jora, J. A. Nóbrega, J. J. R. Rohwedder, C. Pasquini: *Double tungsten coil atomic absorption spectrometer based on an acousto-optic tunable filter.* Spectrochimica Acta Part B: Atomic Spectroscopy *103–104* (2015), 1–8.

[3] h. Tavallali, H. Norozikhan: *Design of cold vapor system and assembled on atomic absorption spectrometer for mercury determination in several waste water samples.* International Journal of ChemTech Research *1* (2009), No. 2, 390–393.

[4] X. T. Yang, Y. X. Zhang, Y. Wang: *Tow novel equipments of zeeman background correction for atomic absorption spectrophotometer.* Chinese Journal of Analytical Chemistry *39* (2011), No. 10, 1517–1520.

[5] M. Xia, T. J. Ying: *Indirect determination of lactoferrin in milk powder by atomic absorption spectrophotometer.* Chinese Journal of Pharmaceutical Analysis *31* (2011), No. 1, 173–175.

[6] Y. G. Zhang, M. Xiao, Y. H. Dong, Y. Jiang: *Determination of soil exchangeable base cations by using atomic absorption spectrophotometer and extraction with ammonium acetate.* Spectroscopy and Spectral Analysis *32* (2012), No. 8, 2242–2245.

[7] X. Y. Bian, R. X. Zhu, Z. T. Wang: *Software design for atomic absorption spectrometer based on LabVIEW and database.* Microcomputer Information *24* (2008), No. 16, 117–119.

[8] S. K. Lu, D. X. He, X. P. Li, S. Tian: *Adaptability of atomic absorption spectrophotometer based on semi-floating optical base for vehicle application.* Chinese Journal of Analysis Laboratory *30* (2011), No. 4, 26–29.

[9] J. Wu, J. H. Zhang, X. S, Zhu: *A self-made circulating water cooling system of atomic absorption spectrometer.* Chinese Journal of Spectroscopy Laboratory *28* (2011), No. 6, 3268–3270.

[10] T. G. Kazi, N. Jalbani, J. A. Baig, G. A. Kandhro, H. I. Afridi, M. B. Arain, M. K. Jamali: *Assessment of toxic metals in raw and processed milk samples using electrothermal atomic absorption spectrophotometer.* Food and Chemical Toxicology *47*, (2009), No. 9, 2163–2169.

[11] I. A. M. Shaibal, F. Khanom, M. A. Rahman, A. M. Shafiqul Alam: *Separation and determination of metals in mixed solvent system on anion exchanger using atomic absorption spectrophotometer.* Pakistan Journal of Analytical & Environmental Chemistry *6* (2005), No. 2, 35–41.

[12] Z. M. Memon, A. M. Shah, T. G. Kazi: *Study of calcium in active pulmonary tuberculosis patients by flame atomic absorption spectrophotometer*. Indo-American Journal of Pharmaceutical Research *4*, (2014), No. 11, 45–48.

[13] Z. F. Du, Y. Qiu: *Discussion of improving energy of 4600 atomic absorption spectrophotometer with a tandem atomizer*. Optical Instruments (2011), No. 4, 34–39.

[14] S. Nimmagadda, A. Jyothi: *Detection and identification of chemical agent using atomic absorption spectrophotometer*. International Journal of Research in Engineering and Technology *2* (2013), No. 5, 764–768.

[15] X. Zheng: *Application of automatic sampler mixed mouth function of shimadzu AA–7000 serises atomic absorption spectrometer*. Chemical Analysis and Meterage (2014), No. 6, 23–29.

Received May 22, 2017

Acta Technica *62* No. 1A/2017, 361–370

A parallel algorithm based on CPU/GPU dynamic coordination control and scheduling[1]

Hanyang Jiang[2,3], Danhua Wang[4]

Abstract. CPU/GPU dynamic coordination technology is gradually applied to the development of parallel algorithms, but the current algorithm has some shortcomings in terms of efficiency and power consumption. Therefore, it is necessary to further study the parallel algorithm based on dynamic coordination control and scheduling. Based on the power cap technology, this paper sets up the device frequency and the single computing node of the synchronization system by studying the synchronization system of the computer, controlling DVFS and mapping mode. In order to avoid power failure and load imbalance, this paper has developed a new empirical model of performance and synchronization system, these models make the most of the power of the system to reduce the power consumption to a predetermined level, Good settings can be done.

Key words. Parallel algorithm, CPU, GPU, dynamic coordination.

1. Introduction

The central processing unit is a call to the electronic circuit inside the computer, and shows the logic input and output commands as compared with the basic arithmetic education, and executes the computer program [1]. The computer industry uses this term at least since 1960, where the central processing unit traditionally refers to the processor and, more specifically, the basic elements of the processing unit and the control unit, the computer and the external components, such as the main memory area and the circuit need to be separated. The graphics processing unit is a dedicated electronic circuit that is designed to be quickly manipulated, capable of changing memory-created images, and a display device designed to speed

[1]Funding for research projects of The Education Department of Hunan Province (16C0227) and the Science and Technology Plan Project of Hunan Province (2016TP1020)

[2]Hengyang Normal University, Hengyang, 421002, China

[3]Hunan Provincial Key Laboratory of Intelligent Information Processing and Application, Hengyang, 421002, China

[4]Hengyang Normal University, Hengyang, 421002, China

up the output buffer [2]. GPU is an embedded system that can be used for mobile phones, personal computers, workstations and game consoles. Modern GPUs are very effective in computer graphics operations and image processing, and their highly parallel architectures enable large blocks of data to be processed in parallel, which is more efficient than using a common algorithm. In the personal computer, GPU can be installed on the video card, or can also be installed on the motherboard, CPU can also be integrated CPU.

On June 30, 1945, before the invention of ENIAC, the mathematician John von Neumann published the first draft of the report, named EDVAC [3]. This is the outline of the computer stored program, in August 1949, EDVAC design eventually completed, you can perform some types of instructions. EDVAC's written program will be stored in high-speed computer memory, rather than in the physical line of the computer. This overcomes the shortcomings of ENIAC, which is a serious flaw in reconfiguring the computer to perform new tasks and takes a lot of time and effort. Improved cache and bypass can maintain the shared memory capacity, to achieve the parallel operation of the thread.

Manchester ran the first program in the computer in 1949, the CPU can be customized to design, play a huge role, and sometimes can be used as part of a single computer [4]. However, the CPU custom design of this method of specific application space is limited, general-purpose processor production quality has been greatly developed. The era of standardized discrete transistors and minicomputers has begun, with the popularity and rapid development of ICs. The chip allows for more complex CPU designs that can be manufactured for nanometer tolerances. Standardized miniaturization of the CPU increases the use of digital devices in modern life, far beyond the application settings, resulting in a lot of specific computers.

2. Materials and methods

In this article, we present an effective power capping technique and a computer synchronization system based on DVFS coordinated mapping technology [5]. Complex performance and system energy consumption is because the frequency of the CPU is different, the frequency of the GPU conforms to the mapping relationship. In exploring the operating space of the parameters, we need to proactively establish a system with limited power that needs to be executed before mapping DVFS settings and tasks. In order to realize the mapping function of orientation and system setting, the performance task is proposed and the new empirical model is identified to verify the technical practicability of heterogeneous system. The fewer configuration files used, these models allow us to get the best parameters for a given power series constraint.

2.1. Power management technology

The capping power is the core technology of the computer power management system. Remove the power pulses of the components and the computer, keep the given nodes, and constrain the computer power consumption [6]. At the level of the

component, there has been an upper limit on the power system and CPU memory that have been proposed. At different levels, limiting the power of personal computing nodes is an effective means of achieving system computing power enhancement, large-scale calculation is very important [7]. Through technology-based power capping technology, we are able to optimize the application's running capacity, which is running on the Internet server's available power capacity.

We use the optimized compiler to mark the database we provide and use it for evaluation and calculation. For the development of mixed applications, we use the parallel code in the benchmark suite, combined with the Rodinia and BLAS libraries [8]. Using the GPU's computing functions and the CPU-side parallel computing code. The hybrid algorithm uses the CPU to provide the results for the user. In the hybrid performance, the data elements only need to be executed when a given task is needed to change the mapping of the GPU. In the experiment, we assume that we can change the percentage of CPU activity and reduce the GPU running memory. It is shown in Fig. 1.

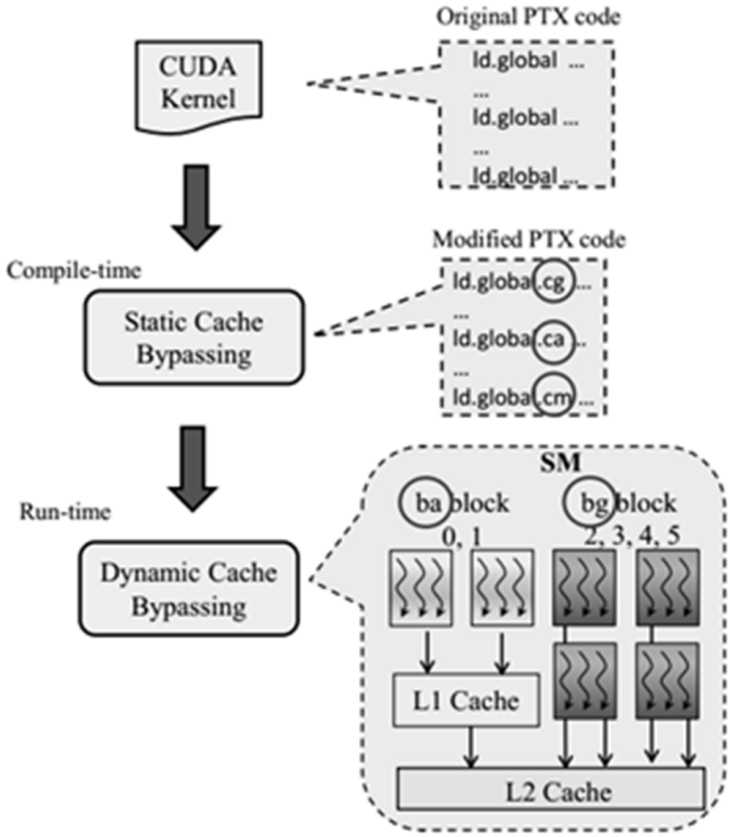

Fig. 1. Static bypassing classifies global loads into three categories using tags ca, cg, and cm

2.2. GPU heterogeneous systems

In this paper, we consider using the limit technique to calculate the power of each node, assuming the structure of the machine [9]. The structure includes a CPU and a GPU. CPU and GPU commercial production has been able to support dynamic voltage and frequency scaling technology, through the management of DVFS, the computer's power consumption can be integrated in the measurement device to install a dedicated hardware counter to read. Provided by the business software interface. Previous research reports indicate that the power displayed by components such as motherboards and hard drives can produce relatively small fluctuations under different workloads. Since CPUs and GPUs are the primary source of nodes, dynamically calculating power fluctuations will be considered the goal of power management.

Estimation of the execution time of the first I kernel K_i hybrid computation, where rcpu and rgpu are not zero, we make the following two assumptions:

- The actual execution time on CPU or GPU is proportional to the number of mapping tasks,

- Global obstacles need to be executed after each parallel kernel; we can estimate the execution time of the I kernel with the following equation

$$K_i = \max\left\{K_i^{\mathrm{c}}(f_{\mathrm{cpu}}, f_{\mathrm{gpu}}) \times \frac{r_{\mathrm{cpu}}}{100}, K_i^{\mathrm{g}}(f_{\mathrm{cpu}}, f_{\mathrm{gpu}}) \times \frac{r_{\mathrm{gpu}}}{100}\right\}. \tag{1}$$

The cache not only reduces access latency and power consumption, it also means that a particular hardware area consists of different parts [10]. For example, the computer's architecture uses a unified cache and shared project memory. The uniform design increases the size of the cache, meaning that the size of the shared memory can be reduced. However, this may affect performance, and the reduction in shared memory volume will reduce the number of active threads [11]. In contrast, the improved cache can bypass the maintenance of shared memory capacity, enhance the parallel performance of the thread. It is shown in Fig. 2.

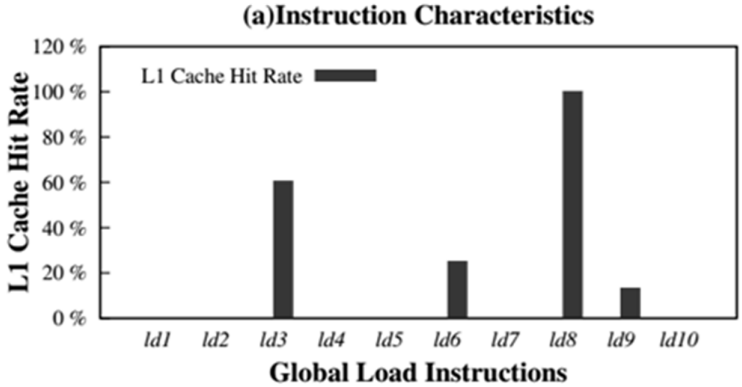

Fig. 2. Motivation for coordinated cache bypassing using SPV application

2.3. Parallel computing

Parallel computing of two CPUs and GPUs can mix data and improve the efficiency and performance of the energy of the synchronous compute nodes [12]. Recently, with the advent of portable GPU programming environments, such as OpenCL and OpenACC, many researchers have proposed a variety of compilation and execution systems to take full advantage of the data parallel processing capabilities. We evaluated the selected applications and BLAS libraries for the Rodinia benchmarks. When the compiler or database is running, connect with the CPU's capabilities. Therefore, we must manually change the mapping mechanism of heterogeneous tasks using a variety of compilers.

In this example, the CPU activity percentage is 0.3 and the GPU's task completion is 0.7. Since the parallel data task can be divided into unit tasks associated with the various elements of the data, we have to control the percentage of activity for each device to provide computing power. Previous studies have shown that the system can adjust the compiler's ability to map load to load. Depending on the computing power of the computer, depending on the percentage of detailed tasks, the use of GPU to achieve relative acceleration is applicable to different applications. It is shown in Fig. 3.

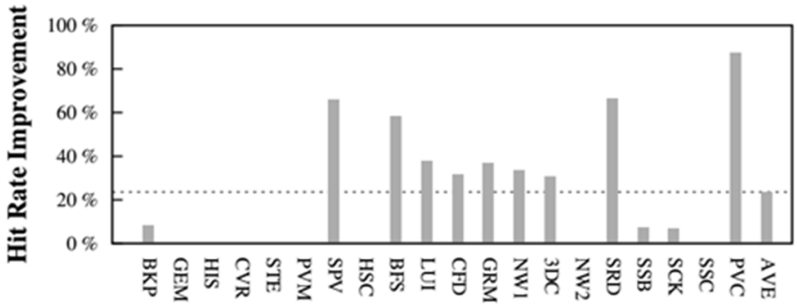

Fig. 3. L1 Cache Hit Rate Improvement (16 kB)

3. Results

The focus is on coordinating DVFS to achieve heterogeneous system task mapping [13]. To do this, under the existing adaptive synthesis method, the program is mapped to the feedback controller. In this method, a large number of parameters need to be adjusted in operation to explore the wider parameter space. Under the current architecture of the CPU / GPU, an additional capacity between the data memory and the memory is required to accommodate the task-mapped environment, which results in significant performance degradation [14]. In order to avoid this problem, we use the positive method to study the characteristics of the parameter space. Typical GPU application behavior does not perform substantially, using iterative algorithms to change the operation of many GPU applications. These facts

tell us that there is a desire to use a positive approach to coordinate task mapping between CPU/GPU and synchronization systems.

3.1. Power pack

In the proposed power capping technique, it is necessary to determine the operating frequency of the CPU and GPU, according to the percentage mapped to the CPU and GPU in the active program. To summarize the power cap technology, let's save the configuration file information for the application running on the CPU and the GPU in order for us to change the set parameters before executing the application. The information includes the empirical model and the timing of the forecast execution, and utilizes the maximum power mix of the CPU and GPU implementation. The model allows all possible settings to perform a detailed analysis of all possible settings for the mapping parameters. Predict the best parametric model, we run the application to find that the system can overcome the power constraints, and because the parameter prediction can eliminate the power dissipation error, which is shown in Fig. 4.

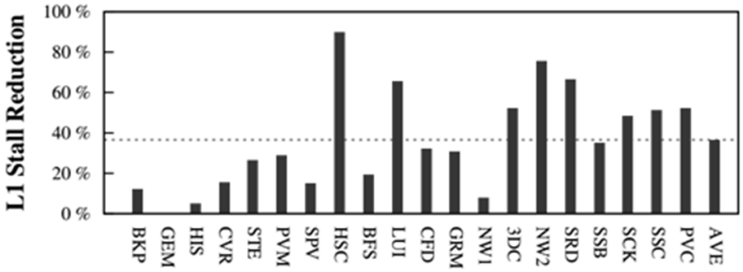

Fig. 4. Reduction on pipeline stall caused by L1 cache congestion (16 kB)

While this is rare, the research experience with this model is sufficient because we can use the existing technical force to adjust the frequency of the CPU at runtime to prevent unauthorized behavior. The response controller is responsible for adjusting the parameters. In this case, adjusting the frequency of the CPU alone does not result in large performance degradation, since the value is close to the chase high limit of the energy supply, and the adjustment of the frequency is within the specified range. We use the Linux cpufreq command to change the CPU frequency and use the nvidiasmi command to change the frequency of the GPU.

3.2. Experimental module

The power configuration information includes the number of compute nodes for the CPU and GPU. We also collect the parallel execution time of each kernel's execution function. We analyzed the execution time of the standard, compared with the execution time of the GPU at the highest frequency. Therefore, the implementation of the model can be applied to the data analysis, the use of different databases are different. When you install the application, we can get the analysis information of

the system. The system must support measurement of node energy consumption and allow the energy consumption of the CPU and GPU to be calculated, which is shown in Fig. 5.

However, this ignores the data caching capabilities of the analysis system and may ignore the good data area. Instead, by changing the location of the bypass cache data, make sure that the useful data is left in the global view. In addition, we can bypass the co-ordination of the work required to achieve data cache coordination. Recently, Professor Chen proposed an adaptive cache management technology, by protecting the limited distance within the wire to achieve cache protection to improve the performance of the cache. Similar to our findings, they have proven that the cache can effectively alleviate the transmission pressure and reduce the difficulty of purely linear execution of the program. Instead, our data is coordinated around the cache by identifying the static nature of the bypass, coordinating the local area with the overloaded area, and dynamically adjusting the local cache in the thread block.

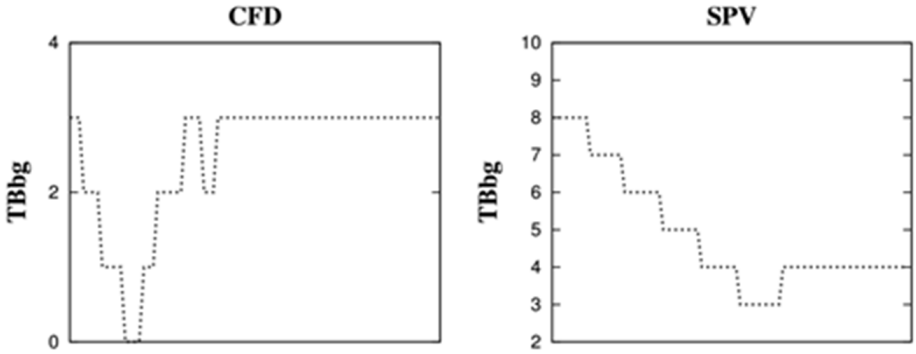

Fig. 5. TB_{bg} modulation

3.3. Execution time algorithm

By estimating the execution time of the kernel and combining the hybrid computation method, we make the following two assumptions: The actual execution time of the computer is proportional to the number of mapping tasks, and global errors need to be resolved after executing each parallel kernel The In this case, the faster equipment must wait for the other device to run. Using the two hypothetical information, we can estimate the time of the implementation of the kernel, in line with the following equation, the analysis of the collected information, through our study of empirical models and parameters, we set up the parameters to achieve the best parameter settings, Each power value constrains the best parameter in the storage list, so you need to create a table.

In addition, it takes a lot of time to build the data table, using the exhaustive search algorithm to get the best parameter settings, because we can quickly estimate the maximum execution time and estimate the actual power consumption of any parameter model. Before executing the application, get the optimal set of parameters at run time by looking up the table. However, the larger cache does not solve all

the problems. The application cache does not help improve the performance of the cache and the success rate of the calculation. But it is useful to improve the cache, because it can help reduce the stall of the pipeline.

3.4. Analysis and discussion

The GPU has been widely used to accelerate the speed of generic applications. However, making full use of GPU performance is not a simple matter. The biggest obstacle is to achieve performance optimization. GPU modeling and performance optimization, through multi-tasking and data conversion modeling, to achieve optimal parameter control, the use of the most advanced technology and memory layout program to design the chip. In all the optimization techniques, the memory system becomes more and more common, the optimization program access mode can change the irregular memory, and the application ported to the GPU. In the experiment, we used a single node and multi-core CPU to handle the problem. To get more information about the experiment, we measured the energy consumption associated with the total number of machines.

The CPU and GPU power measurement and analysis, we use the software to read the relevant hardware devices on the counter, get energy consumption information. For the bypass memory cleanup cache, for data congestion and limited cache resources, the effective way is to reduce the high speed of the pressure. Both static and dynamic methods can be used on general purpose processors. CPU technology is mainly used as a caching experimental model, cache hit rate does not always exist prediction model, including large-scale parallel processing, memory resource dispersion problem. Recent research explores the problem of GPU bypass caching. From the perspective of the cache bypass technology analysis of the data access mode and load the memory, shortening the compile time.

4. Conclusion

In order to improve the efficiency of the algorithm and reduce the power consumption of the system, this paper uses the power cap technology to study the synchronization system of the computer, control the DVFS and mapping mode, set the frequency of the synchronization system equipment and the single Computational nodes, and finally an effective power capping parallel algorithm is proposed to reduce the power consumption of the system to a predetermined level. We run five data parallel applications on a single machine, and the experimental results show that our proposed power cap algorithm is ideal for performance. At the same time, in order to avoid power failure and load imbalance, we develop new mathematical models to improve the performance of the synchronization system, which allows us to make the best settings. The parallel algorithm proposed in this paper greatly reduces the power consumption of the computer system, and has a wide application prospect. However, there are some shortcomings in the running speed and accuracy of the algorithm, the future will continue to improve the speed and accuracy of the algorithm.

References

[1] W. Shen, L. Sun, D. Wei, W. Xu, H. Wang, X. Zhu: *A hybrid parallel algorithm for computer simulation of electrocardiogram based on a CPU-GPU cluster.* Proc. IEEE/ACIS, International Conference on Computer and Information Science, 16–20 June 2013, Niigata, Japan, IEEE Conference Publications (2013), 167–171.

[2] F. Yang, T. N. Shi, H. Chu, K. Wang: *The design and implementation of parallel algorithm accelerator based on CPU-GPU collaborative computing environment.* Advanced Materials Research *529* (2012), Chapter. 4, 408–412.

[3] T. H. Chang, M. Alizadeh, A. Scaglione: *Real-time power balancing via decentralized coordinated home energy Scheduling.* IEEE Transactions on Smart Grid *4* (2013), No. 3, 1490–1504.

[4] G. J. Lu, Y. Yan, J. Y. Zhao: *Motion coordination control system with dual CPU based on ARM.* Journal of Mechanical & Electrical Engineering (2012), No. 08, 691 to 697.

[5] Y. Ma, L. Wang, A. Y. Zomaya, D. Chen,R. Ranjan: *Task-tree based large-scale mosaicking for massive remote sensed imageries with dynamic DAG Scheduling.* IEEE Transactions on Parallel and Distributed Systems *25* (2014), No. 8, 2126–2137.

[6] B. Chen, Y. Xu, J. Yang, H. Jiang: *A new parallel method of Smith-Waterman algorithm on a heterogeneous platform.* Proc. International Conference on Algorithms and Architectures for Parallel Processing, 21–23 May 2010, Busan, South Korea, Algorithms and Architectures for Parallel Processing, (LNCS) *6081* (2010) 79–90.

[7] K. Li, J. Liu, L. Wan, S. Yin, K. Li: *A cost-optimal parallel algorithm for the 0-1 knapsack problem and its performance on multicore CPU and GPU implementations.* Parallel Computing *43* (2015), 27–42.

[8] T. H. Bai, Y. G. Li, L. Y. Chen, Y. L. Wang: *Parallel optimization of geometric correction algorithm based on CPU-GPU hybrid architecture.* Applied Mechanics and Materials *543–547* (2014), No.Chapter. 6, 2804–2808.

[9] S. N. M. Shah, M. N. b. Zakaria, N. Haron, A. K. B. Mahmood, K. Naono: *Design and evaluation of agent based prioritized dynamic round Robin Scheduling algorithm on computational grids.* AASRI Procedia *1* (2012), 531–543.

[10] J. Li, B. Guo, Y. Shen, B. Li, J. Wang, Y. Huang, Q. Li: *GPU-memory coordinated energy saving approach based on extreme learning machine.* Proc. IEEE International Conference on High Performance Computing and Communications, IEEE International Symposium on Cyberspace Safety and Security, IEEE International Conference on Embedded Software and Systems, 24–26 August 2015, New York, NY, USA (2015), 827–830.

[11] L. Bukata, P. Šůcha, Z. Hanzálek: *Solving the resource constrained project scheduling problem using the parallel tabu search designed for the CUDA platform.* Journal of Parallel and Distributed Computing *77* (2015), 58–68.

[12] H. Guan, J. Yao, Z. Qi, R. Wang: *Energy-efficient SLA guarantees for virtualized GPU in cloud gaming.* IEEE Transactions on Parallel and Distributed Systems *26* (2015), No. 9, 2434–2443.

[13] K. Wang, Y. Huai, R. Lee, F. Wang, X. Zhang, J. H. Saltz: *Accelerating pathology image data cross-comparison on CPU-GPU hybrid systems.* Proceedings VLDB Endowment *5* (2011), No. 11, 1543–1554.

[14] M. Zouari, C. Diop, E. Exposito: *Multilevel and coordinated self-management in autonomic systems based on service bus.* Journal of Universal Computerence Science *20* (2014), No. 3, 431–460.

Received May 22, 2017

Acta Technica *62* No. 1A/2017, 371–380

A balancing artificial bee colony algorithm for constrained optimization problems[1]

Zhen Wang[2], Yuelin Gao[2]

Abstract. To solve constrained optimization problems, a balancing Artificial Bee Colony (BABC) algorithm is proposed in this paper. It is important to balance constraints and objective function during iterations by population-based algorithm. The feasible rules are the main constraint handling method employed in this paper. To balance the constraints and objective function, the replacement mechanism and the mutation strategy are added. Furthermore, the opposite learning initialization is introduced to make the initial colony scattered evenly on the search area. And the best-lead search equation is used in onlooker bee phase to improve the convergent speed. The BABC algorithm is tested on 18 test functions with 30-D at IEEE CEC2010. The experimental results are compared with other state-of-art algorithms, which suggest that the BABC algorithm outperforms or performs similarly to other algorithms.

Key words. Constrained optimization, Artificial bee colony algorithm, feasibility rule.

1. Introduction

The research to find better optimization algorithms of constrained optimization problems arose from science and engineering has never stopped. Since science and engineering constrained optimization problems are getting complicated, the significant attentions are paid on efficient and effective algorithm. In recent years, population-based algorithms have been widely used to deal with constrained optimization problems. Currently, a population-based algorithm called artificial bee colony (ABC) algorithm is proposed to simulating the behavior of foraging bees, which is widely used for solving many kinds of optimization problems and real world problems including constrained optimization problems [1].

[1]This work is supported by National Nature Science Foundation of China (No. 61650104, No. 61561001), 2016 scientific research project of North Minzu University (No. 2016SXKY03) and the key research projects of North Minzu University (2015KJ10).

[2]Institute of Mathematics and Information Science, North Minzu University, Yinchuan 750021, China

Since most of the population-based algorithms are originally designed for unconstrained optimization problems, one of the main concerns of using these algorithms for solving constrained optimization problems is how to select the promising individuals for solution iteration. In most cases, the individuals in the population with better fitness function values may not be feasible, which makes the constraints handling method combined in the algorithm is much more important. Generally speaking, methods dealing with the constraints can be divided into five groups.

Methods based on transforming unfeasible solutions into feasible ones with some operators. Michalewicz and Schoenauer [2] discussed difficulties connected with solving the general nonlinear programming problem and provide a constraints handling method.

Methods based on penalty functions. Thakur et al. [3] proposed a modified real coded genetic algorithm for constrained optimization with penalty function method. Elsayedet et al. [4] applied the concept of training and testing with a self-adaptive multi-operator based evolutionary algorithm to find suitable parameters with penalty function method.

Methods based on feasibility rules. Deb [5] first proposed the feasibility rules for binary tournaments in Genetic Algorithms. Tuba and Bacanin [6] introduced modifications to the seeker optimization algorithm to control exploitation/exploration balance and hybridized it with elements of the firefly algorithm that improved its exploitation capabilities for constrained optimization problems with feasibility rules.

Methods based on stochastic ranking. Rodrigues [7] presented a new technique to handle constraints in the solution of optimization problems by evolutionary algorithms - the Balanced Ranking Method (BRM).

Other hybrid methods. Gao et al. [8] defined the best fitness value among feasible solutions in current population as gbest and converted the original COPs to multi-objective optimization problems (MOPs) with one constraint. Wang et al. [9] incorporated the objective function information into the feasibility rules for solving constrained optimization problems with evolutionary optimization.

All these methods have their own advantages. Among all the constraints handling methods, the well-known feasibility rule is widely used because of the simplicity. Since feasible solutions are preferred unfeasible ones, the algorithms often lack diversity in population. An effective selection method should balance the information obtained by objective function and constrained functions during searching progress, which can maintain the diversity of the population.

In this paper, a balancing artificial bee colony (BABC) algorithm is proposed to overcome shortcomings mentioned above. In BABC algorithm, a modified ABC algorithm serves as the search engine and the well-known feasibility rule is used as the constraints handling method. In addition, the replacement mechanism and mutation strategy are used to compare individuals based on objective function. Furthermore, the information of objective function has also been used to guide the search. The performance of the BABC algorithm has been tested on 18 benchmark test functions collected in IEEE CEC2010 and compared with other state-of-the-art algorithms [9].

The reminder of the paper is organized as follows. In Section 2, a balancing artificial bee colony algorithm for solving constrained optimization problem is intro-

duced. In Section 3, the proposed algorithm is compared with other algorithms. In Section 4, a conclusion is provided.

2. Methodology

Generally, for minimization problems, a constrained optimization problem can be formulated as follows:

$$\begin{array}{ll} \min f(x), & x = (x_1, x_2, ..., x_n) \in R^n \\ \text{subject to} & l_i \leq x_i \leq u_i,\ i = 1, ..., n, \\ & g_j(x) \leq 0 \text{ for } j = 1, ..., q, \\ & h_j(x) = 0 \text{ for } j = q+1, ..., m. \end{array}$$

The objective function f is defined on an n-dimensional rectangle S in $R^n (S \subseteq R^n)$. Domains of variables are defined by their own upper and lower bounds. A feasible region $F \subseteq S$ is defined by m constraints, and x is defined on the feasible region. If there exists an inequality constraint that satisfies $g_j(x) = 0,\ j = 1, ..., q$ for any $x \in F$, the constraint is called active constraint at point x. All equality constraints are considered active at all points of F.

In the original ABC algorithm, the swarm consists of three kinds of artificial bees: employed bees, onlooker bees and scout bees. Employed bees explore the food source and share the information to the onlooker bees in the hive. Onlooker bees select a food source and exploit it based on the information shared by employed bees. The employed bee whose food source has been abandoned becomes a scout bee to search a new food source. For constrained optimization problems, the feasibility rules are used as the constraints handling method in ABC algorithm. However, in the method based on feasibility rules, the feasible solution prefers unfeasible solution, so that it will cause premature convergence. How to balance the constraints and objective function is a basic problem when solving constrained optimization problems by the ABC algorithm. Denote the food source number as SN, the position of the ith food source as $x_i,\ (i = 1, \cdots, SN)$, which is a D-dimensional vector. In the following subsections, the BABC algorithm for constrained optimization problems is described in detail to overcome the shortages described above.

2.1. Opposition-based learning initialization

It is important to generate an even initial population of swarm intelligence-based algorithms, which can affect the convergent speed and solution quality. In the initialization, there is no information about the distribution of solution. Therefore, the initial population needs to be scatted evenly on searching space to make sure the algorithm can search the whole space uniformly. In original ABC algorithm, the initial population is generated randomly in the searching space, which cannot ensure the evenly distributed population initialization. To conquer this issue, the initial population is generated by using opposition-based learning initialization. Notice that opposition-based learning method can simultaneously generate a solution

and its opposite [10], which can make the initial population be scattered evenly over the searching space. The algorithm for generating an initial population based on opposition-based learning initialization method is given as follows.

Algorithm 1: Generation of initial population.

Step 1: Set the population size SN and the individual counter $i = 1, j = 1$.
Step 2: Randomly generate a population $X(SN)$ by

$$x_{ij} = x_{\min,j} + \text{rand}(0,1)\left(x_{\max,j} - x_{\min,j}\right),$$
$$i \in \{1, 2, \cdots, SN\}, j \in \{1, 2, \cdots, D\}. \tag{1}$$

Step 3: For $i = 1, \cdots, SN; j = 1, \cdots D$, generate a population $OX(SN)$ by

$$ox_{ij} = x_{\min,j} + x_{\max,j} - x_{i,j}.$$

Step 4: Among the $X(SN)$ and $OX(SN)$, select SN individuals having the smallest costs as the initial population.

2.2. Searching equation

It is well known that the exploration ability and exploitation ability are both crucial for the search equations to find the optima in searching space, and the tow abilities are contradict to each other. It is well known that the search equation is good at exploration and poor at exploitation in original ABC algorithm. In order to balance the exploration ability and exploitation ability, two kinds of searching equations are used in BABC algorithm.

At the employed bee stage, the original searching equation is also used to keep the exploration ability, that is

$$v_{ij} = x_{ij} + \phi_{ij}(x_{ij} - x_{kj}), \tag{2}$$

where k, j are randomly selected indices, $k \in \{1, 2, ..., SN\}$, $k \neq i$, $j \in \{1, 2, ..., N\}$, and $\phi_{ij} \in [-1, 1]$ is a random number.

At onlooker bee stage, the searching equation is modified as best guided searching equation proposed by Zhu et al. [11] to enhance the exploitation ability, that is

$$v_{ij} = x_{ij} + \phi_{ij}(x_{ij} - x_{kj}) + \varphi_{ij}(x_{\text{best},j} - x_{lj}), \tag{3}$$

where $k, l \in \{1, 2, ..., SN\}$ is a random selected index which is different from i, $j \in \{1, 2, ..., D\}$ is a randomly selected index, $x_{\text{best},j}$ is the global best solution, $\phi_{ij} \in [-1, 1]$ and $\varphi_{ij} \in [0, 1.5]$ are both uniformly distributed random numbers.

At the scout bee stage, the individual is generated randomly within the range of the boundaries of the parameters by (1).

2.3. Replacement mechanism and mutation strategy

By replacing some individuals from the population, the replacement mechanism attends to alleviating the greediness of the feasibility rule. It can maintain the diversity of the population and balance the constraints and objective function. First, divide the population into S parts with the same size and sort it based on the objective function value in descending order. Second, choose the individual with the maximum degree of constraint violation from the first part and the individual with the minimum degree of constraint violation from A, where the set A consists of the individuals that cannot survive at the employed bee and onlooker bee stages. Third, compare the objective function value of the two selected individuals, and store the minimum one into the population, the other stored into A. Repeat the above step on all S parts of population respectively. Therefore, the replacement mechanism can be described as the following algorithm:

Algorithm 2: Replacement mechanism

Sort population in descending order according to the objective function values and divide it into S parts with the same size;

$i = 1$
while A is not empty and $i < S$

Select the individual x_a with the maximum degree of constraint violation from the ith part of population;
Select the individual x_b with the minimum degree of constraint violation from A;
if $f(x_b) < f(x_a)$

Replace x_a with x_b and delete x_b from A;

end if
$i = i + 1$
end while

Consider the premature issue, a simple mutation strategy is used when all the individuals in the population are unfeasible. The details are as follows:

Algorithm 3: Mutation strategy

if all the individuals in the population are unfeasible

Randomly select an individual x_c from population;
Generate a random integer number k between 1 and D, and let the kth dimension of x_c be equal to a value randomly chosen from $[L_k, U_k]$. Thus obtain a mutation individual x_d;
Choose the individual x_e with the maximum degree of constraint violation in population;
if $f(x_d) < f(x_e)$

Replace x_e with x_e;

end if
end if

2.4. BABC algorithm

In BABC algorithm, the probability of a food source being selected by an onlooker bee is given by:

$$p_i = \begin{cases} 0.5 + \left(\frac{\text{fit}_i}{\sum_{i=1}^{SN} \text{fit}_i}\right) \times 0.5 & \text{if solution is feasible,} \\ \left(1 - \frac{\text{violation}_i}{\sum_{i=1}^{SN} \text{violation}_i}\right) & \text{if solution is unfeasible,} \end{cases} \tag{4}$$

where violation_i is the penalty value of the solution x_i. The ith fitness value fit_i for a minimization problem is defined as

$$\text{fit}_i = \begin{cases} \frac{1}{1+f_i}, & f_i \geq 0, \\ 1 + \text{abs}(f_i), & f_i < 0, \end{cases} \tag{5}$$

where f_i is the objective function value of the ith solution.

Therefore, the solution procedure of the BABC algorithm is as follows:

Algorithm 4: Balancing artificial bee colony algorithm

Step 1: Initialize the food source by algorithm 1 and set all the parameters in the algorithm.

Step 2: The employed bees search the new food source according to (2). Evaluate the objective function value, fitness value and violation value of this food source. Then, use the feasibility rule to make a choice between the new food source and the old one. If the new food source is preferred to the old one, the new one replaces the old one.

Step 3: Calculate the selective probability according to (5) and select a food source for onlooker bees. Then, the onlooker bees search the new food source according to (3). And evaluate the objective function value, fitness value and violation value of this food source. Then, use feasibility rule to make a choice between the new food source and the old one. If the new food source is preferred to the old one, the new one replaces the old one.

Step 4: Replace some individuals according to the replacement mechanism introduced by **Algorithm 2**.

Step 5: Implement the mutation strategy introduced by **Algorithm 3**.

Step 6: If there is an abandoned food source, replace it with a new food source discovered by the scout bee.

Step 7: Check whether the termination criteria are satisfied. If they are, stop searching and output the final food position; otherwise, return to **Step 2**.

3. Result analysis and discussion

In this section, the effectiveness of the BABC algorithm is empirically evaluated on a set of benchmark test functions with 18 benchmark test functions with 30-D developed in IEEE CEC2010. Note that all objective functions of these benchmark

test functions should be minimized. The parameters settings of BABC algorithm are as follow: colony size (SN) is 80, maximum cycle number (MCN) is 7500, the value of limit is $0.5 * SN * D$. Thus, the maximum number of FEs is 600000. Experiments were repeated 25 times independently.

Table 1 show the statistical results of original ABC algorithm and BABC algorithm for 18 benchmark test functions. In these tables, Best, Mean and Worst represent the best, mean and worst function value over 25 independent runs; Std. represents the stability of algorithm; Percentage represents the percentage of feasible individuals in population. The results show that the BABC algorithm can obtain the optimal solution stability better than original ABC algorithm. From the last column, the percentage values show that the BABC algorithm also has more feasible individuals in population than original ABC algorithm dose.

To further exam the performance of the proposed algorithm, the best solutions are compared with εDEag, SRS-εDEag, ECHT-DE, AIS-IRP, DyHF, FROFI and CMODE. All the comparison results show in Table 2. According to the mean results, it is shown that BABC algorithm performs equal or better than εDEag, SRS-εDEag, ECHT-DE, AIS-IRP, DyHF, FROFI, CMODE and ABC. The compared results show that the proposed algorithm has the better performance on constrained optimization problems.

It is well known that the performance of any evolutionary algorithm on constrained optimization problem is highly affected by the constraint handling method. In fact, the algorithm using feasibility rules lack of objective function information used in the population. In BABC algorithm, we combine the objective function information through searching procedure, such that the proposed algorithm can efficiently and effectively solve the constrained optimization problems.

4. Conclusion

In this paper, we present a balancing ABC algorithm for constrained optimization problems, called BABC. In BABC, the information of objective function has been used to alleviate the greediness and improve the robustness of the well-known feasibility rule by the replacement mechanism and the mutation strategy. To improve the convergent speed, the opposite learning initialization on initial stage and the best-lead search equation on onlooker bee stage are used. Experiments are performed on benchmark test sets from IEEE CEC2010. The comparative studies indicate that:

i) the opposite learning initialization is a promising way to deal with the diversity of initial population;

ii) the best-lead search equation adding in original ABC algorithm make the algorithm to have the capability to improve the convergent speed during evolution;

iii) the replacement mechanism and mutation strategy can balance the information of both constraints and objective function, and increase the diversity of population.

In conclusion, the BABC algorithm can be efficiently used for solving constrained optimization problems. In the future, there are some directions that should be noticed:

i) to design new constrained handling model for solving more complicated high-dimension and large-scale constrained optimization problems;

ii) to combine with advanced discrete processing methods for discrete constrained optimization problems.

Table 1. Statistical results over 25 independent runs

Fun	Algorithm	Best	Mean	Worst	Std	Percentage
C01	ABC	–5.79E–01	–5.54E–01	–5.30E–01	1.49E–02	1.00
	BABC	–5.64E–01	–4.75E–01	–3.66E–01	4.71E–02	1.00
C02	ABC	2.80E+00	3.94E+00	4.75E+00	5.44E–01	0.33
	BABC	1.89E+00	3.71E+00	4.33E+00	5.18E–01	0.97
C03	ABC	2.63E+02	6.79E+02	1.51E+03	3.49E+02	0.00
	BABC	4.74E+03	3.60E+04	1.08E+05	2.60E+04	0.00
C04	ABC	1.32E+00	2.51E+00	4.79E+00	9.16E–01	0.00
	BABC	3.80E+01	1.87E+04	2.03E+05	4.97E+04	0.00
C05	ABC	6.95E–05	2.43E–03	8.45E–03	1.76E–03	0.00
	BABC	1.97E–03	4.21E+02	5.31E+02	1.11E+02	0.83
C06	ABC	5.53E–04	3.04E–03	7.81E–03	1.89E–03	0.00
	BABC	8.29E–05	4.42E+02	5.61E+02	1.49E+02	0.78
C07	ABC	1.63E–02	1.43E+00	1.51E+01	3.09E+00	1.00
	BABC	1.29E+07	1.48E+09	1.19E+10	3.06E+09	1.00
C08	ABC	2.50E–02	3.93E+00	4.79E+01	1.01E+01	1.00
	BABC	1.69E+09	2.06E+10	4.35E+10	1.21E+10	1.00
C09	ABC	8.40E–05	1.97E+12	4.94E+13	9.87E+12	0.00
	BABC	4.04E–04	1.92E+13	3.61E+13	8.79E+12	0.85
C10	ABC	1.10E–04	4.39E+12	4.25E+13	1.24E+13	0.00
	BABC	1.24E+13	2.19E+13	3.64E+13	6.64E+12	0.92
C11	ABC	1.04E–03	3.40E–01	1.84E+00	4.39E–01	0.00
	BABC	2.67E+04	1.28E+06	1.97E+07	3.91E+06	0.00
C12	ABC	–8.68E+02	–4.21E+02	2.51E+02	3.84E+02	0.07
	BABC	2.78E+01	2.27E+10	2.91E+11	7.22E+10	0.00
C13	ABC	–6.45E+01	–6.18E+01	–6.01E+01	1.16E+00	0.97
	BABC	–5.51E+01	–4.33E+01	–2.40E+01	8.23E+00	1.00
C14	ABC	1.64E+13	6.57E+13	1.19E+14	2.84E+13	1.00
	BABC	1.09E+14	2.07E+14	2.86E+14	4.86E+13	1.00
C15	ABC	1.76E+14	3.26E+14	4.80E+14	7.14E+13	0.60
	BABC	1.16E+14	2.60E+14	3.77E+14	6.50E+13	1.00
C16	ABC	1.13E+00	1.17E+00	1.21E+00	1.97E–02	0.22
	BABC	1.06E+00	1.13E+00	1.17E+00	2.88E–02	1.00
C17	ABC	9.07E+02	1.36E+03	2.32E+03	2.96E+02	0.13
	BABC	7.10E+02	1.13E+03	1.74E+03	2.75E+02	0.97
C18	ABC	1.85E+04	3.02E+04	4.25E+04	5.38E+03	0.37
	BABC	1.56E+04	2.59E+04	3.51E+04	5.08E+03	0.99

Table 2: The best solution obtained by εDEag, SRS-εDEag, ECHT-DE, AIS-IRP and BABC

Fun	εDEag	SRS-εDEag	ECHT-DE	AIS-IRP	BABC
C01	–8.21E – 01	–8.21E – 01	–8.00E – 01	–8.20E – 01	–4.75E – 01
C02	–2.15E+00	–2.19E+00	–1.99E+00	–2.21E+00	3.71E+00
C03	2.88E+01	2.87E+01	9.89E+01	6.68E+01	3.60E+04
C04	8.16E – 03	5.70E – 03	–1.03E – 06	1.98E – 03	1.87E+04
C05	–4.50E+02	–4.63E+02	–1.06E+02	–4.36E+02	4.21E+02
C06	–5.28E+02	–5.29E+02	–1.38E+02	–4.54E+02	4.42E+02
C07	2.60E – 15	2.70E – 15	1.33E – 01	1.07E+00	1.48E+09
C08	7.83E – 14	4.90E – 14	3.36E+01	1.65E+00	2.06E+10
C09	1.07E+01	2.43E+00	4.24E+01	1.57E+00	1.92E+13
C10	3.33E+01	3.29E+01	5.34E+01	1.78E+01	2.19E+13
C11	–2.86E – 04	–2.99E – 04	2.60E – 03	–1.58E – 04	1.28E+06
C12	3.56E+02	2.13E+02	–2.51E+01	4.29E – 06	2.27E+10
C13	–6.54E+01	–6.59E+01	–6.46E+01	–6.62E+01	–4.33E+01
C14	3.09E – 13	1.04E – 13	1.24E+05	8.68E – 07	2.07E+14
C15	–8.21E – 01	–8.21E – 01	–8.00E – 01	–8.20E – 01	–4.75E – 01
C16	–2.15E+00	–2.19E+00	–1.99E+00	–2.21E+00	3.71E+00
C17	2.88E+01	2.87E+01	9.89E+01	6.68E+01	3.60E+04
C18	8.16E – 03	5.70E – 03	–1.03E – 06	1.98E – 03	1.87E+04

Table 3: The best solution obtained by FROFI, DyHF, CMODE, ABC and BABC

Fun	FROFI	DyHF	CMODE	ABC	BABC
C01	–8.21E – 01	–8.21E – 01	–8.21E – 01	–5.54E – 01	–4.75E – 01
C02	–2.00E+00	5.74E – 01	9.75E – 01	3.94E+00	3.71E+00
C03	2.87E+01	3.03E+12	2.18E+01	6.79E+02	3.60E+04
C04	–3.33E – 06	8.25E+00	6.72E – 04	2.51E+00	1.87E+04
C05	–4.81E+02	2.95E+12	2.77E+02	2.43E – 03	4.21E+02
C06	–5.29E+02	–2.10E+01	–4.96E+02	3.04E – 03	4.42E+02
C07	0.00E+00	1.59E – 01	5.24E – 05	1.43E+00	1.48E+09
C08	0.00E+00	4.72E+00	3.68E – 01	3.93E+00	2.06E+10
C09	4.30E+01	1.50E+13	1.72E+13	1.97E+12	1.92E+13
C10	3.13E+01	1.57E+13	1.60E+13	4.39E+12	2.19E+13
C11	–3.92E – 04	–1.68E – 01	9.50E – 03	3.40E – 01	1.28E+06
C12	–1.99E – 01	–1.59E+01	–3.46E+00	–4.21E+02	2.27E+10
C13	–6.83E+01	–6.61E+01	–3.89E+01	–6.18E+01	–4.33E+01
C14	9.80E – 29	2.41E+12	9.31E+00	6.57E+13	2.07E+14
C15	2.16E+01	5.49E+13	1.51E+13	3.26E+14	2.60E+14
C16	0.00E+00	7.41E – 01	6.30E – 02	1.17E+00	1.13E+00
C17	1.59E – 01	6.04E+02	3.12E+02	1.36E+03	1.13E+03
C18	4.87E – 01	1.18E+04	7.36E+03	3.02E+04	2.59E+04

References

[1] D. Karaboga, B. Akay: *A modified artificial bee colony (ABC) algorithm for constrained optimization problems.* Applied Soft Computing *11* (2011), No. 3, 3021–3031.

[2] Z. Michalewicz, M. Schoenauer: *Evolutionary algorithms for constrained parameter optimization problems.* IEEE Journal Evolutionary Computation *4* (1996), No. 1, 1–32.

[3] M. Thakur, S. S. Meghwani, H. Jalota: *A modified real coded genetic algorithm for constrained optimization.* Applied Mathematics and Computation *235* (2014), 292 to 317.

[4] S. M. Elsayed, R. A. Sarker, D. L. Essam: *Training and testing a self-adaptive multi-operator evolutionary algorithm for constrained optimization.* Applied Soft Computing *26* (2015), 515–522.

[5] K. Deb: *An efficient constraint handling method for genetic algorithms.* Computer Methods in Applied Mechanics and Engineering *186* (2000), Nos. 2–4, 311–338.

[6] M. Tuba, N. Bacanin: *Improved seeker optimization algorithm hybridized with firefly algorithm for constrained optimization problems.* Neurocomputing *143* (2014), 197 to 207.

[7] M. de Castro Rodrigues, B. S. L. M. P. de Lima, S. Guimarães: *Balanced ranking method for constrained optimization problems using evolutionary algorithms.* Information Sciences *327* (2016) 71–90.

[8] L. Gao, Y. Zhou, X. Li, Q. Pan, W. Yi: *Multi-objective optimization based reverse strategy with differential evolution algorithm for constrained optimization problems.* Expert Systems with Applications *42* (2015), No. 14, 5976–5987.

[9] Y. Wang, B. C. Wang, H. X. Li, G. G. Yen: *Incorporating objective function information into the feasibility rule for constrained evolutionary optimization.* IEEE Transactions on Cybernetics *46* (2016), No. 12, 2938–2952.

[10] Q. Xu, L. Wang, N. Wang, X. Hei, L. Zhao: *A review of opposition-based learning from 2005 to 2012.* Engineering Applications of Artificial Intelligence *29* (2014) 1–12.

[11] G. Zhu, S. Kwong: *Gbest-guided artificial bee colony algorithm for numerical function optimization.* Applied Mathematics and Computation *217* (2010), No. 7, 3166–3173.

Received June 6, 2017

Acta Technica *62* No. 1A/2017, 381–390

The application of digital image processing technology in glass bottle crack detection system[1]

Kuang Tai[2]

Abstract. In order to solve the current mass production of glass bottles and the stringent requirements of quality problems, this paper adopts digital image processing technology is applied to the detection of glass bottle crack, in order to establish a complete glass bottle crack detection system. The image preprocessing, image segmentation and feature extraction are used to monitor the crack in the glass bottle. Through the implementation of related algorithms and the construction of the frame, a rapid detection system of glass bottle cracks has been obtained. The experimental results show that the digital image processing has strong practicability in detecting the crack of glass bottle. This system greatly improves the detection speed and accuracy, and can bring great convenience for manufacturers.

Key words. Digital image processing, glass bottle crack detection, feature extraction, two-value image.

1. Introduction

The detection methods of glass bottle cracks are mainly as follows: artificial detection, sensor based inspection, and non-contact inspection based on machine vision. Artificial inspection costs a lot of human resources, and the human eyes cause fatigue and other nonresistance factors, so the accuracy of the detection cannot be well guaranteed. The precision of sensor based detection is higher. However, the instrument cost is too high and the flexibility is not high. In the two aspects, the machine vision inspection method has great advantages.

Chen Hanqing mentioned that in the today's society dominated by computer technology, digital image processing has received great attention (Chen et al. 2013) [1]. Digital image processing first appeared in 1950s. Because of the rapid processing of images by computers, computer technology has been applied to graphics and image information processing. The initial application of image processing is to improve the

[1]This work is supported by Zhejiang Natural Science Foundation of China (No. LZ15F030002).
[2]Zhejiang College of Security Technology, Wenzhou, 325016, China

quality of images, and to improve the visual effects for human objects. Zhang Hong found that with the further development of image processing technology, extensive attention in many applications has been received and milestone progress has been achieved, such as aerospace, biomedical engineering, and even artificial intelligence (Zhang et al. 2015) [2].

Through the screening and image segmentation and other operations of the head images of the part taken by the CCD camera, the core part and crack were extracted, which successfully improved the detection efficiency of threaded parts head crack (Yang et al. 2013) [3]. Because of the successful application of crack detection in many fields, digital image processing technology is also used in the detection of glass bottle mouth. Ding Ting obtained the best threshold according to the iterative method, extracted the features and imported rectangular displacement sensor (Ding et al. 2007) [4]. The crack point was searched by double circle method, and the crack was determined by field scanning method. Practice has proved that the application of digital image processing in crack treatment of glass bottle mouth is very successful. Due to the quality of the picture affected by many factors, Chen Tong made more attempts on the basis of the original (Chen et al. 2013) [5]. In order to improve the efficiency of the system, Li Juncheng made accurate judgment on the glass bottle crack through a series of operations, such as the pretreatment of glass bottle image, the image segmentation and the rough positioning of the center of the bottle mouth (Li et al. 2015) [6]. In the detection of glass fiber reinforced plastic composites, Glud captured white light images from the specimen, used transmission light to detect cracks in the image, then processed the cracks and calculated their cracks within the duration of the test (Jia et al. 2016) [7]. With the development of computer technology, great progress has been made in crack detection based on digital image processing.

2. State of the art

With the development of computer software and hardware, the theory and method of digital image processing have been improved day by day. Therefore, its application fields are gradually expanding, from the original aviation, aerospace and other specialized fields to other industries closely related to human daily life. Many glass bottle crack detection systems based on digital image processing have been established and perfected step by step. Chen Yuanyan used CA-MPE-1000 black and white image acquisition card to obtain the 8-bit grey image of the detected glass bottle (Chen et al. 2001) [8]. In order to reduce the research scope, the bottle neck region with the crack might be fixed relative to the whole image. He used field averaging to preprocess the glass bottle to eliminate most of the random noises. Since the black and white images cannot obtain the grey threshold directly, we choose the method of setting the threshold. This method is not suitable to realize the binary images of the position object and the background point, which is the percentage of the total pixel. Therefore, the grey scale histogram is selected to better judge the threshold in this topic. Only the domain average method cannot eliminate the small error, so a median filtering method is added to make the image better recognition.

On the basis of previous studies, Luke chose to add a median filter to suppress the noise of the image, and the median filter method could better protect the image edge information. Grey histogram was adopted to set the threshold (Lu et al. 2015) [9]. This method could find the most suitable threshold so that the binary image was more suitable for feature extraction. The roundness index was used to determine whether the image was a crack image. The method was fast and accurate, and it could well meet the needs of actual production. But for the region of interest, if the interference spot or background brightness was too large, it would lead to the wrong result of the algorithm. In order to solve this problem, Yan Taishan adopted the new intelligent model of neural network, which provided a new framework for industrial inspection system (Yan 2005) [10]. The crack detection system of glass bottle was realized by BP neural network structure, which improved the flexibility of environment change, the fault tolerance, the learning and adaptive ability of the system. Through the training of a large number of samples, it could well meet the situation of large interference with good judgment.

3. Methodology

The subject is in accordance with the flow chart, as shown in Fig. 1, for the glass bottle crack detection.

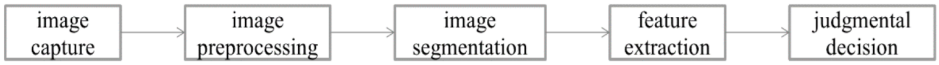

Fig. 1. Operation process of glass crack detection system

3.1. Image acquisition

Yu Fashan proposed that, because the camera could capture the moving image in real time, it converted the optical signal into a two-dimensional electrical signal (Yu et al. 2013) [11]. The digital image could be obtained by converting the image acquisition card with A/D conversion function, which could meet the needs of actual production. Therefore, the camera image is usually taken to obtain the glass bottle image.

3.2. Image preprocessing

In actual production, the quality of the image does not reach the ideal state because of the illumination condition and the image transformation. Therefore, the quality of the image is reduced to a certain extent. Li Li concluded that before the analysis of the image, the quality of the image should be improved (Li et al. 2016) [12]. In order to reduce the image noise, the image needs to be processed smoothly. In this paper, we choose the smoothing method and median filtering method to process the image, which can filter the noise effectively and protect the edges of the image better. The basic idea of the domain averaging method is to replace the

greyscale of each pixel with the average of several pixels. It is assumed that there is image $F(x, y)$ with $N \times N$ pixels, and another image $g(x, y)$ is obtained after smoothing. The $g(x, y)$ is determined by the formula

$$g(x, y) = \frac{1}{M} \sum_{(m,n)\in x} f(x, y) \tag{1}$$

where $x, y = 0, 1, 2...$ is a collection of coordinates at the midpoint of the field, but it does not include (x, y) points. And M is the total number of coordinate points in the collection. The formula (1) indicates that the grey value of the pixel is determined by the average value of the predetermined field.

Figure 2, left part shows an example of the original image and right part depicts the same image after processing by domain filtering.

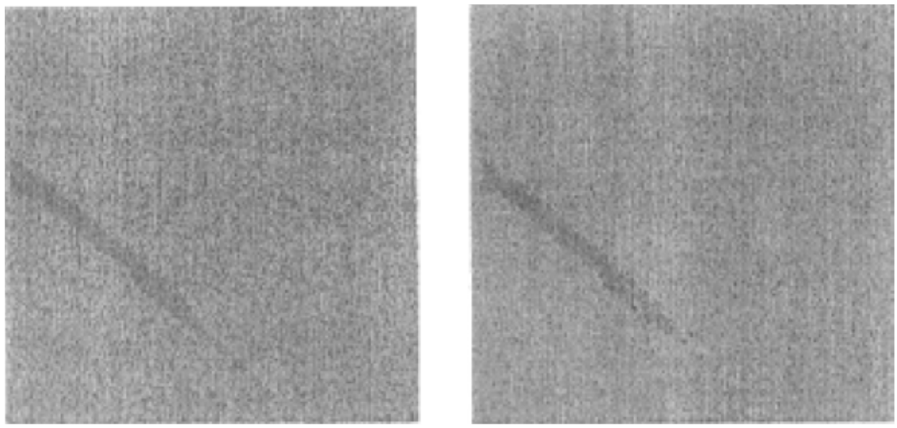

Fig. 2. Original image (left) and image after processing by domain filtering (right)

By comparing the image processed by the original image and the domain filter, we can see that the algorithm can eliminate the noise and make the edge smooth, but the image becomes more blurred. Because the image noise of glass bottle is not strong enough, the image sharpness and edge strength are highly demanded in the following work. To improve this, we have added the use of median filtering.

Median filter is a kind of nonlinear spatial filter, which has good effect on eliminating the interference of isolated points. The basic principle of median filtering method is to use a median of each sample point in the field instead of digital image or in a sequence of values.

The field of a particular length or shape of a point is called a window. At this point, two-dimensional windows in some forms are used. Let $\{x_{i,j}, (i, j) \in I^2\}$ represent the grey values of each point of the digital image. In the filter window A, two-dimensional median filter can be defined as

$$y_{i,j} = \mathrm{Med}\{x_{i,j},\ (i, j) \in I^2\} = \mathrm{Med}\{x_{(i+r),(j+s)},\ (r, s) \in A,\ (i, j) \in I^2\}, \tag{2}$$

where A is a two-dimensional median filter window.

Median filter is used in image processing. By setting a filter window, it traverses the points on the image. Replace the value of the center point of the window with the median value of the original values in each window.

Single use of the domain average method and median filtering method cannot meet the desired requirements. In order to obtain better image, it is found by comparing Fig. 3, left and right parts that the combination of one domain averaging method and four median filtering can filter the original noise in the image to a great extent. Moreover, the edge information of the crack image is well saturated, so that the edge is strengthened. Through the image preprocessing of the crack image, the subsequent feature extraction can be carried out more smoothly.

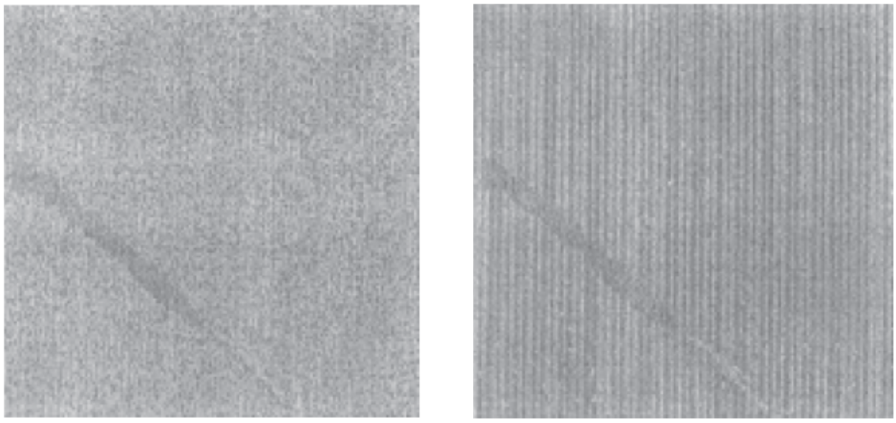

Fig. 3. Original image (left) and image after median filtering (right)

3.3. Image segmentation

In order to make computers better for image recognition and processing, the most important thing is to segment a large amount of information. The purpose of image segmentation is to divide the image space into some meaningful areas. The computation speed is greatly improved by studying only the regions of interest. Feng Xue believed that image segmentation included discontinuous detection, threshold processing, region processing, morphological processing, watershed method and so on (Feng et al. 2014) [13]. Each method has its advantages and disadvantages. In order to improve speed, we choose threshold processing.

Since the range of grey values of the objects and backgrounds to be processed is different, the grey values of each pixel in the image are compared with the threshold by using the threshold setting method. The pixel grey value which is greater than the threshold is set to 255, and the pixel grey value which is less than the predicted pixel is set to be 0. A new grey scale image can be obtained. This method is simple in calculation and can obtain good results. It can close and connect the needed area without overlapping erroneous judgment. The choice of threshold is very important, which affects the quality of image segmentation. This subject uses grey image binarization principle to segment the processed image, and separates the

crack image from the background, so as to prepare for the feature extraction.

The image after the binarization process is depicted in Fig. 4.

Fig. 4. Image after binarization processing

3.4. Feature extraction

Feature extraction is an important part of digital image processing and computer vision, and it is the key step of feature matching. Grey scale information of image is used to detect the corner and edge points of grey scale and gradient transform. In this paper, we need to extract the crack in the image to make the later judgment.

Jia Ping found that in his study, since the feature points of the crack were different from the background, the crack in the image was determined by giving some parameters of the characteristic points of the glass crack (Jia et al. 2013) [14]. According to the characteristics of the grey value of the glass crack image, the geometric features of the segmented image are analyzed and measured. In these characteristics, there are some quantities that can be represented by numbers, such as area, perimeter, etc., which can be used as the basis for judging the existence of cracks. The features are extracted by feature extraction and used for image recognition and understanding.

In an image that has been segmented, the area of the target can be simply defined as the number of pixels contained in the target boundary. By scanning the entire target area, the grey value is calculated to be one pixel total.

$$A = \sum_{x=1}^{N} \sum_{y=1}^{M} f(x, y)\,, \tag{3}$$

At the same time, the perimeter of the crack can be obtained by finding the sum of the pixels of the outer boundary of the image.

After obtaining the area and perimeter of the crack, we can calculate the roundness of the crack. Since the shape of the crack is generally slender, the characteristic

parameter roundness can be used as an index to determine whether there is crack or not.

Cai Qing mentioned that roundness was defined as (Cai et al. 2017) [15]

$$C = \frac{p^2}{4\pi A}, \tag{4}$$

where A represents the area of the object and p represents the perimeter of the object:

$$\text{Area} \in \begin{cases} \text{circle, when} & C = 1, \\ \text{thin, when} & C > 1. \end{cases} \tag{5}$$

If the calculated target circularity conforms to the standard range, it can be judged as crack. According to the result, whether there are cracks in glass bottles is determined. They are displayed and stored in the appropriate files to facilitate subsequent production needs.

3.5. Software design

Because VS has the advantages of simple interface and good programming language, Visual Studio 2010 is used as the development platform to realize the function of each module in this paper. The process of image processing includes the image acquisition and display, image processing, analysis and image storage. In order to meet the needs of actual production, the basic functions of the system are image preprocessing, image segmentation, feature extraction and crack detection. Through the comparison results of the original image and the processed image, a decision is made. Specific modules and implementations are shown below, in Fig. 5.

4. Result analysis and discussion

Several experiments have shown (see Table 1) that the roundness of the edge of the crack spot is maintained at about 0.35, and the length of the crack is maintained at about 0.80, so that the principle of fast determination of the boundary crack can be obtained. If such an area of light appears in an image, the roundness of its edge is between 0.30 and 0.50, and the fine length is between 0.70 and 0.85, there is a spot in the image that is reflected by the crack, which indicates that there is a crack region in this image. Through the conclusion, we can test the crack of glass bottle more quickly in actual production.

Table 1: Ten samples of glass bottles: crack detection, roundness and fine length

number	1	2	3	4	5	6	7	8	9	10
roundness (cm)	0.33	0.30	0.34	0.32	0.40	0.38	0.33	0.36	0.33	0.31
slightness (cm)	0.81	0.78	0.75	0.81	0.74	0.71	0.80	0.78	0.82	0.83

In addition to the above conclusions, it has been proved by many practices that the combination of domain filtering method and median filtering method can make

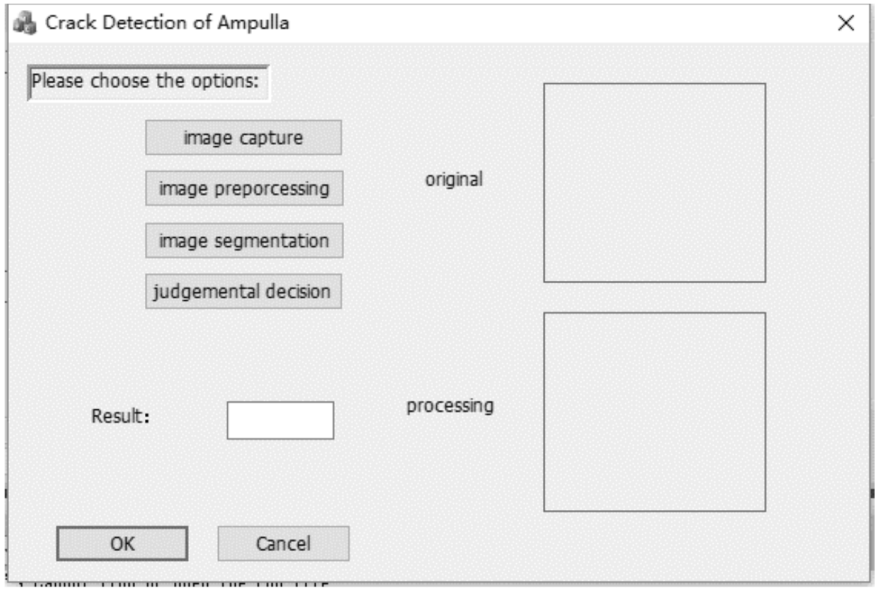

Fig. 5. Interface of glass bottle crack detection system

image processing more delicate, which is more suitable for subsequent feature extraction. Judging whether there is a crack in the glass bottle by roundness, it has a high accuracy rate. For the detection of 300 samples, the detection system only misjudges 1 bottle without cracks, the error detection rate is 0.3 %, and the omission rate is zero. At the same time, the speed of the detection system is very high. By setting timers in the program, the detection of each glass bottle needs only about 40 ms, while the average rate is 100 ms. The speed is more than doubled, and it can well meet the needs of the actual production test of the glass bottle. A typical result can be seen if Fig. 6.

5. Conclusion

This paper aimed to establish a glass bottle crack detection system based on digital image processing to help manufacturers improve the quality of products. The noise of the picture was suppressed and the edge of the image was smoothed by means of averaging and median filtering. Then we drew grey histogram to set the threshold, and made binarization processing of the image. Finally, the crack on the binary image was detected and judged to obtain the result that whether the glass bottle had cracks. Through the research of this subject, some conclusions were drawn. In the process of image preprocessing, considering the factors of computation speed and processing accuracy, the image quality could be better by one domain filtering and three median filtering. At the same time, due to the particularity of the crack image, the corresponding threshold could be set to determine whether there was a crack in the image.

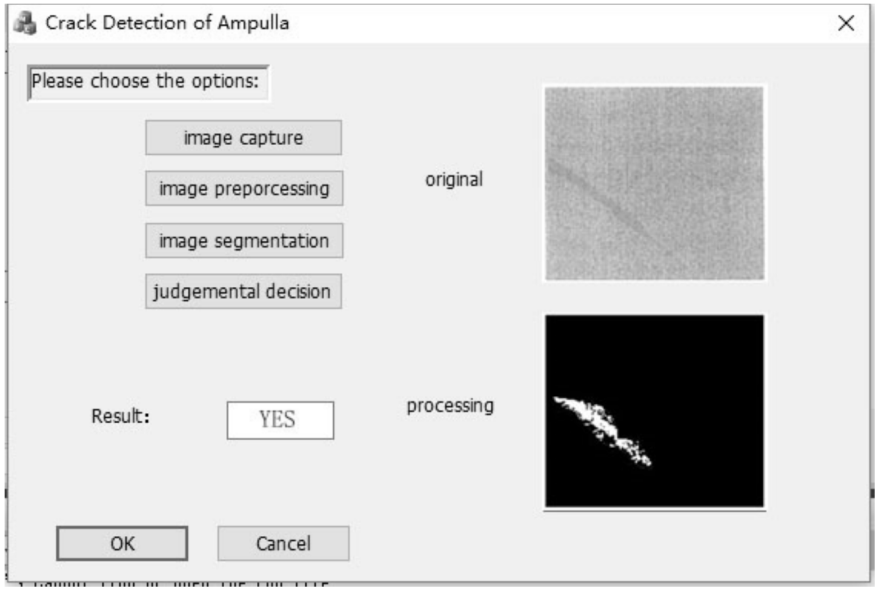

Fig. 6. Results of glass bottle crack detection system

The designed glass bottle crack detection system based on digital image processing technology can be widely applied in practical production, which breaks the limitations of traditional methods, such as time-consuming and long time, and improves the user's competitiveness in the industry. As the system is still in the initial stage of establishment, it cannot meet the realization and improvement of some functions, and there is a gap between it and the expectation. And the threshold chosen by the algorithm itself has to be proved by a great deal of practice. We hope that in future practice, the resolution of the image itself will be enhanced and the detection efficiency will be higher.

References

[1] H. C. Chen, S. S. Kuo, S. C. Sun, C. H. Chang: *A distinguishing arterial pulse waves approach by using image processing and feature extraction technique.* Journal of Medical Systems *40* (2016), No. 10, 215.

[2] H. Li, T. Zhao, N. Li, J. Du: *Feature matching of multi-view 3d models based on hash binary encoding.* Neural Network World: International Journal on Neural and Mass—Parallel Computing and Information Systems *27* (2017), No. 1, 95–105.

[3] M. Xia, W. Lu, J. Jang, Y. Ma, W. Yao, Z. Zheng: *A hybrid method based on extreme learning machine and k-nearest neighbor for cloud classification of ground-based visible cloud image.* Neurocomputing *160* (2015), 238–249.

[4] F. Liang, Y. Xu, M. Zhang, L. Zhang: *A POCS algorithm based on text features for the reconstruction of document images at super-resolution.* Symmetry *8* (2016), No. 4, 102.

[5] W. Lu, W. Zong, W. Xing, E. Bao: *Gait recognition based on joint distribution of motion angles.* Journal of Visual Languages & Computing *25* (2014), No. 6, 754–763.

[6] X. X. Zhou, T. Yan: *Applied-information technology in random naming system based on image processing and application.* Advanced Materials Research *1046* (2014), 440 to 443.

[7] X. Chen, W. Cheng: *Facial expression recognition based on edge detection.* Journal of Computer Science and Engineering Survey *6* (2015), No. 2, 1.

[8] A. Alrashdan, S. Motavalli, B. Fallahi: *Automatic segmentation of digitized data for reverse engineering applications.* IIE Transactions *32* (2000), No. 1, 59–69.

[9] J. Wang, A. K. Asundi: *A computer vision system for wineglass defect inspection via Gabor-filter-based texture features.* Information Sciences *127* (2000), Nos. 3–4, 157–171.

[10] T. S. Yan: *Crack detection model of glass bottles based on BP artificial neural network.* Sci-Tech Information Development & Economy *15* (2005), No. 15, 182–183.

[11] X. Peng, X. Li: *An online glass medicine bottle defect inspection method based on machine vision.* Glass Technology—European Journal of Glass Science and Technology Part A *56* (2015), No. 3, 88–94.

[12] M. H. Ma, G. D. Su, J. Y. Wang, Z. Ni: *A glass bottle defect detection system without touching.* Proc. International Conference on Machine Learning and Cybernetics, 4–5 Nov. 2002, Beijing, China *2*, 628–632.

[13] F. Duan, Y. N. Wang, H. J. Liu, Y. J. Li: *A machine vision inspector for beer bottle.* Applications of Artificial Intelligence *20* (2007), No. 7, 1013–1021.

[14] P. Jia, N. Xu, Y. Zhang: *Automatic target recognition based on local feature extraction.* Optics and Precision Engineering *21* (2013), No. 7, 1898–1905.

[15] L. Wang, C. Li, Q. Sun, D. Xia, C. Y. Kao: *Active contours driven by local and global intensity fitting energy with application to brain MR image segmentation.* Computerized Medical Imaging and Graphics *33* (2009), No. 7, 520–531.

Received June 6, 2017

Acta Technica *62* No. 1A/2017, 391–400

Research on graphic design based on digital media[1]

Yanjun Shi[2], Cheng Feng[2], Yanfang Shen[2]

Abstract. The application of digital media technology has promoted the technical reform in the art field of our country. Under the background of digital media, graphic design is developing rapidly. In order to promote the application of digital media technology in graphic design field, firstly, the research status of digital media and graphic design at home and abroad was introduced in this paper. Then, the multivariate statistical analysis method was applied, and the process of the relationship between digital media and graphic design was expounded. Finally, the data obtained from the multivariate analysis model was analyzed and conclusions were drawn. The results show that the application of digital media technology enriches the means of graphic design, but it has less influence on design thinking and content. According to the research results, the influence of digital media on graphic design was summarized, the direction of improvement was pointed out, and some references were provided for graphic design thinking and content optimization.

Key words. Digital media, graphic design, multivariate analysis.

1. Introduction

In recent years, China's economy and society have been greatly developed, especially in the field of science and technology. The application of computer technology has brought about tremendous impacts on China's economy and society, and has brought about tremendous changes in the lives of our people. The popularization of computer technology and Internet technology has led our country into the digital era.

The advent of the digital media era has provided greater technical support for the development of visual arts and multimedia fields in China, and due to the rapid development of multimedia technology, China has made unprecedented progress in the field of art. Graphic design is one of the most important parts of art. To a great extent, the technology of digital media has promoted the development and

[1]The project of the education science project in Hebei province (the VTE—CDIO Education mode of animation vocational education) 1250186.

[2]Handan University, Handan, Hebei, China, 056001

progress of graphic design in our country. Digital media technology initially has brought great liberation and convenience for the staff of graphic design industry in our country. However, for graphic designers, the most important impact of digital media technology on graphic design industry is that it has led to a qualitative leap in the transmission of design ideas. China's digital media started relatively late. Although it has been generally recognized by our people, how to better understand the impact of digital media on China's graphic design industry and enhance its application effect is still an important topic for our researchers to study deeply.

Based on this, through the construction of multiple-regression analysis model, the graphic design in the background of digital media was analyzed and studied in this paper.

2. State of the art

Foreign scholars have studied digital media technology earlier, while Chinese scholars have fewer achievements, and most of the research results are too theoretical, and there are some deficiencies in the depth and breadth of the research content.

The study of digital time by foreign scholars can be traced back to the 1960s. Hua has proposed that the development of digital media technology will one day replace the traditional media, and people will usher in the digital era [1]. ADI has believed that digital media technology has important implications for modern manufacturing and design industries, and at the same time, he has practically expounded the relationship between the existing digital media technology and graphic design [2]. Gate has believed that media art and media technology are closely related to each other, and meanwhile, he has comprehensively introduced and expounded the development process and major problems of media art in the last century [3]. Discussed was the relationship among new media technology and modern art creation and design teaching, and it was believed that the emergence of digital media technology has historic significance for the design industry [4]. From the point of view of art aesthetics, LAN has expounded the important influence of digital media technology on advertisement design and television art [5].

The above studies are the introduction and discussion of the development process and the influence of digital media technology. Although these studies have conducted a more detailed discussion of the digital media era, there is a lack of research on the practical application of digital technology in graphic design in the era of digital media. Therefore, the in-depth study of the relationship between digital media and graphic design is of great significance. Therefore, in view of the shortcomings of the existing research, a multiple regression analysis model is proposed in this paper, and the graphic design and digital media are analyzed and studied. In addition, in the third part, the specific contents of the research object and the construction of the multiple-regression analysis model are expounded. In the fourth part, the specific data of the multiple-regression analysis model is obtained, and the data results are analyzed. And the fifth part is a summary of the full text.

3. Methodology

Through the method of multiple regression analysis, the graphic design of digital media era was mainly studied in this paper. Some experts thought that in the regression analysis, if there are two or more than two independent variables, it is called the multiple-regression [6]. In fact, a phenomenon is often associated with a number of factors, and it is more effective and more practical to predict or estimate the variables by using the optimal combination of multiple independent variables than with only one independent variable. Therefore, multiple-linear regression is more practical than single linear regression. It was believed that the basic principle and basic calculation process of multiple-linear regression are the same as that of unary linear regression. However, due to the number of independent variables, the calculation is very troublesome, which should rely on statistical software in practical applications [7].

Knight has thought that the units may be different because of the independent variables. For example, in a graphic design level relationship, designer's salary level, education level, occupation, region, family burden and so on will affect the level of graphic design, and the units of these factors are obviously different. Therefore, the magnitude of the coefficient of the independent variable does not explain the magnitude of the factor. To put it simply, the regression coefficient obtained in Yuan is less than the one in 100 yuan in the case of the same wage income, but the effect of the designer's wage level on graphic design will not change. Therefore, each independent variable should be unified into the unit [8]. According to Oswald, the common standard used in theoretical research has this function. Specifically, all variables, including dependent variables, are firstly translated into standard scores and then carried out in linear regression, and the regression coefficients obtained at this time can reflect the importance of the independent variables [9]. The regression equation at this time is called the standard regression equation. The regression coefficient is called the standard regression coefficient, which is expressed as

$$Z_y = \beta_1 \times 1 + \beta_{2Z} \times 2 + \cdots + \beta_{kZ} \times k\,.$$

Here, β with different subscripts are independent variables, Z is the dependent variable and k is the regression coefficient.

The method of constructing multivariate analysis model follows.

Firstly, the multiple regression analysis is different from the single linear analysis and the two element linear analysis. In the multiple regression analysis, the following formula should be applied to compare and test the fitting degree of regression equation, so as to determine whether the regression equation matches the object and content of the study

$$y = a + bx\,.$$

Here, y is the fitting degree, a is one yuan regression coefficient, b is two yuan regression coefficient, and x is the regression variable.

Secondly, according to the results of the above fitting operation, the coefficient of decision is adjusted, and the regression equations used in the study can't be

determined until the resulting fit is high enough. Then, the significance tests should be carried out according to the formula

$$b = \sum xy - n \sum x \sum y \text{div} \left[\sum x^2 - n \left(\sum x \right)^2 \right]$$

to ensure the accuracy of the research results and to lay a good foundation for modeling. Symbol n denotes the number of variables.

Thirdly, the regression coefficients are used to set and select the regression coefficients and variables, and then, the residual analysis is carried out according to the formula

$$a = \sum y - \frac{b}{n} \sum x \,.$$

Here, $\sum y$ denotes the residual value of fitness, and $\sum x$ is the residual sum of regression variables. The residual analysis is mainly used to achieve the normal distribution of the original data, so as to check again significant differences on the basis of ensuring the regression operation.

Fourthly, the regression data obtained by the above steps is input into the SPSS statistical software, and after the operation of the software, the final operation results are obtained, thus providing a good reference for the research of this paper.

The SPSS statistical analysis software mentioned above has a higher frequency of application in theoretical research. Zhou has believed that the basic functions of statistical analysis software include data management, statistical analysis, chart analysis and output management [10]. Figure 1 shows the interface of the SPSS statistical software.

Fig. 1. SPSS statistical software interface

There are many statistical analysis methods for this software, and the statistical analysis methods include simple basic statistical analysis and more complex multivariate statistical analysis, such as the basic statistical analysis, frequency analysis, correlation analysis, regression analysis, cluster analysis, factor analysis and other

statistical analysis methods. Petti has believed that the most important feature of SPSS statistical software are its graphical capabilities. The graphical performance of this analysis software is very good, which can not only help the user analyze the data and get the corresponding analysis results, but also can make graphical statistics of the results of the data, so as to enable users to have a more vivid understanding of the rules of statistical results [11]. SPSS software can generate bar graph, scatter diagram and normal distribution map according to the data, which is helpful for users to understand the statistical results more intuitively. In addition, through the interface, SPSS statistical analysis software can convert data, and carry out statistical analysis. Drucker has believed that SPSS statistical analysis software has a particular graphics system, which can draw graphics on the basis of the data and its results, so as to achieve the different requirements of different users [12]. From the drawing point of view, SPSS statistical software and graphic design have certain commonalities, and the study of graphic design with this software is beneficial for designers to better understand the research results, so as to promote the continuous development of graphic design industry.

SPSS statistical analysis software has a good interface and simple way of operation. Washington has believed that in this software, only data entry and some commands are implemented by keyboard input, while most operations are done by using menus, buttons, and dialog boxes. In the process of using the software, the user only needs to realize the statistical analysis of large amounts of data and achieve the result through the mouse instruction according to the actual demand, and at the same time, users can also get statistical data tables and statistical analysis change icons on the basis of the analysis results [13]. The data analysis and icon analysis can be visually displayed through the screen, and can also be printed on the data analysis tables and charts. Huang has believed that SPSS statistical analysis software has a complete and comprehensive function of data analysis and statistics and contains a statistical type and more than one hundred and thirty kinds of statistical functions [14]. Figure 2 shows the results of the SPSS statistical software application example. SPSS statistical analysis software covers multivariate statistical analysis from simple to complex, such as data exploration, analysis, contingency table analysis, etc. Moreover, SPSS statistical analysis software includes not only conventional statistical analysis methods, but also a variety of multivariate statistical analysis methods, which is very helpful to the users who are not good at mathematics to a certain extent. Steinberg has thought that users can use SPSS statistical analysis software for data analysis without understanding the statistical process of statistical analysis software [15].

4. Result analysis and discussion

The multivariate analysis results obtained by the methods described above are shown in Table that shows the data analysis of the variance analysis and residual analysis of the regression equation. The data shows that the variance and residual error of the regression analysis equation are within a reasonable range, but the mean variance is higher, and the degree of variation is higher, and there is a certain

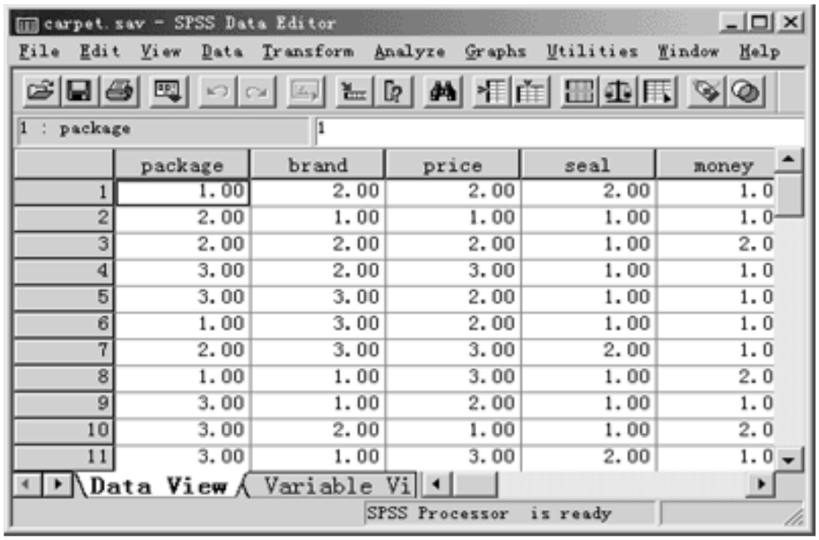

Fig. 2. SPSS statistical software application interface

colinearity problem. Because there is a certain interaction between variables, the degree of variation of individual variables affects the accuracy of the results of the entire regression equation. Once the colinearity problem exists in the regression equation, the significance test of the regression equation is performed to ensure the accuracy of the regression equation.

Table 1. Results of regression analysis of variance

Coefficient	Sum of squares	Freedom	Mean square deviation
Regression	42.823	3	14.274
Residual	0.530	10	0.053

According to the colinearity problem of the regression equation described above, a regression test of the regression coefficients was made. The results are shown in Table 2. The data shows that there was a linear relationship between the standard error and the regression coefficient, and the significance test results accorded with the analysis requirement. It can be seen that the coefficients of the regression equation can meet the requirements, and it is feasible to apply the regression equation to the study of digital media and graphic design. At the same time, the results obtained by regression equation have high reference value.

Table 2. Results of regression coefficient test

Model	Standard error	Partial regression coefficient	T
1	7.852	12.322	3.383
2	–0.566	0.174	12.551
3	–1.206	0.501	-0.213

Through the analysis of variance and the significance test of regression equation, on the basis of ensuring the feasibility of the regression equation, the original parameters were entered into the analysis data obtained by SPSS statistical analysis software, as shown in Table 3. Data shows that the application of digital media technology improves the type and quantity of graphic design software, and the function of graphic design software is more powerful. At the same time, the application of digital media technology stimulates the designers' spatial imagination to a certain extent, thus promoting the continuous optimization of their design thinking. In addition, from the point of view of color richness, the application of digital media technology further refines the color hierarchy, which has a very important positive impact on designers. The variety of colors greatly enhances the visual effects of graphic design.

Table 3. Results of SPSS statistical analysis

Serial number	1	2	3	4	5	6	7	8	9	10
1	1.92	408	2.0	10	2.0	155	4.42	0.96	2.02	1.50
2	2.15	412	1.8	8	2.1	140	4.15	0.95	2.10	1.21
3	2.35	421	2.1	11	2.6	156	4.89	0.94	2.65	1.62
4	3.22	432	2.9	12	2.9	175	3.54	0.88	2.45	1.72
5	3.61	456	2.2	16	3.2	180	3.67	0.93	3.01	1.42
6	4.01	526	3.1	7	4.1	150	2.86	0.81	2.77	1.78
7	3.97	550	2.0	9	2.4	161	2.22	0.78	2.98	1.56
8	3.78	563	2.4	9	2.6	170	2.85	0.77	3.12	1.37
9	4.34	604	4.5	7	6.2	137	4.12	0.95	2.45	1.89
10	2.13	634	6.0	13	6.3	156	3.12	0.65	3.09	1.29

As shown in Figs. 3 and 4, the comparative analysis bar graph produced by the statistical software showed the data results more intuitively. By comparing the results of figures 3 and 4, it can be seen that the application of digital media technology had a certain influence on the design performance and the mode of transmission of graphic design. Comparatively speaking, the influence of digital media technology on graphic design performance varied greatly, and showed the trend of increasing year by year. However, the influence of digital media technology on the propagation of graphic design was fluctuating, although it increased, the growth was not stable. The influence of digital media technology on graphic design was mainly composed of three aspects: design means, design contents and design thinking. The impact of digital media technology on graphic design was significant, which can be verified by the richness of design software, and the influence of digital media technology on graphic design was mainly reflected in the two-way communication between designers and customers. The graphic design of digital media technology can better convey and display the designer's design concept and actual effect to the customers.

To sum up, with the advent of the digital media era, the application of digital media technology in graphic design is beneficial to the performance of graphic design, the promotion of the performance, and the optimization of the mode of communication. And digital media technology has a positive influence on enriching graphic design tools and promoting graphic design effects. However, as a technical means,

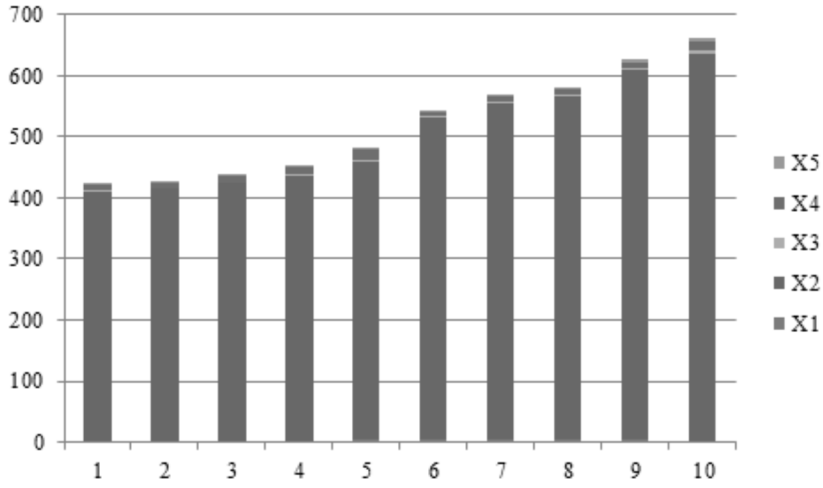

Fig. 3. Analysis of data comparison

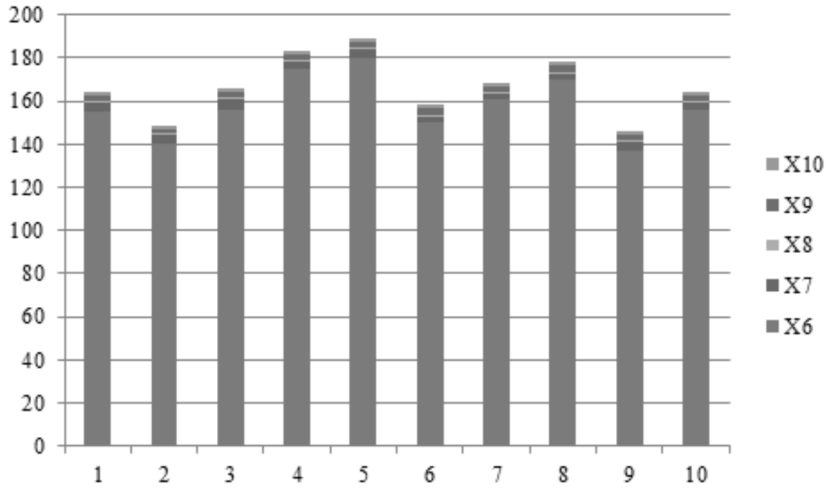

Fig. 4. Analysis of statistical results

the impact of digital media on the design connotation is reflected by quantitative data, and there is a certain error, and the impact will take a long time to validate, and therefore, the degree of positive influence of digital media technology on the design thinking and design content of graphic design is still lacking. The same problems also exist in the study of the influence of digital media technology on graphic design communication, and as a result, although there is some credibility, there are still some errors in the effect of digital media technology on the thinking and content of graphic design. However, the errors do not prevent the research results of the relationship between digital media technology and graphic design. Therefore, it is believed that digital media technology has a higher positive impact on graphic

design, and enterprises and designers can continuously optimize the design content and design thinking on the basis of constantly expanding design tools.

5. Conclusion

In order to enhance the effective application of digital media in graphic design, through the construction of multiple-regression analysis model, the influence of digital media on graphic design was analyzed and studied, and finally, the following main conclusions were obtained in this paper: digital media technology has influence on graphic design, performance, and communication mode, but it has little influence on design performance and communication mode. From the point of view of design performance, digital media technology has a better influence on graphic design, but it has no obvious but positive influence on design content and design thinking.

To sum up, multiple regression analysis model is simple, practical and easy to calculate, but the model of the research object of the professional requirements are higher. The method of multiple regression analysis used in this paper is helpful to make clear the direction of applying digital media to improve graphic design. However, the way of measuring the impact of design thinking and design content is more complex, and therefore, although there is certain reference value in this study, there are still some shortcomings. In future studies, the effectiveness of multiple regression analysis can be improved by increasing the model parameters and improving the comprehensiveness of the parameters, resulting in more credible results.

References

[1] L. Spiegel: *Back to the drawing board: graphic design and the visual environment of television at midcentury.* Cinema Journal *55* (2016), No. 4, 28–54.

[2] R. P. Hamlin: *The consumer testing of food package graphic design.* British Food Journal *118* (2016), No. 2, 379–395.

[3] V. A. Douglas, A. Aultman Becker: *Encouraging better graphic design in libraries: a creative commons crowdsourcing approach.* Journal of Library Administration *55* (2015), No. 6, 459–472.

[4] I. Visser, L. Chandler, P. Grainger: *Engaging creativity: Employing assessment feedback strategies to support confidence and creativity in graphic design practice.*Art, Design & Communication in Higher Education *16* (2017), No. 1, 53–67.

[5] D. Riposati, G. D'Addezio, A. Chesi, F. DiLaura, S. Palone: *Graphic design and scientific research: the experience of the INGV Laboratorio Grafica e Immagini.* Proc. EGU General Assembly Conference Abstracts, 17–22 April 2016, Vienna, Austria, *18*, 7183.

[6] M. T. Ryianti, T. N. Erwin, S. H. Suriani: *Implementing project based learning approach to graphic design course.* American Journal of Education Research *5* (2017), No. 5, 559–563.

[7] R. Harland: *Some important things to say about graphic design education.* Art, Design & Communication in Higher Education *16* (2017), No. 1, 3–6.

[8] P. Viegas: *Kapa magazine, 1990—1993: A survey on postmodern graphic design and appropriation.* Blucher Design Proceedings *1* (2014), No. 5, 265–271.

[9] U. Felix: *A multivariate analysis of students' experience of web based learning.* Australian Journal of Educational Technology *17* (2001), No. 1, 21–36.

[10] J. Zhou: *Expression of traditional graphic design elements in new media art.* Packaging Engineering *34* (2013), No. 2, 28–32.

[11] A. Moreno, C. Navarro, R. Tench, A. Zerfass: *Does social media usage matter? An analysis of online practices and digital media perceptions of communication practitioners in Europe.* Public Relations Review *41* (2015), No. 2, 242–253.

[12] T. Jombart: *adegenet: a R package for the multivariate analysis of genetic markers.* Packaging Engineering *24* (2008), No. 11, 1403–1405.

[13] D. V. Shah, J. N. Capella, W. R. Neuman: *Big data, digital media, and computational social science: Possibilities and perils.* ANNALS of the American Academy of Political and Social Science *659* (2015), No. 1, 6–13.

[14] P. N. Howard, M. M. Hussain: *The role of digital media.* The role of digital media *22* (2011), No. 3, 35–48.

[15] D. V. Dimitrova, A. Shehata, J. Strömbäck, L. W. Nord: *The effects of digital media on political knowledge and participation in election campaigns: Evidence from panel data.* Communication Research *41* (2014), No. 1, 95–118.

Received June 6, 2017

Acta Technica *62* No. 1A/2017, 401–410

Application and simulation analysis of C++ in sweep robot control program

Xiaorong You[1,2], Hao Pei[1]

Abstract. The purpose of this study is to further optimize the planning path, to improve the existing D*Lite algorithm. The reverse search connection path optimization method is used, and the existing D*Lite algorithm in the steering angle of 45 integer multiple limit is canceled. The smooth path of the planning process is to reduce the ground robot movement process of the number of steering and path length. And through simulation to verify the effectiveness of the optimized D*Lite algorithm. At the end, in the Visual C++ environment, the path planning of optimized D*Lite algorithm is programmed on the environment map. The multiple obstacles are added on the environment map, and the path planning capability of the optimized D*Lite algorithm is verified in the complicated environment. The results show that the security improvement strategy and path optimization method can improve the security and path optimization. Therefore, we concluded that the optimized D*Lite algorithm has advantages in ensuring the safety of the sweeping robot and reducing the length of the path.

Key words. C++, sweeping robot, D*Lite algorithm, path optimization.

1. Introduction

With the gradual integration of intelligent appliances into the family life, the application of the ground mobile robot in the life gradually increases, which intelligent sweeping robot is widely used in the home [1]. As a service robot, sweeping robot can replace the traditional manual cleaning work, and the market prospect is broad [2]. At present, domestic sweeping robot rarely has navigation and positioning function, and it lacks effective path planning [3]. It is cheap but is characterized by inefficient cleaning. How to make the sweeping robot moves safely and reliably in a dynamic environment and quickly calculates the shortest path has become an important issue in sweeping robot research.

At present, many researchers in the world study the path planning of sweeping robot. The D*Lite algorithm is an optimized version of the LPA* algorithm [4]. The

[1]Department of Electrical and Mechanical Engineering, Changzhou Textile Garment Institute, No. 5 Gehu Road Changzhou, Jiangsu, 213164, China
[2]Corresponding author

search direction is changed from the target position to the current robot position. And it is more suitable for the robot dynamic path planning in the process of moving [5]. Based on the study of existing D*Lite algorithm, two kinds of space can be improved, including the security improvement of path planning and the optimization of path. D*Lite algorithm uses search method of eight grid, the planned path angle is an integer multiple of 45 °, and it is not suitable for the practical application of the sweeping robot. This paper gives the detection and optimization methods, the optimized path reduces the number of steering and the distance of the robot. And the steering angle can be any angle. Based on the existing grid map, the characteristics of the simulated laser scanning range finder are programmed in the Visual C++ environment. And the path calculation of the optimized D*Lite algorithm is completed. Based on the path calculated in Visual C++ on the sweeping robot, the actual verification of path planning is completed.

2. Materials and methods

2.1. Sweeping robot path planning algorithm

The Sweeping robot path planning algorithm was a safe optimal path from the current location to the target location in the environment map. If the environment was all known, and the location and size of the obstacle information were known, the path planning algorithm could be used to calculate the shortest path and avoid the optimal path, which was the global path planning. If only part of the environmental information was known, or the environment was not known, at this time, the robot configuration sensor only could be relied to perceive the surrounding environment. In the process of walking the robot, the detection of obstacles to avoid obstacles is the local path planning.

The first one is the A* path planning algorithm principle. A* algorithm is a heuristic search algorithm, using the evaluation function $f(n)$ to analyze the current location to the destination location of the path. Priority search of the highest-valued path nodes, in rare cases, it needed to search the entire environment map in order to get the best path. A* algorithm path assessment function was as follows: $f(n) = g(n) + h(n)$, where $f(n)$ evaluates whether the position node n reaches the destination, $g(n)$ is the actual value required from the starting point to the position n and $h(n)$ is the mobile cost estimate of position n to the target location.

The second one is the LPA* algorithm that was used to maintain the three parameters, including $g(s)$, Rhs(s) and $h(s)$ values in path planning. Here, $g(s)$ is the distance from node s to the starting position. And this is equal to G value in the A* algorithm. Symbol Rhs(s) is the estimated value of the parent node of the current node. And the $g(s)$ value is assigned to the node when the grid Rhs(s) value is calculated. Symbol $h(s)$ is the same as the H value in A* and it represents the estimated value of the current node to the target position. The Rhs(s) value is a new variable introduced by the LPA* algorithm, which is calculated as follows. If

Pred(s) is the parent node of node s, then

$$\mathrm{Rhs}(s) = \min[\mathrm{Pred}(s) + 1]\,.$$

The third is the D*Lite algorithm, whose implementation process is shown in Fig. 1.

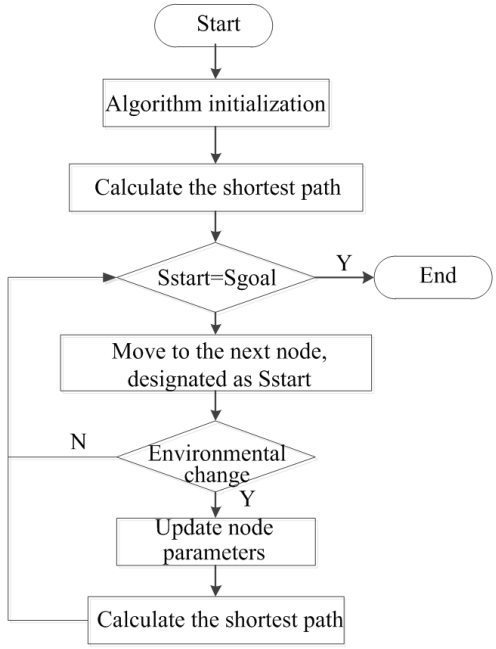

Fig. 1. Path planning flow chart of D*Lite

*2.2. Optimized D*Lite algorithm*

After analysis on the existing D*Lite algorithm, there are two main problems about the algorithm. Firstly, the algorithm for robot safety considerations were not perfect, and the algorithm of the path of the results had the existence of security risks. Secondly, the path of the D*Lite plan had too many twists and turns, and it did not optimize and smooth the planned path. In addition, the limit of the robot path was an integer multiple of 45 ° and did not conform to the actual motion characteristics of the robot.

2.2.1. Path optimization method. In the raster map, there were complex obstacles, such as concave obstacles. The first path search entered the concave barrier internal search path, finally, the conclusion could be gotten that this road cannot pass. In order to reduce the number of grids that were unnecessary to enter the recesses and reduce the number of path searches, the temporary barrier grid mark was used to avoid unnecessary raster search. Path optimization used a strategy that

was similar to D*Lite to optimize the shortest path that had been planned from the target grid to the starting grid. The steps were as follows.

First, the target location grid and the following two path nodes were analyzed. And the three nodes were analysed to check whether the two paths of the three nodes can be optimized as a path and check the security path rules. Second, if the new path met the security path rule described in the previous section, then the two paths in the three nodes were changed to two nodes and one path. And the two nodes were kept and the next node was added to continue checking whether three new nodes and two paths could be optimized. Third, if the new path did not conform to the path safety rule, therefore, there was an obstacle ridge and the barrier grid binding position. Then the optimization of the three shortest path nodes was completed. The first joined node was removed (the path node closest to the target grid) and the next node was added. Fourth, the steps 2 and step 3 were carried out circularly to check whether there was an optimized path until the originating node was reached. Finally, when the path changed, from the path change node to the surrounding affected by the path of the node could be carried out the search and optimization of the optimized path until the need to pick up the need to optimize the path so far.

The reverse path was the "path straightened" within the visible range of the path, it aimed at reducing the number of turns and the length of the path. Before the path fusion, firstly determine whether the fusion path to meet the safety rules to ensure the safety of the path. The direction selection of the path fusion was consistent with the search direction of the path. That was the searching fusion from the target position to the robot's current position. Therefore, in the process of sweeping robots was close to the target, the need to merge and update the path was decreasing. At the same time, path fusion was the path optimization based on the existing D*Lite algorithm, which can guarantee the optimality and correctness of the path planning results.

*2.2.2. Optimized D*Lite search process.* The optimized D*Lite algorithm was roughly consistent with the D*Lite algorithm [6]. The optimized D*Lite algorithm checked for unsecured paths during path calculations and improved to a secure path. After completing the shortest path planning, the reverse search link optimization was made to paths, so that the path length reduced, the path smoothness improved and the number of steering purposes reduced. The complete algorithm was executed as follows.

First, the $h(s)$ value for all rasters was initialized and the target node was placed in the queue. The h(start) value of starting position is 0, and the starting position was incremented by one for each of the eight rasters of the surrounding grid. From one grid to another, the vertical or diagonal grid $h(s)$ value difference was 1. Until the full value of the entire raster was initialized. Initialized all grid Rhs(s) values and $g(s)$ values were infinite. The target node was placed in the priority queue. The second was to calculate the shortest path. The target node became the first locally discontinuous node. From the target node, the $k(s)$ parameter of the eight rasters around was calculated, and Rhs(s) was assigned to $g(s)$ if $g(s)$ was greater

than Rhs(s). Before choosing the next grid to be extended, it was firstly determined whether there was a problem with the two safety path rules that violated the combination of the barrier through the barrier grid and the sharp corners passing through the obstacle grid. In addition, the grid with the smallest $k(s)$ was selected from the priority queue again as the grid to be expanded. And it was judged whether the new grid to be expanded conformed to the security path rule. The node extension that had the smallest $k(s)$ and conformed to the safe path rule was repeatedly selected until the Rhs(start) was equal to the g(start). The third was the path generating. It was moved from the current position to the grid with the smallest $g(s')+c(s', s\text{start})$ value, and s' is Succ(s). The fourth was the path optimization. From the target position, each time the three consecutive nodes were performed to judge the path optimization, and the security judgments was made to optimized path. If obeyed the path security rules, then the path optimization was given up. The first access to the path node was removed and the next path node was added until it was optimized to the originating node. The last was to check the environmental changes. During the movement of the swept robotic robot, the change of the raster map was detected, the $k(s)$ of the changing grid was updated, and the raster recalculation parameter was changed by the raster map change. Then according to the steps 3 to find the new path light and following the step 4 to complete the path optimization.

*2.2.3. Optimized D*Lite algorithm simulation.* In order to make a clear comparison between the two aspects of security improvement and path optimization for the optimized D*Lite algorithm, the results of the improved D*Lite algorithm for path planning security improvement were firstly verified, see Table 1. And then based on the result of path planning that was totally improved, the path optimization was carried out.

Table 1. Comparison of the security improved D*Lite algorithm and the original algorithm planning path

Evaluation parameters	Existing D*Lite algorithm	D*Lite algorithm with security strategy
The number of turns	8	10
Steering angle (°)	495	675
Path length (m)	15.6	21.6

The fully improved path avoided the security issues mentioned above, but the path length and the number of turns were increased while the security path was improved. According to the characteristic of robot in the practical application that it can complete any steering angle, based on the path security, the reverse connection path fusion method was used. Starting from the target node, each time three nodes were selected to determine whether they can be merged into one path. After merging, the three path nodes will be reduced to two nodes, and the intermediate nodes were removed. If the original two paths were folded, then the path after the fusion will no longer be reduced, which reduced the number of paths and the path length of

the path. The robot walked in accordance with the fusion path after the degree of turning, it was no longer limited to the integer multiple of the 45 °. The path evaluation parameters after the execution path optimization with the existing D*Lite algorithm and the security improved D*Lite algorithm were compared in Table 2.

Table 2. Optimized D*Lite algorithm and existing algorithm and path comparison results using security policy

Evaluation parameters	Existing D*Lite algorithm	D*Lite algorithm with security strategy	Path-optimized D*Lite algorithm
The number of turns	8	10	2
Steering angle (°)	495	675	169
Path length (m)	15.6	21.6	15

The final optimization D*Lite path planning algorithm used a security strategy while the reverse search path optimization was performed on the path results. The data in table 2 showed that compared with the existing D*Lite algorithm, the optimized D*Lite algorithm had fewer steering and steering angles. Especially, when the number of turns was reduced to only twice and the steering angle was reduced to less than half of the algorithm. The path length was required to be bypassed by the use of a safety-improved path in the position where the position of the obstruction combination and the sharp corners of the obstacle. So that the path was not significantly reduced, and it was slightly lower than the path length of the original algorithm. In practice, the length of the walking path of the sweeping robot, the steering angle and the number of turns affected the length and energy consumption of the sweeping robot to the target. Therefore, the optimized D*Lite algorithm had an effective path optimization for the existing D*Lite algorithm aiming at the practical characteristics of sweeping robots [7].

2.3. Platform introduction

The laser scanning range finder was added into the basic hardware platform, which was in-depth study to the environment modeling, path planning and other directions. In the sweeping robot path planning research, the sensor system was one of the core [8]. The verification platform used a notebook as the center of information collection, processing and control. The lower computer was mainly responsible for driving the motor movement, collecting infrared proximity sensors and ultrasonic range finder data. Algorithm validation platform PC used a laptop computer to install the windows operating system and Vissual C++ 2008 development environment. The laptop was connected directly to the laser range finder via the USB port. The lower unit was equipped with six ultrasonic and infrared sensors and gyroscopes, acceleration sensors. In order to ensure the safety of the robot body, the grid map expansion amount was about the same as the length of the robot body

and the larger value in the width of the robot. In the process of the path planning environment map construction, the size of the robot was the basis for the obstacle expansion of the grid map. In order to protect the safety of the robot body, the grid map expansion was about half the value of the robot body length and the larger width. In this paper, after installing the laser range finder at the front of the robot, the length was about 460 mm and the width was about 450 mm.

*2.4. Experimental results of the optimized D*Lite algorithm*

The experiment used the optimized D*Lite algorithm to do the final verification work of the path planning on the robot platform. First, according to the laboratory environment to draw the grid map, the data was acquired in Vissual by programming simulation laser scanning range finder, the optimized D*Lite algorithm in the drawing of the grid map to calculate the shortest path from the starting point to the target location. And then the path planning results were imported into the sweeping robot to test the actual walking effect of the optimized D*Lite algorithm.

2.4.1. Experimental grid map. The laboratory environment was divided into a number of small squares, according to the body size 48 cm of the length and 46 cm of the width, the square grid that the length and width were 10cm was selected. The obstruction will extend to the surroundings by two grids that cannot pass through the grid. It was important to prevent the robot from moving and obstruct the collision, and the robot was narrowed to occupy a grid.

*2.4.2. Optimize the running result of the D*Lite algorithm in the raster map.* It can be seen from the experiment that after the acquisition of the environment map became smaller, the path turning point that was calculated by the algorithm became more and more. It can be seen that the amount of environmental information that was obtained by the laser sensor that was installed by the sweeping robot had a great influence on the path planning process during the movement of the sweeping robot. When the sweeping robot moved to the target position, the laser range finder constantly detected the new environmental information to join the raster map. When the obstacle appeared on the path to be walking, the path planning algorithm updated the parameters and the calculation of the raster node. The effective maximum measurement distance of the laser sensor used in this experiment was 4095 mm, the high measurement accuracy could be gotten in the effective measurement range. When the laser scanning range finder used the maximum measurement distance, the amount of environmental information was obtained. And the path planning had less steering times and path lengths, and the path planning results were better. At the same time, in the experiment, when the obstacle was extended, the margin of the ground robot was set aside, and the unsafe path was improved accordingly. In order to obtain better path planning results, the next test used the laser scanning rangefinder to measure the maximum distance measurement of environmental information. The environment map in the experiment was the path planning under the condition that the global raster map was known. The path planning algorithm

was relatively simple to complete the path planning on the known raster map. The ground moving robot traveling in the practical application environment can only rely on the distance data measured by the laser sensor. And the data measured by the laser sensor was the obstacle to face the data of the front of the laser sensor and cannot obtain the appearance dimension of the obstacle. The result of the shortest path was based on the acquisition of the global environment map. Therefore, the laser scanning range finder will affect the planning result of the environment. The self-localization of the sweeping robot was also a problem in practical application.

3. Results

In the known raster map, the starting position and target position of the ground robot was specified. The optimized D*Lite algorithm calculated the shortest path from the start point to the end point. Because the detection environment was large, the most of the obstacle information could be gotten during the movement. The path that was planned by optimized D*Lite algorithm was close to the shortest path, the number of path steering was only three times, and the path smoothness was high. Path planning details was in Fig. 2. When the path planning algorithm detected that there is an obstacle on one of the two sides of the next node in the process of going to the target, and the optimized algorithm changed the path from the neighboring grid.

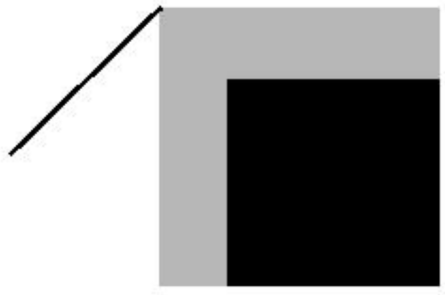

Fig. 2. Optimized D*Lite algorithm for planning the security path

On the basis of the map in Fig. 2, the raster map of the barrier joint point was added, and the algorithm of the optimization of the barrier grid was verified. The calculated path is shown in Fig. 3. The optimized algorithm regards the barrier of the barrier grid as non-accessible when the optimized D*Lite algorithm detects that there is the barrier junction when it moves to the next position.

Simple grid map of the algorithm validation was not very full, the actual environment had more obstacles. Then the path of the planning employed more practical significances. Figure 4 is the map after adding obstacles.

When the ground robot moved to the target position, the laser range finder constantly detected the new environment information to join the grid map. When the obstacle appeared on the path to be walking, the path planning algorithm updated

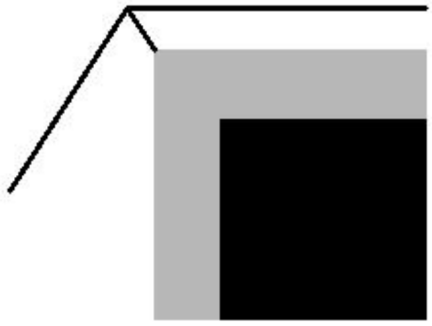

Fig. 3. Optimized D*Lite algorithm for planning a secure path (adding a barrier junction)

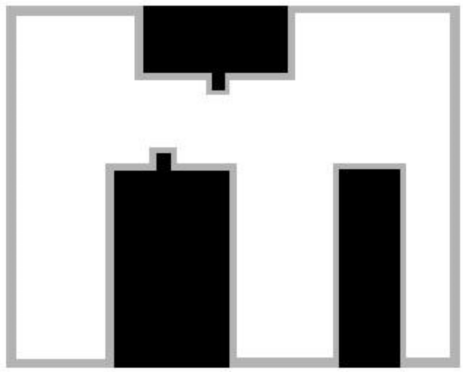

Fig. 4. Map after adding obstacles

the parameters and calculation of the raster node. From the experiment, it can be seen that the optimized D*Lite algorithm can still be used to plan a feasible shortest path in the chaotic environment.

The optimization of the D*Lite algorithm was carried out by using the optimized D*Lite algorithm to simulate the data acquisition characteristics of the laser scanning range finder on the grid map with the global environment. A new obstacle was added to the map to verify the effect of optimizing the D*Lite algorithm on path planning on complex barrier maps. In the simulation, the amount of environmental information of the laser scanning rangefinder was adjusted, and the comparison result showed that the path calculation algorithm of the sweeping robot was shorter and smoother. Because the limitation of the environment to obtain information and the accuracy of the robot self-positioning were not high, so the mapping laboratory environment map was used. The simulation results of the algorithm were simulated in Visual C++, and the optimized D*Lite algorithm was simulated. The route was imported into the sweeping robot to verify the safety and optimization of the moving route from the departure location to the target location. The experimental results showed that the improved strategy and path optimization method can improve the path security and path optimization.

4. Conclusion

In this paper, the path planning algorithm in unknown environment is studied, and the improvement of path planning security and path optimization are made. Based on the existing D*Lite algorithm, the total improvement and path optimization are carried out. The experimental results show that the total improvement strategy and the path optimization method can be used to improve the path.

It can also be concluded that the optimized D*Lite algorithm can calculate the optimal path from the current position to the target location according to the known environmental information. The simulation results show that the path of the algorithm has higher security. The path length, the number of steering and the steering angle are reduced and the smoothness of the path is improved. At the same time, the optimized D*Lite algorithm has advantages in ensuring the safety of the sweeping robot and reducing the length of the path

References

[1] W. Zhong, X. Tao, J. Lu: *Study of key technology for pipeline cleaning robot.* Modular Machine Tool & Automatic Manufacturing Technique (2013), No. 4.

[2] M. M. Bian, L. J. Zhang, L. L. Bian: *Design of mobile robot remote control.* Advanced Materials Research *1030–1032* (2014), Chapter 6, 1453–1456.

[3] A. Ulusoy, S. L. Smith, X. C. Ding, C. Belta, D. Rus: *Optimality and robustness in multi-robot path planning with temporal logic constraints.* International Journal of Robotics Research *32* (2013), No. 8, 889–911.

[4] H. Lee, A. Banerjee: *Intelligent scheduling and motion control for household vacuum cleaning robot system using simulation based optimization.* Proc. IEEE Winter Simulation Conference (WSC), 6–9 Dec. 2015, Huntington Beach, CA, USA, IEEE Conference Publications (2015), 1163–1171.

[5] Y. Zhang, D. W. Gong, J. H. Zhang: *Robot path planning in uncertain environment using multi-objective particle swarm optimization.* Neurocomputing *103* (2013), 172 to 185.

[6] L. Yang, J. Qi, D. Song, Y. Xia: *Survey of robot 3D path planning algorithms.* Journal of Control Science and Engineering (2016), No. 1, 1–22.

[7] M. R. K. Ryan: *Exploiting subgraph structure in multi-robot path planning.* Journal of Artificial Intelligence Research *31* (2008), No. 1, 497–542.

[8] X. Wang, Y. Shi, D. Ding, X. Gu: *Double global optimum genetic algorithm–particle swarm optimization-based welding robot path planning.* Engineering Optimization *48* (2016), No. 2, 299–316.

Received June 6, 2017

Acta Technica *62* No. 1A/2017, 411–420

Performance simulation of electronically controlled cooling system for automotive engines

Jiao Hongtao[1]

Abstract. The past engine cooling system is limited by the drive mode, and the fan speed depends on the engine speed, which is difficult to automatically adjust the temperature through the engine. However, the movement condition of the car is constantly changing, which will lead to engine cooling difficulties or excessive cooling, and at the same time, it will also cause the engine to stop working, increase the fuel consumption. Based on this, in this paper, the performance simulation of the electronically controlled cooling system for automotive engines was researched. Firstly, the design process of intelligent control system of cooling system was introduced briefly; secondly, relevant researches on the control of electronically controlled cooling system based on automotive engines were carried out; thirdly, the software design research of electric cooling system based on automotive engines was conducted, and the actual inspection was carried out. The results showed that the critical ratio K_s was decreasing and the simulation results were in accordance with the actual requirements.

Key words. Automobile engine, cooling system, electromechanical control, performance simulation.

1. Introduction

At present, the vast majority of automotive engines adopt the forced circulating water cooling treatment system. Engine cylinder head and cylinder block have the water jacket. Then, the pump inhales water from the outside of the machine, and generates pressure, makes the cool water flow in the water jacket, eliminates the heat of the adjacent parts. After the heating of the cooling water, the water's temperature is increased, and then it enters into the front of the radiator. With the progress of the car and the suction of the fan, the cold air outside puts the radiator cooling water into the atmosphere through the radiator. When the cooling water in the radiator is cooled down, it can enter into the water jacket circulation again under the action of the pump. In view of this situation, in the text, the

[1]Zhengzhou Railway Vocational & Technical College, Henan, Zhengzhou, 450052, China

Y80-based automotive engine electronically controlled cooling system was studied deeply. The intelligent control system of cooling system is an important foundation of the research. Therefore, this paper first studies relevant design standards and types of the cooling system intelligent control system. Then, the control planning of electronically controlled cooling system for automotive engines is analyzed, and some results are gained. Finally, the software design of electronic controlled cooling system based on automotive engine is studied in detail, and the experiment is carried out. The experimental results show that the oscillation period and the critical scale factor K_{s} of the system are determined by using the proportional adjustment link. The proportional coefficient K_{p} is automatically controlled by the microcontroller system, then, it increases gradually. This shows that the actual needs can be satisfied, and the simulation of the engine can be accurately achieved, which has a very good application prospect.

2. State of the art

The most commonly used clutch fan in the wind speed adjustment technology is the silicone oil clutch fan, in the design, the viscous liquid drive is applied, and then, the liquid viscous shear can be cut by the dynamic viscosity of the force and the shear film, its rate is proportional to the oil film and inversely proportional to the thickness, that is, as long as the thickness of the oil film is small enough, the oil film area is large enough to pass through large forces [1]. In the course of work, according to keep the same role of the shear film thickness, the role of the fan speed adjustment can be achieved by cutting the area. The clutch fan can control the engine operating temperature in the range of 80–90 °C, compared with the traditional fan, it has significant energy saving effect, besides, the clutch is small and easy to install, at present, this kind of fan is widely used in vehicles [2], and it is very popular in the silicone clutch vehicles at home and abroad [3]. In 1980s, there were electric cooling fans. The fan is no longer powered by the engine, while the electric fans are adopted, the fan can achieve changes in operating speed, avoid the fan power loss caused by the engine drive cooling, shorten the engine warm-up time, and reduce heat in accordance with the engine temperature and load conditions [4]. Electric adjustment technology is the hot spot in recent years. The earliest car electric cooling fan appeared in the patent document in March, 1981, the patent first proposed to replace the engine crankshaft with an electric cooling fan through a V-type drive cooling fan [5]. The heat system can control the temperature of the coolant and the temperature of the air conditioning condenser by ECU [6]. The system can control the fan speed according to the cooling water temperature and the operating conditions of the air conditioning system separately. On the basis of that the domestic car manufacturers are absorbing new advanced cooling systems abroad, the new cooling systems are developed [7]. In addition, research institutions also research and develop actively. Shandong Agricultural University has been engaged in the study of engine cooling control. In 2000, a new electronic thermostat was developed, and then, the single-chip control engine cooling theory was put forward, that was, the fan could work under the static, low and high speed conditions [8].

3. Methodology

3.1. Design of intelligent control system for cooling system

Cooling system can use the pump as a driving force, so that the cooling liquid in the body can conduct the forced circulation. The pump is installed in front of the cylinder and the coolant is placed in the water jacket of the cylinder, and then into the cylinder head. Finally, the thermostat is taken out from the outlet pipe of the cylinder head to complete the coolant cycle [9]. When the coolant temperature is below 66 °C, the coolant is pumped back from the outlet pipe through the pump and pumped into the body for an hour. When the outlet temperature reaches 76 °C, the thermostatic control valve is fully opened, and the cooling liquid enters the radiator for heating through the thermostat, this is a long cycle [10]. Figure 1 is a schematic diagram of an automotive engine.

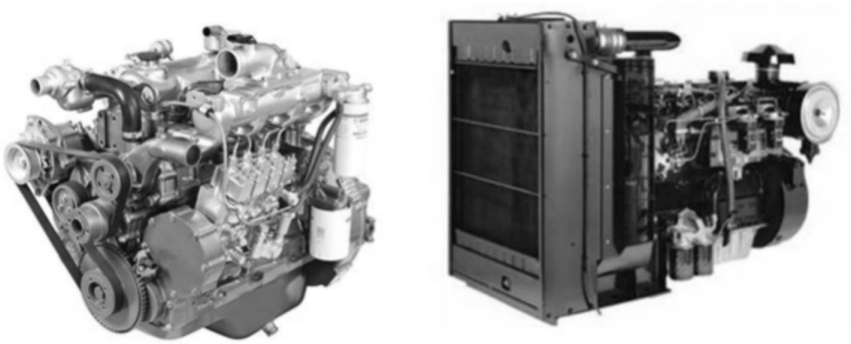

Fig. 1. Sketch map of automotive engines

As can be seen from Fig. 1, the cooling system consists of a radiator, a fan, a water pump and a thermostat, as well as consisting of a closed system including a flow path in a pipe and cylinder [11]. In a conventional cooling system, the fan is driven by the crankshaft of the engine, so the speed is relatively fixed. The problem of the traditional axial fan to the DC motor fan is driven by the pump to the DC motor [12]. In addition, compared with the conventional control system, the intelligent control system also adds microcontrollers and temperature sensors, and the speed of the fan motor is controlled by the microcontroller according to the coolant at different temperatures [13]. This paper focuses on micro control device system. The system is mainly composed of signal acquisition, clock circuit, temperature setting, LED temperature display, power supply circuit, motor drive, buzzer alarm and other components, and the specific composition is shown in Fig. 2.

3.2. Control of electronically controlled cooling system based on automotive engines

The temperature value of the electronically controlled cooling system for automotive engines is set as the setting value of the whole system. Then, the actual

temperature detected by the NTC temperature sensor is compared with the set value [14]. And the comparison result is input to the PID temperature controller. In order to control the deviation between the two PWI output signals, the controller changes the fan and adjusts the measured parameters, so it always changes the direction of the set value. Figure 3 is the system's control schematic diagram.

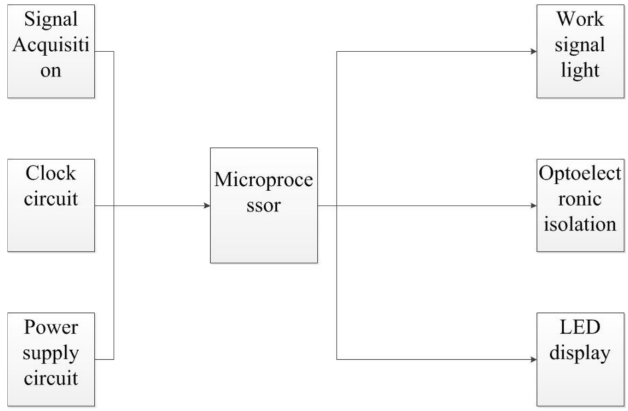

Fig. 2. Composition of intelligent control system

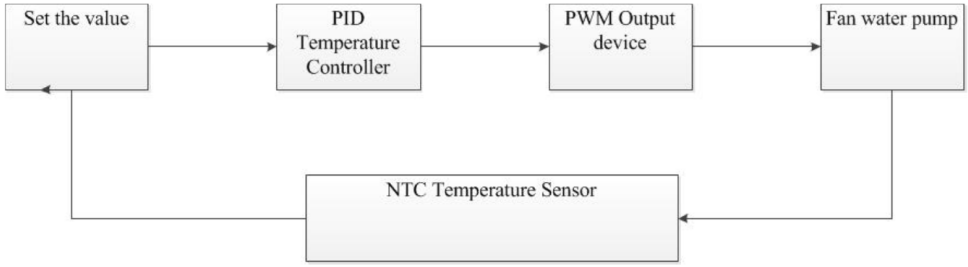

Fig. 3. Composition of intelligent control system

As the NTC temperature sensor conducts the real-time monitoring on water's temperature changes, and feedback back to the controller for the real-time comparison, so that the set temperature and the actual water temperature can be closely linked, therefore, the system constitutes a negative feedback closed-loop control system [15]. This method can not only change the controlled parameters quickly, but also conduct the corresponding adjustment, combines the PID control algorithm and PWM output mode, so as to improve the control accuracy, and the temperature control system adopts a wider control method. In a variety of electromechanical systems, the DC motor has good start, braking and speed control performances. Besides, the DC speed control technology has been widely used in in all aspects of the industry, aerospace fields. The most commonly used direct current speed control technology is pulse width modulation (PWM) DC speed control technology, which has high precision, fast response, wide speed range, wear and other characteristics. Through the pulse width modulation (PWM) control motor armature voltage, DC

motor speed expression is

$$n = \frac{U - IR}{K\Phi}, \tag{1}$$

where n denotes the revolutions per time, U is the voltage, I denotes the current, R stands for the resistance, Φ is the magnetic flux and K is a constant.

The vast majority of DC motors use the switch drive mode. The switch drive mode allows the semiconductor power device to be in a switching state, then, the motor armature voltage is controlled by pulse width modulation (PWM), so as to achieve the required speed.

3.3. Software design of electronically controlled cooling system based on automotive engines

The control software of the electrically controlled system of the automotive engine adopts the modular structure design, and each function block is independent, which needs to be expanded in accordance with needs. In the structure, the software is composed of the main program, interrupt procedures and multiple subroutines. The first order subroutine is: interrupt service subroutine, A/D sampling subroutine, digital filter subroutine. The second order subroutine is: temperature setting subroutine, table conversion subroutine and operation subroutine. The third subroutine is voltage checklist subroutine, checklist subroutine, delay subroutine. The specific features are shown in Table 1.

Table 1. Modular structural design components

First order subroutine	Interrupt service subroutine, A/D sampling subroutine, digital filter subroutine, digital Pm regulator subroutine, PWM output subroutine, alarm subroutine
Second order subroutine	Temperature setting subroutine, table conversion subroutine, operation subroutine, BCD code conversion subroutine, display subroutine
Third order subroutine	Voltage checklist subroutine, temperature checklist subroutine, LED checklist subroutine, delay subroutine

In the real-time control of the system, the microprocessor is calibrated at regular intervals, and the interval is called the sampling period. In each sampling period, the controller performs sampling and coding of continuous signals and digital operations according to the control law, and then, it enters into a continuous signal by converting the results of the output register into a decoder digital signal (that is, PWM conversion process). Through the NTC sensor and temperature acquisition circuit, the temperature signal converts the physical signals into electrical signals, and then, converts them into digital by A/D. The voltage signal is converted to a temperature value by scale. Besides, the AD-CMP-CON operation is used to define analog input pins and digital I/O pins. Then, the ADPD bit that is 1 is set to start sampling; turn on or off is based on needs; ADR is set to start AD conversion; and

the conversion result is read from ADDATA; the interrupt flag bit ADIF is cleaned up, and before the next sampling, two time intervals need to be waited at least.

For analog signals, especially flow, pressure, component content and other processes, there should be a better digital filter. For example, in winter, the engine's cooling water temperature is higher, while the cooling water temperature in summer is lower. The system provides a possible support for the user to set the cooling water temperature. The keyboard interrupt is the highest priority, which is the need for real-time man-machine exchange. When the key is pressed, the system executes the critical interrupt subroutine from the currently executing program. Delaying 10 seconds is to get rid of the tremble, so as to avoid the wrong operation of the button. This is a commonly used switch signal software anti-jamming measures. If the key is pressed, the INTO interrupt subroutine is executed. Pressing the button once displays the currently set temperature value and flash. Pressing the button again, the circulation can be set accordingly at the same time of setting the value and the flash next time. When the key is pressed for 3 seconds, the flashing temperature value is stored in the program and the target value of the system is considered. At the same time, returning to the main program interrupts, before continuing to interrupt the program, the digital tube at this time can display the current measured temperature value.

4. Result analysis and discussion

According to the parameters obtained, the operation was carried out in the speed control system, and the control effect was observed. If the control effect could not meet the control requirements, based on the following principles, the parameters could be adjusted according to the following rules. Increasing the scale coefficient K_{p} would speed up the system's response speed, but the system would produce a large overshoot, or even produce oscillation. Then, increasing the integration time T_{i} was conducive to reducing overshoot, reducing oscillation and making the system more stable; however, the system transition time was also increased. In addition, increasing the differential time constant T was helpful to speed up the response of the system, so that the overshoot was reduced and the stability was increased. However, the system's ability to suppress the disturbance was weakened and the response to the disturbance was more sensitive. The calculated KI values were placed in the simulation model, as shown in Fig. 4.

In the transfer function of the zero-order holder, T was the sampling period. Based on the above principle, in the PID control system model, the target value of 80 °C and the simulation time of 2000 seconds were input, then, the PID parameters were gradually adjusted, particularly $T = 3.36\,\mathrm{s}$, $K_{\mathrm{p}} = 1\,\mathrm{s}$, setting 002, $KI = 0.008\,\mathrm{s}$. The digital PID control parameter adjustment task was to determine the parameters of the digital PID. For simple control systems, these parameters could be determined by using theoretical calculations. However, due to the complexity of the speed control system of automotive engines, the mathematical model was not very accurate. In this paper, the extended critical grading method was used to adjust the parameters, and the final PID parameters were obtained by combinatorial empirical method.

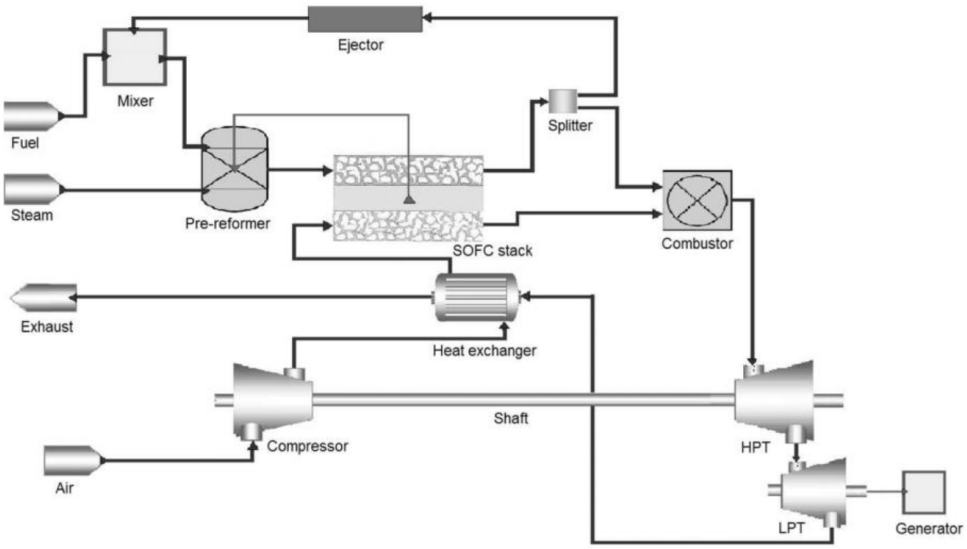

Fig. 4. Simulation model diagram of PID control system

In the digital control system, the sampling period was a more important factor, and the selected sampling period should be considered with the PID parameters. Firstly, the sampling period was selected to meet the following requirements: far less than the object disturbance cycle; much smaller than the time constant; try to shorten the sampling period, improve the quality of supervision. In this system, the PID regulation control process was completed in a periodic interrupt state, so the size of the sampling period must ensure that the interrupt service routine operated normally. Without affecting the operation of the interrupt program, the sampling period $T = 0$ (T being the vehicle engine's pure delay time) was adopted.

Determination of the critical oscillation period: when the digital PID parameters were initially determined, the differential control function and integral control function of the digital controller in the PID control circuit of the speed control system were eliminated, and the condition was the sampling period. The oscillation period and the critical scale factor K_s of the system were determined by using a proportional adjustment link (shown in Fig. 5). The proportional coefficient K_p was automatically controlled by the microcontroller system and it gradually increased.

It could be seen from Fig. 5 that the critical ratio K_s was decreasing, and finally, it tended to zero illimitably. Control degree was based on analog adjusters, then, the quantitative measurement of digital control systems and analog adjusters could achieve the synthesis of control effects of the same object. Control effect was to use a certain integral criteria, and then, the response was conducted in accordance with the system specified input. As mentioned before, the length of the sampling period would affect the control quality of the system, both the two were best tuning, while the quality of the digital control system was lower than the control quality of the simulation system. In other words, the control degree parameter was always

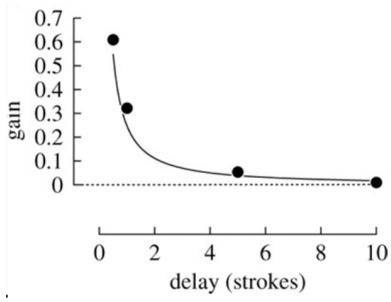

Fig. 5. Parameter change curve

greater than 1, and the greater the control degree was, the worse the quality of the corresponding digital control system was.

5. Conclusion

Conventional cooling systems often cause the phenomenon of the temperature imbalance in the cold start of the engine. In this paper, in view of the existing shortcomings of the automobile engine cooling system, the microcomputer and advanced control method were proposed to control. According to research the cooling system, it is proposed to use electromechanical control method for control. Then, through the test, research, design and simulation of the control system, the operation system based on the electrically controlled cooling for automotive engines was successfully designed. Firstly, the purpose and significance of the research were discussed, and the significance of controlling the engine coolant was described. Then, the research status of the engine cooling system at home and abroad was introduced, the problems in this field were analyzed, next, the factors affecting the cooling system were analyzed, the overall structure and hardware circuit of the cooling system were devised. This article can provide some relevant theoretical basis for motor engineers of the automobiles. Due to the limitation of time and my personal ability, there are still some shortcomings in this paper. For example, the computer in this control system is independent, which neither communicates with the engine and chassis control computer, nor conducts the centralized control on the system and other control systems of the vehicle by using the computer.

References

[1] O. Veneri, C. Capasso, S. Patalano: *Experimental study on the performance of a ZEBRA battery based propulsion system for urban commercial vehicles.* Applied Energy *185* (2017), Part 2, 2005–2018.

[2] E. S. Mohamed: *Development and analysis of a variable position thermostat for smart cooling system of a light duty diesel vehicles and engine emissions assessment during NEDC.* Applied Thermal Engineering *99* (2016), 358–372.

[3] X. Tao, K. Zhou, J. R. Wagner, H. Hofmann: *An electric motor thermal man-*

agement system for hybrid vehicles: modelling and control. International Journal of Vehicle Performance *2* (2016), No. 3, 207–227.

[4] S. P. Datta, P. K. Das: *Performance of an automotive air conditioning system with the variation of state-of-charge of the storage battery.* International Journal of Refrigeration *75* (2017), 104–116.

[5] Y. Yang, N. Schofield, A. Emadi: *Integrated electromechanical double-rotor compound hybrid transmissions for hybrid electric vehicles.* IEEE Transactions on Vehicular Technology *65* (2016), No. 6, 4687–4699.

[6] S. S. Naini, J. A. Huang, R. Miller, J. R. Wagner, D. Rizzo, S. Shurin, K. Sebeck: *A thermal bus for vehicle cooling applications-design and analysis.* SAE International Journal of Commercial Vehicles *10* (2017), No. 1, 122–131.

[7] Y. Yang, T. Wright, M. Herbison, C. Gallagher, S. Little, A. Jaciw-Zurakowsky: *Design and analysis of an electromechanical actuator for the valve train of a camless internal combustion engine.* International Journal of Mechanisms and Robotic Systems *2* (2015), No. 2, 169–181.

[8] S. Twaha, J. Zhu, Y. Yan, B. Li: *A comprehensive review of thermoelectric technology: Materials, applications, modelling and performance improvement.* Renewable and Sustainable Energy Reviews *65* (2016), 698–726.

[9] K. I. Wong, P. K. Wong, C. S. Cheung: *Modelling and prediction of diesel engine performance using relevance vector machine.* International Journal of Green Energy *12* (2015), No. 3, 265–271.

[10] S. S. Butt, R. Prabe, H. Aschemann: *Robust nonlinear control of an innovative engine cooling system.* IFAC-PapersOnLine *48*, (2015), No. 14, 235–240.

[11] E. Ganev: *Selecting the best electric machines for electrical power-generation systems: high-performance solutions for aerospace more electric architectures.* IEEE Electrification Magazine *2* (2014), No. 4, 13–22.

[12] J. Ruan, P. D. Walker, P. A. Watterson, N. Zhang: *The dynamic performance and economic benefit of a blended braking system in a multi-speed battery electric vehicle.* Applied Energy *183* (2016), 1240–1258.

[13] V. V. Kokotovic, C. Buckman: *Electric water cooling pump sensitivity based adaptive control.* SAE International Journal of Commercial Vehicles *10* (2017), No. 1, 331 to 339.

[14] M. C. George, C. Buckman: *A new efficient PFC CUK converter fed BLDC motor drive using artificial neural network.* Artificial Intelligent Systems and Machine Learning *8* (2016), No. 8, 291–295.

[15] X. F. Zheng, C. X. Liu, Y. Y. Yan, Q. Wang: *A review of thermoelectrics research—-Recent developments and potentials for sustainable and renewable energy applications.* Renewable and Sustainable Energy Reviews *32* (2014), 486–503.

Received June 6, 2017

Acta Technica *62* No. 1A/2017, 421–432

Application of cross correlation algorithm in micro sensor detection

Zhu Yanqin[1]

Abstract. With the increasingly widespread application of micro sensors in daily life, how to give better play to the role of micro sensors in various fields has become the focus of attention. In order to better promote the development of micro sensors in detection, the cross correlation algorithm was applied to the digital closed-loop control system of micro sensors in this paper, and the adjustment test of language coding, simulation software, and development boards was carried out. The results show that the fusion application of cross correlation algorithm in the micro sensor industry can help to achieve detection function and improve performance standards, and can also provide effective experience for the application of cross-correlation algorithms in other fields.

Key words. Cross-correlation algorithm, micro sensor, detection, application.

1. Introduction

Micro sensors have been widely used electronic devices in recent years, the principle of which is the sensors that consist of physical and chemical reactions and mechanisms and microfabrication techniques on the basis of semiconductor material [1]. Micro sensors are divided into different species according to different attributes. For example, according to whether there is energy, they are divided into source micro sensors and passive micro sensors [2]. According to the factors of sound, they can be divided into phase micro sensors, acoustic harmonic sensors and amplitude micro sensors [3]. In addition, micro sensors can be divided into antigen micro sensors, biological micro sensors, hormone micro sensors and biomass micro sensors according to their uses [4]. Moreover, there are many classifications, such as optics, electricity, chemistry and so on, which are not discussed below. Micro sensors have been developing rapidly in recent years because of intelligence, low loss, simple synthesis and small size. The smallest size of the microsensor is up to a few millimeters [5].

However, for the rapid development of micro sensors, the research on its principle, technology and application is far from enough. Nowadays, the micro sensor is developing toward digital, scientific and technological, high security, high accuracy,

[1]Huizhou Economics and Polytechnic College, Huizhou, Guangdong, 516057, China

intelligence, automation, miniaturization, low loss, energy saving and environmental protection [6]. Since micro sensors are fabricated by micro mechanical technology, the size of micro components can reach sub-micron size, and so it is called "micro scale effect" [7]. However, there are also many problems such as severe signal attenuation, large amount of loss and interference of external factors, which set many obstacles for the reception and transmission of signals [8].

Based on the related basic theories, the problems and difficulties existing in the application of micro sensors were discussed in this paper. Through field programmable gate array, cross correlation algorithm was integrated into the application of micro sensors. The non-interfering signals in all the signals received by the micro sensor were detected and effectively selected. And some references were provided for the application of cross-correlation operation and the function of micro sensor.

2. State of the art

According to the literature, the so-called micro sensors can be divided into chemical micro sensors, physical micro sensors and biological micro sensors on the basis of their different measurement objects [9]. Chemical micro sensors are generally based on the charged nature of ions. At present, the application of ion sensors in the fields of medicine, chemistry and biological products has become more mature [10]. The physical micro sensor transmits the physical information of the object through the frequency of the sound wave, such as magnetic field, amplitude, angular velocity, temperature, and other factors [11]. But its application scope is not very extensive, and the specific application methods need further exploration and research. Biological micro sensor is the process of mapping DNA probes to target DNA by using changes in physical properties such as light waves and sound waves. In this way, the process of synthesis and the process of polymerization of nucleotides are clearly displayed, which solves many problems for the biological community and even the medical community [12]. Some studies have shown that the application of micro sensors has become the most mature, stable and practical microelectromechanical devices [13].

The cross-correlation method can reflect the correlation of two random variables at different times, which can describe the relation between the variable A in time T_1 and the variable B in time T_2, so as to facilitate the transmission and acquisition of information. At present, the cross correlation operations play an important role in the following aspects: first of all, the cross-correlation calculation can be used to determine the delay time and improve the efficiency of the industry [14]. Moreover, the cross correlation operations can identify transmission paths, and a number of peaks in the function are analyzed and identified synthetically [15]. Third, the cross-correlation operation can detect any interference signal, which can select the target signal among many signals, so as to eliminate the external interference and provide the accuracy of detection. Fourth, the micro sensor pulse system always maps the measurement results, and for the interference signal, the system will eliminate all the interference signals. In this way, it is not difficult to find that cross correlation

algorithm can be used in micro sensor applications with a multiplier effect. Therefore, how to apply cross-correlation algorithm to micro sensors is the most important aspect of our research.

3. Methodology

Taking silicon micro sensor as an example, the application of cross-correlation algorithm to detect weak signals in micro sensors was described in this paper.

3.1. 3.1 Design of correlation system detection module

First of all, in order to find the resonant point of an electric thermal shock sensor, a closed electrical loop system was designed in this paper, as shown in Fig. 1. The output signal of the micro sensor was formed by the signal to be measured, the interference signal whose frequency is 50 % of the signal to be measured and the interference noise of an electric thermal shock micro-sensor. The method of detecting the measured signals by cross-correlation algorithm is as follows:

The input signal of the micro sensor is $X(t)$. Its components include noise signal $N(t)$, same frequency coupling sine interference signal $S_{\mathrm{w}}(t)$ and sine noninterference signal $S_{2\mathrm{w}}(t)$. Thus, it can be expressed by the formula

$$X(t) = S_{\mathrm{w}}(t) + S_{2\mathrm{w}}(t) + N(t)\,. \tag{1}$$

The multifrequency control signal is $Y_{2\mathrm{w}}(t)$. According to the formula (1), the relation between the input signal of the micro sensor and multifrequency control signal is

$$\begin{aligned} R_{xy}(n) &= X(t) \times Y(t+n) \\ &= [S_{2\mathrm{w}}(t) + S_{\mathrm{w}}(t) + N(t)] \times Y_{2\mathrm{w}}(t+n) \\ &= S_{2\mathrm{w}}(t) \times Y_{2\mathrm{w}}(t+n) + S_{\mathrm{w}}(t) \times Y_{2\mathrm{w}}(t+n) + N(t) \times Y_{2\mathrm{w}}(t+n) \\ &= R_{s_{2\mathrm{w}}Y_{2\mathrm{w}}} + R_{s_{\mathrm{w}}Y_{2\mathrm{w}}} + R_{NY_{2\mathrm{w}}}\,. \end{aligned} \tag{2}$$

The multifrequency control signal in the formula is the sine signal $S_{2\mathrm{w}}(t)$. There is no cross correlation between the multifrequency control signal $Y_{2\mathrm{w}}(t)$ and the noise signal $N(t)$. So when n is infinite, $R_{S_{\mathrm{w}}Y_{2\mathrm{w}}}$ is viewed as approximately equal to 0, and $R_{xy}(n) \approx R_{S_{2\mathrm{w}}Y_{2\mathrm{w}}}$. In this way, the extracted functions are represented by programming:

$$R_{xy}(m) = \frac{1}{N} \sum_{n=0}^{N-1} x(n)y(n-m)\,, \tag{3}$$

where m is an infinite integer. The function $R_{xy}(M)$ is converted to a sine function with the same period as the sampled signal. Thus, the resonant point of the micro

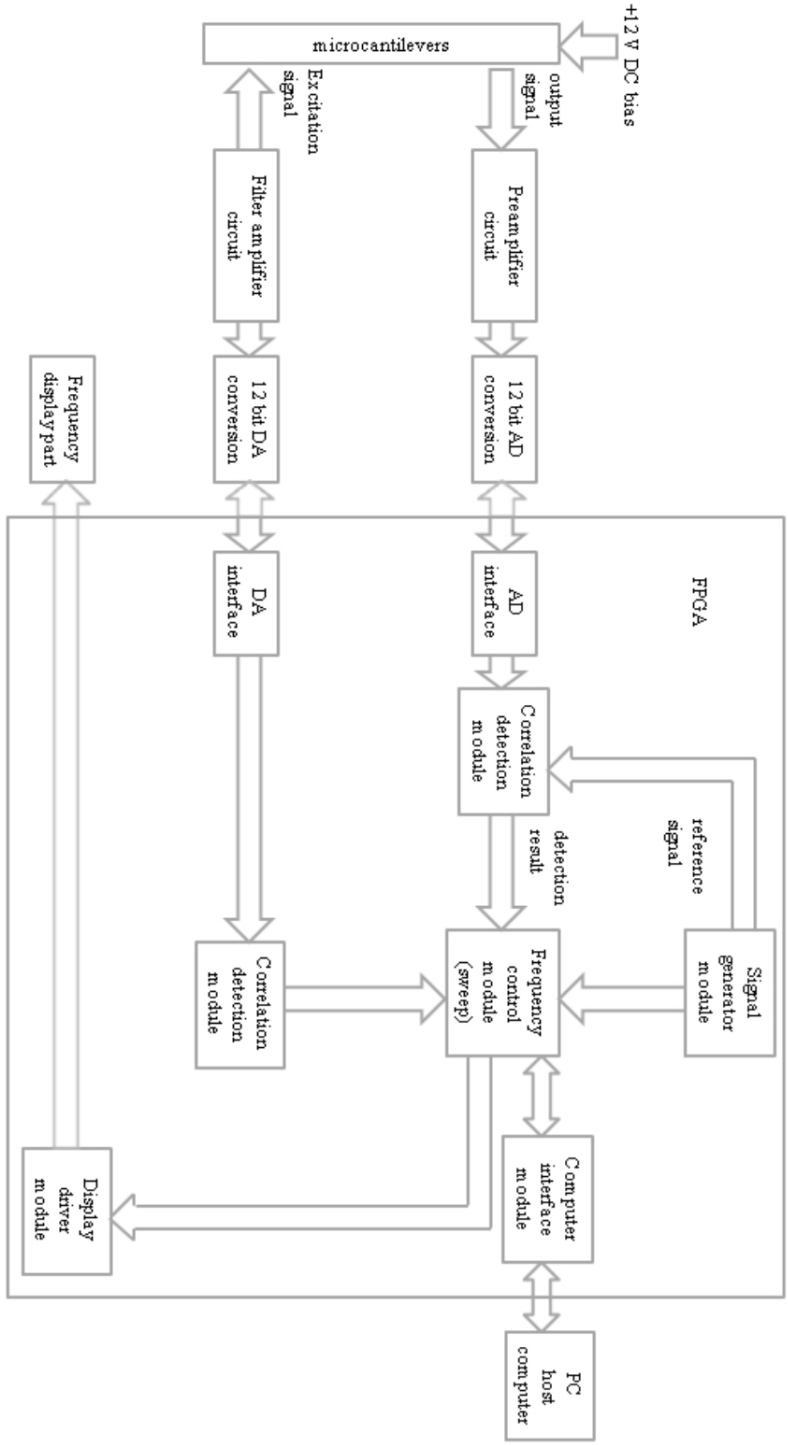

Fig. 1. Closed-loop electric system of sensor

sensor is obtained. The smaller is the mean absolute value of the autocorrelation function, and the smaller is the absolute value, the smaller is the output intensity of the sensor. Then, when the absolute value is the maximum, the corresponding frequency point is the resonance point.

The above design was simulated and analyzed by Matalab software. The start time was $t = 5e - 6$, the end time was $t = 12.8e - 4$, and the time interval was consistent with the start time. 240 points were set as detection points, and according to multi frequency contrast signals $Y_{2\mathrm{w}}(t) = \cos(2\pi \times \omega t)$, all selected signals in the input signals were as follows $S_{2\mathrm{w}}(t) = \cos(2\pi\omega t)$. The same frequency coupling sine interference signal was $S_{\mathrm{w}}(t) = \cos(\pi\omega t)$. In the formula $\omega = 14000$, and simulation charts can be obtained.

3.2. Implementation of cross-correlation operations by the use of FPGA

The purpose of this paper is to extract the target signal mixed in the noise without being affected by the same frequency coupling interference signal. The FPGA can only handle digital signals. Therefore, firstly, the signals collected by micro sensors were converted into digital signals. And FPGA was used to control the collected signals. The converted digital input signal and the multifrequency control signal were passed to the RAM of the FPGA corresponding address until a sufficient amount of data information was obtained.

In cross correlation operation, the following formula was used

$$\underset{xy}{\hat{R}}(k) = \frac{1}{N} \sum_{n=0}^{N-1} x(n)y(n-k)\,. \tag{4}$$

It is known that the cross-correlation operations of digital signals follow the rules: multiplication first, followed by the addition. Then, by using the nature of the real time signals of the target signals, each operation only selects half of the data for cross-correlation calculation, thus ensuring that the number of data information for each cross-correlation operation is equal. In doing division, FPGA is prone to greater errors. Therefore, in order to get the maximum value for each section, the operation divided by N was canceled in this paper, and then the formula was converted to

$$\underset{xy}{\hat{R}}(k) = \sum_{n=0}^{N/2} x(n)y(n-k)\,. \tag{5}$$

However, in practice, there was a problem that time could not be delayed. In order to solve this problem, the cross-correlation operation was used to read the corresponding data. When reading the data, the RAM address bar of the stored data was changed. Finally, the result data were compared and analyzed. The larger the target signal in the micro sensor output signal was, the greater the calculated result was, the two showed the proportional relation. When the maximum corresponding frequency point was the resonant point of the micro sensor, the maximum value of

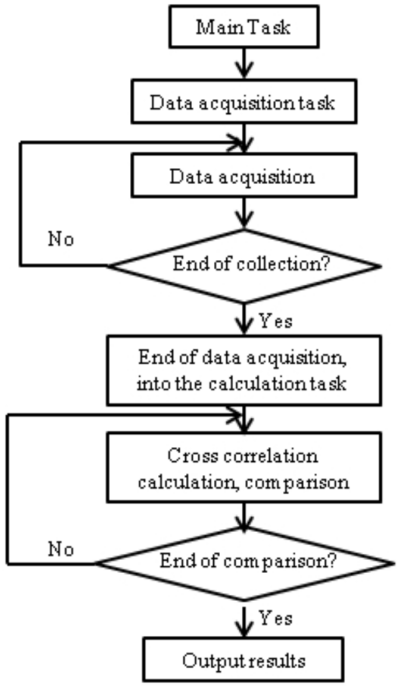

Fig. 2. Closed-loop electric system of sensor

the operation result and the corresponding n were recorded simultaneously. The experimental technical route is shown in Fig. 2.

4. Result analysis and discussion

4.1. Design results of the relevant system detection module

The simulation diagram is shown in Figs. 3–6. Figure 3 shows the correlation between the multi frequency control signal and the preset detected signal. Figure 4 shows a case where multiple frequency contrast signals are correlated with the same frequency coupled sinusoidal interference signals. Figure 5 shows the correlation between the multi frequency control signal and the interference input signal. Figure 6 is the comparison of the results in Figs. 3, 4, and 5. From the results of Fig. 3, when the input signal contained only interference signals, the results of cross-correlation operations were smaller. The results of cross-correlation calculation of the same frequency coupling sinusoidal interference signal and multi frequency control signal were very close to that of the multi frequency control signal and the preset detection signal. It can be seen, that at the theoretical design level, the detection of the micro sensor input signals with the same frequency coupling interference can be effectively extracted by cross-correlation calculation. And there is some theoretical support for this method.

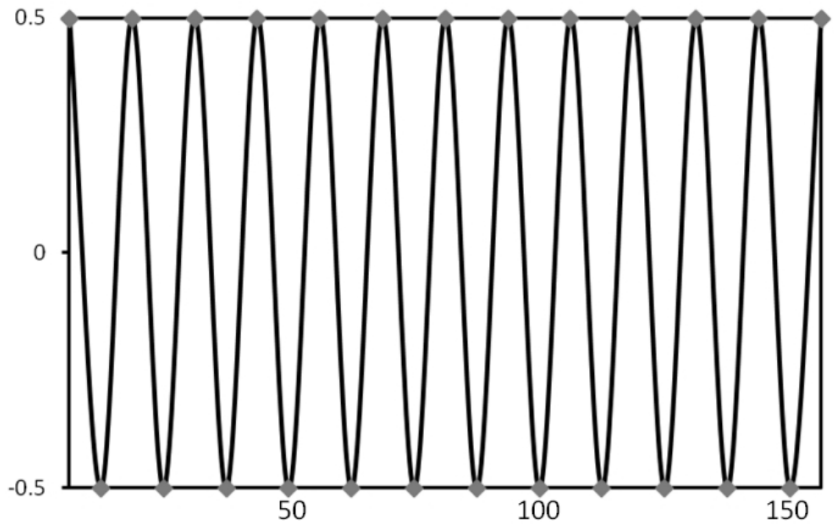

Fig. 3. Cross-correlation between multi frequency control signal and preset detected signal

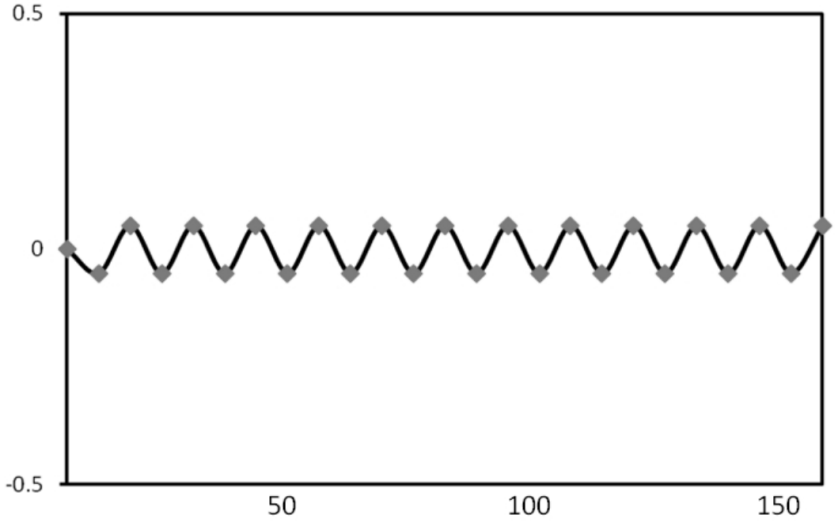

Fig. 4. Cross correlation operation of multi frequency control signal and sinusoidal interference signal with same frequency coupling

4.2. Using FPGA to achieve cross-correlation results

The object of this experiment was the sine wave band of 13.5 kHz. A total of 16 data was obtained at the frequency of 200 kHz, as shown in Table 1. The cross correlation operation was carried out on two groups of data, and the results showed that $n = 2$, Max = 1676267.

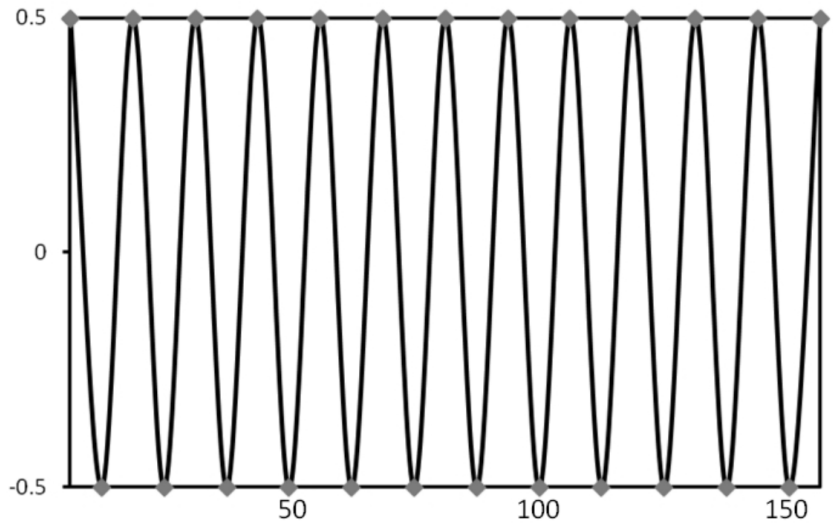

Fig. 5. Cross-correlation computation between multifrequency control signals and interference input signals

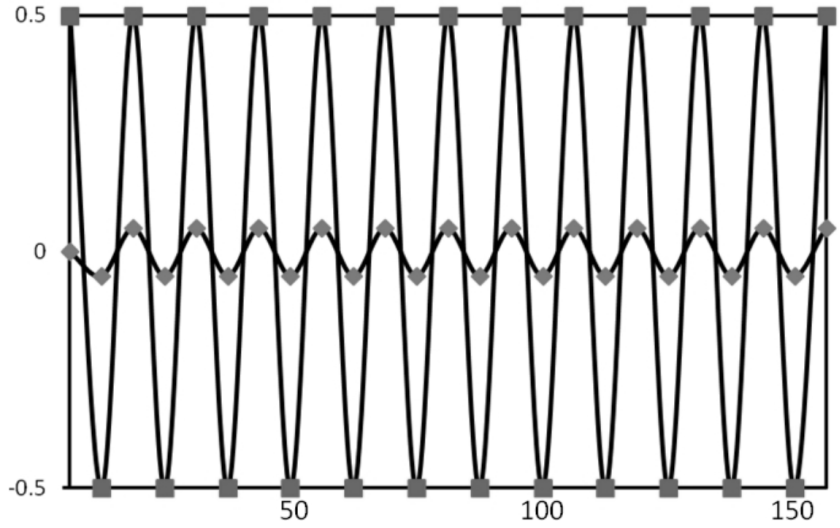

Fig. 6. Unified results

Table 1. Two sets of input signal data

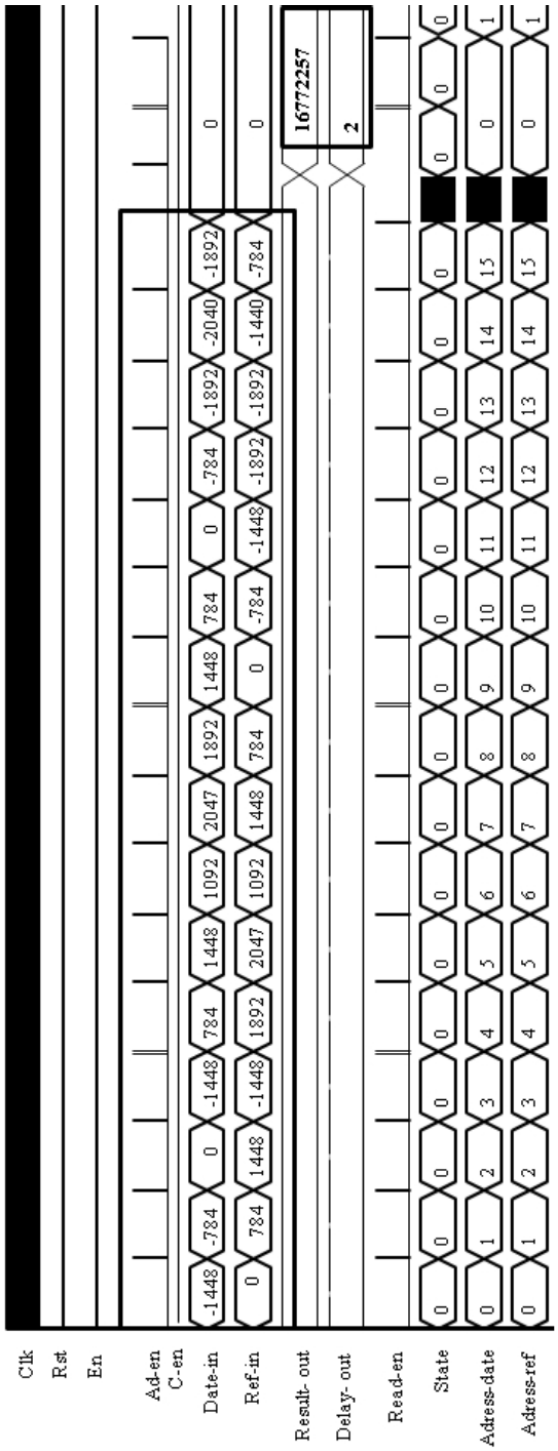

Fig. 7. Simulation results

Address	Data in	Ref in	Address	Data in	Ref in	Address	Data in	Ref in
0	-1445	0	6	2024	1445	12	-1445	-2024
1	-739	739	7	1887	739	13	-1887	-1887
2	0	1445	8	1445	0	14	-2024	-1445
3	739	1887	9	739	-739	15	-1887	-739
4	1445	2024	10	0	-1445			
5	1887	1887	11	-739	-1887			

Quartus II software was used to carry out simulation experiments, as shown in Fig. 7. The upper two sets of data were input data, and the two party data was the simulation data for application. It can be seen that the theoretical value is consistent with the simulation results.

After the system was debugged, the system was applied to the control system of the silicon resonant micro sensor. After open loop detection, scanning was performed, but the signal was not locked and thus re detected.

5. Conclusion

In order to study the application of the cross-correlation algorithm in the detection of micro sensors, this paper takes silicon micro sensors as an example. Firstly, the feasibility of cross-correlation computation applied to micro sensors is analyzed and verified theoretically. Then, the design and application of cross correlation operation in silicon micro sensor is realized by FPGA. Through Verilog programming language code, and the use of Quartus II software simulation experiments and debugging, and finally obtained the frequency characteristic curve. The conclusion of the study are as follows: through the cross-correlation algorithm can be extracted in the mixed noise signal, which is not affected by the same frequency coupling interference signal. The frequency and number of samples are in line with the corresponding standards. However, the application of the cross-correlation algorithm in the detection of micro sensors is still in the initial stage, and the distance to create products that are really applied in military and other fields still needs further research and demonstration. But the conclusions and results obtained in this paper can provide some reference for future research.

References

[1] T. T. Shen, L. Zhu, L. Kong, L. X. Zhang, C. H. Rao: *Real-time image shift detection with cross correlation coefficient algorithm for correlating Shack-Hartmann wavefront sensors based on FPGA and DSP.* Applied Mechanics and Materials. *742* (2015), 303–311.

[2] J. Galbally, S. Marcel, J. Fierrez: *Image quality assessment for fake biometric detection: Application to iris, fingerprint, and face recognition.* IEEE Transactions on Image Processing *23* (2014), No. 2, 710–724.

[3] L. Francioso, C. de Pascali, E. Pescini, M. G. De Giorgi, P. Siciliano: *Modeling, fabrication and plasma actuator coupling of flexible pressure sensors for flow*

separation detection and control in aeronautical applications. Journal of Physics D: Applied Physics *49* (2016), No. 23, paper 235201.

[4] B. C. Roberts, E. Perilli, K. J. Reynolds: *Application of the digital volume correlation technique for the measurement of displacement and strain fields in bone: A literature review.* Journal of Biomechanics *47* (2014), No. 5, 923–934.

[5] D. Waithe, M. P. Clausen, E. Sezgin, C. Eggeling: *FoCuS-point: software for STED fluorescence correlation and time-gated single photon counting.* Bioinformatics *32* (2015), No. 6, 958–960.

[6] J. Goulden, A. Bewick: *The application of the AZtec EBSD System to the study of strain in the SEM.* Microscopy and Microanalysis *22* (2016), No. 53, 18–19.

[7] V. V. Zaharov, R. H. Farahi, P. G. Snyder, B. H. Davison, A. Passian: *Karhunen–Loève treatment to remove noise and facilitate data analysis in sensing, spectroscopy and other applications.* Analyst *139* (2014), No. 22, 5927–5935.

[8] M. Kitzunezuka, K. S. J. Pister: *Cross-correlation-based, phase-domain spectrum sensing with low-cost software-defined radio receivers.* IEEE Transactions on Signal Processing *63* (2015), No. 8, 2033–2048.

[9] A. Bhardwaj, L. Sam, Akanksha, F. J. Martin-Torres, R. Kumar: *UAVs as remote sensing platform in glaciology: Present applications and future prospects.* Remote Sensing of Environment *175* (2016), 196–204.

[10] R. Sen, Y. Lee, K. Jayarajah, A. Misra, R. K. Balan: *GruMon: Fast and accurate group monitoring for heterogeneous urban spaces.* Proc. 12th ACM Conference on Embedded Network Sensor Systems, 03–06 Nov. 2014, Memphis, TN, USA, 46–60.

[11] W. H. Tien, D. Dabiri, J. R. Hove: *Color-coded three-dimensional micro particle tracking velocimetry and application to micro backward-facing step flows.* Experiments in Fluids *55* (2014), No. 3, 1684.

[12] D. Scheffler, A. Hollstein, H. Diedrich, K. Segl, P. Hostert: *AROSICS: An automated and robust open-source image co-registration software for multi-sensor satellite data.* Remote Sensing, *9* (2017), No. 7, 676.

[13] Z. Zhang, T. Pang, Y. Yang, H. Xia, X. Cui, P. Sun, B. Wu, Y. Wang, M. W. Sigrist, F. Dong: *Development of a tunable diode laser absorption sensor for online monitoring of industrial gas total emissions based on optical scintillation cross-correlation technique.* Optics Express *24* (2016), No. 10, A943–A955.

[14] I. D. S. Miranda, A. C. C. Lima: *Impulsive sound detection directly in sigma-delta domain.* Archives of Acoustics *42* (2017), No. 2, 255–261.

[15] R. Zhang, C. Mu, X. Gao, H. Xia, X. Cui, P. Sun, B. Wu, Y. Wang, M. W. Sigrist, F. Dong: *A fusion algorithm of template matching based on infrared simulation image.* Proc. Eighth International Conference on Digital Image Processing (ICDIP), 19th Oct. 2016, Chengu, China, CD-ROM.

Received June 6, 2017

Acta Technica *62* No. 1A/2017, 433–446

The pH value control of clarifying process in sugar refinery based on fuzzy control[1]

Zhangyun Wang[2]

Abstract. With the continuous development of automation technology, the application of the technology has also penetrated into the sugar industry. In this paper, the research status of pH control in sugar factory was analyzed, and the development and application of fuzzy control were illustrated. On the basis of fuzzy adaptive PID control, pH intelligent control system and software and hardware were designed, and the experimental results were analyzed. The experimental results show that the pH intelligent control system can effectively guarantee the stability of pH value in the clarifying process of sugar refinery, and it also has better control effect on temperature. In addition, the feasibility of fuzzy control can be ensured, which will contribute to the application research of pH value control in the clarifying process of sugar factory based on fuzzy control.

Key words. Automation technology, sugar industry, fuzzy control, pH value.

1. Introduction

Since the late 1950s, with the development of a large number of engineering practices, especially the development of space technology, the automation control theory has been developed vigorously. Because of the wide application of automation technology in many fields such as industrial production, electric power, traffic, iron and steel, the production efficiency of various industries has been improved, and the economic benefits have been greatly improved. More and more people believe that the level of automation of an enterprise has become an important indicator of the competitiveness of the entire enterprise market.

In recent years, automation technology has been gradually introduced into the sugar industry. At present, most sugar mills in our country adopt the clarification process of sulfurous acid method. Only a small part of sugar factories adopt carbonate clarification process. Because of the impurities removed by the carbonic acid

[1]This paper is supported by Scientific research project of Guangxi education department in 2014 (No. LX2014611).

[2]Guangxi Vocational and Technical Institute of Industry, Nanning, Guangxi, 530001, China

method is more than that removed by the method of sulfuric acid, the clarification effect of carbonic acid method is better than many KIA sulfuric acid methods [1]. But the production cost of carbonate method is much higher than that of KIA sulfuric acid method. Especially in the production of equipment, the production facility that carbonate method requires is more than that of sulfuric acid method, and the whole process of production is also more complex. Therefore, in the existing technical level, many sugar enterprises choose sulfurous acid method. Subsequently, with the development of science and technology, especially the improvement of automation, the cost of production has been reduced, and the carbonic acid method has been widely used [2].

Whether it is carbonate or sulfurous acid method, the pH value in the clarifying process of the sugar refinery is an important index of the whole section, which is related to the effect of the whole clarification. Recognizing the importance of the pH value in the clarifying process of the sugar refinery, a large amount of research work has been done on the control of pH stability [3]. The lag and inertia link exist in the neutralization process of pH value in sugarcane juice. In 1991, Wu Minghua of South China University of Technology adopted the Dalin algorithm with parameter self-correction to design computer control system, which improved the quality of manual control. Aiming at the problems of neutralization pH value and pH value control of clarified juice, teachers and students of Guangxi University used the fuzzy control algorithm, adaptive dynamic programming and genetic algorithm to optimize the design of control system control, so as to improve the efficiency and accuracy of control [4]. But it was only in the theoretical simulation stage, and the real application was very rare. In the past, due to the relative backwardness of automation technology, there were few on-line inspection devices in the clarifying process of sugar refinery. Most of the detection parameters were adjusted by manual experience, which resulted in low quality sugar content in the finished sugar and low production efficiency of sugar mills [5]. With the development of economy and society, the demand for high quality sugar in domestic and foreign markets is increasing. How to improve the quality of sugar ratio has become a problem for sugar refinery enterprises. To promote the development of production automation in sugar factories has become the focus of research in the field of sugar production.

In the second part of this paper, the research status of pH control in sugar factories was analyzed and summarized, and the development and application of fuzzy control were illustrated. The third part used fuzzy adaptive PID control to design pH intelligent control system in the clarifying process of sugar refinery, and the hardware part and software parts were designed, respectively. In the fourth part, the pH value control and the temperature control performance of the control system were analyzed through the experiment, and its feasibility was studied. In the fifth part, the full text was summarized and the conclusions were drawn, which supported the research of pH value control in the clarifying process of sugar factory based on fuzzy control.

2. State of the art

2.1. Research status of pH control in sugar factory

The clarifying process of a sugar refinery is a complicated nonlinear and large delay link. Nonlinearity is that it is not a linear relation between the pH value of cane juice and the induction voltage of glass electrode. When the pH value is about 7, with the added acid or base, the pH value of sugarcane juice changes rapidly instead of following a certain linear relationship [6]. The large lag link is due to that the pH point and the control point of the pH value is not synchronized. In the clarifying process of sugar cane juice, when pre lye inflows into the reaction tank until overflow, the detection point of neutralization juice pH value is reached. On the one hand, this process leads to the non-synchronization of the pre gray pH value and the test point of neutralization pH value. On the other hand, it leads to the large common lag in the process of control. The widely used pH measuring device in the sugar factory is glass electrode [7]. Glass electrode has the characteristics of high precision, fast response and strong stability, which can meet the requirements of complex environment. However, because the experimental equipment with the glass electrode can simulate the research process of pH value intelligent control system in the clarifying process of sugar refinery, it has the disadvantages of high resistance and easy to produce fouling. Therefore, in order to ensure the accuracy and stability of the measurement, the glass electrodes must be cleaned periodically [8]. Aiming at the problems existing in pH value measurement in sugar factory, based on the complex working environment, Song Yunpeng of Guangxi University designed the pH value measurement circuit, and successfully solved the pH measurement system exist impedance matching and electromagnetic interference and other problems, which could quickly and accurately collect the pH value of sugarcane juice. However, by analyzing the technological process of the clarifying process of the sugar refinery, it is found that the pH value measurement itself is a nonlinear link, and the pH control part has the characteristics of uncertainty and large lag.

It is difficult to solve the nonlinear and large lag of pH value. Therefore, pH control is recognized as one of the most difficult processes to control. In view of the difficult control problems of the pH value in the clarifying process of the sugar factory, a set of pH value computer integrated control system was developed by Wu Minghua of South China University of Technology, and it was put into operation in Guangdong Lecong sugar refinery. It could solve the problem of pH value control in the clarifying process of sugar refinery, and the control quality of pH value in neutralization process was greatly improved [9]. Later, Huang Xueying and other people made further improvements to the SS983 type neutralization pH automatic measuring control system, and a series of tests were carried out on the improvement of the measurement part, host circuit design, updating of electronic components, control software, the cleaning system and the ash additive, the selection of the ash adding controller, and the change of the technological process. In addition, they launched a new version. It has been proved by the practice of more than 20 sugar factories that in addition to the original advantages of the new system, the

system also has a strong anti-interference ability, long electrode life, gray control more reasonable, and juice pH more stable, and smaller fluctuations [10]. Huacheng auto control equipment factory in Qinzhou designed the pH automatic detection device of double glass electrode. The system used double glass electrodes to measure and clean in turn, which solved the problem of glass electrode measurement accuracy reduction caused by the glass electrode fouling. It has improved the accuracy of pH measurement in sugar factories, and has been applied in many sugar factories in Guangxi, Guangdong, Yunnan and other provinces. The following diagram in Fig. 1 describes the process of sulfurous acid process.

2.2. The development and application of fuzzy control

Control fuzzy is a computer digital control technology based on fuzzy set theory, fuzzy linguistic variables and fuzzy logic inference. In 1965, the famous American expert L. A. Zadeh established the fuzzy set theory based on control theory. In 1973, L. A. Zadeh defined the fuzzy logic control and related theorems of University of Cambridge. In 1974, at the University of Cambridge, E. H. Mamdani's fuzzy controller realized the application of steam engine control for the first time [11]. Through the analysis of the basic process of the water crisis in the chemical plant of University of Electronic Science and Technology in 2002, MATLAB fuzzy tool was used to reflect the pH control simulation based on the characteristics of big inertia and pure lag. And the simulation results showed that fuzzy control could achieve good control effect. In 2007, Cao Youwei of Dalian University of Technology analyzed the problem of pure hysteresis in the process of large inertia temperature control. The fuzzy temperature controller was designed based on 89C51 single chip microcomputer, which solved the problem of difficulty in tuning the PID parameters of temperature control [12]. The waste water treatment system with pH value had the characteristics of large inertia, pure time delay, nonlinear and fuzzy control, which was combined with the prediction of Smith. The fuzzy controller was established to control Smith sewage treatment system pH, using Simulink simulation, which had good control effect [13]. In 2010, Li Gang of Central South University applied fuzzy control into the dual tank water level control, to compare the control effect of the traditional PID algorithm and fuzzy control algorithm in the dual tank water level control, and it was proved that fuzzy control was more conducive to solving the problems of large lag and nonlinearity in the level control. In the same year, Xie Shihong of Shaanxi University of Science and Technology proposed a fuzzy PID control algorithm for on-line adjustment of parameters in view of the nonlinearity and hysteresis of acid-base neutralization process. The method adjusted the parameters of the PID controller on-line according to the real-time deviation of the control process, and analyzed the deviation and deviation change rate to set the fuzzy rules [14]. Experiments showed that the method could adapt to the global change of pH value and overcome the influence of fluctuation of acid-base neutralization flux. In 2011, Wang Baolu of Guangxi University designed fuzzy logic PID controller based on OPC technology and applied it to pH value control in clarifying process of sugar refinery. The experimental results showed that the fuzzy logic PID control had a

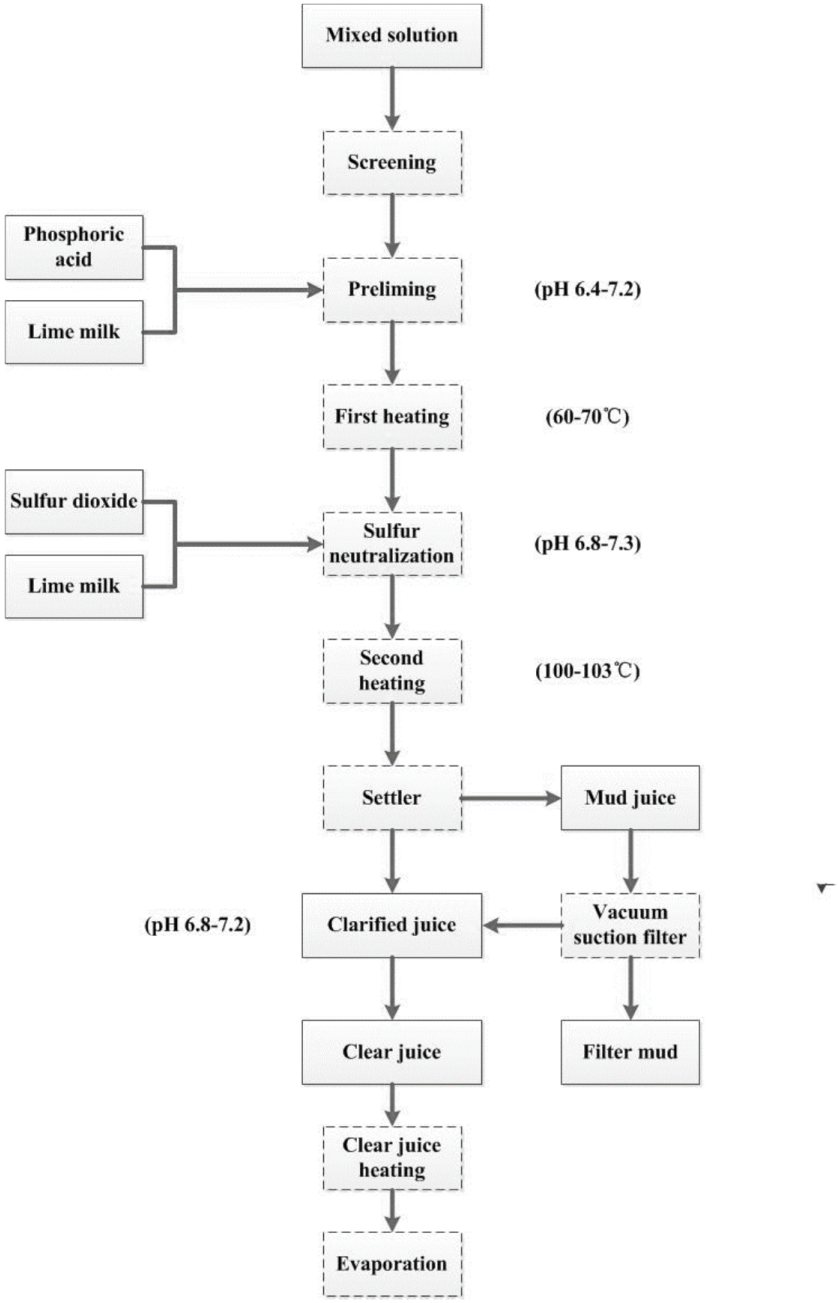

Fig. 1. Process flow diagram of sulfurous acid process

good control effect on the pH value in the clarifying process of the sugar refinery, and it also had certain application value. In the same year, Yan Feng of Beijing Tech-

nology and Business University analyzed the time variation and hysteresis in the air conditioning system, and designed and simulated the parameter self-tuning fuzzy controller in the environment of the MATLAB software based on the basic characteristics of fuzzy control technology and classical PID control. The experimental results showed that the controller had faster response and smaller steady-state error [15]. In 2003, Li Hongzhong in Lanzhou Jiaotong University applied the fuzzy control method into the intelligent traffic light system. By controlling the traffic rate of the single intersection, the average delay time of the waiting traffic was reduced, and the environmental protection, energy saving and economic access were realized.

3. Methodology

3.1. Fuzzy adaptive PID control

Figure 2 shows the composition of the fuzzy controller.

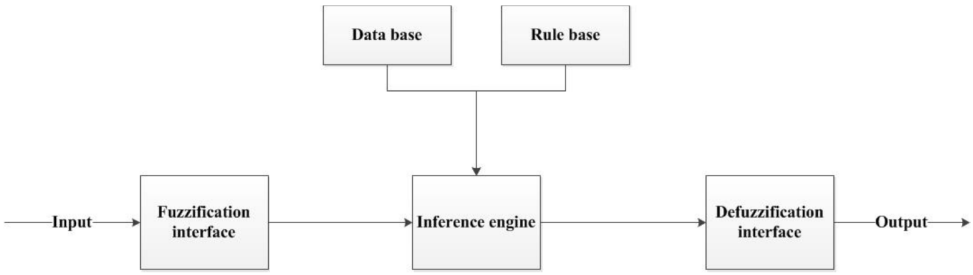

Fig. 2. Composition of fuzzy controller

By calculating the current system error and the rate of error change, fuzzy rules are used to carry out fuzzy reasoning, and the parameters are adjusted after defuzzification. The core of fuzzy PID control design is to summarize the technical knowledge and practical experience of engineering designers, and to establish the appropriate fuzzy rules table. The output values of the control quantity are adjusted respectively according to the three parameters of scale, integration and differential. The fuzzy adaptive PID controller has a deviation of e and a deviation change rate Δe, and the outputs are ΔK_{p}, ΔK_{i} and ΔK_{d}. Among them, G_{l} and $G_{\Delta \mathrm{l}}$ are quantization factors, G_{Kp}, G_{Ki} and G_{Kd} are scale factors, and the range is selected according to the input and output range of objects. Quantities ΔK_{p}, ΔK_{i} and ΔK_{d} obtained by fuzzy inference that adapts to the control object are as the parameter increments of K_{p}, K_{i} and K_{d}, respectively. According to the state of the controlled object, the PID parameters can be adjusted on-line. The fuzzy adaptive PID controller adjusts the PID parameters as follows:

$$K_{\mathrm{p}} = K_{\mathrm{p}}^{'} + \Delta K_{\mathrm{p}}\,,$$

$$K_{\mathrm{i}} = K_{\mathrm{i}}^{'} + \Delta K_{\mathrm{i}}\,,$$

$$K_{\mathrm{d}} = K_{\mathrm{d}}^{'} + \Delta K_{\mathrm{d}}\,, \tag{1}$$

where $K_{\mathrm{p}}^{'}$, $K_{\mathrm{i}}^{'}$ and $K_{\mathrm{d}}^{'}$ are the initialized PID parameters.

The fuzzy adaptive PID finds the fuzzy relation between the three parameters of the PID and the deviation e and the deviation change rate Δe. During the operation, the three parameters are modified online according to the fuzzy control principle by continuously detecting e and Δe. When the control parameters are different, the controlled object has good dynamic and static performances.

3.2. Hardware design of control system

The hardware platform of the control system mainly includes PC104 industrial control computer, pH value detection and control module, temperature detection, control module, and flow detection module. The hardware structure of the control system is shown in Fig. 3.

PC104 is an industrial computer bus standard specially defined for embedded applications. The PCM-3587, PCL-2101 and PCL-9402 modules used in this paper all support the PC104 bus standard. Therefore, in the hardware design of the control system, the three are connected in stack mode to form an industrial controller based on the PC104 bus standard. The core control part adopts PCM-3587 industrial control board which is produced by Dark blue Science and Technology Ltd. It is a low power X86 embedded motherboard designed for PC104 industrial computer bus standards. CPU uses DM&P SOC Vortex86DX, and integrates the north bridge, the south bridge, SPI, BIOS, LPC, serial/parallel port, high-speed USB2.0, OTG, Ultra-DMAIDE, and lOM/lOOM ethernet. The Vortex86DX processor uses an external display chip. This is an ultra-low power graphics chipset with a total power consumption between 1 and 1.5 W, supporting the VGA display resolution of 1600×1200. PCM-3587 has good downward compatibility, which is widely used in the field of embedded development. In the field of hardware requiring small volume, low power consumption and low cost, the modules based on PC104 bus standard have been widely used.

3.3. Software design of control system

The software realization of the control system mainly includes the design of the monitoring interface, the communication between the host computer and the lower computer, and the design and embedding of the control algorithm. The monitoring interface design contains Kingview monitoring design and touch-screen human-computer interaction interface design. The Kingview monitor design part realizes the connection between Kingview and database, and it can monitor real-time data and historical data query. Touch-screen design can achieve real-time display of online data, manual control and automatic control switching. The .dll file of the fuzzy controller is written in the VC++6.0 environment. The .dll file is embedded in the VisSim simulation modeling software, and the temperature control module and the pH value control module are set up. The software framework of the control system

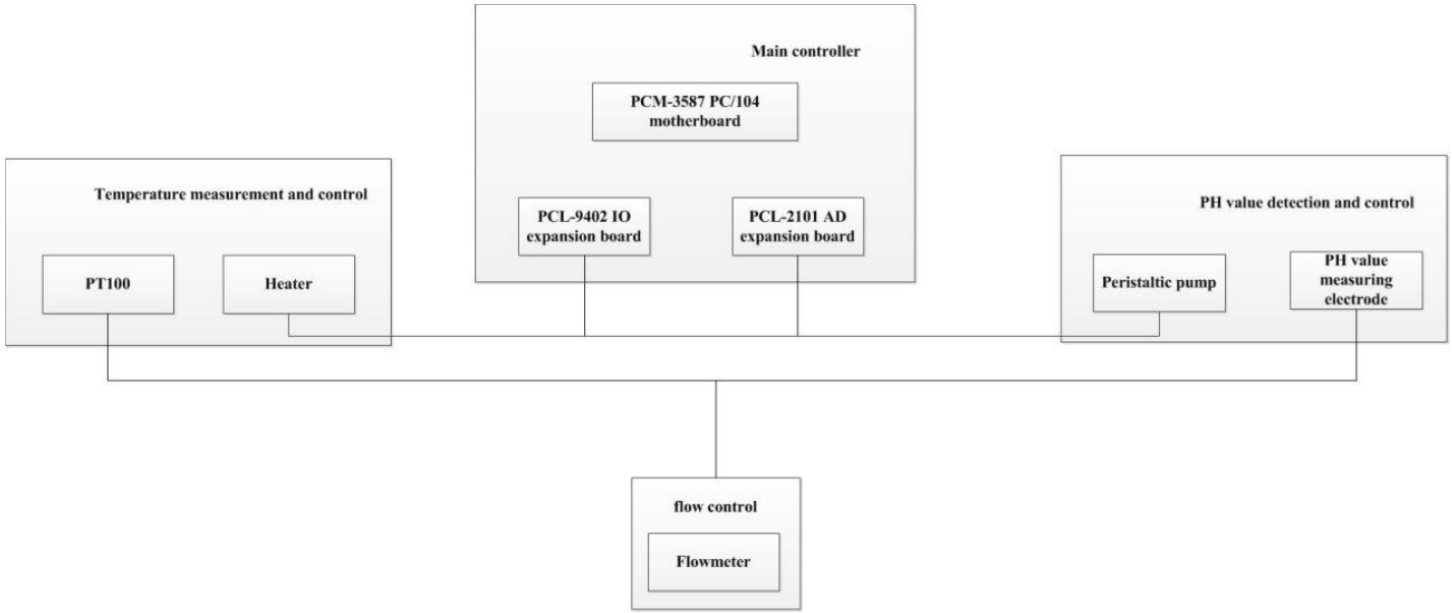

Fig. 3. Hardware structure of the system

is shown in Fig. 4.

The Modbus protocol was the first global bus protocol for industrial sites invented by Schneider electric in 1979. The protocol supports traditional RS-232, RS-422, RS485, and Ethernet devices. At present, many industrial devices use Modbus protocol as communication standard. The controller communicates with the host computer using the Modbus RTU protocol. The Modbus RTU protocol uses a master-slaver query mode. On a communication line, the host sends a query command from the machine to determine whether to reply the message by analyzing whether the command is sent to itself. In the control system, each slaver has a unique address. As a result, the same query instruction does not correspond to multiple responses. In the VC++6.0 environment, the driver programs of the controller are developed to realize the communication with the host computer ModbusRTU. The implementation process of communication is as follows.

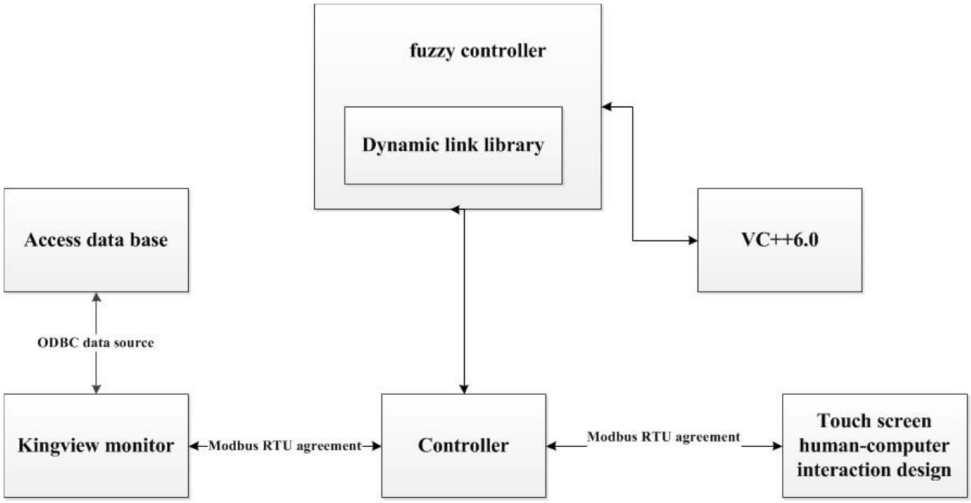

Fig. 4. Software function framework

The format of the Modbus RTU message frame is shown in Table 1.

Table 1. Format of message frames

Address field	Function domain	Data domain	Check field
1bit	1bit	N bits	2bits

4. Result analysis and discussion

The pre lye was sent into the reaction tank through the direct current to simulate the lagging link of actual production in sugar factory. According to the error and the error change rate of the measured value and the given value of the neutralization juice, the pH fuzzy controller obtained the control output by querying the fuzzy rule table. The PWM wave pulse was used to regulate the flow of alkaline juice,

and the pH value of neutral juice was stable near the desired index. Before the pH value control experiment, the pH value measuring and controlling device was used to measure several buffer solutions with different pH values. The purpose of the test was to test the sensitivity and accuracy of the glass electrode for different pH values. The buffer value of pH was 9.18, 6.86 and 4, respectively; disodium hydrogen phosphate, sodium tetra borate and dipotassium hydrogen phosphate were used to prepare the buffer solution. The glass electrode was placed in a neutral solution for 1–2 minutes before the experiment, with the purpose to ensure that the surface of the glass electrode was cleaned and to remove the residual solution before. The glass electrodes were successively placed in solutions with pH values of 4, 6.86 and 9.18. The detection effect is shown in Fig. 6.

As shown in Fig. 6, at the initial time, a glass electrode was used to detect a buffer solution of pH value of 4, and the pH value was about 3.93, and the error was about 1.7 %. After 1 minute, the glass electrode was placed in a buffer solution of pH 6.86, and the response time was about 10 seconds; then the pH value increased gradually, and it finally stabilized at about 6.9 with the error of 0.6 %. When the pH value was stable, the glass electrode was placed in a buffer solution of pH 9.18, the response time was about 8 seconds, and the pH value was detected to be about 9.15 with the error of 3 %. The experiments were repeated, and it was found that the experimental results were basically consistent with the first one. PH measurement results showed that the performance of glass electrode, pH signal acquisition board and signal amplifier board was reliable, and the hardware part of pH detection met the design requirements.

PH value fuzzy controller was adopted to control pH value of neutralization juice. In order to simulate the change law of pH value in clarifying process of sugar refinery, a hydrochloric acid solution with a pH value of 6.5 was used to simulate the pre lye, and the sodium hydroxide solution with a pH value of 12.8 was used as neutralization reagent to control pH value of neutralization juice in the experimental process. The given value of neutral juice was 7. Experimental results are shown in Fig. 7.

According to the test results of the temperature control in Fig. 8, in the course of the experiment, the 1800 W electric heater was used to control the pre lye. In the initial state, the temperature of pre lye was 32 °C or so, and the temperature setting index of pre lye was 65 °C. The traditional PID control method was used to control the temperature, and the temperature of pre lye generated fluctuations. The stability of PID control effect was better than that of fuzzy control when the system was in steady state. Experimental results show that the pre lye temperature control fuzzy control algorithm had good control effect.

5. Conclusion

The control of the pH value in the clarifying process of the sugar refinery plays a key role in the quality of the final product of the sugar refining. The lack of automation technology in the production process of the sugar factory has led to low production efficiency and low product yield, which has affected the production and management level of the sugar enterprises. With the continuous development of

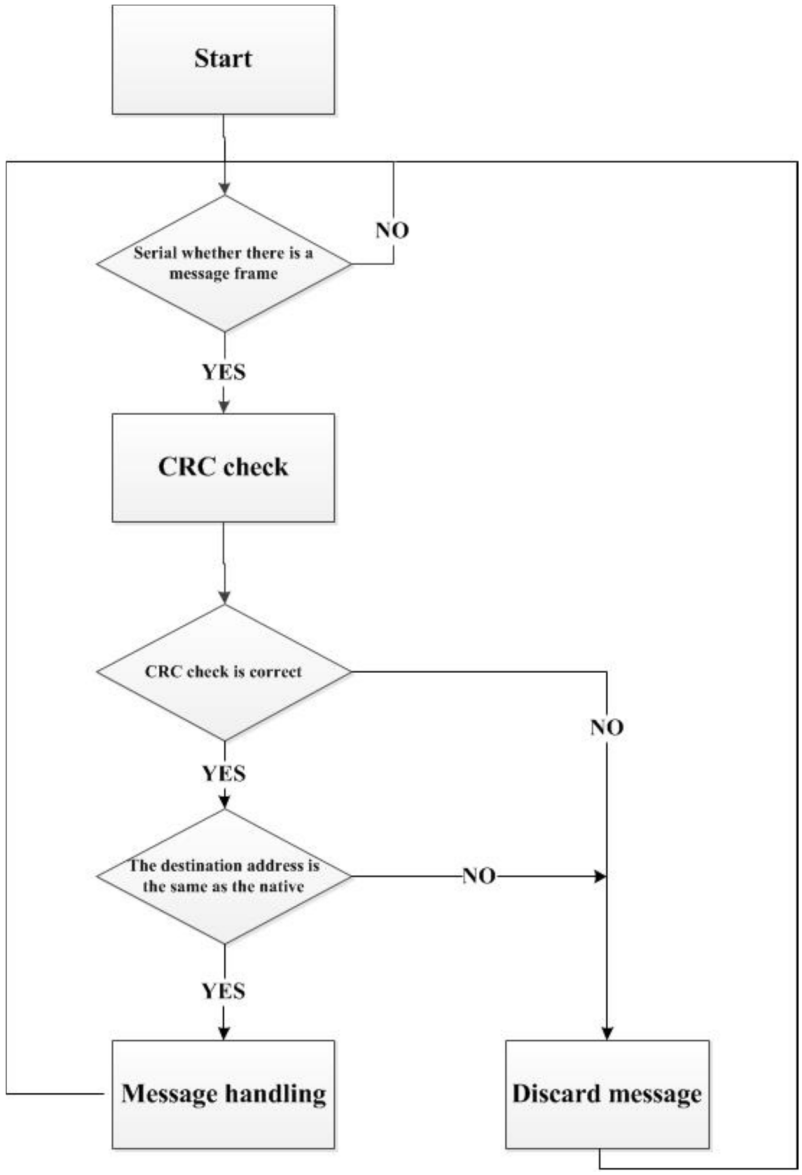

Fig. 5. Modbus communication flow chart

society and the continuous progress of automation technology, it has been promoted in research, application and sugar industry. How to better control the pH value in the clarification section of sugar refinery has become an important problem. In this paper, a pH value intelligent control system was designed on the simulation experimental device in the clarifying process of sugar refinery. The simulation device could truly reflect the actual technological process of the clarifying process of the

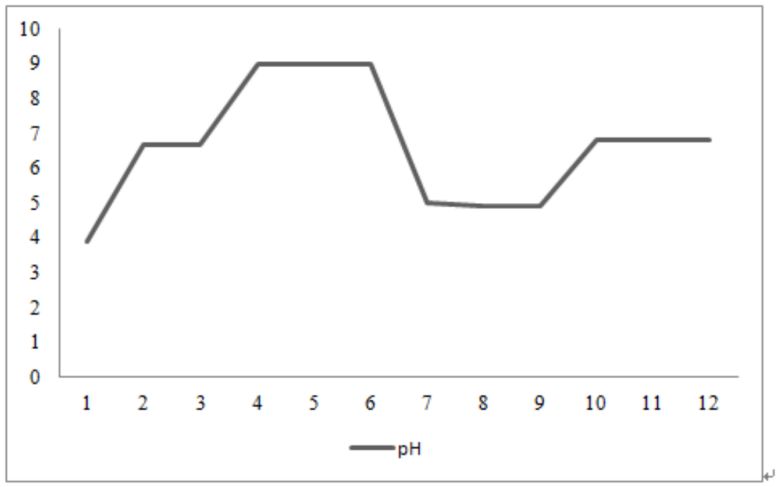

Fig. 6. PH value detection chart

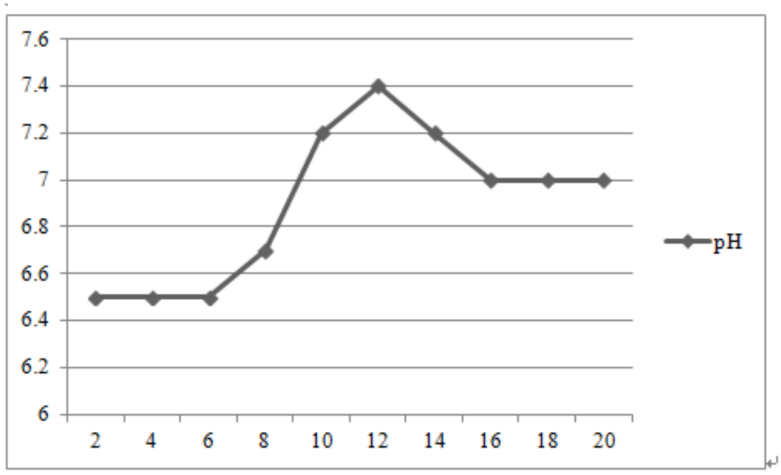

Fig. 7. Neutral juice pH control effect diagram

sugar refinery, and effectively reflect the existing problems. On this basis, the fuzzy control algorithm was used to control the condition index and realize the design of the related hardware system, including AD acquisition program, Modbus communication program, the software design, and the temperature control module. With the help of the pH intelligent control system, the control simulation of the clarifying process of the sugar refinery was carried out, and the control effect of the control system on the pH value and temperature was preliminarily verified. Therefore, the study is of practical significance to improve the research level of pH value control in the clarifying process of sugar refinery based on fuzzy control.

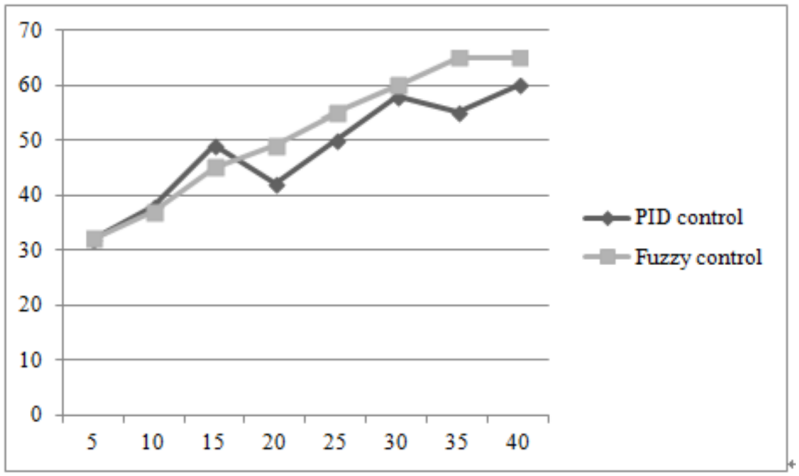

Fig. 8. Temperature control test chart

References

[1] A. U. Aquino, M. G. A. C. Bautista, R. G. Baldovino, E. J. Calilung, E. Sybingco, E. P. Dadios: *A neuro-fuzzy mixing control model for the cooking process of coconut sugar*. Proc. 9th International Conference on Computer and Automation Engineering (ACM), 18–21 Feb. 2017, Sydney, Australia, 211–220.

[2] D. Nguyen, V. Gadhamshetty, S. Nitayavardhana, S. K. Khanal: *Automatic process control in anaerobic digestion technology: A critical review*. Bioresource Technology *193* (2015), 513–522.

[3] M. Sujaritha, S. Annadurai, J. Satheeskumar, K. Sharan, L. Mahesh: *Weed detecting robot in sugarcane fields using fuzzy real time classifier*. Computers and Electronics in Agriculture *134* (2017), 150–171.

[4] L. Anojkumar, M. Ilangkumanar, S. M. Hassan: *An integrated hybrid multi-criteria decision making technique for material selection in the sugar industry*. International Journal of Multicriteria Decision Making *6* (2016), No. 3, 247–268.

[5] S. Birle, M. Hussein, T. Becker: *On-line yeast propagation process monitoring and control using an intelligent automatic control system*. Engineering in Life Sciences *15* (2015), No. 1, 83–95.

[6] V. Blomenhofer, F. Gross, J. Procelewska: *Water quality management in the food and beverage industry by hybrid automation using the example of breweries*. Water Science and Technology: Water Supply *132* (2013), No. 2, 427–434.

[7] S. Bachche: *Deliberation on design strategies of automatic harvesting systems: A survey*. Robotics *4* (2015), No. 2, 194–222.

[8] A. H. Najafabadi, M. Shahrokhi: *Model predictive control of blood sugar in patients with type-1 diabetes*. Optimal Control Applications and Methods *37* (2016), No. 4, 559–573.

[9] N. Perrot, C. Baudrit, J. M. Brousset, P. Abbal, H. Guillemin, B. Perret, E. Goulet, L. Guerin, G. Barbeau, D. Picque: *A decision support system coupling fuzzy logic and probabilistic graphical approaches for the agri-food industry: prediction of grape berry maturity*. PloS one *10* (2015), No. 7, paper e0134373.

[10] T. Hermann: *Industrial production of amino acids by coryneform bacteria*. Journal of Biotechnology *104* (2003), Nos. 1–3, 155–172.

[11] P. Grant: *A new approach to diabetic control: fuzzy logic and insulin pump technology*. Medical engineering & physics *29* (2007), No. 7, 824–827.

[12] T. Siimes, P. Linko, C. von Numers, M. Nakajima, I. Endo: *Real-time fuzzy-knowledge-based control of Baker's yeast production.* Biotechnology and Bioengineering *45* (1995), No. 2, 135–143.

[13] J. I. Horiuchi: *Fuzzy modeling and control of biological processes.* Journal of Bioscience and Bioengineering *94* (2002), No. 6, 574–578.

[14] V. Petridis, V. Kaburlasos: *FINkNN: A fuzzy interval number k-nearest neighbor classifier for prediction of sugar production from populations of samples.* Journal of Machine Learning Research *4* (2003), No. 1, 17–37.

[15] M. J. Araúzo-Bravo, J. M. Cano-Izquierdo, E. Gómez-Sánchez, M. J. López-Nieto, Y,À. Dimitriadis, J. L. Coronado: *Automatization of a penicillin production process with soft sensors and an adaptive controller based on neuro fuzzy systems.* Control Engineering Practice *12* (2004), No. 9, 1073–1090.

Received June 6, 2017

Acta Technica *62* No. 1A/2017, 447–458

Application of simulation material for water-resisting soil layer in mining physical simulation[1]

Jie Zhang[1], Bin Wang[2], Tao Yang[2]

Abstract. In order to study the failure mechanism of water-resisting soil layer under both coal excavation and seepage effect, a new kind of experimental material for fluid-solid physical simulation (FPS) has been established. The material adopts river sand and clay as the aggregates, besides engine oil and low-temperature grease are used as the gelatinizing agents. According to relevant property testing on the experimental material, the mechanical parameters and seepage parameters of the material totally match the parameters of the soil layer, and meets the requirements of the fluid-solid coupling experiment. A FPS model has been constructed to simulate coal excavation under water-bearing strata with the specific material. The results indicated that movement and failure mechanism of the water-resisting soil layer agree with the in-situ monitoring results. In addition, revolution law of mining-induced crack also matched the actual data. The mechanism of submarine seepage and its parameters on the material and the prototype are similar. Meanwhile, the model demonstrates that selection of the material and coupling parameters are effective and correct.

Key words. Water-resisting soil layer, physical simulation, fluid-solid coupling, simulation material, mining-induced destroy.

1. Introduction

Physical simulation, as an experimental methodology combining simulation theory and dimensional analysis, was introduced to solve mining problems [1]. As we know that fluid-solid coupling is interaction between fluid (water) and solid (rock and soil) in geotechnical engineering [2]. The coupling effect contains deformation and failure of the rock and soil and flow characteristics from the fluid [3]. So we mainly study evolution mechanism of mechanical behavior and seepage trait after rock and soil failure with fluid flowing [4]. Many field of engineering technology would relate

[1]The authors acknowledge the National Natural Science Foundation of China (Grant: No. 5147173).

[2]School of Energy, Xi'an University of Science and Technology, Xi'an, 710000, China

the fluid-solid problems like mining engineering, petroleum engineering, hydraulic and hydro-Power engineering and so on [5]. An accurate mechanism on fluid-solid coupling can control failure of water-resisting soil layer by mining excavation [6]. We studied the mechanism on fluid-solid coupling by theoretical analysis and numerical simulation. Now fluid-solid physical simulation is a new way. In the way, we can determine experimental settings such as single factor or multi-factor. Particularly, in the fluid-solid physical simulation with multi-factor, we need design fluid feature into the research course but not general simulation by only solid material.

Simulation principle of fluid-solid coupling needs determine simulation coefficients of elastics mechanics and hydromechanics of fluid-solid media desperately in the same settings with fluid-solid coupling theoretical model for continuous medium. When we determine the simulation coefficients, simulation constants in the hydromechanics should be replaced with simulation constants in the elastics mechanics, which can achieve fluid-solid coupling simulation.

$$\begin{cases} [T]\{H\} + [S]\left\{\frac{\partial H}{\partial t}\right\} + \{I\} = 0, \\ \{R\}[B]\{\Delta\delta\}_{\epsilon} = \frac{n\gamma}{E_{\mathrm{w}}}\Delta H, \\ \{F_{\mathrm{w}}\} + \{\Delta F_{\mathrm{w}}\} = [K]\cdot[\{\delta\}_{\epsilon} + \{\Delta\delta\}_{\epsilon}], \end{cases} \tag{1}$$

where $[T]$, $[S]$ and $\{M\}$ are transmission matrix, storage matrix and converge column matrix, respectively. Symbols $\{R\}$, $[B]$ and δ_{ϵ} are unit vector, unit stain vector and unit displacement vector, respectively. Symbols n, γ and H are crack rate of rock-masses, water unit weight and underwater head, respectively. Symbols $\{F_{\mathrm{w}}\}$ and $\{\Delta F_{\mathrm{w}}\}$ are equivalent nodal force by body force from water seepage and relevant equivalent node force increment. Finally, $[K]$ is the global stiffness matrix for the simulation model.

According to simulation theory in elastics mechanics, $C_{\mathrm{G}} = C_{\mathrm{E}} = C_{\lambda}$. Besides, geometry, stress and inertia force simulation settings are $C_{\mathrm{u}} = C_{\mathrm{l}}$, $C_{\mathrm{G}} = C_{\mathrm{E}} = C_{\gamma}C_{\mathrm{l}}$ and $C_{\mathrm{t}} = \sqrt{C_{\mathrm{l}}}$ apart.

According to simulation theory in hydromechanics, converge column, seepage coefficient and storage rate simulation settings are, respectively

$$C_{\mathrm{I}} = \frac{1}{C_{\mathrm{t}}} = \frac{1}{\sqrt{C_{\mathrm{l}}}},\ C_{\mathrm{KX}} = C_{\mathrm{KY}} = C_{\mathrm{KZ}} = \sqrt{\frac{C_{\mathrm{l}}}{C_{\gamma}}},\ C_{\mathrm{S}} = \frac{C_{\mathrm{t}}C_{\mathrm{I}}}{C_{\mathrm{H}}} = \frac{1}{C_{\gamma}C_{\mathrm{l}}}.$$

The main ingredients of red clay aquiclude are red-brown clay, loam, mineral composition is mainly based chlorite, 11 % sand, 51 % silt, 38 % clay, void ratio is 0.6∼0.89, it is silty clay, compact structure, is in hard plastic state, and it has the high strength and low compressibility. The results of physical and mechanical parameters of soil samples are shown in Table 1.

In order to test the seepage deformation characteristics of soil under seepage flow, through the water head pressure applied, to Measure the hydraulic pressure on the soil. Main completed the clay try, grain size analysis, fluid density and water

content, plastic limit and penetration test. Step by step under the set seepage water pressure on the upper load to stable. In the seepage water pressure for l0 kPa, 20 kPa, 30 kPa, 40 KPa cases of head seepage deformation test showed that the basic seepage deformation were positively correlated, stronger water-resisting layer. The experimental results are shown in Table 2.

Table 1. Physical and mechanical parameters on red clay

Physical properties				Mechanical properties			
Water content W (%)	Void ratio e	Porosity n (%)	Cohesive force c (kPa)	Internal friction angle φ (°)	Coefficient of compressibility (MPa^{-1})	Modulus of compression Es (MPa)	Unconfined compressive strength qn (kPa)
11.3∼17	0.6∼0.89	38∼46.1	42∼98	27.8∼33	0.1∼0.25	8∼21	110∼151

Table 2. Water-physical property of red clay

Lithology	Liquid limit W_1 (%)	Plastic limit (Wp) (%)	Permeability coefficient K (mm/h)	Saturability Sr (%)	Coefficient of collapsibility δ (s)	Flee welling ratio δct (%)
Red clay	25.1∼31.5	16.6∼18.3	10.24∼26.25	40.2∼65.5	0∼0.005	1∼18

In the physical simulation experiment, proper material selection would be crucial for the experiment. With relevant simulation theory, simulation material should satisfy the simulation principle for fluid-solid coupling and other basic properties. Specially, the simulation material for the fluid-solid coupling need be non-hydrophilic, low permeability and plastics deformation. Moreover, non-hydrophilic material is similar with the prototype in the mechanics characteristics aspect. We have finished related simulation material on rock-water two-phase experiment and confirmed low fusibility high quality paraffin (42 °–54 °) as the gelatinizing agents [7]. Simultaneously, simulation material should meet sealing, which do not influence the movement mechanism of rock and soil layer. In the end, we need simulate failure mechanism of the rock and soil layer and crack evolution characteristics. The crack would emerge by the mining excavation rather than artificial water seepage channel and water seepage through the crack should be visual.

In general, we made specimens with various matching on the aggregate and gelatinizing agent and obtained related mechanical and seepage parameters. We determine the aggregate by the prototype composition, property and experimental purpose. According to former research results, river sand and clay can get low strength simulation material. River sand mainly offers strength and brittleness. With the same relative density, internal friction angle of the river sand is larger due to larger superficial roughness of sand particle. When sand particle is oversize, permeability of the simulation material would increase remarkably. On the contrary, fine sand

which has larger surface area, would integrate with the gelatinizing agent better. Material made by various particle size sand would reduce the void rate and when Cu>5, seepage rate of the material would decrease obviously. So the material should choose the river sand with good psephicity and small particle size.

Clay mainly represents plastics trait. According to geological investigation in coal mine restrict, north part of Shaanxi Province, China, stone loess is comprised by loam and sub-sand. Hipparion red soil is consist by clay, sandy clay with compact structure. Considering high content of mineral in the water-resisting clay, crack be induced by the coal excavation would be close promptly, so we should choose the clay with low permeability and solid deformation behavior .

Engine oil and low-temperature grease were chosen as the gelatinizing agents. Engine oil, which is the machine oil addicting thickening agent and lubricant additive presenting semi-solid state mechanical parts lubricant, was applied for controlling non-hydrophilia of the material. Besides, low-temperature grease called mineral grease, which was white or faint yellow cream, provided large plastic deformation. The grease had good stickiness, lipophilicity, high density and good waterproofness.

2. Materials and methods

2.1. Strength and water-physical property test

Strength and water-physical property test of the material would be crucial in the simulation material experiment. We adopted the technical geotechnical facilities to make the material specimens. Particularly, the gelatinizing agents, which has obvious influence on the material strength. We employed high precision physical balance to weigh up related indigents. Based on experimental matching, the aggregates and gelatinizing agents would be blended evenly with automatic agitator kettle. Simultaneously, we heated and stirred the mixture for two reasons: in one hand, the aggregates can mix with the gelatinizing agents after fusion; on the other hand, the mixture would be heated evenly. In order to ensure the specimens quality and take apart the specimen, we would smear lubricant on the internal surface of specimen mould before manufacturing the specimens, which can guarantee the specimen quality. The heated experimental materials were easy to bond the mould, so we used bi-partition mould to make cylinder specimens. The mixture would pour into the mould, and we tamped it tightly. When the experimental materials have been cooled, we took apart the relative mould. The specimens needed to be conserved due to low strength after taking apart the moulds. Each group with various matching has triple specimens being numbered for subsequent testing. We set ratio sand (S) with soil (T) 1:1 as initial value and obtained the mechanics and water-physical properties being influenced by the engine oil and low-temperature grease. Next, we altered the matching of the aggregates to obtain relevant impact on the properties. Fig. 1 to Fig. 2 indicated the relevant experiments. The results were shown that the specimen would disintegrate after 48 hour soaking. The experimental material was non-hydrophilia obviously. When the specimens were compressed, dilatation was clear in the center of specimens, which was similar with failure behavior of

the water-resisting layer. Moreover, liquid limit moisture content of the material is 34.01 %, plastic limit moisture content is 25.21 %. Plastic index (IP) is 8.8 and liquidity index is ranged from 0.25 to 0.75 with good plasticity.

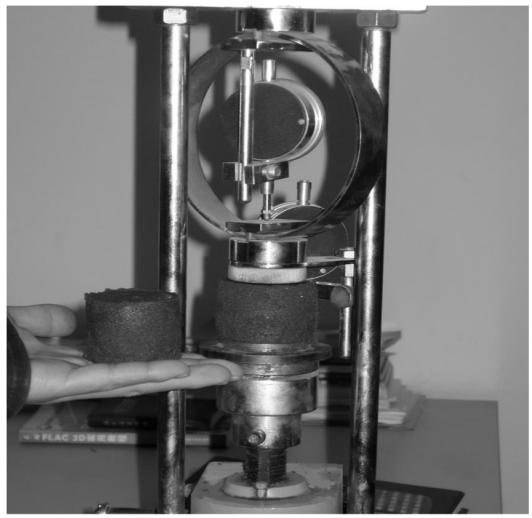

Fig. 1. Compressive strength testing

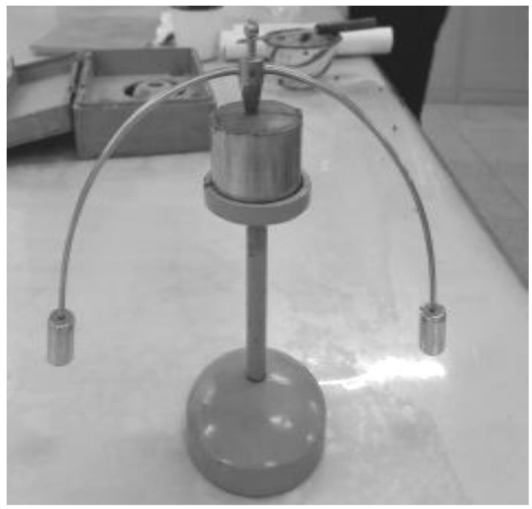

Fig. 2. Liquid and plastic limit testing

2.2. Material experiment analysis

Based on former abundant testing results, we have known the mechanics and water-physical properties of the materials basically. We schemed the various match-

ing of sand and soil including 2:1, 1:1, 1:2, 1:3 and 1:5. Simultaneously, the gelatinizing agent ratio adopted 4:1, 6:1, 8:1 and 10:1. The relative results are shown below.

Material strength influence by the ratio between sand and soil. When the gelatinizing agent ratio was constant, sand as the aggregate had large impact on the material mechanics characteristics. Values of material strength and elastic modulus would increase to specific value and then decrease remarkably with the ratio decreasing. When the ratio was 2:1, the specimen strength was lower due to inadequate cement of the aggregates. When the ratio was 3:1, curve tendency after peak value was similar. When the gelatinizing agent ratio increased from 6:1 to 10:1, the gelatinizing agent had huge effect on deformation behavior of the materials. Fig. 3 shows stress-strain curve with various the ratio between sand and soil, when the gelatinizing agent ratio were 6:1 and 10:1, respectively.

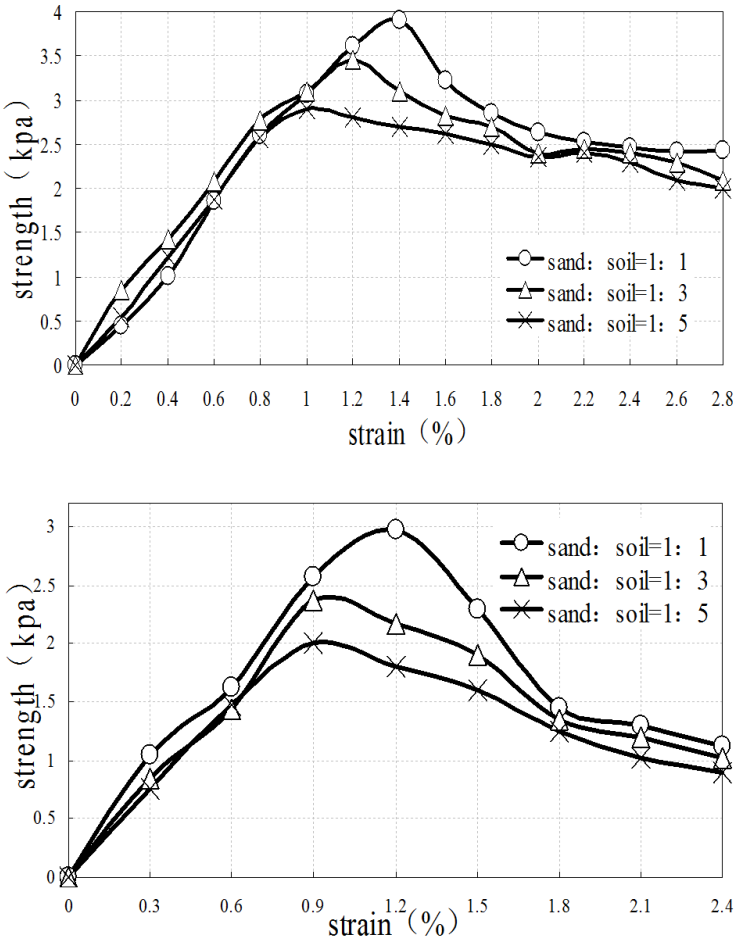

Fig. 3. Stress-strain curve in various ratios between sand and soil: up–gelatinizing agent ratio 10:1, bottom–gelatinizing agent ratio 6:1

Material strength influence by engine oil and low-temperature grease. Here, the influence was mainly performance on the plasticity of the material by engine oil, and low-temperature grease has large effect on the permeability behavior of the material. When we just use single kind of the gelatinizing agent, material strength always decreased with ratio between the aggregate and the gelatinizing agent decreasing. However, we adopted both gelatinizing agents for the simulation materials, which was better for the permeability experiment. Fig. 4 indicates stress-strain value on grease ratio with ratio between sand and soil 1:3 and 1:5.

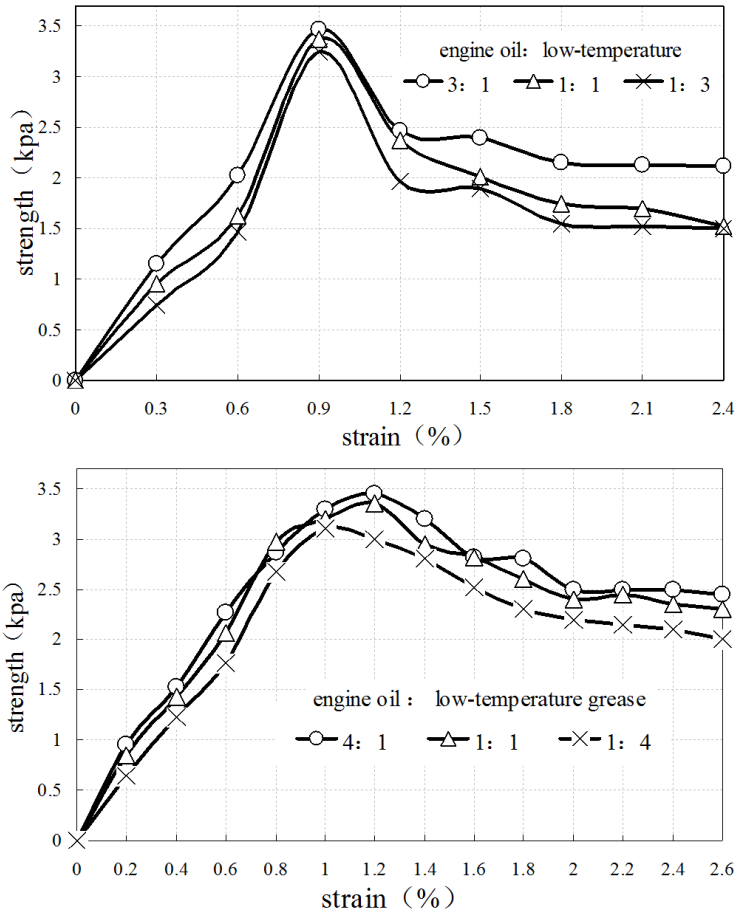

Fig. 4. Ratio between sand and soil 1:3: up–ratio between sand and soil 1:3, bottom–ratio between sand and soil 1:5

Material strength influence by ratio between the aggregate and the gelatinizing agent. In each specimen, the ratio between engine oil and low-temperature grease was 1:1 generally. With the same ratio between sand and soil, the strength of material would decrease obviously with ratio between the aggregate and the gelatinizing agent. Specially, ratio between sand and soil was down to 1:3, the curve kept steady

remarkably. When the ratio continued to decrease, post-peak value decrease quickly with distinct plasticity. Fig. 5 depicts stress-strain curve with ratio between sand and soil 1:1 and 1:3.

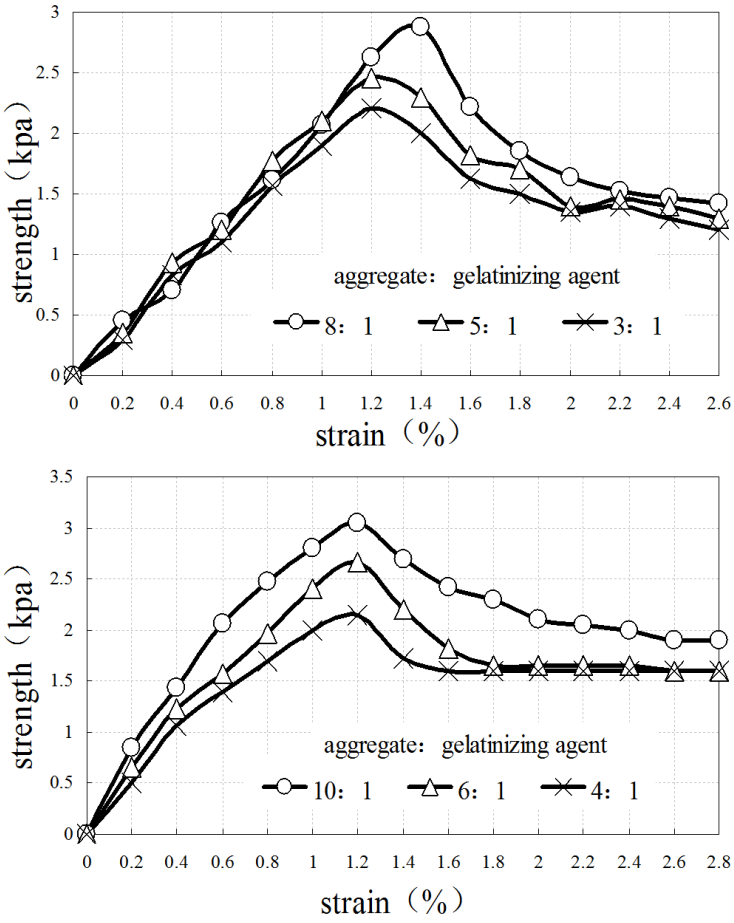

Fig. 5. Stress-strain curve in various ratios between the aggregate and gelatinizing agent: up–ratio between sand and soil 1:1, bottom–ratio between sand and soil 1:3

Proper analysis on material matching. In general, the strength of the material would decrease with increment of the ratio between sand and soil, between the aggregate and the gelatinizing agent. Stress-strain curves with various matching were totally similar with the curve from the prototype, which can satisfy the experiment settings well. With multi-target orthogonal experiment, the experiment should meet two index requirements. Firstly, proportion between engine oil and low-temperature grease should be equal, because that the grease ratio has few impact on the mechanics property of materials. From the above analysis, the specimens with ratio between sand and soil 1:5, whose mechanics property were similar with the property of soil furthest. So, we finally decided the reasonable matching, which is ratio between

sand and soil 1:5, the grease ratio 1:1. However, ratio between the aggregate and the gelatinizing agent should be conformed further by the permeability testing.

2.3. Material permeability testing

Material permeability testing mainly ensured the ratio between the aggregate and the gelatinizing agent. According to Darcy law, we adopted hydraulic conductivity methodology to measure permeability coefficient of the material. The relative formula for permeability coefficient is

$$K = \frac{QL}{t_n S(h+L)}\,. \tag{2}$$

Here, K is the permeability coefficient (mm/h), L is the thickness of experimental material (mm), h is the thickness of the water layer (mm) and t_n is time interval (hours). Symbol Q can be calculated by the formula

$$Q = \frac{Q_1 + Q_2 + Q_3 + \cdots + Q_n}{n}\,, \tag{3}$$

where Q is the average amount of water (mm^3). $Q_1, Q_2, Q_3, \cdots, Q_n$ are amounts of water in each permeability (mm^3). Symbol S means the cross-section area (mm^2). After 48 hours uf soaking, we started the testing and use water drum to gather the permeable water. The model needed 1 hour to achieve steady status and then we launched timer and read the data each one hour the values of Q_1, Q_2,$\cdots$, Q_n. Table 1 contains permeability coefficients in eight groups with various gelatinizing agent amount, ordered from large to small. We can conclude that the smaller proportion of the gelatinizing agent, the larger permeability coefficient, which indicates that the more loose the material, the larger permeability coefficient. Combining indigent and structure analysis on the soil group, we can conclude that the more compact structure of the soil group, the more weak permeability coefficient.

Permeability coefficient value of field soil is 10.24–26.25 mm/h by the testing . Geometry simulation constant is 100 and weight simulation constant is 1.56 in the experiment. Considering fluid-solid coupling simulation principle, permeability coefficient simulation constant is 6.4. So we can calculate permeability coefficient of the simulation material is 1.62–4.10 mm/h. Analyzing the data in the Table 3, the experimental material satisfies requirements in the simulation experiment and is similar with the soil.

3. Results

3.1. Investigation on geological settings and model schemes

Destruction of geological environment by coal excavation is more and more serious in Shenfu coal district. Particularly, we focus on the destruction of water resource. When height of excavated coal is about 2 m and water-resisting l layer is weak clay

strata, actual operation could achieve water protection mining, if the water-resisting layer would recover water-resisting performance after slight failure. So, we studied evolution mechanism of water flowing cracks in the soil layer and analyzed the cracks effect on water-resisting property. Next, protection measurement on water-resisting layer has been proposed finally after mastering relation between soil layer failure and overlying water body. The measurement can promote substantial and rational development of regional economics, and have important theoretical significance and application value . We set No. 2–2 working face as research area. Here, average angle of the coal seam is 1.5 degrees and excavated height is 2.0 m. Overlying strata is loose layer and 15 m hipparion red soil in tertiary. The soil in the research area has a tight structure and is medium hard. Void ratio of the soil is 0.70–0.83 and relevant permeability coefficient is 0.0058–0.6300 m/d. Besides, phreatic layer lies above the loose layer . Main mechanical parameter for overburden strata is in Table 4.

Table 3. Permeability coefficient of each experimental material

Ratio between aggregate and gelatinizing agent		4:1	5:1	6:1	7:1	8:1	9:1	10:1	11:1
Permeability coefficient (mm/h)	Specimen 1	1.25	1.48	1.69	2.31	2.85	3.63	3.91	4.32
	Specimen 2	1.21	1.41	1.61	2.29	2.86	3.50	3.89	4.28
	Specimen 3	1.19	1.46	1.68	2.33	2.89	3.58	3.85	4.31
	Average	1.22	1.45	1.66	2.31	2.87	3.57	3.88	4.30

Table 4. Mechanical parameters of overlying strata above working face

Serial number	Lithology	Thickness (m)	Density (10^3 kg/m3)	Tensile strength (MPa)	Elastic modulus (GPa)
8	Loose phreatic aquifer	20.0	1.6	-	2.0
7	Red soil layer	15.0	2.3	1.84	6.0
6	Medium sandstone	6.0	2.4	4.89	18.0
5	Siltstone with medium and fine sandstone	10.0	2.3	4.84	13.0
4	Medium sandstone	6.0	2.4	4.89	18.0
3	Siltstone	4.0	2.5	3.90	8.0
2	CityplaceSandy mudstone	4.0	2.5	3.62	7.0
1	Siltstone	2.0	2.4	3.90	6.0
0	Coal seam	2.0	1.3	0.70	1.5

We have established the fluid-solid coupling physical simulation model with geometry scale 1:100. The specific excavation method simulated actual longwall mining and the excavated height of coal seam was 2.0 m. We set 30 m boundary coal pillars which lied both in left and right sides of the model. Fig. 6 indicates model situation before and after the model excavation.

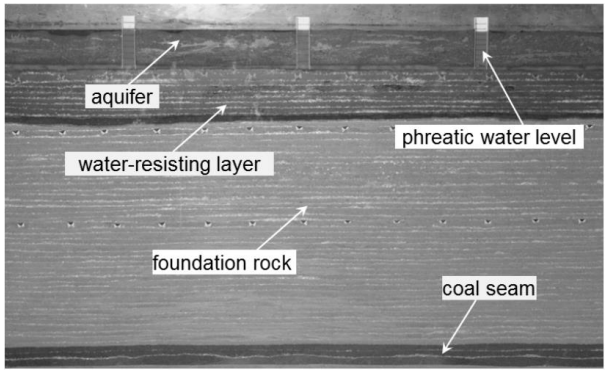

Fig. 6. Actual physical simulation model

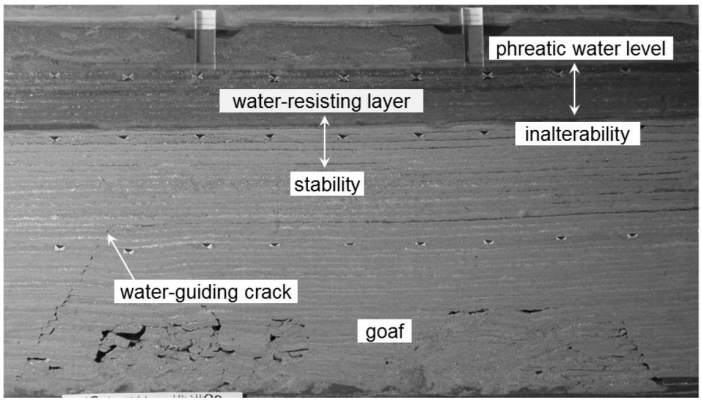

Fig. 7. Model status after coal seam excavation

3.2. Model result analysis

The experiment results indicated that coal roofs emerge a large-scale collapse when the working face advances 7 m and the collapse height reaches up to 15 m or so. With the working face advancing increasingly, periodical collapse of the coal roof is presented and mining-induced cracks gradually develop upward until the working face advances 150 m. Generally speak, final height of caving zone is about 20 m and the height of fissure zone can be up to 36 m. In particular, few small cracks has been developed into bottom of the water-resisting layer. Remarkable submerge has happened in the soil layer, however, cracks never connect the soil layer. In whole experiment, phreatic water level kept steady.

4. Conclusion

This paper developed a new physical material for fluid-solid coupled experiment based on fluid-solid coupling theories. We selected relevant materials for aggregates and gelatinizing agents. Moreover, the matching testing was also attempted and analyzed mechanical and water-physical properties. Finally, we adopted valid simulation materials and related matching. Main conclusions are following as:

Deduced simulation settings for elastic mechanics of rock mass and hydromechanics of water with fluid-solid coupling mathematics model. The theoretical basis for fluid-solid coupling is ensured with related simulation principle.

According to mechanical property and material matching testing, we offer relevant experimental materials, which are non-hydrophilia well and stable deformation performance. Considering coupling test data, the experimental materials can satisfy requirements for fluid-solid coupled model.

Built up the simulation model setting 2–2 coal seam as research area. Water-resisting layer is still steady with coal seam excavation. Water inrush and leakage seldom happened in the working face. The experimental results showed that movement and failure of overlying strata and crack evolution mechanism by the model coincided with the actual situation. Also, permeability laws and its parameters were also similar with in-situ monitoring results.

References

[1] J. Zhang, Y. Tao, T. Yunpeng, B. Wang: *Experimental test for destruction law of aquiclude under action of mining and seepage.* Rock and Soil Mechanics *36* (2015), No. 1, 219–224.

[2] J. Zhang, Y. Xueyi, C. Lianhua: *Failure mechanism of soil layer in long wall face intermission advance in shallow seam mining.* Journal of Hunan University of Science & Technology (Natural Science Edition *27* (2008), No. 6, 801–804.

[3] S. F. Xue, X. H. Tong, B. Q. Yue: *Progress of seepage rock mass coupling theory and its application.* Journal of the University of Petroleum *24* (2000), No. 2, 109–115.

[4] J. Zhang, Z. J. Hou, P. W. Shi: *Simulation materials experiment of the coupling seepage field and stress field in underground engineering.* Journal of Liao Ning Technical University *24* (2005), No. 5, 639–642.

[5] X. Miao, H. Pu, H. Bai: *Principle of water-resisting key strata and its application in water-preserved mining.* Journal of China University of Mining & Technology *37* (2008), No. 1, 1–4.

[6] J. Zhang, Z. J. Hou: *Experimental study on simulation materials of the solid-liquid coupling.* Chinese Journal of Rock Mechanics and Engineering *23* (2004) No. 18, 3157–3161.

[7] X. Miao, R. H. Chen, H. Bai: *Fundamental concepts and mechanical analysis of water-resisting key strata in water-preserved mining.* Journal of China Coal Society *32* (2007), No. 6, 561–564.

Received June 6, 2017

Acta Technica *62* No. 1A/2017, 459–470

Optimization design and motion simulation of multi-link mechanism based on mechanical press[1]

Jinmei Wu[2], Han Peng[2], Haicheng Zhu[2]

Abstract. Multi-link mechanism of mechanical press has gradually become an important technology for the development of machinery industry in the current era. However, there are still many shortcomings in the theory and operation of this technology. The theory of multi-link mechanism of mechanical press in China was summarized and compared with the traditional presses. Mechanical horses were taken as examples, and the relevant major influencing factors were identified and optimized. The results show that the optimized mechanical horse is more stable. The purpose of this study is to provide scientific support for the improvement of the theory of multi-link mechanism of mechanical press in China and to provide a positive impact on the development of machinery industry in China.

Key words. Mechanical press, multi-link mechanism, optimization design, motion simulation
.

1. Introduction

In the present era, with the rapid development of the world economy, science and technology has become an important productive force in the development of the times. It is very important for the development and promotion of various industries in the world. As the first productive forces in the economic development of the present era, the development of various kinds of science and technology is the inevitable demand of economic and enterprise development in the present era. It is also an important driving force for the development of a national or regional industry, which further combines with the traditional enterprise industry, so as to achieve the comprehensive improvement of a country or region. Nowadays, many

[1]This work was supported by the Higher Key Scientific Research Projects of Henan province in China—Trajectory optimization and deformation control of green environmental protection thin wall parts (Grant No. 17A460020).

[2]School of Mechanical Engineering, North China University of Water Resources and Electric Power, Zhengzhou, 450046, China

industries have begun to introduce advanced science and technology step by step, and design more products which are suitable for the development of the times. These products have brought a very important influence on the development of the world and society. This study will mainly be based on the optimization design of multi-link mechanism of mechanical press and its application to motion simulation, so as to provide some theoretical basis or technical support for the development of some simulation products in China.

2. State of the art

With the development of economy, machinery industry has gradually become an important economic pillar industry in a country or region. The development of the machinery industry is of great importance to the promotion of the economic level of a country or region [1]. Especially the introduction and application of new related innovative technologies, which began to introduce more new mechanical theories into the development of mechanical design industry and bring a very important impetus to the development and progress of these industries, the continuous improvement of mechanical design theory and the development of technology make more mechanical products begin to be constantly designed, and the related design concept is constantly optimized, and the product performance is higher [2]. The related theory and design scheme of product design is one of the important production links in the design of mechanical products. Under the application of new design concepts and technologies, the design of today's mechanical products is more efficient and unified, which is more suitable for the needs of various mechanical facilities [3]. Multi-link mechanism of mechanical press which is designed by machinery in the modern times is a design concept with more design technology and first opportunity, which has the important development significance for the development of many industries.

The multi-link mechanism of mechanical presses can effectively promote the use of other industries and products because it has practical and more advanced technology, and its performance is better for other related equipment [4]. In many industries, the mechanical press multi-linkage mechanism has been gradually quoted. In particular, in the design of related products for motion simulation, mechanical press multi-linkage mechanism with more consideration for the application of disabled crowd simulation sports equipment can be further applied to assistive devices in disabled persons through the related products designed by this technology [5]. Many research scholars believe that because it can better simulate the movement of the normal population, this kind of sports equipment with simulation performance makes the design mode of the simulation sports equipment more rational and scientific, and further provides some technical support for further efficient use of related products, provides theoretical basis for the design and improvement of more related products [6].

3. Methodology

In today's era, with the continuous development of mechanical technology, the introduction of more and more new science and technologies has made many enterprises gradually pursue more precise related parts and accessories [7]. As the development of various industries makes a larger number of mechanical products parts began to be gradually demand, this trend has further promoted the development of machinery industry, making its industry-related technology and theoretical standards continue to enhance and improve, as a result, the economic strength of the present world is further enhanced (Fig. 1).

Since entering the new century, the continuous improvement and progress of economic level in China have made the comprehensive national strength of the country greatly improved and developed. Especially since the reform and opening to the outside world, the state has further introduced advanced technology from western developed countries. With the continuous improvement of comprehensive economic strength in China and the gradual increase of communication with the outside world, China's related products and technologies are gradually extended to other countries [8]. In this trend, China's various industries have a great degree of development. As an important pillar industry in China, the machinery manufacturing industry can provide some spare parts and assembly process for more industry development, so as to gradually increase its importance, further promote the further research and discussion of China's related theory and technology for the industry [9]. In the current era, more advanced technology has gathered the mechanical manufacturing technology, which has made great progress in the manufacture of machinery in our country, and has made great achievements. Since the new century, with the increasing importance of the industry in China, the machinery manufacturing industry has been further promoted and progressed. At the same time, the research on the theory and technology of the industry is more systematic and scientific. The degree of organic combination of production has gradually improved. However, the relevant technology and theory have been greatly improved. At the same time, some uncoordinated phenomenon is further exposed. It can be seen from the generalization of the times, although our country already has a lot of mechanical multi-linkage mechanism related technologies in the current era, many enterprises have continued the application of the traditional mechanical multi-link technology, and the application of the multi-link technology of the mechanical press is less. Even in many industries, the multi-link technology of mechanical press, which has a great advantage, has been gradually applied to the actual industrial development, due to the lack of understanding and cognition of relative theoretical knowledge of the technology, the algorithm of analysis is more using vector algebra or matrix method. These more backward analytical algorithms do not provide an accurate analysis of the relevant model, and further provide a degree of distress for subsequent mechanical programming and theoretical optimization [10]. These algorithms make the workload and work more difficult, which further limits their usefulness. The controllability of the design program is gradually reduced, so it cannot better meet the actual needs. In many enterprises, because the operation of the technology is more complex, the op-

erator is not proficient in the relevant technology, and the man-machine interaction cannot be more coordinated, so that the use and operation of multi-link mechanism of mechanical press in our country is still relatively backward. In view of this series of uncoordinated phenomena, the relevant theories and techniques of this technology need to be constantly optimized. It is of great importance to put forward relevant proposals which are more suitable for the operation of this technology. Especially in view of its complex operation and operation principle, it is an important trend for the development of this technology to optimize its related structure and optimize its related process [11]. The input and modification of the parameters of the visual working mechanism are difficult, and the man-machine interaction is poor. In view of this situation, this study mainly used the mechanical press multi-link mechanism as the object of study, and further analyzed and discussed the mathematical expressions of the relevant data indexes in the operation of this kind of running mechanism through reading the relevant data. On this basis, through the reference to relevant optimization methods, in this paper, a new multi-link press technology which is more suitable for the development of industry and field in modern times was further determined [12]. Finally, the relevant actual cases were introduced to analyze the obtained results to prove the accuracy of the research and conclusions. In our country, the related theory and technology of mechanical multi bar linkage technology is imperfect, and this study is mainly to further analyze its related characteristics. The purpose of this study is to provide theoretical basis for the development of related technologies in China and to provide some reference for the continuous improvement and promotion of the comprehensive strength and related theories of related industries in China, so as to provide scientific support for the development of China's comprehensive economic level.

Fig. 1. Development of China's machinery industry

The four-block single-drive mechanical mechanism design was taken as an exam-

ple. The design of the multi-link mechanism of the mechanical press and the related design scheme of the motion simulation were studied. Firstly, the relevant design scheme of the mechanical design was summarized and analyzed. The main design options included the choice of movement mode and drive mode. The summary results are shown in Table 1.

Table 1. Analysis of the design scheme of four legged single drive mechanical horse mechanism

Design level	Relevant requirements
Movement mode	1. Deduce kinematic equations conveniently
	2. With a certain strength and load capacity
	3. The control is simple, and the structure is easy to process
Drive mode	1. Motor drive
	2. Hydraulic drive
	3. Air pressure drive
Shape design	1. Long 879 mm
	2. Width 208 mm
	3. High 720 mm

Then, the simulation of the mechanical design was designed. The relevant model formula is shown below. After optimizing the machine, the mechanical design before and after optimization was analyzed and compared.

$$\theta_1 = 180 - \arccos \frac{OF^2+OA^2-2OF\cdot OA\cdot\cos\angle FOA+EA^2-EA^2}{2\cdot EA\cdot\sqrt{OF^2+OA^2-2\cdot OF\cdot OA\cdot\cos\angle FOA}}+ \\ + \arcsin\left[\frac{OF}{FA}\sin\angle FOA\right] - \angle EAB\,. \tag{1}$$

Here, OF and OA, respectively, represent the mechanical arm and link length; ∠ FOA represents the included angle formed by the mechanical arm movement, and EA represents the length error between different lengths of mechanical arm.

4. Result analysis and discussion

The related concepts and technologies of mechanical press multi-link are not relatively new concepts and techniques, which have been applied in our country for several decades, and have already entered our country's market emergency system construction earlier (Fig. 2). China's first research and description of related technologies and theories date back to the last century [13]. In 1950, in China, the company began to refer the related technology to its manufacturing industry, and formed the higher production efficiency through its slow drawing speed and faster formation of equal characteristics. Nowadays, the multi-link mechanism of mechanical pressure has gradually replaced the traditional mechanical technology, thus gradually becoming one of the important development directions of the machinery manufacturing industry in our country.

Fig. 2. Development of multi-link for mechanical presses

Compared with the traditional principle of mechanical manufacturing, multi-link mechanical pressure applied in our country has made great improvement and progress, through the analysis and generalization of the relevant data, and the main advantages of this are the performance level, the design cost, the drawing speed, the depth of drawing, the drawing and the mold productivity. The results are shown in Table 2. Through the analysis of its main characteristics, the theory of the technology can be further improved and provide a theoretical basis for the better application of it in practical production and life [14]. From the analysis results, it can be seen that for the mechanical press, the multi-linkage mechanism has a great improvement in comparison with the traditional press. The introduction of this kind of pressure mechanism can further provide some technical support for the development and development of the related machinery and equipment in the development industry, so that the mechanical manufacturing can effectively reduce the waste of related materials which may be caused in the related product manufacturing process, and further improve the efficiency and speed of the machinery manufacturing, effectively increase the quality and production of the products, and further apply the products for later products, provide some technical support and scientific basis for the application of late-related products, which in theory proves that the new mechanical manufacturing technology can meet the application and development of other industries [15].

Then, through the analysis of the shortage of mechanical pressure multi-link technology in China, the general results were obtained, as shown in Fig. 3.

In this study, the mechanical horse products designed by an industry in China were analyzed and taken as examples. The relevant information was read and summarized, and the friction between its components was ignored without considering the weight of the various parts of the mechanical horse itself. The maximum displacement of the relevant parts in a certain direction was taken as the function target, the

parameters of the whole mechanical parts were analyzed, and the structural parameters of each component were further optimized. The optimization results of each parameter are shown in Table 3. Through the simulation of the relevant parameters of the mechanical horse products, then all the bars were simulated and calculated. In the case of the Loc_Y value, the value of Loc_Y was taken as the maximum value of –198 mm and the minimum value of –215 mm.

Table 2. Analysis of the advantages of multi-link mechanism of mechanical presses

Analysis level	Traditional presses	Multi-link presses
Structural level	The contact speed of the sliding block is fast, the possibility of tearing material is increased, the noise and vibration are larger, and the heat inside the mould is stronger, and the die life is short.	The contact speed of the sliding block is slow, the possibility of tearing the material is reduced, the noise and vibration are reduced, and the heat inside the die is reduced, and the service life of the die is prolonged.
Design cost	Higher.	Due to the change of the drive part, the other parts are still standard designs, and the motion curve can be modified according to the requirements of the work piece, thus reducing the cost.
Deep drawing speed	Deep drawing speed is relatively high and uneven; the space velocity is relatively slow, the production efficiency is low.	The drawing speed is relatively low and uniform; the space velocity is faster and the production efficiency is higher.
Drawing depth	70 mm	320 mm
	The crank radius and the crank torque are larger, so that the press structure is relatively loose, the overall size increases, and the weight of the machine is increased.	Crank radius and crank torque is small, so that the press structure is compact, the overall size is reduced, thus reducing the weight of the machine.
Drawing forming	Relatively low strength steel	High strength steel
Mold productivity	Relatively low	Higher

Then, based on the optimization value, the parametric analysis of the optimization point and coordinate direction of all the indexes of the mechanical horse product was further carried out, and the sensitivity of all the parameters was analyzed. The results are shown in Table 4. As can be seen from the results that through the analysis of the sensitivity, the values of DV_10, DV_11 and DV_12 were large, which indicated that these three indexes had great influence on the design of me-

chanical horses. Therefore, in the design of the mechanical horse products, these three indicators need to be more attention to effectively improve the quality of the product.

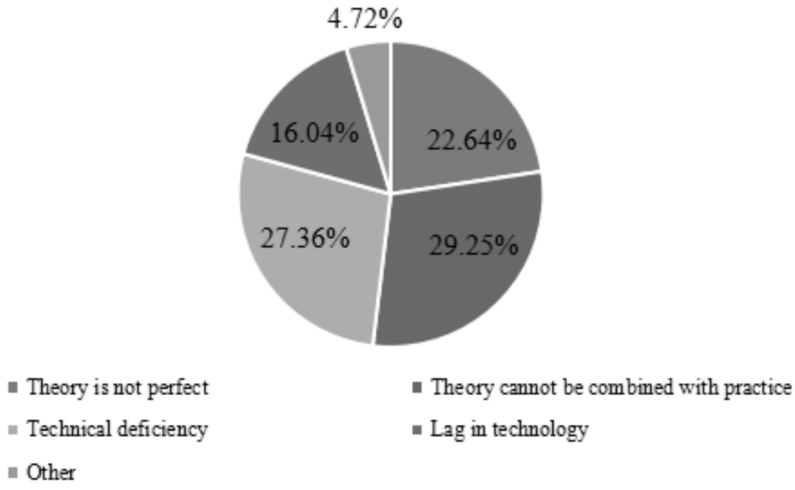

Fig. 3. The shortage and defect of multi-link technology of mechanical press in our country

Table 3. Analysis of the advantages of multi-link mechanism of mechanical presses

	Loc_X	Loc_Y	Loc_Z
POINT_B	(DV_1)	(DV_2)	200.0
POINT_C	(DV_3)	(DV_4)	200.0
POINT_D	(DV_5)	(DV_6)	200.0
POINT_E	(DV_7)	(DV_8)	200.0
POINT_F	(DV_9)	(DV_10)	200.0
POINT_H	(DV_11)	(DV_12)	200.0

Through the analysis of the sensitivity, the relevant important indexes were determined, and the indexes were optimized. The optimization results are shown in Table 5 and Fig. 4. Through optimization, it is found that the relevant indicators have better stability, and other related characteristics have also been greatly developed and improved.

5. Conclusion

With the development of the world economy, many technologies have been developed and improved to a great extent. Under the trend of this world, China's economy and various industries have developed and improved to a great extent.

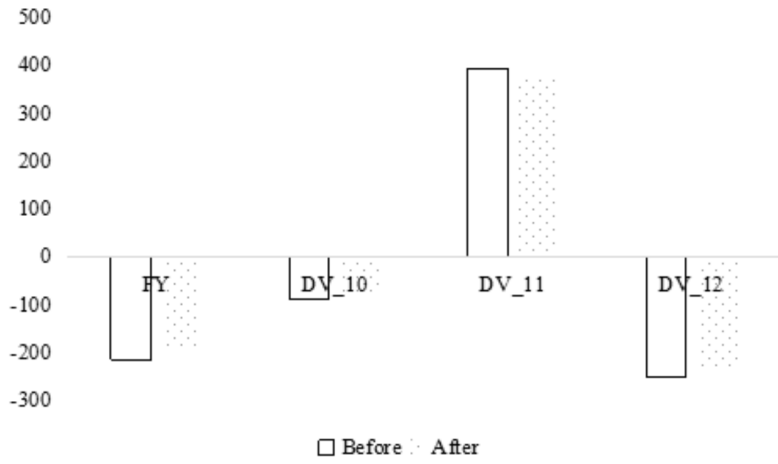

Fig. 4. A comparative analysis of the results of the optimization of the indicators

The development of these industries also provides a certain impetus and positive impact for the promotion of China's overall economic strength. Especially as an important pillar industry in China, the development of machinery design industry is of great significance to the promotion of China's comprehensive strength.

In today's era, as a new mechanical design method, the multi-link mechanism of mechanical press provides more important influence for the development of machinery industry. However, the relative theories and techniques of this kind of technology in our country are still relatively weak.

Table 4. Maximum displacement sensitivity of the optimum design variables of the D point at the end of the leg mechanism in the Y direction

Design variable	Optimization point	Coordinate direction	FY sensitivity
DV_1	POINT_B	X	1.0
DV_2	POINT_B	Y	1.0
DV_3	POINT_C	X	–1.2
DV_4	POINT_C	Y	–1.1
DV_5	POINT_D	X	–0.5
DV_6	POINT_D	Y	0.6
DV_7	POINT_E	X	0.6
DV_8	POINT_E	Y	–0.2
DV_9	POINT_F	X	0.8
DV_10	POINT_F	Y	–3.5
DV_11	POINT_H	X	–3.9
DV_12	POINT_H	Y	–3.6

Table 5. Comparative analysis of each indicator optimization

	FY	DV_10	DV_11	DV_12
Before optimization	–215	–89.7	393	–253
After optimization	–189	–85.3	374	–228

In view of this deficiency, the related concepts of multi-link mechanism of mechanical press were summarized. The multi-link presses were analyzed and compared with traditional presses, and their advantages were found. Mechanical horse was taken as an example, the related results were analyzed, the sensitivity of all of its indicators was analyzed and the main indicators were optimized based on the sensitivity. The results proved that the optimized index is more stable. The research aims to provide some theoretical basis and scientific support for the development of China's machinery construction industry. Because the technology has a wide range of application, the research is only on one side are discussed, and research has certain limitation, but still can be used as a reference for related research.

References

[1] G. U. Feng, O. W. Gao: *Design of a servo mechanical press with redundant actuation.* Chinese Journal of Mechanical Engineering *22* (2009), No. 4, 574–579.

[2] L. Jian, W. Jianxin, Y. Wenqi, Y. Baolin: *Optimization design of the six-link transmission mechanism used in mechanical press.* CFHI Technology (2011), No. 1, 7–10.

[3] J. Yao, W. Zhou, W. Guo: *Modular analysis of kinematics performances for multi-link mechanical presses.* Forging & Stamping Technology (2008), No. 6, 28.

[4] J. Yu, Y. Hu, R. Fan, L. Wang, J. Huo: *Mechanical design and motion control of a biomimetic robotic dolphin.* Advanced Robotics *21* (2007), Nos. 3–4, 499–513.

[5] H. Li, Y. Zhang: *Seven-bar mechanical press with hybrid-driven mechanism for deep drawing; Part 1: kinematics analysis and optimum design.* Journal of Mechanical Science and Technology *24* (2010), No. 11, 2153–2160.

[6] G. Figliolini, M. Ceccarelli: *A novel articulated mechanism mimicking the motion of index fingers.* Robotica *20* (2002), No. 1, 13–22.

[7] S. Qingyu, L. Jian, Y. Wenqi: *Mechanical press six-link mechanism design based on multi-objective.* Transactions of the Chinese Society for Agricultural Machinery *43* (2012), No. 4, 225–229.

[8] C. Alexandru: *The kinematic optimization of the multi-link suspension mechanisms used for the rear axle of the motor vehicles.* Proceedings of the Romanian Academy-Series A *10* (2009), No. 3, 244–253.

[9] S. K. Dwivedy, P. Eberhard: *Dynamic analysis of flexible manipulators, a literature review.* Mechanism and Machine Theory *41* (2006), No. 7, 749–777.

[10] N. Lobontiu: *Distributed-parameter dynamic model and optimized design of a four-link pendulum with flexure hinges.* Mechanism and Machine Theory *36* (2001), No. 5, 653–669.

[11] P. Yu-hai: *Analysis on the motion characteristics of drawing press working mechanism based on the virtual prototype.* Machinery Design & Manufacture (2013), No. 3, 211–213.

[12] Q. Zhang, H. Zhou, Y. Tian: *Kinematic simulation and trajectory optimization for the enclosed five-bar feeding mechanism of sewing machine.* Machine Design and Research *22* (2004), No. 6.

[13] J. Knapczyk, M. Maniowski: *Optimization of 5-rod car suspension for elastokinematic and dynamic characteristics.* Archive of Mechanical Engineering *57* (2010), No. 2, 133–147.

[14] N. Schvalb, B. B. Moshe, O. Medina: *A real-time motion planning algorithm for a hyper-redundant set of mechanisms.* Robotica *31* (2013), No. 8, 1327–1335.

[15] C. Zhou, Z. Cao, S Wang, M. Tan: *A marsupial robotic fish team: Design, motion and cooperation.* China Technological Sciences *53* (2010), No. 11, 2896–2904.

Received June 6, 2017

Acta Technica *62* No. 1A/2017, 471–482

Layered space-time coding (LSTC) technology and its application in mobile communication systems[1]

Lijun Han[2]

Abstract. With the increasing demand for wireless mobile communications and increasing number of users, wireless communication services have also been increased from the original language services to the multimedia services, but the characteristics of communications have restricted its development. In order to improve the efficiency and quality of its communication, the research on the layered space-time coding technology and its application in mobile communication systems were proposed in this dissertation. Through the construction and simulation application of layered space-time coding, it can be seen that the layered space-time coding can reduce the number of error bits in the system and increase the diversity and coding gain of the system, moreover, the amplitude of the gain increases accordingly with the increase of the number of transmitting and receiving antennas. Therefore, layered space-time coding technology can effectively improve the utilization of communications and quality of services in mobile communication systems.

Key words. Layered space-time, coding technology, mobile communication system, technology research.

1. Introduction

With the continuous progress of human society and the continuous development of science and technology, modern communication technology has very obvious individual characteristics, and mobile communication can adapt to and meet the needs of modern communications, which is one of the fastest growing technologies in the world. The continuous development of mobile communication technology is to realize the purpose that people can communicate with any person at any place and any time [1]. With the advent of the information age, information transmission is becoming more and more important in various communication technologies, and

[1]The study was supported by research fund for civil-military integration in Shaanxi province (17JMR27); Project of Shaanxi province education department (16JK1280); Weinan normal university characteristic discipline construction project: photoelectric detection and Qin dong industry (14TCXK06); Natural science research project of Weinan Teachers University (17YKS05)

[2]School of Mathematics and Physics, Wei Nan Normal University, Wei Nan, China

it is also the support technology of other technologies. Therefore, the demand for information technology in various countries is getting higher and higher, and more efforts are devoted to the development of modern communication technologies and the construction of modern comprehensive communication networks.

But in mobile communication technologies, the channel has very complex characteristics, and it needs to be transmitted by multiple functions in the process of information expositions; in addition, there are many fading phenomena in the process of transmissions, which seriously affect the performance of mobile communications [2]. With the popularization and promotion of the information technology, the users of mobile technology continue to increase. The communication service has developed from the simple voice service to the multimedia communication service, which makes the communication spectrum resources become tense. Therefore, how to improve the utilization rate of spectrum resources and reduce the degree of declines under the influence of various factors has become a hot spot and focus of researches, and it has also promoted the continuous development of communication technologies [3].

2. State of the art

In the long history of communication technology, if the history of the improvement of frequency usage is the phylogeny of wireless communication, the history of the improvement of frequency utilization and the expansion of the number of users is the phylogeny of mobile communication. This development process not only meets the increasing demand, but also improves the density of global mobile communications and the efficiency of frequency utilizations [4]. The history of mobile communication can be divided into three stages. The first stage was marked by the emergence of the first analog cellular mobile phone, which was represented by the analog and frequency division multiple access cellular system technology in northern Europe, the United States and the United kingdom. However, it has the disadvantages of small capacity, the single service and the poor security, etc., and it is not consistent with the rapid development of mobile communication businesses [5]. Therefore, in order to get better development, communication technology entered the second generation of digital mobile devices, and capacity and function were improved through the digital technology. However, the second generation digital mobile communication technology is divided into European system and North American system, and the implementation technologies of the two systems are different and incompatible with each other. Although it has multi-mode and multi-frequency terminal products, it still cannot achieve the purpose of communications at any time and place and with any person [6]. In 1985, the third generation digital mobile communication concept was proposed by ITU, the earliest name was the future public land mobile communication system, then its name was changed into the international mobile communication system IMT-2000, because the system was commercially available and the frequency band was 2000 MHz [7]. The goal of the third generation mobile communications is to achieve seamless coverage, connectivity and roaming in all areas of the world with a unified frequency band, thereby improving the quality of services and the security performance of mobile communications and providing

users with multimedia business services, so that the terminal mobile phone structure is simpler and more convenient to carry, its price is more affordable, and the adaptability is stronger [8]. This undoubtedly can solve the problems of the first and second generation mobile communication systems, however, the core network of the third generation mobile communication is still based on the core network structure of the second generation mobile communication system, therefore, the third generation mobile communication system is considered to be a transitional stage [9]. In the following research, the focus of researches is to improve the communication quality and speed of data transmissions.

3. Methodology

Multipath propagation and frequency selective fading are typical characteristics of wireless transmissions, which will be seriously disturbed in the process of data transmissions, resulting in overall performance degradations [10]. In the past solutions, the main focus is on the elimination of multipath propagation factors, and the effect is limited. Diversity technology is the most effective way to improve the multipath effect, and its primary function is to provide a copy of the signal in some forms, while for the receiving end, multiple independent or highly unrelated paths carry out the transmission of the same signal and merge according to a specific method, so that the probability of judgment error is greatly reduced [11]. In this process, diversity has two implications for decentralized transmission and centralized processing. The most important condition in decentralized transmission is the correlation, which mainly depends on the channel condition during transmissions. The main implementation of centralized processing is to design signal processing at both ends of transceivers [12]. In diversity technology, there are different technical classifications through different classification standards. Table 1 shows the technical classification of diversity techniques.

As shown in Table 1, time diversity and frequency diversity are the symbols which carry the information are sent repeatedly through different time slots. In this case, the spacing of the adjacent two slots is greater than the correlation time$\Delta t$of the channel. Or the interleaving is carried out by using error correcting coding, so that the signal will introduce redundancy in the time domain to achieve time diversity [13]. If the signal is transmitted in a multi-carrier manner, the spacing between the two carriers which are adjacent is greater than the related bandwidth Δf of channel. Therefore, it can be seen from the above that time diversity and frequency diversity can improve the performance of the whole communication system on the basis of the reduction of frequency utilizations. Spatial diversity can be achieved by the simultaneous use of multiple transmitting antennas and multiple receiving antennas without decreasing the frequency [14]. The main principle is that multiple antennas are placed at one or two terminals of the transmitter and receiver, and the distance between each antenna is far enough. Typically, it is 10 times of the carrier wavelength. In this case, antennas are unrelated, so that the multiple independent communication channels between the receiver and transmitter can be built. What can be seen from above is that the spatial diversity does not introduce redundancy

in the time domain, and it does not introduce redundancy in the frequency domain during the process of diversity, so that the utilization rate of the frequency is not reduced, and the transmission is improved.

Table 1. Technical classification of diversity techniques

Diversity classification and standard	Diversity type			
Diversity purpose	Macro diversity is achieved through level design of systems, such as power control, so as to achieve long-term anti-decline purposes			
	Micro diversity is a technique that can resist short-term fading and cover a large number of signal processing			
Signal transmission mode	Explicit diversity, for example, delaying the diversity schemes			
	Implicit diversity, such as the coded interleaving schemes			
The form of obtaining multiple signals	Time diversity	It uses the channel time selectivity, and the main forms are the channel coding, interleaving and ARQ retransmission, which has better fast fading times		
	Frequency diversity	The frequency selectivity of the channel is mainly achieved by merging different multipath delay components on the same signal, such as equalization, frequency hopping and Rake reception (DS-CDMA). But the diversity gain is limited in non-frequency selective channels		
	Space diversity	Space angle diversity	Smart antenna	
		Polarization diversity	Vertical and horizontal polarization (single antenna implementation	
		Space position diversity	Receiving diversity	Selective diversity (Max, SNR) and handoff diversity
				Linear combination diversity (MMSE, MRC)
			Transmitting diversity	Feedback mode (weighted emission in TDD system)
				Feed-forward and training method (space-time / combination of frequency coding and optimal reception of channel estimations)
				Blind schemes (combining channel coding with phase sweeping and frequency offset, and it requires extended bandwidth)

Space coding techniques in space diversity can be divided into trellis space-time codes, packet space-time codes and layered space-time code coding techniques. Layered space-time code (LST) can solve the problems existing in the wireless channel through the propagation of wireless channel, so that it can be used in more abundant propagation path environments [15]. The system in layered space-time codes does not process fading at the beginning of the signal, but it considers them as different sub channels in different propagation paths, so that they can transmit information in parallel. At the same time, the multiplicative interference and the signal interference are eliminated by the linear decision feedback equalizer at the receiving end of the information through the fading characteristics of different channels. This is an effective solution to high-speed data transmission of wireless communications, which has a broad application prospect.

In the process of layered space-time coding for mobile communications, the encoding process is simple, and coding error correction is also required. In order to keep the efficiency of information transmission, encoding is adopted to reduce the bit error rate by means of encoding and decoding, which requires the decoder to be relatively simple and friendly. Although the layered space-time codes have great advantages in bandwidth utilizations, the characteristic matrix in the acceptance process of signals will depend on the channel, thus resulting in adverse effects on the performance of the system, reducing the performance of the system, and limiting its future development. Layered space-time decoding has two kinds of maximum likelihood decoding and zero forcing detection and decoding. Considering the characteristics of the two kinds of decoding, the maximum likelihood decoding is chosen to be studied and analyzed.

According to the error correcting decoding theory, the channel coding input sequence can be set as M, and the output sequence of a channel encoder that is the input sequence of the channel can be set as C. At the same time, the input of the channel decoder that is the output sequence of the channel is R, the output sequence of the channel decoder is $\hat{M}$, and the interference sequence is E. In the process of decoding, the decoder will generate an estimation sequence $\hat{C}$ that is related to C base on R, and when $\hat{C} = C$ and $\hat{M} = M$, the decoding of the decoder is correct. When the given receive sequence is R, the error probability of the conditional decoding of the decoder is defined as the formula

$$P\left(E\left|R\right.\right) = P\left(\hat{C} \neq C\left|R\right.\right). \tag{1}$$

The error probability of the decoder can be obtained by formula (1), as shown in the equation

$$P_E = \sum_R P\left(E\left|R\right.\right) P\left(R\right). \tag{2}$$

In the formula, the $P\left(R\right)$ is the probability of acceptance of R, and it is independent of the decoding mode, thus, the decoding error probability is minimized by

the best decoding laws, as shown in two following formulae

$$\min P_E = \min_R P\left(E\left|R\right.\right) = \min_R P\left(\hat{C} \neq C\left|R\right.\right), \tag{3}$$

$$\min_R P\left(\hat{C} \neq C\left|R\right.\right) \Rightarrow \max P\left(\hat{C} = C\left|R\right.\right). \tag{4}$$

What can be seen from the formula is that the input R needs to choose the maximum code word C_i though the decoder in 2^k code words, so that which can be used as the estimation sequence $\hat{C}$ of C in $P\left(\underset{\mathrm{i}}{\hat{C}} = C\left|R\right.\right)$, and $i = 1, 2, ..., 2^k$. Then it is in accordance with the Bayes formula, as shown in the formula

$$P\left(C_r\left|R\right.\right) = \frac{P\left(C_i\right)P\left(R\left|C_i\right.\right)}{P\left(R\right)}. \tag{5}$$

It can be found that if the probability $P\left(C_i\right)$ of the information transmitting terminal for the firing of each code word is the same, and $P\left(R\right)$ has nothing to do with the way of decoding, then

$$\max_{i=1,2,\ldots,2^{\mathrm{k}}} P\left(C_i\left|R\right.\right) \Rightarrow \max_{i=1,2,\ldots,2^{\mathrm{k}}} P\left(R\left|C_i\right.\right). \tag{6}$$

Thus, if the decoding rules in a decoder can select one which can make the formula (6) become the largest in the 2^k code words, the decoding rule is the maximum likelihood decoding, and $P\left(R\left|C\right.\right)$ is the likelihood function. Because there is a monotonic relation between $\log_b x$ and x, the following formula is derived:

$$\max_{i=1,2,\ldots,2^{\mathrm{k}}} P\left(C_i\left|R\right.\right) \Rightarrow \max_{i=1,2,\ldots,2^{\mathrm{k}}} \log_b P\left(R\left|C_i\right.\right). \tag{7}$$

In the formula, $\log_b P\left(R\left|C_i\right.\right)$ is the log-likelihood function.

As shown in the following equation, the logarithmic relief ratio of the layered code information bits is:

$$\Lambda\left(b\right) = \log \frac{\sum_{b=1} \prod_{j=1}^{N} \exp\left(-\frac{r_j - \sum_{j=1}^{N_j} \alpha_{i,j} c_i^2}{N_0}\right)}{\sum_{h=1} \prod_{j=1}^{N} \exp\left(-\frac{\left|r_j - \sum_{j=1}^{N_j} \alpha_{i,j} c_i\right|^2}{N_0}\right)}. \tag{8}$$

In the formula, r_j is the information received by the jth antenna, c_i is the signal transmitted by the ith antenna, and $\alpha_{i,j}$ is the channel characteristic factor that is transmitted by the ith antenna and received by the jth antenna.

If C and E are used to represent two different code word matrices, C is the code word matrix to be transmitted, and $\mathrm{prob}\left(C \to E\right)$ represents the 2-2 average error probability between the two matrices. As a result, in a fast fading environment, the

upper limit of prob $(C \to E)$ is shown in the formula

$$\text{prob}\,(C \to E) \le \prod_{r=1}^{l} \left(1 + |c_\tau - e_\tau|^2 \frac{E}{4N_0}\right)^{-m}. \tag{9}$$

In a slow fading environment, the upper limit of prob $(C \to E)$ is shown in the formula

$$\text{prob}\,(C \to E) \le \prod_{r=1}^{\max(C-E)} \left(1 + \Lambda_k \frac{E}{4N_0}\right)^{-m}. \tag{10}$$

Among them, Λ_k is the eigenvalue of the matrix $(C-E)(C-E)^+$.

4. Result analysis and discussion

In this paper, the layered space-time coding technology and its application in mobile communication system were studied. Therefore, simulation experiments were carried out for the proposed hierarchical space-time coding formula model. The performance of layered space-time coding was analyzed and studied by transmitting and receiving signals through wireless communication systems. The following parameters were selected according to the actual radio information transmission:

Firstly, the channel environment was a slow fading channel; value was QPSK modulation; the number of antennas was equal to that of the receiving antenna and the transmitting antenna, namely, $N = M = 2 \text{or} N = M = 4$; error correction codes were 8-status Turbo codes or non-codes, and the polynomial produces by Turbo codes was: $g_0(D) = 1 + D^2 + D^3$ and $g_1(D) = 1 + D + D^3$. According to the layered space-time coding process and the simplified calculation process, the contrast of the bit error rate was obtained, as shown in Figs. 1 and 2. What can be seen from Figs. 1 and 2 is that when the number of antennas was 2, the maximum likelihood algorithm did not make a significant improvement on the overall performance of the system for the non-coding system; when the number of antennas was 4, the maximum likelihood algorithm didn't significantly improve the frame error rate for the non-coding system, but the bit error rate of the system was improved, and it was obviously decreased. This means that the number of error bits that may occur in each frame is decreasing, and it can help to improve the overall performance of the system.

As shown in Figs. 3 and 4, the performance of the maximum likelihood algorithm and the ZF detection algorithm were compared. The two algorithms were in the 8-status Turbo code environment. Figure 3 shows the comparison of the frame error rates of the two algorithms, and Fig. 4 shows a comparison of the bit error rates. As can be seen from the comparison in Fig. 3, the frame error rate of the Turbo code concatenation was 10^{-2}. When the number of transmitting and receiving antennas was 4, the maximum likelihood algorithm obtained gains and the gain amplitudes were in the range of 9-12 dB. When the number of antennas received was 2, the maximum likelihood algorithm gains were about 2 dB. What can be seen from Fig. 3

is that the algorithm's advantages were not obvious, but the advantages shown in Fig. 4 were obvious. On the one hand, the algorithm improved the error propagation caused by decoding layer by layer to a certain extent, and reduced the number of error bits in the system; on the other hand, the number of error bits of per frame was more likely to be used by level connections of the system.

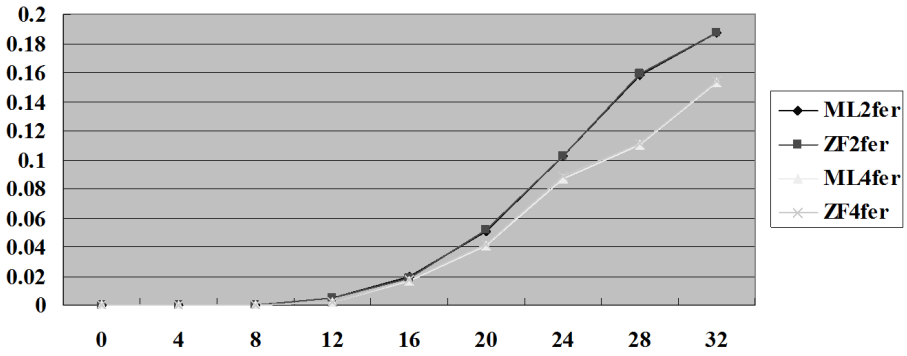

Fig. 1. Comparison of bit error rates of ML and ZF without encoding the system

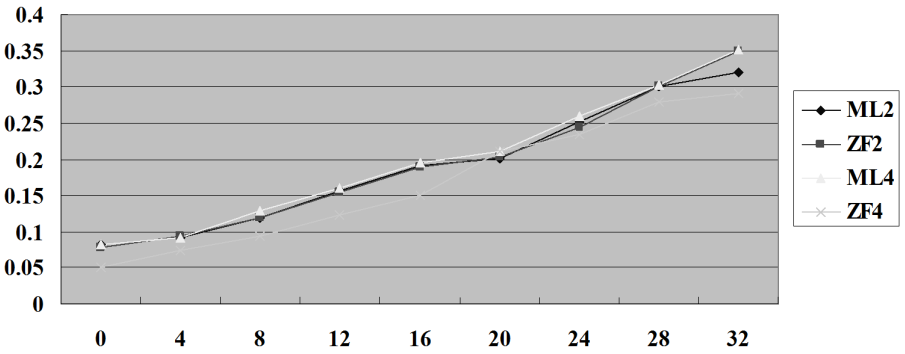

Fig. 2. Comparison of the performance of the non-coding system ML and ZF

Then, the performance of the system was compared when the number of transmitting and receiving antennas was 2 and 4 respectively. When the maximum likelihood algorithm was used, the diversity gain and coding gain obtained by the system whose number of transmitting and receiving antennas was 4 were larger than that of the system whose number of transmitting and receiving antennas was 2. As for the ZF algorithm, when the number of transmitting and receiving antennas was 2, the performance of the system was better than that of the system whose number of transmitting and receiving antennas was 4. The reason is that the performance of ZF algorithm is more dependent on the detection accuracy of the upper layer, so when the antenna number increases, it will likely reduce the accuracy, thus resulting in the gain loss of the diversity and encoding of the system. As far as the maximum likelihood algorithm is concerned, the algorithm is different from the ZF algorithm.

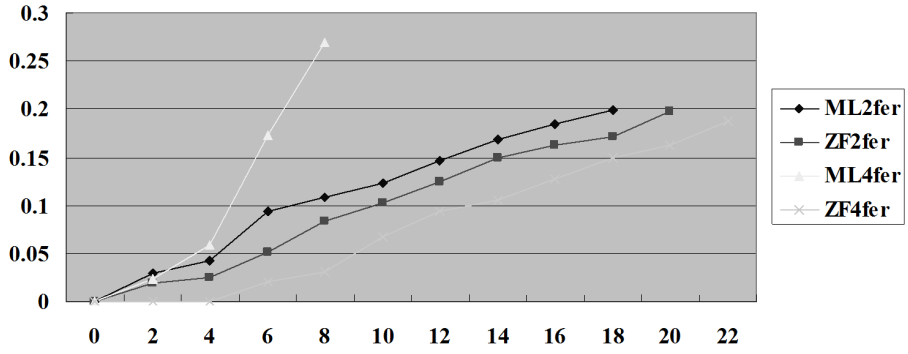

Fig. 3. Comparison of bit error rates of coded systems ML and ZF

Although the probability of error propagation also presents, the algorithm considers the influence of the channel characteristic matrix and noise in equilibrium, so as to improve error propagations, and when the number of transmitting and receiving antennas increases, the gain is more pronounced.

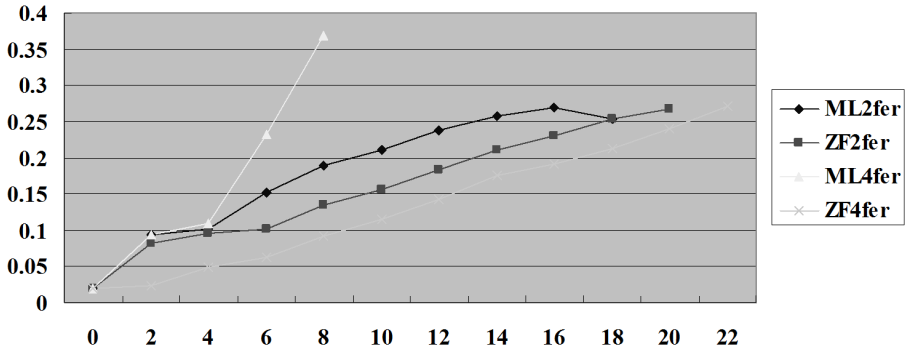

Fig. 4. Comparison of performances of coding systems ML and ZF

To sum up, layered space-time coding can effectively improve the performance of the system by using the channel propagation characteristics, reduce the number of error bits in each channel and improve the diversity and coding gain of the system, thus achieving the probability of error propagations of the system. Although the maximum likelihood algorithm studied in this paper can improve the performance of the system, it has high complexity, and it is difficult to calculate and operate, so it needs further improvements and researches.

5. Conclusion

With the continuous progress of human society, the demand for mobile communications is higher and higher, so as to meet the communication needs of individuals.

At the same time, the users of mobile communications develop rapidly, and the services have been increased from the original language services to the multimedia services. How to improve the efficiency and service quality of mobile communications has become the focus of future development. Therefore, research on the layered space-time coding technology and its application in mobile communication systems were proposed in this thesis. The layered space-time coding, decoding and other modules were built, and the wireless communication features were used to improve the efficiency and quality of communications. Compared with other diversity techniques, the simulation results show that layered space-time coding technology can be hierarchically constructed without reducing the efficiency of frequency usage. Furthermore, the maximum likelihood algorithm can reduce the number of error bits and increase the diversity and coding gain by using the characteristics of wireless communications. And the more the number of transmitting and receiving antennas is, the greater the amplitude of the gain is, and the better the performance of the system is. However, the layered space-time coding model constructed in this paper still has deficiencies, and it has a high degree of fickleness, which will cause some restrictions on its future development, so it needs further improvements and researches.

References

[1] S. A. Sattarzadeh, A. Olfat: *Bounds on the throughput performance of PU2RC and its application in mode switching.* IEEE Transactions on Vehicular Technology *61* (2012), No. 2, 876–882.

[2] S. Bhunia, I. S. Misra, S. K. Sanyal, A. Kundu: *Performance study of mobile WiMAX network with changing scenarios under different modulation and coding.* International Journal of Communication Systems *24* (2011), No. 8, 1087–1104.

[3] J. Chen, X. Z. Ke, N. Zhang, N. Lu: *Adaptive multi-layer space-time coding in FSO-MIMO.* Laser Technology *37* (2013), No. 2, 158–164.

[4] A. Alexiou, M. Haardt: *Smart antenna technologies for future wireless systems: Trends and challenges.* IEEE Communications Magazine *42* (2004), No. 9, 90–97.

[5] A. Nosratinia, T. E. Hunter, A. Hedayat: *Cooperative communication in wireless networks.* IEEE Communications Magazine *42* (2004), No. 10, 74–80.

[6] S. Uehara, E. J. M. Noriega: *Trends in EFL technology and educational coding: A case study of an evaluation application developed on livecode.* JALT CALL Journal *12* (2016), No. 1, 57–78.

[7] L. A. Jones, H. Z. Tan: *Application of psychophysical techniques to haptic research.* IEEE Transactions on Haptics *6* (2013), No. 3, 268–284.

[8] L. K. Bansal, A. Trivedi: *Comparative study of different space-time coding schemes for MC-CDMA systems.* International Journal of Communications Network and System Sciences *3* (2010), No. 4, 418–424.

[9] A. K. Hasan, A. A. Zaidan, R. Salleh, O. Zakaira, B. B. Zaidan, S. M. Mohammed: *Throughput optimization of unplanned wireless mesh networks deployment using partitioning hierarchical cluster (PHC).* Lecture Notes in Engineering and Computer Science *2176* (2009), No. 1, 907–911.

[10] A. Foster, J. Harms, B. Ange, B. Rossen, B. Lok, S. Lind, C. Palladino: *Empathic communication in medical students' interactions with mental health virtual patient scenarios: A descriptive study using the empathic communication coding system.* Austin Journal Psychiatry Behavior Science *1*, (2014), No. 3, paper 1014.

[11] J. Hamodi, R. Thool, K. Salah, A. Alsagaf, Y. Holba: *Performance study of mobile TV over mobile WiMAX considering different modulation and coding techniques*. International Journal of Communications Network and System Sciences *7* (2014), No. 1, 10–21.

[12] D. Gesbert, M. Shafi, D. Shiu, J. P. Smith, A. Naguib: *From theory to practice: An overview of MIMO space-time coded wireless systems*. IEEE Journal on Selected Areas in Communications *21* (2003), No. 3, 281–302.

[13] M. Y. Naderi, H. R. Rabiee, M. Khansari, M. Salehi: *Error control for multimedia communications in wireless sensor networks: A comparative performance analysis*. Ad Hoc Networks *10* (2012), No. 6, 1028–1042.

[14] G. J. Foschini: *Layered space-time architecture for wireless communication in a fading environment when using multi-element antennas*. Bell Labs Technical Journal *1*, (1996), No. 2, 41–59.

[15] L. Gyarmati, T. A. Trinh: *Cooperative strategies of wireless access technologies: A game-theoretic analysis*. Pervasive and Mobile Computing *7* (2011), No. 5, 554–568.

Received June 6, 2017

Acta Technica *62* No. 1A/2017, 483–494

Application of ISP technology in the design of intelligent instruments

Linbin Wu[1], Jian Yang[1,2]

Abstract. Intelligent signal processing (ISP) technology provides very important technical support for the design of intelligent instrument and meter in our country. In order to improve the application effect of ISP technology in the design of intelligent instrument and meter, the research status of ISP technology at home and abroad was firstly introduced, and then the construction and method of DMC and PID control algorithm model were expounded, finally, the data obtained from the model operation was analyzed and the conclusion was drawn. The results show that the DMC control algorithm has high application feasibility, and the application of ISP technology improves the stability of the output value of intelligent instrument. Based on the research results, the effect of algorithm model and technology application was summarized and the direction of improvement was clarified, so that some references were provided for the improvement of application effect of ISP technology.

Key words. ISP technology, intelligent instrument, instrument design.

1. Introduction

In recent years, the development of science and technology in our country is relatively fast. The rapid development of communication technology, network technology and semiconductor technology has brought important technical support for the development and design of intelligent instrument and meter system, and ISP technology has been one of the most important development techniques in system programming.

The emergence of ISP technology is the inevitable result of the development of system programming technology. The development of science and technology has greatly promoted the continuous prosperity of the intelligent equipment industry. Nowadays, all kinds of equipment, instruments and meters have been widely used in industrial production and daily life in the era of intelligent, and how to meet the needs of users for intelligent instruments and meters has become the main goal of the designers of intelligent instruments and meters. From the point of view of design,

[1]Key Laboratory of Earthquake Geodesy, Institute of Seismology, CEA, Wuhan 430071, China
[2]Corresponding author

system programming technology plays a very important role in the whole design process of intelligent instrument and meter. ISP technology is widely used in all kinds of system programming technology, which is mainly related to its unique technical advantages and strong applicability. In addition, ISP technology has played a very important role in the development of digital systems. Therefore, how to further improve the effectiveness of ISP technology in the design of intelligent instrument and meter has become a very important topic to research.

Based on this, the application of ISP technology in the design of intelligent instrument and meter was analyzed and studied by constructing the model of control algorithm.

2. State of the art

Foreign scholars began to study ISP technology earlier, while the research on system programming technology starts late in our country, which is mainly because of the late development of computer network technology in China.

Miao proposed ISP technology originated in the semiconductor business, initially, the application of this technology focused mainly on the design and manufacturing of semiconductor products [1]. Wang believed that the emergence of ISP technology broke the shackles of traditional design technology, and played a revolutionary role in system programming [2]. Susa proposed that the application of ISP technology was simple and did not require more complicated basic equipment and process [3]. Ispled described the design features and intelligent applications of ISP technology, and he believed that this technology could be integrated with other systems in the design of instrumentation so as to achieve better design results [4]. Liu proposed that ISP technology was closely related to fuzzy logic control and artificial neural networks [5]. Ran described the application of ISP technology in intelligent sensor design, and proved the application of this technology in the design of intelligent instrument and meter to a certain extent [6].

The above studies are the introduction and discussion of the origin, development and application of ISP technology, although these studies have a detailed exposition of ISP technology, the research of this technology is too theoretical and lack of examples in the design of intelligent instruments and meters. Therefore, in view of the shortcomings of the existing research, the control algorithm model was proposed, and the application of ISP technology in the design of intelligent instrument and meter was analyzed and studied. In addition, the object of study and the specific content of the control algorithm model was described in the third part of this paper, and the specific data of the control algorithm model and simulation test was obtained and the data results were analyzed in in the fourth part; the last part was about the summary of the paper and the relevant conclusions.

3. Methodology

The application of ISP technology in the design of intelligent instrument and meter was studied mainly by constructing the integrated control algorithm model of intelligent instrument. Most intelligent instruments are integrated control algorithms, such as Schneider Electric's inverter and PLC are integrated with PID control algorithm, so that the usability of the instrument is stronger, and the composition of the control loop is simpler. The design of the intelligent instrument in this paper also integrated two control algorithms: PID algorithm and DMC algorithm.

Limited believed that PID controllers (also known as PID regulators) controlled by the ratio (P), integral (I) and differential (D) in process control are the most widely used automatic controllers [7]. They have the advantages of simple principle, simple realization, wide application scope, independent control parameters and simple selection of parameters. Moreover, it can be proved that PID controller is an optimal control for the typical object of process control - "the first order lag + pure lag" and "the second order lag + pure lag" control object. There are three simple PID control algorithms in the control point, which are incremental algorithm, position algorithm, and differential first. Chinmoy believes that although these three PID algorithms are simple, they have their own characteristics and can basically meet most of the requirements of general control [8].

Table 1 shows the basic control parameters of the PID algorithm. Mohanrao held that algorithm of PID controller design is the most commonly used controller, and the control system is composed of PID controller and controlled object [9]. PID controller is a kind of linear controller, there is difference between the input setting value and the output feedback value constitutes the feedback bias, the better control effect can be obtained by correcting the deviation, and the control law can be deduced according to this basic principle.

Table 1. PID control parameters

Mode	Channel	Set point	Parameter KP	Parameter TI	Parameter TD
0/1/2	0–7	0–100	0–100	0–100	0–100

The construction process of the PID control algorithm model is as follows:

Firstly, the following formula is applied to calculate the control increment parameter.

$$\Delta MV(t) = K_{\mathrm{p}} \left[DV(t) + \frac{1}{T_i} \int DV(t)\,\mathrm{d}t + T_{\mathrm{D}} \frac{\mathrm{d}(DV(t))}{\mathrm{d}t} \right]. \tag{1}$$

Here, t is the sensing time of intelligent instrument, M is the control quantity of algorithm model, V is the data delay, D is a variable coefficient, and $\Delta MV(t)$ is the control increment.

Secondly, the following formula is applied to calculate the control quantity of the control algorithm model, and the time constant and the deviation coefficient are the

main parameters for calculating control quantity and control rate.

$$MV(t) = MV(t) + \Delta MV(t)\,. \tag{2}$$

Thirdly, generally speaking, the controller of intelligent instrument and meter is usually designed by the programming language C. According to this practical situation, the control algorithm parameters obtained by the above operations was needed to be discretized, so as to obtain the specific sampling data points and computing time. The discretization operation is shown in the equation

$$\Delta MV(k) = K_{\mathrm{p}}\left[e(k) + \frac{T}{T_i}\sum_{i}^{k} e(i) + \frac{T_{\mathrm{d}}}{T}(e(k) - e\,(k-1))\right]. \tag{3}$$

Here, k is the sampling time point, T is the computing time, p is the initial sampling time, and e is the output parameter of the instrument controller.

Fourthly, after the discretization operation, the obtained sampling period and time point are needed to use the following formula to further process the algorithm model, so as to obtain the algorithm base model with higher accuracy.

$$\Delta MV = \Delta MV(k-1) + q_0 e(k) + q_1 e(k-1) + q_2 e(k-2)\,, \tag{4}$$

where q is the value of sample period.

Fifthly, the following formula is used to determine the final algorithm model. In general, the algorithm model obtained by operation has a better control effect and more stable control rate. At the same time, tracking speed and accuracy are also important indexes to measure the effectiveness of the algorithm model.

$$\Delta MV = K_{\mathrm{p}}\left\{[e(k) - e(k-1)] + \frac{T}{T_i}e(k) + \frac{T_{\mathrm{d}}}{T}\left[e(k) - 2e(k-1) + e(k-2)\right]\right\}, \tag{5}$$

where T_{d} is the sampling time for the peak amount of control.

DMC, dynamic matrix control, is a computer based control technique, which is an incremental algorithm and the unit-step response based on the system, and it is applicable to stable linear systems. The dynamic characteristics of the system have pure hysteresis and do not affect the direct application of the algorithm. Deng believed that the standard DMC control algorithm is a very successful application in control systems based on DMC, however, there is a big problem when it is applied directly to the network environment [10]. In the case of low network load, the network delay is very small, the impact on the control system is almost negligible, and so the DMC algorithm has fast response, smooth transition and good control effect. Table 2 shows the basic parameter of the DMC control algorithm. Paul believed that the control structure of DMC is mainly composed of prediction model, rolling optimization, error correction and closed-loop control [11]. The predictive control algorithm is divided into model predictive control, generalized predictive control, and predictive control with internal model structure. The core idea of any algorithm includes three parts: prediction model, receding horizon optimization and

feedback correction.

Table 2. DMC algorithm parameters

Manual value	Size of DMC forecast step	The period of sampling	Size of DMC control step	DMC control parameters
0–4	0–100	100–10000	0–100	0.001–0.1

Liu believed that predictive control is a model-based control algorithm, this model is called predictive model [12]. The function of the prediction model is to predict its future output according to the object's historical information and future inputs. As a result, the future control strategy arbitrarily can be given as in the case of system simulation, the output changes of the observation object under different control strategies can be used to compare the quality of these control strategies, and the optimal control strategy is determined and controlled. The prediction model is constructed as follows: firstly, the sampling and sorting of the raw data are performed according to the unit step response of the controlled object, and the sampling period is also determined. In general, sampled data is the raw data for model nonparametric tests. Secondly, the linear processing of data analysis is carried out, and the concrete operation of model control increment is completed according to the following formula (6), finally, data output of the prediction model and value of model output is obtained.

$$\tilde{y}_1\left(k+\frac{i}{/}k\right)=\tilde{y}_0\left(k+\frac{i}{/}k\right)+a_i\Delta u(k)\,. \tag{6}$$

Here, k and i are the regression coefficients and increment coefficients of the control variables, $\tilde{y}_0\left(k+\frac{i}{/}k\right)$ is the model output value, and $a_i\Delta u(k)$ is the sampling sequence.

Predictive control is an optimization control algorithm, which is to determine the optimal future control role through a certain performance indicators, this performance indicator relates to the future behavior of the system. Aboozar believed that the optimization of predictive control is very different from the discrete optimal control in the traditional sense, which is mainly manifested in the optimization of predictive control that is a priority interval for receding horizon optimization [13]. At each sampling point, the optimization interval moves forward at the same time. Therefore, predictive control isn't based on a global optimization performance index, but at each point there is an optimal performance index relative to that time. The relative form of the performance indicators at different times is the same, but the absolute form and the time zone included are different. Therefore, optimization isn't carried out off-line at once, but is carried out online repeatedly in predictive control, that is called rolling optimization. The optimization process is on-line optimization over time repeatedly. Wang believed that every step is to achieve a static optimization, but it is dynamic optimization from the overall perspective [14]. This is the meaning of rolling optimization, and also the fundamental point of predictive control that is different from the traditional optimal control. The process of rolling optimization is that the starting point of a certain time is determined as the starting

point and the control increment is calculated, and then the forecast value is calculated according to the following formula, and finally the optimal index is determined by comparing the predicted value.

$$\Delta u(k) = (B_T Q B + r)^{-1} B^T Q \left[w_p(k) - \tilde{Y}_{p0}(k) \right] . \tag{7}$$

Here, B and Q control the optimization factor and the dynamic coefficient of the variable, w is the setting value of the control increment, $\tilde{Y}_{p0}$ is the input value of the sampling time, and $\Delta u(k)$ is the predictive value of the rolling optimization.

Zhang believed that predictive control is a closed-loop optimization control algorithm, after a series of future control roles are identified by optimization, it is usually not the full implementation of these control functions, but only the control of this moment to prevent the deviation of the model from the ideal state due to model mismatch or environmental interference [15]. At the next sampling time, the actual output of the object is detected first, the model based prediction is corrected by using this real-time information, and then the new optimization is carried out. The form of feedback correction is various, no matter what kind of correction form, the optimization of predictive control is based on the actual system and tries to predict the dynamic behavior of the system accurately in the optimization. Therefore, the optimization in predictive control not only is based on the model, but also uses the feedback information, thus closed-loop optimization is constituted. In the application of the DMC algorithm model, the feedback correction usually is used the following formula to correct the error through the detection of actual output and the predicted value.

$$\tilde{Y}_{\text{cor}}(k+1) = \tilde{Y}(k) + He(k+1) , \tag{8}$$

where $\tilde{Y}_{\text{cor}}(k+1)$ is the feedback error of $k+1$ sampling time points, $\tilde{Y}(k)$ is the sampling output prediction value, and H is the feedback correction coefficient.

The method of constructing PID and DMC control algorithm was used and the experiment was simulated to study the application effect of ISP technology in intelligent instrument design. ISP technology is widely used in the design of intelligent instrument and meter, and its application is more complicated. The method of model control algorithm research can be simulated in a certain extent so as to ensure the accuracy of the application of the algorithm model and provide a more favorable reference basis and basis for the study.

4. Result analysis and discussion

The results of the algorithm model analysis obtained by the methods described above are shown in several tables.

Table 3 shows the data results of the intelligent instrument test by using ISP technology, which is obtained through PID control algorithm model and DMC control algorithm model respectively. The data show that the accuracy of the data obtained by the DMC control algorithm model is higher. So it can be seen that the

DMC control algorithm model has a high feasibility in the research of ISP technology application.

Table 3. Comparative analysis of model output values

Frequency	PID output value	DMC output value
50	100.10	4.9997
50	100.50	2.4995
50	101.10	1.0001
50	100.02	0.5000

The rolling optimization method described in the third part above was used to carry on the model computation and the simulation test after the DMC model was carried on the scroll optimization. The results of the data obtained comparison are shown in Fig. 1. The data showed that the change trend of the test results of the three experimental models was more obvious after rolling optimization, and the trends of the three experimental models had a higher similarity. It was obvious that the data obtained by the algorithm after rolling optimization was more convincing, and the overall output level of the intelligent instrument was obviously lower than that of the original model. The stability of the simulated test output of the intelligent instrument was still poor. Therefore, the feedback correction was applied below to further improve the algorithm model and test results.

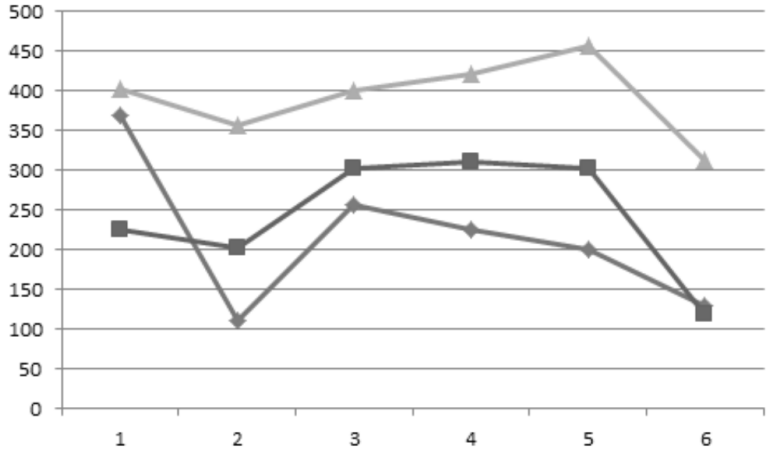

Fig. 1. Rolling optimization data of algorithm model

As shown above, the simulated results obtained after feedback correction of the control algorithm model are shown in Fig. 2. The data showed that the data stability of the DMC algorithm model and the simulation test was better, and the data change trend of the three test algorithm models was stable. Therefore, the optimized DMC model was used to test the influence of ISP technology on the design of intelligent instrument and meter.

In order to better verify the application of ISP technology in the design of intelli-

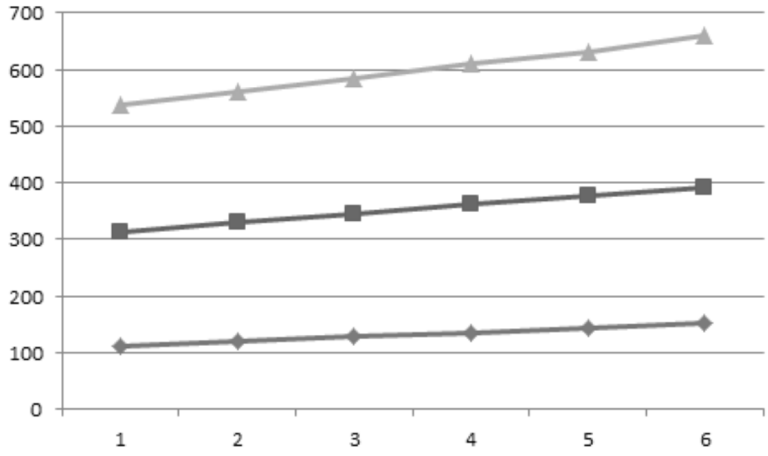

Fig. 2. Comparative analysis of the feedback data of the algorithm model

gent instrument and meter, in this paper, the intelligent arithmetic model was used to test the three basic indexes of voltage, current and power, which weren't designed by using ISP technology. The test results are shown in Table 4. The data showed that the average voltages, current and power index of common intelligent instruments changed greatly, however, the range of change was relatively small and the test results of raw data were less stable, therefore, the stability of ordinary intelligent instruments needed to be improved.

Table 4. Experimental results of application of ISP technology

U (V)		I (A)		P (VA)	
Standard value	Measured value	Standard value	Measured value	Standard value	Measured value
100	100.80	5	4.8997	500	500.12
100	100.50	5	5.0002	500	489.96
100	101.10	5	4.8999	500	498.89
100	100.02	5	4.8959	500	500.02
100	100.06	5	5.1010	500	510.10
100	101.02	5	5.2021	500	479.20

Table 5 shows the specific data of the voltage, current and power obtained by the instrument after the improved design of the general intelligent instrument described above by using ISP technology. The test value and the standard value of the three parameters of the intelligent instrument were improved by the ISP technology, and the range of change was small and could be negligible, so it could be seen that the stability of the test output of the intelligent instrument designed by ISP technology

was high.

Table 5. Experimental results of ISP technology application

U (V)		I (A)		P (VA)	
Standard value	Measured value	Standard value	Measured value	Standard value	Measured value
100	100.10	5	4.9997	500	500.09
100	100.20	5	5.0002	500	499.96
100	100.10	5	4.9999	500	499.89
100	100.02	5	4.9959	500	500.02
100	100.06	5	5.0010	500	500.10
100	100.08	5	5.0021	500	499.20

To sum up, the intelligent instrument designed by this technology has a better stability and higher practicability, so the application of ISP technology for the design of intelligent instruments can improve the overall performance of the instrument. However, because the application of ISP technology in intelligent instrument and meter is related to the adjustment of artificial neural network threshold, although this problem has some influence on the application of ISP technology in the design of intelligent instrument and meter, the degree of influence is small and can be ignored. Therefore, the author believes that the application of ISP technology in intelligent instrument design is better, but its scope of application still needs to be further expanded. First of all, ISP technology will be applied to the sensor circuit design and extended to other intelligent instrumentation device design from the perspective of sensor design. Secondly, the simulation research of ISP technology in the design of intelligent instrument and meter should be strengthened from the point of view of artificial neural network, so as to improve the actual application effect of technology. Finally, the control parameters should adjusted in the design process, so that the technical advantages can be actively applied to the instrument design, the functionality of the intelligent instrument and meter can be promoted, and the intelligent production of the device can be promoted.

5. Conclusion

In order to improve the application effect of ISP technology in the design of intelligent instrument and meter, the influence of ISP technology on the design of intelligent instrument and meter was analyzed and studied by building a multi-control algorithm model. Finally, the main conclusions were as follows: the data results obtained by performing simulation tests of the DMC control algorithm model have high accuracy. The application of ISP technology can improve the accuracy and stability of the output of intelligent instruments and meters to a certain extent, but the technique still has the problem of adjusting the threshold of the artificial

neural network.

To sum up, the model of the control algorithm used in this paper has a high rationality and comprehensiveness, the application of the algorithm model is beneficial to the application of ISP technology to improve the design direction of intelligent instruments. However, there are still problems that are not conducive to the adjustment of the threshold of the artificial neural network. Therefore, although this study has a certain reference value, there are still some shortcomings. In the future research, the application scope of system programming technology should be expanded and the application effect of ISP technology in intelligent instrument design should be enhanced by reasonably adjusting the control parameters of instruments and meters.

References

[1] Z. Miao, M. Lu, X. Hu, Z. You: *Development and application of intelligent monitoring and controlling system of cotton-picking machine based on virtual instrument technology.* Transactions of the Chinese Society of Agricultural Engineering *30* (2014), No. 23, 35–42.

[2] J. Y. Wang, S. Z. Li: *ISP technology's application in remote upgrade for the intelligent instruments.* Advanced Materials Research *542–543* (2012), No. Chapter 6, 711–716.

[3] Y. Xu, H. X. Lv, Y. Xie, R. X. Yao: *Intelligent instrument's course design based on visual instrument.* Advanced Materials Research *718–720* (2013), No. Chapter 7, 2259–2263.

[4] C. Pan, H. Ding, H. Y. Wang: *The research and design of instrument management system based on wireless HART technology.* Applied Mechanics and Materials *241–244* (2013), Chapter 18, 2350–2353.

[5] Q. Lifang: *Design of remote upgraded intelligent instrument based on ISP technology.* Electronic Measurement Technology (2007), No. 02, 039.

[6] X. E. Chen, J. G. Zhang, Y. J. Liu: *Research on the intelligent control and simulation of automobile cruise system based on fuzzy system.* Mathematical Problems in Engineering (2016), No. 5, 1–12.

[7] N. Sasidharan, N. M. Madhu, J. G. Singh, W. Ongsakul: *An approach for an efficient hybrid AC/DC solar powered Homegrid system based on the load characteristics of home appliances.* Energy and Buildings *108* (2015), 23–35.

[8] P. Chinmoy, T. Okabe, K. Vimalathithan, S. Narahari), M. Jeyabharath, S. Wang, C. John): *Identification of factors influencing injury severity prediction (ISP) in real world accident based on NASS-CDS.* International Journal of Automotive Engineering *6* (2015), No. 4, 119–125.

[9] J. G. P. Reddy, K. R. Reddy: *Design and simulation of cascaded H-bridge multilevel inverter based DSTATCOM.* International Journal of Engineering Trends and Technology *3* (2012), No. 1, 737–743.

[10] Z. H. Deng, Y. H. Zhu: *The design and implementation of a handling-robot.* Applied Mechanics and Materials *644–650*, (2014), No. Chapter 1, 290–293.

[11] S. Paul, R. Jain, M. Samaka, J. Pan: *Application delivery in multi-cloud environments using software defined networking.* Computer Networks *68* (2014), 166–186.

[12] B. Liu, G. Cong, Y. Zeng, D. Xu, Y. M. Chee: *Influence spreading path and its application to the time constrained social influence maximization problem and beyond.* IEEE Transactions on Knowledge and Data Engineering *26* (2014), No. 8, 1904–1917.

[13] A. Jamalnia, H. A. Mahdiraji, M. R. Sadeghi, S. H. R. Hajiagha, a. Feili: *An integrated fuzzy QFD and fuzzy goal programming approach for global facility location-*

allocation problem. International Journal of Information Technology & Decision Making *13* (2014), No. 02, 263–290.

[14] G. J. Wang, X. H. Cheng, Z. X. Wang: *Terminal design of the intelligent data acquisition system based on USB interface*. Applied Mechanics & Materials *380–384*, (2013), Chapter 7, 3629–3632.

[15] H. Ma, X. Tang, F. Xiao, X. Zhang: *Phase noise analysis and estimate of millimeter wave PLL frequency synthesizer*. International Journal of Infrared and Millimeter Waves *26* (2005), No. 2, 271–278.

Received June 6, 2017

Acta Technica *62* No. 1A/2017, 495–506

Design and implementation of energy management system software in green building

Hongyan Zhang[1], Zhiping Zhou[1]

Abstract. Construction energy consumption has been tied up with traffic and industrial energy consumption at this stage, and has become one of the three major energy users in China. In view of the current problems of prominent energy consumption and the lack of energy management software system in our country, as well as the lack of energy data in the actual operation of green intelligent buildings, the design method of software management system was put forward in this paper, and then the mature software engineering method was used to develop the energy management which can meet the requirement of green building energy saving; finally, in the experiment, it was proved that the energy consumption data analysis module was the main part in the energy management software. Through the statistical analysis and research of the building energy consumption, the energy consumption of the building model was compared and analyzed, so that the equipment efficiency and energy consumption of the building were defined, and the corresponding management and optimization measures were put forward, so as to provide a theoretical reference for the development of green building energy-saving management software.

Key words. Green building, energy management system, management software.

1. Introduction

Because of the huge population base and rapid development of social economy in China, the consumption of resources in China is serious. China has become one of the energy consuming countries in the world. The serious consumption of resources leads to the vicious development of human living environment, which seriously affects people's life and health. Facing such an era background, the government has introduced a series of policies to encourage green development to promote green construction and create a healthy living environment. Green building is a leap in the development of intelligent buildings, and there are obvious differences between the two. The so-called intelligent building is a building that uses high technology to meet the needs of people, while the green building is based on intelligent architecture,

[1]Software Department, Hebei Software Institute, Baoding, Hebei, 71000, China

which covers human life for the pursuit of natural development. That is to say, green building is the integration of intelligent building and environmental consciousness. The formation of green buildings mainly depends on the self-discipline of society to promote green economy, reduce energy consumption, and improve the utilization rate of energy. From the technical point of view, green building is a requirement for technological development and an important achievement of economic reform. The choice of materials for green building is quite severe, which mainly adopts the new energy-saving and environmental protection materials, integrates with the development of the times, and combines with the characteristics of the development of intelligent buildings, so as to effectively monitor and control the system information.

2. State of the art

Green buildings refer to buildings that increase resource utilization but reduce energy consumption, from which, users try their best to reduce resource consumption and save resources, so as to achieve efficient and healthy construction [1]. On the other hand, green building covers a wide range, which is closely related to technology, equipment, materials and environment [2]. In recent years, China's government agencies have introduced a number of green building support policies, and highlighted the importance of green building energy efficiency. Facing such a development situation, we should try our best to realize the new leap of green energy saving construction, so as to promote the steady development of society. Focusing on the development of green building in the world, the annual resource consumption of office buildings is down by about twenty percent with the development of building automation system [3]. According to relevant statistics, few intelligent buildings can achieve energy-saving effect in our country. However, most the energy saving systems in smart buildings are just BAS systems, which can detect the control status of equipment, but the effect is not obvious, and the loss of capital is also raised. Therefore, the development of energy-saving buildings has become a major problem faced by China's construction industry to reduce consumption. In the current technological context, breakthroughs in new technologies are based only on Intelligent buildings, and the energy monitoring system is embedded in intelligent building to realize the optimized management of energy [4]. The development of the leading green building energy management system at home and abroad is based on many of the latest technologies in the Internet community, such as cloud computing, Internet of things and other advanced technologies [5]. Through energy management systems of the Internet of things and cloud computing, the various sensors and controllers within the building group can be fully connected. On the basis of intelligent control and system integration on the construction site, the scattered single buildings are connected into building groups for real-time data statistics, analysis and processing, and the energy consumption of the building group is unified controlled to realize the integration of intelligent building energy control function. And a large number of buildings can form a unified control of energy consumption in a smart city [6].

3. Methodology

In building, the purpose of using energy is to provide comfortable, safe and convenient service for all kinds of personnel in the building, that is, which is people-oriented. Energy efficiency should be analyzed both in terms of real energy consumption data, and the relationship between energy use and human use. Therefore, in addition to the traditional energy transmission efficiency, the concept of energy utilization efficiency should be introduced [7].

The formula for the efficiency of energy transmission is

$$\eta_t = \frac{E}{E_0} \times 100\,\%\,, \tag{1}$$

where E_0 represents the total energy output within the building, and E represents the total energy obtained by the end device.

Energy efficiency is used to indicate the extent to which energy is transferred to the end of the system, that is, the place where people move [8]. The efficiency of energy utilization depends on the distribution and mode of activity of people in buildings (the distribution and activity of personnel are different in different areas of a building, and the frequency of distribution and activity is different at different time periods), which can be expressed by discrete data, and the average efficiency of energy can be obtained by summation method [9]. If the energy is fully utilized, the utilization efficiency is 1, otherwise, it is 0. The area in the building is divided into n units, with hours as time units, and the average energy utilization efficiency can be expressed as

$$\bar{\eta}_t = \frac{(\sum_{k=0}^{n} \delta_{kt})}{nt} \times 100\,\%\,, \tag{2}$$

where $\delta_{kt} \in \{0, 1\},\ k \in (0, n),\ t \in (0, 23)$, δ_{kt} represents the energy efficiency of a given period of time, k represents the zone number and t represents the time period.

For type 2, the meaning of the expression is very clear but cannot be measured accurately, which can only be estimated by the method of estimation, and the energy in the building is always measured at a certain time delay. Therefore, there is no definite method of measuring energy efficiency, which is more based on experience. By recording long-term energy usage, the energy management system can obtain approximate representation of energy efficiency through statistical methods, which is also an original intention of building an energy management system [10].

Another way to achieve energy efficiency is that with the improvement of building intelligence, the passenger flow analysis technology is used to monitor the distribution and activity of personnel in real time, so as to determine the efficiency of energy utilization.

Figure 1 shows the ideal green building with an energy management system.

Building energy management systems, referred to as BEMS, can monitor buildings' energy efficiency and energy use and energy consumption equipment, build building energy information database, and analyze and process it on the basis of database, so as to realize the diagnosis of energy efficiency and control of energy consumption.

The system data classification diagram is shown in Table 1.

Fig. 1. Ideal green building with an energy management system

Table 1. BEMS data classification map

Environmental data	Temperature humidity sensor	
	Illumination sensor	
Energy consumption data	Item metering ammeter	Electricity for air conditioning
		Electricity for lighting outlet
		Power consumption
		Special power consumption

The whole BEMS includes 4 function subsystems, such as detection system, control system, measurement system and analysis system.

Test system: environment temperature, humidity and illumination of building are collected. The energy consumption (air conditioning equipment and lighting equipment) is embodied by the real-time representation of the environmental conditions of each building's use space.

Metering system: through the collection of energy consumption data of air conditioning, lighting, sockets, power, electricity and special power, the amount of energy consumed in buildings is measured by analogue measurement.

Control system: on the basis of measurement and detection, the results of measurement and measurement are compared and analyzed. Through building control system (BAS), intelligent optimization control of energy consumption equipment is carried out according to feedback control theory.

Analysis system: on the basis of appeal measurement and test database, a variety of energy consumption analysis reports and statements are provided, thus forming the basis for building energy efficiency reform.

In the aspect of energy saving, the system can detect the abnormal use of energy and adjust the running state of the equipment in time through real-time on-line monitoring, so as to ensure the comfort of the indoor environment, and eliminate the waste of energy. The system control process is shown in Fig. 2.

The system is divided into five layers, such as data monitoring and collection, data

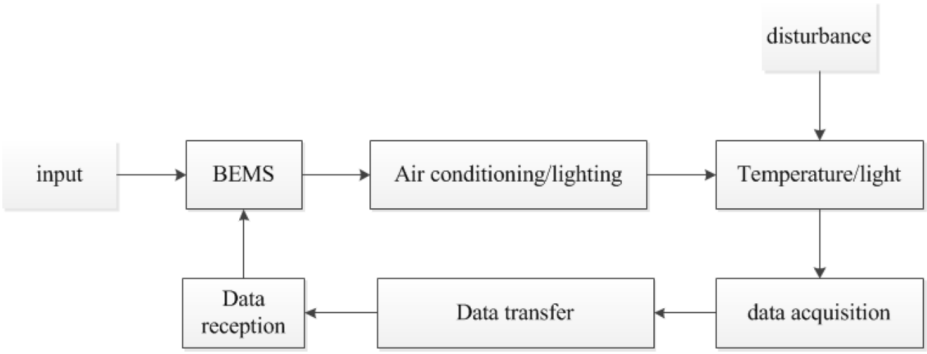

Fig. 2. BEMS system control flow chart

transmission, data interpretation, system evaluation and performance optimization, as shown in Table 2.

Table 2. Hierarchy of BEMS systems

The fifth layer	Energy-saving optimization layer	System operation optimization, parameter optimization, start stop, optimization and so on
The fourth layer	System evaluation layer	Building energy consumption analysis, energy saving potential assessment
The third layer	Data interpretation layer	Protocol interface development, data packet analysis, data storage
The second layer	Data transport layer	Zigbee, RS485 and other transport protocols
The first layer	Data acquisition layer	Environmental variables, equipment, electricity consumption and other energy information

The data acquisition layer is composed of three parts, namely, data acquisition subsystem, data transfer station, and data center, and the data acquisition subsystem is mainly responsible for monitoring and collecting energy consumption of the building facade, including an analysis software. The data relay station is responsible for receiving and caching the energy consumption information corresponding to the management area, and should upload it to the data center at the same time General data transfer stations can omit data processing and permanent storage capabilities. The data center is to receive and store the data information submitted by the transfer station in the corresponding management area, and then to display and publish it after processing.

In the process of gathering energy consumption data, two types are involved: the classified energy consumption and the sectional energy consumption. The classified energy consumption refers specifically to the type of energy consumed by state or-

gans, office buildings and large public buildings, which is convenient to carry out data collection and arrangement, including power consumption, natural gas consumption, tap water consumption, etc. Based on the specific categories of building energy usage, there are 6 indicators for classifying energy consumption, including power consumption, water consumption, gas consumption, heating capacity, and cooling capacity and other energy consumption. For example, coal and oil are renewable energy sources. The sectional energy consumption refers to the amount of specific energy consumed by intelligent buildings in accordance with energy projects, which is convenient for data collection and arrangement on the basis of project use, such as lighting, electricity and power consumption, as shown in Table 3.

Table 3. Sampling of energy consumption data

Electricity for lighting outlet	A functional area in a building; all lighting
Electricity for air conditioning	A device for supplying air or warm air to a building. Generally speaking, the air conditioning electricity is composed of two parts, namely has two sub items, respectively, hot and cold stations, electricity and air-conditioning terminal power
Power consumption	All equipment that can provide power support, such as elevators, ventilators, pressure equipment, etc.
Special power consumption	Outside the building function of unconventional equipment, electricity, usually special electricity consumption is relatively large, and at the same time, concentration is relatively high

In the data transmission layer, data of sensors and meters are transmitted, and the data transmission mode is mainly divided into two ways: wire transmission and wireless transmission. In actual buildings, data transmission is still widely used for its stability and reliability.

Through the data collector, the data is stored in the relational database SQL Server in accordance with the required transmission mode. The friendly interaction in current intelligent energy management is to process data through the program and to display it through the application. The data is analyzed by the transmission command of the display layer, and the statistical data and parameter reports are obtained.

In the energy management system, 6 report modules are used, such as energy consumption report, energy consumption ranking, energy consumption comparison, monthly average report, deviation analysis, cost report and so on, so as to assess the use of energy.

Intelligent lighting and air conditioning systems are used as energy saving optimization systems. In the system, the fixed time switch is arranged on the intelligent lighting, so that the electric energy can't generate superfluous waste, and the energy saving target is achieved. Air-conditioning parameters are set up to ensure that temperature and humidity can be maintained within a certain value, so as not to waste

energy. And the temperature of fresh air and return air is adjusted automatically according to temperature and humidity, so as to achieve the goal of energy saving.

4. Result analysis and discussion

After the development of the energy management system software, it was applied in the new office building of a design institute. Through the actual use of users, the system function indicators were tested, and the actual system data was used to test the system performance.

Firstly, some related reports in the system evaluation layer were obtained, as shown in Figs. 3 and 4.

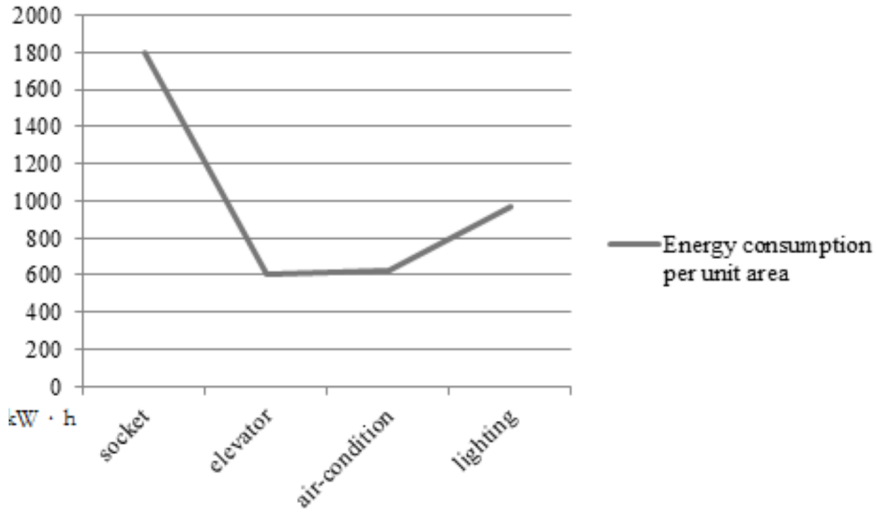

Fig. 3. Energy consumption report

Through the energy consumption report of energy management system produced on time, daily, monthly and annual, users can grasp all kinds of energy consumption. Through energy consumption indicators such as unit area, energy consumption and other indicators, the abnormal values of energy consumption can be found out. These energy consumption reports are also basic data supports for energy statistics and energy audits.

Energy ranking shows the energy consumption value of different equipment in each month, in which, the energy consumption can be observed in different months, and the energy consumption of different energy sources can be ranked. The energy efficient equipment and the lowest energy consumption equipment can be found through the energy consumption sequencing of the energy management team in different time ranges.

Secondly, the test of energy management system software was divided into 2 parts: function test and performance test. In functional testing, software integrity was the main test content, so as to test whether the software can meet the design

goals, and whether the functions should to be implemented in the requirement analysis. In performance testing, the software's data processing time, space performance indicators were the main testing contents. And the function test was tested by manual operation. In the performance test, the actual data device was used for input and output tests, and the corresponding time consumption was calculated, and the results were obtained, as shown in Table 4 and Table 5.

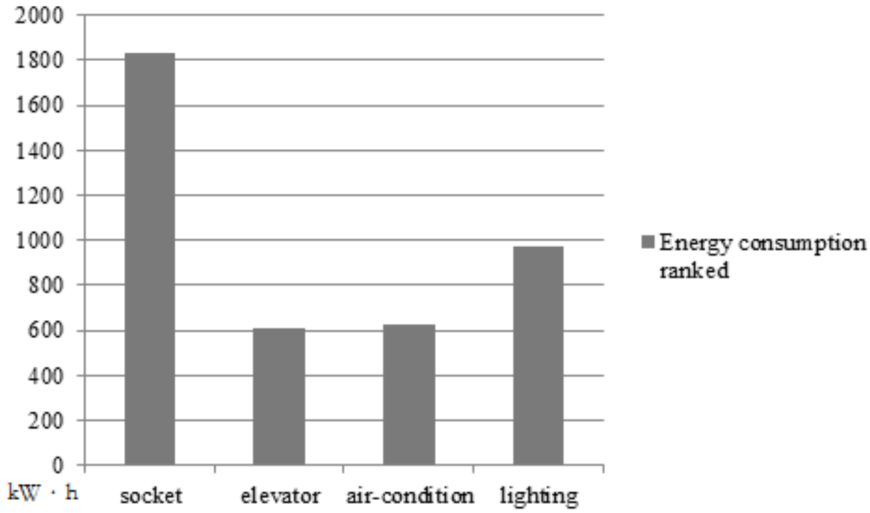

Fig. 4. Energy ranking

Table 4. Results of system function test

Test item	Test result
Monitoring the operation status of the main equipment in the energy system	Have
Setting energy system parameter function	Have
Centralized control, operation and adjustment of main equipment	Have
Comprehensive balance, reasonable allocation and optimized dispatching function of energy system	Have
Dealing with exceptions, failures, and accidents	Have
Basic energy data management function	Have
Real time short time archiving, database archiving and instant query function for actual data of energy operation	Have

Through the above tables, it can be seen that the building energy allocation is more flexible. The energy management system can change the energy allocation of buildings according to external conditions, energy supply, user demand and economic

cost. The energy management system has many advantages, the first is to strengthen the energy system scalability, the energy management system can connect all the lower energy subsystems, and carry out comprehensive fault-tolerant control and energy use planning for all kinds of energy units in the building, which is easy to extend the system; the second is the openness of building energy systems, the energy management system is an open system, which makes the building energy system more convenient to connect with other building systems and exchange data, so as to achieve the purpose of integrated management; the third is the convenient management, energy management systems can save data and time on manual data acquisition, manual control, and error checking of building energy systems, while the non-professional managers can also master system manipulation in a very short period of time; the fourth is to improve energy saving effect, an obvious advantage of the energy management system can find the ideal energy consumption of each device through data analysis and control strategy design, and reasonably determine the set value of the running state of the equipment, automatically adjust the operation mode of equipment and control equipment start and stop time, so as to effectively reduce the energy consumption of building the system.

Table 5. Performance test results

Test item		Test result
1) System performance design index	Support simultaneous online customers	>10
	Number of connected control systems	>10
	The total number of control nodes in the connected control system	>20000
	The number of simultaneous changes in the number of control nodes in a connected control system	>500 dots per second
2) Time characteristic requirement	Client interface data updates (from the underlying device data update - changes in user interface data intervals)	<=5 s
	System real time data transfer time (the time delay from the underlying device data update - new data obtained by the system)	<=2 s
	System control command transfer time (refers to the user from the interface to send operation commands - the underlying device to accept the delay of the command)	<=5 s
	A storage record stored in a database (the time delay from which the underlying device data is updated - the system obtains new data from the device and stores it in the database)	<=5 s
	Update access to dynamic data	<=5 s
	All data in the system	<=60 s

5. Conclusion

Through the analysis of the control principle of central air-conditioning system for large building energy users, the core viewpoints of energy saving and energy efficiency improvement were derived in this paper. Starting from the whole, the central air-conditioning management system that can save energy and reduce energy consumption was analyzed, so as to realize the development of system energy consumption and system cold load, and the following conclusions were obtained.

Through the analysis of building energy management system, the general development of the system data interface was realized, the information storage function of the system was developed, the system software design was completed, and the purpose of reducing energy consumption was achieved. In this system, each parameter of the software was monitored in real time, and the processing and storage of the transmitted data were done at the same time. By referring to the parameter information and the control effect of the system, the relevant engineers analyzed the specific conditions of the system operation in a given time range, and calculated the utilization of the energy. And through the database comprehensive integration of energy use, the energy control strategy was optimized. In addition, real-time maintenance of the system was realized, and the related faults were inquired, thus providing important reference for solving the problem and optimizing the system.

However, there are still some deficiencies in the development of the system, and the application of the whole platform has not yet fully realized. Different projects should be improved. For example, in the future development, some of the following functions of the software can also be realized: the memory configuration of the database should be optimized, its use performance should be improved, a detailed design plan should be formulated, and the system should be tested, so as to realize the generalization of system interface, to integrate with other systems in the life, such as office system, parking management system and so on, thus promoting the all-round development of intelligent building.

References

[1] P. Palensky, D. Dietrich: *Demand side management: Demand response, intelligent energy systems, and smart loads.* IEEE Transactions on Industrial Informatics *7* (2011), No. 3, 381–388.

[2] Y. K. Chen, Y. C. Wu, C. C. Song, Y. S. Chen: *Design and implementation of energy management system with fuzzy control for DC microgrid systems.* IEEE Transactions on Power Electronics *28* (2013), No. 4, 1563–1570.

[3] H. Dagdougui, R. Minciardi, A. Ouammi, M. Robba, R. Sacile: *Modeling and optimization of a hybrid system for the energy supply of a "Green" building.* Energy Conversion and Management *64* (2012), No. 3, 351–363.

[4] D. H. Sun, S. L. Han, Y. Yang: *Application of embedded database in wireless temperature sensor network.* Instrument Technique and Sensor *30* (2009), No. 08, 57–59.

[5] M. H. Li, J. Wang, Y. W. Qu: *Designed of sewage monitor system based on WINCC and ZigBee.* Control Engineering of China *20* (2013), No. 2, 324–326.

[6] S. N. Han, G. M. Lee, N. Crespi: *Semantic context-aware service composition for*

building automation system. IEEE Transactions on Industrial Informatics *10*, (2014), No. 1, 752–761.

[7] A. Costa, M. M. Keane, J. I. Torrens, E. Corry: *Building operation and energy performance: Monitoring, analysis and optimisation toolkit.* Applied Energy *101* (2013), 310–316.

[8] L. F. Wang, W. Zhu, Y. Rui: *Intelligent multiagent control system for energy and comfort management in smart and sustainable buildings.* IEEE Transactions on Smart Grid *3* (2012), No. 2, 605–617.

[9] B. Sun, P. B. Luh, Q. S. Jia, Z. Jiang, F. Wang, C. Song: *Building energy management: Integrated control of active and passive heating, cooling, lighting, shading, and wentilation systems.* IEEE Transactions on Automation Science and Engineering *10* (2013), No. 3, 588–602.

[10] M. D. L. Rongge: *Implementation method of ASP.net-based the three layers.* Microcomputth Applications (2002), No. 3, 120–124.

Received June 6, 2017

Acta Technica *62* No. 1A/2017, 507–520

Modeling and analysis of complex pipe network taking into account the vulnerability of pipe network[1]

Han Zhixia[2]

Abstract. The detection of the vulnerability of the existing pipe network often depends on the analysis of a sufficient number of samples. However, the new pipe network vulnerability has massive emergence, and at the beginning of the emergence, due to the limited number of samples, the existing method cannot quickly detect the new type of pipe network vulnerability and its variants. In this paper, the anomaly degree and similarity of the fluid flow passage behavior in the pipe network flow dependency network is analyzed, the risk of pipe network vulnerability detection and estimation is introduced, and a method for the modeling of the pipe network vulnerability of complex pipe network through complex network is put forward. This method only requires a small proportion of training samples to achieve accurate pipe network vulnerability detection, which is more applicable for the new pipe network vulnerability detection than the existing methods. Based on our empirical analysis of 8.340 normal pipe network flows and 7.257 pipe network vulnerability flows, the proposed method has significantly improved the vulnerability detection effect of the pipe network compared to that of the traditional statistical classifier based modeling method. Even under the condition that the training samples are only 1 % of the total sample size, this method still can achieve the error rate of 5.55 %, which is by 36.5 % lower than that of the traditional method.

Key words. Passage behavior, pipe network vulnerability detection, complex pipe network, pipe dependency network.

1. Introduction

According to the worldwide monitoring statistics, in 2014 the new pipe network vulnerabilities was 317 million, and the total number of pipe network vulnerabilities had reached 1.7 billion [1]. The rapid increase in the number of new pipe network

[1]This work was support by the Industrial Research Project of Shaanxi Science and Technology Agency (No.2014K05-47) of Research of Leakage Monitoring Application Technology of Water Supply Pipe Network Based on Complex System Theory.

[2]Electronics & Electric Engineering College, Baoji University of Arts and Sciences, Baoji, Shaanxi, 721016 China

vulnerabilities has posed challenge to the pipe network vulnerability detection. The detection of pipe network vulnerability often depends on the analysis of a sufficient number of samples and their variants, and on this basis to automatically extract the rules or features based on human experience or statistical learning methods, and to update the existing detectors [2–6]. As the collection and analysis of a sufficient number of relevant samples often take a relatively long time, the existing modeling methods cannot quickly detect the new pipe network vulnerability and its variants, the massive emergence of new pipe network vulnerabilities still pose a continuing threat to the whole society.

At the early stage of the emergence of the new pipe network vulnerability, the number of emerging samples is often few, which cannot provide sufficient information for the current pipe network vulnerability modeling methods. After a large number of samples emerge, due to the lack of effective prevention in the early stage, serious security incidents may occur from time to time [7]. At the same time, no matter the methods based on human experience, or the methods that make use of the statistical learning, they are both based on sufficient known samples. The method on the basis of human experience creates the behavior rules and feature codes that can be applied for the identification of the vulnerability of the new type of pipe network through analyzing the behavior of the new samples and the sequence of commands according to the knowledge experience. The method of manual analysis has high accuracy, but it is time consuming and has low self-adaptability. With the study and application of statistical learning theory, statistical learning method has provided an effective tool for pipe network vulnerability rules and feature extraction [2, 3, 4, 6]. Such methods often rely on a sufficiently known set of samples, that is, the program sample which has been determined as normal or malicious program sample. For the label determination of the new type of pipe network vulnerability, it often requires the manual analysis at first so as to ensure the accuracy. As manual analysis is very time consuming, it is highly difficult to ensure that a sufficient set of known samples can be obtained within a short time. How to ensure the accuracy of the pipe network vulnerability detection under the condition of only a small number of known samples is a key problem to respond to the current situation of the rapid growth of new pipe network vulnerability.

In order to solve this problem, this paper makes use of the complex pipe network method, on the basis of the analysis of the dependency relationship of the data flow of the system objects, puts forward a kind of modeling method for the pipe network vulnerability with the combination of the anomaly degree and similarity of the pipeline flow behavior. This method can ensure the ideal accuracy in a small number of known samples by the incremental training. In the past research, it was found that the network object model could be analyzed and evaluated from the perspective of the network structure, and the importance of the system object could be analyzed and evaluated effectively through the network modeling of the data flow dependencies among the system objects, and thus effectively identify the important objects in the system in the perspective of security [8]. In this paper, on the basis of the importance of system object evaluation, the key point of pipeline flow behavior is defined by using the importance of program access object, so as to analyze the

anomaly degree of pipeline flow behavior. At the same time, the data dependency network under the whole system has provided the basis for the evaluation of the similarity of the system objects, which can help us analyze the similarity of the behavior of the fluid flow from the perspective of the access object, so as to further provide the basis for the judgment of whether the program is normal or anomaly, that is, the more similar the program of the passage activity is, and the more similar the label will be. Combined with the anomaly degree and similarity of the pipeline flow behavior, we make use of the method of the complex pipe network to realize the effective modeling method for the pipe network vulnerability under the current situation of a large number of unknown samples.

The complex pipe network is an incremental sample forecasting method. On the basis of the definition of the estimated risk, the samples of the complex network are predicted from the unmarked samples. Based on the pipeline flow behavior anomaly, we have constructed a statistical learning classifier for the prediction of the label of unknown samples. At the same time, by analyzing the similarity of pipeline flow behavior, we can obtain the estimation risk of the unknown sample prediction label. We have identified the unknown samples of complex networks, so as to predict the labels as the ones for the unknown samples, and use them as the known samples to further improve the classifier based on the degree of passage behavior anomaly. The strategy of this complex network can continuously improve the classifier for pipe network vulnerability detection, and further reduce the estimation risk on this basis. Therefore, it can ensure the accuracy of the sample even in the case of a small number of samples, and can also achieve relatively ideal accuracy, reduce the cost of manual analysis of samples and speed up the response to the vulnerability of the new pipe network, which is more applicable to respond to the situation of the rapid growth of the new pipe network vulnerability at present. Through the experimental verification of the passage behavior of 8.340 daily normal pipeline flow life cycles and 7.257 actual pipe network vulnerabilities, the method proposed in this paper has shown a significant increase in the detection effect when compared with the method that adopts the original statistical classifier method only.

2. Modeling of the vulnerability of active pipe network based on the complex network

2.1. Modeling of the vulnerability of pipe network based on passage behavior anomaly degree

The vast majority of pipe network vulnerability through the sensitive operation of important objects is able to achieve its infection or damage the operating system. Here we define the modification of objects and the creation of fluid flow operations as sensitive operations, characterized by the flow of fluids through which the sensitive operations are performed. Then we make use of the statistic learning classifier to classify the normal pipeline flow and the pipe network vulnerability, so as to solve the problem of pipe network vulnerability detection. First of all, we define the key detection points for fluid flow behavior anomaly detection, which are the most

important C objects (the C objects with the highest important value) among all the objects that execute the sensitive operation. We construct a characteristic vector x with the length C for each fluid flow, in which, x_i $(1 \leq i \leq C)$ stands for the importance of the ith important object among all objects that perform the sensitive operation in the flow of the fluid. This eigenvector has described the critical detection point information for the fluid flow. We found in the experiment that, under the condition of $C = 5$, relatively good pipe network vulnerability detection performance can be obtained in the two aspects of the true positive rate and false positive rate. Therefore, all the experiments in this paper are carried out under the condition of $C = 5$.

2.2. Complex pipe network based on the complex network

The complex pipe network is an important field in machine learning, and the research of incremental sample marking method has been studied. Complex networks based on complex network method was first proposed by Zhu et al [9]. Given the part of the marked samples, through the complex pipe network from unmarked samples to identify the samples that can be labeled. Unlike the random selection, this method selectively selects the unlabeled samples as labeled samples in a new round of learning and is therefore also called the semi-supervised learning.

Under the strategy of complex network estimation, we make use of the greedy choice to carry on the complex pipeline network on the unlabeled sample. Unknown samples are predicted by training the classifier according to the key detection points of known samples. At the same time, according to the similarity of unlabeled samples, the estimated risk of each unlabeled sample is measured. The unlabeled sample with the least estimated risk is chosen as the labeled sample, the classifier is relearned, and the process is repeated until all samples are marked. If the similarity value is reasonable, it can help the learner to improve the learning process and achieve better classification effect. Based on the estimated risk defined by the following equation, the complex pipe network based on the complex network is a process of greedy searching for the unknown samples that meet the following conditions:

$$\arg\min_{i \in U} \hat{R}_i$$

in which

$$\hat{R}_i = \frac{1}{2} \sum_{j \in L} \frac{\mathrm{Sim}\left(v_i, v_j\right)}{\sum_k \mathrm{Sim}\left(v_i, v_k\right)} \left(h\left(i\right) - h\left(j\right)\right)^2 . \tag{1}$$

Here, L (labeled) stands for the set of labeled samples, that is, the fluid passage flow with the normal and malicious labels known, and U (unlabeled) stands for the unlabeled sample set. Algorithm 1 describes the process of active network vulnerability detection based on complex network in this paper. In which, in step 4, we use the statistical learning classifier to obtain the pipe network vulnerability detection model (classifier h) based on the passage flow behavior anomaly degree. And then, under the strategy of the complex network, the passage behavior similarity is used to identify the unlabeled fluid flow with the smallest estimated risk, and the selected

fluid flow is marked according to the predicted result of h. The fluid flow samples with predictive labels are added to the training set L and retested in the anomaly-based pipe network vulnerability detection model until all the unlabeled fluid flow samples are labeled accordingly.

Algorithm 1: Vulnerability detection of active pipe network based on the complex network

Inputs: Initial labeled sample L^0, unlabeled sample U, and the number of complex pipe network samples per round K.

Output: Label of the sample in U.

1: $L = L^0$, the real label of $h(j) = j$, $\forall j \in L^0$.

2: Calculate the similarity of each sample i in U and each sample j in L, [Sim (v_i, v_j).

3: While unlabeled sample do exist in U, then

4: Make use of statistical classifier to conduct training on L, and classifier h can be obtained.

5: Use classifier h to predict the sample labels in U.

6: Calculate the estimated risk $\hat{R}_i$ for each sample in U, see equation (1)

7: For $i = 0 \to K - 1$ do

8: Select $k \leftarrow \arg\min_i \hat{R}_i$, see equation (1) .

9: $L \leftarrow L \bigcup \{k\}$.

10: $U \leftarrow U / \{k\}$.

11: end for

12: end while

In Step 6 of the complex pipe network process, the complexity of the algorithm is $O(|U||L|)$, that is, $\mathrm{O}(n^2)$. In order to reduce the complexity of the algorithm, we have performed pruning on the calculated similarity. In this paper, we adopt Top-V pruning: through setting N for the sample $i \in U$, N samples with the largest similarity to i are selected, that is, the local manifold structure of unlabeled samples is constructed. This method first appeared in the LLE method of Roweis and Saul. Based on our observations in the experiment, when $N = 3$, the detection effect has the most significant improvement. The experimental results described in this paper are obtained under the condition of $N = 3$.

The method of complex pipe network can effectively deal with the situation that the number of known normal and malicious fluid flow is limited, and the model is established through the strategy of complex network. This method can effectively respond to the situation of the rapid growth of pipe network vulnerability in the current Internet environment.

3. Experimental analysis

3.1. Experimental design

The experiment is mainly carried out from three aspects: 1) The influence of different similarity evaluation methods (the influence of Sim (v_i, v_j) on the detection

results; 2) The influence of different classifiers (h) on the detection results; 3) The influence of different initial training set size (L^0) on the detection results. We first test the similarity of nodes under the three different network structures proposed in Section 3.2, and compare the influence of different evaluation methods on the detection results. In this experiment, we adopt the nearest neighbor as the statistical learning classifier for pipe network vulnerability detection. Then, we use two different classifiers, k nearest neighbors and random forests to analyze the effect of the classifier on the detection results. The initial training set size is often the main factor affecting the performance of the classifier. In order to cope with the current rapid increase in the number of pipe network vulnerabilities, we need to achieve better detection results even in the small initial training set. Therefore, we finally analyze the results of different initial training set to illustrate the practicality of our method. In all the experiments, we have conducted 10 experiments at the specified initial training set size to ensure the randomness of the experiment.

To evaluate the effect of the detection, we adopt the false positive rate and the true positive rate to evaluate the detection results, and use the accuracy and error rate to compare the detection results of different methods. Specifically, assuming that the number of samples actually judged to be malicious by the modeling method is FP, the number of samples actually being malicious is TP; in the samples that are actually normal samples in the modeling method, the number of actually normal sample is TN, and the number of actually malicious samples is FN. The false positive rate, true positive rate, accuracy and error rate are defined as follows:

False positive rate $= \frac{FP}{TN+FP}$, True positive rate $= \frac{TP}{TP+FN}$,
Accuracy $= \frac{TP+TN}{TP+FN+TN+FP}$, Error $= \frac{FP+FN}{TP+FN+TN+FP}$.

3.2. Experimental results

3.2.1. Influence of different similarity evaluation methods on the results. We compare the effect of node similarity evaluation on the vulnerability of pipe network under the three different network structures proposed in Section 3.2. As shown in Fig. 1, two initial training sets with different sizes are selected as

$$\left|L^0\right| / \left(\left|L^0\right| + |U|\right) ,$$

which are compared with the nearest neighbor classifier in the k nearest neighbors classifier, without using (baseline, training the classifier only on the initial training set) and using the complex pipe network method under the test results. At the same time, we have also compared the influence of the sample size of the complex pipe network on the detection results, that is, the ratio of the step size

$$K = \left(\left|L^0\right| + |U|\right) ,$$

in the input of Algorithm 1. 10 experiments have been conducted under each experiment setting, and Fig. 1 shows the average accuracy and the standard deviation of 10 experiments.

As shown in Fig. 1, upper part, when only 1 % sample are selected as the initial

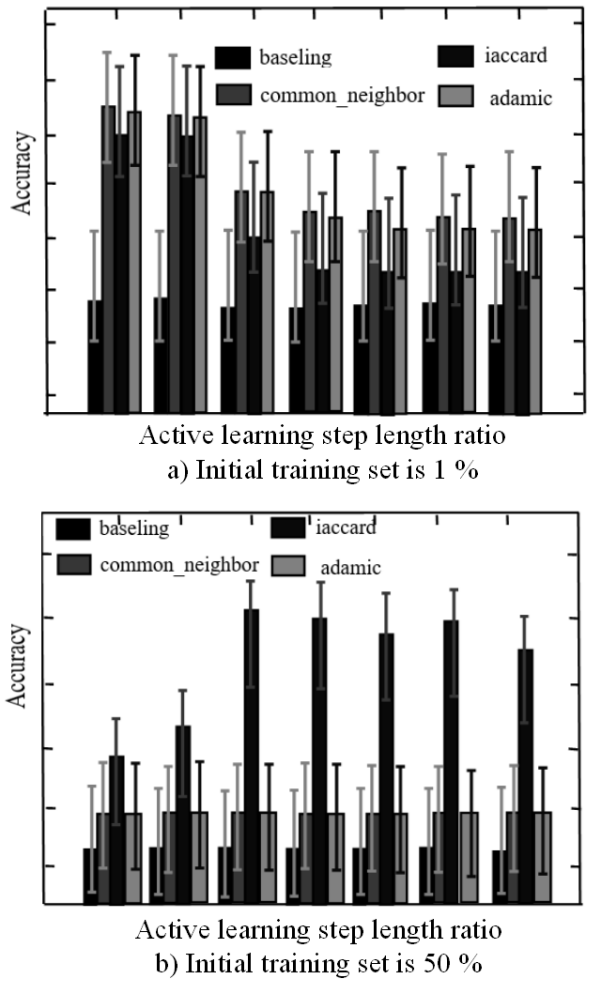

Fig. 1. Accuracy of the similarity evaluation in different complex pipe network sample step length ratio: up–initial training set size is 1 %, bottom–initial training set size is 50 %

training set, the method of the complex pipe network decreases with the increase of the sample ratio of the complex pipe network. The baseline method is less effective than the 95 % confidence interval for the detection accuracy of the complex pipe network method when 1 % or 2 % of the samples are collected in each round of the complex pipe network, indicating that in both cases the three complex pipe network methods are significantly superior to those without the application of the complex pipe network. Moreover, the similarity evaluation method using public neighborhoods is superior to the other two evaluation methods. On the other hand, it can be seen from Fig. 1, bottom part, that, under the condition of selecting 50 % sample as the initial training set, the method of the three kinds of complex pipe network in all

complex pipe network sample ratio is significantly superior to the methods without the application of the complex pipe network. In addition, the Jaccard coefficient similarity evaluation method is superior to the other two evaluation methods in contrast to Fig. 1, upper part. At the same time, with the increase of the proportion of complex pipe network samples, the accuracy of the method based on the public network and Adamic's complex pipe network did not change significantly. Based on the observation in Fig. 1, it is inferred that different similarity evaluation methods have different effects on the detection of the vulnerability of the pipe network under different training set sizes. In order to verify this hypothesis, Figure 2 shows the detection accuracy of the complex pipeline network method under different initial training sets under the two steps of the complex pipe network ratio (1 % and 50 %) and the three similarity evaluations.

Comparing Fig. 2, upper part and Fig. 3, bottom part, the accuracy of the complex pipe network method is the same as that of the initial training set under the two steps of the complex network. And Jaccard coefficient can get better detection accuracy than public neighborhood and Adamic in the case of known large training samples. Under the known initial training set, the method of complex network based on public neighborhood can get better detection accuracy. Furthermore, the detection of pipeline vulnerability is often concerned with the detection of false alarm rate and true positive rate.

3.2.2. Influence of the initial training set size and complexity of the pipe network sample ratio on the results. From the experiments in the previous section, we find that the number of samples of the same complex pipe network has different effects on the detection results under the initial training set of different sizes. Moreover, the number of samples in each round of complex pipe network will directly affect the number of rounds needed to complete all the sample forecast, thus affecting the efficiency of pipe network vulnerability detection. In order to further understand the impact of each round of complex pipe network on the detection results, Figure 3 shows the initial test sample accuracy of the nearest neighbor classifier in different initial training setting after the calibration of each round of complex pipe network. It can be seen from Figure 3 that, when a small training set (1 %) is known, a complex network of small samples (1 %, 2 %) per round in the previous rounds of complex pipe network processes Can effectively guarantee the accuracy rate. This shows that the complex network can provide an effective sample network for the pipe network vulnerability detection complex network strategy to improve the accuracy of pipe network vulnerability detection. However, there are some common passage behaviors of the current classifier in the fluid flow sample that cannot distinguish the samples effectively based on the complex network method according to the complex network. It requires us to propose more effective classification methods to further improve the detection results. On the other hand, when the training set is known to be sufficient (50 %), as shown in Fig. 3, bottom part, the previous rounds of complex pipe network can effectively improve the detection accuracy. However, when the number of complex pipe network samples is small (1 %, 2 %), the accuracy of the last few rounds of learning also shows significant declination. We further analyze the

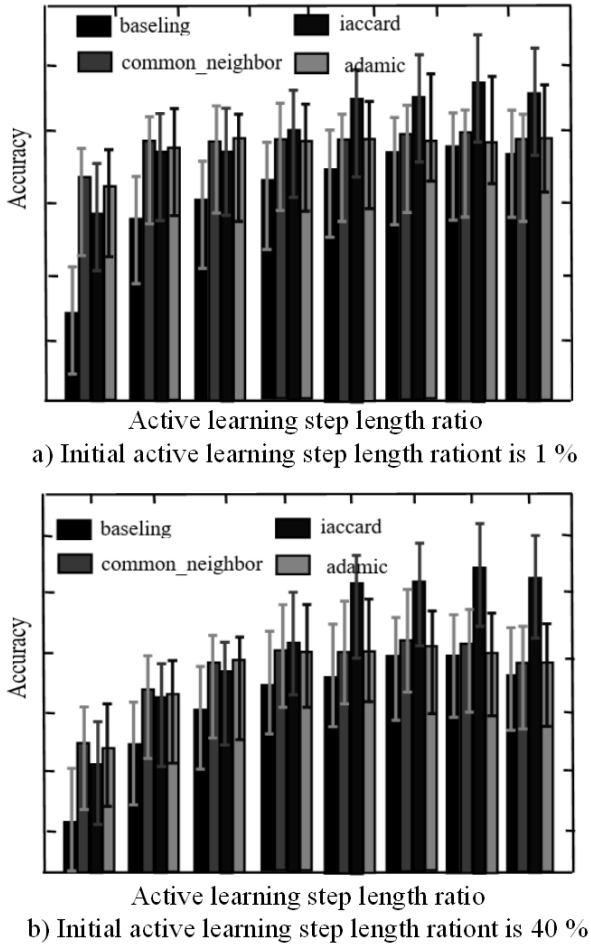

Fig. 2. Accuracy of similarity evaluation under different initial training set: up–initial active learning step length ratio is 1 %, bottom–initial active learning step length ratio is 40 %

complex pipe network processes with 1 % and 50 % of the initial training set and 1 % step size. We find that in the last few rounds of the complex pipe network process, the estimated risk of unknown samples, equation (1), appears to rise markedly. Also, samples with higher estimated risk are similar to the behavior of many unlabeled samples, where false predictions directly lead to subsequent errors in other unlabeled samples that resemble them. In general, the number of high-risk fluid flows is small on the basis of the complex pipeline network method. In the actual pipe network vulnerability environment, the samples with higher risk can be estimated by manual analysis to match the complicated pipe network, which can more effectively complete the pipe network vulnerability examination.

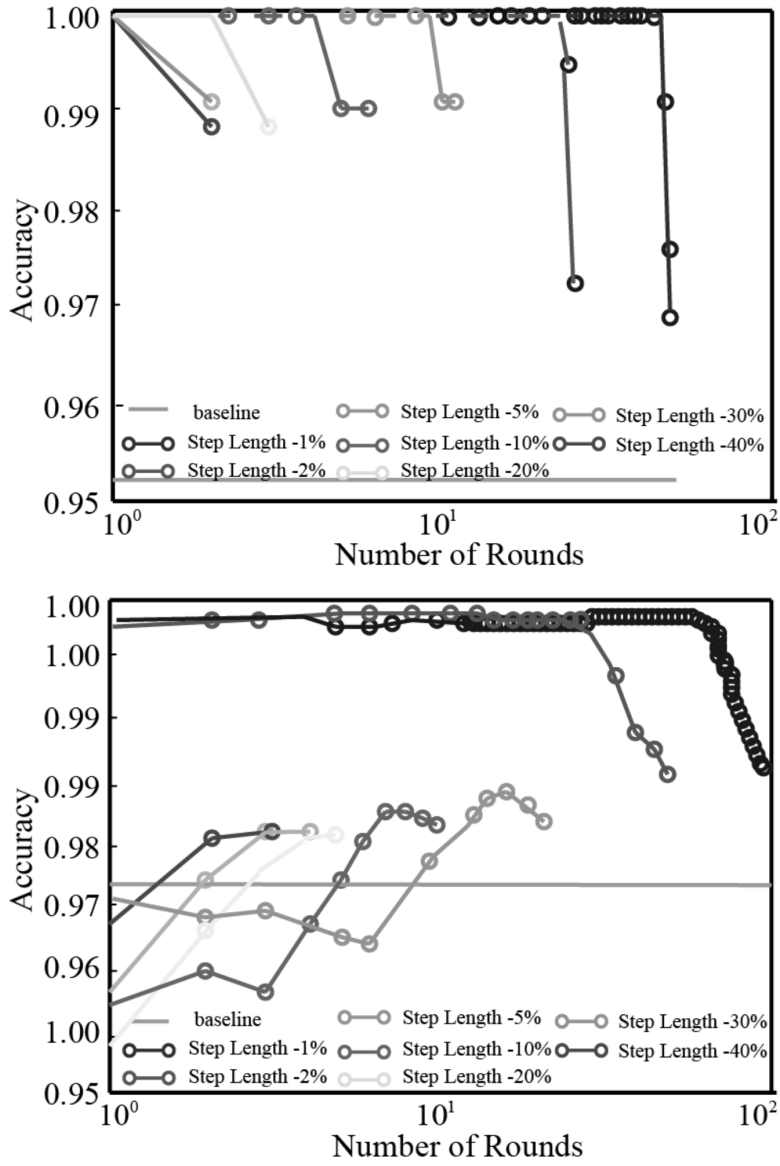

Fig. 3. Accuracy of the initial test sample after the calibration of the nearest neighbor classifier for each round of complex pipe network: up–initial training set of public neighborhoods is 1 %, bottom–initial training set of Jaccard coefficient is 50 %

In order to provide the basis for the selection of the pipe network vulnerability modeling methods under different real environments, we analyzed the best detection method under the initial training set of different sizes. Table 1 shows the method with the baseline (classifier, similarity evaluation method) under different experi-

mental settings (initial training set size, complex pipe network step length ratio).

Each cell in rows 2–8 of Table 1 shows the initial training set size represented by the column in which the line stands for the lowest average detection error rate for the complex pipe network step length ratio (Classifier - similarity), and the average error rate of the method. Line 9 shows the classifier with the lowest error rate in both classifiers (nearest neighbor, random forest) and its detection error rate without adding the complex pipe network. In addition, we have emphasized the complex network of pipe networks with the lowest average error rate in each column.

Table 1. Modeling method with the minimum error rate under different initial training set sizes and the average error rate

Complex pipe network step length ratio	Initial training set					
	1 %	2 %	5 %	10 %	20 %	50 %
1 %	knn-cn	knn-cn	knn-ada	knn-jac	knn-jac	knn-jac
	5.55 %	4.75 %	4.59 %	4.30 %	3.64 %	3.10 %
2 %	knn-cn	knn-cn	knn-cn	knn-jac	knn-jac	knn-jac
	5.70 %	4.75 %	4.56 %	4.19 %	3.36 %	2.80 %
5 %	rf-cn	knn-cn	knn-cn	knn-jac	knn-jac	knn-jac
	7.06 %	4.95 %	4.53 %	3.95 %	2.92 %	0.91 %
10 %	rf-cn	knn-cn	knn-ada	knn-jac	knn-jac	knn-jac
	7.16 %	5.54 %	4.66 %	3.78 %	2.90 %	0.94 %
20 %	rf-cn	knn-cn	knn-cn	knn-jac	knn-jac	knn-jac
	7.10 %	5.62 %	4.74 %	3.90 %	2.78 %	1.24 %
30 %	rf-cn	knn-cn	knn-cn	knn-jac	knn-jac	knn-jac
	7.16 %	5.68 %	4.95 %	3.96 %	2.67 %	0.94 %
40 %	rf-ada	knn-cn	knn-cn	knn-jac	knn-jac	knn-jac
	7.03 %	5.77 %	4.97 %	4.02 %	2.65 %	1.17 %
Baseline	rf	knn	knn	knn	knn	knn
	8.74 %	6.80 %	5.80 %	5.22 %	4.96 %	4.80 %
Error rate reduction ratio	36.50 %	30.15 %	21.90 %	27.59 %	46.57 %	81.04 %

For example, when only 1 % of the training samples are known, the neighbor neighborhood classifier with 1 % sample per round of the complex network has the lowest average detection error rate of 5.55 %, using the common neighborhood as the similarity evaluation. The last row shows that the complexity of the pipe network method with the lowest average error rate can reduce the error rate relative to the baseline using only the classifier. It can be seen that, when the size of the training

set is known to increase, the step length ratio of the complex pipe network can be improved to obtain better detection results. Similar to the observations described above, the similarity evaluation based on the common neighbor is better when the number of training set samples is less ($\leq$5 %). When the training set is larger ($\geq$10 %), The similarity evaluation based on Jaccard coefficient can obtain better detection result. At the same time, we find that, when the ratio of the step length ratio of the complex pipe network is selected to be close to the initial training set, no matter which kind of classifier or similarity evaluation method is selected, complex pipe network method can always reduced the detection error rate significant. In our experiment, the pipe network vulnerability modeling method of the complex pipe network has reduced the error rate by 40.6 % compared with the modeling method using only the classifier; in the case of only 1 % known samples, the error rate is decreased by 36.5 %.

4. Conclusion

At the beginning of the emergence of new pipe network vulnerability, the number of samples that are available for analysis is limited, which has presented a challenge for the timely and effective detection of the new pipe network vulnerabilities and their variants. In this paper, a method of pipe network vulnerability modeling based on the complex pipe network in combination with the anomaly degree and similarity of the passage behavior of the fluid flow is proposed from the data dependency network accessed by the resources in operating system. We have analyzed the data dependency relationship of the resource passage behavior and constructed the data dependency network to describe the resource access of the whole system. In addition, though analyzing the network structure, the important resource object for the fluid flow access is identified, and the pipe network vulnerability modeling method based on passage flow behavior anomaly degree is designed. At the same time, the similarity of the fluid flow passage behavior is measured under the network structure, and the classifier for pipe network vulnerability detection is studied incrementally by using the method of complex pipe network, so as to put forward a new method for the modeling of the pipe network vulnerability in combination with the anomaly degree and similarity of the passage behavior of the fluid flow. Through the experimental verification of 8.340 normal pipe network flows and 7.257 pipe network vulnerability samples of Windows XP sp3 user, we found that, the method of the complex pipe network has improved the performance of the pipe network vulnerability detection compared to the traditional method based on statistical classifier. In addition, the error rate of the method proposed in this paper is reduced by 36.5 % compared with the traditional method based on the statistical classifier under the condition of only 1 % known samples. The results show that our method can effectively respond to the situation of the rapid growth of the new pipe network vulnerability at present.

References

[1] Q. Shuang, M. Zhang, Y. Yuan: *Node vulnerability of water distribution networks under cascading failures.* Reliability Engineering & System Safety *124* (2014), 132–141.

[2] Q. Shuang, M. Zhang, Y. Yuan: *Performance and reliability analysis of water distribution systems under cascading failures and the identification of crucial pipes.* PloS ONE *9* (2014), No. 2, 88445.

[3] S. Esposito, S. Giovinazzi, L. Elefante, I. Iervolino: *Performance of the L'Aquila (central Italy) gas distribution network in the 2009 (M_w 6.3) earthquake.* Bulletin of Earthquake Engineering *11* (2013), No. 6, 2447–2466.

[4] G. Beaulieu, D. Austin, M. L. Leonard: *Do nest exclosures affect the behaviour of Piping Plovers (Charadrius melodus melodus) and their predators?* Canadian Journal of Zoology *92* (2014), No. 2, 105–112.

[5] A. J. Whelton, T. Nguyen: *Contaminant migration from polymeric pipes used in buried potable water distribution systems: A review.* Critical Reviews in Environmental Science and Technology *43* (2013), No. 7, 679–751.

[6] R. Wang, D. G. Feng, Y. Yang, P. R. Su: *Semantics-based malware behavior signature extraction and detection method.* Journal of Software *23* (2012), No. 2, 378–393.

[7] D. Valis, K. Pietrucha-Urbanik: *Contribution to diffusion processes application in the area of critical infrastructure security assessment.* Applied Mechanics and Materials *436* (2013), No. Chapter 6, 539–548.

[8] S. A. Welsh, Z. J. Loughman: *Upstream dispersal of an invasive crayfish aided by a fish passage facility.* Management of Biological Invasions *6* (2015), No. 3, 287–294.

[9] D. Valis: *Contribution to assessments of impacts on the critical infrastructure.* Applied Mechanics and Materials *656* (2014), No. Chapter 5, 578–587.

Received June 6, 2017

Acta Technica *62* No. 1A/2017, 521–530

Design of high-speed acquisition system based on computer fuzzy image and information data

Guo Lei[1], Gao Zhigang[2]

Abstract. In order to meet the requirements of fuzzy image display, performance prediction accuracy and collection efficiency in various fields, high-speed acquisition system based on computer fuzzy image and information data was designed in this paper. In the design of this system, the rasterization operation on the fuzzy image data was carried out by the fuzzy image processing module of the system, and the obtained black and white pixel images were rendered. The rendered black and white pixel images were partially and integrally filled with color respectively by the vertex shader and the pixel shader in the color fill module, and the full color image of the obtained fuzzy image was transmitted to the computer monitor for display. Kalman filter was used to process the fuzzy image information data. The final experimental results show that the system designed in this paper has high display effects, accurate behavior prediction and collection efficiency.

Key words. Fuzzy image, high-speed acquisition system, system design.

1. Introduction

The high-speed acquisition system of image information data is widely used in the fields of public security, fire protection, aviation and spaceflight. Restricted by the speed of object motion, the high-speed motion objects have a high probability of producing blurred images. In many cases, the information contained in the blurred image is very important, so the high-speed acquisition of the fuzzy image data has become the focus of the scientific research organizations. High-speed acquisition system of fuzzy image data from previous studies used a variety of acquisitions, but they were unable to meet the requirements of fuzzy image display, behavior prediction and the collection efficiency of the system in various fields. In the image acquisition system, the real-time processing is the core of the system. In traditional image acquisition system, the system design of "camera-image card-computer" is usually adopted. The image algorithm is implemented by computer software, which

[1]Xi'an Aeronautical University, Xi'an 710077, China
[2]College of Astronautics, Northwestern Polytechnical University, Xi'an 710072, China

can meet the practical application in low speed and single sensor image acquisition. However, in a high-speed image acquisition system, the frame speed of the high speed camera usually reaches 100-200 frames per second. In the multi sensor visual testing system, the serial operation of sensors, the input and output ports, the transmission speed and all algorithms can only be implemented by software with many other restrictions, so it is difficult to guarantee the real-time performance of the system.

2. State of the art

At present, great progress has been made in the design of high speed data acquisition system. However, the focuses of the performance of the high speed data acquisition system for blurred images in the past were different, but they were all unable to achieve the high-performance design. For example, the high-speed acquisition system for blurred image information based on FC-AE-ASM is a high-speed acquisition system of fuzzy image information designed on the basis of aviation information collection system, and it can realize super high-speed acquisition of fuzzy image information data. The whole system has high prediction level and display level, and its collection efficiency is acceptable, but it is expensive, so it is less used in daily enterprises [1]. High-speed acquisition system of blurred image based on PXI bus carried out the design of display terminal for fuzzy image restoration, used the display processor optimization of acquisition high performance resources, and realized the display of high-level fuzzy image by the system, but the collection efficiency of this system still has more rooms for improvement [2]. On the basis of guaranteeing the display level, the high-speed acquisition system of the fuzzy image data based on FPGA and USB can effectively improve the processing and storage efficiency of the system by using FPGA and USB. But the functions of the system are simple, so it is only suitable for fields without high demands for high-speed acquisition system of fuzzy image. In order to improve the display effect, performance prediction accuracy and collection efficiency of the system, a high-speed acquisition system of high-performance fuzzy image data is designed [3]. In addition, machine vision has been developed in recent years. It uses charge coupled devices or CMOS cameras to ingest images and convert them into image signals, and then sends them to the image processing system, so as to obtain morphological information captured targets, such as pixel distribution, brightness, color, and to change them into the digital signal (Li et al. 2015) [4]. Through image enhancement, image segmentation and other means of processing, it can extract target features, and then make judgments and give control actions and other measures. Machine vision is widely used in many fields, such as face recognition, tracking and localization, real-time monitoring, printed product quality inspection, image coding, security surveillance and so on, and it plays an increasingly important role [5].

3. Methodology

The high-speed acquisition system of fuzzy image data has many hardware devices. The system uses the visual processor, the coordinate processor, the fragment processor, and shader to collect fuzzy image information data and uses the Kalman filter for auxiliary operation, so the system can achieve the high-level display of blurred images by the system, accurate prediction of behavior, and high-speed acquisition. The operating flow of the whole system can be observed by computer [6].

The fuzzy image processing module uses the visual processor, the frame buffer, the coordinate processor and the fragment processor to process the data of fuzzy image. Visual processor unit (GPU) is a kind of display chip especially for image processing and computer CPU image processing (Guo et al. 2014) [7]. In the processing of the fuzzy image information, the acquisition of the target image coordinate is the basic work of the visual processor. The coordinate value of the target image is processed by the coordinate processor and is then transmitted to the frame buffer for temporary storage. The coordinate processor first transforms the stereo coordinates of the target image into two-dimensional coordinate, then converts the blurred image into the raster image by the rasterization operation and carries out the block restoration on the raster image, thereby resulting in black and white pixels [8].

In order to read black and white pixels information of fuzzy image, it is necessary to connect the frame buffer through the bidirectional diagnostic control interface and display the processing result directly on the computer screen [9]. Black and white pixel images need to be rendered to match the hue of the blurred image. Figure 1 shows the structure of the rendering pipeline of the blurred image processing module.

As can be seen from Fig. 1, the rendering of the visual processor is performed mainly by coordinate processors and fragment processors. The amount of memory that a coordinate processor and a fragment processor can hold is extremely low, so they can only process the black and white pixel image data of the blurred image in real time, and the output of the results will be stored in the frame buffer. The coordinate processor processes the coordinate values of the black-and-white pixel image information data, and the processing result is transmitted to the fragment processor. At the same time, the visual processor transmits the original blurred image information to the fragment processor via its own interface. The fragment processor simulates its texture memory before receiving the original fuzzy image information data, so as to improve the computing power of the fragment processor, which is convenient to the zero offset rendering of black and white pixels by the fuzzy image processing module [10].

The color flow of vertex shader to black and white pixel images and the processing flow of fuzzy image processing module are corresponding. A fuzzy image processing module is used to process the blurred image, and the processing results are transmitted to the vertex shader for real-time color filling [11]. The structure of the vertex shader is shown in Fig. 2.

As can be seen from the diagram, vertex shaders have strong computing abilities, and they can handle four different types of registers at the same time. Color spaces

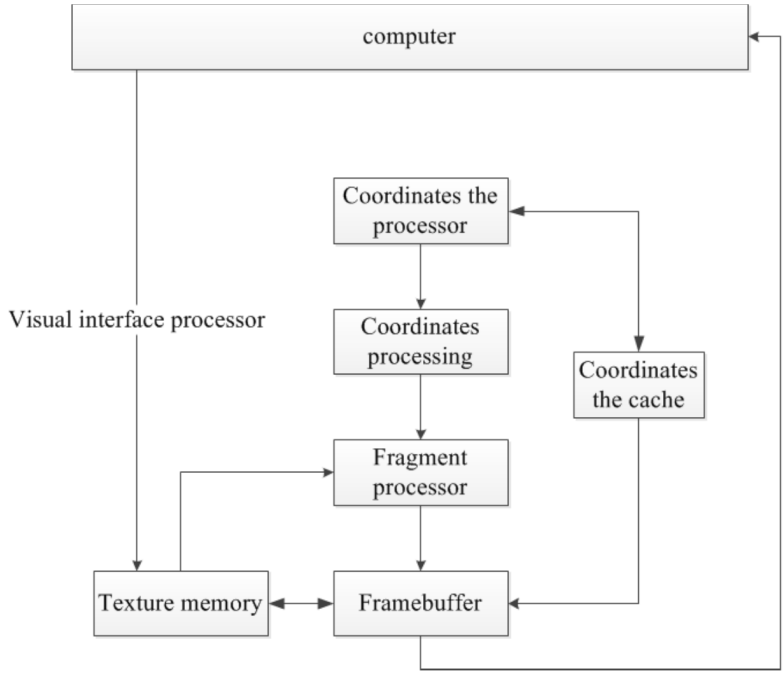

Fig. 1. Structure of the rendering pipeline of the blurred image processing module

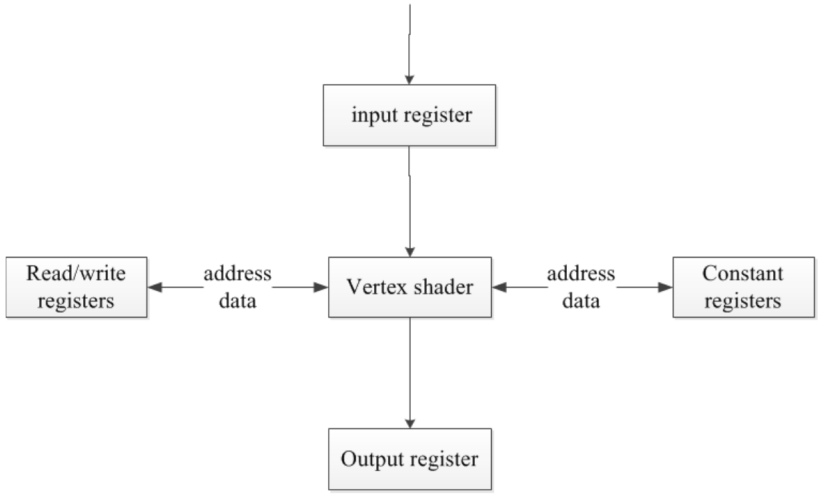

Fig. 2. Structure diagram of vertex shader

are usually divided into four types: red space, blue space, green space and three primary colors. The colors in the original blurred image are classified into four color spaces, and each color space is selected by a different register, so there are 4 different types of registers in the vertex shader. Registers store fuzzy image color information

data, and other fuzzy image information data are also stored completely in real time. The input register stores data such as vertex coordinates, prediction displacement and prediction speed; the output register stores the color fill results of the vertex shader; the register and constant register are directly controlled by computer; the computer stores the coloring algorithm and language of the high-speed acquisition system of the fuzzy image information. Registers are also often used as temporary storage areas for data information of target objects in blurred images.

The pixel shader processes the rendered black and white pixel images in two ways: texture memory sampling and pixel computing. The pixel shader operator can provide add, multiply, dot product and so on for the high-speed acquisition system for blurred image information, and texture memory sampling and pixel computing are performed in the arithmetic unit. The operator samples the texture coordinates in the original fuzzy image data, and then obtains the important information data by pixel calculation. The pixel shader fills the black and white pixel images with large areas of color based on pixel results. At the same time, the filling result of the vertex shader is also passed to the pixel shader's storage register, and the operator combines the fill results of the two shaders to produce full color images. Finally, through the output register, the full color image information of the blurred image is transmitted to the computer display.

Kalman filtering is an optimal estimation method based on linear function observation data, and each processing process of the fuzzy image information data is well stored. When the system processes the fuzzy image information again, it will refer to the previous processing flow, and compare and perfect the reference value and the actual processing result, until the optimal processing result is obtained.

The fuzzy image model is constructed and the Kalman filter is used to analyze the fuzzy image parameters, so as to divide the fuzzy image information data and combine them into a plane fuzzy image, and the reason is that the information data plane blurred image is more intuitive.

Supposing that the length and width of a rectangular fuzzy image $g(k, j)$ to be processed are the ranges of horizontal and vertical coordinates of fuzzy image in model M, N, k, j respectively, the image split after the initial blurred image can be shown as$f(k, j)$, as shown in the formula

$$f(k, j) = Af(k - 1, j) + v(k - 1, j)\,. \tag{1}$$

Here, A is the fuzzy image matrix, and its value is related to k under special conditions; v is the estimated value of preprocessing of fuzzy image and it is often expressed as a unary regression function. With the deformation treatment to formula (1), the fuzzy image estimation $g(k + 1)$ can be obtained, as formula

$$g(k + 1) = HAf(k - 1, j) + Hv(k - 1, j) + n(k, j)\,. \tag{2}$$

Here, $k \in [0, M]$, $j \in [0, N]$, and k and j are natural numbers; H is transfer matrix of split image in blurred image and $n(k, j)$ is the estimated value of fuzzy image processing by Kalman wave filtering.

According to formulae (1) and (2), the restoration equation of the blurred image

is shown in the formula

$$f(k) = f(k-1) + K(k)e(k)\,. \tag{3}$$

In the above formula, $e(k)$ is the difference between the actual value and the estimated value, so it is called the estimated optimization value; $K(k)$ is the weighting function of $e(k)$, and its value is equal to the inverse matrix of H. The bigger $K(k)$ is, the higher the sharpness of the image collected by the high-speed acquisition system of the blurred image information data will be and the smaller the system acquisition error will be. Using the following expressions, $K(k)$ can be obtained in this way

$$K(k) = P_1(k)H^{\mathrm{T}}[HP_1(k)H^{\mathrm{T}} + R(k)]^{-1}\,, \tag{4}$$

$$P_1(k) = AP(k-1)A^{\mathrm{T}} + Q(k-1)\,, \tag{5}$$

$$P(k) = P_1(k) + K(k)HP_1(k)\,. \tag{6}$$

Here, T represents one-dimensional length of the fuzzy image, $P(k)$ is the minimum estimation bias matrix for optimal gain, $P_1(k)$ is the estimation bias matrix of $Af(k-1)$, Q is the covariance function of v and R is the covariance function of n.

In order to reduce the computational complexity of the fuzzy image data high-speed acquisition system, the one-dimensional image collected by the system should be restored. Now that the one dimensional images are moving in uniform rectilinear motion; based on the Kalman wave filtering, $HAf(k-1)$ can be calculated, and then the estimated optimization value of $e(k)$ can be obtained, using the formula

$$e(k) = g(k) - HAf(k-1)\,. \tag{7}$$

The recovered estimate is shown in the formula

$$f(k) = e(k) + Af(k-1)\,. \tag{8}$$

4. Result analysis and discussion

In the experiment, the display level, the performance prediction accuracy and the collection efficiency of the high-speed image acquisition system designed by the fuzzy image data were verified. The verification method was that the high-speed acquisition system with high performance of fuzzy image information was compared with the system designed in this paper. The selected contrast systems were the high-speed image acquisition system based on PXI bus and the high-speed acquisition system based on FPGA and USB for the fuzzy image information.

The experiment tested the display effect of the three systems, on the blurred image first. Figure 3 shows initial fuzzy images that needed high-speed acquisition of information data. With the acquisition of the blurred image by the three systems under the same conditions, the output results were obtained, as shown in Figs. 4–6.

Fig. 3. Initial fuzzy image

Fig. 4. Output image of high-speed acquisition system of blurred image information based on FPGA and USB

As can be seen from Figs. 4–6, the high-speed acquisition system of fuzzy image information based on FPGA and USB could barely display the license plate of the blurred image in the experiment under the same conditions. But in the complex fuzzy image, it could be seen as invalid display. Therefore, on the basis of guaranteeing the display level, the high-speed acquisition system of the fuzzy image data based on FPGA and USB effectively improved the processing and storage efficiency of the system by using FPGA and USB. But the functions of the system were simple, so it was only suitable for fields without high demands for high-speed acquisition system

of fuzzy image. The high-speed acquisition system of fuzzy image information based on PXI bus had good display effects, but it carried out the design of display terminal for fuzzy image restoration, used the display processor optimization of acquisition high performance resources, and realized the display of high-level fuzzy image by the system. So the collection efficiency of this system still has more rooms for improvement. Compared with the two systems, the display effects of this system are closer to the real object, so the system has excellent display effects.

Fig. 5. Output image of high-speed acquisition system of fuzzy image information based on PXI bus

Fig. 6. Output image of the system presented in this paper

The experiment also used the prediction of the behavior of the cars in figure 4 by these three systems (the direction of the north was 0°), and analyzed the working

hours of the three systems statistically. Table 1 shows a comparison table of the behavior prediction of three systems, and Table 2 shows the statistical table of the total use time of three systems.

Table 1. A comparative table of behavior predictions for three systems (°)

	Based on PXI bus	Based on FPGA and USB	System in this paper
Actual direction of the car	-90	-90	-90
Predicted vehicle direction	-86	-88	-90
The actual running direction of the front wheel	-60	-60	-60
Predicted front wheel running direction	-57	-58	-60
Actual running direction of the rear wheel	-40	-40	-40
Predicted rear wheel running direction	-56	-56	-40

Table 2. A statistics table of total usage statistics for three systems (ms)

Experimental data acquisition system	Processing time	Acquisition time	Total useful time
Based on PXI bus	16	10	26
Based on FPGA and USB	11	8	19
System in this paper	9	5	14

As shown in Table 1, the prediction accuracies of the three systems were remarkable, but the prediction accuracy of the system in this paper reached 100 %, so the system had extremely good predictive abilities. Table 2 shows that the total working time of the system in this paper on the blurred image in Fig. 4 was 14 ms, which was lower than that of the high-speed acquisition system based on fuzzy image data of FPGA and USB for 5 ms and lower than that of the high-speed acquisition system based on fuzzy image data of PXI bus as 12 ms. So it was proved that the system in this paper has the advantage of high collection efficiency. The experimental results show that the system designed in this paper has better display performances, the accuracy of prediction and the collection efficiency.

5. Conclusion

The system designed in this paper used fuzzy image processing module to raster the data of fuzzy image and to render images of black and white pixels, and used Kalman filter to deal with fuzzy information of image data. Through this study, the

following conclusions were obtained: the efficient processing of high-speed acquisition system of fuzzy image data of the fuzzy image data is based on the high speed and accurate acquisition of fuzzy image data. If the processing result is not accurate, all the works performed by the collector are invalid. The system uses Kalman filter to process the fuzzy image information data, so the data are more easily to be collected. After the visual processor is rendered, the image data of black and white pixel still has some differences with the original fuzzy image information data. Combining vertex shader and pixel shader and filling black and white pixel image can guarantee the display effect of fuzzy image data high-speed acquisition system on fuzzy image, and also can improve the collection efficiency of the system. However, there are still some defects that need to be improved in this paper. For example, the high-speed acquisition system and the computer network system can be combined to achieve real-time data acquisition and delivery.

References

[1] Z. J. Geng: *Rainbow three-dimensional camera: New concept of high-speed three-dimensional vision systems.* Optical Engineering *35* (1996), No. 2, 376–383.

[2] R. Castañeda-Miranda, E. Ventura-Ramos, R. del Rocío Peniche-Vera, G. Herrera-Ruiz: *Fuzzy greenhouse climate control system based on a field programmable gate array.* Biosystems Engineering *94* (2006), No. 2, 165–177.

[3] Q. Zhou, J. Ma, Y. Dong, J. Li: *Design of the image acquisition system based on the low power microcontroller.* Electronic Measurement Technology *98* (2014), No. 03, paper 023104.

[4] J. Dubois, D. Ginhac, M. Paindavoine, B. Heyrman: *A 10 000 fps CMOS sensor with massively parallel image processing.* IEEE Journal of Solid-State Circuits *43* (2008), No. 3, 706–717.

[5] K. H. Ang, G. Chong, Y. Li: *PID control system analysis, design, and technology.* IEEE Transactions on Control Systems Technology *13* (2005), No. 4, 559–576.

[6] A. Telesca, F. Carena, W. Carena, S. Chapeland, V. Chibante Barroso, F. Costa, E. Dénes, R. Divià, U. Fuchs, A. Grigore, C. Ionita, C. Delort, G. Simonetti, C. Soós, P. Vande Vyvre, B. von Haller: *System performance monitoring of the ALICE data acquisition system with Zabbix.* Journal of Physics: Conference Series *513* (2014), No. 6, paper 062046.

[7] Y. N. Wang, T. Chen, Z. D. He, C. Z. Wu: *Review on the machine vision measurement and control technology for intelligent manufacturing equipment.* Control Theory & Applications *3* (2015), No. 03, 273–286.

[8] M. Delbracio, P. Musé, A. Almansa: *Non-parametric sub-pixel local point spread function estimation.* Image Processing On Line *10* (2012), No. 2, 8–21.

[9] Y. Y. Lei, L. I. Zhi: *Design of data acquisition system based on producer/consumer.* Machinery (2011), No. 09.

[10] M. N. Inanici: *Evaluation of high dynamic range photography as a luminance data acquisition system.* Lighting Research & Technology *38* (2006), No. 2, 123–136

[11] F. Ran, H. Yang, S. P. Huang: *Design of real-time color video capture system for area array CCD.* Optics and Precision Engineering *18* (2010), No. 1, 273–280.

Received June 6, 2017

Acta Technica *62* No. 1A/2017, 531–540

Hierarchical phrase machine translation decoding method based on tree-to-string model enhancement[1]

Ximeng Wen[2]

Abstract. Statistical machine translation model based on the syntax has gained unprecedented growth over the last ten years. In order to study the hierarchical phrase machine translation decoding method based on tree-to-string model enhancement, the hierarchical phrase model was used as the basic model in this paper. The tree-to-string model was used as a supplementary of hierarchical phrase model to increase the size of the translation inference space. And statistical machine translation decoding technology was mainly studied. Several decoding strategies including exact decoding strategy based tree, fuzzy decoding strategy based tree and decoding strategy based string were proposed. Finally, the experimental results on the NIST Chinese English translation task confirmed that the method studied in this paper could improve the translation performance of the baseline hierarchical phrase system effectively. For example, the data on newswire and web were raised by 1.3 and 1.2 BLEU points, respectively.

Key words. Hierarchical phrase model, tree-to-string model, machine translation decoding.

1. Introduction

The most successful statistical Machine translation model based syntax is a synchronous context free grammar based on hierarchical phrase model. In this model, no target language or source language syntax information is used to restrict translation in the process of extracting translation rules, so as to satisfy the learning of a large number of translation rules. However, the number of translation rules cannot be extended. Therefore, in order to control the number of translation rules, they are made within the acceptable range of the machine. The most common method is to set some restrictions in the extraction and use of hierarchical phrases, so as to achieve this effect. For example, the source language span referenced in decoding cannot exceed a threshold value. These restriction rules have already achieved good

[1]This work is supported by project from Education department of Hainan province, Automobile English (NO. Hyjc2011-11).

[2]Hainan College of Vocation & Technique, Haikou, Hainan, 570100, China

results and can even help the hierarchical phrase system to be practical. When the syntax needed to translate is complex or problems that need to be dealt with are dependent on long distance dependencies, these limitations also lead to a significant reduction in the processing power of hierarchical phrase systems. In order to better solve this problem and make the hierarchical phrase system have better translation and decoding performance, there are generally two ways to consider. The first is to add syntactic features of the target language to the system. The second is to combine hierarchical phrases with tree-to-string systems based on the idea of system integration. And the second method is the method which this article carries on the thorough discussion.

2. State of the art

Many scholars have begun to study and explore the language between machine translation since the beginning of the design and manufacture of the first computer. Rule-based methods were the mainstream method of machine translation research until 90s [1]. The statistical machine translation method was based on the content of Brown and other papers in 1993. The word based statistical machine translation method was first proposed innovatively [2]. This approach is a reversal of the process of translation and considers the target language sentence E as the input of the channel, it distorts through the noise channel, and the output side outputs the source language sentence, that is to say, it is needed to find the target language sentence to product F. At some level, the translation model and the language model reflect the fidelity and fluency of translation. At the time, the performance of this translation method exceeds that of rule-based SYSTRAN system, which attracts many researchers' interest [3]. Since then, more and more scholars have begun to do research on large-scale bilingual corpus analysis, probabilistic translation model exploration and model parameter research, which has opened up the era of machine translation and made many important breakthroughs. Phrase model performance growth has slowed down in recent years. This is mainly because only the size of the translation granularity is changed but there is no fundamental solution to the problem of remote reordering and lack of global information, which makes the model exhibit a plateau trend [4]. Yamad proposed the first statistical machine translation model based on syntax in 2001. In 2005, Chiang combined the model based phrase with the idea of tree structure and proposed an efficient decoding algorithm based on hierarchical phrase model and line graph analysis. The model is modeled based on simultaneous upper and lower independent grammars and does not use any of the displayed annotation information [5].

3. Methodology

Hierarchical phrase model relies on synchronous context free grammar (SCFG). A synchronous context free grammar can describe the generative process of bilingual strings containing hierarchical structures [6]. Formally, a synchronous context free

grammar is represented as a regular system called (N, W_s, W_t, R). Among them, N represents a set of non-terminating symbols, W_s and W_t represent termination symbols (or vocabulary) collections of source language and target language. Symbol R represents a production set [7]. Each production in R corresponds to a SCFG rule in the form of $X \to (\alpha, \beta, \sim)$. The resulting left-hand X represents a non-terminating character, α at the right hand represents a source language terminator and non-termination sequences, which is called the source language side, β represents the terminator and non-termination sequence of a target language, which is called the target language side. Finally, $\sim$ represents a one-to-one correspondence between non-terminating characters in α and β. Typically, $\sim$ can be represented as a non-subscript index [8].

Probabilistic synchronous context free grammars can be automatically extracted from word aligned data by using heuristic information [9]. For example, firstly, the initial set of translated phrases can be extracted, and then these initial phrases are used to obtain the translation rules of the hierarchical phrases (i.e., translation rules containing variables). After getting the SCFG rule, the SCFG rules can be used to decode the new sentence and complete the translation of the unknown sentence. An example of a SCFG rule that is extracted from a word - aligned example is given. Among them, rules of h_7, h_1 and h_3 correspond to a translation deduction, which can cover the whole bilingual sentence pair [10]. The decoding problem of hierarchical phrase model can also be treated as syntactic analysis. In other words,the source language side of SCFG is used to analyze the input sentences, and then to construct a SCFG derivation forest (or a hyper-graph structure). The translation model and the language model are used to derive the score, and the optimal derivation and output are obtained in the derivation forest [11].

In real systems, some constraints are introduced to enable the decoding process to be completed within an acceptable time usually. The details are as follows: When decoding, a hierarchical phrase rule can be applied to span size, which is called span limit. The usual limit is 10. The order of a rule (the number of variables allowed by the rule) is usually not more than two. Rule source language side variables can't appear continuously (except for glue rules). Rules must be Wie lexicalization rules (except for glue rules) and so on [12].

Tree-to-string translation model makes the translation process defined as the transformation from the source language to the target language string syntax tree. This translation process can be represented by a series of tree-to-string translation rules [13]. A tree-to-string rule r can be represented as $(s_r, t_r, \sim)$. Among them, s_r represents the source language fragment of the rule. The leaf node of s_r is either a terminator or variable (non-terminator). Symbol t_r represents the target language terminator and sequence of variables of a rule and $\sim$ represents a one-to-one correspondence between the leaf variables in s_r and the variables in t_r. The specific expression is shown in the following formula

$$\mathrm{VP}(\mathrm{VV}(\text{increase})x_1 : NN) \to \text{increases}(x_1)\,. \tag{1}$$

Formula (1) represents a tree-to-string translation rule. The "VP(VV(increase)x_1: NN)" represents the source language syntax tree fragment. "increases (x_1)" is the

target string. x_1 of two sections indicates that variables should correspond to each other.

The extraction of translation rules from tree-to-string is usually achieved by the GHKM method. The basic idea of GHKM method is to use the word alignment information to extract the minimum translation rules from the source language tree and target string [14].

The basic idea of integrating from the tree-to-string model integrated into the hierarchical phrase model is as follows: Hiero and GHKM are used to extract translation rules from bilingual data, at the same time, the extracted translation rules (tree-to-string) extracted by the GHKM method are added to the hierarchical phrase system to supplement the baseline SCFG. It should be noted that this method is different from the traditional system fusion and the mixed translation model, it does not simply equate different models (hierarchies phrases and trees to strings), and then fuse them together. Instead, the hierarchical phrase model is used as the underlying model, and then a small number of tree-to-string rules are used to enforce it [15]. In fact, the advantage of tree-to-string model is used to help the hierarchical phrase model improve its shortcomings, but it is not a symmetric system fusion method. Fig. 1 shows the basic framework of this method. The method uses both Hiero and GHKM methods to obtain rules and get a "larger" SCFG in the rule extraction phase. These SCFG rules of sentence words and syntactic information are used to decode the new sentence.

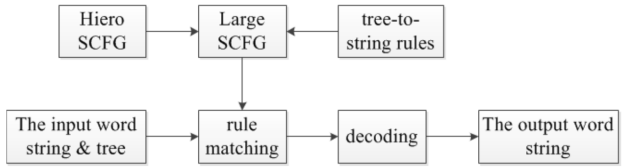

Fig. 1. Framework of tree-to-string model integration in hierarchical phrase system

As shown in Fig. 1, the method used in this paper requires simultaneous extraction of SCFG rules and tree-to-string rules extraction. These two kinds of rules can be obtained by using standard Hiero rule extraction method and GHKM rule extraction method respectively. However, tree-to-string translation rules and SCFG rules have different forms. Therefore, if you want to use tree-to-string translation rules in hierarchical phrase systems, you need to translate them into SCFG rules. Thus, it is possible to indirectly use the tree-to-string translation model information in a decoder based SCFG.

The conversion from tree-to-string rules to SCFG rules is very straightforward. For a given tree-to-string translation rule $(s_r, t_r, \sim)$, the sequence of leaf nodes corresponding to the source language side s_r is used as the source language side of the generated SCFG rule. And t_r and $\sim$ are kept unchanged in the SCFG rule. After that, all syntactic symbols in the rule are replaced by syntactic tags (such as X) used in hierarchical phrase systems, and the rules of SCFG are obtained. Thus, each tree-to-string translation rules will correspond to the only one SCFG rule after the above transformation. Therefore, the above results after translating of the original SCFG and the tree-to-string translation rules are merged to obtain a larger SCFG

rule.

Furthermore, the rules in the merged SCFG are divided into two types of rules. The type 1 rule is a rule that can be extracted by the Hiero. That is to say, all the rules in the baseline hierarchical phrase system are the first type rules. The second type rule is a rule that Hiero cannot extract, but it can be translated from tree-to-string translation rules.

In summary, the basic idea of the tree-to-string model is to obtain the phrase structure tree of the source language by a parser. And then, the tree-to-string alignment template is used to map the phrase structure tree of the source language into the string of the target language. In tree-to-string alignment templates (referred to as TAT), z is a three tuple $tildeT, \tilde{S}, \tilde{A}$). This three tuple describes the alignment relationship $\tilde{A}$ between the source language syntax tree $\tilde{T} = T(f_1^{\Gamma})$ and the target language string $\tilde{S} = S(e_1^{\Gamma})$. In this relation, T is used to represent a syntactic tree, and $T(z)$ is used to represent tree-to-string alignment of trees in template z. Similarly, $S(z)$ stands for tree-to-string alignment of strings in template z. The source language string f_1^{Γ} is the leaf node sequence of T. It may contain either a terminator or a non-terminating (part of speech mark or phrase structure class). The target language string e_1^{Γ} can also contain either a terminator or a non-terminator (placeholder).

The alignment relation $\tilde{A}$ is defined as a subset of the Descartes product of the source language and the target language symbol position, which is shown in the formula

$$\tilde{A} \subseteq \{(j,i) : j = 1 \cdots J', i = 1 \cdots I'\}. \tag{2}$$

Tree-to-string alignment templates can be divided into three categories according to the degree of lexicalization:

The first is the lexicalization alignment template. Leaf node and target language string of any source language syntax tree are all terminators.

The second is a partially lexicalization aligned template. Leaf node and the target language string of the source language syntax tree contain both the non-terminator and the terminator.

The third is a non-lexical alignment template. Leaf nodes and target language symbols of any source language syntax tree are non-terminating characters.

4. Result analysis and discussion

The experiment in this paper was carried out in the Chinese English translation task of NIST. The experiment used 2 million 700 thousand pairs of bilingual data. NiuTrans Hierarchy was chosen as the basic system of experiment, the decoder of the system was based on CKY algorithm, and the beam pruning and cubic pruning were used to speed up the decoder. The feature weights were automatically tuned on the development set by using minimum error rate training. All translation rules were obtained by standard Hiero extraction methods. The maximum span allowed in decoding and basic phrase rule extraction was 10.

The GHKM rules provided by NiuTrans were used to extract module for tree-to-

string rule extraction. Tree-to-string translation rules were extracted from a high-quality quantum set (500 thousand sentences) in training data. Each rule allowed up to 5 terminators and 5 variables at most. In addition, the tree-to-string rule was pruned by using translation probabilities. Pruning included the rule of discarding the forward translation probability which was less than 0.02 and the rule of non-lexicalization of discarding the forward translation probability which was less than 0.10.

Table 1 and Table 2 show the BLEU values for different experiments.

Table 1. BLEU value of Newswire translation system

	Tune	MT08	MT12	MT08.p	All test
	1181	691	400	688	1779
Standard hierarchical phrase base system	36.70	32.50	33.30	31.90	32.79
Exp01+ syntax soft constraint (feature)	36.84	32.44	33.30	31.99	32.83
Exp01+ removes span constraint	36.80	32.54	33.32	31.99	32.86
Exp03+ tree-to-string rule	37.19	33.06	33.79	32.27	33.20*
Exp04+ tree-to-string characterization	37.26	33.15	33.82	32.39	33.28**
Exp04+ fuzzy syntax mark	37.24	33.20	33.90	32.39	33.32**
Exp04+ fuzzy tree structure	37.45	33.39	33.97	32.66	33.49**
Exp04+ fuzzy tree structure & syntax mark	37.47	33.42	34.08	32.78	33.57**
Keywords Exp04+ based decoding	37.61	33.63	34.12	32.88	33.69**
Source language tree constraint	34.90	31.04	31.98	30.05	31.23**
Exp08 is done on span >10	37.12	33.20	33.63	32.20	33.17
Exp08+ left child optimization two fork	37.95	34.01	34.66	33.47	34.13**
Exp08+ right child optimization two fork	37.68	33.57	34.23	32.93	33.70**
Exp08+ forest based two forks	37.99	35.96	34.62	33.55	34.15**

Note: * or ** indicates a significant increase in baseline exp01 compared to the test set, P <0.05 or 0.01

Three baseline systems were selected for effective comparison. Exp01- standard hierarchical phrase system was NiuTrans Hierarchy. On the basis of exp01, if syntactic constraints were soft, exp02- used a better feature set, {NP+, NP=, VP+, VP=, PP+, PP=, XP+, XP=}. Exp03- was in exp01 decoding. When the source language fragment conformed to the syntactic structure, the span constraint was removed. This approach can be viewed as the simplest use of source language syntactic information in hierarchical phrase systems.

Table 2. BLEU value of Web translation system

	Tune	MT08	MT12	MT08.p	All test
	483	666	420	682	1768
Standard hierarchical phrase base system	31.80	23.90	21.90	25.00	24.21
Exp01+ syntax soft constraint (feature)	31.91	23.84	22.06	25.03	24.26
Exp01+ removes span constraint	31.85	23.95	21.86	25.00	24.22
Exp03+ tree-to-string rule	32.24	24.20	22.43	25.42	24.59
Exp04+ tree-to-string characterization	32.35	24.27	22.40	25.51	24.64*
Exp04+ fuzzy syntax mark	32.46	24.33	22.43	25.59	24.70**
Exp04+ fuzzy tree structure	32.60	24.46	22.48	25.65	24.81**
Exp04+ fuzzy tree structure & syntax mark	32.67	24.53	22.55	25.80	24.90**
Keywords Exp04+ based decoding	32.70	24.64	22.77	25.81	24.99**
Source language tree constraint	31.20	22.56	20.07	23.27	22.56
Exp08 is done on span >10	32.22	24.24	22.33	25.27	24.53
Exp08+ left child optimization two fork	33.04	24.99	23.04	26.24	25.44**
Exp08+ right child optimization two fork	32.77	24.60	22.87	25.86	25.07**
Exp08+ forest based two forks	33.02	24.94	23.07	26.30	25.48**

It can be seen from Table 1 and Table 2 that adding syntactic soft constraints (exp01) can lead to small performance gains over multiple test sets. On the one hand, this result confirms that source language syntax information is useful for machine translation. On the other hand, the results also show that simple syntactic features (without introducing new rules or increasing decoding space) cannot effectively improve the performance of hierarchical phrase system. In addition, removing the span constraint in exp03 will lead to certain BLEU improvements. The experimental results also verify that reducing span constraints is helpful for systems based syntactic constraint.

In addition, the running speeds of different decoding methods (tree-to-string rules and features were added for the baseline system, using string based decoding was used and the two forks method was added) were measured, as shown in Table 3.

Table 3 shows the average speed at which all the data is processed by the system. It can be seen that the translation speed of the system was only decreased by 10 % after introducing syntactic rules, which was consistent with the expected results. The introduction of less syntactic rules did not increase the system burden too much. On the other hand, when a string based decoding was introduced, the system run at

a half rate. The result is primarily for all span memory calculations due to string based decoding, and the system does not constrain the decoding family by decoding the syntax structure just as tree based decoding does. As a result, the system is burdened heavily.

Table 3. Operating speeds of different decoding methods

Number	system	Speed
Exp01	Standard hierarchical phrase base system	1.11 Sentence per second
Exp05	+Tree-to-string features and rules	1.01 Sentence per second
Exp09	+ decoding based String	0.47 Sentence per second
Exp12	+ left child priority two fork	0.42 Sentence per second

Table 3 shows the average speed at which all the data is processed by the system. It can be seen that the translation speed of the system was only decreased by 10 % after introducing syntactic rules, which was consistent with the expected results. The introduction of less syntactic rules did not increase the system burden too much. On the other hand, when a string based decoding was introduced, the system run at a half rate. The result is primarily for all span memory calculations due to string based decoding, and the system does not constrain the decoding family by decoding the syntax structure just as tree based decoding does. As a result, the system is burdened heavily.

In addition to examining the BLEU values of system output results, the use of different types of rules in optimal translation derivations were studied, as shown in Table 4.

Table 4. Percentage of different rule matching methods used

Rule matching method	Baseline (%)	+ Tree-to-string (%)	+ Binary tree (%)
String based	100	73	55
Tree based	0	27	45

5. Conclusion

The research focus of this thesis is the decoding of syntactic information of source language in hierarchical phrase system. The decoding strategy of tree-to-string rules in hierarchical phrase system was studied, and the corresponding decoding strategy was proposed. On the basis of the hierarchical phrase translation model, the number of string translation model was added as a supplementary model. Through the comparison of the experimental results of different decoding strategies, it can be found that the combination of the binary syntax tree and the decoding based on string can achieve maximum performance improvement. The conclusions can be obtained through this study that the biggest advantage of tree-to-string translation model is that the rules (and all variables) follow the syntax tree constraints. For example, all of the variables are required to cover legitimate and complete unit syn-

tactic sub-trees. Therefore, decoding of tree-to-string translation does not require forcing to join the constraint of the rule span. In addition, due to the use of source language syntax tree, the constraints such as the number of variables, the number of continuous variables in the source language, and the necessary lexicalization of rules in hierarchical phrases can be eliminated in tree-to-string translation models. Although good results have been achieved in this paper, there were still some problems that needed to be further studied in the future such as how to improve the accuracy of long sentence dependency analysis.

References

[1] W. Wang, J. May, K. Knight, D. Marcu: *Re-structuring, re-labeling, and re-aligning for syntax-based machine translation.* Journal Computational Linguistics *36* (2010), No. 2, 247–277.

[2] L. Adam: *Statistical machine translation.* ACM Computing Surveys (CSUR) *40* (2008), No. 3, article 8.

[3] D. Chiang: *Hierarchical phrase-based translation.* Journal Computational Linguistics *33* (2007), No. 2, 201–228.

[4] R. Q. Zhang, K. J. Yasuda, E. Sumita: *Chinese word segmentation and statistical machine translation.* Journal ACM Transactions on Speech and Language Processing *5* (2008), No. 2, Article No. 4.

[5] F. J. Och, H. Ney: *The alignment template approach to statistical machine translation.* Journal Computational Linguistics *30* (2004), No. 4, 417–449.

[6] F. J. Och, H. Ney: *A systematic comparison of various statistical alignment models.* Journal Computational Linguistics *29* (2003), No. 1, 19–51.

[7] C. Tillman, H. Nye: *Word reordering and a dynamic programming beam search algorithm for statistical machine translation.* Journal Computational Linguistics *29* (2003), No. 1, 97–133.

[8] H. Alshawi, S. Bangalore, S. Douglas: *Learning dependency translation models as collections of finite-state head transducers.* Computational Linguistics *26* (2000), No. 1, 45–60.

[9] P. F. Brown, J. Cocke, S. Della Pietra, V. J. Della Pietra, F. Jelinek, J. D. Lafferty, R. L. Mercer, P. S. Roossin: *A statistical approach to machine translation.* Journal Computational Linguistics *16* (1990), No. 2, 79–85.

[10] P. F. Brown, S. A. Della Pietra, V. J. Della Pietra, R. L. Mercer: *The mathematics of statistical machine translation: Parameter estimation.* Journal Computational Linguistics–Special issue on using large corpora: II *19*, (1993), No. 2, 263–311.

[11] K. Knight: *Decoding complexity in word-replacement translation models.* Journal Computational Linguistics *25* (1999), No. 4, 607–615.

[12] K. Church, R. Patil: *Coping with syntactic ambiguity or how to put the block in the box on the table.* Journal Computational Linguistics *8* (1982), Nos. 3–4, 139–149.

[13] A. V. Aho, J. D. Ullman: *Syntax directed translations and the pushdown assembler.* Journal of Computer and System Sciences *3* (1969), No. 1 37–56.

[14] A. L. Berger, S. A. Della Pietra, V. J. Della Pietra: *A maximum entropy approach to natural language processing.* Journal Computational Linguistics *22*, (1996), No. 1, 39–71.

[15] D. Wu: *Stochastic inversion transduction grammars and bilingual parsing of parallel corpora.* Journal Computational Linguistics *23* (1997), No. 3, 377–403.

Received June 6, 2017

Acta Technica *62* No. 1A/2017, 541–552

Electric vehicle control system based on CAN bus

Han Peng[1]

Abstract. The purpose of this paper is to develop a theoretical basis for improving electric vehicle control system which based on controller area network (CAN) bus. Based on the CANOPEN protocol, electric vehicle control system was analyzed, which mainly focused on DS301and DS302 sub protocol. The method is to design a electric vehicle control system of by CANOPEN network. Then, strategy for electric vehicle control was studied and operation mode and working condition of electric vehicle was concluded. Finally, hardware and software systems of electric vehicle control system were designed. Mainly, hardware concerning flyback power supply and main controller were debugged. Modular method was adopted when designing software. Software was classified into five modules to design according to its function. The experimental results show that the electric vehicle system based on CAN bus is suitable for the development of both hardware and software. Based on the above finding, it is concluded that electric vehicle control system was improved to a certain extend.

Key words. Electric vehicle, CAN bus, control system.

1. Introduction

Transportation is more and more convenient with the rapid development of automobile industry in recent years. However, more and more environment and energy issues are emerging [1], which interferes heavily in the quality of people's lives. For example, some regions in the world are instable and global economy development is influenced because of unbalanced petroleum distribution. Besides, automobile industry account for a large proportion of the world's greenhouse gases because a large amount of fossil fuel is assumed. Moreover, vehicle emissions such as respirable suspended particulates, carbon monoxide and oxynitride would increase the incidence of respiratory disease [2–3]. For these reasons, electric vehicle is needed. Comparing with traditional vehicle, electric vehicle has many advantages, such as environmental-friendly, easy to drive, high efficiency, and low noise. There are no engine, transmission and exhaust system. Besides, electric vehicle can charge in off-peak hours of power demand, which can reduce power shortage in peak hours [4].

[1]School of Mechanical Engineering, North China University of Water Resource and Electric Power, Zhengzhou, 450045, China

Electric vehicle can be dated back to 1880s, which developed rapidly until 1920. Since 1920s, electric vehicle is gradually replaced by automobile because more and more petroleum was exploited and there are more and more studies about automobile. However, since 1950s, electric vehicle industry was attached great importance again because more attention was paid to oil crisis, environmental protection and rational used of energy [5]. Electric vehicle is a complex systematic engineering, which needs a reliable control system with superior performance to comprehensively coordinate and control the work of various components [6]. Therefore, study on design of electric vehicle control system is of great important to the development of electric vehicle technology. Many scholars at home and abroad have studied electric vehicle control system.

For example, a new controller is researched and developed [7], which can be used to reduce vibration by disturbing observer and enhance stability of power transmission system of electric vehicle using electrical machine. The control slip rate of electric vehicle with changing parameters was controlled by sliding-mode [8]. Based on Nissan LEAF blade electric vehicles (BEV), Kawamura and his partners integrated its two forward gears to set dynamic model and economic model [9]. Different driving control strategies for three models were designed based on different driving conditions [10]. The strategy for automatic mode identification is studied based on fuzzy control system. Thus, electric vehicle control system based on CAN bus was to be studied to improve control system [11].

2. Materials and methods

2.1. Application of CANOPEN protocol in electric vehicle

For those electric vehicles in use, several electronic control units are controlled by main controller through CAN bus [12], for example, electric machine, ABS/ESP unit, automotive dashboard, battery controllers, air conditioner controller, and controllers of door, window and windshield wiper. In common, electric vehicle bus is made up of two or three CAN bus. A high-speed CAN bus is used to connect main controller to electric machine driver while one or two other low-speed CAN buses are used communication between main controller and low-speed signals. Thus, for the system studied only two electric machines were controlled by main controller through CAN bus (see Fig. 1) and the other parts will be worked out in the future work.

Basic CANOPEN network is built according to DS301 sub protocol of CANOPEN protocol, which is able to distribute identifier, establish object dictionary, initialize SDO and PDO communication objects, and establish state machine and management objects of NMT network. However, with the most basic network functions, this network was unable to meet requirements of complex system. Thus, start-up procedures of CANOPEN network was designed based on DS302 sub protocol of CANOPEN protocol and electric machine control protocol stack was built based on DS402 sub protocol of CANOPEN protocol for the application of CAN bus to electric vehicle.

DS301 sub protocol defines state machine for network management and ways

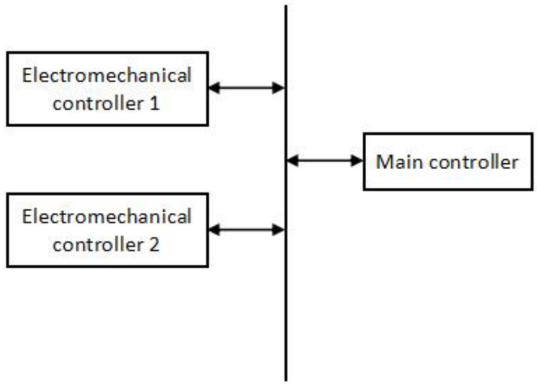

Fig. 1. CAN Bus structure of electric vehicle

to switch node network state. Simple systems such as vo module can be start-up with this procedure while complex system such as electric machine driver, should be start-up with an improved start-up procedure to ensure all nodes were started-up safely. Under CANOPEN protocol, main engine need to reset communication of sub-ordinate computer before starting up sub-ordinate computer node. State of sub-ordinate computer node should be checked by NMT main machine before sending instruction to reset communication [13] because equipment such as machine controller would enter a special working mode similar to manual mode when NMT main engine suddenly lost connection.

Figure 2 shows start-up procedure of CANOPEN network based on DS302 sub protocol. Configuration audit for software version under DS302 sub protocol was ignored because network structure of this system was simple. Currently, the system studied controlled two cooperative-working electric machine controllers whose sub-ordinate computer node was set as necessary and states need to be reviewed before start-up when configuration network.

2.2. Electric vehicle control strategy

Electric vehicle control system was made up of several components and sub-systems, including electric machine controller, energy management system (EMS), vehicle control system, accelerator pedal and brake pedal. This control system was based on vehicle control unit, which transmits and exchanges information with CAN bus. Figure 3 shows structure of the vehicle control system.

Electric vehicle has four gears, which operation can be classified into such five modes with the used of accelerator pedal and brake pedal as neutral position, normal driving pattern, braking mode, failure mode for protection and start mode [14]. After processing signals of key, pedal, gears and signals of other sensors according to control strategy, electric vehicle controller identified the corresponding model and passed the corresponding instruction into corresponding control unit to control the vehicle accordingly. According to those five models, seven working conditions can be

achieved, such as parking, braking, charging, reversing, driving, starting and limb driving mode, which basically included all working conditions of electric vehicle and met the basic driving function of vehicle. Vehicle control system determines specific working conditions mainly according to key signal (Key-On), accelerate pedal signal (APP), driving gear signal (Gear-D), minimum power for vehicle normal operation (SOC-Low), reversing gear signal (Gear-R), charging request signal (Charge-Req), braking pedal signal (BPP), defective cells (Fault1, Fault2), and battery signal (SOC) [15].

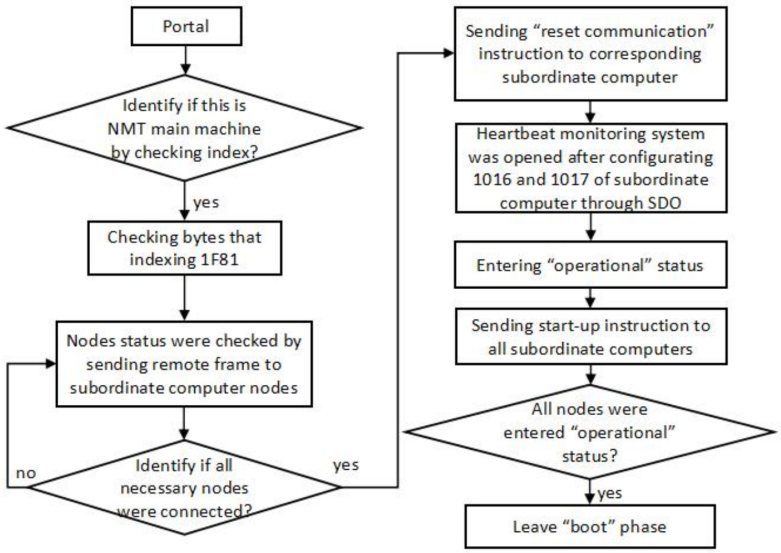

Fig. 2. Flow chart of main engine start-up procedure of the studied system

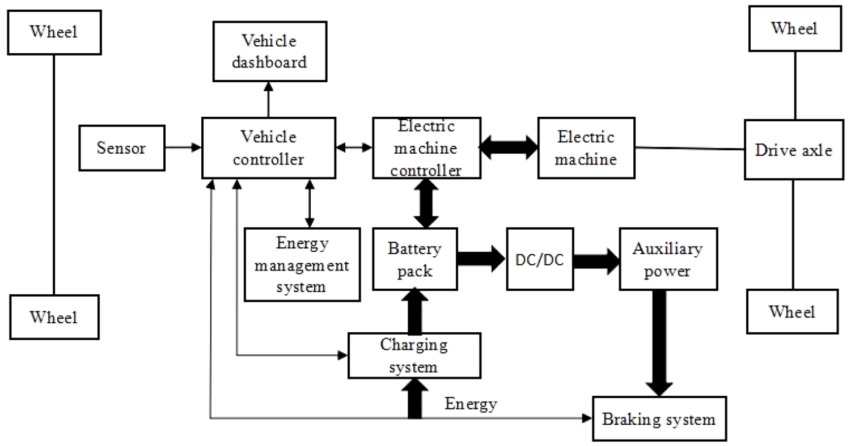

Fig. 3. Structure of electric vehicle control system (Thick arrows stands for energy flow; thin arrow stands for control signal; straight line stands for mechanical joint)

3. Experimental results and discussion

3.1. Hardware design for electric vehicle control

The electric vehicle system was powered by 72 V storage battery which was directly connected to direct current (DC) bus of electric machine. However controller chips need to be powered by low voltage of S V/3.3 V, so switch signal for MOSFET switch tube should be more than ten volts. Thus, a battery was designed to convert 72 V into SV or 12 V. In the system designed, current of 1.2 A was needed by SV and 0.6 A was needed by 12 V. Simple LDO linear chip was inappropriate for declining voltage because of large output current and great voltage differences between 72 V and 12 V. Thus, fly-back DC/DC power with high-frequency transformer was used. Figure 4 shows topological structure of fly-back DC/DC power.

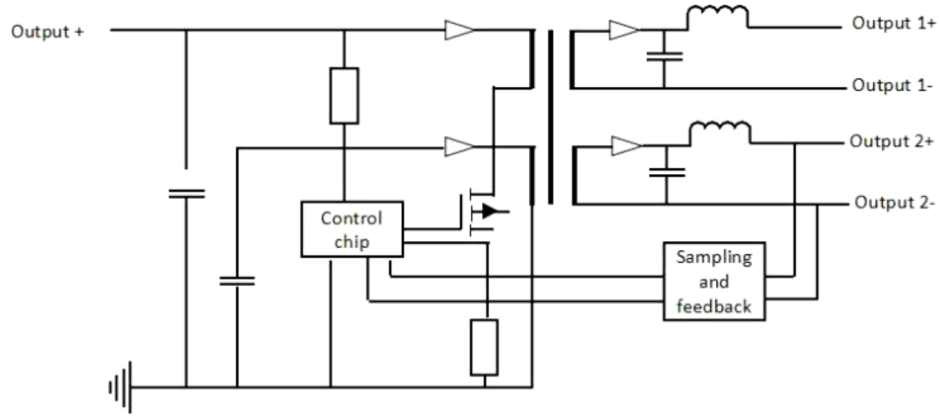

Fig. 4. Topological structure of fly-back DC/DC power

Function of high-frequency transformer was similar to power inductor which storage energy when MOS breakover and release energy to secondary side when MOS turned off. Totally, there were four parallel branches for windings. One of them was subsidiary loop output used to supply power for chip control loop. Two of them were output windings connected to load, outputting 12 V and SV voltage respectively. SV winding was designed as feedback loop because it supplied power for digital circuit which needs relatively higher accuracy.

MCU of TMS320F28035 type was used as central controller of main controller of electric vehicle. Signals listed in below Table 1 should be detected by main controller. Interface circuit for digital signal detection was simple, which can connected to GPIO interface of MCU after partial pressure followed by Π-shaped filter circuit. Vehicle speed signal, pulse signal, was connected to ECAP pin of MCU. 3.3 V power supply was used by MCU and voltage range of AD interface was 0–3.3 V. Power of common electronic pedal sensor and electronic steering sensor were supplied by SV and the range of outputted analog signal was 0–5 V. Thus, analog signal cannot be directly input in MCU. Figure 5 shows AD interface circuit. Electric machine controller was

configured by main controller through CAN bus. Figure 6 shows CAN interface circuit of main controller.

Table 1. Semaphores to be detected by main controller of electric vehicle

Sigals	Signal type	Voltage range
Vehicle speed	Pulse	0–5 V
Switch	Number	0–5 V
Direction switch	Number	0–5 V
The reserved switch	Number	0–5 V
Signal of accelerator pedal	Simulation	0–5 V
Signal of brake pedal	Simulation	0–5 V
Turning signal	Simulation	0–5 V
Temperature measurement	Simulation	0–5 V

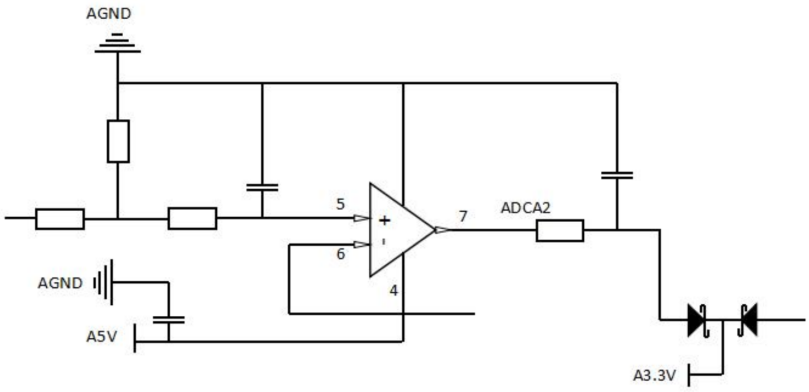

Fig. 5. Schematic diagram of AD interface circuit

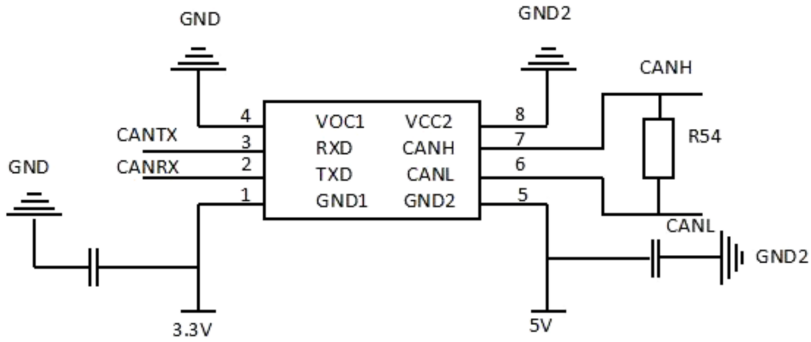

Fig. 6. Chip circuit of CAN bus interface

3.2. Software design for electric vehicle control system

Software was of great importance for vehicle controller because all parts of vehicle were controlled by software. Different modules were used to design software according to software functions. Based on different functions, software of vehicle controller was classified into such three hierarchies as management, executive and interface. Figure 7 shows hierarchy structure.

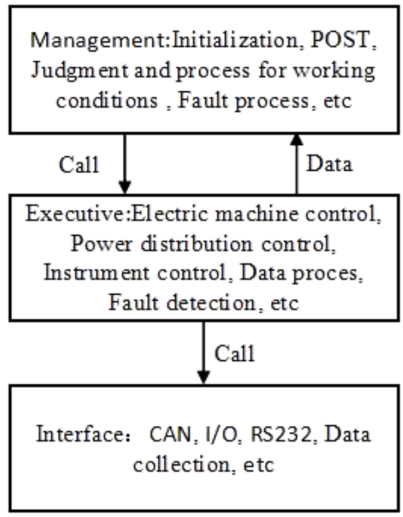

Fig. 7. Software overall structures

Main program was the key of software design, which was used to identify working status of vehicle according to collected operational information and real-time status of vehicle. Figure 8 shows flow chart of main program.

Subprogram design, power-on-self-test (POST), fault detect, failure process, and judgment and process of working conditions were tackled in subprogram design. First, all modules of controller should be initialized before operating procedures. Figure 9 shows specific modules' content and initializing sequence. POST was needed after initialization and following Fig. 10 shows POST flow chart. To ensure security, fault detection was made for all parts of system and Fig. 11 shows failure detection flow chart. If it detected failures, failure process was needed. If there are no failures, it moves to judgment and process for work condition. Vehicle working condition was determined according to collected operation information and real-time status of all parts of vehicle. Then, corresponding instructions were given to control normal operation of vehicle.

3.3. Design of electromagnetic compatibility (EMC)

Frequency converter and motor are two serious electromagnetic interference sources of electric vehicle. The frequency converter consists of two parts, the main loop and

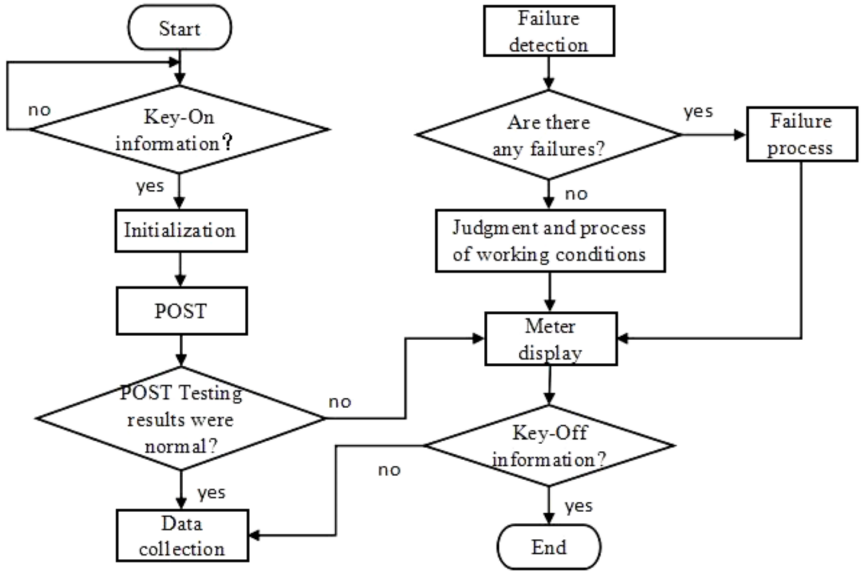

Fig. 8. Flow chart of main program

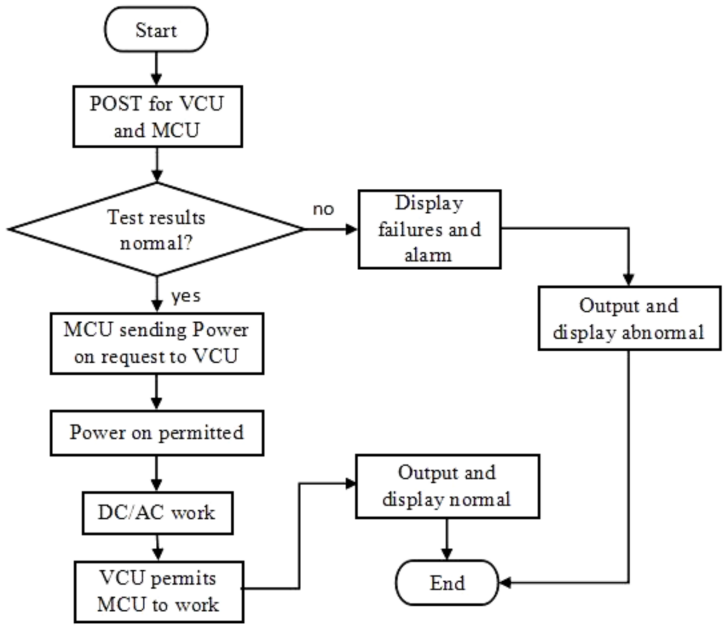

Fig. 9. Flow chart of POST

the control loop. The main circuit of frequency converter is mainly composed of rectifier circuit, inverter circuit and control circuit, in which rectifier circuit and inverter

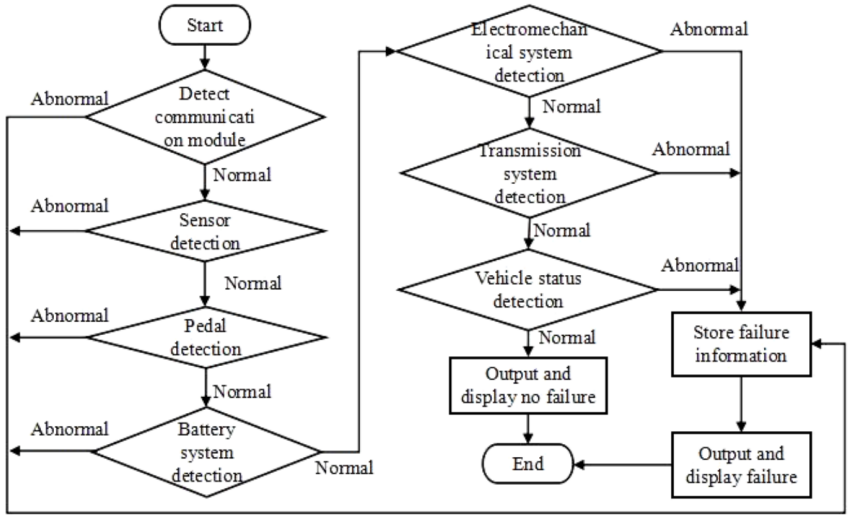

Fig. 10. Flow chart of failure detection

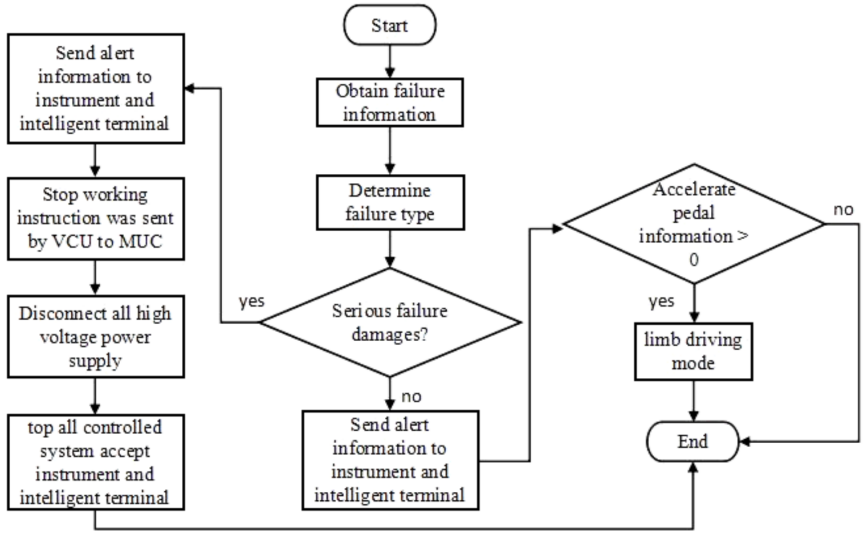

Fig. 11. Flow chart of failure processing

circuit are composed of power electronic devices. The power electronic device has nonlinear characteristics. When the inverter is running, it has to do fast switching, resulting in higher harmonics. Therefore, the output waveform of the inverter contains a large number of higher harmonics besides the fundamental wave. No matter what kind of interference, the higher harmonic is the main reason for the interference of the inverter. Therefore, the converter itself is the harmonic interference source, so it will affect the power side and the output side of the device. Higher order har-

monics have strong radiation effects. If the harmonic energy is directly broken or entered into the digital equipment by other means, then it will disturb the normal operation of the equipment, increase its failure rate, and affect the service life of the equipment. The motor is an inductive device. When the motor works, it will produce strong pulse flow. At the same time, it can spread in the power network and radiate into the surrounding space. The opening, stopping and load change of the motor will change the working current and produce the pulse current, especially the rectifier motor. This interference is represented by an irregular pulse stream with a spectrum of about l0 kHz–1 GHz. Other electromagnetic interference sources include microprocessors, microcontrollers, electrostatic discharges, and instantaneous power actuators, such as electromechanical relays, switching power supplies, and lightning. In a microcontroller system, the clock circuit is usually the largest wideband noise generator, and this noise is scattered across the spectrum. With the application of a large number of high speed semiconductor devices, the edge hopping rate is very fast, and this circuit can produce harmonic interference up to 300 MHz.

All electronic circuits can receive transmission of electromagnetic interference. Although some of the electromagnetic interference can be received directly by radio frequency, most of them are received by instantaneous conduction. In digital circuits, critical signals are most susceptible to electronic interference. These signals include reset, interrupt, and control signals. The low level amplifier, the control circuit and the power supply adjustment circuit are also susceptible to noise. In order to design electromagnetic compatibility and meet electromagnetic compatibility standards, designers need to minimize radiation to enhance their susceptibility to radiation and interference immunity. Both emission and interference can be classified according to the combination of radiation and conduction. Radiation woe is very common in high frequency, but conduction path is more common in low frequency.

4. Conclusion

Vehicle control system was studied based on CAN bus. Basic structure for CAN bus was built based on DS301 sub-protocol. Then, start-up procedure of CANOPEN network for electric vehicle control system was built according to reference protocol DS302. Electric vehicle operation was classified into five modes and seven working conditions according to its four gears and use of accelerate pedal and brake pedal. Finally, hardware and software of electric vehicle control system were designed. Hardware of flyback power supply and main controller were debugged during hardware design. Modular method was adopted in software design. According to its functions, software was classified into three different hierarchies, including management, executive and interface, to be designed by different modulus. Then, main program and sub-program including initialization, POST, failure detection and process, and judgment and process of working condition were designed.

However, further study is needed because of limited research conditions, time and knowledge. It is at preliminary design phase for software and hardware design of vehicle controller. More efforts were needed in the future study to design a complete and practical controller.

References

[1] M. Sarancha: *An analysis of regional strategies and programs in the framework of the development of automobile tourism in the Central Federal District.* Universities for Tourism and Service Association Bulletin *9* (2015), No. 1, 34–41.

[2] E. Magaril, R. Magaril: *Improving the environmental and performance characteristics of vehicles by introducing the surfactant additive into gasoline.* Environmental Science & Pollution Research *23* (2016), No. 17, 17049–17057.

[3] I. J. Lu, S. J. Lin, C. Lewis: *Decomposition and decoupling effects of carbon dioxide emission from highway transportation in Taiwan, Germany, Japan and South Korea.* Energy policy *35* (2007), No. 6, 3226–3235.

[4] J. Peng, H. He, W. Liu, H. Guo: *Hierarchical control strategy for the cooperative braking system of electric vehicle.* Scientific World Journal (2015), No. 4, ID 584075.

[5] Y. Wang, L. H. Hui, B. Liu: *The study of intelligent scheduling algorithm in the vehicle ECU based on CAN bus.* Open Cybernetics & Systemics Journal *9* (2015), No. 1, 1461–1465.

[6] H. Zhao, G. F. Li, N. H. Wang, S. L. Zheng, L. J. Yu, Y. Gao: *Research status of several key technologies for the development of electric vehicles.* Applied Mechanics and Materials *160* (2012), No.Chapter 3, 361–365.

[7] J. M. Rodriguez, R. Meneses, J. Orus: *Active vibration control for electric vehicle compliant drivetrains.* Annual Conference of the IEEE Industrial Electronics Society (IECON), 10–13 November 2013, Vienna, Austria, IEEE Conference Publications (2013), 2590–2595.

[8] T. Goggia, A. Sorniotti, L. de Novellis, A. Ferrara, P. Gruber, J. Theunissen, D. Steenbeke, B. Knauder, J. Zehetner: *Integral sliding mode for the torque-vectoring control of fully electric vehicles: Theoretical design and experimental assessment.* IEEE Transactions on Vehicular Technology *64* (2015), No. 5, 1701–1715.

[9] C. Lv, J. Zhang, Y. Li, Y. Yuan: *Mode-switching-based active control of powertrain system with nonlinear backlash and flexibility for electric vehicle during regenerative deceleration.* Institution of Mechanical Engineers, Part: D, Journal of Automobile Engineering *229* (2015), No. 11, 1429–1442.

[10] Y. Chen, W. Liu, Y. Yang, W. Chen: *Online energy management of plug-in hybrid electric vehicles for prolongation of all-electric range based on dynamic programming.* Mathematical Problems in Engineering (2015), ID 368769.

[11] H. Wang, Q. Song, S. Wang, P. Zeng: *Dynamic modeling and control strategy optimization for a hybrid electric tracked vehicle.* Mathematical Problems in Engineering (2015), ID 251906.

[12] J. Wang, Q. N. Wang, P. Y. Wang, J. N. Wang, N. W. Zou: *Hybrid electric vehicle modeling accuracy verification and global optimal control algorithm research.* International Journal of Automotive Technology *16* (2015), No 3, 513–524.

[13] D. Guilbert, M. Guarisco, A. Gaillard, A. N'Diaye, A. Djerdir: *FPGA based fault-tolerant control on an interleaved DC/DC boost converter for fuel cell electric vehicle applications.* International Journal of Hydrogen Energy *40* (2015), No. 45, 15815 to 15822.

[14] C. X. Song, F. Xiao, S. X. Song, S. L. Peng, S. Q. Fan: *Stability control of 4WD electric vehicle with in-wheel motors based on integrated control of electro-mechanical braking system.* Applied Mechanics and Materials *740*, (2015), No.Chapter 3, 206–210.

[15] B. Weeks, J. Xu, B. Cao, Q. Li, Q. Yang: *Compound-type hybrid energy storage system and its mode control strategy for electric vehicles.* Journal of Power Electronics *15* (2015), No. 3, 849–859.

Received June 6, 2017